land

Planning for Sustainable Urban and Land Development

Edited by
Zongcai Wei, Yuting Liu and Andrzej Biłozor

mdpi.com/journal/land

MDPI

Planning for Sustainable Urban and Land Development

Planning for Sustainable Urban and Land Development

Guest Editors

Zongcai Wei
Yuting Liu
Andrzej Biłozor

Guest Editors

Zongcai Wei	Yuting Liu	Andrzej Biłozor
School of Architecture	School of Architecture	Department of
South China University of	South China University of	Socio-Economic Geography
Technology	Technology	University of Warmia and
Guangzhou	Guangzhou	Mazury in Olsztyn
China	China	Olsztyn
		Poland

This is a reprint of the Special Issue, published open access by the journal *Land* (ISSN 2073-445X), freely accessible at: https://www.mdpi.com/journal/land/special_issues/Z2TH91666P.

For citation purposes, cite each article independently as indicated on the article page online and as indicated below:

Lastname, A.A.; Lastname, B.B. Article Title. *Journal Name* **Year**, *Volume Number*, Page Range.

Contents

About the Editors

Zongcai Wei

Zongcai Wei is a professor at the Department of Urban Planning, School of Architecture, South China University of Technology (China). He is also a core member of the State Key Laboratory of Subtropical Building and Urban Science. His research interest covers big data and smart cities, housing and community planning, travel behavior, urban development, and spatial planning. He is the Principal Investigator of several key research projects and urban planning projects and has published over 100 journal papers in these research fields. He currently serves as the Deputy Head of Department of Urban Planning. He is also an Early Career Editorial Board Member of several reputable professional journals, such as Chinese Geographical Science, Economic Geography (in Chinese), and Tropical Geography (in Chinese). In addition to this, he is an active member of several academic committees, including Youth Working Committee of the Geographical Society of China, Territorial Spatial Planning Research Committee of the Chinese Society of Natural Resources.

Yuting Liu

Yuting Liu is a Professor at the Department of Urban Planning, School of Architecture, South China University of Technology, and a core member of the State Key Laboratory of Subtropical Building and Urban Science. His research focuses on urban and rural development and planning, housing policy and community planning, urban renewal, and socio-spatial differentiation. He serves as the Executive Deputy Director of the Guangdong-Hong Kong-Macao Greater Bay Area Planning Innovation Research Center. He is an active member of several academic committees, including the Urban Geography Committee of the Geographical Society of China and the Urban-Rural Governance and the Policy Research Committee of the Urban Planning Society of China. Additionally, he has been the planning consultant for various governments within Guangdong Province.

Andrzej Biłozor

Andrzej Biłozor is a professor at the Department of Socio-Economic Geography at the Institute of Spatial Management and Geography, Faculty of Geoengineering, University of Warmia and Mazury in Olsztyn (Poland). His research interests are mainly focused on spatial planning, urban analysis, optimization of urban space, spatiotemporal analysis, fuzzy set theory, and changes in land use and land cover. These activities concern the development of methods for investigating the phenomena of city planning and sustainable development, the evaluation of spatial conflicts, and the optimization of spatial processes. He is the author of more than 80 scientific papers on the subject and actively leads and participates in scientific projects. He has also been an academic teacher for many years, teaching in this field.

Article

Exploring the Relationship between Urbanization and Eco-Environment Using Dynamic Coupling Coordination Degree Model: Case Study of Beijing–Tianjin–Hebei Urban Agglomeration, China

Xuying Wu, Yanjun Zhang * and Xiaoyan Li

College of Earth Sciences, Jilin University, Changchun 130061, China; wuxuying0827@163.com (X.W.); lxyan@jlu.edu.cn (X.L.)

* Correspondence: yanjunzhang@jlu.edu.cn

Abstract: The continuous and rapid development of global urbanization has brought great pressure to eco-environments. It is particularly serious in mega urban agglomerations, which determine the development process of urbanization in the world and affect the international competitiveness of countries. Taking the mega urban agglomerations with few research cases as the research area to explore the relationship between urbanization and eco-environment is vital to realize global sustainable development and optimize the development direction and trend of world urbanization. It is of great significance to assume the historical task of shifting the center of the world economy and the main position of the "Belt and Road" construction for China, and enhance its international competitiveness, as well as accelerate China's high-quality development of new urbanization and the realization of ecological civilization. Previous studies mostly used the static coupling coordination degree (SCCD) model, which has limitations in describing complex interactions. This study used the dynamic coupling coordination degree (DCCD) model to analyze relationships in Beijing–Tianjin–Hebei urban agglomeration (BTH) from 2003 to 2019, which is one of China's mega urban agglomerations. For the first time, we explain the progressiveness of the DCCD model from the construction concept, theoretically analyze the rising and falling laws of DCCD in break-in development stage, and propose the concepts of "benign transition" and "non-benign transition" when DCCD changes from break-in development to utmost development. Results show that BTH's urbanization increased in fluctuation, with significant regional differences. The eco-environment was relatively good, but there are potential risks. The DCCD showed an S-shaped curve. Break-in development was the main type of DCCD. Moderate urbanization development and small degree of eco-environment sacrifice were necessary for "benign transition". After the "benign transition" is realized, the high-level symbiosis of DCCD and the mutual promotion can be achieved through technical improvement. According to the identification results of the main controlling factors, the DCCD can be regulated by subsystems.

Keywords: sustainable development; dynamic coupling coordination degree; mutual promotion of urbanization and eco-environment; mega urban agglomerations; Beijing–Tianjin–Hebei urban agglomeration

1. Introduction

The 2018 Revision of World Urbanization Prospects indicated that global population could add another 2.5 billion people to urban areas by 2050 [1]. Of this, China will add 255 million urban dwellers [1], accounting for 10.2% of the global growth. The development of global urbanization is advancing rapidly. The eco-environment is facing great pressure. It is very acute in China, which is urbanizing rapidly. Especially, BTH is facing more serious pressure on resources and eco-environment, as one of China's mega urban agglomerations. Balancing the relationship between urbanization and eco-environment will determine

the world urbanization development process, affect the international competitiveness of countries, and is vital to realizing the United Nations 2030 Agenda for Sustainable Development. It is of great significance to assume the historical task of shifting the center of gravity of the world economy and the main position of the "Belt and Road" construction for China, and enhance its international competitiveness as well as accelerate China's high-quality development of new urbanization and the realization of ecological civilization. However, there are three shortcomings in the existing research on urbanization and eco-environment. (1) Insufficient attention has been paid to changes in the leading factors of urbanization and eco-environment. The analysis of the internal driving factors of CCD is not deep enough. (2) More studies use the SCCD model to quantify the relationship of urbanization and eco-environment [2–5]. In fact, their relationship is an open, unbalanced, dynamic fluctuation system with nonlinear interaction and self-organizing ability [6,7]. The interactions are extremely complex [8–10]. The SCCD model has some limitations in describing this relationship. (3) There are few case studies on the interaction between urbanization and eco-environment in mega urban agglomerations, and it is urgent to carry out research to meet the needs of the world and the countries.

Research on the relationship between urbanization and eco-environment has emerged since the 1990s. At present, a circular path of "empirical research–law summary–theory construction–empirical research" has been established [2,11]. The subjects involved include ecology, geography, management, economics, and environmental science. The research area is mainly ecologically fragile, urbanized, and metropolitan, covering multiple scales including world, national, provincial, urban, and regional [12]. And the research pays more attention to the coercion impact of urbanization on the eco-environment. The important achievements in theoretical research mainly include "Environmental Kuznets curve" [13–15], "Ecological Footprint Theory" [16–19], and "Eco-environment Pressure-State-Response model". The empirical research includes the single-dimension research of eco-environment protection and governance in the process of urbanization, the coupling and coordination research of urbanization and eco-environment, the coupling law disclosure, the coordination relationship evaluation, the simulation analysis, and the prediction analysis. It is generally accepted that there is an extremely complex interaction and stress relationship between urbanization and eco-environment. The main performance is that urbanization has a coercive or promoting effect on the eco-environment through population growth, economic development, energy consumption, technological progress, urban management, and construction land expansion. And the eco-environment has a restrictive or carrying effect on urban development through resource carrying, environmental capacity, ecosystem services, environmental equity, and policy intervention [8,20]. That is, the development of urbanization is inevitably accompanied by the change of eco-environment, which is comprehensive and phased [7,21]. In the early stage of urbanization development, the comprehensive quality of eco-environment deteriorated, including the excessive consumption and destruction of atmosphere, water, land, organisms, resources, and energy. It even induced structural variation and functional loss of the entire ecosystem. In the middle and later stages of urbanization development, the quality of eco-environment improved. Meanwhile, the eco-environment, as the carrier and support of human activities, provides the material basis for the development of urbanization. Its material quantity and carrying capacity restrict the development of urbanization. The relationship between urbanization and eco-environment has received extensive attention.

The coupling coordination degree (CCD) model is the mainstream method to study the relationship between urbanization and eco-environment, accumulating many research results. Wu et al. found that the urbanization development in line with the eco-environment carrying capacity can avoid their mutual detriment, in their study on urbanization and eco-environment CCD [22]. Tian et al. found that there is an inverted U-shaped curve of CCD between urbanization and eco-environment [23]. Liu et al. found that urbanization hindered the further improvement in CCD [24]. There are many studies that have reached similar conclusions [14,25–27].

From 1978 to 2019, China's urbanization rate has increased from 17.92% to 60.60% [28], and is expected to reach 76.0% by 2050 [29]. In the past few decades, China's traditional urbanization development has successfully solved the problem of "fast or not fast" [30]. However, the attention given to eco-environment was not enough, and a series of eco-environment problems appeared, such as soil degradation and desertification [31,32], water and energy shortage [33–35], climate warming [36–38], loss of biological habitat [39–41], air pollution [42–44], and so on. In the new era, China's urbanization development is in the transition period from the rapid growth stage to the quality improvement stage in the late stage, with the emphasis on high-quality development [30]. The high-quality development of China's urbanization will not only determine the future of China, but also determine the development process of global urbanization. "Efficient, low-carbon, ecological, environmental protection, conservation, innovation, wisdom and safety" is the specific path to promote the high-quality development of new urbanization [30,45]. Accelerating the construction of urban agglomerations and improving their development quality is an important carrier for high-quality development of new urbanization [30,45,46]. The Central Urbanization Work Conference, the Party's "19th National Congress" report meeting and so on have clear instructions on this. As a highly developed spatial integrated urban form, urban agglomeration represents the advanced stage of industrialization and urbanization. In China, the urbanization development in the past decades at the cost of eco-environment has made it a high incidence area of ecological and environmental problems. Among them, mega urban agglomerations are the representative. Their development presents unsustainable high-density agglomeration, high-speed expansion, high-intensity pollution, and high risk of resource and environmental protection threats [45]. Mega urban agglomerations are the strategic core area of national economic development and the main area of national new-type urbanization. They bear the historical responsibility of carrying the shift of the center of gravity of the world economy. As the hub for China to enter the world and the gateway for the world to enter China, it is profoundly affecting China's international competitiveness and will determine the new pattern of world politics and economy in the 21st century. China's mega urban agglomerations have low levels of development, low levels of resource and environmental protection, low regional economic aggregate, heavy environmental pollution, and prominent ecological problems, compared to the world's most developed megacities. It is not yet able to take up the historic task of shifting the center of the world economy and building the main position of the "Belt and Road" [45]. There are few case studies on the interaction between urbanization and eco-environment in mega urban agglomerations, and it is urgent to carry out research to meet the needs of the world and the countries [45]. The BTH, the Yangtze River Delta urban agglomeration, and the Pearl River Delta urban agglomeration are the three major mega urban agglomerations in China. These regions have the most dynamic economy, the highest degree of openness, the strongest innovation capacity, and the largest number of foreign population, and their comprehensive development level is in an absolute advantage. Among them, the BTH is facing more serious resource and eco-environment stress pressure. Focusing on the BTH, in-depth analysis of the urbanization and eco-environment development and their CCD status is of great significance to assume the historical task of shifting the center of gravity of the world economy and the main position of the "Belt and Road" construction for China, and enhance its international competitiveness, as well as accelerate China's high-quality development of new urbanization and the realization of ecological civilization.

This paper took BTH from 2003 to 2019 as the research area. Firstly, we constructed the evaluation index system of urbanization and eco-environment. Secondly, we used the DCCD model rather than the SCCD model to analyze their relationship. We analyzed the spatial–temporal changes of urbanization, eco-environment, and DCCD. We paid attention to the impact of subsystems on urbanization and eco-environment. We analyzed the characteristics changes of DCCD emphatically. Combined with the analysis of urbanization, eco-environment, and DCCD, we explored the possibility of realizing the benign interaction of urbanization and eco-environment by adjusting the subsystems. This study has some

features. (1) We further developed the DCCD model on urbanization and eco-environment. (2) We analyzed the urbanization, eco-environment, and DCCD in depth from the subsystems level. (3) We clarified the existing problems of BTH. (4) We identified the weaknesses and strengths of the urbanization and eco-environment subsystems. (5) We made up for the deficiencies of existing research. We provide reference for the sustainable development of mega urban agglomerations and regional cities, and alleviate the contradiction between urbanization and eco-environment.

This paper verifies the scientificity and advancement of the DCCD model in the study of the relationship between urbanization and eco-environment from two dimensions of construction concept and empirical case. It further promotes the application of the DCCD model in the research field of the relationship between urbanization and eco-environment. Based on the evaluation results of the DCCD model, two new theoretical concepts of the relationship between urbanization and eco-environment are proposed: "benign transition" and "non-benign transition". Meanwhile, this paper deeply explores the relationship between urbanization and eco-environment from the subsystems level. The key to realizing the mutually promoting relationship between urbanization and eco-environment is found. This study provides a more scientific and accurate research idea for the related research on the relationship between urbanization and eco-environment. The research results have important reference significance for the study of the relationship between urbanization and eco-environment, and have important practical significance for the realization of benign interaction between the two.

2. Methods

2.1. Study Area

BTH is located at the intersection of the longitudinal axis of the "coastal channel" and the "Beijing–Harbin and Beijing–Guangzhou Channel" in China's "two horizontal and three vertical" urbanization strategy pattern. The geopolitical relationship between BTH and the two major newly industrialized countries, Japan and South Korea, and the strategic position of the core region of Northeast Asia formed there are very important. BTH is an important part of China's economic core region and the core region leading China's participation in global economic competition. Including Beijing, Tianjin, Shijiazhuang, Tangshan, Qinhuangdao, Handan, Xingtai, Baoding, Zhangjiakou, Chengde, Cangzhou, Langfang, and Hengshui, altogether there are 13 cities. The core areas are Beijing and Tianjin. As the capital of China, Beijing is one of the most dynamic and open regions in the world, as well as the political, cultural, international exchange, and technological innovation center of China. Tianjin is an international port city, an ecological city, and a northern economic center. The total area of BTH is 217,156 km^2. The terrain is high in the northwest and low in the southeast, and the main landform types include plateaus, mountains, and plains. The eco-environment in plateau, mountainous, and hilly areas is relatively fragile, and the plain area is one of China's important grain-producing areas (Figure 1).

As one of the three major urban agglomerations leading the high-quality development in China, BTH shoulders the dual mission of balanced north–south and coordinated development within the region. Its historical development went through four stages [47]. (1) Since the Liao and Jin Dynasties, the Gyeonggi region with Beijing as the core developed as a whole. (2) Since modern times, the Gyeonggi region with Tianjin as the economic center of the north has developed as a whole. (3) After the founding of new China, the industrialization and administrative economy formed a pattern of regional competition. (4) Since 2014, BTH collaborative development has become a national strategy, opening up a new situation of regional cooperation and development. At present, the driving role of BTH in the hinterland of the north is limited, the development gap between the north and the south continues to widen, and the degree of collaborative development of BTH is still in the stage of further deepening. In terms of policy and system, from the 1980s to now, the cooperation policy of the three places of Beijing, Tianjin, and Hebei has

gradually evolved into a formal system integration [48]. There are four stages. (1) The preliminary stage of cooperation led by the informal cooperation agreement between the governments of the three places (from 1980s to 2014). (2) The initial stage of coordinated development with formal systems such as the top-level planning of central ministries as the main, and local policies as the auxiliary (2014–2017). (3) In-depth coordinated development stage of continuous improvement in supporting policies at the executive level (2017–2022). (4) High-quality coordinated development phase of cross-regional cooperation supporting policies for advantageous driving forces (2022 to present). Judging from the historical development and institutional evolution of BTH, it is urgent for BTH to accelerate the benign interaction between urbanization and eco-environment at present, and it is also a key period of its development.
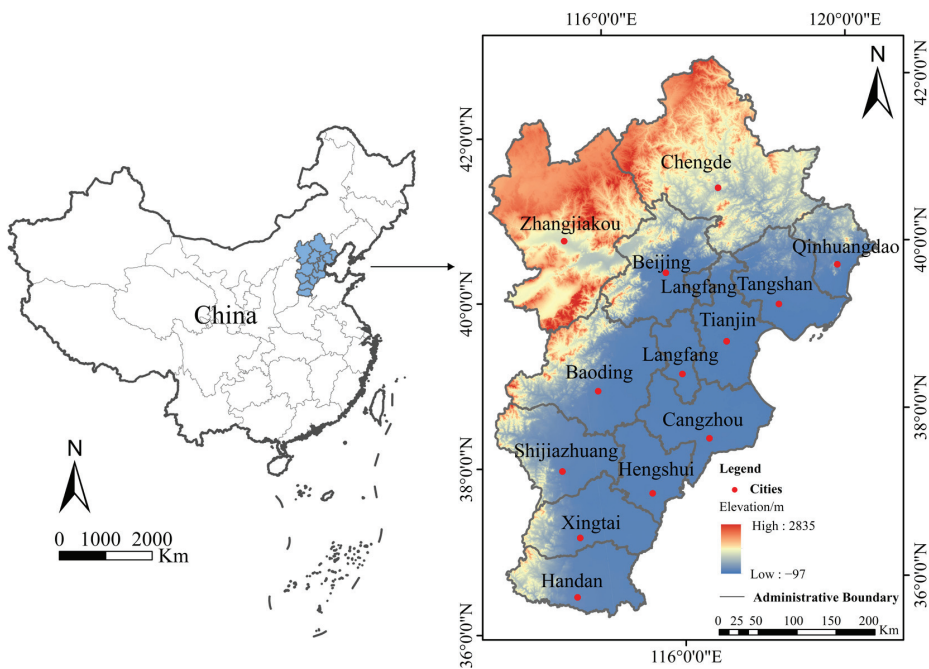
Figure 1. Spatial distribution map of study area.

2.2. Construction of Index System and Data Sources

Different disciplines have different definitions of urbanization, but it is generally believed that the connotation of urbanization mainly includes population change, economic development, spatial expansion, and social culture [21]. Therefore, this paper divided the urbanization into population, economic, spatial, and social urbanization. The concept of eco-environment varies greatly in different scenarios. This paper studies the urban eco-environment; most of its problems are related to human activities. It mainly means the summation of natural factors that affect human development and survival, including water, land, gas, resources, energy, etc. This paper divided the eco-environment into resources, environment load and ecological civilization construction. Then, combined with the data availability, development status, and strategic positioning of BTH, we carried out the principal component and independence analysis of the indicators in existing research. We selected relatively independent indicators with rich connotation to form an indicator system for urbanization and eco-environment and used the entropy weight method to ascertain the index weight (Tables 1 and 2).

Table 1. Evaluation index system and weight of urbanization.

System	Subsystem	Weight	Indicators	Unit	Attribute	Weight
Urbanization	Population urbanization	0.2276	Natural population growth rate	‰	+	0.3669
			Proportion of employees in the secondary industry	%	+	0.3056
			Proportion of employees in the tertiary industry	%	+	0.3276
	Economic urbanization	0.2755	Per capita GDP	CNY	+	0.2294
			Proportion of the secondary industry output in GDP	%	+	0.2106
			Proportion of the tertiary industry output in GDP	%	+	0.2631
			Consumer price index (CPI)	%	+	0.2969
	Social urbanization	0.2886	Per capita total retail sales of consumer goods	CNY	+	0.2365
			Disposable income of urban residents Per capita	CNY	+	0.2511
			Buses per 10,000 people number	Vehicle	+	0.2553
			Practicing (assistant) doctors per 10,000 number	Person	+	0.257
	Spatial urbanization	0.2083	Built-up area per capita	m^2	+	0.3341
			Road area per capita	m^2	+	0.3435
			City population density	Person/km^2	−	0.3224

Table 2. Evaluation index system and weight of eco-environment.

System	Subsystem	Weight	Indicators	Unit	Attribute	Weight
Eco-environment	Resources	0.3114	Coverage rate of green space in built-up area	%	+	0.363
			Per capita total grain output	kg	+	0.3441
			Park green area per capita	m^2	+	0.2929
	Environment load	0.4074	Industrial wastewater discharge per capita	t	−	0.3298
			Industrial sulfur dioxide emissions per capita	t	−	0.3391
			Household electricity consumption per capita	KW·h	−	0.3312
	Ecological civilization construction	0.2812	Wastewater treatment rate	%	+	0.2619
			Comprehensive utilization rate of general industrial solid waste	%	+	0.2883
			Artificial afforestation area	ha	+	0.4497

The research data come from China Urban Construction Statistical Yearbook, China Cities Statistical Yearbook, China Price Statistics Yearbook, China Forestry Statistical Yearbook, China Statistical Yearbook and, China Regional Economic Statistics Yearbook, China Environment Statistical Yearbook, China Population and Employment Statistics Yearbook, and statistical bulletins of economic and social development of each city.

2.3. Construction of DCCD Model

Urbanization and eco-environment systems change as a nonlinear process [7,48,49]. Combined with Lyapunov's first approximation theorem, to ensure the stability of nonlinear system development, the general function of the urbanization and eco-environment system change process can be approximately expressed as Equations (1) and (2) [48].

$$f(U) = \sum_{i=1}^{n} a_i x_i, \ i = 1, 2, 3 \cdots, n \tag{1}$$

$$f(E) = \sum_{j=1}^{n} a_j x_j, \ j = 1, 2, 3 \cdots, n \tag{2}$$

The relationship of urbanization and eco-environment is a complex interactive force. It is a complex system composed of the urbanization system $f(U)$ and the eco-environment system $f(E)$. Combined with the general system theory [50], the evolution equations of this system can be described as (3) and (4):

$$A = \frac{df(E)}{dt} = \alpha_1 f(E) + \alpha_2 f(U), \ V_A = \frac{dA}{dt} \tag{3}$$

$$B = \frac{df(U)}{dt} = \beta_1 f(E) + \beta_2 f(U), \ V_B = \frac{dB}{dt} \tag{4}$$

In Equations (3) and (4), U and E are the urbanization and eco-environment level. Table 3 shows the classification criteria of U and E. A and B are the evolution states of urbanization and eco-environment. α_1 and α_2 are the influence coefficients of eco-environment and urbanization on the evolution state of the urbanization system. β_1 and β_2 are the influence coefficients of eco-environment and urbanization on the evolution state of the eco-environment system. V_A and V_B are the evolution speed of the two. The evolution speed of the composite system is the function of V_A and V_B, so $V = f(V_A, V_B)$. Therefore, taking V_A and V_B as control variables, the DCCD is explored by analyzing the changes of V.

Table 3. Classification standard of urbanization and eco-environment.

Value	0–0.5	0.5–0.6	0.6–0.7	>0.7
U/E type	Weak	Genera	Developing	Developed

The evolution of the composite system conforms to the S-type development mechanism [49]. The dynamic coupling coordination relationship between urbanization and eco-environment changes periodically, and the change of V is caused by V_A and V_B. The evolution trajectories of V_A and V_B can be projected on a two-dimensional plane (V_A, V_B) for analysis (Figure 2). The ellipse is the evolution trajectory of V, and the angle θ between V_A and V_B can be expressed as Equation (5).

$$\theta = \text{arctg}\left(\frac{V_A}{V_B}\right) \tag{5}$$

θ is the DCCD. According to the θ, we divide the evolution state and DCCD of the composite system into four types: low-level symbiosis; break-in development; utmost development; and high-level symbiosis.

(1) Low-level symbiosis: $-90° < \theta \leq 0°$. The urbanization development is slow. The eco-environment does not restrict the urbanization. The urbanization influence on eco-environment is marginal.

(2) Break-in development: $0° < \theta \leq 90°$. Along with the urbanization development rate increase, the stress on the eco-environment begins to appear. The eco-environment increasingly restricts the urbanization. The contradiction between the two has appeared, but it is not serious.

(3) Utmost development: $90° < \theta \leq 180°$. Rapid urbanization has resulted in huge consumption of resources and eco-environment deterioration. The eco-environment obviously limits the urbanization. The contradiction between the two is prominent. This contradiction will be alleviated with the technical improvement.

(4) High-level symbiosis: $-180° < \theta \leq -90°$. The relationship of urbanization and eco-environment gradually turns from mutual coercion to mutual promotion.
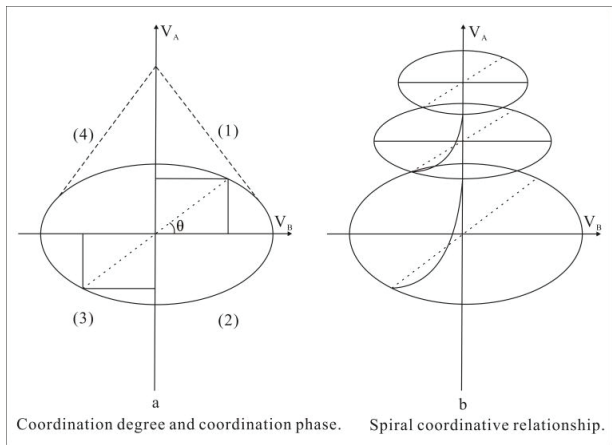
Figure 2. Coordination coupling process of urbanization and eco-environment.

Overall, the DCCD model regards urbanization and eco-environment as a composite system. First, it fully considers the nonlinear change process of urbanization and eco-environment, and the stability of the nonlinear system movement process. It can highlight the complex development and interaction of them. Second, it fully considers that the evolution of urbanization and eco-environment are determined by their own and external influences. DCCD model results are more sensitive to the changes of various factors and their interactions. Third, according to the urbanization and eco-environment evolution speed, rather than their development status, it analyzes the composite system changes, and then studies the coupling coordination relationship of them. It can better reflect their dynamic relationship. Fourth, the composite system evolution meets the combined S-shaped development mechanism. The DCCD model assumes that the urbanization and eco-environment relationship presents periodic changes. The results can better reflect the phased and periodic characteristics of the DCCD. The DCCD model is a more advanced model that can consider the dynamic, stage, and periodic characteristics [51,52]. The development and application of the DCCD model bring the coupling relationship research to a new height.

2.4. Geographic Detector

Geographic detector is a tool used to detect spatial differentiation and reveal driving factors [53,54]. It is less restricted by data conditions, has no linear assumption, and has clear physical meaning. Therefore, it is widely used in many fields such as natural and social sciences. This paper analyzes the influence of urbanization and eco-environment subsystems on DCCD by using the geographic detector. The formula is as follows [54]:

$$q = 1 - \frac{1}{n\sigma^2} \sum_{i=1}^{m} n_i \sigma_i^2 \tag{6}$$

where q represents the influence of subsystems on DCCD, $q \in [0, 1]$, and the larger the value is, the greater the influence of the subsystem. n is the sample number; σ^2 is the discrete variance of DCCD; and when $\sigma^2 \neq 0$, the model holds.

3. Results

3.1. Analysis of Urbanization and Eco-Environment

From 2003 to 2019, the urbanization level of BTH showed a fluctuating upward trend, with significant regional differences. In 2003, the starting point of urbanization among cities was different (0.23–0.39). The higher the starting point, the smaller and more stable the urbanization growth. By 2019, there were only two cities with an urbanization level of developed type, seven cities with general type, and four cities with developing type. The development of the four subsystems was unbalanced. The leading factor of urbanization has changed to social urbanization; it started with population urbanization (Figure 3, Table 3).
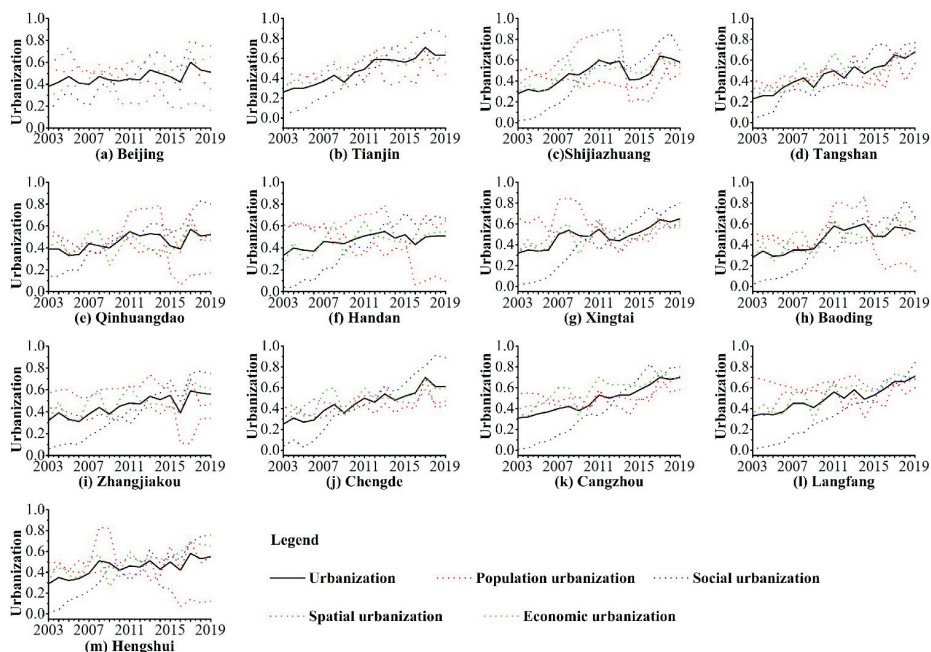
Figure 3. Changes in urbanization and its subsystems during 2003–2019.

Population urbanization and social urbanization development could be divided into two stages. Spatial urbanization development was different among cities. The economic urbanization development was consistent with the urbanization, and had little impact on the urbanization.

For population urbanization: The boundary of Shijiazhuang, Handan, Xingtai, Zhangjiakou, and Chengde was 2007, and the boundary of the other cities was 2010. In the first stage, population urbanization development occurred in advance, which drove the rapid development of urbanization. In the second stage, population urbanization gradually lagged, and the restriction effect on urbanization emerged.

For social urbanization: The boundary of Langfang was 2015, while the boundary of the other cities was 2012. In the first stage, social urbanization was seriously backward. It was the main factor hindering the high-quality urbanization development. However, the social urbanization had received much attention. Its growth rate has gradually accelerated. In the second stage, social urbanization level continued to increase, becoming the most important factor to promote the urbanization.

The spatial urbanization in Tianjin, Tangshan, Chengde, and Cangzhou was coordinated with urbanization. The spatial urbanization in other cities had stage characteristics, which could be divided into two stages. The boundary of Beijing and Hengshui was

2009, Handan and Xingtai was 2011, Langfang was 2016, and Shijiazhuang, Qinhuangdao, Baoding, and Zhangjiakou was 2014. In the first stage, spatial urbanization was developing in advance; it was the primary factor driving the urbanization development. In the second stage, with China paying more and more attention to the conservation and intensive and efficient use of land, the disorderly expansion of urban land was seriously curbed. The spatial urbanization of BTH has declined significantly. By 2019, the spatial urbanization in Beijing, Qinhuangdao, Handan, Baoding, Zhangjiakou, and Hengshui lagged significantly. The spatial urbanization in other cities was highly coordinated with urbanization.

From 2003 to 2019, the eco-environment level of BTH showed a fluctuating upward trend, with a large increase and fast growth rate. Especially since 2012, its rise was particularly obvious. By 2019, its eco-environment was generally good. There were 11 cities with an eco-environment level of developed type and 1 city with general type and developing type, respectively (Figure 4, Table 3).
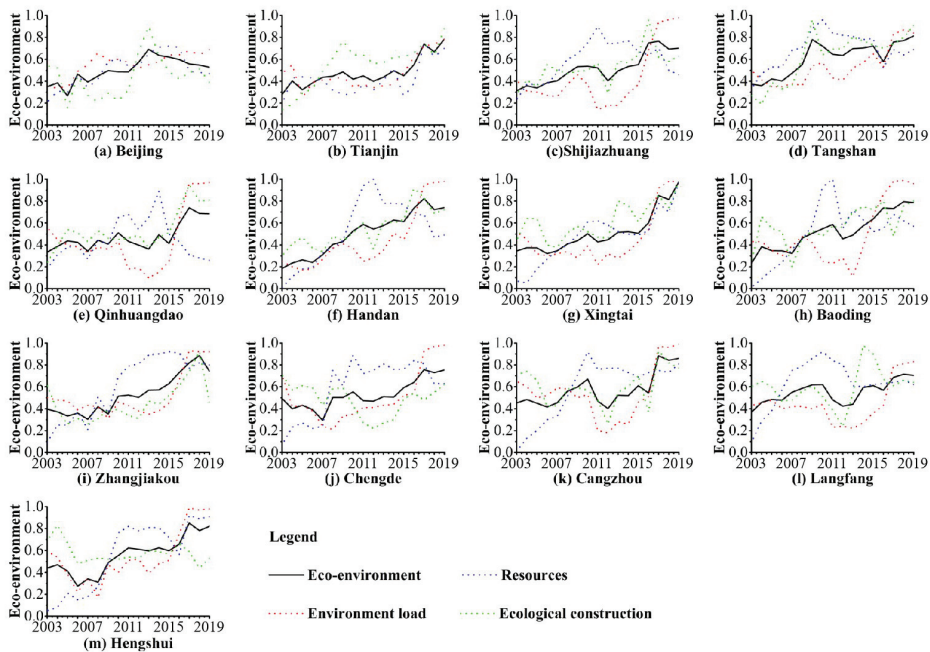
Figure 4. Changes in eco-environment and its subsystems during 2003–2019.

The resources subsystem in Beijing fluctuated around the eco-environment, and had no obvious influence on eco-environment. The development of resource subsystem in Tianjin mostly lagged behind the eco-environment. However, Tianjin's ecological civilization construction level was relatively high, which could fully eliminate the negative impact of environment load and resources subsystem. After 2016, its coordination with environment load, ecological civilization construction, and eco-environment was significantly improved. The resources subsystem in other cities experienced a "low–high–low" development process. Firstly, the development of resources subsystem was lower than that of environment load, ecological civilization construction, and eco-environment. It was the primary factor limiting the improvement in eco-environment. Secondly, the development of resources subsystem was significantly higher than that of environment load, ecological civilization construction, and eco-environment, which drove the rapid rise of eco-environment. Then, the development of resources subsystem in Tangshan, Xingtai, Zhangjiakou, Chengde, Cangzhou, Langfang, and Hengshui was relatively coordinated with eco-environment and other subsystems. The development of resources subsystem

in Shijiazhuang, Qinhuangdao, Handan, and Baoding lagged behind seriously, with an obvious downward trend.

The environment load in Beijing was mostly higher than resources, ecological civilization construction, and eco-environment. Especially after 2012, the environment load increased significantly and the ecological civilization construction was weak. Beijing has become the city with the worst eco-environment among BTH. The environment load in Tianjin was slightly lower than the eco-environment, and its negative impact was small. The environment load in other cities changed from backward to advanced. Before 2016, the environment load obviously lagged behind resources, ecological civilization construction, and eco-environment. Its negative impact on eco-environment could be basically eliminated. After 2016, the environment load grew rapidly and obviously advanced. The eco-environment had a certain degree of decline.

The ecological civilization construction in Tianjin, Shijiazhuang, Tangshan, Qinhuangdao, Handan, Xingtai, and Baoding was higher than eco-environment, which had a positive impact on the eco-environment improvement. Ecological civilization construction lagged behind the eco-environment, and needs to be strengthened in other cities.

Further analysis showed that the development of resources, environment load, and ecological civilization construction in Tianjin was relatively balanced. Its coordination with the eco-environment was relatively high. In other cities, it is necessary to curb the rise of environment load and strengthen the ecological civilization construction so as to drive the development of resources subsystem and improve the resilience and quality of eco-environment.

3.2. Analysis of DCCD

We used OriginPro 9.1 to solve the urbanization and eco-environment curve fitting. The fitting results are shown in Table 4. Combining Equations (3)–(5) obtained the DCCD of urbanization and eco-environment (Figure 5). The results showed that there was a dynamic coupling and coordination relationship between urbanization and eco-environment, and the DCCD showed an S-shaped curve. Meanwhile, the DCCD in BTH was significantly different among cities.
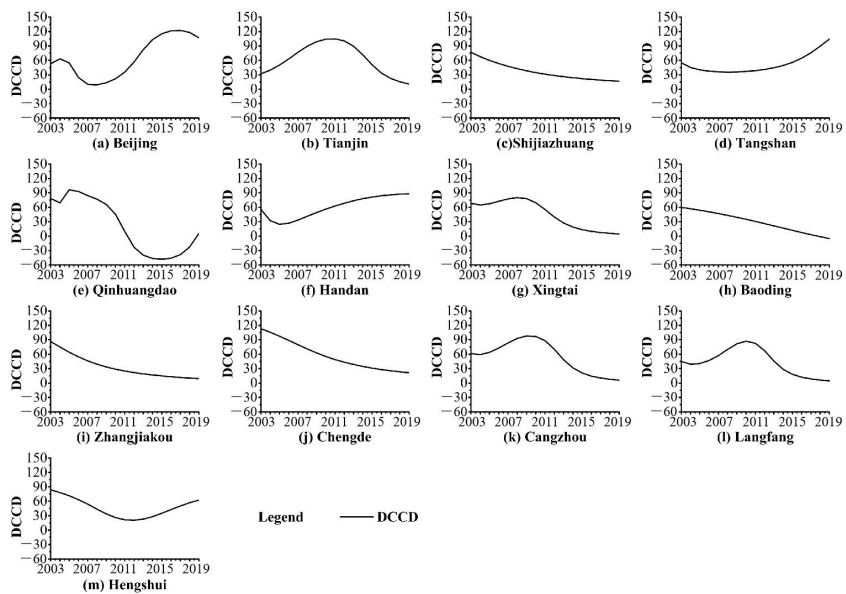

Figure 5. The evolution of DCCD during 2003–2019.

Table 4. Curve fitting of urbanization and eco-environment.

City	Urbanization	R^2	Eco-Environment	R^2
Beijing	$U = -2 \times 10^{-5}x^4 + 0.0008x^3 - 0.01x^2 + 0.0514x + 0.3447$	0.52	$E = 7 \times 10^{-6}x^5 - 0.0003x^4 + 0.0042x^3 - 0.0224x^2 + 0.0586x + 0.3041$	0.84
Tianjin	$U = -0.0007x^2 + 0.0391x + 0.2028$	0.93	$E = 0.0004x^3 - 0.0102x^2 + 0.0794x + 0.2229$	0.89
Shijiazhuang	$U = 0.2554x^{0.2903}$	0.71	$E = 0.0005x^2 + 0.0165x + 0.3139$	0.82
Tangshan	$U = 0.2013x^{0.3868}$	0.9	$E = -0.0018x^2 + 0.0577x + 0.279$	0.77
Qinhuangdao	$U = 7 \times 10^{-5}x^4 - 0.0027x^3 + 0.0322x^2 - 0.1242x + 0.4973$	0.63	$E = 0.0021x^2 - 0.018x + 0.4211$	0.72
Handan	$U = 6 \times 10^{-6}x^5 - 0.0002x^4 + 0.003x^3 - 0.017x^2 + 0.0579x + 0.3038$	0.82	$E = 7 \times 10^{-6}x^4 - 0.0004x^3 + 0.0064x^2 + 0.0103x + 0.1723$	0.96
Xingtai	$U = 0.2935x^{0.2458}$	0.76	$E = 4 \times 10^{-5}x^4 - 0.001x^3 + 0.0098x^2 - 0.0271x + 0.3716$	0.94
Baoding	$U = -0.0014x^2 + 0.0441x + 0.1967$	0.78	$E = 0.0005x^2 + 0.0229x + 0.2668$	0.89
Zhangjiakou	$U = -0.0003x^2 + 0.0202x + 0.2956$	0.73	$E = 0.0019x^2 - 0.0025x + 0.348$	0.93
Chengde	$U = -0.0002x^2 + 0.0284x + 0.2229$	0.89	$E = 0.0021x^2 - 0.0162x + 0.4559$	0.81
Cangzhou	$U = 0.2538x^{0.3173}$	0.85	$E = 0.0004x^3 - 0.0087x^2 + 0.06x + 0.3742$	0.72
Langfang	$U = 0.2834x^{0.2728}$	0.83	$E = 0.0005x^3 - 0.0122x^2 + 0.1001x + 0.288$	0.69
Hengshui	$U = 2 \times 10^{-5}x^4 - 0.0004x^3 + 0.0009x^2 + 0.0349x + 0.2517$	0.75	$E = 0.0017x^2 - 0.0004x + 0.3852$	0.81

The DCCD of urbanization and eco-environment in BTH has three types: low-level symbiosis; break-in development; and utmost development. There was no high-level symbiosis. The occurrence frequency of low-level symbiosis was low, only Qinhuangdao (2012–2018) and Baoding (2018–2019) had this type. Break-in development was the main type of DCCD in BTH. The utmost development was found in Beijing (2014–2019), Tianjin (2009–2012), Tangshan (2018–2019), Qinhuangdao (2005–2006), Chengde (2003–2005), and Cangzhou (2008–2010). By 2019, only Beijing and Tangshan were the utmost development type. Tianjin, Chengde, and Cangzhou were break-in development type, and the DCCD decreased gradually. The DCCD in Qinhuangdao experienced a changing process of utmost development, break-in development, low-level symbiosis, and break-in development. It showed that the utmost development of DCCD in BTH was relatively low in sustainability.

When the DCCD was transitioning from break-in development to utmost development, the urbanization and eco-environment of Beijing, Tianjin, Tangshan, Qinhuangdao, Chengde, and Cangzhou were in small-speed reverse development. That is, relatively stable development speed and small-degree urbanization or eco-environment sacrifice were necessary to achieve utmost development. The DCCD of Handan, Zhangjiakou, Langfang, and Hengshui approached 90° in 2017–2019, 2003 and 2010. However, the transition from break-in development to utmost development was not achieved. The main reason was the high rate of urbanization or eco-environment change (Figures 3 and 4). This further supported the above research conclusions.

For the rise and fall of DCCD in the break-in development stage, urbanization and eco-environment were in a state of simultaneous rise or decline. On this premise, the development of urbanization and eco-environment can be divided into two situations. (1) The development rate of urbanization was lower than that of eco-environment. With the gradual increase in the extent that the urbanization development rate was lower than that of eco-environment, the DCCD decreased and approached 0°. On the contrary, the DCCD increased and approached 45°. (2) The development rate of urbanization was higher than that of eco-environment. With the gradual increase in the extent that the urbanization

development rate was higher than that of eco-environment, the DCCD increased and approached 90°. On the contrary, the DCCD decreased and approached 45°.

Theoretical analysis showed the following: (1) When urbanization and eco-environment are both in a rising state and the DCCD approaches 90°, the DCCD will realize the transformation from break-in development to utmost development if urbanization development maintains a steady rising trend and eco-environment quality declines slightly. (2) When urbanization and eco-environment are both in a declining state and the DCCD approaches 90°, the DCCD will realize the transformation from break-in development to utmost development if urbanization keeps a steady downward trend and eco-environment quality rises slightly. This paper called the first state "benign transition", and called the second state "non-benign transition". In fact, the coordinated development of DCCD in BTH was a "benign transition". That is, when the utmost development of DCCD was realized, its urbanization development was in a steady upward trend, and the eco-environment quality was slightly declining.

The above analysis results show that it is not advisable to blindly emphasize urbanization or eco-environment development. To realize the "benign transition" of DCCD from break-in development to utmost development, a moderate and steady advance development of urbanization and a small degree of eco-environment quality sacrifice are necessary. Therefore, determining how to grasp the degree of advance development of urbanization and sacrifice of eco-environment quality, and realize and maintain the relatively coordinated and stable development of urbanization and eco-environment are the key to realize the utmost development of DCCD. Only when the utmost development is realized is it possible to achieve the high-level symbiosis of DCCD through technological improvement and realize the mutual promotion of urbanization and eco-environment.

3.3. Identification of Main Driving Factors

This paper detected the driving force of urbanization and eco-environment subsystems on DCCD by geographic detector (Table 5). In the calculation results, the factor detector module automatically outputs independent variable values p and q, which are data randomness probability and factor influence value, respectively. This paper holds that when $p \leq 0.01$ and $q \geq 0.5$, the factor is the main control factor of the DCCD.

Social urbanization was the common factor that affected the DCCD in BTH. The influence value of social urbanization was particularly prominent, ranking second in Beijing, Tangshan, and Qinhuangdao, and first in the other ten cities. This showed that the changes of DCCD were closely related to the social urbanization. The urbanization development of BTH has entered the social urbanization leading stage.

The influence scope of spatial urbanization was relatively wide. Seven cities' main control factors included the spatial urbanization, namely, Beijing, Qinhuangdao, Handan, Baoding, Zhangjiakou, Cangzhou, and Hengshui. Cangzhou's spatial urbanization development was relatively moderate from 2003 to 2019. When the spatial urbanization was in advance or lagged behind, its level could be adjusted in time, and the spatial urbanization was consistent with the urbanization development. Therefore, spatial urbanization was one of the main controlling factors of DCCD in Cangzhou. Spatial urbanization was the main control factor of DCCD in the other six cities, mainly because their spatial urbanization changed from significantly advanced to seriously lagged. The spatial urbanization of these cities had seriously restricted the improvement in urbanization. Ensuring the economical and intensive use of space, appropriately improving the spatial urbanization level was conducive to the optimization of DCCD. The economic urbanization was the main control factor of DCCD in Beijing and Cangzhou. This was because the economic urbanization of these two cities maintained a state of advanced development from 2003 to 2019. It was one of the main driving factors for the urbanization development. The DCCD of Beijing and Cangzhou was sensitive to the changes of economic urbanization. The influence of population urbanization on DCCD in BTH was not significant. This is mainly because BTH is an important part of China's economic core region, its population urbanization has

a high coordination with urbanization, and there is no long-term or serious advance or lag development.

Table 5. Detection results of main control factors of DCCD.

City	Index	Population Urbanization	Economic Urbanization	Social Urbanization	Spatial Urbanization	Resources	Environment Load	Ecological Civilization Construction
Beijing	q	0.68	0.76	0.82	0.86	0.79	0.35	0.73
	p	0.02	0.01	0.01	0.00	0.02	0.49	0.02
Tianjin	q	0.49	0.64	0.90	0.48	0.43	0.48	0.61
	p	0.50	0.09	0.00	0.15	0.25	0.10	0.05
Shijiazhuang	q	0.13	0.75	0.79	0.10	0.46	0.79	0.58
	p	0.97	0.04	0.01	0.91	0.28	0.02	0.15
Tangshan	q	0.08	0.61	0.87	0.50	0.75	0.11	0.92
	p	0.92	0.04	0.00	0.14	0.17	0.88	0.00
Qinhuangdao	q	0.24	0.18	0.73	0.92	0.10	0.66	0.40
	p	0.75	0.75	0.01	0.00	0.93	0.06	0.48
Handan	q	0.27	0.56	0.88	0.87	0.73	0.67	0.80
	p	0.46	0.14	0.00	0.00	0.05	0.04	0.01
Xingtai	q	0.22	0.44	0.85	0.33	0.82	0.18	0.65
	p	0.61	0.31	0.00	0.36	0.00	0.76	0.07
Baoding	q	0.09	0.51	0.93	0.78	0.74	0.67	0.51
	p	0.93	0.18	0.00	0.01	0.02	0.16	0.23
Zhangjiakou	q	0.50	0.64	0.87	0.86	0.64	0.80	0.59
	p	0.21	0.08	0.00	0.01	0.04	0.01	0.26
Chengde	q	0.25	0.48	0.96	0.55	0.57	0.69	0.27
	p	0.84	0.46	0.00	0.29	0.14	0.05	0.71
Cangzhou	q	0.40	0.74	0.87	0.71	0.84	0.77	0.29
	p	0.69	0.01	0.00	0.01	0.00	0.02	0.78
Langfang	q	0.39	0.56	0.89	0.70	0.48	0.64	0.28
	p	0.50	0.11	0.00	0.03	0.22	0.15	0.86
Hengshui	q	0.11	0.55	0.88	0.68	0.69	0.63	0.30
	p	0.93	0.18	0.00	0.01	0.08	0.21	0.88

Moreover, 61.54% of cities had no eco-environment subsystems as the main control factor. This indicated that urbanization played a dominant role in the coupling and co-ordination relationship between urbanization and eco-environment of BTH. Meanwhile, five cities in BTH had the eco-environment subsystem as the main control factor, and its influence value was relatively high ($q > 0.8$). The ecological civilization construction was the main control factor of DCCD in Tangshan and Handan. The urbanization of Tangshan showed a continuous upward trend, and the eco-environment occasionally deteriorated under the influence of urbanization (Figures 3 and 4). The good development of the ecological civilization construction had fully eliminated the negative influence of the environment load and enhanced the ability of Tangshan to quickly restore the eco-environment. The ecological civilization construction provided a guarantee for the continuous rise of DCCD. The urbanization of Handan developed slowly (Figure 3), and its DCCD changes were more dependent on the eco-environment. Handan's environment load continued to rise, and the resources subsystem decreased significantly. Therefore, the ecological civilization construction level determined whether the eco-environment deteriorated or not, and had a great influence on the change trend of DCCD (Figures 4 and 5). The resources subsystem was the main control factor of DCCD in Xingtai and Cangzhou. The reasons were as

follows: Xingtai's urbanization development showed a large fluctuation and rising trend, and Cangzhou's urbanization development showed a rapid and continuous rising trend (Figure 3). These two cities' urbanization developments brought great pressure to the eco-environment. The ecological civilization construction fluctuated greatly. The elimination of the negative impact of urbanization on eco-environment was more dependent on the resources subsystem. The environment load was the main control factor of the DCCD in Zhangjiakou. This was because its ecological civilization construction was relatively backward, the resources subsystem could not fully eliminate the negative impact of the environment load, and environment load was sensitive to the changes of urbanization. To realize the regulation and control of the DCCD, these five cities should pay attention to the changes of urbanization and eco-environment simultaneously.

Comprehensive analysis showed that the identification results of the main control factors could accurately reflect the driving force of subsystems on urbanization, eco-environment, and DCCD. When the imbalance between the development of urbanization and eco-environment appeared, the situation of each subsystem could be adjusted according to the identification results of the main controlling factors, to realize the optimization and adjustment of urbanization, eco-environment, and DCCD.

4. Discussion

The continuous and rapid development of global urbanization brought great pressure to the eco-environment. It is important to have a deep understanding of the relationship between urbanization and eco-environment, especially in mega urban agglomerations where the most representative and studied cases are extremely scarce. This will determine the process of urbanization in the world, affect the international competitiveness of countries, and hold the key to the realization of the United Nations 2030 Agenda for Sustainable Development. It is also an important part of the global countries achieving green, low-carbon, and sustainable development. With the rapid development of global urbanization, the contradiction between urbanization and eco-environment in various countries is becoming more prominent, and their interaction is becoming more complex. The SCCD model commonly used in previous studies and the research method that only analyzes the relationship between urbanization and eco-environment system cannot meet the profound needs of the research on the relationship between urbanization and eco-environment. Different from the previous studies that only analyzed urbanization and eco-environment changes, this paper deeply analyzed urbanization, eco-environment, and their subsystems changes, as well as the relationship between them. The DCCD model was used instead of the SCCD model to analyze the relationship between urbanization and eco-environment. Meanwhile, China's urbanization is developing rapidly and is in an accelerated stage. BTH is one of the three major urban agglomerations and a representative of the rapid development of urbanization in China. It is also a region facing more serious resource and eco-environment stress in China's mega urban agglomerations. The BTH in China was selected as the research area, and the research results are more representative and meaningful for reference. This paper can make up for the deficiencies of the existing research and provides a new research idea and methodological reference for studies on the relationship between urbanization and eco-environment.

However, in the research of urbanization and eco-environment coupling coordination relationship, the application of DCCD model was few, and the correlation analysis was not deep. The conclusions of this paper need more studies that are theoretical and cases from different countries and regions to support them. When the DCCD model is used to analyze the relationship between urbanization and eco-environment, we should take some measures: (1) Focus on strengthening the relevant theoretical research. (2) Expand the scope of the study area to clarify the similarities and differences of the DCCD changes in different development levels and different types of countries and cities. The practical implication of this study includes the following two aspect: theoretical and empirical aspects.

4.1. Practical Implication to Theoretical Research

This paper explained the progressiveness of the DCCD model from the construction concept and theoretically analyzed the rising and falling laws of DCCD in break-in development stage for the first time. This was confirmed in this study. Moreover, the changes of DCCD in break-in development stage of existing studies also conformed to this law [49,52,55]. We propose the concept of "benign transition" and "non-benign transition" when the DCCD changes from break-in development to utmost development for the first time. Meanwhile, it was found that moderate and steady advance development of urbanization and small degree eco-environment sacrifice are the key to achieve the "benign transition". The theoretical analysis of this paper and the empirical analysis of existing research both show that the realization of "benign transition" is the premise of achieving the high-level symbiosis of DCCD through technological improvement, and is the key to realizing the mutual promotion between urbanization and eco-environment. Determining how to grasp the degree of urbanization advance development and eco-environment quality sacrifice, timely adjust their priority, and balance their relationship are important issues for sustainable development.

This finding is of great significance: (1) The changes of DCCD between urbanization and eco-environment may be predicted and regulated. (2) By regulating urbanization and eco-environment development, the key point of "benign transition" from break-in development to utmost development can be found. (3) When the DCCD passed the key point of "benign transition", the technological improvement will become an important means of sustainable development, and the mutual promotion of urbanization and eco-environment is expected to be realized.

4.2. Practical Implication to Empirical Research

BTH's urbanization development had entered the leading stage of social urbanization. Its social urbanization development was advanced. Urbanization development needs to take the social urbanization improvement as the breakthrough point in the short term to promote the development of other subsystems, balance the relationship among subsystems, reduce regional differences, and realize the improvement in urbanization level. In addition, Beijing's urbanization level has changed from ranking second at the beginning of this study to ranking lowest at the end of this study. The unbalanced urbanization development between Beijing, Tianjin, and Hebei restricted the outward relaxation of Beijing's noncapital functions. The improvement in urban agglomeration urbanization level is a long-term and complex systematic project, which must take urban agglomeration as the main form, complement the weak points, and promote coordination. It is necessary to draw on the development experience of cities with a high level of urbanization, such as Langfang (0.71), Cangzhou (0.70), and Tangshan (0.68), to promote high-quality development within each city. Efforts should be made to enhance industrial complementary and industrial chain extension between cities, seize the major strategic opportunities brought about by the new scientific and technological revolution for industrial transformations, solve the problem that the industrial structure of some cities is too heavy on industry, and promote the overall urbanization quality of urban agglomeration.

The DCCD of Beijing and Tangshan was of utmost development, and its development trend was decreasing and increasing, respectively. Beijing needs to curb the decline of DCCD through the diversion of noncapital functions. Tangshan should improve the utilization efficiency of resources through scientific and technological progress and maintain the rising trend of DCCD. The other 11 cities were in the critical period of DCCD's transformation from break-in development to utmost development. DCCD was gradually rising in Qinhuangdao, Handan, and Hengshui, which was expected to achieve the "benign transition" by maintaining the steady development of urbanization and slightly sacrificing the eco-environment. In the other cities, the DCCD gradually decreased, and there was a risk of regression from break-in development to low-level symbiosis. Combined with the urbanization and eco-environment analysis, the eco-environment of these cities provided

space for urbanization development. These cities should moderately increase the speed of urbanization and pay attention to the eco-environment carrying capacity improvement, maximize the protection of urbanization development, and turn the development of DCCD from declining to increasing.

The DCCD of Beijing, Tianjin, Tangshan, Qinhuangdao, Chengde, and Cangzhou was the utmost development type in 2014–2019, 2009–2012, 2018–2019, 2005–2006, 2003–2005, and 2008–2010, respectively. However, the transition from utmost development to high-level symbiosis has not been realized. The key to the transformation from utmost development to high-level symbiosis still lies in the promotion of scientific and technological level. In the long run, technical and policy support for the sustainable development of BTH is extremely important [56].

To achieve and maintain the utmost development type of DCCD faster and better, even the high-level symbiosis, it is necessary to conduct a comprehensive and accurate analysis of urbanization, eco-environment, their subsystems, and DCCD. On the premise of fully understanding the development status and changing trend, the relationship between urbanization and eco-environment can be optimized through the adjustment of subsystems. Simple spatial–temporal changes or single-angle analysis cannot guide the optimization of urbanization, eco-environment, and DCCD. For example, according to the spatial–temporal changes of urbanization and eco-environment, BTH had a good eco-environment quality, which can rapidly promote the urbanization development. However, the analysis of urbanization and eco-environment subsystems found that from 2003 to 2019, the ecological civilization construction level of Beijing, Zhangjiakou, Chengde, Cangzhou, Langfang, and Hengshui lagged behind the eco-environment. It needed to be strengthened. At the end of the study period, the development of resources subsystem in Beijing, Shijiazhuang, Qinhuangdao, Handan, and Baoding obviously lagged behind, and had a downward trend. Meanwhile, except for Tianjin, the environment load in BTH grew rapidly and was obviously advanced. In other words, all the cities except Tianjin had potential eco-environment risks. All these indicated that the further development of urbanization could not be separated from the continuous attention to eco-environment. It is necessary to analyze urbanization, eco-environment, and their relationship from the subsystems level.

5. Conclusions

This paper took the mega urban agglomeration with a few cases as the research area, and used the more advanced DCCD model in this research field to explore the relationship between urbanization and eco-environment. We verified the scientificity and advancement of the DCCD model in the study of the relationship between urbanization and eco-environment from the two dimensions of construction concept and empirical case. New concepts were proposed. Meanwhile, we further promoted the application of the DCCD model in the research field of the relationship between urbanization and eco-environment. We analyzed the urbanization, eco-environment, and DCCD from the subsystems level, providing a deeper analysis than before. We found the key to realizing the mutually promoting relationship between urbanization and eco-environment. We provide a more scientific and accurate research idea for the related research on the relationship between urbanization and eco-environment. This paper makes up for the deficiency of the existing research from the aspects of empirical research and theoretical research. Some important conclusions are drawn:

(1)   From 2003 to 2019, the urbanization level of BTH showed a fluctuating upward trend, with significant regional differences. The urbanization starting point among cities was different (0.23–0.39). The higher the starting point, the smaller and more stable the urbanization growth. The development of population, economic, social, and spatial urbanization subsystems was unbalanced. The leading factor of urbanization had changed from population to social urbanization.

(2)   From 2003 to 2019, the eco-environment level of BTH showed a fluctuating upward trend, with a large increase and fast growth rate. Its rise was particularly obvious,

especially since the Chinese government in 2012 raised the construction of ecological civilization to an unprecedented strategic height. By 2019, the eco-environment of BTH was generally good. Tianjin's resources, environment load, and ecological civilization construction development was balanced. Its subsystems' coordination with the eco-environment were relatively high. All other cities need to curb the rise of environment load and strengthen their ecological civilization construction. Meanwhile, the impact of ecological civilization construction and environment load on resources and eco-environment had a relative lag.

(3) There was a dynamic coupling and coordination relationship between urbanization and eco-environment in BTH. The DCCD showed an S-shaped curve. Break-in development was the main type of the DCCD in BTH. BTH's urbanization development was in an accelerating stage, and the contradiction between urbanization and eco-environment was becoming increasingly serious. Moderate and steady advance development of urbanization and a small-degree eco-environment sacrifice are the key to achieve the "benign transition" of DCCD from break-in development to utmost development. Only when the utmost development is realized is it possible to achieve the high-level symbiosis through the technological improvement and realize the mutual promotion between urbanization and eco-environment.

(4) Social urbanization was the common factor that affected the DCCD between urbanization and eco-environment in BTH, and its influence value was particularly prominent. Meanwhile, the urbanization, eco-environment, and DCCD could be regulated by monitoring and adjusting the subsystems.

Author Contributions: Conceptualization, X.W. and Y.Z.; methodology, X.W.; software, X.W.; validation, Y.Z. and X.L.; formal analysis, X.W. and Y.Z.; investigation, X.W.; resources, Y.Z. and X.L.; data curation, X.W., Y.Z. and X.L.; writing—original draft preparation, X.W.; writing—review and editing, X.W.; visualization, X.W.; supervision, Y.Z.; project administration, Y.Z.; funding acquisition, X.W., Y.Z. and X.L. All authors have read and agreed to the published version of the manuscript.

Data Availability Statement: Data are contained within the article.

Conflicts of Interest: The authors declare no conflicts of interest.

References

1. UN 2018 Revision of World Urbanization Prospects 2018. Available online: https://www.un.org/zh/desa/2018-revision-world-urbanization-prospects (accessed on 12 September 2022).
2. -Ma, Y. Examining the Coupling Degree and Interactive Stress between Urbanization and Eco-Environment in Yangtze Rover Economic Belt. *Resour. Environ. Yangtze Basin* **2020**, *29*, 275–286. [CrossRef]
3. Ariken, M.; Zhang, F.; Ngai, W.C.; Hsiang, K. Coupling coordination analysis and spatio-temporal heterogeneity between urbanization and eco-environment along the Silk Road Economic Belt in China. *Ecol. Indic.* **2021**, *121*, 107014. [CrossRef]
4. Guo, B.; Wei, C.; Yu, Y.; Liu, Y.; Li, J.; Meng, C.; Cai, Y. The dominant influencing factors of desertification changes in the source region of Yellow River: Climate change or human activity? *Sci. Total Environ.* **2022**, *813*, 152512. [CrossRef] [PubMed]
5. Liu, W.; Jiao, F.; Ren, L.; Xu, X.; Wang, J.; Wang, X. Coupling coordination relationship between urbanization and atmospheric environment security in Jinan City. *J. Clean. Prod.* **2018**, *204*, 1–11. [CrossRef]
6. Fang, C. Dissipative Structure Theory and Geography System. *Aird L. Geogr.* **1989**, *12*, 51–56. [CrossRef]
7. Fang, C.; Yang, Y. Basic laws of the interactive coupling system of urbanization and ecological environment. *Arid Land Geogr.* **2006**, *29*, 1–8. [CrossRef]
8. Cui, X.; Fang, C.; Li, J.; Liu, H.; Zhang, Q. Progress in dynamic simulation modeling of urbanization and ecological environment coupling. *Prog. Geogr.* **2019**, *38*, 111–125. [CrossRef]
9. Fang, C.; Cui, X.; Liang, L. Theoretical analysis of urbanization and eco-environment coupling coil and coupler control. *Dili Xuebao/Acta Geogr. Sin.* **2019**, *74*, 2529–2546. [CrossRef]

10. Ren, Y.; Fang, C.; Li, G.; Sun, S.; Bao, C.; Liu, R. Progress in local and tele-coupling relationship between urbanization and eco-environment. *Acta Geogr. Sin.* **2020**, *75*, 589–606. [CrossRef]

11. Ren, Y.; Cao, W.; Zhang, Y.; Su, H.; Wang, X. Spatio-temporal coupling characteristics of urbanization and ecological environment in three major urban agglomerations along the Yangtze River Economic Belt. *Resour. Environ. Yangtze Basin* **2019**, *28*, 2586–2600.

12. Fang, C.; Liu, H.; Li, G. International progress and evaluation on interactive coupling effects between urbanization and the eco-environment. *J. Geogr. Sci.* **2016**, *26*, 1081–1116. [CrossRef]

13. Aslanidis, N.; Iranzo, S. Environment and development: Is there a Kuznets curve for CO_2 emissions? *Appl. Econ.* **2009**, *41*, 803–810. [CrossRef]

14. Shahbaz, M.; Sbia, R.; Hamdi, H.; Ozturk, I. Economic growth, electricity consumption, urbanization and environmental degradation relationship in United Arab Emirates. *Ecol. Indic.* **2014**, *45*, 622–631. [CrossRef]

15. Dongfeng, Y.; Chengzhi, Y.; Ying, L. Urbanization and sustainability in China: An analysis based on the urbanization Kuznets-curve. *Plan. Theory* **2013**, *12*, 391–405. [CrossRef]

16. Rees, W.; Wackernagel, M. Urban ecological footprints: Why cities cannot be sustainable—And why they are a key to sustainability. *Environ. Impact Assess. Rev.* **1996**, *16*, 223–248. [CrossRef]

17. Burke, B.M. Our ecological footprint: Reducing human impact on the earth. *Popul. Environ.* **1997**, *19*, 185–189. [CrossRef]

18. Galli, A.; Wiedmann, T.; Ercin, E.; Knoblauch, D.; Ewing, B.; Giljum, S. Integrating Ecological, Carbon and Water footprint into a "Footprint Family" of indicators: Definition and role in tracking human pressure on the planet. *Ecol. Indic.* **2012**, *16*, 100–112. [CrossRef]

19. Fang, K.; Heijungs, R.; De Snoo, G.R. Theoretical exploration for the combination of the ecological, energy, carbon, and water footprints: Overview of a footprint family. *Ecol. Indic.* **2014**, *36*, 508–518. [CrossRef]

20. Cui, X.; Fang, C.; Liu, H.; Liu, X.; Li, Y. Research progress of coupling dynamic simulation theory and method of urbanization and ecological environment. *Acta Geogr. Sin.* **2019**, *74*, 1079–1096. [CrossRef]

21. Liu, Y.; Li, R.; Song, X. Grey associative analysis of regional urbanization and eco-environment coupling in China. *Acta Geogr. Sin.* **2005**, *60*, 237–247.

22. Wu, X.; Zhang, Y.; Wang, L. Coupling relationship between regional urban development and eco-environment: Inspiration from the old industrial base in Northeast China. *Ecol. Indic.* **2022**, *142*, 109259. [CrossRef]

23. Tian, Y.; Zhou, D.; Jiang, G. Conflict or Coordination? Multiscale assessment of the spatio-temporal coupling relationship between urbanization and ecosystem services: The case of the Jingjinji Region, China. *Ecol. Indic.* **2020**, *117*, 106543. [CrossRef]

24. Liu, X.; Guo, P.; Yue, X.; Zhong, S.; Cao, X. Urban transition in China: Examining the coordination between urbanization and the eco-environment using a multi-model evaluation method. *Ecol. Indic.* **2021**, *130*, 108056. [CrossRef]

25. Zheng, Z.; Wu, Z.; Chen, Y.; Yang, Z.; Marinello, F. Exploration of eco-environment and urbanization changes in coastal zones: A case study in China over the past 20 years. *Ecol. Indic.* **2020**, *119*, 106847. [CrossRef]

26. Feng, Y.; He, S.; Li, G. Interaction between urbanization and the eco-environment in the Pan-Third Pole region. *Sci. Total Environ.* **2021**, *789*, 298–324. [CrossRef]

27. Zhao, J.; Liu, Y.; Zhu, Y.; Qin, S.; Wang, Y.; Miao, C. Spatiotemporal differentiation and influencing factors of the coupling and coordinated development of new urbanization and ecological environment in the Yellow River Basin. *Resour. Sci.* **2020**, *42*, 159–171. [CrossRef]

28. National Bureau of Statistics 2006–2019, Urbanization Rate. Available online: http://www.stats.gov.cn/ (accessed on 21 December 2021).

29. United Nations Department of Economic and Social Affairs. 2014 Revision of World Urbanization Prospects. 2014. Available online: https://www.un.org/en/development/desa/publications/2014-revision-world-urbanization-prospects.html (accessed on 23 December 2021).

30. Fang, C. Basic rules and key paths for high-quality development of the new urbanization in China. *Geogr. Res.* **2019**, *38*, 13–22. [CrossRef]

31. Egidi, G.; Zambon, I.; Tombolin, I.; Salvati, L.; Cividino, S.; Seifollahi-Aghmiuni, S.; Kalantari, Z. Unraveling latent aspects of urban expansion: Desertification risk reveals more. *Int. J. Environ. Res. Public Health* **2020**, *17*, 4001. [CrossRef]

32. Salvati, L.; Karamesouti, M.; Kosmas, K. Soil degradation in environmentally sensitive areas driven by urbanization: An example from Southeast Europe. *Soil Use Manag.* **2014**, *30*, 382–393. [CrossRef]

33. Hossain, M.B.; Mertig, A.G. Socio-structural forces predicting global water footprint: Socio-hydrology and ecologically unequal exchange. *Hydrol. Sci. J.* **2020**, *65*, 495–506. [CrossRef]

34. Li, Z.; Zhou, Y.; Li, K.; Xiao, H.; Cai, Y. The spatial effects of city-level water-energy nexus: A case study of Hebei Province, China. *J. Clean. Prod.* **2021**, *310*, 127497. [CrossRef]

35. Shen, L.; Cheng, S.; Gunson, A.J.; Wan, H. Urbanization, sustainability and the utilization of energy and mineral resources in China. *Cities* **2005**, *22*, 287–302. [CrossRef]

36. Huang, Q.; Lu, Y. The Effect of Urban Heat Island on Climate Warming in the Yangtze River Delta Urban Agglomeration in China. *Int. J. Environ. Res. Public Health* **2015**, *12*, 8773–8789. [CrossRef] [PubMed]

37. Ouyang, Z.; Sciusco, P.; Jiao, T.; Feron, S.; Lei, C.; Li, F.; John, R.; Fan, P.; Li, X.; Williams, C.A.; et al. Albedo changes caused by future urbanization contribute to global warming. *Nat. Commun.* **2022**, *13*, 3800. [CrossRef]

38. Sun, Y.; Hu, T.; Li, C. Contribution of Global warming and Urbanization to Changes in Temperature Extremes in Eastern China Geophysical Research Letters. *Geophys. Res. Lett.* **2019**, *46*, 11426–11434. [CrossRef]

39. Magura, T.; Kiss, E.; Lövei, G.L. No consistent diversity patterns in terrestrial mammal assemblages along rural-urban forest gradients. *Basic Appl. Ecol.* **2021**, *52*, 38–45. [CrossRef]

40. Rickman, J.K.; Connor, E.F. The effect of urbanization on the quality of remnant habitats for leaf-mining Lepidoptera on Quercus agrifolia. *Ecography* **2003**, *26*, 777–787. [CrossRef]

41. Sol, D.; Bartomeus, I.; González-Lagos, C.; Pavoine, S. Urbanisation and the loss of phylogenetic diversity in birds. *Ecol. Lett.* **2017**, *20*, 721–729. [CrossRef] [PubMed]

42. Luo, X.; Sun, K.; Li, L.; Wu, S.; Yan, D.; Fu, X.; Luo, H. Impacts of urbanization process on PM2.5 pollution in "2+26" cities. *J. Clean. Prod.* **2021**, *284*, 124761. [CrossRef]

43. Zhang, X.; Han, L.; Wei, H.; Tan, X.; Zhou, W.; Li, W.; Qian, Y. Linking urbanization and air quality together: A review and a perspective on the future sustainable urban development. *J. Clean. Prod.* **2022**, *346*, 130988. [CrossRef]

44. Zhao, C.; Wang, B. How does new-type urbanization affect air pollution? Empirical evidence based on spatial spillover effect and spatial Durbin model. *Environ. Int.* **2022**, *165*, 107304. [CrossRef] [PubMed]

45. Fang, C.; Zhou, C.; Gu, C.; Chen, L.; Li, S. Theoretical analysis of interactive coupled effects between urbanization and eco-environment in mega-urban agglomerations. *Acta Geogr. Sin.* **2016**, *71*, 531–550. [CrossRef]

46. Fang, C. China's Urban Agglomeration and Metropolitan Area Construction Under the New Development Pattern. *Econ. Geogr.* **2021**, *41*, 1–7. [CrossRef]

47. Liu, L.; Gao, C.; Wang, W.; Wang, D.; Liang, X. The High-Quality Coordinated Development of the Beijing-Tianjin-Hebei Region: Evolution Cause, Power Mechanism, and Future Prospects. *Local Gov. Gov.* **2023**, *5*, 61–71. [CrossRef]

48. Liu, H.; Fang, C.; Li, Y. The Coupled Human and Natural Cube: A conceptual framework for analyzing urbanization and eco-environment interactions. *Dili Xuebao/Acta Geogr. Sin.* **2019**, *74*, 1489–1507. [CrossRef]

49. Qiao, B.; Fang, C. The dynamic coupling model of the harmonious development between urbanization and eco-environment and its application in arid area. *Acta Ecol. Sin.* **2005**, *25*, 3003–3009.

50. Bertalanffy, L.V. *General System Theory-Foundation, Development, Applications*, Reversion ed.; George Braziller: New York, NY, USA, 1987.

51. Chen, Y.; Zhao, L. Exploring the relation between the industrial structure and the eco-environment based on an integrated approach: A case study of Beijing, China. *Ecol. Indic.* **2019**, *103*, 83–93. [CrossRef]

52. Zhao, Y.; Wang, S.; Zhou, C. Understanding the relation between urbanization and the eco-environment in China's Yangtze River Delta using an improved EKC model and coupling analysis. *Sci. Total Environ.* **2016**, *571*, 862–875. [CrossRef] [PubMed]

53. Cao, F.; Ge, Y.; Wang, J. Optimal discretization for geographical detectors-based risk assessment. *Gisci. Remote Sens.* **2013**, *50*, 78–92. [CrossRef]

54. Wang, J.; Xu, C. Geodetector: Principle and prospective. *Acta Geogr. Sin.* **2017**, *72*, 116–134. [CrossRef]

55. Wang, S.; Ma, H.; Zhao, Y. Exploring the relationship between urbanization and the eco-environment—A case study of Beijing-Tianjin-Hebei region. *Ecol. Indic.* **2014**, *45*, 171–183. [CrossRef]

56. Fang, C.; Cui, X.; Li, G.; Bao, C.; Wang, Z.; Ma, H.; Sun, S.; Liu, H.; Luo, K.; Ren, Y. Modeling regional sustainable development scenarios using the Urbanization and Eco-environment Coupler: Case study of Beijing-Tianjin-Hebei urban agglomeration, China. *Sci. Total Environ.* **2019**, *689*, 820–830. [CrossRef] [PubMed]

County-Level Spatiotemporal Dynamics and Driving Mechanisms of Carbon Emissions in the Pearl River Delta Urban Agglomeration, China

Fei Wang [1], Changjian Wang [2,3,*], Xiaojie Lin [2,4], Zeng Li [2] and Changlong Sun [5,*]

[1] School of Resources and Planning, Guangzhou Xinhua University, Guangzhou 510520, China; wangfei1323@xhsysu.edu.cn
[2] Guangdong Provincial Key Laboratory of Remote Sensing and Geographical Information System, Guangzhou Institute of Geography, Guangdong Academy of Sciences, Guangzhou 510070, China; linxj01@126.com (X.L.); lzeng2023@gdas.ac.cn (Z.L.)
[3] Guangdong–Hong Kong-Macau Joint Laboratory for Smart Cities, Shenzhen 518061, China
[4] Water Resources Bureau of Fuding, Fuding 355200, China
[5] School of Economics and Management, Wenzhou University of Technology, Wenzhou 325000, China
* Correspondence: wangcj@gdas.ac.cn (C.W.); 20200436@wzu.edu.cn (C.S.)

Abstract: Encouraging cities to take the lead in achieving carbon peak and carbon neutrality holds significant global implications for addressing climate change. However, existing studies primarily focus on the urban scale, lacking more comprehensive county-level analyses, which hampers the effective implementation of differentiated carbon mitigation policies. Therefore, this study focused on the Pearl River Delta urban agglomeration in China, adopting nighttime light data and socio-economic spatial data to estimate carbon emissions at the county level. Furthermore, trend analysis, spatial autocorrelation analysis, and Geodetector were adopted to elucidate the spatiotemporal patterns and influencing factors of county-level carbon emissions. Carbon emissions were predominantly concentrated in the counties on the eastern bank of the Pearl River Estuary. Since 2010, there has been a deceleration in the growth rate of carbon emissions in the region around the Pearl River Estuary, with some counties exhibiting declining trends. Throughout the study period, construction land expansion consistently emerged as a predominant factor driving carbon emission growth. Additionally, foreign direct investment, urbanization, and fixed asset investment each significantly contributed to the increased carbon emissions during different development periods.

Keywords: City- and county- level carbon emissions; Pearl River Delta; nighttime light data; construction land expansion; Geodetector

1. Introduction

The issue of global climate change poses one of the most formidable challenges to humanity [1–5]. The Paris Agreement establishes the goal of limiting increases in the global average temperature to less than 2 °C above pre-industrial levels, with an ambitious aim to strive for less than 1.5 °C, thereby mitigating the risks and impacts associated with climate change [6–10]. The international community has actively engaged in discussions on scientific measures to mitigate emissions, resulting in over 150 countries proposing carbon peak or carbon neutral targets. Cities, being the epicenters of human economic and social activities, constitute merely 3% of the earth's land but contribute more than 75% to global GDP and account for over 70% of worldwide greenhouse gas emissions [11]. The peaking of urban carbon emissions has emerged as a pivotal concern in climate change mitigation efforts. As the leading emitter of carbon globally, over 85% of China's total carbon emissions originate from its cities, thereby necessitating focused measures to curb CO_2 emissions within urban areas [12,13]. Therefore, with cities as the primary source of carbon emissions, it is imperative to investigate the origins of urban carbon emissions and

promote the development of environmentally friendly, low-carbon cities. This approach has become crucial for China in achieving its "double carbon" goal and ensuring sustainable economic and social progress. Research on urban carbon emissions primarily encompasses comprehensive carbon emission accounting, spatiotemporal dynamics of carbon emissions, and investigation into the driving mechanisms behind such emissions. Accurate assessment of carbon emissions is a focal point in both domestic and international research efforts, as it serves as the foundation for comprehensively understanding the spatiotemporal dynamics and influencing factors of carbon emissions. Clarifying the influencing factors of carbon emissions is crucial for effectively controlling and mitigating carbon emissions.

The calculation of carbon emission data with higher spatial and temporal resolution, as well as the achievement of more detailed, accurate, and timely carbon emission simulation, are currently at the forefront of scientific research and represent significant national priorities. Due to the lack of comprehensive and reliable carbon emission data in China, researchers primarily rely on statistical data such as energy statistical yearbooks and relevant statistical yearbooks to estimate carbon emissions at national [14], provincial [15,16], and urban levels [12,17] using the inventory analysis method provided by IPCC. Due to the relative scarcity of statistical data, researchers have tried to make carbon emission estimates using other datasets. Elvidge et al. initially identified a correlation between the brightness values in night light data and greenhouse gas emissions [18]. Subsequently, night-time imagery was employed by Doll et al. as a surrogate variable to represent socioeconomic status and carbon emissions [19]. Ghosh et al. integrated the Defense Meteorological Satellite Program's Operational Linescan System (DMSP-OLS) data and population spatial grid data to reconstruct a high-resolution (1 km) global distribution map of energy-related carbon emissions [20]. By incorporating point source data and night light data, Oda et al. compiled a comprehensive inventory of global carbon emissions from 1980 to 2007 at a resolution of 1 km [21]. Su et al. developed a normalized approach for assessing China's city-level energy-related carbon emission DMSP-OLS nighttime light imagery [22]. Compared with DMSP-OLS night light remote sensing data, the National Polar-Orbiting Partnership's Visible Infrared Imaging Radiometer Suite (NPP-VIIRS) has a higher spatial resolution [23]. The utilization of NPP-VIIRS nighttime light data, which overcomes the primary limitations of DMSP-OLS nighttime light data, enables the investigation of urban carbon issues at a more refined spatial scale. Zhang et al. applied the power function approach to fit the nonlinear relationship between NPP-VIIRS and DMSP-OLS, subsequently conducting an analysis of the spatiotemporal differentiation characteristics of urban carbon emissions in Northwest China [24].

However, as cities continue to expand, spatial disparities within urban areas have become increasingly significant, and the distribution of carbon emissions has undergone significant changes. Previous attempts at implementing carbon emission reduction policies based on urban spatial units have not yielded the desired results. The inconsistency of statistical caliber and the lack of smaller-scale statistical data pose challenges in meeting the requirements of current refined carbon governance. To address the limitations of traditional carbon emission estimations based on statistical data, numerous scholars have started exploring more efficient and accurate methods for estimating carbon emissions. Chen et al. employed the particle swarm optimization–back propagation (PSO-BP) algorithm to construct a fusion model integrating two types of county-level night light data, namely DMSP-OLS and NPP-VIIRS, for the purpose of inverting China's county-level carbon emissions from 1997 to 2017 [25]. They utilized a power function regression model to establish the relationship between NPP-VIIRS and DMSP-OLS night light data, thereby estimating CO_2 emissions for 334 prefectural cities in China from 1992 to 2017 [26]. Zhu et al. adopted a deep learning method on DMSP-OLS and NPP-VIIRS nighttime light datasets to estimate county-level carbon emissions in China from 1997 to 2019, the fitting effects of which are better than those obtained in previous studies based on traditional statistical methods [27]. Xiang et al. applied a regression model to NPP-VIIRS nighttime light data to analyze spatiotemporal changes in carbon emissions at the district and county levels of

Jiangsu Province in China [28]. Jiang et al. identified an asymmetric U-shaped relationship between daily mean temperatures and carbon intensities on county-level data from 2000 to 2019 based on spline regressions. The carbon emissions dataset was sourced from the Open-source Data Inventory for Anthropogenic Carbon Dioxide (ODIAC), which is a high-spatial-resolution (1 km × 1 km) global emission data product [29]. Xie et al. analyzed the spatial–temporal characteristics of carbon budget and carbon compensation rate at the county level in the Yellow River Basin; carbon source data were mainly obtained from the China Carbon Accounting Database (CEAD, https://www.ceads.net.cn/ (accessed on 6 June 2022)) [30].

Currently, there exists a wealth of research findings on the spatiotemporal dynamics of carbon emissions. Zhou et al. [31] and Ke et al. [32] employed the spatial autocorrelation analysis method to examine the spatial spillover effect of urban carbon emissions in China. Cheng et al. investigated spatiotemporal dynamics and influencing factors of provincial carbon emission intensity in China from 1997 to 2010 [33]. The current methods employed to study these factors include IPAT, STIRPAT, LMDI, IDA, and SDA [34–38]. However, these methods only provide insights into the degree of influence exerted by different factors and fail to elucidate the spatial differentiation mechanisms underlying carbon emissions. Consequently, researchers have turned their attention towards analyzing this mechanism from a spatial perspective using techniques such as the geographical weighted regression model (GWR) [13], spatial econometric model [39], and Geodetector [40,41], among others. Many scholars have conducted analyses on the driving mechanisms of carbon emissions at a national scale in various countries, including China. These studies reveal that factors such as urbanization [42], economic density [43], construction land [44,45], road density [46], household consumption [47], foreign investment [48,49], foreign trade [50], fixed asset investment [51,52], local government expenditure [53,54], and other variables significantly influence carbon emissions. By examining the driving factors of carbon emissions in different provinces and regions of China, it is evident that urbanization [55], household consumption [56], foreign trade [57], fixed asset investment [58], and other factors exert a strong impact on carbon emissions.

The current carbon emission data are primarily calculated based on energy statistical data at the municipal level and above, with a lack of spatially refined research. The DMSP-OLS and NPP-VIIRS nighttime light datasets have facilitated great progress in the simulation of carbon emissions at the county level. However, the dependence on nighttime light data to estimate carbon emissions may introduce considerable uncertainties, especially in areas with minimal industrial activity. Building upon previous research on the spatialization of carbon emissions using nighttime light data, this study has further integrated multiple sources of spatial data such as population and economy to enhance cross-validation and calibration processes, thereby achieving more precise simulations of carbon emissions. The traditional linear model, in addition, predominantly employs static models like power functions or polynomial regression to invert the relationship between nighttime light and carbon emissions. However, these models fail to capture nonlinear dynamic relationships, and they overlook the technical advantages of machine learning in integrating multi-source data. Additionally, the driving mechanism behind carbon emissions is mainly studied at provincial and urban scales, resulting in insufficient analysis of regional impact mechanisms at finer scales.

Therefore, this study aims to construct a multi-scale refined carbon emission dataset coupled with multiple sources of data. By constructing a multifactorial analysis framework, we aim to promote understanding of the district- and county-scale driving mechanisms for carbon emissions while proposing differentiated paths for emission reduction. The Pearl River Delta is at the forefront of reform and opening up, characterized by rapid economic and social development as well as a significant population increase [59]. It stands out a region in China with a highly accelerated urbanization process while also serving as a major contributor to carbon emissions. Therefore, effectively controlling carbon emissions in the Pearl River Delta plays a crucial role in achieving China's dual-carbon target. The swift

urbanization and industrialization within the Pearl River Delta have resulted in substantial consumption of natural resources, leading to high levels of carbon emissions. Furthermore, variations in economic and social development among different cities have contributed to disparities in carbon emissions. However, there remains a lack of research on both the spatial distribution pattern and driving mechanisms behind county-level carbon emissions within this region. Hence, analyzing key influencing factors for carbon emissions from an urban development perspective holds great practical significance for understanding the dynamics within the Pearl River Delta.

2. Materials and Methods

2.1. Materials for Spatial Simulation of Carbon Emissions

The Defense Meteorological Satellite Program's Operational Linescan System (DMSP-OLS) and National Polar-Orbiting Partnership's Visible Infrared Imaging Radiometer Suite (NPP-VIIRS) nighttime light data were adopted in this study.

The carbon emission data utilized in this study for the period spanning from 2000 to 2019 at the provincial level were sourced from the CEAD research data, which was derived using sectoral and reference methods provided by the IPCC (https://www.ceads.net.cn/data/province/ (accessed on 6 June 2022)). It calculated CO_2 emissions from 17 types of fossil fuels and 47 energy-related sectors across the 30 provinces of mainland China from 1997 to 2019. The data can be downloaded from the CEAD (https://www.ceads.net/ (accessed on 6 June 2022)).

The population kilometer grid data utilized in this study are the 2000, 2005, 2010, 2015, and 2019 releases of population kilometer grid data by the Resources and Environmental Science Data Platform of Chinese Academy of Sciences (https://www.resdc.cn/DOI/DOI.aspx?DOIID=32 (accessed on 6 June 2022)). The GDP kilometer grid data employed in this study are the 2000, 2005, 2010, 2015, and 2019 releases of GDP kilometer grid data by the Resources and Environmental Science Data Platform of Chinese Academy of Sciences (https://www.resdc.cn/DOI/DOI.aspx?DOIID=33 (accessed on 6 June 2022)).

The provincial and urban GDP and permanent resident population of Guangdong Province utilized in this study were sourced from the Statistical Yearbook of Guangdong Province, spanning from 2001 to 2020 (http://stats.gd.gov.cn/ (accessed on 6 June 2022)), while the district and county GDP and total population data were sourced from the China County Statistical Yearbook, Guangdong Provincial Statistical Yearbook, and municipal Statistical Yearbook of Guangdong Province for the same period. Some missing data was supplemented using information from the statistical bulletin of national economic and social development corresponding to specific districts and counties.

The DMSP-OLS (the period from 1992 to 2013) and NPP-VIIRS (the period from 2012 to the present) night light data were preprocessed separately in this research. The simulation model of the two types of night light data and the nonlinear relationship between the night light DN value and carbon emissions were constructed by PSO-BP [25,26,60]. The PSO-BP algorithm was employed for the first time in the modeling process to acquire night light data with a long-term and consistent 1 km × 1 km resolution, resulting in the acquisition of comparable long-term time series data from 2000 to 2019. The simulation model exhibited a goodness-of-fit value of 0.97544, indicating excellent fitting accuracy. The PSO-BP algorithm was employed for the second time in the modeling process to establish a correlation between simulated carbon emission data and statistical accounting carbon emission data. By integrating night light data with multi-source data (population grid data and GDP grid data), a correlation between simulated carbon emission data and statistical information was established. The estimation of grid-level carbon emissions through a detailed calculation process is outlined in our authorized invention patent (ZL202310240626.9). The estimation model demonstrated a high goodness-of-fit value of 0.99274, enabling accurate prediction of carbon emissions at the grid level.

Using ArcGIS 10.1 software, the long-term series 1 km × 1 km gridded carbon emission dataset was overlaid with the administrative regions of cities and counties in the Pearl River

Delta urban agglomeration. This allowed us to obtain city-level and county-level carbon emission datasets for this urban agglomeration from 2000 to 2019. Since current carbon emission datasets based on statistical data are primarily at the provincial and municipal levels, this study compared the city-level carbon emission data with existing city-level carbon emission accounting data to mutually verify the simulation results. We compared city-level carbon emission data from CEAD, which considered both fossil fuel-related emissions from 47 socioeconomic sectors and 17 types of fossil fuels, as well as process-related emissions from cement production [61]. We also compared city-level carbon emission data from the China High-Resolution Emission Database (CHRED, www.cityghg.com or www.ceeio.com (accessed on 6 June 2022)), which included point emission sources and gridded emission data (with a spatial resolution of 1 km and 10 km) [62,63]. In comparison with previous studies [61–65], some errors in calculating carbon emissions were identified due to the lack of city-level statistical data. However, the obtained carbon emissions for these urban agglomerations align roughly with previous studies' total amounts and trends in most cities. Therefore, conducting subsequent studies on the carbon emissions of these urban agglomerations was considered feasible.

2.2. Trend Analysis Based on SLOPE

With the passage of time, carbon emissions exhibit a tendency towards growth, while any decrease or change remains inconspicuous. The present study aimed to develop a linear regression model for analyzing the temporal trend of carbon emissions [28,66]. By calculating the slope value over a 20-year period from 2000 to 2019, it examined the linear trend in carbon emissions in each district and county, thereby analyzing annual changes in carbon emissions. The least squares method is employed to estimate the specific formula for determining the linear trend:

$$SLOPE = \frac{n \times \sum_{i=1}^{n} x_i C_i - \sum_{i=1}^{n} x_i \sum_{i=1}^{n} C_i}{n \times \sum_{i=1}^{n} x_i^2 - \left(\sum_{i=1}^{n} x_i \right)^2} \tag{1}$$

where n represents the total number of years (20), x_i denotes the year i, and C_i signifies the CO_2 emissions in year i. A positive value for SLOPE indicates an increasing trend in carbon emissions over time t, while a negative value suggests a downward trend. The magnitude of SLOPE reflects the rate at which carbon emissions change; a larger absolute value corresponds to a faster growth or decline rate, whereas a smaller absolute value signifies slower growth or decline [66].

2.3. Exploratory Spatial Data Analysis

The method of Exploratory Spatial Data Analysis (ESDA) can unveil the spatial autocorrelation and spatial dependence of geographical phenomena within a specific region, as well as similar phenomena in its neighboring regions [67,68]. Among the commonly used ESDA methods, global spatial autocorrelation and local spatial autocorrelation are analyzed separately in this paper to examine carbon emissions in this urban agglomerations.

Global spatial autocorrelation analysis aims to determine whether a geographical phenomenon exhibits spatial autocorrelation and dependence by analyzing its overall spatial distribution. Currently, the primary indices used to measure global spatial autocorrelation are global Moran's *I* and Geary's *C*. In this study, the global Moran's *I* index is employed to unveil the global spatial autocorrelation of carbon emissions in this urban agglomeration. The global Moran's *I* index assesses the similarity of attribute values between each unit and its surrounding area, providing a comprehensive measure of spatial autocorrelation for the entire research area [69]. The specific formula is as follows:

$$Global\ Moran's\ I = \frac{n\sum\limits_{i=1}^{n}\sum\limits_{j\neq1}^{n}w_{ij}\left(X_i - \overline{X}\right)\left(X_j - \overline{X}\right)}{\left(\sum\limits_{i=1}^{n}\sum\limits_{j=1}^{n}w_{ij}\right)\sum\limits_{i=1}^{n}\left(X_i - \overline{X}\right)^2} \tag{2}$$

The Global Moran's *I* represents the global Moran's *I* index, where *n* denotes the number of spatial units. X_i and X_j represent the observed values of variable *X* in space units *i* and *j*, respectively, while $\overline{X}$ signifies the mean value of *X*. The w_{ij} is a spatial weight matrix, with a value of 1 when X_i and X_j are adjacent, and 0 otherwise. The range for Global Moran's *I* is [−1, 1]. A negative value indicates a negative correlation in spatial distribution between observed values; a zero value suggests no correlation; whereas a positive value implies a positive correlation. Furthermore, the absolute magnitude reflects both the strength of correlation and level of agglomeration.

The Global Moran's *I* index only captures the overall level of spatial agglomeration and dispersion of attribute values within a region, serving as a statistical measure representing the general spatial distribution. On the other hand, local spatial correlation enables us to identify specific patterns of spatial agglomeration for different geographical phenomena, thereby reflecting the localized heterogeneity of these phenomena [70]. Commonly employed indicators for measuring local spatial correlation include the local Moran's *I* index and the local Geary's *C* index. In this study, we utilize the Local Moran's *I* index to analyze the spatial variations between each region and its surrounding areas, with its specific formula presented as follows:

$$Local\ Moran'\ I_i = \frac{\left(X_i - \overline{X}\right)}{m_o}\sum_j w_{ij}\left(X_i - \overline{X}\right) \tag{3}$$

$$m_o = \sum_j^n \left(X_i - \overline{X}\right)/n \tag{4}$$

The positive value of Local Moran's I_i indicates the presence of either high–high or low–low clustering in the *i* spatial unit, while the negative value suggests the presence of either high–low or low–high clustering.

The significance test of Local Moran's *I* was conducted using the following formula:

$$Z(I_i) = \frac{I_i - E(I_i)}{\sqrt{\text{var}(I_i)}} \tag{5}$$

The symbol $Z(I_i)$ denotes the significance level of spatial autocorrelation. $E(I_i)$ represents the expected value of Moran's *I* index, and $\text{var}(I_i)$ signifies the variance under the null hypothesis of no spatial autocorrelation.

2.4. Geodetector

The term "spatial heterogeneity" refers to the uneven distribution of various geographical phenomena in space, which represents the spatial manifestation of natural and socio-economic processes [71,72]. By analyzing spatial variance, the geodetector can be utilized to identify the spatial stratification heterogeneity of a single variable and explore potential causal relationships between two variables. The principle behind the geodetector is that if an independent variable *X* has an impact on a dependent variable *C*, then there tends to be consistency in their spatial distributions. The degree of this spatial consistency can be determined by the determination force q_x of measure factor *X*.

$$q_x = 1 - \frac{1}{N\sigma^2}\sum_{Z=1}^{L} N_Z \sigma_Z^2 \tag{6}$$

$$\sigma_Z^2 = \frac{1}{N_Z - 1} \sum_{N_Z-1}^{N_Z} \left(C_{z,i} - \overline{C_z}\right)^2 \tag{7}$$

$$\sigma^2 = \frac{1}{N - 1} \sum_{j=1}^{N} \left(C_j - \overline{C}\right)^2 \tag{8}$$

The determinant index q_x influences the factors of carbon emission. The σ_Z^2 represents variance in the Z layer. The σ^2 represents variance in the whole study area for the dependent variable C. N_Z denotes the number of samples containing dependent variable C in region Z. N signifies the number of samples of dependent variable C contained in the entire research area. Lastly, L indicates the number of layers in independent variable X. In this study, a large q value demonstrates that the factor affects more of the changes in county-level emissions.

3. Results

3.1. Spatial–Temporal Patterns and Trends of Carbon Emissions in the Pearl River Delta Urban Agglomeration

3.1.1. The Temporal Dynamics of Carbon Emissions in the Pearl River Delta Urban Agglomeration

From 2000 to 2019, the total carbon emissions of this urban agglomeration exhibited a consistent upward trajectory, fluctuating from 151 million tons in 2000 to 400 million tons in 2019, representing a substantial increase of 2.64 times (Figure 1). This was accompanied by an average annual growth rate of 5.25%. Over this period, per capita carbon emissions rose from 3.53 tons in 2000 to reach a peak at 5.21 tons in 2019, displaying a general inverted U-shaped trend. Following rapid increases until reaching its zenith around the year 2009, carbon emissions subsequently experienced fluctuations and declines, with minimal changes since the year 2015. Notably, carbon emission intensity in this urban agglomeration demonstrated a remarkable downward trend, plummeting from emitting approximately 1.57 tonnes/10,000 CNY in the year of inception (2000) to merely half that amount at just about 0.50 tonnes/10,000 CNY by the end of our study period (2019). These findings underscore active efforts undertaken by this urban agglomeration towards promoting energy and industrial transformation and upgrading while concurrently enhancing energy utilization efficiency and driving down carbon emission intensity.

3.1.2. Spatial Distribution Pattern of Carbon Emissions in the Pearl River Delta Urban Agglomeration

From 2000 to 2019, the total carbon emissions of these urban agglomerations exhibited a consistent upward trajectory, with carbon emissions primarily concentrated in the vicinity of the Pearl River estuary and gradually expanding outward. The eastern bank of the Pearl River demonstrated significantly higher levels of carbon emissions compared to its western counterpart, while the ecological barrier area outside the Pearl River Delta displayed considerably lower emissions than those observed around the estuary (Figure 2). During this period, Guangzhou, Foshan, Dongguan, Shenzhen, and other cities experienced rapid development in their early industrial enterprises, resulting in relatively high overall carbon emissions for these cities. Similarly, Huizhou, Zhongshan, Jiangmen, Zhaoqing, and Zhuhai also witnessed substantial growth due to their rapid industrial development stage; however, their total emission levels remained comparatively lower than those recorded by other cities.

3.1.3. Evolution of City-Scale Carbon Emission Patterns in the Pearl River Delta Urban Agglomeration

The carbon emissions of various cities within these urban agglomerations were computed based on spatial findings, as illustrated in Figure 3. Predominantly concentrated around the Pearl River Estuary, the carbon emissions within these urban agglomerations are primarily attributed to Guangzhou, consistently accounting for the largest proportion from 2000 to 2019 at approximately 20%. Foshan, Dongguan, and Shenzhen emerged as

significant contributors to carbon emissions, while Huizhou, Jiangmen, and Zhongshan experienced rapid growth in their emission levels. Conversely, Zhuhai and Zhaoqing exhibited relatively lower levels of carbon emissions. (1) In 2000, the carbon emissions of this urban agglomeration accounted for 77% of the total carbon emissions in the Guangdong province. Guangzhou, Dongguan, and Foshan emerged as major contributors to carbon emissions, with shares of 20.67%, 19.31%, and 16.46%, respectively, within this urban agglomeration, while Zhaoqing and Zhuhai exhibited relatively lower levels of carbon emissions. (2) In 2005, the Pearl River Delta emerged as a prominent gateway for international trade and witnessed remarkable growth of numerous enterprises, characterized by high energy consumption. The carbon emission levels in the Pearl River Delta escalated from 151 million tons in 2000 to 239 million tons in 2005. Amongst these emissions, Guangzhou, Dongguan, and Foshan accounted for the largest shares, at 21.21%, 16.04%, and 15.95%, respectively, while Zhaoqing and Zhuhai exhibited comparatively lower carbon emission levels. During the period between 2000 and 2005, Huizhou and Zhaoqing experienced the most rapid increase in carbon emissions, with average annual growth rates of approximately 18.09% and 14.18%, respectively. As a consequence of implementing the dual-transfer policy initially proposed in 2004, which aimed to gradually relocate labor-intensive industries dispersed throughout the Pearl River Delta towards eastern/western regions as well as mountainous areas within Northern Guangdong Province, there was an expansion of Guangdong's overall carbon emissions beyond just those originating from within the Pearl River Delta, thus leading to a decrease in total carbon emissions within this urban agglomeration province-wide. (3) In 2010, the carbon emissions of this urban agglomeration increased to 336 million tons. Guangzhou, Foshan, and Dongguan remained as the three cities with the highest carbon emissions in the Pearl River Delta, accounting for 21.19%, 16.03%, and 15.31% of regional carbon emissions, respectively. Zhuhai and Zhaoqing had the lowest carbon emissions, at 0.15 million tons and 16 million tons, respectively, in 2010. The cities experiencing the most rapid growth in carbon emissions over the past five years were Zhaoqing, Zhuhai, and Huizhou, which saw increases by factors of approximately 1.60, 1.50, and 1.47, respectively. (4) In 2015, the carbon emissions of this urban agglomeration reached a total of 354 million tons. As a result of the implementation of national carbon control measures in 2014, there was only a marginal increase compared to the 336 million tons recorded in 2010. Guangzhou, Foshan, and Dongguan are identified as the three cities with the highest carbon emissions, accounting for approximately 21.65%, 15.12%, and 14.76% of the overall regional carbon emissions, respectively. The growth rate of carbon emissions across all cities was relatively slow, while collectively contributing to about 70.74% of the province's total carbon emission. (5) In 2019, the carbon emissions of this urban agglomeration rose to 400 million tons, with Guangzhou, Dongguan, and Foshan remaining as the primary contributors, accounting for 21.48%, 14.51%, and 13.81% of the total regional carbon emissions, respectively. Zhongshan, Huizhou, and Zhaoqing experienced significant growth in carbon emissions at average annual rates of 4.44%, 4.25%, and 4.11%, respectively.

3.1.4. Spatial Pattern Analysis of Carbon Emissions at the County Level in the Pearl River Delta Urban Agglomeration

This paper employs a trend analysis to examine the temporal variation characteristics of carbon emissions in various districts and counties. Specifically, we calculate the SLOPE of carbon emissions from 2000 to 2019 using this method, and we apply ArcGIS software's natural break point grading method (Jenks) to classify each county's carbon emission change trend into five types: the type with the slowest growth rate, the type with a slower growth rate, the type with a medium-speed growth rate, the type with a fast growth rate, and the type with a rapid growth rate. To further analyze this slowdown phenomenon in urban agglomerations within the Pearl River Delta region after 2010, we separately calculated inclination values for carbon emissions during two periods (2000–2010 and 2010–2019) for each county. The results are presented in Figures 4 and 5.
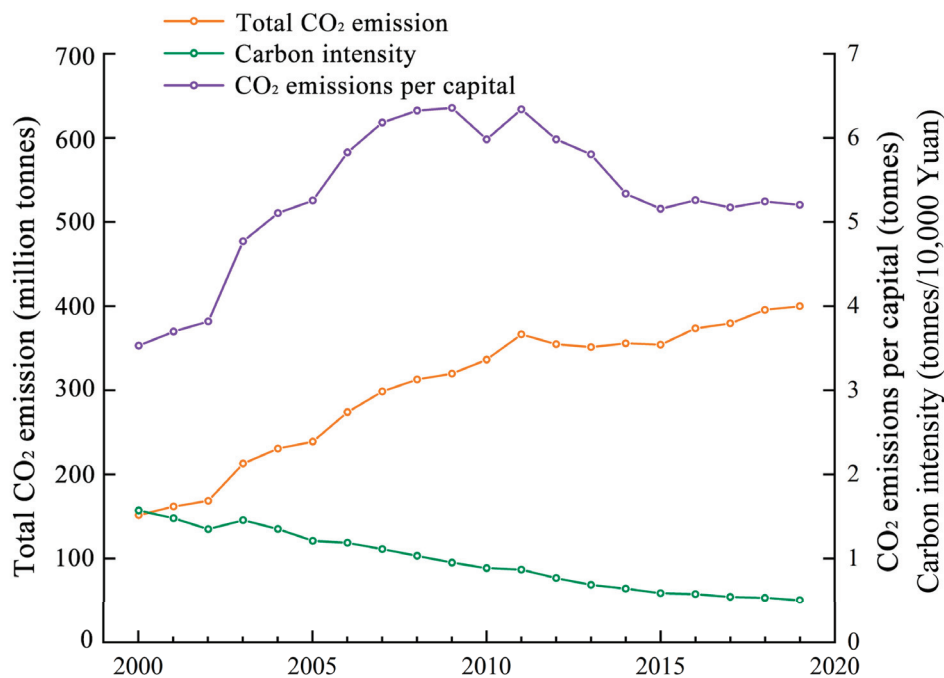
Figure 1. Evolution trend of total carbon emission, per capita carbon emission and carbon emission intensity in the Pearl River Delta urban agglomeration from 2000 to 2019.

From 2000 to 2010, owing to the rapid development of the Pearl River Delta, carbon emissions witnessed a substantial increase in most districts and counties of Guangzhou, Foshan, Huizhou, and other cities. The western bank of the Pearl River experienced a moderate growth rate in carbon emissions, while the northern region of Zhaoqing displayed a relatively sluggish growth trend. From 2010 to 2019, as industrial transformation and upgrading continued to progress in the Pearl River Delta, there was a deceleration in the growth rate of carbon emissions around the Pearl River Estuary. Notably, Shunde District in Foshan, Southern Group in Zhongshan, Yantian District in Shenzhen, and Duanzhou District in Zhaoqing exhibited a downward trajectory for carbon emissions. Conversely, the western bank of the Pearl River demonstrated a comparatively slower growth trend with an expanding area experiencing rapid growth of carbon emissions. This phenomenon primarily manifested itself within certain districts and counties on both banks of the river; for instance, Jiangmen and Zhuhai showcased an accelerated growth trend (Table 1).

Based on the spatial analysis of carbon emissions, the county-level carbon emissions of this urban agglomerations were calculated and presented in Figure 6. Being the most economically developed region in Guangdong Province, this urban agglomeration experienced a rapid increase in carbon emissions, with high-value areas primarily concentrated around the Pearl River Estuary. Foshan Nanhai District, Shunde District, Huizhou Huiyang District, Huicheng district, Shenzhen Longgang District, Guangzhou Baiyun District, Panyu District, and Zengcheng District exhibited significant levels of carbon emissions, exceeding 12 million tons in 2019. Additionally, Dongguan and Huizhou also demonstrated substantial carbon emissions. Notably, the east bank of the Pearl River displayed significantly higher carbon emission levels compared to its western counterpart, while most districts and counties in Guangzhou, Dongguan, Huizhou, and Shenzhen witnessed a rapid increase in their respective carbon emissions. Conversely, Jiangmen, Zhuhai, and Zhaoqing, on the west bank of the Pearl River, had relatively low carbon emissions. Foshan Nanhai district and Shunde district stood out as the two regions with the highest carbon emissions in the Pearl River Delta.
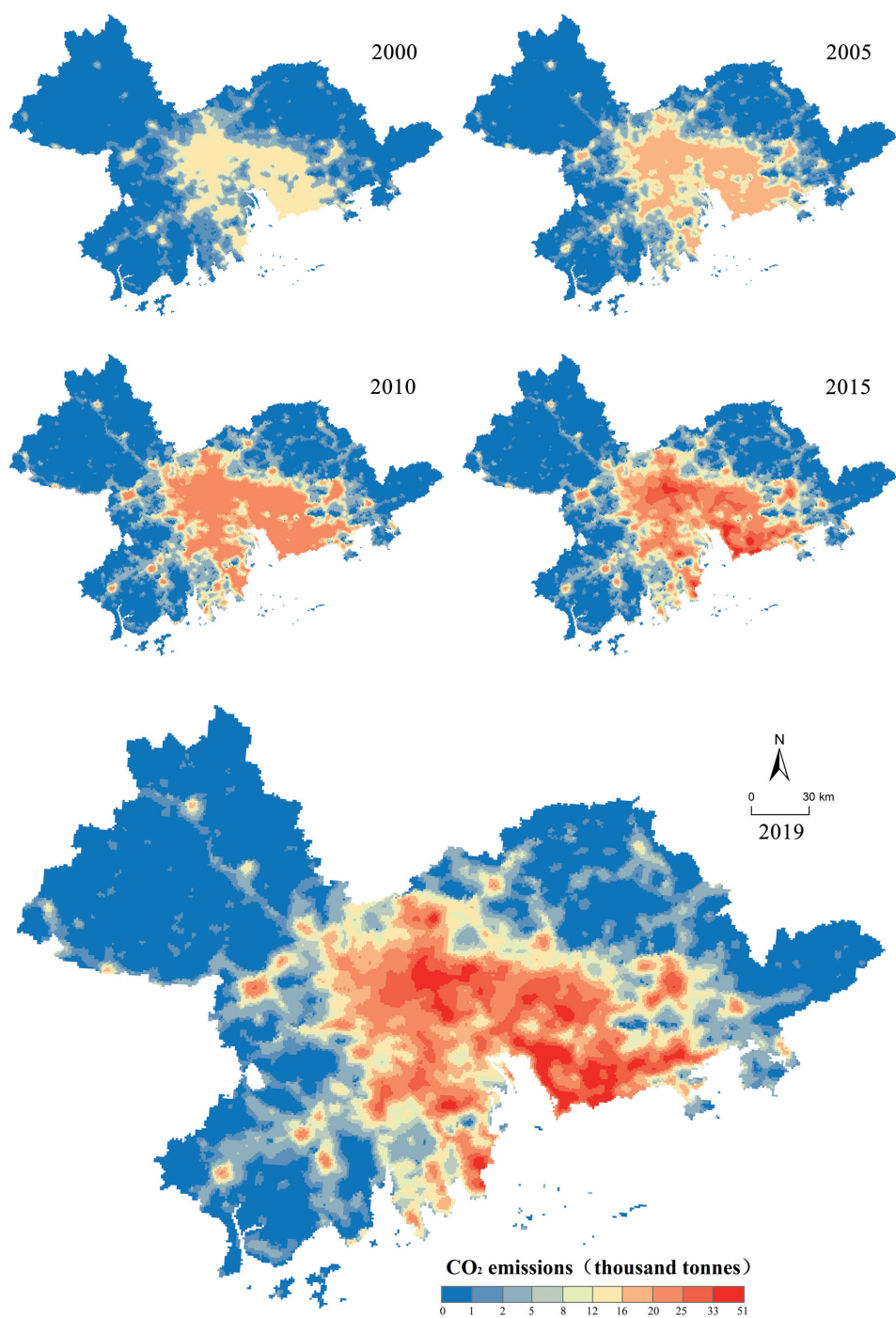
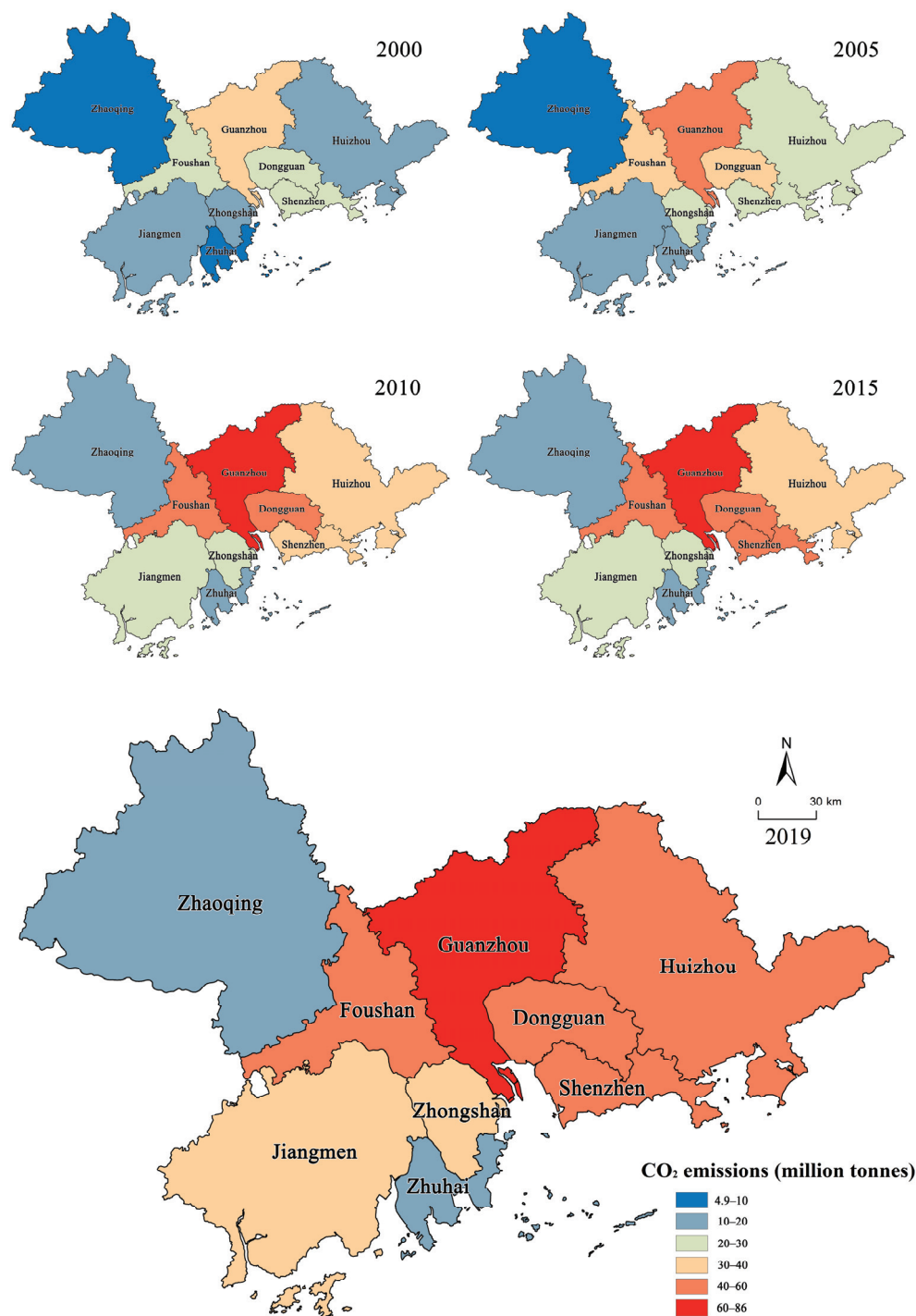**Figure 2.** Results of spatialization of carbon emissions in the Pearl River Delta urban agglomeration.

Figure 3. Spatial distribution of carbon emissions in the Pearl River Delta by cities from 2000 to 2019.
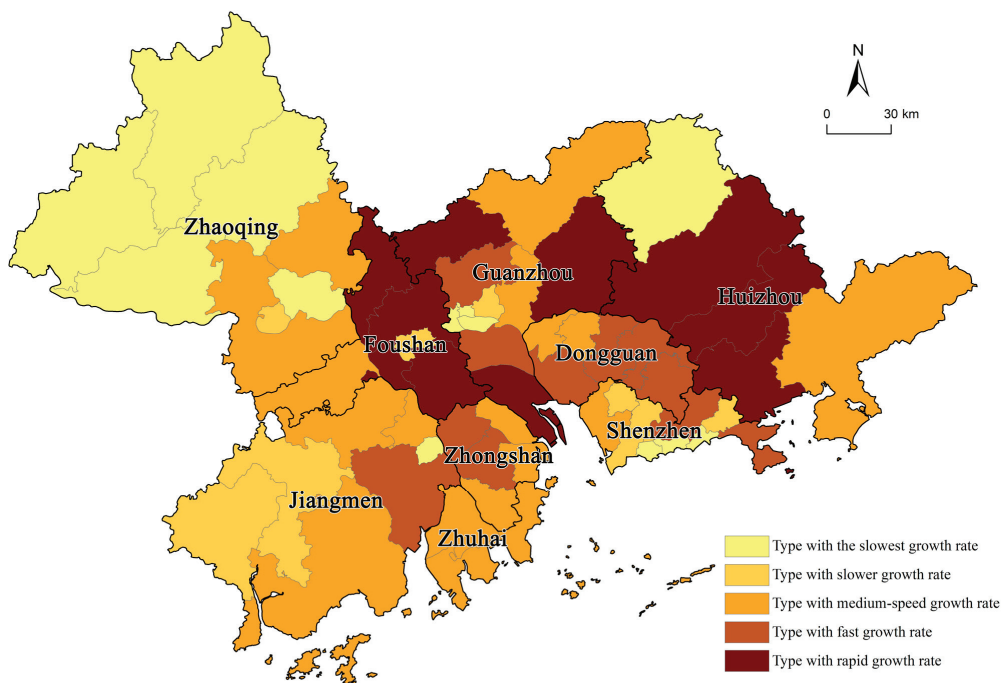
Figure 4. Trends in carbon emissions in the Pearl River Delta from 2000 to 2010.
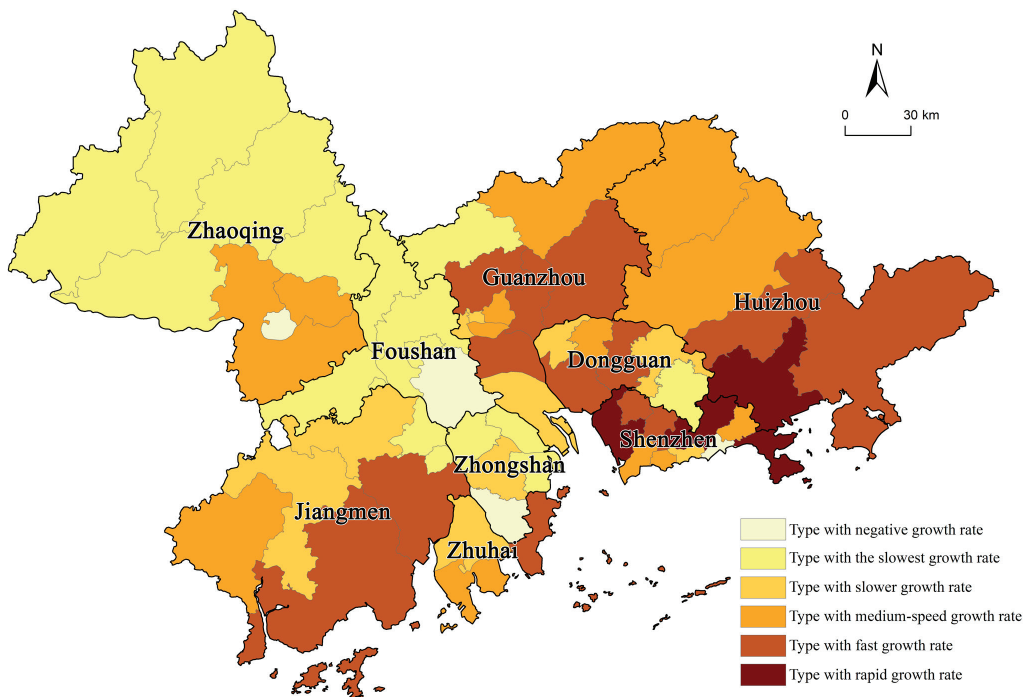

Figure 5. Trends in carbon emissions in the Pearl River Delta from 2010 to 2019.

<div align="center">

Table 1. Types of carbon emission growth in Pearl River Delta urban agglomeration by stage.

</div>

Growth Type	During 2000–2010	During 2010–2019
Decreasing growth rate		Yantian District, Duanzhou District, Shunde District, Southern Group in Zhongshan
		Mean value of the SLOPEs is −0.0211
Slowest growth rate	Futian District, Longmen County, Haizhu District, Dinghu District, Yantian District, Liwan District, Yuexiu District, Luohu District, Jianghai District, Guangning County, Huaiji County, Fengkai County, Deqing County	Jianghai District, Guangning County, Huaiji County, Fengkai County, Deqing County, Huadu District, Sanshui District, Northeast Group in Zhongshan, Eastern Group in Zhongshan, Chancheng District, Gaoming District, Pengjiang District, Pengjiang District, Nanhai District, Northwest Group in Zhongshan, Southeast Area in Dongguan, Sihui City
	Mean SLOPE value = 0.0701	Mean SLOPE value = 0.0193
Slower growth rate	Tianhe District, Nanshan District, Pingshan District, Enping City, Duanzhou District, Kaiping City, Guangming District, Longhua District, Chancheng District	Liwan District, Yuexiu District, Luohu District, Nansha District, Kaiping City, Heshan City, Central Group in Zhongshan, Eastern Industrial Park Area in Dongguan, Water Township New Town Area in Dongguan, Doumen District
	Mean SLOPE value = 0.1601	Mean SLOPE value = 0.0581
Medium growth rate	Urban area in Dongguan, Conghua District, Jinwan District, Gaoyao District, Bao'an District, Southern Group in Zhongshan, Heshan City, Water Township New Town Area in Dongguan, Doumen District, Huangpu District, Xiangzhou District, Taishan City, Huidong County, Northeast Group in Zhongshan, Eastern Group in Zhongshan, Gaoming District, Pengjiang District, Sihui City	Futian District, Longmen County, Boluo County, Haizhu District, Tianhe District, Nanshan District, Pingshan District, Enping City, Dinghu District, Urban Area in Dongguan, Conghua District, Jinwan District, Gaoyao District
	Mean SLOPE value = 0.3176	Mean SLOPE value = 0.1022
Fast growth rate	Longgang District, Central Group in Zhongshan, Eastern Industrial Park Area in Dongguan, Songshan Lake Area in Dongguan, Baiyun District, Panyu District, Xinhui District, Northwest Group in Zhongshan, Southeast Area in Dongguan	Binhai Area, Songshan Lake Area in Dongguan, Baiyun District, Huangpu District, Panyu District, Zengcheng District, Xinhui District, Guangming District, Huicheng District, Longhua District, Xiangzhou District, Taishan City, Huidong County
	Mean SLOPE value = 0.4888	Mean SLOPE value = 0.1925
Rapid growth rate	Boluo County, Huiyang District, Shunde District, Nansha District, Zengcheng District, Huicheng District, Huadu District, Sanshui District, Nanhai District	Baoan District, Longgang District, Huiyang District
	Mean SLOPE value = 0.7873	Mean SLOPE value = 0.3671

This study utilizes the Global Moran's *I* analysis tool provided by GeoDa 1.22 software to compute the global Moran's *I* index for carbon emissions at the county level in this urban agglomeration from 2000 to 2019. The findings are presented in Figure 7. The global Moran's *I* index for county-scale carbon emissions in Pearl River Delta exhibits positive values, and their Z-values pass the significance test. Throughout the study period, districts and counties demonstrate significant spatial autocorrelation characteristics regarding carbon emissions, indicating that areas with higher (lower) carbon emissions tend to be surrounded by other areas with higher (lower) levels as well. From 2000 to 2014, the Moran's I index for carbon emissions in this urban agglomerate followed an inverted U-shaped trend and stabilized after 2014. The degree of spatial concentration of carbon emissions within each district and county experienced an initial increase followed by a gradual decrease. After 2014, due to national efforts towards carbon control promotion and industrial transformation/upgrading

initiatives targeting high-carbon emission regions, there was a tendency towards greater consistency in terms of carbon emission levels within this area.
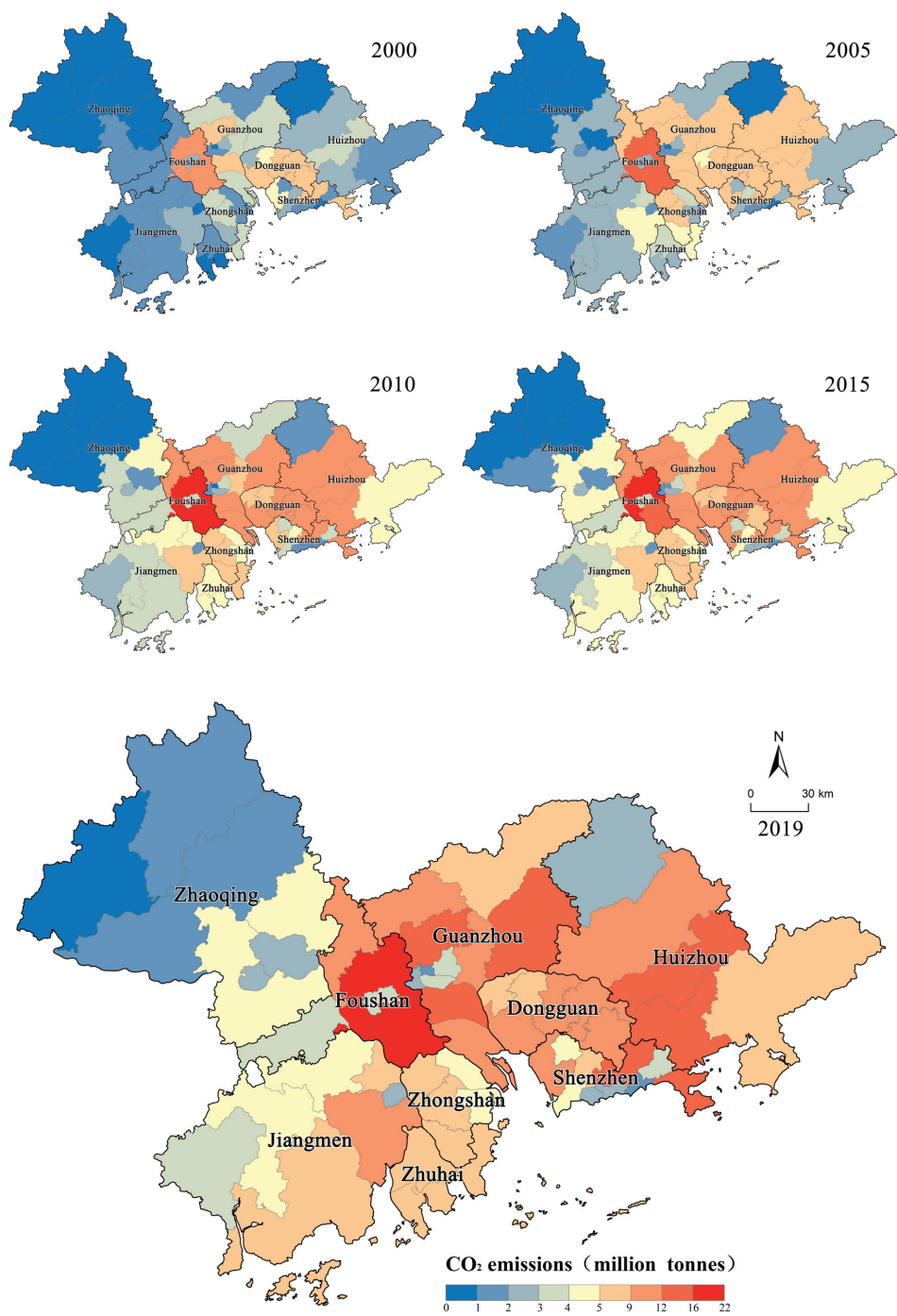

Figure 6. Spatial distribution of carbon emissions in sub-counties of the Pearl River Delta.

Figure 7. Moran's *I* index of Pearl River Delta urban agglomeration.

In order to further investigate the local spatial correlation of carbon emissions in this urban agglomeration at the regional and county levels, GeoDa and ArcGIS software were utilized to generate Local Moran's *I* spatial distribution maps for carbon emissions in 2000, 2005, 2010, 2015, and 2019. According to Equations (3)–(5), the Local Moran's *I* index was calculated to analyze the spatial variations between each region and its surrounding areas. The positive value of Local Moran's *I* index indicates the presence of either high–high or low–low clustering, while the negative value suggests the presence of either high–low or low–high clustering. The results are presented in Figure 8. Overall, there are distinct agglomeration characteristics observed in carbon emissions at the county level within this urban agglomeration. These characteristics can be categorized as high–high concentration regions and low–low concentration regions. The high–high concentration regions primarily exist around the estuary of the Pearl River, where development zones are optimized for industrial production and daily life activities that require significant energy consumption resulting in large carbon emissions. Moreover, these high–high concentration areas exhibit an eastward diffusion trend, with Huizhou having the majority of districts and counties showing high–high concentrations. Low–low-concentration areas mainly surround the periphery of these high–high concentrated areas, while most districts and counties in Zhaoqing demonstrate consistently low–low concentrations. Due to accelerated construction efforts towards an ecological industry system in Zhaoqing, the number of districts and counties with consistently low concentrations has remained stable. In summary, there is a decreasing spatial disparity observed regarding carbon emissions within Pearl River Delta.

3.2. Driving Mechanisms of Carbon Emissions in the Pearl River Delta Urban Agglomeration

Based on regional characteristics and data availability, this study has selected indicators to analyze the driving mechanisms of carbon emissions in the Pearl River Delta. The total carbon emissions of the counties within this urban agglomeration in 2010, 2015, and 2019 were chosen as independent variables. Additionally, nine indicators representing

seven factors at the county scale corresponding to these years were selected as explanatory factors and dependent variables (Table 2). Geodetector was adopted to elucidate the influencing factors of county-level carbon emissions.
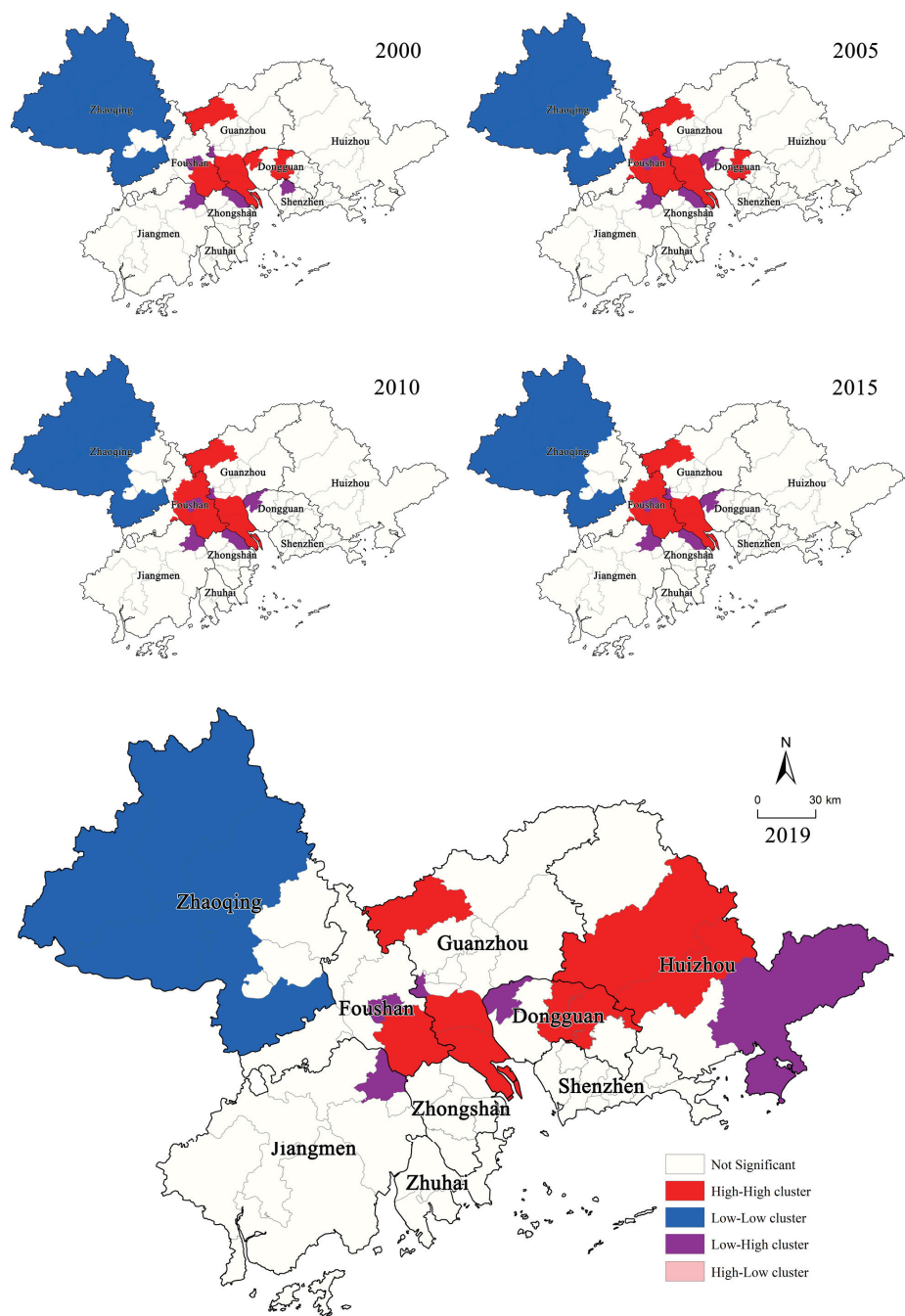

Figure 8. Spatial and temporal evolution of carbon emissions in the Pearl River Delta.

Table 2. Description of indicators.

Factors	Variables	Variable Interpretation Instructions
Population urbanization	Urbanization (UPOP)	Size of permanent urban population in each district and county (unit: 10,000)
Economic development	Economic density (DGDP)	The ratio of GDP of each district and county to each district and county area (unit: yuan/km^2)
Economic globalization	Foreign direct investment (FDI)	The actual amount of foreign direct investment used in each district and county (unit: 10,000 USD)
	Foreign trade (TEXIM)	Total amount of import and export trade of each district and county (unit: 100 million CNY)
Land use	Construction land (UAREA)	Total area of construction land in each district and county (unit: km^2)
	Road density (DROAD)	The ratio of the total mileage of the road network of each district and county to the area of the district and county (unit: km/km^2)
Household consumption	Total retail sales of consumer goods (TRSCG)	Total retail sales of consumer goods per capita in each district or county (unit: CNY/person)
Investment in fixed assets	Investment in fixed assets (FAI)	Investment in fixed assets of each district or county (unit: 10,000 CNY)
Government expenditure	Local government expenditure (GPBE)	Local government expenditure of each district or county (unit: 10,000 CNY)

3.2.1. Single-Factor Detection Results

The driving factors contributing to spatial differentiation of carbon emissions in this urban agglomeration were identified using geographic detectors. According to Equations (6)–(8), the *q* value of each factor was calculated. A larger *q* value indicated that the factor explained more of the change in county-level carbon emissions. The results of single factor detection are presented in Table 3 and Figure 9.

Table 3. Explanatory power of each driving factor in different years.

Variables	Explanatory Power (*q* Value)		
	2010	**2015**	**2019**
UPOP	0.359 ***	0.533 ***	0.541 ***
DGDP	0.245 ***	0.259 ***	0.284 ***
UAREA	0.886 ***	0.896 ***	0.898 ***
DROAD	0.313 ***	0.285 ***	0.252 **
TRSCG	0.279 *	0.309 ***	0.404 ***
FDI	0.461 ***	0.241 *	0.348 **
TEXIM	0.343 ***	0.386 ***	0.343 **
FAI	0.423 ***	0.466 ***	0.548 ***
GPBE	0.506 ***	0.495 ***	0.368 ***

Note: The significance levels for ***, **, and * are 0.01, 0.05, and 0.1, respectively, indicating statistical significance.

The explanatory power of factors in descending order in 2010, as presented in Table 3 and Figure 9, was observed to be construction land > local government expenditure > foreign direct investment > investment in fixed assets > urbanization > foreign trade > road density > household consumption > economic density. In 2015, the descending order of explanatory power shifted to construction land > urbanization > local government expenditure > investment in fixed assets > foreign trade > household consumption > road density > economic density > foreign direct investment. Similarly, in 2019, the descending order of explanatory power was found to be construction land > investment in fixed assets > urbanization > household consumption > local government expenditure > foreign

direct investment > foreign trade > economic density > road density. Throughout the study period, it is noteworthy that construction land (UAREA) consistently exhibited the highest influence, and its explanatory power increased progressively over time. Other factors demonstrated varying changes in their respective explanatory powers. For instance, indicators such as investment in fixed assets, urbanization, household consumption, and economic density displayed significant increases during all three study periods, while indicators like foreign direct investment, road density, and local government expenditure experienced a decline.
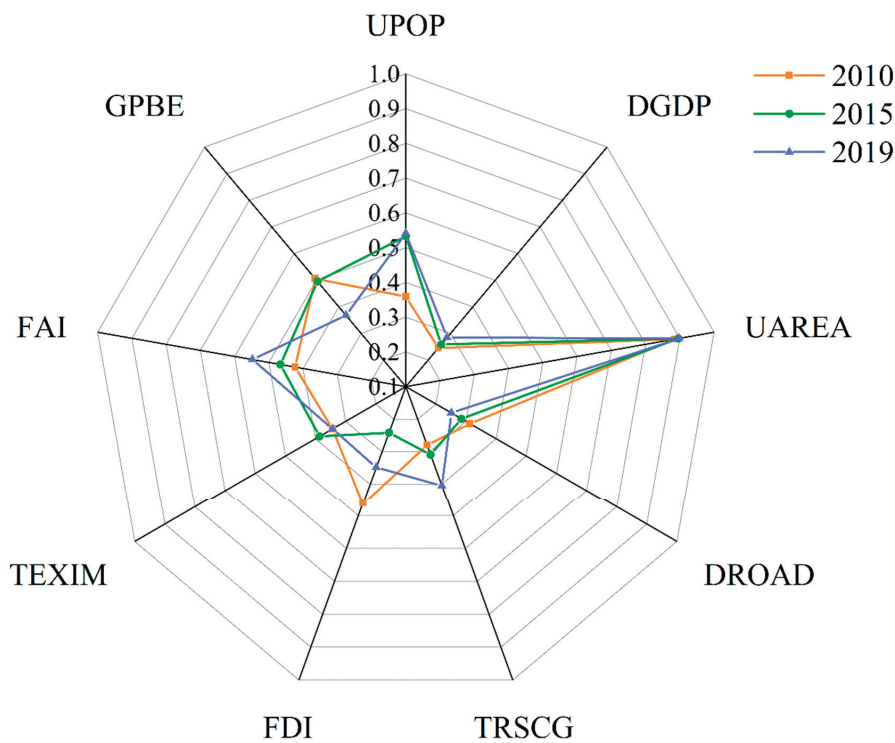

Figure 9. Explanatory power of each driving factor based on the *q* value.

The land use indicator exerted a significant influence on the spatial differentiation of carbon emissions in this urban agglomeration. Throughout the study period, construction land consistently demonstrated the highest explanatory power, with its *q* value progressively increasing from 0.886 in 2010 to 0.898 in 2019. On the one hand, the expansion of urban construction land caters to the demands of economic growth and urbanization within this urban agglomeration. However, it also engenders substantial energy consumption and carbon emissions. From 2010 to 2019, there was a rapid expansion in construction land area within this urban agglomeration, particularly between 2010 and 2015 when this expansion was most pronounced. Consequently, there was a significant increase in explanatory power observed in 2015 compared to that of 2010; subsequently, although there was a slight deceleration in the growth rate for construction land areas from 2015 to 2019, the explanatory power continued to exhibit marginal improvement.

The indicator representing population urbanization exerted a significant influence on the spatial differentiation of carbon emissions in the Pearl River Delta, with their explanatory power significantly enhanced over the study period. The explanatory power of urbanization increased from 0.359 in 2010 to 0.541 in 2019. The rapid development of the

Pearl River Delta facilitated an elevation in its level of urbanization, attracting a substantial influx of labor forces and resulting in a concentration effect on population. The permanent population of the Pearl River Delta surged from 56.315 million in 2010 to 65.648 million in 2019, while its level of urbanization rose from 73.1% to 85.5%. The heightened consumption demand stemming from urbanization and population concentration drive an increase in energy consumption requirements, which profoundly impacts carbon emissions within the urban agglomeration.

3.2.2. Multifactor Interaction Detection Results

After examining the individual impact of each factor on the spatial variation of carbon emissions in this urban agglomeration, an analysis was conducted to explore the influence of multifactor interactions, as depicted in Figures 10–12.
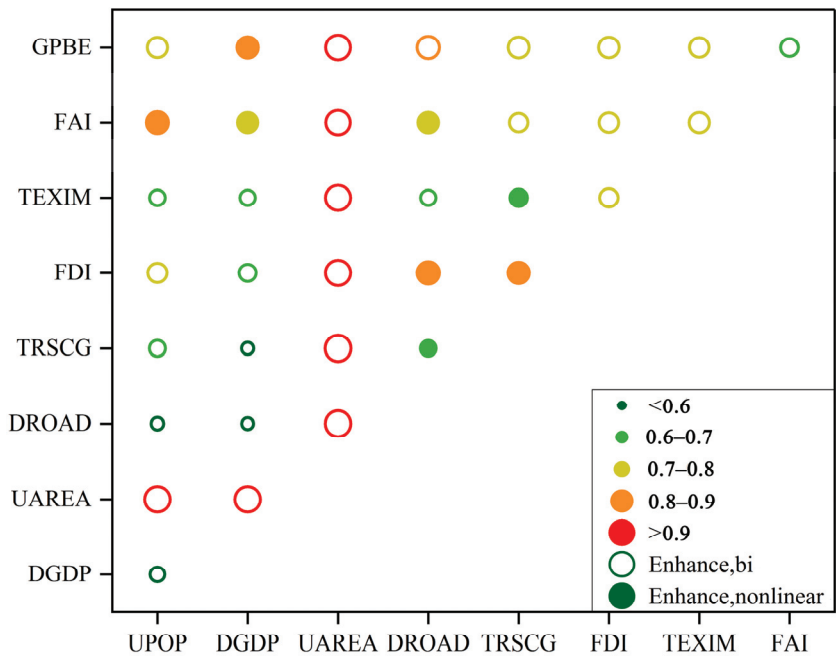

Figure 10. Multifactor interaction detection results in 2010. Note: The color and size depicted in the figure represent the explanatory power of factor interactions. The hollow circle signifies an enhanced interaction relationship between two factors, while the solid circle represents a nonlinear enhanced interaction relationship between two factors.

The influence of all factors on the spatial differentiation of carbon emissions significantly increased under interaction. Due to the robust detection and explanatory power of construction land (UAREA) as a single factor, the explanatory power of all other factors substantially improved after interacting with UAREA, reaching over 0.9. The interaction between other factors was also strong, enhancing the influence of low-explanatory-power factors detected via single-factor analysis. In 2010, household consumption and economic density had low single-factor detection influences of 0.279 and 0.245 respectively. However, their explanatory powers exceeded 0.7 when interacting with investment in fixed assets and local government expenditure (Figure 10). In 2015, economic density and foreign direct investment had low single-factor explanatory power, with *q* values of 0.259 and 0.241, respectively. However, after interacting with urbanization and local government expenditure, their explanatory powers reached approximately 0.8 (Figure 11). In 2019,

local government expenditure, which initially had weak explanatory power, surpassed 0.7 under the interaction of factors such as urbanization, investment in fixed asset, and local government expenditure (Figure 12).
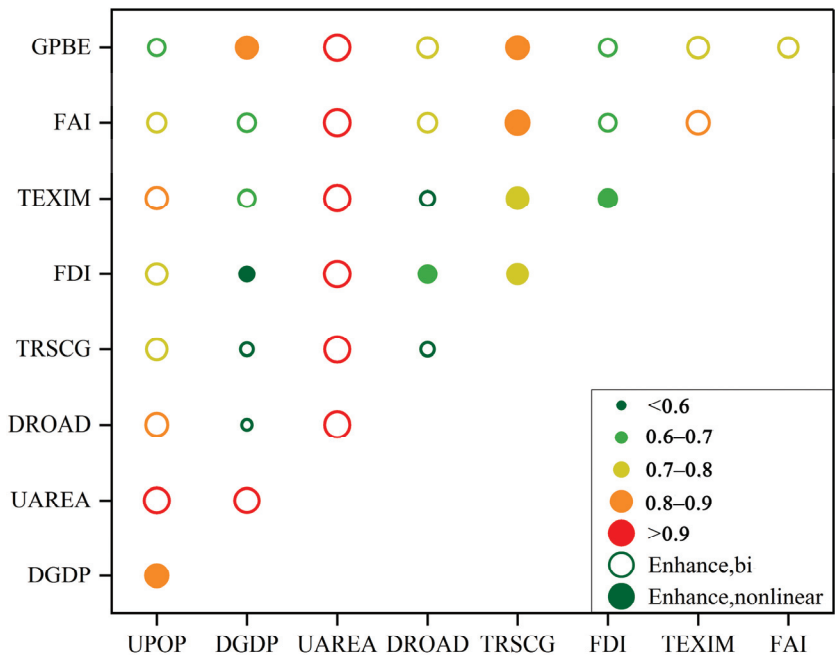

Figure 11. Multifactor interaction detection results in 2015.
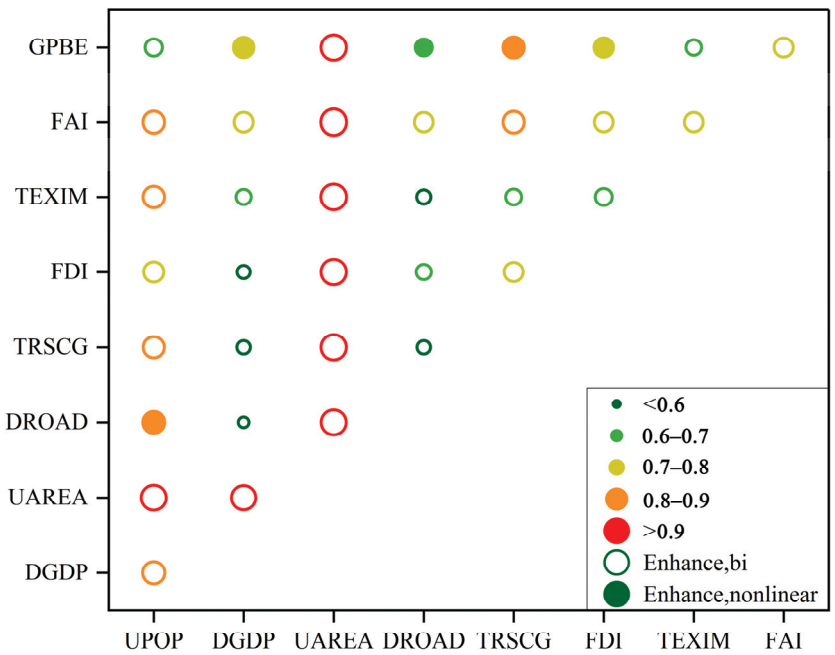

Figure 12. Multifactor interaction detection results in 2019.

The explanatory power of land use and population urbanization indicators on carbon emissions exhibits a high degree of spatial differentiation across all study periods, particularly in 2015 and 2019. Notably, when interacting with economic density, the explanatory power is significantly enhanced. These findings highlight the close relationship between population urbanization, economic growth, and land use patterns in the Pearl River Delta regarding carbon emissions' spatial distribution. The rapid economic development within this urban agglomeration has been accompanied by steady progress in the urbanization process, leading to increased population concentration and continuous expansion of urban construction land. Consequently, domestic energy demand has surged alongside high levels of energy consumption for both production and lifestyle purposes, resulting in substantial carbon emissions. Additionally, indicators representing investment in fixed assets and local government expenditure exhibit strong interactions with most influencing factors. Furthermore, foreign trade demonstrates intertwined relationships with indicators related to population urbanization, land use patterns, and household consumption. As the process of urbanization deepens continuously while opportunities within the Pearl River Delta progress further; infrastructure improvements have been witnessed alongside enhancements in household consumption, providing favorable conditions for foreign trade activities to thrive. This increase in foreign trade scale has subsequently attracted a significant influx of production factors while accelerating the pace of urbanization.

4. Conclusions

The PSO-BP algorithm, integrated with multi-source data including remote sensing, population, and economy, was employed in this study to construct a multi-scale and multi-level spatial database of carbon emissions in this urban agglomeration. This enabled the transformation of carbon emission spatial distributions from administrative boundaries to kilometer grids and facilitated the accurate implementation of the "dual carbon" target. Trend analysis and exploratory spatial data analysis (ESDA) were utilized to systematically examine the spatiotemporal characteristics of carbon emissions at the city and county levels from 2000 to 2019. The spatiotemporal dynamics of carbon emissions in this urban agglomeration were analyzed at the city, district, and county levels. Furthermore, a comprehensive framework for analyzing multiple influencing factors such as urbanization, economic growth, land use, household consumption, foreign trade, fixed asset investment, and government expenditure was established to promote understanding of the county-level driving mechanisms behind carbon emissions.

Carbon emissions in this region exhibit distinct spatial patterns, characterized by high–high and low–low concentrations. Carbon emissions were predominantly concentrated in the counties surrounding the Pearl River Estuary, with significantly higher emission levels observed in counties on the eastern bank of the Pearl River compared to those on the western bank. Overall, there was a partial reduction in spatial disparities regarding carbon emissions.

In 2010, 2015, and 2019, construction land consistently emerged as the most influential factor, with its explanatory power progressively increasing over time. The explanatory power of other factors varied with their changing dynamics. The interaction effect significantly amplified the effect of various factors on the spatial differentiation of county level carbon emissions, particularly enhancing the impact of low-explanatory-power single factors.

With the continuous economic and social development of the Pearl River Delta urban agglomeration, construction land expansion significantly influences the county-level carbon emissions of this region. Moreover, the escalating demand for land to accommodate high-carbon projects will inevitably result in substantial carbon emissions. Therefore, local governments should rigorously regulate land requirements for high-carbon projects such as thermal power plants and refining and chemical plants while concurrently enhancing spatial utilization efficiency for industrial land and energy infrastructure with high carbon footprints. Additionally, local governments should bolster investments in clean energy

initiatives and advancements in energy-saving and emission-reduction technologies. This includes improving the energy efficiency of transportation systems, buildings, water supply networks, and power supply facilities to curtail both energy consumption levels and associated carbon emissions.

5. Discussion

In this research, a spatial simulation of carbon emissions based on multi-source data was conducted with the support of PSO-BP. The focus of this study was to investigate the spatiotemporal dynamics and driving mechanisms of carbon emissions in this urban agglomeration at both district and county levels. The aim was to provide a decision-making basis and reference for the low-carbon development path not only for this urban agglomeration but also for other urban agglomerations. However, this research still has following shortcomings:

(1) The spatial simulation of carbon emissions primarily relies on a top-down approach. Despite the coupling of high-precision population and economic spatial data, there is still room for further improvement in the spatial accuracy of carbon emissions data. In future studies, it is recommended to consider incorporating a combination of bottom-up and top-down approaches to enhance the integration of multi-source POI data, big data from industrial enterprises, high-precision land use data, etc., thereby enhancing the accuracy of spatial simulations for carbon emissions.

(2) Energy consumption, energy structure, and other factors directly impact carbon emissions. However, obtaining data on energy consumption is challenging due to the varying statistical caliber at the city, district, and county levels. To enhance the accuracy of statistical accounting for carbon emissions in future research, it is recommended to conduct field surveys on energy consumption data at the district and county levels, as well as the enterprise and household levels.

(3) The driving mechanisms of carbon emissions identified in this study primarily focused on the internal influencing factors of urban agglomerations. With the implementation of the new dual-cycle development pattern, there is increased connectivity between the internal and external aspects of urban agglomerations. Therefore, it is essential to enhance research on the impact of external influencing factors on local carbon emissions in urban agglomerations.

Institutional Review Board Statement: Not applicable.

Informed Consent Statement: Not applicable.

Data Availability Statement: The authors have not obtained permission to publish the data. Therefore, the data can be obtained from the corresponding author upon reasonable request.

Conflicts of Interest: The authors declare no conflicts of interest.

References

1. McNutt, M. Time's up, CO$_2$. *Science* **2019**, *365*, 411. [CrossRef] [PubMed]
2. Bulkeley, H. Governing climate change: The politics of risk society? *Trans. Inst. Br. Geogr.* **2001**, *26*, 430–447. [CrossRef]
3. Adger, W.N. Social Capital, Collective Action, and Adaptation to Climate Change. *Econ. Geogr.* **2003**, *79*, 387–404. [CrossRef]
4. Thomas, C.D.; Cameron, A.; Green, R.E.; Bakkenes, M.; Beaumont, L.J.; Collingham, Y.C.; Erasmus, B.F.N.; de Siqueira, M.F.; Grainger, A.; Hannah, L.; et al. Extinction risk from climate change. *Nature* **2004**, *427*, 145–148. [CrossRef] [PubMed]
5. Nordhaus, W.D. A Review of the Stern Review on the Economics of Climate Change. *J. Econ. Lit.* **2007**, *45*, 686–702. [CrossRef]
6. Meinshausen, M.; Lewis, J.; McGlade, C.; Gütschow, J.; Nicholls, Z.; Burdon, R.; Cozzi, L.; Hackmann, B. Realization of Paris Agreement pledges may limit warming just below 2 °C. *Nature* **2022**, *604*, 304–309. [CrossRef]
7. Roelfsema, M.; van Soest, H.L.; Harmsen, M.; van Vuuren, D.P.; Bertram, C.; den Elzen, M.; Höhne, N.; Iacobuta, G.; Krey, V.; Kriegler, E.; et al. Taking stock of national climate policies to evaluate implementation of the Paris Agreement. *Nat. Commun.* **2020**, *11*, 2096. [CrossRef]
8. Schneider, L.; Duan, M.; Stavins, R.; Kizzier, K.; Broekhoff, D.; Jotzo, F.; Winkler, H.; Lazarus, M.; Howard, A.; Hood, C. Double counting and the Paris Agreement rulebook. *Science* **2019**, *366*, 180–183. [CrossRef]
9. Rogelj, J.; Huppmann, D.; Krey, V.; Riahi, K.; Clarke, L.; Gidden, M.; Nicholls, Z.; Meinshausen, M. A new scenario logic for the Paris Agreement long-term temperature goal. *Nature* **2019**, *573*, 357–363. [CrossRef]
10. Tanaka, K.; O'Neill, B.C. The Paris Agreement zero-emissions goal is not always consistent with the 1.5 °C and 2 °C temperature targets. *Nat. Clim. Chang.* **2018**, *8*, 319–324. [CrossRef]
11. Acuto, M.; Parnell, S.; Seto, K.C. Building a global urban science. *Nat. Sustain.* **2018**, *1*, 2–4. [CrossRef]
12. Dhakal, S. Urban energy use and carbon emissions from cities in China and policy implications. *Energy Policy* **2009**, *37*, 4208–4219. [CrossRef]
13. Li, Z.; Wang, F.; Kang, T.; Wang, C.; Chen, X.; Miao, Z.; Zhang, L.; Ye, Y.; Zhang, H. Exploring differentiated impacts of socioeconomic factors and urban forms on city-level CO$_2$ emissions in China: Spatial heterogeneity and varying importance levels. *Sustain. Cities Soc.* **2022**, *84*, 104028. [CrossRef]
14. Streets, D.G.; Jiang, K.; Hu, X.; Sinton, J.E.; Zhang, X.-Q.; Xu, D.; Jacobson, M.Z.; Hansen, J.E. Recent Reductions in China's Greenhouse Gas Emissions. *Science* **2001**, *294*, 1835–1837. [CrossRef]
15. Chen, Y.; Wang, J.; Xu, L.; Ye, S. Spatio-temporal Variations and Influencing Factors of Energy Efficiency in Fujian Province. *J. Fujian Norm. Univ. Nat. Sci. Ed.* **2024**, *40*, 20–29.
16. Zhang, Q.; Lin, J.; Wang, Q.; Chen, D.; Zhou, T.; Dang, N.; Zhuang, X.; Li, Y.; Luo, D. The Impact of Main Functional Area Strategy on Regional Energy Consumption Carbon Emission: A Case Study of Fujian Province. *J. Fujian Norm. Univ. Nat. Sci. Ed.* **2024**, *40*, 30–43.
17. Qi, X.; Huang, R.; Jia, Y.; Huang, Q. Analysis of Spatial and Temporal Characteristics and Driving Factors of Carbon Emissions at the County Level in Coal Resource-Based Areas:Take Shanxi Province as an Example. *J. North China Inst. Water Conserv. Hydroelectr. Power Soc. Sci. Ed.* **2024**, *40*, 1–11. [CrossRef]
18. Elvidge, C.D.; Baugh, K.E.; Kihn, E.A.; Kroehl, H.W.; Davis, E.R.; Davis, C.W. Relation between satellite observed visible-near infrared emissions, population, economic activity and electric power consumption. *Int. J. Remote Sens.* **1997**, *18*, 1373–1379. [CrossRef]
19. Doll, C.N.H.; Muller, J.P.; Elvidge, C.D. Night-time imagery as a tool for global mapping of socioeconomic parameters and greenhouse gas emissions. *Ambio* **2000**, *29*, 157–162. [CrossRef]
20. Ghosh, T.; Elvidge, C.D.; Sutton, P.C.; Baugh, K.E.; Ziskin, D.; Tuttle, B.T. Creating a global grid of distributed fossil fuel CO$_2$ emissions from nighttime satellite imagery. *Energies* **2010**, *3*, 1895–1913. [CrossRef]
21. Oda, T.; Maksyutov, S. A very high-resolution (1 km × 1 km) global fossil fuel CO$_2$ emission inventory derived using a point source database and satellite observations of nighttime lights. *Atmos. Chem. Phys.* **2011**, *11*, 543–556. [CrossRef]
22. Su, Y.; Chen, X.; Li, Y.; Liao, J.; Ye, Y.; Zhang, H.; Huang, N.; Kuang, Y. China's 19-year city-level carbon emissions of energy consumptions, driving forces and regionalized mitigation guidelines. *Renew. Sustain. Energy Rev.* **2014**, *35*, 231–243. [CrossRef]
23. Shi, K.; Yu, B.; Huang, Y.; Hu, Y.; Yin, B.; Chen, Z.; Chen, L.; Wu, J. Evaluating the Ability of NPP-VIIRS Nighttime Light Data to Estimate the Gross Domestic Product and the Electric Power Consumption of China at Multiple Scales: A Comparison with DMSP-OLS Data. *Remote Sens.* **2014**, *6*, 1705–1724. [CrossRef]
24. Zhang, L.; Lei, J.; Wang, C.; Wang, F.; Geng, Z.; Zhou, X. Spatio-temporal variations and influencing factors of energy-related carbon emissions for Xinjiang cities in China based on time-series nighttime light data. *J. Geogr. Sci.* **2022**, *32*, 1886–1910. [CrossRef]
25. Chen, J.; Gao, M.; Cheng, S.; Hou, W.; Song, M.; Liu, X.; Liu, Y.; Shan, Y. County-level CO$_2$ emissions and sequestration in China during 1997–2017. *Sci. Data* **2020**, *7*, 391. [CrossRef]
26. Chen, J.; Gao, M.; Cheng, S.; Liu, X.; Hou, W.; Song, M.; Li, D.; Fan, W. China's city-level carbon emissions during 1992–2017 based on the inter-calibration of nighttime light data. *Sci. Rep.* **2021**, *11*, 3323. [CrossRef]
27. Zhu, N.; Li, X.; Yang, S.; Ding, Y.; Zeng, G. Spatio-temporal dynamics and influencing factors of carbon emissions (1997–2019) at county level in mainland China based on DMSP-OLS and NPP-VIIRS Nighttime Light Datasets. *Heliyon* **2024**, *10*, e37245. [CrossRef]

28. Xiang, C.; Mei, Y.; Liang, A. Analysis of Spatiotemporal Changes in Energy Consumption Carbon Emissions at District and County Levels Based on Nighttime Light Data—A Case Study of Jiangsu Province in China. *Remote Sens.* **2024**, *16*, 3514. [CrossRef]

29. Jiang, L.; Yang, L.; Wu, Q.; Zhang, X. How does extreme heat affect carbon emission intensity? Evidence from county-level data in China. *Econ. Model.* **2024**, *139*, 106814. [CrossRef]

30. Xie, Z.; Wang, L.; Zhao, R.; Xiao, L.; Ding, M.; Yao, S.; Chuai, X.; Rong, P. County-level carbon budget and carbon compensation in the Yellow River Basin: A perspective with balancing efficiency and equity. *Environ. Dev. Sustain.* **2024**. [CrossRef]

31. Zhou, C.; Wang, S. Examining the determinants and the spatial nexus of city-level CO_2 emissions in China: A dynamic spatial panel analysis of China's cities. *J. Clean. Prod.* **2018**, *171*, 917–926. [CrossRef]

32. Ke, N.; Lu, X.; Kuang, B.; Zhang, X. Regional disparities and evolution trend of city-level carbon emission intensity in China. *Sustain. Cities Soc.* **2023**, *88*, 104288. [CrossRef]

33. Cheng, Y.; Wang, Z.; Ye, X.; Wei, Y.D. Spatiotemporal dynamics of carbon intensity from energy consumption in China. *J. Geogr. Sci.* **2014**, *24*, 631–650. [CrossRef]

34. York, R.; Rosa, E.A.; Dietz, T. STIRPAT, IPAT and ImPACT: Analytic tools for unpacking the driving forces of environmental impacts. *Ecol. Econ.* **2003**, *46*, 351–365. [CrossRef]

35. Brizga, J.; Feng, K.; Hubacek, K. Drivers of CO_2 emissions in the former Soviet Union: A country level IPAT analysis from 1990 to 2010. *Energy* **2013**, *59*, 743–753. [CrossRef]

36. Wang, H.; Ang, B.W.; Su, B. Assessing drivers of economy-wide energy use and emissions: IDA versus SDA. *Energy Policy* **2017**, *107*, 585–599. [CrossRef]

37. Wang, C.; Wang, F.; Zhang, X.; Yang, Y.; Su, Y.; Ye, Y.; Zhang, H. Examining the driving factors of energy related carbon emissions using the extended STIRPAT model based on IPAT identity in Xinjiang. *Renew. Sustain. Energy Rev.* **2017**, *67*, 51–61. [CrossRef]

38. Wang, F.; Wang, C.; Chen, J.; Li, Z.; Li, L. Examining the determinants of energy-related carbon emissions in Central Asia: Country-level LMDI and EKC analysis during different phases. *Environ. Dev. Sustain.* **2020**, *22*, 7743–7769. [CrossRef]

39. Li, Z.; Chen, X.; Ye, Y.; Wang, F.; Liao, K.; Wang, C. The impact of digital economy on industrial carbon emission efficiency at the city level in China: Gravity movement trajectories and driving mechanisms. *Environ. Technol. Innov.* **2024**, *33*, 103511. [CrossRef]

40. Xu, L.; Du, H.; Zhang, X. Driving forces of carbon dioxide emissions in China's cities: An empirical analysis based on the geodetector method. *J. Clean. Prod.* **2021**, *287*, 125169. [CrossRef]

41. Liao, K.; Huang, W.; Wang, C.; Wu, R.; Hu, Y. Spatio-Temporal Evolution Features and Impact Factors of Urban Expansion in Underdeveloped Cities: A Case Study of Nanchang, China. *Land* **2022**, *11*, 1799. [CrossRef]

42. Su, Y.; Wu, J.; Ciais, P.; Zheng, B.; Wang, Y.; Chen, X.; Li, X.; Li, Y.; Wang, Y.; Wang, C.; et al. Differential impacts of urbanization characteristics on city-level carbon emissions from passenger transport on road: Evidence from 360 cities in China. *Build. Environ.* **2022**, *219*, 109165. [CrossRef]

43. Liu, S.; Shen, J.; Liu, G.; Wu, Y.; Shi, K. Exploring the effect of urban spatial development pattern on carbon dioxide emissions in China: A socioeconomic density distribution approach based on remotely sensed nighttime light data. *Comput. Environ. Urban Syst.* **2022**, *96*, 101847. [CrossRef]

44. Wang, S.; Liu, X.; Zhou, C.; Hu, J.; Ou, J. Examining the impacts of socioeconomic factors, urban form, and transportation networks on CO_2 emissions in China's megacities. *Appl. Energy* **2017**, *185*, 189–200. [CrossRef]

45. Shi, K.; Xu, T.; Li, Y.; Chen, Z.; Gong, W.; Wu, J.; Yu, B. Effects of urban forms on CO_2 emissions in China from a multi-perspective analysis. *J. Environ. Manag.* **2020**, *262*, 110300. [CrossRef]

46. Li, Y.; Lv, C.; Yang, N.; Liu, H.; Liu, Z. A study of high temporal-spatial resolution greenhouse gas emissions inventory for on-road vehicles based on traffic speed-flow model: A case of Beijing. *J. Clean. Prod.* **2020**, *277*, 122419. [CrossRef]

47. Duan, C.; Zhu, W.; Wang, S.; Chen, B. Drivers of global carbon emissions 1990–2014. *J. Clean. Prod.* **2022**, *371*, 133371. [CrossRef]

48. Khan, M.K.; Teng, J.-Z.; Khan, M.I.; Khan, M.O. Impact of globalization, economic factors and energy consumption on CO_2 emissions in Pakistan. *Sci Total Environ.* **2019**, *688*, 424–436. [CrossRef]

49. Zhang, Y.; Zhang, S. The impacts of GDP, trade structure, exchange rate and FDI inflows on China's carbon emissions. *Energy Policy* **2018**, *120*, 347–353. [CrossRef]

50. Lin, H.; Wang, X.; Bao, G.; Xiao, H. Heterogeneous Spatial Effects of FDI on CO_2 Emissions in China. *Earths Future* **2022**, *10*, e2021EF002331. [CrossRef]

51. Hertwich, E.G. Increased carbon footprint of materials production driven by rise in investments. *Nat. Geosci.* **2021**, *14*, 151–155. [CrossRef]

52. Zhao, X.; Zhang, X.; Shao, S. Decoupling CO_2 emissions and industrial growth in China over 1993–2013: The role of investment. *Energy Econ.* **2016**, *60*, 275–292. [CrossRef]

53. Cheng, S.; Chen, Y.; Meng, F.; Chen, J.; Liu, G.; Song, M. Impacts of local public expenditure on CO_2 emissions in Chinese cities: A spatial cluster decomposition analysis. *Resour. Conserv. Recycl.* **2021**, *164*, 105217. [CrossRef]

54. Xu, C.; Xu, Y.; Chen, J.; Huang, S.; Zhou, B.; Song, M. Spatio-temporal efficiency of fiscal environmental expenditure in reducing CO_2 emissions in China's cities. *J. Environ. Manag.* **2023**, *334*, 117479. [CrossRef]

55. Wang, Q. Effects of urbanisation on energy consumption in China. *Energy Policy* **2014**, *65*, 332–339. [CrossRef]

56. Wu, S.; Lei, Y.; Li, S. CO_2 emissions from household consumption at the provincial level and interprovincial transfer in China. *J. Clean. Prod.* **2019**, *210*, 93–104. [CrossRef]

57. Zhang, Z.; Zhao, Y.; Su, B.; Zhang, Y.; Wang, S.; Liu, Y.; Li, H. Embodied carbon in China's foreign trade: An online SCI-E and SSCI based literature review. *Renew. Sustain. Energy Rev.* **2017**, *68*, 492–510. [CrossRef]

58. Zhang, X.; Zhao, Y. Identification of the driving factors' influences on regional energy-related carbon emissions in China based on geographical detector method. *Environ. Sci. Pollut. Res.* **2018**, *25*, 9626–9635. [CrossRef]

59. Su, Y.; Chen, X.; Wang, C.; Zhang, H.; Liao, J.; Ye, Y.; Wang, C. A new method for extracting built-up urban areas using DMSP-OLS nighttime stable lights: A case study in the Pearl River Delta, southern China. *GISci. Remote Sens.* **2015**, *52*, 218–238. [CrossRef]

60. Chen, J.; Liu, J.; Qi, J.; Gao, M.; Cheng, S.; Li, K.; Xu, C. City- and county-level spatio-temporal energy consumption and efficiency datasets for China from 1997 to 2017. *Sci. Data* **2022**, *9*, 101. [CrossRef]

61. Shan, Y.; Guan, Y.; Hang, Y.; Zheng, H.; Li, Y.; Guan, D.; Li, J.; Zhou, Y.; Li, L.; Hubacek, K. City-level emission peak and drivers in China. *Sci. Bull.* **2022**, *67*, 1910–1920. [CrossRef] [PubMed]

62. Zhang, L.; Ruan, J.; Zhang, Z.; Qin, Z.; Lei, Z.; Cai, B.; Wang, S.; Tang, L. City-level pathways to carbon peak and neutrality in China. *Cell Rep. Sustain.* **2024**, *1*, 100102. [CrossRef]

63. Cai, B.; Liang, S.; Zhou, J.; Wang, J.; Cao, L.; Qu, S.; Xu, M.; Yang, Z. China high resolution emission database (CHRED) with point emission sources, gridded emission data, and supplementary socioeconomic data. *Resour. Conserv. Recycl.* **2018**, *129*, 232–239. [CrossRef]

64. Zhou, Y.; Li, K.; Liang, S.; Zeng, X.; Cai, Y.; Meng, J.; Shan, Y.; Guan, D.; Yang, Z. Trends, Drivers, and Mitigation of CO_2 Emissions in the Guangdong–Hong Kong–Macao Greater Bay Area. *Engineering* **2023**, *23*, 138–148. [CrossRef]

65. Zhou, Y.; Shan, Y.; Liu, G.; Guan, D. Emissions and low-carbon development in Guangdong-Hong Kong-Macao Greater Bay Area cities and their surroundings. *Appl. Energy* **2018**, *228*, 1683–1692. [CrossRef]

66. Song, Y.; Ma, M.; Veroustraete, F. Comparison and conversion of AVHRR GIMMS and SPOT VEGETATION NDVI data in China. *Int. J. Remote Sens.* **2010**, *31*, 2377–2392. [CrossRef]

67. Anselin, L. Spatial Econometrics: Methods and Models. *J. Am. Stat. Assoc.* **1990**, *85*, 160.

68. Haining, R. Spatial data analysis in the social and environmental sciences. *Environ. Int.* **1991**, *17*, 618.

69. Liu, Q.; Wang, S.; Zhang, W.; Zhan, D.; Li, J. Does foreign direct investment affect environmental pollution in China's cities? A spatial econometric perspective. *Sci Total Environ.* **2018**, *613–614*, 521–529. [CrossRef]

70. Anselin, L. Local Indications of Spatial Association—LISA. *Geogr. Anal.* **1995**, *27*, 93–115. [CrossRef]

71. Wang, J.-F.; Zhang, T.-L.; Fu, B.-J. A measure of spatial stratified heterogeneity. *Ecol. Indic.* **2016**, *67*, 250–256. [CrossRef]

72. Wang, J.F.; Li, X.H.; Christakos, G.; Liao, Y.L.; Zhang, T.; Gu, X.; Zheng, X.Y. Geographical Detectors-Based Health Risk Assessment and its Application in the Neural Tube Defects Study of the Heshun Region, China. *Int. J. Geogr. Inf. Sci.* **2010**, *24*, 107–127. [CrossRef]

Synergistic Enhancement of Carbon Sinks and Connectivity: Restoration and Renewal of Ecological Networks in Nanjing, China

Renfei Zhang, Hongye Li and Zhicheng Liu *

School of Landscape Architecture, Beijing Forestry University, Beijing 100083, China;
renfei_zhang@bjfu.edu.cn (R.Z.); lihongye_la@163.com (H.L.)
* Correspondence: zhicheng_liu@bjfu.edu.cn

Abstract: Urbanization has led to a reduction in green space, weakening the region's carbon sink capacity and stability and bringing a series of ecological problems, making the restoration and improvement of the ecological environment crucial. This study used Nanjing, China, as a case to construct an ecological network by applying Morphological Spatial Pattern Analysis (MSPA) and the Linkage Mapper (LM) tool based on circuit theory. The connectivity of ecological patches was evaluated by calculating the delta potential connectivity index (dPC). The CASA model (Carnegie–Ames–Stanford approach) was applied to quantify carbon sequestration in Nanjing. We propose an innovative carbon sink index (CSI) that integrates three indicators: capacity, efficiency, and variability. This index assesses the carbon sink function of ecological patches from both static and dynamic perspectives. Using the Future Land Use Simulation (FLUS) model, we simulated carbon sequestration changes in 2035, providing insights for risk assessment and future optimization strategies. The results reveal a significant positive correlation between node connectivity and both carbon sink capacity and efficiency, indicating that enhancing connectivity at key nodes can effectively improve its carbon sequestration. On this basis, by coupling dPC and CSI indices to classify ecological network nodes, we proposed four strategies for optimization: ecological conservation, structural connectivity, carbon sink improvement, and synergistic enhancement. Finally, by adding 26 ecological stepping stones, 32 ecological corridors, and optimizing landscape components, we achieved dual improvements in both the structural and functional aspects of the ecological network. After optimization, the network connectivity increased by 1.6% and the carbon sink increased by 3.82%, demonstrating a significant improvement. This study emphasizes that by protecting, enhancing, and restoring ecological spaces, the carbon sequestration function and stability of urban ecological networks can be effectively improved. These findings provide valuable insights for the scientific management of ecological spaces in urbanized areas.

Keywords: carbon sink index; landscape connectivity; ecological network optimization; multi scenario simulation; urban planning

1. Introduction

As urbanization continues to accelerate globally, cities are confronting unprecedented climate and ecological challenges [1]. The ongoing expansion of urban land often encroaches on natural ecosystems, leading to habitat fragmentation [2,3], biodiversity loss [4], and the decline of ecosystem services and stability [5]. These changes reduce the carbon sequestration potential of green spaces and limit the effectiveness of regional ecological

networks as carbon sinks [6,7]. With China's commitment to sustainable development and carbon neutrality goals [8], there is a pressing need to restore and improve the ecological environment. Optimizing urban ecological structures and promoting sustainable urban development are therefore central areas of current research.

Ecological network construction has become a crucial conservation strategy, playing an essential role in ecological environment restoration. The core principle is to maintain connectivity between isolated and fragmented ecological sources and corridors, ensuring the continuous provision of ecological services and carbon sink functions [9,10]. Researchers generally follow a process of "source identification, resistance surface construction, and corridor extraction" in ecological network construction [11–13]. Ecological sources, often patches with complete landscape structures and strong ecological functions, are identified using methods like MSPA [14], which precisely locates areas vital for landscape connectivity [15]. The minimum cumulative resistance model is commonly used to determine ecological corridors [16], identifying optimal pathways for biological movement. However, it falls short in defining the spatial extent and key nodes of these corridors. To address this, circuit theory, drawn from physics, has been applied in ecological networks [17]. By simulating biological movement as electrical current, circuit theory helps identify critical locations and sets corridor width thresholds based on the intensity and frequency of the current, providing a more accurate picture of ecological connectivity [18–20].

Many studies highlight the significance of ecological networks in enhancing the carbon sequestration potential of green spaces [21–23]. These networks provide a critical spatial foundation for the material and energy cycles within urban areas, supporting ecological processes that are integral to low-carbon development and carbon balance [24]. From a network perspective, quantifying the spatiotemporal changes in carbon sequestration due to land-use changes, ecological networks offer valuable insights into how carbon sinks and sources can be balanced to promote sustainable urban growth [25]. Research has demonstrated that modifications in green space network structure can enhance carbon sequestration by enhancing ecosystem resilience, energy flow, and overall functionality [26–28]. Vegetation, which plays a central role in carbon sequestration, is influenced by various environmental factors [29,30]. Healthy ecosystems promote a positive circulation of materials and energy [31–33], and in degraded urban ecosystems, the construction of ecological corridors and stepping stones can enhance plant growth conditions, boosting their carbon absorption potential [34,35]. Therefore, restoring and renewing urban ecological networks is essential for repairing damaged local ecosystems and serves as a strategic approach to large-scale landscape restoration, which is critical for achieving carbon balance [36].

Despite growing interest, research that links carbon sinks with ecological networks remains in the early stages. Most existing studies focus on modeling specific years of ecological space networks, with little attention given to the interactions between ecology and carbon sequestration at the urban scale [37]. Additionally, research on carbon storage at the spatial level tends to focus on land use variability, neglecting the enhancement of individual patch quality [38]. Moreover, there is a lack of scientific frameworks for quantitatively evaluating the structural and functional interactions of ecological networks [39,40]. The existing research often relies on single aggregate indicators to measure carbon sequestration in green spaces, overlooking the complexity and dynamic nature of ecosystems [41]. To clarify the role of urban green spaces in the carbon cycle and guide future urban development, there is an urgent need for a framework that integrates the structural characteristics of green spaces with carbon sequestration potential while promoting network optimization.

Building on previous research and addressing knowledge gaps, this study aims to accomplish the following: (1) establish an ecological network optimization framework that couples green space structure with carbon sink function, considering their dynamic

complexities; (2) use Nanjing as a case study to analyze the connectivity of ecological nodes and the spatiotemporal variation in carbon sinks; and (3) link landscape patch connectivity with carbon sequestration to identify strong and weak ecological nodes and propose targeted optimization strategies. By quantitatively evaluating the effects of these strategies on carbon sequestration and network connectivity, this study aims to enhance the carbon sink potential of urban ecological spaces, improve local environmental quality, and provide valuable insights for sustainable urban development planning.

2. Materials and Methods

2.1. Study Area

Nanjing, a pivotal city within China's Yangtze River Delta urban cluster, is located in the southwestern part of Jiangsu Province. As the capital of Jiangsu Province, it spans an area of 6587.02 km^2, covering 11 municipal districts. The city's geographic coordinates range from 31°14″ to 32°37″ north latitude and 118°22″ to 119°14″ east longitude (Figure 1). By the end of 2023, Nanjing's permanent population reached 9.55 million, with a GDP of 1.74 trillion CNY, ranking second in Jiangsu Province and third within the Yangtze River Delta region. The subtropical warm climate provides ample sunshine throughout the year, with an average annual temperature of 15.4 °C and annual precipitation of 1100 mm. Nanjing's landscape is dominated by plain valleys and low altitude hills, with an average elevation of 28 m and a maximum elevation of 418 m. Nanjing is rich in natural resources, with 31% forest coverage and 11.4% water resources, providing abundant carbon sink potential.
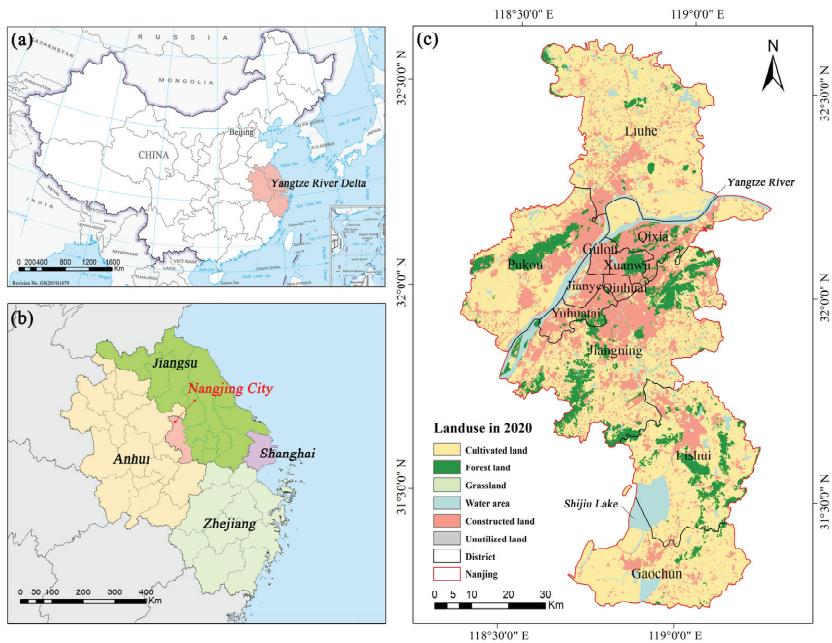
Figure 1. Geographic location analysis of Nanjing, China. (**a**) Geographic location of Yangtze River Delta in China; (**b**) Geographic location of Nanjing in the Yangtze River Delta; (**c**) Land use of Nanjing in 2020.

The Nanjing municipal government attaches great importance to the construction of low-carbon cities, prioritizing ecological restoration and enhancing carbon sink functions. However, rapid urbanization has led to the loss of ecological spaces, a decline in biodiversity,

the degradation of water and soil quality [42], atmospheric pollution, and heat island effects, posing serious challenges to the carbon sink function of ecosystems [43]. Since 2013, Nanjing has implemented various ecological restoration efforts, including the development of greenways, green space planning, and greening projects along the Yangtze River. However, the overall trend of ecosystem degradation has not been fundamentally reversed [44,45]. In light of these challenges, it is necessary to quantitatively evaluate the carbon sink of green spaces from a systematic and multidimensional perspective and propose targeted optimization strategies to address ecological issues in the process of urbanization.

2.2. Data Sources and Processing

This study primarily used multiple datasets from three periods in 2000, 2010, and 2020, as shown in Table 1. According to the classification formulated by the Chinese Academy of Sciences, the land-use data were reclassified into six types: cultivated land, forest land, grassland, water area, construction land, and unutilized land. The climate and environment data include elevation, slope, temperature, precipitation, and solar radiation. Utilizing the Google Earth Engine platform and remote sensing images, the NDVI index was calculated. Socioeconomic data include population, GDP, roads, and transportation stations. All data were uniformly processed using the WGS_1984_UTM_Zone_51N projection coordinate system, with a spatial resolution of 30 m × 30 m.

Table 1. List of research data and sources.

Data	Subdata	Year (s)	Accuracy/(m)	Sources
Land use	LUCC	2000, 2005, 2010, 2020	30	GlobeLand30 (https://zenodo.org/records/12779975, accessed on 1 May 2024)
Remote sensing	Landsat5	2000, 2010	30	GSCloud (http://www.gscloud.cn/, accessed on 1 May 2024)
	Landsat8	2020	30	
Climate and environmental	DEM	2020	30	GSCloud
	Slope	2020	30	Calculated by DEM
	NDVI	2000, 2010, 2020	30	calculated by Landsat
	Temperature and Precipitation	2000, 2010, 2020	1000	CMA (https://data.cma.cn/, accessed on 1 May 2024)
	Solar radiation	2000, 2010, 2020	1000	TerraClimate (https://www.climatologylab.org/, accessed on 1 May 2024)
Socioeconomic	Population density and GDP	2020	1000	CAS (https://www.resdc.cn/, accessed on 1 May 2024)
	Stations and Road network	2020	30	OSM (https://www.openstreetmap.org/, accessed on 1 May 2024)
Planning	Land-use demand	2035	-	Nanjing Territorial Spatial Master Plan (2021–2035)
	Ecological protection red line	2035	-	Territorial Spatial Planning of Jiangsu Province (2021–2035)

2.3. Study Design

This study was conducted in four phases (Figure 2). The first phase involved the construction and connectivity evaluation of the ecological network (See Section 2.3.1 for details). MSPA was used to screen ecological sources, and the Linkage Mapper (LM) tool of circuit theory was used to construct ecological networks. On this basis, we quantitatively

evaluated its structural connectivity. The second phase focused on the measurement and indicator construction of the carbon sink (See Section 2.3.2 for details). The CASA model was used to calculate the carbon sinks, supplemented by empirical values to calculate water carbon sinks. A carbon sink index was proposed to be constructed based on static and dynamic dimensions. The third phase was land-use simulation (See Section 2.3.3 for details). The FLUS model was applied to predict carbon sink changes over the next 15 years under the inertia development and master plan scenarios in 2035 to assess the carbon sink variation for 2020 and to provide a foundation for optimizing the network. The fourth phase focused on the optimization framework for the ecological network (See Section 2.3.4 for details). With the goal of enhancing both the carbon sink function and structural connectivity, the study identified the optimal and worst ecological nodes and proposed optimization strategies. By combining the current situation, planning requirements, and future development scenarios of Nanjing, an implementation path to enhance the city's ecological resilience and carbon sink function was proposed.
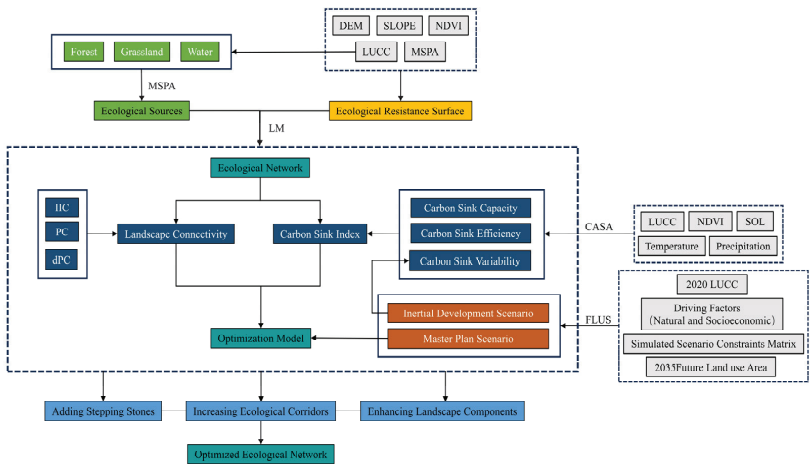
Figure 2. Framework diagram of ecological network optimization research in Nanjing city.

2.3.1. Construction and Connectivity Evaluation of Ecological Network

MSPA is a method based on morphological algorithms used to identify key patches in ecosystems. It classifies pixels into seven landscape types: core, islet, perforation, edge, bridge, loop, and branch, aiming to improve the scientific identification of ecological patches and corridors from the perspective of spatial connectivity [46]. In this study, we used the Guidos Toolbox 3.3 software to analyze land-use data from 2000, 2010, and 2020. Forests, grasslands, and water areas were treated as foreground, and cultivated lands, construction lands, and unutilized lands were considered background. An 8-neighborhood analysis method was adopted to extract core areas larger than 1 km^2 as ecological sources. The interactions between ecological sources are influenced by landscape surface resistance, which is determined by both natural factors and human disturbances [47,48]. To accurately describe the distribution of resistance, this study integrated five key factors: MSPA classification, land-use type, NDVI index, slope, and elevation. The Delphi method was used to scientifically determine the weight of each factor (Table A1), and the fuzzy affiliation tool was used for data normalization. The cumulative resistance surface was generated using the raster calculator in ArcGIS 10.6. Finally, the ecological sources and cumulative resistance surface were input into the LM model [49,50]. This model identifies the least-cost

paths between ecological sources, effectively integrating fragmented ecological patches and forming a cohesive ecological network [51].

Geographically adjacent ecological sources have stronger resistance to disturbances due to their modularity and proximity [52]. As a core indicator for measuring the degree of connectivity between ecosystem patches, landscape connectivity is crucial for assessing ecosystem stability and functional integrity [53–55]. After the successful construction of an ecological network, this study analyzed the characteristics of landscape connectivity using patches as the basic unit. The integral index of connectivity (IIC) and potential connectivity (PC) of the patches were calculated using the Conefor 2.6 platform, and the relative change rate of the potential connectivity (dPC) after each patch disappeared was measured to assess the criticality of each patch in the ecological network structure. The calculation formulas are as follows.

$$IIC = \frac{1}{A_L^2} \sum_{i=1}^{n} \sum_{j=1}^{n} \frac{a_i a_j}{1 + nl_{ij}} \tag{1}$$

$$PC = \frac{1}{A_L^2} \sum_{i=1}^{n} \sum_{j=1}^{n} a_i a_j P_{ij}^* \tag{2}$$

$$dPC = \frac{(PC - PC_{remove})}{PC} \times 100\% \tag{3}$$

where n is the total number of patches; a_i and a_j are the areas of landscape patches i and j; nl_{ij} refers to the number of shortest path connections between patches i and j; P_{ij}^* is the maximum value of the path probability product between patches i and j; A_L is the area of the study area; PC_{remove} is the index of potential connectivity after removing a certain type of landscape element. *IIC* and *PC* values range from 0 to 1, with lower values indicating lower landscape connectivity. The higher the *dPC* value, the more important the patch is for landscape connectivity.

2.3.2. Measurement and Index Construction of Carbon Sink

The CASA model is a solar energy utilization model based on land cover, vegetation classification, and climatic data, which describes the temporal variation of carbon fluxes within terrestrial ecosystems [56,57]. This model calculates the net primary production (NPP) of vegetation based on photosynthetically active radiation and actual light energy utilization efficiency. NPP represents the plants' own carbon sequestration capacity and provides a basis for estimating the carbon sink of ecosystems [58]. The CASA model considers the effects of spatiotemporal heterogeneity and environmental stress on photosynthesis, and compared to the InVEST model, it is more accurate in estimating carbon storage in urban green spaces [59]. This study mainly refers to the CASA model improved by Zhu [60], and its calculation formulas are as follows.

$$NPP(x,t) = APAR(x,t) \times \varepsilon(x,t) \tag{4}$$

$$APAR(x,t) = SOL(x,t) \times FPAR(x,t) \times 0.5 \tag{5}$$

where *APAR* represents the photosynthetically active radiation (MJ·m^{-2}), ε is the actual light energy utilization (gC·MJ^{-1}). *SOL* is the total solar radiation photosynthetically active radiation (MJ·m^{-2}), *FPAR* is the proportion of photosynthetically active radiation absorbed by vegetation, and 0.5 is the proportion of solar active radiation available to vegetation. (*x,t*) denotes the *x* image element at time *t*. *SOL* and *FPAR* were calculated based on remote sensing and meteorological data. Referring to the existing local studies and the research results of Zhu Wenquan's CASA model [60], the light energy utilization rate of cultivated land was taken as 0.542 g·MJ^{-1}, forest land was taken as 0.985 g·MJ^{-1}, grassland was taken

as 0.608 g·MJ^{-1}, water area was taken as 0, and construction and unused land was adopted as a uniform value of 0.389 g·MJ^{-1}.

Watershed carbon sequestration is a small proportion of total carbon fluxes and involves ecological processes that differ only at larger spatial scales. Therefore, in this study, watershed carbon sequestration was measured by the empirical coefficients method used by previous authors for sediment rates in river and lake systems [61–64] (Table 2).

Table 2. Carbon sink rate of wetlands in the Yangtze River Delta region.

Wetland Types	Carbon Sink Rate (tCO$_2$·km^{-2}·a^{-1})
Lake	199.31
Riverine	277.31
Everglade	498.36

Carbon sink is a vital component of the ecological functions of green spaces, and its effectiveness is complex and multifaceted. In planning research, it is crucial to adopt a multi-dimensional quantitative analysis approach to build a comprehensive and diverse evaluation system. This allows for an accurate assessment of the challenges that green spaces face in carbon sequestration during urban development, providing a foundation for targeted optimization. This study innovatively proposed the carbon sink index (CSI), which integrates both static and dynamic dimensions. Static indicators reflect the strength of carbon sequestration capacity, while dynamic indicators capture the extent of change influenced by internal and external factors. The construction of CSI comprehensively covered the three core characteristics of carbon sink capacity, efficiency, and variability in green spaces.

The carbon sink capacity index (CSCI) is a key metric for evaluating the carbon sequestration potential of urban green spaces. Its variations are primarily influenced by the spatial layout and components of green spaces [65,66], allowing for the precise quantification of how each patch contributes to the overall carbon sink. The carbon sink efficiency index (CSEI) measures the effectiveness of urban green spaces in converting input resources into carbon sequestration. Referring to the concept of forest carbon sink efficiency [67], this metric quantifies the amount of carbon sequestered per unit area, revealing insights into the landscape composition, community structure complexity, and ecological quality of the green space [66]. In addition, the carbon sink variability index (CSVI) tracks changes in carbon sequestration from 2020 to 2035 under an inertia development scenario. By capturing fluctuations in carbon sink performance, the CSVI serves as an early warning system, supporting future carbon sink management strategies and decision-making.

2.3.3. Scenario Simulations of Land Use

Since the 1990s, spatial simulation models have been increasingly applied in the study of landscape patterns and ecological processes [68]. Among these, the FLUS model is widely adopted due to its high accuracy, bidirectional logic, and strong scenario-based guidance. This model integrates neural networks and cellular automaton with adaptive inertia mechanism [69,70]. Firstly, the model calculates the suitability probabilities for land use based on user-input driving factors using an artificial neural network (ANN) algorithm. Secondly, the FLUS model optimizes the traditional cellular automata model, improving the accuracy of land-use predictions under the influence of multiple factors [71]. In this study, we selected 10 natural and social driving factors, including elevation, slope, population density, GDP, distance to urban centers, distance to major, secondary, and tertiary roads, and distance to airports and train stations. These data sources are detailed in Table 1.

This simulation established two contrasting scenarios: the inertia development scenario and the master plan scenario. In the inertia development scenario, urban expansion continuously encroaches on surrounding green spaces, disrupting ecological corridors between nodes and weakening the overall functionality of the ecological network [72]. This scenario aims to highlight the feedback mechanisms of green spaces under severe challenges and provides a scientific basis for ecological risk warning [73]. In contrast, the master plan scenario focused on exploring the ecological potential space, based on Nanjing's land-use plan for 2035, proposing a sustainable development strategy [74]. The land-use demand for the inertia development scenario relied on the CA-Markov model [75], calculated with data from two periods in 2005 and 2020. The future land use and ecological protection red line were set according to the master plan.

A cost matrix (Table A2) is used to constrain land-use transitions. For land types that cannot be converted to other types, the corresponding value of the matrix is set to 0. If conversion is allowed, the value is set to 1. The model's accuracy is validated using the Kappa coefficient and FOM index. The Kappa value ranges from 0 to 1, with values greater than 0.75 indicating high simulation accuracy. When the Kappa value meets the required threshold, a higher FOM value suggests better simulation performance [76,77]. Finally, the simulated land use in 2035 is processed by the MSPA and LM models to construct the ecological network. The CSCI and CSVI values are then estimated for each scenario, providing a comprehensive evaluation of the ecological network's carbon sink potential.

2.3.4. Optimization Framework of the Ecological Network

To restore and enhance the ecological network, we examined the carbon sink capacity and connectivity of ecological sources. The CSI was used to measure the carbon sink function of these sources, while the dPC index assessed their structural connectivity. Based on these indices, we first examined the relationship between carbon sinks and connectivity, and then proposed a strategy to enhance both in synergy. During the coupling process of these two indices, we identified the top 20% of patches in terms of CSI and dPC as strong ecological nodes and the bottom 20% as weak ecological nodes. Optimization strategies were then developed based on the performance of patches in both indices, including ecological conservation, structural strengthening, carbon sink improvement, and synergistic enhancement (Figure 3). Finally, we compared the connectivity and carbon sink before and after the optimization of the ecological network to validate the effectiveness of the proposed strategies.
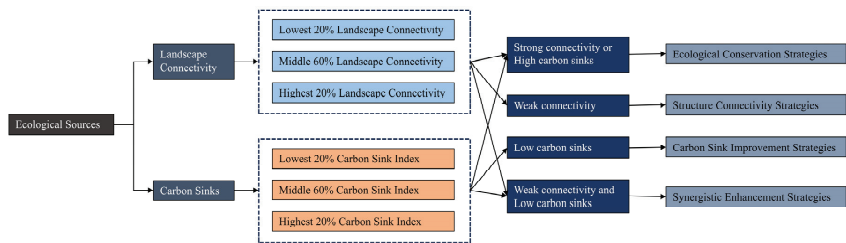
Figure 3. Optimization strategies for ecological networks in Nanjing.

3. Results

3.1. Construction and Analysis of Ecological Network in Nanjing City

3.1.1. Nanjing Ecological Spatial Network

The MSPA results show that the number of ecological sources identified in 2000, 2010, and 2020 were 88, 100, and 78, respectively, with corresponding areas of 966.08 km^2,

1053.50 km^2, and 877.51 km^2. Notably, the increase in the number of sources in 2010 was primarily due to the large-scale conversion of cultivated land to water areas in the southern part of the study area. With the help of ArcGIS platform, we weighed and overlaid five types of factors to generate comprehensive resistance distribution maps for Nanjing in 2000, 2010, and 2020. Based on the LM model, we generated ecological corridors, with 195 corridors in 2000, 208 in 2010, and 180 in 2020. Combined with the screened ecological sources, we constructed the ecological network for the study area (Figure 4). It was found that large-scale ecological sources in Nanjing are primarily distributed south of the Yangtze River, while the sources north of the river are smaller and scattered. The distribution of corridors aligns with the sources land pattern, being sparse in the north and denser in the south. The region to the west of the Yangtze River exhibits a more fragmented network structure, mainly due to the absence of large green spaces to serve as a structural framework. Over the past two decades, the overall number of sources and corridors in Nanjing initially increased but then declined, and the acceleration of urbanization has significantly affected the distribution pattern of ecological spaces.

Figure 4. Construction of the ecological network in Nanjing. (**a**) Ecological sources of Nanjing in 2000, 2010, and 2020; (**b**) Resistance surfaces of Nanjing in 2000, 2010, and 2020; (**c**) Ecological network of Nanjing in 2000, 2010, and 2020.

3.1.2. Nanjing Ecological Network Connectivity Analysis

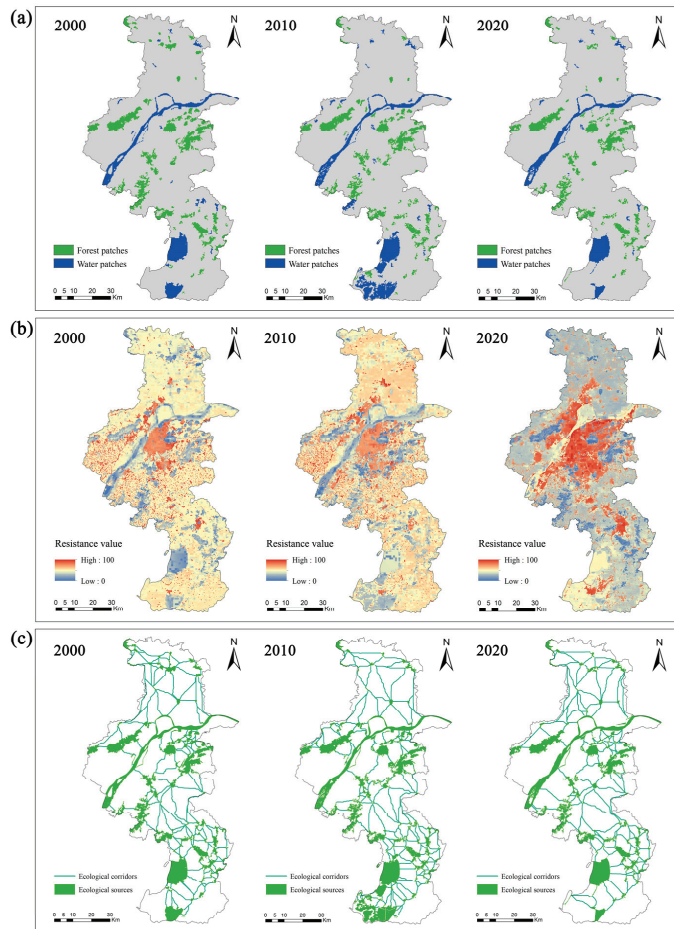Based on the analysis using the Conefor26 platform, we obtained the IIC index and PC indices of the ecological network in 2000, 2010, and 2020, with values of 2.18, 2.59, 2.09 (IIC) and 3.66, 4.68, 3.14 (PC), all of which showed a trend of initially increasing and then significantly decreasing. In 2020, the spatial distribution of patch importance indices (dPC) is shown in Figure 5, where patches are numbered in ascending order of area. The results showed that patches with high dPC values were primarily concentrated around Shijiu Lake (patch 77) and the Yangtze River (patch 78), as well as large forest patches along the riverbanks (patches 76 and 75). These areas form the core groups of the ecological network. Patches with moderate dPC values (patches 51, 69, 73, 74, etc.) were mainly located on the southern edge of the urban area. In contrast, smaller patches distributed widely in the north and south exhibited lower dPC values and lacked structural connectivity, indicating the fragmentation of the ecological network.
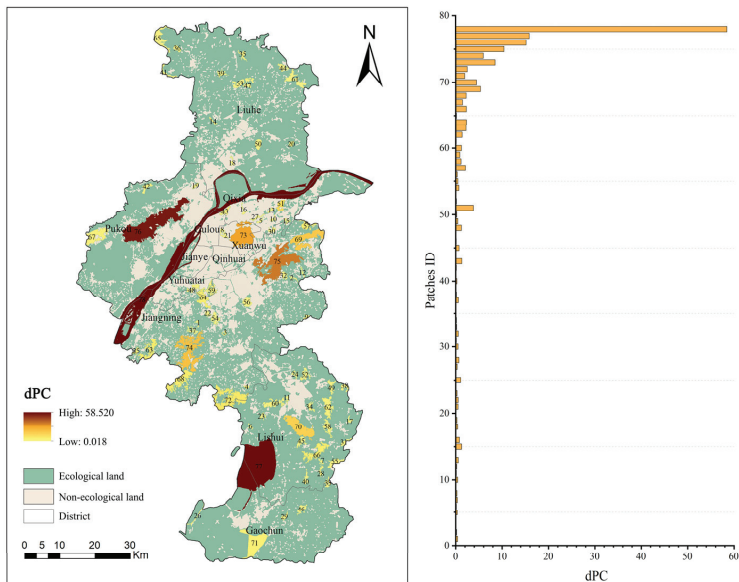
Figure 5. Spatial distribution of dPC index for ecological sources of Nanjing in 2020.

3.2. Comprehensive Evaluation of Carbon Sink by Multi-Scenario Simulation in Nanjing

3.2.1. Results of Land-Use Simulations

We used the FLUS model to simulate land use of Nanjing for 2035 and compared the spatial patterns under two different scenarios: inertial development (Scenario I) and master plan (Scenario II) (Figure 6a). Through calculation, the Kappa coefficient of the FLUS model reached 0.763 and the FOM coefficient was 0.302, verifying the accuracy of the model and its parameters for predicting future land-use changes in Nanjing. In Scenario I, the construction land expanded dramatically, increasing by 10.83%. This growth comes at the cost of a drastic reduction in cultivated land and forest land, with cultivated land decreasing by 513.96 km^2 and forest land decreasing by 71.60 km^2. This indicated that under the inertia development model, urban expansion directly led to a considerable reduction in ecological space. In contrast, in Scenario II, the construction land increased by 7.03%, and although the cultivated land decreased by 406.04 km^2, the forest land increased by 41.62 km^2. Both scenarios showed a decrease in water system areas, with Scenario I experiencing a more severe decline.
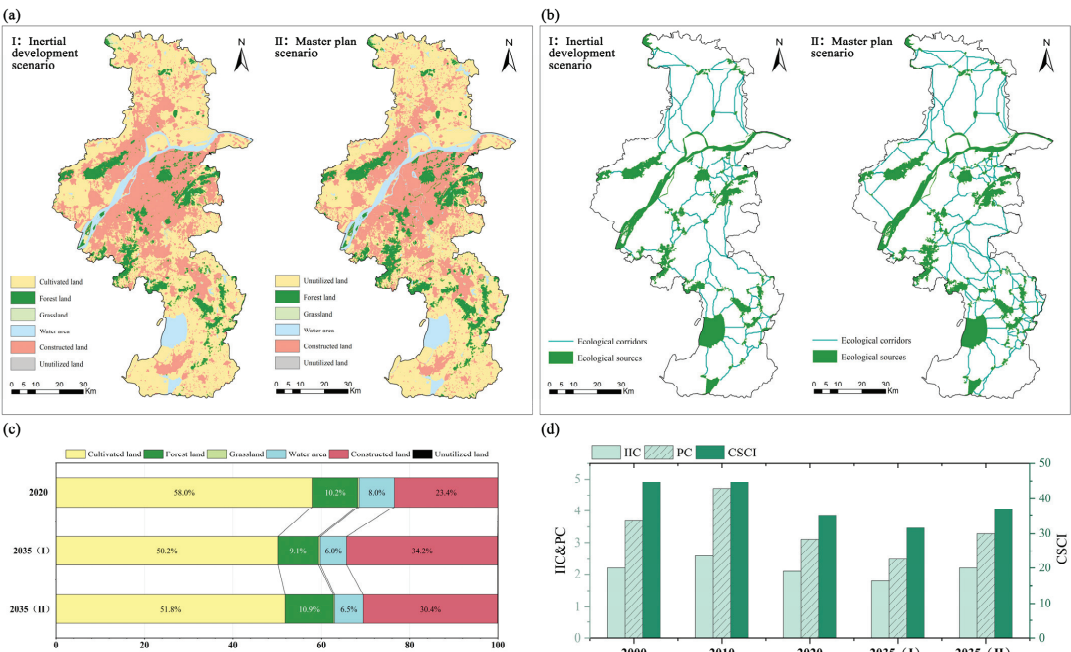
Figure 6. Land use and ecological network under simulated scenarios of Nanjing in 2035. (**a**) Land use under simulated scenarios of Nanjing in 2035; (**b**) Ecological network under simulated scenarios of Nanjing in 2035; (**c**) Comparison of land-use area before and after simulation in Nanjing; (**d**) Comparison of carbon sinks and connectivity before and after simulation in Nanjing.

Figure 6b illustrates the ecological network under the two scenarios for 2035. Scenario II demonstrates a denser ecological network and a more stable localized group structure compared to Scenario I. Specifically, in Scenario I, there were 53 ecological source patches and 104 corridors, both of which had decreased compared to 2020. The primary changes in the network occurred in the central and northern regions, where the loss of core patches led to a sharp reduction in the number of corridors. In Scenario II, the total number of ecological source patches increased to 83, and the number of corridors reached 179. This represents an increase in source patches from 78 in 2020, and the corridor count was similar to 2020 levels. Scenario II showed significant improvements at the northern and southern ends. The northern corridors have become more homogeneous due to the appearance of small patches and effectively connect the original ecological network gap areas. The improved network performance at the southern was reflected in the corridor structure becoming more compact, especially in the localized clusters centered around Shijiu Lake, where connections between patches have become more uniform. Additionally, small patches have emerged in previously vacant areas west of the Yangtze River, indicating that the master plan scenario has enhanced the ecological network's coverage across the city.

Calculating the carbon sinks of the ecological sources under the two scenarios, it was found that the carbon sink capacity of Scenario II increased from 349,000 tons in 2020 to 368,000 tons, reflecting a 5.4% increase. In contrast, the carbon sink capacity of Scenario I decreased to 316,000 tons, representing a reduction of 9.5%. From Scenario I to Scenario II, the carbon sink capacity increased by 52,000 tons, equivalent to 14.9% of the 2020 value. This result clearly demonstrates the significant advantage of the master plan scenarios in enhancing carbon sink capacity, emphasizing the importance of following the plan for urban development and ecological construction.

3.2.2. Evaluation of Carbon Sink Index

Figure 7 illustrates the spatial distribution pattern of carbon sink capacity, efficiency, and variability of ecological sources in 2020. The study showed that the carbon storage was positively correlated with patch area. Small patches (<10 ha) have lower carbon storage, while large patches (>20 ha) exhibit higher carbon sequestration capacity. Large forest patches, with their superior ecological quality and structural components, have more significant ecological benefits. Notably, forest patches such as 76, 75, 74, 73, and 72 display higher carbon sequestration efficiency. In contrast, waterbody patches (such as 77 and 78) and many smaller patches show lower carbon sequestration efficiency, especially in areas like Qixia, Jiangning, Lishui, and Liuhe districts. From a spatial evolution perspective, the total carbon storage in ecological sources has been on a downward trend from 2000 to 2020, with an overall decrease of 21.7%. The most significant decline occurred between 2010 and 2020, as large patches were severely affected, leading to a sharp drop in overall carbon sequestration.
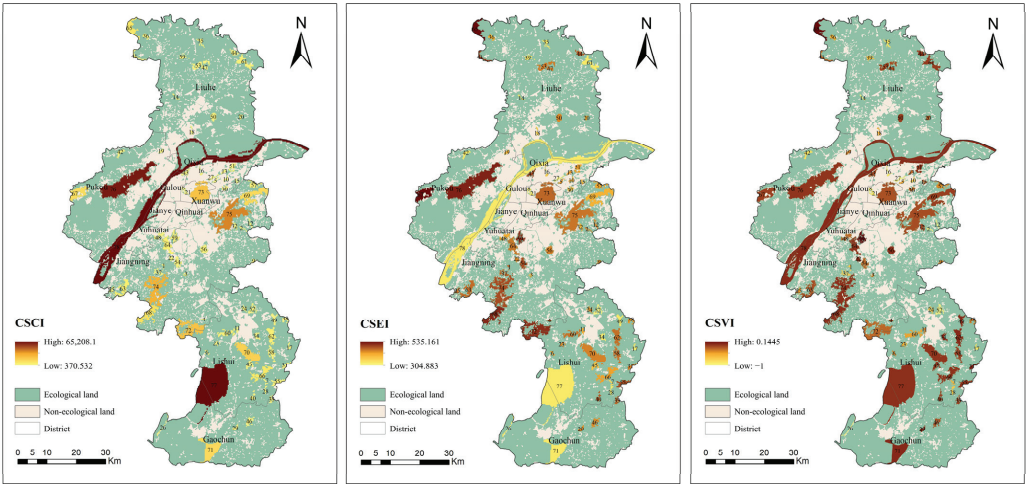
Figure 7. Spatial distribution map of carbon sink capacity, efficiency, and variability for ecological sources of Nanjing in 2020.

To further evaluate the carbon dynamics of ecological sources, this study projected the change rates in carbon storage for each patch from 2020 to 2035, which was used as the carbon sink dynamics index. Under the inertial development scenario, 93.6% of the patches showed a decrease in carbon storage by 2035, with a more pronounced decline in smaller patches, especially in northern Liuhe district, southern Lishui district, and near the central urban areas. Large patches, with their mature green spaces and higher ecological quality, demonstrated stronger resilience, while smaller patches were more vulnerable and faced higher risks.

Figure 8 presents the integrated carbon sink index of patches based on the capacity, efficiency, and the variability from 2020 to 2035. The results reveal that patches 78, 76, 67, 65, and 74 have the highest carbon sink rankings and are the key ecological source sites in Nanjing. Conversely, patches in Lishui, Liuhe, and Gaochun districts, especially smaller patches like 52, 48, 27, 10, and 19, have lower integrated carbon sink values and urgently need restoration and enhancement. Interestingly, despite lower total carbon storage in smaller patches like 65 in the north and 55 in Lishui, their overall carbon sink performance is favorable. The analysis of their sub-indicators shows high carbon sequestration efficiency

and change rates, suggesting good ecological quality and a positive future trend. These patches could serve as models for ecological improvement in other small and medium-sized patches.
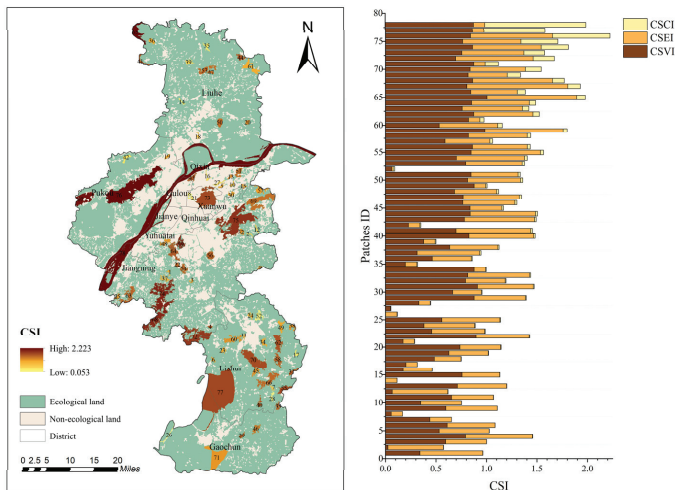
Figure 8. Spatial distribution map of carbon sink index for ecological sources of Nanjing in 2020.

3.3. Optimization and Validation of Ecological Networks

3.3.1. Correlation Analysis Between Carbon Sinks and Connectivity

We obtained the dPC and comprehensive carbon sink index for each ecological source in 2020. To further investigate the potential impact of dPC on the ecosystem's carbon sink capacity, we used Spearman correlation analysis to assess the relationship between carbon sink index and dPC. The results revealed a significant positive correlation between dPC and both carbon sink capacity and efficiency (Figure 9). This suggests that increasing the connectivity of ecological nodes can enhance their carbon sink capacity. Based on this, we propose an optimization strategy that integrates the carbon sink index and connectivity, aiming to strengthen both the structure and function of the ecological network in a complementary way.
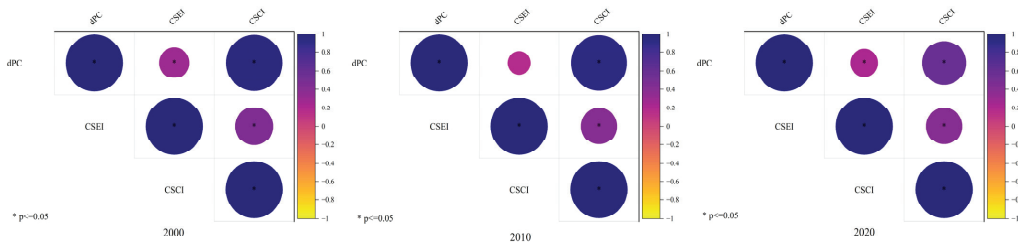
Figure 9. Correlation analysis between carbon sinks and connectivity for ecological sources of Nanjing.

3.3.2. Optimization of Ecological Network

The study deeply explored the coupling relationship between carbon sink index (CSI) and structural connectivity (dPC) based on the ecological source data of Nanjing in 2020 and accordingly identified four categories of ecological sources that need targeted optimization. Under the guidance of the upland planning and 2035 simulation scenarios, we carried out a bidirectional optimization of Nanjing's ecological network in terms of function and structure and mapped the optimization pattern (Figure 10).

1.   Strategies for Ecological Conservation
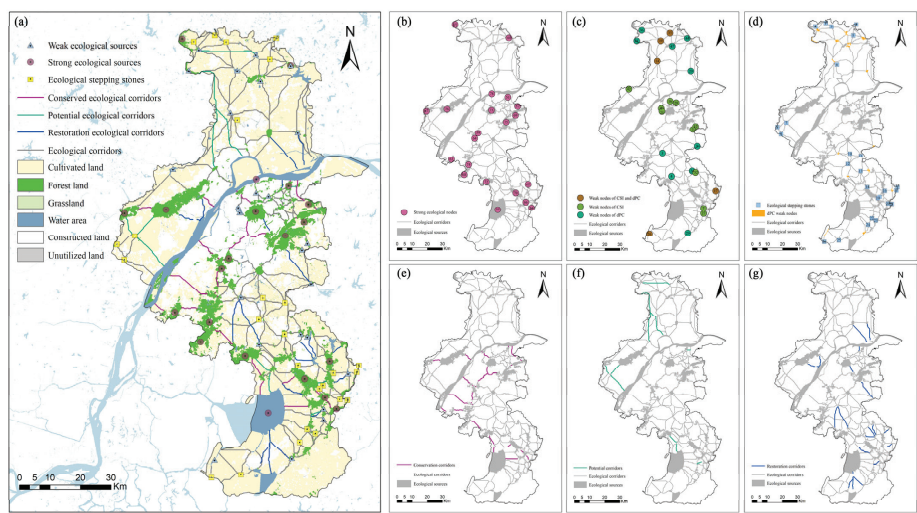
Figure 10. Optimization strategies of ecological network in Nanjing. (**a**) Overall plan for optimizing the ecological network in Nanjing; (**b**) Distribution map of ecological strong nodes in Nanjing; (**c**) Distribution map of ecological weak nodes in Nanjing; (**d**) Distribution map of added ecological stepping stones in Nanjing; (**e**) Distribution map of ecological conservation corridors in Nanjing; (**f**) Distribution map of ecological potential corridors in Nanjing; (**g**) Distribution map of ecological restoration corridors in Nanjing.

For the 21 ecologically strong nodes with CSI or dPC in the top 20%, we adopted an ecological conservation strategy. These nodes are mostly larger scale patches with higher ecological maturity. The Yangtze River (Node 78), a key aquatic ecosystem in the Yangtze River Delta region, plays a crucial role in water conservation, climate regulation, and biodiversity preservation. Similarly, Shijiu Lake (Node 77), a wetland habitat for many bird species, is essential for maintaining ecological balance in the southern region. For these important wetland patches, we propose waterway management and restoration measures to improve their ecological quality. Meanwhile, forest patches such as Nodes 76, 75, and 74, as the primary carbon storage green spaces in Nanjing, should reduce the interference of human activities and formulate strict protection policies to ensure their natural state and ecological continuity. Grasslands distributed between forest patches, which are important habitats for wildlife and significant carbon sinks, should be managed to support natural regeneration, with controlled grazing to ensure their long-term sustainability. Moreover, we place special emphasis on protecting 26 structural corridors that connect ecological strong nodes. Measures such as controlling urban expansion and optimizing landscape composition within the corridors are crucial to maintaining their connectivity and ecological functions.

2.   Strategies for Structural Connectivity

For the 15 nodes with dPC in the latter 20%, we implemented a strategy to enhance structural connectivity. These nodes are primarily located in the northern Liuhe district and the southern Lishui and Gaochun districts. To increase connectivity, we screened small wetlands, water bodies, and forest areas with a landscape shape index greater than 2 and an area larger than 0.3 km2 as stepping stones, totaling 21 locations. In response to the fragmented network structure in the western Yangtze River region and parts of Lishui, we added five additional stepping stones (locations 7, 8, 9, 12, and 13), bringing the total

number of stepping stones to 26. Additionally, we enhanced connectivity by introducing more ecological corridors. The 11 new corridors in the simulated 2035 master plan scenario can be regarded as potential corridors for future planning, which are mainly located in the northern part of Nanjing, the central region to the west of the Yangtze River, and the southern Lishui district. Furthermore, we restored 21 corridors that existed in 2010 but were broken and made extinct in 2020, mainly distributed in the north of the Yangtze River, around the old city, around the sub-city of Lishui, and south of Shijiu Lake, which are habitual pathways for biological migration and information interaction [73]. In total, 32 ecological corridors, including both potential and restoration types, will be added.

3. Strategies for carbon sink improvement

For the 15 weak nodes in the bottom 20% of the CSI, we adopted a carbon sink improvement strategy. Based on the characteristics of patches in terms of carbon sink capacity, efficiency and variability, targeted optimization measures were proposed (Figure 11). For patches with low carbon sink capacity, such as patches 8, 21, and 16 in the central urban area, which are limited by area expansion, it is suggested to enhance the carbon sink capacity by optimizing the landscape components. In the central and southern parts of the city, patches 2, 12, 7, and 17, which are forest areas, could benefit from linking surrounding green spaces to expand their size and create continuous ecosystems. For wetland patches 14, 39, and 28, large-scale ecological restoration is recommended, supported by the development of eco-tourism industries and suburban parks, to effectively increase the size of habitat patches, so as to enhance carbon storage.
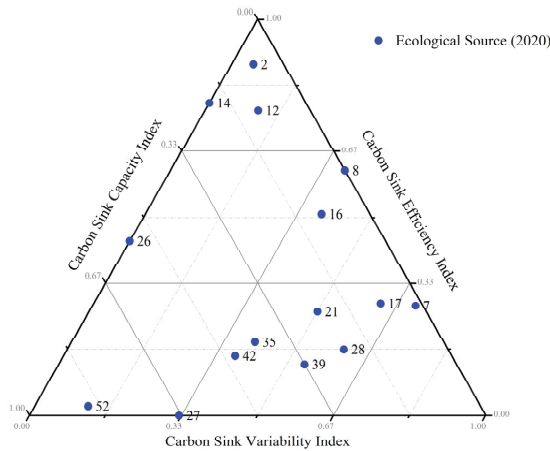
Figure 11. Ternary diagram of carbon capacity-efficiency-variability for 15 weak carbon sink nodes in Nanjing.

For patches with poor carbon sink efficiency, such as patches 27, 52, 17, and 7, the focus should be on improving the structural composition. Specific measures include optimizing community composition, adjusting age structure, and enhancing spatial arrangement. This could involve increasing the proportion of trees and shrubs, promoting evergreen and deciduous trees, and favoring high-carbon vegetation to improve community carbon storage. Additionally, increasing the proportion of younger trees can enhance carbon sink potential, while improving vertical plant structure and building layered plant communities will further strengthen carbon sink capacity. For wetland patches 21, 28, 39, 35, and 42, increasing the proportion of forest, grassland, and aquatic plants is essential to improve carbon sink efficiency.

Regarding carbon sink variability, patches 2, 12, 14, 26, 27, and 52 show weak performance. Simulation results indicate that these patches will experience significant reduction in area by 2035 due to surrounding land-use encroachment, particularly patches 14 and 26, where water systems are almost entirely lost, leading to sharp declines in carbon sink capacity. These patches, mostly located on the outskirts and in rural areas, represent regions with high ecological risk. Future development in these regions should be carefully controlled. If development activities are required, internal composition enhancement strategies should be applied to mitigate the carbon sink loss caused by the reduction in patch size.

4. Strategies for Synergistic Enhancement

For the five dual-weak nodes, where both CSI and dPC fall within the bottom 20%, we applied a collaborative optimization strategy. These nodes are mostly small water patches with low carbon sink density, distributed at the northern and southern ends of the study area, which are characterized by higher ecological risk. To address these issues, we recommend focusing on ecological restoration to enhance the carbon sequestration capacity of wetlands. Additionally, improving connectivity with nearby major water systems is essential to create a specialized water network, thereby boosting both ecological function and connectivity.

3.3.3. Optimized Verification

The carbon sequestration of the optimized ecological network was estimated, with the efficiency of the updated source sites and corridors calculated based on the average values for forest, grassland, and water patches in 2020. The optimized ecological sources showed an increase of 11,019.6 tons in carbon sequestration. Of this, 7162.2 tons resulted from the addition of ecological stepping stones, while 2857.3 tons came from improvements in the internal composition of the sources. The carbon sequestration in ecological corridors increased by 2740.2 tons, resulting in a total improvement of 13,759.8 tons of the entire ecological network. This represents a 3.82% increase in total carbon sequestration compared to the pre-optimization values, demonstrating a significant improvement (Table 3).

Table 3. Changes in carbon sink before and after optimization of Nanjing's ecological network.

Types	Unoptimized (t)	Optimized (t)
Ecological sources of carbon sink	349,433.48	360,453.03
Ecological corridors carbon sink	104,97.61	132,37.85

The number of optimized ecological sources increased to 114, covering a total area of 894.20 km^2, which represents a 1.9% growth compared to the pre-optimization area. The number of ecological corridors also grew to 232, with a total length of 1330.99 km, reflecting a 15.54% increase. Guided by the optimization strategy, the PC index and IIC index have improved by 1.6% and 0.5%, indicating a notable enhancement in the overall structural connectivity of the ecological network (Table 4).

Table 4. Changes in structural indices before and after optimization of Nanjing's ecological network.

Types	2020	2035-I	2035-II	Optimized
Number of ecological sources	78	53	83	114
Area of ecological sources (km^2)	877.51	796.47	915.75	894.20
Number of ecological corridors	180	104	179	232
Length of Ecological Corridor (km)	1151.93	923.33	1150.51	1330.99
PC (10^{-3})	3.14	2.53	3.22	3.19
IIC (10^{-3})	2.09	1.78	2.15	2.10

4. Discussion

4.1. Significance of Coupling Carbon Sinks in Ecological Network Research

The integration of ecological networks and carbon sinks is increasingly seen as a pivotal approach for addressing climate change and biodiversity loss simultaneously. Research on this integration emphasizes its significant role in generating synergies, enhancing ecological connectivity, and improving carbon storage capacity. Numerous studies have shown that landscapes with connected green spaces have higher carbon sequestration efficiency compared to isolated patches [78,79]. For instance, in the European Union, the Natura 2000 network not only conserves biodiversity but also facilitates carbon storage across protected areas. Similarly, China's "ecological redline" policy focuses on restoring ecosystems through protected corridors, incorporating carbon sink functions into national conservation strategies [80]. These integrated efforts demonstrate that strengthening ecological connectivity can directly enhance carbon sink efficiency.

In this study, we integrate carbon sinks with ecological networks by coupling CSI with dPC. This approach allows for the precise identification of critical and vulnerable nodes in Nanjing's ecological network, enabling the formulation of targeted optimization strategies. Previous research on ecological networks has typically focused on singular aspects such as security or connectivity [81,82], often overlooking the multidimensional variations in patch function. This has led to an incomplete understanding of the ecological attributes of these areas [51]. By incorporating carbon sinks, this study offers a more comprehensive methodology, enabling a more accurate and holistic strategy for enhancing various types of patches, ensuring a more efficient use of resources and a more effective implementation.

The construction of the CSI in this research incorporates both static and dynamic dimensions, forming a multi-dimensional evaluation system that captures total carbon sequestration, efficiency, and dynamic changes. This system provides a comprehensive reflection of carbon storage capacity and future risks. To model these dynamic changes, the study used the FLUS model to simulate two land-use scenarios for 2035: the inertia development scenario, which serves as a risk alert, and the master planning scenario, which guides optimization. By considering these scenarios, the optimization strategies proposed in this study are both forward-looking and sustainable, ensuring the long-term improvement of ecological connectivity and carbon sink in Nanjing's urban environment.

4.2. Effectiveness of Ecological Network Optimization Strategies

Compared to the initial network, the optimized network shows significant improvements in connectivity and carbon sequestration. The optimization successfully addresses issues such as the lack of direct connections between ecological patches and fragmented corridors. The focus of the optimization strategy is to enhance the efficiency of nodes and corridors while maintaining the integrity of the original network. This approach maximizes ecosystem service value with minimal land expansion by improving the functionality and stability of existing ecological elements at a low construction cost.

The optimization strategy proposed in this study aims to build a healthier and more stable ecosystem from four aspects: ecological conservation, structural connectivity, carbon sink improvement, and synergistic enhancement. Ecological conservation nodes are typically the most crucial and sensitive areas in the ecosystem, and maintaining their ecological function is vital for the stability of the entire system [83]. The structural connectivity strategy focuses on adding stepping stones and ecological corridors. Small patches are often overlooked in conservation due to their higher risk of extinction [84], but they can serve as essential stepping stones, promoting species migration, providing habitats and shelters [85], and improving overall connectivity within the network. Research has shown that patch connectivity is significantly correlated with carbon sink capacity and efficiency,

meaning that enhancing connectivity not only strengthens the ecosystem's resilience but also promotes carbon sequestration.

The carbon sink improvement strategy aims at repairing damaged patches. Research has found that carbon sink capacity is positively correlated with patch size, and increasing the area and complexity of blue-green patches can significantly improve carbon sequestration benefits. Highly aggregated, adjacent, and connected blue-green patches are associated with greater carbon storage potential [86]. Therefore, optimizing landscape composition, linking adjacent patches, and expanding patch sizes can substantially improve the ecosystem's carbon sink capacity, offering a robust response to climate change. Lastly, the synergistic enhancement strategy targets the double-weak nodes in the ecosystem through integrated management measures, reducing ecological risks and ensuring the stability of the entire system.

4.3. Challenges in the Implementation of Optimization Strategies

The optimization strategy for ecological networks involves the creation and restoration of certain corridors, which are derived from circuit theory within the LM model. However, in real urban environments, the addition of new corridors may face several challenges. A primary challenge is the scarcity of land resources, particularly in rapidly urbanizing areas where land-use conflicts between ecological network development, urban expansion, and agricultural growth are becoming more prominent [87]. Another key challenge is the technical limitations in optimizing ecological networks. For example, the determination of corridor thresholds is highly sensitive when evaluating network connectivity. Incorrect threshold settings can lead to poor ecological outcomes or excessively high construction costs [88]. Additionally, outdated management practices, such as the lack of dynamic feedback on the network's changes and the validation of its stability and connectivity alongside urban development, hinder the effectiveness of ecological protection measures in adapting to future urban growth.

At the micro-community level, ecological network optimization requires further refinement to support the comprehensive development of green spaces. This involves deeper studies into vegetation community structure, species selection, and physiological responses to enhance the efficiency of carbon cycling within ecosystems [89]. Future research should focus on the specific application of ecological restoration techniques and the establishment of standards for corridor construction to improve the practicality and effectiveness of the strategies. Furthermore, it is critical to consider essential factors such as the number, size, and spatial distribution of ecological sources, along with the distribution of high-resistance zones, which are vital when constructing an ecological network.

4.4. International Significance of Ecological Network Optimization

As a key city in the rapidly urbanizing Yangtze River Delta region, Nanjing faces significant challenges in restoring and renewing its urban green spaces. These spaces are constrained by various external factors, such as urban construction, which makes large-scale ecological development difficult. This study proposes an optimization strategy tailored to Nanjing's unique characteristics, focusing on enhancing smaller ecological spaces and corridors to improve the connectivity and stability of the city's ecological network. In turn, it aims to increase the carbon sequestration of urban green spaces. This strategy not only addresses the gap in carbon sink research for Nanjing but also offers practical guidance for building low-carbon and sustainable cities. It represents a strategic shift from expansion to development within existing urban infrastructure, in line with the principles of sustainable development.

Globally, the development of ecological networks has become crucial for biodiversity conservation and regional ecological security. The International Union for Conservation of Nature (IUCN) and the Convention on Migratory Species (CMS) both emphasize the importance of maintaining and restoring ecological connectivity. Europe's Pan-European Ecological Network (PEEN) connects isolated habitats through ecological corridors, forming a regional and even transnational ecological network system [90]. Nanjing's ecological network optimization strategy aligns with these international practices, demonstrating the global importance and urgency of such initiatives. By adopting this approach, Nanjing can not only enhance its own ecological environment but also serve as a model for other rapidly urbanizing regions, offering valuable insights for their ecological planning efforts. This strategy embodies an integrated approach, where urban planning not only focuses on economic growth but also on environmental sustainability. As the dual role of ecological networks in carbon storage and biodiversity conservation becomes increasingly recognized, the global shift toward nature-based solutions underscores the importance of integrating ecological connectivity into urban planning for long-term disaster resilience and climate adaptation.

4.5. Limitations and Prospects in Technical Methods

Previous studies on Nanjing have evaluated carbon sequestration and anthropogenic carbon emissions, providing a more precise assessment of the regional carbon balance [91,92]. However, this study does not account for carbon emissions and focuses solely on the carbon sink function of the ecological network, which introduces certain limitations. In many studies, the InVEST model has been used to simulate carbon storage [93,94]. This approach simplifies the carbon cycle process and is better suited for large-scale studies. In contrast, this study uses the CASA model, which is specifically designed to simulate carbon cycling. It allows for more detailed parameter adjustments tailored to different study areas, making it better suited for understanding the unique characteristics of specific ecosystems. While the CASA model offers more precise insights, it is data-intensive, operationally complex, and primarily focuses on vegetation carbon sinks, excluding carbon sequestration from water bodies. Due to research constraints, the estimation of water body carbon sinks relies on coefficients from similar regions, which could introduce some degree of error. Future studies should address this limitation by conducting more in-depth surveys and sampling to achieve more accurate assessments.

Additionally, this study uses the FLUS model to predict green space carbon sinks for 2035. However, the model faces challenges in simulating land-use changes in rapidly developing regions with complex urban spatial patterns, leading to unclear spatial differences [95]. Future research could consider using the PLUS model or improving the FLUS model to enhance its accuracy [96,97]. Moreover, since the NDVI data for 2035 cannot be directly observed, this study relies on 2020 data for estimations, which limits the accuracy of predictions. Therefore, future work should focus on developing more accurate methods for carbon sink assessment that can better account for long-term land-use changes and the evolving requirements of ecological network optimization.

5. Conclusions

This study establishes an integrated ecological network optimization framework coupled with carbon sinks. Using Nanjing as a case study, we constructed the ecological network using MSPA and LM tools and evaluated connectivity. The CASA model, combined with water body carbon absorption coefficients, was used to quantify carbon sinks. A three-dimensional evaluation system for green space carbon sinks was established. The FLUS model was applied to predict land-use changes for 2035, offering early warnings

and planning guidance for carbon sink dynamics in ecological sources. By combining connectivity and carbon sink indices, key nodes in the ecological network are identified, and targeted optimization strategies are proposed. The key findings are as follows: (1) Nanjing's ecological space exhibits a clear north–south division. From 2000 to 2020, network connectivity declined, and the total carbon sink in ecological sources decreased by 21.7%; (2) Large patches performed well in both carbon sink volume and efficiency, whereas smaller patches were at a disadvantage. In the 2035 inertia development scenario, 93.6% of the carbon sink in ecological sources declined, with a total reduction of 9.46%. In contrast, under the master plan scenario, the carbon sink volume increased by 4.9%, emphasizing the importance of strategic planning; (3) Node connectivity is significantly positively correlated with both carbon sink capacity and efficiency. Based on this, four optimization strategies are proposed: ecological conservation, structural connectivity, carbon sink improvement, and synergistic enhancement. By adding 26 ecological stepping stones, 32 ecological corridors, and optimizing landscape components, the total carbon sink increases by 3.82% and connectivity improves by 1.6%. This research provides practical pathways for ecological network restoration and carbon sink enhancement in Nanjing and other cities, offering valuable insights in the context of global urban ecological and climate change challenges.

Appendix A

Table A1. Values and weights of ecological resistance surface factors.

Resistance Surface Factors	Categories	Resistance Values	Weights
MSPA	Cores	5	0.24
	Bridges	10	
	Loops	20	
	Branches	30	
	Islets	50	
	Edges	60	
	Perforations	70	
	Background	100	

Table A1. *Cont.*

Resistance Surface Factors	Categories	Resistance Values	Weights
LUCC	Cultivated land	1	0.29
	Forest land	20	
	Grassland	30	
	Water area	50	
	Unutilized land	70100	
	Constructed land		
Slope (°)	-	-	0.15
DEM (m)	-	-	0.12
NDVI	-	-	0.20

Table A2. Land transfer restriction matrix for scenario simulations.

	Inertia Development Scenario (I)						Master Plan Scenario (II)					
	Cu	F	G	W	Co	U	Cu	F	G	W	Co	U
Cultivated land (Cu)	1	1	1	0	1	0	1	1	1	0	1	0
Forest land (F)	1	1	1	0	1	0	1	1	1	0	1	0
Grassland (G)	1	1	1	0	1	0	1	1	1	0	1	0
Water area (W)	1	0	1	1	1	0	1	0	1	1	0	0
Constructed land (Co)	0	0	0	0	1	0	0	0	0	0	1	0
Unutilized land (U)	1	1	1	1	1	1	1	1	1	1	1	1

References

1. Touma, D.; Stevenson, S.; Lehner, F.; Coats, S. Human-driven greenhouse gas and aerosol emissions cause distinct regional impacts on extreme fire weather. *Nat. Commun.* **2021**, *12*, 212. [CrossRef] [PubMed]
2. Chu, M.; Lu, J.; Sun, D. Influence of Urban Agglomeration Expansion on Fragmentation of Green Space: A Case Study of Beijing-Tianjin-Hebei Urban Agglomeration. *Land* **2022**, *11*, 275. [CrossRef]
3. Hou, Y.; Wang, L.; Li, Z.; Ouyang, X.; Xiao, T.; Wang, H.; Li, W.; Nie, X. Landscape fragmentation and regularity lead to decreased carbon stocks in basins: Evidence from century-scale research. *J. Environ. Manag.* **2024**, *367*, 121937. [CrossRef] [PubMed]
4. Newbold, T.; Hudson, L.; Hill, S.; Contu, S.; Lysenko, I.; Senior, R.; Borger, L.; Bennett, D.; Choimes, A.; Collen, B.; et al. Global effects of land use on local terrestrial biodiversity. *Nature* **2015**, *520*, 45–50. [CrossRef] [PubMed]
5. Huang, J.; Song, P.; Liu, X.; Li, A.; Wang, X.; Liu, B.; Feng, Y. Carbon Sequestration and Landscape Influences in Urban Greenspace Coverage Variability: A High-Resolution Remote Sensing Study in Luohe, China. *Forests* **2024**, *15*, 1849. [CrossRef]
6. Zhang, W.; Xu, H. Effects of land urbanization and land finance on carbon emissions: A panel data analysis for Chinese provinces. *Land Use Policy* **2017**, *63*, 493–500. [CrossRef]
7. Zhang, M.; Huang, X.; Chuai, X.; Yang, H.; Lai, L.; Tan, J. Impact of land use type conversion on carbon storage in terrestrial ecosystems of China: A spatial-temporal perspective. *Sci. Rep.* **2015**, *5*, 10233. [CrossRef] [PubMed]
8. Li, W.; Zhang, S.; Lu, C. Exploration of China's net CO_2 emissions evolutionary pathways by 2060 in the context of carbon neutrality. *Sci. Total Environ.* **2022**, *831*, 154909. [CrossRef]
9. Huang, L.; Wang, J.; Fang, Y.; Zhai, T.; Cheng, H. An integrated approach towards spatial identification of restored and conserved priority areas of ecological network for implementation planning in metropolitan region. *Sustain. Cities Soc.* **2021**, *69*, 102865. [CrossRef]
10. Wang, S.; Wu, M.; Hu, M.; Fan, C.; Wang, T.; Xia, B. Promoting landscape connectivity of highly urbanized area: An ecological network approach. *Ecol. Indic.* **2021**, *125*, 107487. [CrossRef]
11. Isaac, N.J.B.; Brotherton, P.N.M.; Bullock, J.M.; Gregory, R.D.; Boehning-Gaese, K.; Connor, B.; Crick, H.Q.P.; Freckleton, R.P.; Gill, J.A.; Hails, R.S.; et al. Defining and delivering resilient ecological networks: Nature conservation in England. *J. Appl. Ecol.* **2018**, *55*, 2537–2543. [CrossRef]
12. Cunha, N.S.; Magalhães, M.R. Methodology for mapping the national ecological network to mainland Portugal: A planning tool towards a green infrastructure. *Ecol. Indic.* **2019**, *104*, 802–818. [CrossRef]
13. Yu, K. Security patterns and surface model in landscape ecological planning. *Landsc. Urban Plan.* **1996**, *36*, 1–17. [CrossRef]

14. Wu, B.; Bao, y.; Wang, Z.; Chen, X.; Wei, W. Multi-temporal evaluation and optimization of ecological network in multi-mountainous city. *Ecol. Indic.* **2023**, *146*, 109794. [CrossRef]

15. Zhang, R.; Zhang, L.; Zhong, Q.; Zhang, Q.; Ji, Y.; Song, P.; Wang, Q. An optimized evaluation method of an urban ecological network: The case of the Minhang District of Shanghai. *Urban For. Urban Green.* **2021**, *62*, 127158. [CrossRef]

16. Wu, X.; Zhang, J.; Geng, X.; Wang, T.; Wang, K.; Liu, S. Increasing green infrastructure-based ecological resilience in urban systems: A perspective from locating ecological and disturbance sources in a resource-based city. *Sustain. Cities Soc.* **2020**, *61*, 102354. [CrossRef]

17. McRae, B.H.; Beier, P. Circuit theory predicts gene flow in plant and animal populations. *Proc. Natl. Acad. Sci. USA* **2007**, *104*, 19885–19890. [CrossRef] [PubMed]

18. Kwon, O.-S.; Kim, J.-H.; Ra, J.-H. Landscape Ecological Analysis of Green Network in Urban Area Using Circuit Theory and Least-Cost Path. *Land* **2021**, *10*, 847. [CrossRef]

19. Peng, J.; Yang, Y.; Liu, Y.; Hu, Y.; Du, Y.; Meersmans, J.; Qiu, S. Linking ecosystem services and circuit theory to identify ecological security patterns. *Sci. Total Environ.* **2018**, *644*, 781–790. [CrossRef]

20. Liu, J.; Yin, H.; Kong, F.; Li, M. Structure optimization of circuit theory-based green infrastructure in Nanjing, China. *Acta Ecol. Sin.* **2018**, *38*, 4363–4372.

21. Zhu, X.; Mu, X.; Hu, G. Ecological network analysis of urban energy metabolic system—A case study of Beijing. *Ecol. Model.* **2019**, *404*, 36–45. [CrossRef]

22. Xia, C.; Chen, B. Urban land-carbon nexus based on ecological network analysis. *Appl. Energy* **2020**, *276*, 115465. [CrossRef]

23. Ahern, J. Urban landscape sustainability and resilience: The promise and challenges of integrating ecology with urban planning and design. *Landsc. Ecol.* **2012**, *28*, 1203–1212. [CrossRef]

24. Zheng, H.; Li, A.; Meng, F.; Liu, G.; Hu, Y.; Zhang, Y.; Casazza, M. Ecological network analysis of carbon emissions from four Chinese metropoles in multiscale economies. *J. Clean. Prod.* **2021**, *279*, 123226. [CrossRef]

25. Xia, L.; Zhang, Y.; Sun, X.; Li, J. Analyzing the spatial pattern of carbon metabolism and its response to change of urban form. *Ecol. Model.* **2017**, *355*, 105–115. [CrossRef]

26. Clauzel, C.; Jeliazkov, A.; Mimet, A. Coupling a landscape-based approach and graph theory to maximize multispecific connectivity in bird communities. *Landsc. Urban Plan.* **2018**, *179*, 1–16. [CrossRef]

27. Lu, F.; Hu, H.; Sun, W.; Zhu, J.; Liu, G.; Zhou, W.; Zhang, Q.; Shi, P.; Liu, X.; Wu, X.; et al. Effects of national ecological restoration projects on carbon sequestration in China from 2001 to 2010. *Proc. Natl. Acad. Sci. USA* **2018**, *115*, 4039–4044. [CrossRef]

28. Guo, H.; Yu, Q.; Pei, Y.; Wang, G.; Yue, D. Optimization of landscape spatial structure aiming at achieving carbon neutrality in desert and mining areas. *J. Clean. Prod.* **2021**, *322*, 129156. [CrossRef]

29. Qiu, Z.; Feng, Z.; Song, Y.; Li, M.; Zhang, P. Carbon sequestration potential of forest vegetation in China from 2003 to 2050: Predicting forest vegetation growth based on climate and the environment. *J. Clean. Prod.* **2020**, *252*, 119715. [CrossRef]

30. Amoatey, P.; Sulaiman, H. Quantifying carbon storage potential of urban plantations and landscapes in Muscat, Oman. *Environ. Dev. Sustain.* **2019**, *22*, 7969–7984. [CrossRef]

31. Wan, B.; Liu, T.; Gong, X.; Zhang, Y.; Li, C.; Chen, X.; Hu, F.; Griffiths, B.S.; Liu, M. Energy flux across multitrophic levels drives ecosystem multifunctionality: Evidence from nematode food webs. *Soil Biol. Biochem.* **2022**, *169*, 108656. [CrossRef]

32. Agbelade, A.D.; Onyekwelu, J.C. Tree species diversity, volume yield, biomass and carbon sequestration in urban forests in two Nigerian cities. *Urban Ecosyst.* **2020**, *23*, 957–970. [CrossRef]

33. Tannier, C.; Bourgeois, M.; Houot, H.; Foltête, J. Impact of urban developments on the functional connectivity of forested habitats: A joint contribution of advanced urban models and landscape graphs. *Land Use Policy* **2016**, *52*, 76–91. [CrossRef]

34. Luo, Y.; Wu, J.; Wang, X.; Peng, J. Using stepping-stone theory to evaluate the maintenance of landscape connectivity under China's ecological control line policy. *J. Clean. Prod.* **2021**, *296*, 126356. [CrossRef]

35. Wu, J.; Zhang, S.; Luo, Y.; Wang, H.; Zhao, Y. Assessment of risks to habitat connectivity through the stepping-stone theory: A case study from Shenzhen, China. *Urban For. Urban Green.* **2022**, *71*, 127532. [CrossRef]

36. Fang, M.; Si, G.; Yu, Q.; Huang, H.; Huang, Y.; Liu, W.; Guo, H. Study on the relationship between topological characteristics of vegetation ecospatial network and carbon sequestration capacity in the Yellow River Basin, China. *Remote Sens.* **2021**, *13*, 4926. [CrossRef]

37. Wan, Y.; Wang, Y.; Gao, M.; Jin, L. An empirical assessment of whether urban green ecological networks have the capacity to store higher levels of carbon. *Sci. Rep.* **2024**, *14*, 3132. [CrossRef] [PubMed]

38. Cui, X.; Wei, X.; Liu, W.; Zhang, F.; Li, Z. Spatial and temporal analysis of carbon sources and sinks through land use/cover changes in the Beijing-Tianjin-Hebei urban agglomeration region. *Phys. Chem. Earth Parts A/B/C* **2019**, *110*, 61–70. [CrossRef]

39. Stokstad, E. Global efforts to protect biodiversity fall short. *Science* **2020**, *369*, 1418. [CrossRef] [PubMed]

40. Zhao, D.; Cai, J.; Xu, Y.; Liu, Y.; Yao, M. Carbon sinks in urban public green spaces under carbon neutrality: A bibliometric analysis and systematic literature review. *Urban For. Urban Green.* **2023**, *86*, 128037. [CrossRef]

41. Wang, M.; Shi, Q. Evaluation index system and empirical study on green carbon sequestration efficiency in urban high density area—A case study of Shanghai Huangpu district. *Chin. Landsc. Archit.* **2016**, *32*, 18–24.

42. Dong, J.; Dai, W.; Shao, G.; Xu, J. Ecological Network Construction Based on Minimum Cumulative Resistance for the City of Nanjing, China. *ISPRS Int. J. Geo-Inf.* **2015**, *4*, 2045–2060. [CrossRef]

43. Zhang, H. *Research on the Ecological Security Pattern of Nanjing Based on Ecological Service Function*; Nanjing Normal University: Nanjing, China, 2018.

44. Guo, T.; Wang, Z. Prediction and multi-scenario simulation analysis of the temporal and spatial evolution of ecosystem carbon storage in Nanjing based on LUCC. *Hubei Agric. Sci.* **2022**, *61*, 33.

45. Sun, X.; Xue, J.; Dong, L. Spatiotemporal change and prediction of carbon storage in Nanjing ecosystem based on PLUS model and InVEST model. *J. Ecol. Rural Environ.* **2023**, *39*, 41–51.

46. Li, Y.; Zhang, Y.; Jiang, Z.; Guo, C.; Zhao, M.; Yang, Z.; Guo, M.; Wu, B.; Chen, Q. Integrating morphological spatial pattern analysis and the minimal cumulative resistance model to optimize urban ecological networks: A case study in Shenzhen City, China. *Ecol. Process.* **2021**, *10*, 63. [CrossRef]

47. Liang, C. *The Multi-Scale Spatial Pattern Optimization of Urban Fringe Based on Ecological Adaptivity: A Case Study of Xiamen*; Tianjin University: Tianjin, China, 2024.

48. Xu, F.; Yin, H.; Kong, F.; Xu, J. Developing ecological networks based on mspa and the least-cost path method: A case study in bazhong western new district. *Acta Ecol. Sin.* **2015**, *35*, 6425–6434.

49. Cao, Y.; Yang, R.; Carver, S. Linking wilderness mapping and connectivity modelling:A methodological framework for wildland network planning. *Biol. Conserv.* **2020**, *251*, 108679. [CrossRef]

50. Wei, B.; Su, J.; Hu, X.; Xu, H.; Zhu, M.; Liu, L. Comprehensive identification of eco-corridors and eco-nodes based on principle of hydrological analysis and Linkage Mapper. *Acta Ecol. Sin.* **2022**, *42*, 2995–3009.

51. Zhang, L.; Yue, W.; Chen, Y. Construction of urban ecological security pattern based on of patch composite characteristics:A case study of Hangzhou. *Acta Ecol. Sin.* **2021**, *41*, 4632–4640.

52. Qiu, S.; Yu, Q.; Niu, T.; Fang, M.; Guo, H.; Liu, H.; Li, S.; Zhang, J. Restoration and renewal of ecological spatial network in mining cities for the purpose of enhancing carbon Sinks: The case of Xuzhou, China. *Ecol. Indic.* **2022**, *143*, 109313. [CrossRef]

53. Vogt, P.; Ferrari, J.R.; Lookingbill, T.R.; Gardner, R.H.; Riitters, K.H.; Ostapowicz, K. Mapping functional connectivity. *Ecol. Indic.* **2009**, *9*, 64–71. [CrossRef]

54. Sahraoui, Y.; Foltête, J.-C.; Clauzel, C. A multi-species approach for assessing the impact of land-cover changes on landscape connectivity. *Landsc. Ecol.* **2017**, *32*, 1819–1835. [CrossRef]

55. Saura, S.; Pascual-Hortal, L. A new habitat availability index to integrate connectivity in landscape conservation planning: Comparison with existing indices and application to a case study. *Landsc. Urban Plan.* **2007**, *83*, 91–103. [CrossRef]

56. Wu, C.; Chen, K.; E, C.; You, X.; He, D.; Hu, L.; Liu, B.; Wang, R.; Shi, Y.; Li, C.; et al. Improved CASA model based on satellite remote sensing data: Simulating net primary productivity of Qinghai Lake basin alpine grassland. *Geosci. Model Dev.* **2022**, *15*, 6919–6933. [CrossRef]

57. Wang, Y.; Xu, X.; Huang, L.; Yang, G.; Fan, L.; Wei, P.; Chen, G. An Improved CASA Model for Estimating Winter Wheat Yield from Remote Sensing Images. *Remote Sens.* **2019**, *11*, 1088. [CrossRef]

58. Ruimy, A.; Saugier, B.; Dedieu, G. Methodology for the estimation of terrestrial net primary production from remotely sensed data. *J. Geophys. Res. Atmos.* **1994**, *99*, 5263–5283. [CrossRef]

59. Wang, R.Y.; Mo, X.; Ji, H.; Zhu, Z.; Wang, Y.S.; Bao, Z.; Li, T. Comparison of the CASA and InVEST models' effects for estimating spatiotemporal differences in carbon storage of green spaces in megacities. *Sci. Rep.* **2024**, *14*, 5456. [CrossRef] [PubMed]

60. Zhu, W.; Pan, Y.; He, H.; Yu, D.; Hu, H. Simulation of maximum light use efficiency for some typical vegetation types in China. *Chin. Sci. Bull.* **2006**, *51*, 457–463. [CrossRef]

61. Liao, L.; Wu, M.; Dai, Z.; Liang, J.; Zuo, P. Research analysis of carbon budgets in coastal wetlands based on bibliometrics. *Mar. Environ. Sci.* **2022**, *41*, 32–39.

62. Ma, Y. *Study on Estimation of Carbon Source and Carbon Sink and Optimization of Spatial Pattern in Chengdu Under the Background of Low-Carbon Construction of Park City*; Beijing Forestry University: Beijing, China, 2022.

63. Peng, X.; Yan, Y.; Sun, Z.; Wang, M.; Liang, F.; Fan, H.; Liu, Q.; Zhang, G.; Luo, M.; Tang, Q. Sediment organic carbon content and its storage in Yancheng coastal salt marshes of Jiangsu Province. *Mar. Sci. Bull.* **2023**, *42*, 407–417.

64. Zhai, X.; Cui, L.; Li, W.; Zhao, X.; Zhang, M.; Kang, X. Research on Carbon Sequestration Value of Typical Wetland Ecosystem in China. *J. Hydroecol.* **2024**, *45*, 1–8. [CrossRef]

65. Li, X.; Jiang, Y.; Liu, Y.; Sun, Y.; Li, C. The impact of landscape spatial morphology on green carbon sink in the urban riverfront area. *Cities* **2024**, *148*, 104919. [CrossRef]

66. Zhang, X.; Huang, H.; Tu, K.; Li, R.; Zhang, X.; Wang, P.; Li, Y.; Yang, Q.; Acerman, A.C.; Guo, N.; et al. Effects of plant community structural characteristics on carbon sequestration in urban green spaces. *Sci. Rep.* **2024**, *14*, 7382. [CrossRef]

67. He, X. *Study on Index System Design and Efficiency Evaluation of Forest Carbon Sink Driven by Data*; Fujian Agriculture And Forestry University: Fuzhou, China, 2024.

68. Lett, C.; Silber, C.; Dubé, P.; Walter, J.N.; Raffy, M. Forest Dynamics: A Spatial Gap Model Simulated on a Cellular Automata Network. *Can. J. Remote Sens.* **1999**, *25*, 403–411. [CrossRef]

69. Liu, X.; Liang, X.; Li, X.; Xu, X.; Ou, J.; Chen, Y.; Li, S.; Wang, S.; Pei, F. A future land use simulation model (FLUS) for simulating multiple land use scenarios by coupling human and natural effects. *Landsc. Urban Plan.* **2017**, *168*, 94–116. [CrossRef]

70. Liang, X.; Liu, X.; Li, X.; Chen, Y.; Tian, H.; Yao, Y. Delineating multi-scenario urban growth boundaries with a CA-based FLUS model and morphological method. *Landsc. Urban Plan.* **2018**, *177*, 47–63. [CrossRef]

71. Li, H.; Chen, H.; Wu, M.; Zhou, K.; Zhang, X.; Liu, Z. A Dynamic Evaluation Method of Urban Ecological Networks Combining Graphab and the FLUS Model. *Land* **2022**, *11*, 2297. [CrossRef]

72. Wu, Z.; Zhang, K.; Wang, H. Construction and Optimization of Green Space Ecological Network under Urban Expansion Scenario Simulation: A Case Study in Some Areas of Nanjing. *Chin. Landsc. Archit.* **2022**, *38*, 56–61.

73. Fan, F.; Liu, Y.; Chen, J.; Dong, J. Scenario-based ecological security patterns to indicate landscape sustainability: A case study on the Qinghai-Tibet Plateau. *Landsc. Ecol.* **2020**, *36*, 2175–2188. [CrossRef]

74. Liao, Z.; Zhang, L. Spatio-temporal analysis and simulation of urban ecological resilience in Guangzhou City based on the FLUS model. *Sci. Rep.* **2023**, *13*, 7400. [CrossRef] [PubMed]

75. Mokarram, M.; Pham, T.M. CA-Markov model application to predict crop yield using remote sensing indices. *Ecol. Indic.* **2022**, *139*, 108952. [CrossRef]

76. Congalton, R.G. A Quantitative Method to Test for Consistency and Correctness in Photointerpretation. *Photogramm. Eng. Remote Sens.* **1983**, *49*, 69–74.

77. Ma, X.; Lin, P.; Chen, M. Simulation of land use spatial layout based on FLUS model: A case study of Huadu District, Guangzhou. *Adv. Soc. Sci.* **2019**, *8*, 1327–1341.

78. Dantas de Paula, M.; Groeneveld, J.; Huth, A. Tropical forest degradation and recovery in fragmented landscapes — Simulating changes in tree community, forest hydrology and carbon balance. *Glob. Ecol. Conserv.* **2015**, *3*, 664–677. [CrossRef]

79. Lu, Z.; Geng, Y.; Li, W.; Yue, R. Integrating spatial carbon factors into ecological network construction in an energy-intensive megaregion toward multi-objective synergy in northern China. *Environ. Impact Assess. Rev.* **2024**, *106*, 107480. [CrossRef]

80. Wang, L.; Zheng, H.; Chen, Y.; Huang, B. Ecological redline policy strengthens sustainable development goals through the strict protection of multiple ecosystem services. *Glob. Ecol. Conserv.* **2024**, *56*, e03306. [CrossRef]

81. Fu, F.; Liu, Z.; Liu, H. Identifying key areas of ecosystem restoration for territorial space based on ecological security pattern: A case study in Hezhou City. *Acta Ecol. Sin.* **2021**, *41*, 3406–3414.

82. Liu, Y.; Yang, S.; Ni, W.; He, J. Comprehensive assessment method on ecological patch importance: A case study in Sichuan Province, China. *Acta Ecol. Sin.* **2020**, *40*, 3602–3611.

83. Kan, H.; Ding, G.; Guo, J.; Liu, J.; Ou, M. Identification of key areas for ecological restoration of territorial space based on ecological security pattern analysis: A case study of the Taihu Lake city cluster. *Chin. J. Appl. Ecol.* **2024**, *35*, 2217–2227.

84. Riva, F.; Fahrig, L. The disproportionately high value of small patches for biodiversity conservation. *Conserv. Lett.* **2022**, *15*, e12881. [CrossRef]

85. Han, L.; Wang, Z.; Wei, M.; Wang, M.; Shi, H.; Ruckstuhl, K.; Yang, W.; Alves, J. Small patches play a critical role in the connectivity of the Western Tianshan landscape, Xinjiang, China. *Ecol. Indic.* **2022**, *144*, 109542. [CrossRef]

86. Yuan, Y.; Guo, W.; Tang, S.; Zhang, J. Effects of patterns of urban green-blue landscape on carbon sequestration using XGBoost-SHAP model. *J. Clean. Prod.* **2024**, *476*, 143640. [CrossRef]

87. Zhang, Y.; Yu, B. Analysis of urban ecological network space and optimization of ecological network pattern. *Acta Ecol. Sin.* **2016**, *36*, 6969–6984.

88. Wang, Y.; Zhao, W.; Liu, C. Optimization and construction of ecological network based on MSPA-Conefor-MCR Path: A case study of Pengze County. *Acta Agric. Univ. Jiangxiensis* **2022**, *44*, 504–518.

89. Ma, L.; Shen, C.; Lou, D.; Fu, S.; Guan, D. Ecosystem carbon storage in forest fragments of differing patch size. *Sci. Rep.* **2017**, *7*, 13173. [CrossRef]

90. Jongman, R.H.G.; Bouwma, I.M.; Griffioen, A.; Jones-Walters, L.; Van Doorn, A.M. The Pan European Ecological Network: PEEN. *Landsc. Ecol.* **2011**, *26*, 311–326. [CrossRef]

91. Liu, C.; Sun, W.; Li, P. Characteristics of spatiotemporal variations in coupling coordination between integrated carbon emission and sequestration index: A case study of the Yangtze River Delta, China. *Ecol. Indic.* **2022**, *135*, 108520. [CrossRef]

92. Chuai, X.; Yuan, Y.; Zhang, X.; Guo, X.; Zhang, X.; Xie, F.; Zhao, R.; Li, J. Multiangle land use-linked carbon balance examination in Nanjing City, China. *Land Use Policy* **2019**, *84*, 305–315. [CrossRef]

93. Wu, W.; Xu, L.; Zheng, H.; Zhang, X. How much carbon storage will the ecological space leave in a rapid urbanization area? Scenario analysis from Beijing-Tianjin-Hebei Urban Agglomeration. *Resour. Conserv. Recycl.* **2023**, *189*, 106774. [CrossRef]

94. Koo, H.; Kleemann, J.; Fürst, C. Impact assessment of land use changes using local knowledge for the provision of ecosystem services in northern Ghana, West Africa. *Ecol. Indic.* **2019**, *103*, 156–172. [CrossRef]
95. Zhao, Q.; Shao, J. Evaluating the impact of simulated land use changes under multiple scenarios on ecosystem services in Ji'an, China. *Ecol. Indic.* **2023**, *156*, 111040. [CrossRef]
96. Xu, X.; Wang, S.; Rong, W. Construction of ecological network in Suzhou based on the PLUS and MSPA models. *Ecol. Indic.* **2023**, *154*, 110740. [CrossRef]
97. Li, P.; Chen, J.; Li, Y.; Wu, W. Using the InVEST-PLUS Model to Predict and Analyze the Pattern of Ecosystem Carbon storage in Liaoning Province, China. *Remote Sens.* **2023**, *15*, 4050. [CrossRef]

Analysis of Surface Urban Heat Island in the Guangzhou-Foshan Metropolitan Area Based on Local Climate Zones

Xiaxuan He [1,2], Qifeng Yuan [1,3], Yinghong Qin [2], Junwen Lu [1,*] and Gang Li [1,*]

1   School of Architecture, South China University of Technology, Guangzhou 510641, China;
    hexiaxuan617@gxmzu.edu.cn (X.H.); yuanqf@scut.edu.cn (Q.Y.)
2   School of Civil Engineering and Architecture, Guangxi Minzu University, Nanning 530008, China;
    yqin1@mtu.edu
3   State Key Laboratory of Subtropical Building and Urban Science, Guangzhou 510640, China
*   Correspondence: lujunwen@scut.edu.cn (J.L.); mrligang1991@scut.edu.cn (G.L.)

Abstract: Understanding the driving mechanisms behind surface urban heat island (SUHI) effects is essential for mitigating the degradation of urban thermal environments and enhancing urban livability. However, previous studies have primarily concentrated on central urban areas, lacking a comprehensive analysis of the entire metropolitan area over distinct time periods. Additionally, most studies have relied on regression analysis models such as ordinary least squares (OLS) or logistic regression, without adequately analyzing the spatial heterogeneity of factors influencing the surface urban heat island (SUHI) effects. Therefore, this study aims to explore the spatial heterogeneity and driving mechanisms of surface urban heat island (SUHI) effects in the Guangzhou-Foshan metropolitan area across different time periods. The Local Climate Zones (LCZs) method was employed to analyze the landscape characteristics and spatial structure of the Guangzhou-Foshan metropolis for the years 2013, 2018, and 2023. Furthermore, Geographically Weighted Regression (GWR), Multi-scale Geographically Weighted Regression (MGWR), and Geographical Detector (GD) models were utilized to investigate the interactions between influencing factors (land cover factors, urban environmental factors, socio-economic factors) and Surface Urban Heat Island Intensity (SUHII), maximizing the explanation of SUHII across all time periods. Three main findings emerged: First, the Local Climate Zones (LCZs) in the Guangzhou-Foshan metropolitan area exhibited significant spatial heterogeneity, with a non-linear relationship to SUHII. Second, the SUHI effects displayed a distinct core-periphery pattern, with Large lowrise (LCZ 8) and compact lowrise (LCZ 3) areas showing the highest SUHII levels in urban core zones. Third, land cover factors emerged as the most influential factors on SUHI effects in the Guangzhou-Foshan metropolis. These results indicate that SUHI effects exhibit notable spatial heterogeneity, and varying negative influencing factors can be leveraged to mitigate SUHI effects in different metropolitan locations. Such findings offer crucial insights for future urban policy-making.

Keywords: local climate zones; surface urban heat island; multi-scale geographically weighted regression; geographical detector; Guangzhou-Foshan metropolitan area

1. Introduction

With the rapid development of urbanization and the ongoing effects of global warming, urban heat island (UHI) issues—where land surface temperatures (LST) in cities are higher than those in surrounding rural areas—are increasingly becoming a major challenge for urban planners and experts in related fields [1–5]. Rapid industrialization typically leads to the expansion of urban construction land, characterized by the conversion of diverse ecological and agricultural land into built environments. This transformation results in an increase in impervious surfaces and a deterioration of the urban thermal environment [6]. Urban areas, as major economic growth centers, attract almost 57% of the world's

population, with 35% of that population being under 15 years old or over 65 years old [7]. In the future, cities are expected to remain highly attractive, with projections indicating that more than 67% of the population will reside in urban areas by 2050 [8]. Therefore, it is essential to explore the complex relationship between urban development and UHI effects, summarizing the various factors influencing the UHI effect and providing a quantitative basis for future urban planning and management.

In recent years, the deterioration of urban thermal environments has prompted extensive research on the mechanisms behind urban heat island (UHI) effects. Many previously overlooked factors such as tree crown shadow areas and historical and economic factors have been reemphasized [9–11]. Additionally, many new analytical methods including random forests, multiple linear regression, and machine learning have been introduced to analyze UHI effects [12–14]. Despite this progress, defining surface urban heat island intensity (SUHII) across different urban areas has become a challenge. Previous studies relied on binary urban-rural classifications or landscape feature analysis methods to measure the intensity of urban heat island (UHI) effects in different types of urban areas, but these surface landscape classification methods lack precision [15,16]. The introduction of local climate zones (LCZs) has addressed this issue, offering a framework for SUHII calculation by categorizing built types into 10 categories (1–10) and land cover types into 7 categories [5,17,18]. Numerous scholars have employed LCZs to study the UHI effects and their mechanisms. For instance, Badaro-Saliba et al. [17] utilized the LCZ scheme to assess the SUHI effects in complex urban regions, highlighting that UHI effects in coastal cities are influenced by factors like building height and impervious surface ratio. Xi et al. [19] analyzed seasonal UHI effects in Hefei city using LCZs, employing geographical detectors and regression analysis to explore the impact mechanisms. Yin et al. [20] studied 1920 blocks in Hangzhou city, utilizing an urban weather generator (UWG), LCZs, and deep learning to analyze the UHII across different local climate zones. This research also provided urban planning and design recommendations, such as limiting the proportion of compact high-rise (LCZ 1) types and increasing green space ratios.

Numerous researchers have established a relatively standardized approach to study SUHI effects and have developed a framework for calculating SUHI intensity [5,15,19,21,22]. This prevalent framework primarily relies on satellite remote sensing of infrared radiation to estimate LST across different local climate zones (LCZs). Temperature differences are then compared to calculate the SUHII. Following this, the relevant factors contributing directly or indirectly to the generation of SUHI are summarized. This framework has been widely applied in various studies. For instance, Shi et al. [23] investigated the SUHII in Wuhan city by computing the temperature difference between LCZs and LCZ D, utilizing the formula of $\Delta T = T_{LCZX} - T_{LCZD}$. While other researchers also calculate SUHII by different formulae such as $\Delta T = T_{LCZX} - T_{LCZB}$ or $\Delta T = T_{LCZX} - T_{LCZA}$ [24–26]. Based on the information above, it is inferred that researchers have basically reached a consensus on the calculation method of SUHII. Through multiple empirical tests and calculations, it is believed that the formula using LCZ D as an indicator of SUHI effect is more reliable.

In exploring the mechanisms of SUHI effects, researchers have summarized various influencing factors and indicators [2,15,27,28]. Moon et al. [29] investigated the relationship between urban green space (UGS) layout and UHI effects, revealing that green space in central urban areas mitigates the UHI effect the most. Peng et al. identified correlations between urban morphology and UHI effects, while Li et al. [30] concluded that block types in different urban renewal areas significantly impact SUHI. Additionally, numerous studies have confirmed that factors such as population density, building density, traffic density, nightlight, and urban morphology significantly influence UHI effects [19,31,32].

Despite the significant achievements in existing research, certain limitations remain that necessitate further exploration. On one hand, when examining the relationship between the Surface Urban Heat Island (SUHI) effect and various Land Cover Zones (LCZ) using ordinary least squares (OLS) or logistic multiple regression analysis, researchers often overlook the spatial heterogeneity of influencing factors at different time periods. This oversight can lead to an inadequate exploration of the impact factors across different locations and times within the city [20,32]. On the other hand, studies analyzing the influencing factors of the SUHI effect typically focus on urban areas or central business districts (CBDs), with few investigations adopting a broader regional perspective. By examining the SUHI effects and their influencing factors from the standpoint of urban agglomerations or metropolitan areas, these studies often result in a limited consideration of the relevant factors [33–36].

To address these research gaps, this study employs a multi-scale geographically weighted regression (MGWR) model to analyze the influencing factors of the Surface Urban Heat Island (SUHI) effect across diverse locations and time periods within the Guangzhou-Foshan metropolitan area. Additionally, Geodetectors are utilized to explore the interactions between influencing factors and their effects on SUHI [37–39]. By comparing multiple models, this research aims to provide a comprehensive analysis of the factors affecting the urban heat island effect in metropolitan areas and offers quantitative suggestions and guidance for future urban renewal and construction efforts. This study seeks to answer the following two questions: (1) What is the influential mechanism of SUHI impact factors across different time periods and locations within a metropolitan area characterized by a complete core-periphery spatial pattern? (2) Which types of Land Cover Zones (LCZ) have positive or negative impacts on SUHI effects, and how do the impacts of different LCZs vary? The remainder of this paper is organized as follows: Section 2 introduces the research materials and methods. Section 3 presents the classification of the LCZ scheme in the Guangzhou-Foshan metropolitan area and explores the influencing factors of various LCZs that impact SUHI effects at different locations and times. Section 4 discusses the key findings of this research, comparing them with previous studies, and proposes planning and policy recommendations to mitigate the SUHI effect. Finally, the concluding section summarizes the findings and offers suggestions for future research directions.

2. Materials and Methods

2.1. Study Area

The core region of this study is the Guangzhou-Foshan metropolitan area, which comprises the two principal cities of Guangzhou and Foshan, located in southern China. These cities serve as key components of the Guangdong-Hong Kong-Macao Greater Bay Area (Figure 1). The metropolitan area spans longitude $112°22'$ E–$113°03'$ E and latitude $22°26'$ N–$23°56'$ N, with a population of approximately 30 million residents and an area of 11,235.12 km^2. This region experiences a subtropical monsoon climate, with average annual temperatures ranging from 21.7 °C to 23.1 °C throughout the year. In the past five years, summer temperatures have peaked at 39.1 °C, indicating a significant increase in the SUHI effect [40,41]. This study focuses on the Guangzhou-Foshan metropolitan area, specifically examining the summers of 2013, 2018, and 2023 as research periods. The SUHI effects and their influencing factors during these three periods were analyzed and compared, providing insights into the mechanisms underlying the SUHI phenomenon.
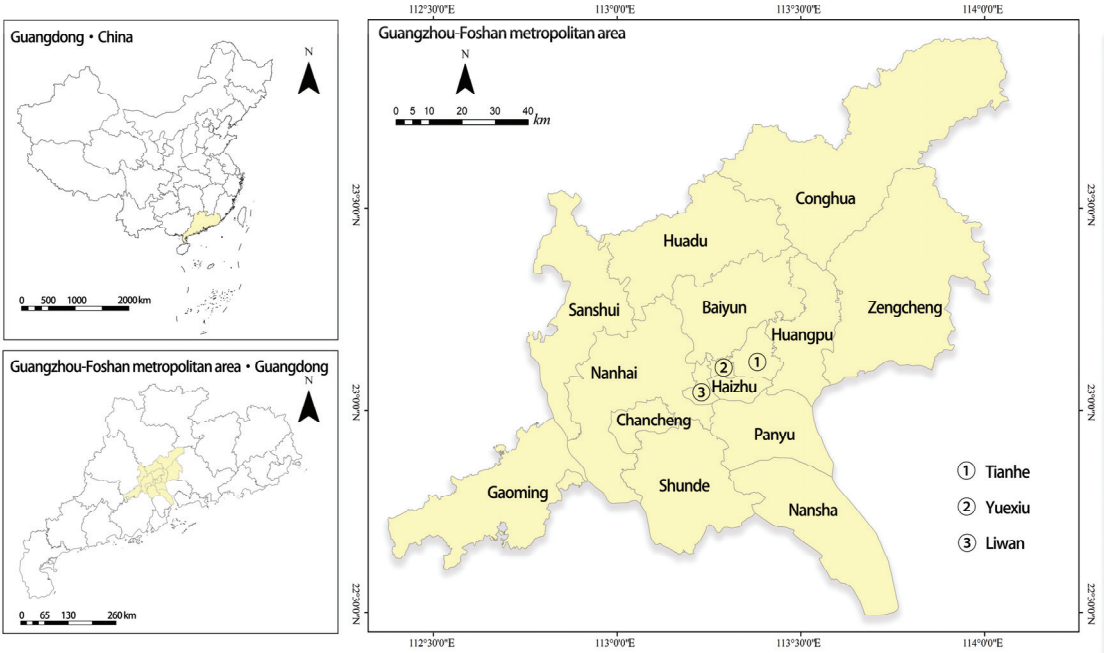
Figure 1. Study area.

2.2. Data Source

As shown in Table 1, the data utilized in this research were obtained from reliable sources. (1) Landsat images were provided by the United States Geological Survey (USGS) from the Landsat-8 satellite, equipped with a Thermal Infrared Sensor (TIRS). The quality of the data was ensured by selecting cloud-free and rain-free images from the summers of 2013, 2018, and 2023 to retrieve land surface temperatures (LST) [42,43]. (2) The Land-Use and Land-Cover Change (LUCC) data were acquired from the Chinese Academy of Sciences, which maintains remote sensing monitoring datasets of annual land use in China (https://www.resdc.cn/Default.aspx, accessed on 15 May 2024). (3) High-quality nighttime light images were obtained from the DMSP-OLS dataset (https://dataverse.harvard.edu/dataset.xhtml?persistentId=doi:10.7910/DVN/GIYGJU, accessed on 15 May 2024) [44]. (4) Annual road data were sourced from OpenStreetMap (OSM). (5) Points of Interest (POI) data were obtained from opensource data from Amap v10.0.5. (6) Digital elevation model (DEM) data were acquired from NASA's dataset (https://www.earthdata.nasa.gov, accessed on 1 May 2024). (7) Gross Domestic Product (GDP) and population data were derived from the China Urban Statistical Yearbook, Guangdong Provincial Statistical Yearbook, Guangzhou Statistical Yearbook, and other sources.

Data	Date	Type	Spatial Resolution	Source
Landsat images	13 June 2013 3 August 2013 12 July 2018 11 August 2018 15 June 2023 22 June 2023	Raster	30 m × 30 m	USGS (https://landsat.visibleearth.nasa.gov, accessed on 4 October 2024)
Road network	2013 2018 2023	Vector		Open Street Map (http://www.openstreetmap.org, accessed on 4 October 2024)
Digital elevation model	2013	Raster	30 m × 30 m	NASA (https://www.earthdata.nasa.gov, accessed on 4 October 2024)
Points of interest (POI)	2013 2018 2023	Vector		Amap (https://www.amap.com, accessed on 4 October 2024)
LUCC	2013 2018 2023	Raster	30 m × 30 m	Chinese Academy of Science (https://www.resdc.cn/DOI, accessed on 4 October 2024)
Nighttime light images	2013 2018 2023	Raster	30 m × 30 m	DMSP-OLS dataset (https://dataverse.harvard.edu/dataset. xhtml?persistentId=doi: 10.7910/DVN/GIYGJU, accessed on 4 October 2024)
Population/GDP	2013 2018 2023	Raster	30 m × 30 m	<China Urban Statistical Yearbook> etc.

2.3. Methods

The methodology of this research consists of four parts (Figure 2): Classification of LCZs: The first step involves classifying the Local Climate Zones (LCZs) in the Guangzhou-Foshan metropolitan area. Training samples for various LCZs were drawn from Google Earth. A combination of LCZ generators and random forest (RF) classification techniques was employed to categorize the surface landscape features of Guangzhou and Foshan into different LCZ types, ensuring a recognition accuracy greater than 75% [45–47]. Calculation of SUHII: The second step calculates the Surface Urban Heat Island Intensity (SUHII) by comparing the land surface temperatures (LSTs) of different LCZs. The LSTs used for this comparison were obtained using a single-window algorithm to analyze high-quality Landsat images [48–51]. Selection of Influencing Factors: The third step involves selecting the influencing factors. Based on previous research and practical experience, this study identified three categories of influencing factors: remote sensing data, urban multi-source big data, and urban panel data [2,15,31]. Exploration of Influencing Mechanisms: The fourth step aims to explore the mechanisms influencing SUHI. Following the steps outlined above, this study intends to identify the influencing factors and mechanisms of SUHI effects through the application of geographically weighted regression (GWR). Additionally, multi-scale geographically weighted regression (MGWR) will be employed to investigate the influencing factors related to the built types of LCZ. Finally, the interactions between these factors will be examined using geographic detectors [21,26,52].

Step 1: Local Climate Zone Classification

LCZ training set

LCZ classification

LCZ
2, 3, 4, 5, 6, 8, 9, 10

Built types

LCZ
A, B, C, D, E, F, G

Land cover types

LCZ generator

Random Forest

No — Accuracy by categories > 75% — No

Yes

LCZ map

Step 2: SUHII Calculation

Landsat ETM Raw Data

Data fetch

Radiation calibration

Geometric correction

Guangzhou-Foshan metropolitan area

Extract by Mask

Thermal infrared radiation brightness value

Surface radiation ratio

Inversion model for real surface temperature

Land surface Temperature (LST)

Surface urban heat island intensity (SUHII)

Creating 300m×300m fish net

SUHII of different types of LCZ

Geographically weighted regression

independent variable

Land cover factors

socioeconomic factors

Urban environmental factors

dependent variable

SUHII of different types of LCZ

influencing machanism on SUHII

Geographic detectors

independent variable

Land cover factors

socioeconomic factors

Urban environmental factors

dependent variable

SUHII of different types of LCZ

The interaction between influencing factors

Multi-scale geographical weighted regression

independent variable

Land cover factors

socioeconomic factors

Urban environmental factors

dependent variable

SUHII of built types of LCZ

influencing machanism on SUHII of built types of LCZ

Step 4: Driving Machanisms of SUHII

Collected data

Remote sensing imagery

Open source data

Urban panel data

NDBI

POI

Population density

NDWI

Road Density

GDP

NDVI

DEM

NPP

Nighttime light

Land cover factors

Urban environmental factors

socioeconomic factors

Influencing factors

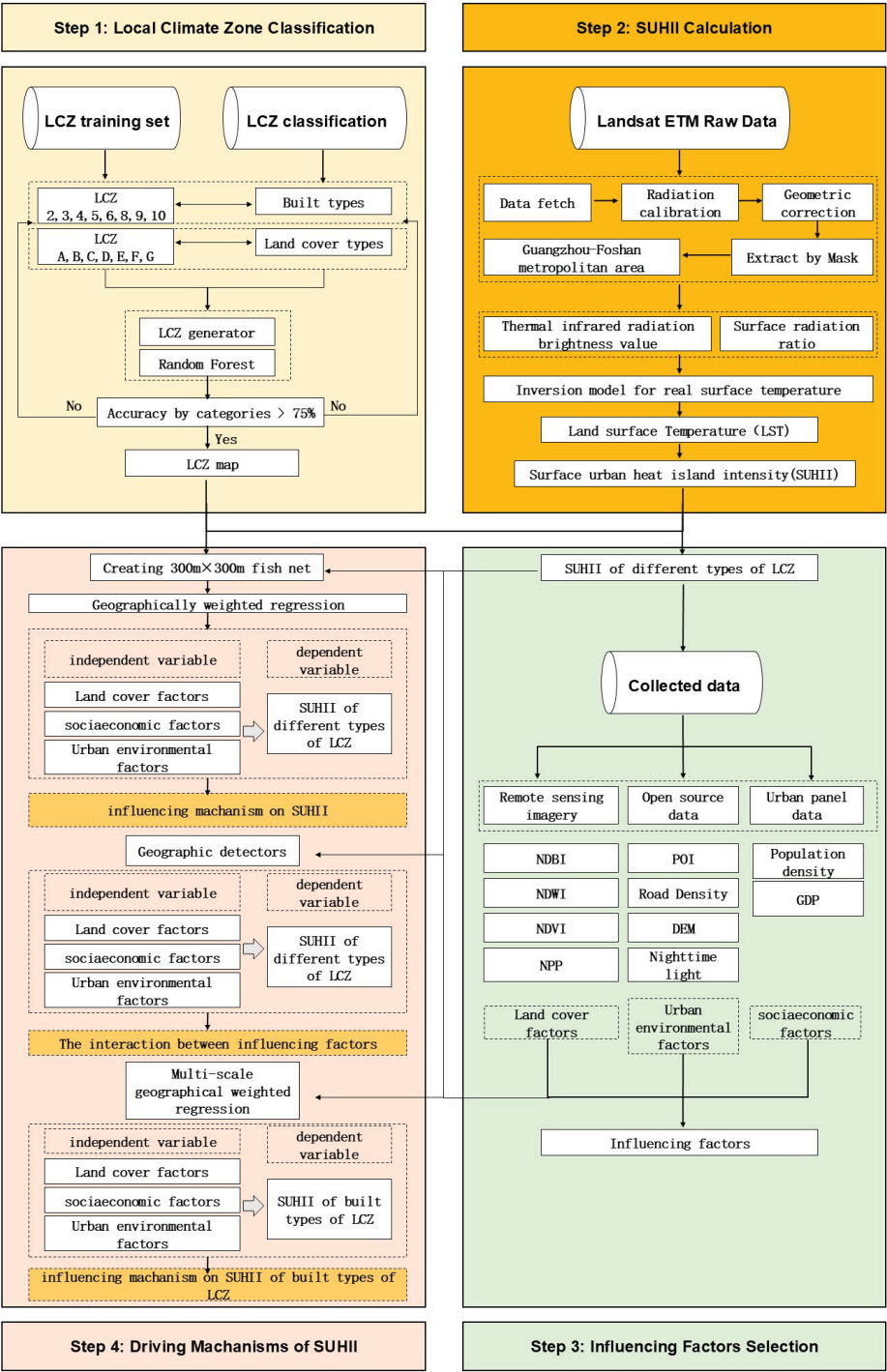**Step 3: Influencing Factors Selection**

Figure 2. The workflow of the research methodology.

2.3.1. Local Climate Zones Measurement

The LCZ generator and random forest classification were the two primary methods employed to create the LCZ mapping in this research [45,53]. The LCZ generator, developed in 2017 based on the World Urban Database and Access Portal Tools (WUDAPT), has been widely used in studies of urban landscape feature analysis and the Urban Heat Island (UHI) effect, as well as in related fields [7,54–58]. The generation logic process involves selecting training sets for different types of LCZs within the research area on Google Maps and exporting these as KML format; the selected area should ideally be within 300 m × 300 m. The generator (https://lcz-generator.rub.de, accessed on 15 May 2024) will select similar images from the WUDAPT database to fit and generate LCZ maps of the target region. In this research, the LCZ classification scheme classified land surface morphology into eight built types and seven land cover types, among which the built types include LCZ 2 (compact midrise), LCZ 3 (compact lowrise), LCZ 4 (open highrise), LCZ 5 (open midrise), LCZ 6 (open lowrise), LCZ 8 (large lowrise), LCZ 9 (sparsely built), LCZ 10 (heavy industry); and the land cover types include LCZ A (dense trees), LCZ B (scattered trees), LCZ C (bush, scrub), LCZ D (low plants), LCZ E (bare rock or paved), LCZ F (bare soil or sand), LCZ G (water) [45,59] (Table 2).

Table 2. List of various types of LCZ training sample examples.
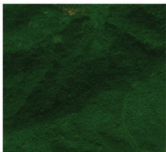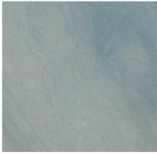
Built Types		Land Cover Types	
LCZ Types	**Training Sample Example**	**LCZ Types**	**Training Sample Example**
LCZ 2 compact midrise		LCZ A dense trees	
LCZ 3 compact lowrise		LCZ B scattered trees	
LCZ 4 open highrise		LCZ C bush, scrub	
LCZ 5 open midrise		LCZ D low plants	
LCZ 6 open lowrise		LCZ E bare rock or paved	

Table 2. *Cont.*

Built Types		Land Cover Types	
LCZ Types	**Training Sample Example**	**LCZ Types**	**Training Sample Example**
LCZ 8 large lowrise		LCZ F bare soil or sand	
LCZ 9 sparsely built		LCZ G water	
LCZ 10 heavy industry			

However, the satellite remote sensing imagery data in WUDAPT database primarily originate from cities in Europe and the Americas, which may render it unsuitable for Asian regions, increasing the likelihood of errors in classifying Asian urban landscapes. To address this issue, this study employed the random forests method to rectify the LCZ maps of the Guangzhou-Foshan metropolitan area produced by LCZ generator. Due to the confusion between LCZ 2 (compact midrise) and LCZ 3 (compact lowrise), as well as confusing LCZ 5 (open midrise) with LCZ 6 (open lowrise) in Asian contexts based on the original WUDAPT LCZ-generator, random forest classification was utilized to reclassify satellite image training samples for these pairs, thereby enhancing the identification accuracy of LCZ types 2, 3, 5, and 6 [60]. For each LCZ type, 5–10 training samples were selected from high-resolution satellite imagery, with adjustments made continuously until the accuracy exceeded 75% [61].

2.3.2. Surface Urban Heat Island Measurement

The measurement of SUHII consists of two steps: (1) computing land surface temperature and (2) comparing the land surface temperature between LCZ X and LCZ D.

Calculating LST involves three parts. First, calculate the fractional vegetation cover index with the following equations [62]:

$$NDVI = (NIR - R)/(NIR + R) \tag{1}$$

$$FC = (NDVI - NDVI_{min})/(NDVI_{max} - NDIV_{min}) \tag{2}$$

where NDVI is Normalized Difference Vegetation Index; NIR indicates the near infrared reflectance; R represents the red band reflectance; FC means the fractional vegetation cover index.

Secondly, calculate black-body radiation brightness value with the following equations:

$$\varepsilon_{surface} = 0.9625 + 0.0614FC - 0.0461FC^2 \tag{3}$$

$$\varepsilon_{building} = 0.9589 + 0.086FC - 0.0671FC^2 \tag{4}$$

where $\varepsilon_{surface}$ is natural surface emissivity and $\varepsilon_{building}$ is urban surface emissivity.

According to the radiation transfer equation and Planck's law, the formula for the black-body temperature (T) in the thermal infrared band is expressed as the following equation:

$$B(T_S) = [L_\lambda - L\uparrow - \tau(1-\varepsilon)L\downarrow]/\tau\cdot\varepsilon \tag{5}$$

where $B(T_S)$ is the temperature of black-body radiant brightness in the thermal infrared band; $L\uparrow$ and $L\downarrow$ represent the upward and downward radiance of the atmosphere; ε indicates land surface emissivity; τ is atmospheric transmittance in the thermal infrared band; and L_λ represents brightness value in the thermal infrared band.

Finally, calculate the LST by $B(T_S)$ with the following equation:

$$LST = K_2/\text{In}(K_1/B(T_S)+1) \tag{6}$$

where LST is land surface temperature; as for K_1 and K_2, according to data from NASA's official website and collaborating websites, it can be inferred that K_1 is $666.09^{w/(m^2\cdot sr\cdot\mu m)}$, $K_2 = 1282.71$ K.

SUHII is defined as the temperature difference between built types LCZ and land cover types LCZ. Considering the characteristics of the Guangzhou-Foshan metropolitan area, LCZ D was selected as the measurement standard for the SUHI effect in this study. The formula for calculation is presented as follows:

$$SUHII = T_{LCZX} - T_{LCZD} \tag{7}$$

where T_{LCZX} represents the temperature of LCZ X and T_{LCZD} indicates the temperature of LCZ D, which consists of low plant surface scenery.

2.3.3. Analysis of Driving Mechanism of SUHI

In previous studies, many scholars have explored the formation mechanisms of urban heat island (UHI) effects based on classifying local climate zones (LCZ). The surface urban heat island intensity (SUHII) in different types of LCZ as a symbolic indicator is often used as the dependent variable. When selecting independent variables, land cover elements are the primary considerations [63]. Some scholars have incorporated urban environment factors on top of the existing land cover factors when conducting urban studies [64–66]. However, as research progressed, the explanatory power of these two factors for SUHI effects proved somewhat insufficient. Subsequently, urban socioeconomic factors were added to the analysis [67–69]. Therefore, in this study, we refer to previous research and comprehensively consider three types of influencing factors: land cover factors, urban environmental factors and social-economic factors (Table 3).

To ensure the depth and comprehensiveness of this study, three kinds of regression models were selected to reveal the impact mechanism of ten independent variables on the SUHI effects in diverse LCZs of the metropolis. Firstly, the GWR model is used to analyze the global characteristics of influencing factors, allowing for the assessment of the average impact of each type of influencing factor on the SUHII of different LCZs, and identifying the most significant factor types within the overall range of the Guangzhou-Foshan metropolitan area. Secondly, based on the GWR model analysis, the MGWR model is employed to further identify the impact of each type of factor on the SUHII of LCZs at different geographical locations. This study examines the effects of different factors in the core, transition, and peripheral areas within the "core-peripheral" metropolitan area. Finally, the geographic detectors (GD) model is used to investigate the interactions between different factors, providing a deeper understanding of how various types of factors influence SUHII of different LCZs.

<div align="center">

Table 3. List of independent variables for SUHII analysis.

</div>

Types	Indicators	Formula	Description
Land cover factors	NDVI	$(NIR - R)/(NIR + R)$	NIR: infrared reflectance; R: red band reflectance
	NDBI	$(SWIR - NIR)/(SWIR + NIR)$	SWIR: Short wave infrared reflectance; NIR: Infrared reflectance
	NDWI	$(Green - NIR)/(Green + NIR)$	Green: Green light band; NIR: Infrared reflectance
	NPP	$GPP - R$	GPP: Gross Primary Productivity; R: The loss of plant respiration
Urban environmental factors	POI kernel density	$f_n(x) = \dfrac{1}{nh} \sum_{i=1}^{n} k\left(\dfrac{x - x_i}{h}\right)$	Where k is the kernel function, h is the smoothing parameter, X is the POI point, and x_i is the sample observation point.
	Road Density (RD)	$D = \sum_{m=1}^{n} (L_m \times V_M)/A_i$	Where D is the line density value, n is the number of lines within the grid point search radius, L is the length of the lines, V is the weight of the lines, and A is the search area centered on the grid point.
	DEM	—	—
	Nighttime light	—	—
Social-economic factors	Population density	—	—
	GDP	—	—

The GWR model was applied to analyze the driving mechanism of SUHI on all types of LCZs, with the final result values ranging between −1 and 1. The closer the result value is to 1, the more positive effect the influencing factor has on SUHI, and the closer the result is to −1, the more negative effect the factor has on SUHII. The formula is as follows:

$$y_i = \beta_0(u_i, v_i) + \sum_{k=1}^{m} \beta_k(u_i, v_i)x_{ik} + \varepsilon_i \tag{8}$$

where y_i represents the SUHII of LCZ X_i; β_0 is intercept; u_i and v_i indicate the longitude and latitude of LCZ X_i; $\beta_k(u_i, v_i)$ is the fitting coefficient of the k explanatory variable of LCZ X_i; x_{ik} means the value of the k explanatory variable at the LCZ X_i; and ε_i is random error term.

The MGWR model is one of the important methods for analyzing spatial heterogeneity. As an optimized model of GWR model, it allows each research variable to have different bandwidths, exploring the impact range and mechanisms of various influencing factors across different geographical spaces. This makes it a more accurate spatial model, resulting in more reliable outcomes. In this study, the MGWR model was exploited to analyze the driving mechanism of SUHII on built types of LCZs, representing the impact of influencing factors on the SUHII of LCZ at different spatial-temporal positions. This study utilizes the MGWR library based on the Python platform [70].

The calculating formula is as follows:

$$y_i = \sum_{j=1}^{k} \beta_{bwj}(u_i, v_i)x_{ij} + \varepsilon_i \tag{9}$$

where bwj represents the bandwidth used for the regression coefficient of the j variable; The vitality index representing the LCZ X_i; y_i represents the SUHII of the LCZ X_i; (u_i, v_i) represents the centroid coordinates of the LCZ X_i; β_{bwj} represents the regression coefficient of the j independent variable of bandwidth in the LCZ X_i; k represents the number of samples; and ε_i represents the random error term.

The GD model was utilized to analyze the driving mechanism of SUHI on all types of LCZs, with its four approaches for analysis: risk detection, factor detection, ecological detection, and interaction detection. This study mainly used factor detection and dual factor interaction detection. In this study, a geographic detector model based on the R language

platform was used, in which the influencing factors were divided into 3–8 categories based on the actual situation [37].

Factor detection can be used to detect the spatial heterogeneity of different types of LCZ. Meanwhile, it can be applied to explore the significance p and correlation q of different influencing factors on SUHI heterogeneity. For the p-value, that under 0.05 indicates a significant impact, that less than 0.01 indicates a more significant impact, while that equal to 0 indicates an extremely significant impact. For the q-value, the specific formula for calculating it is as follows:

$$q = 1 - \frac{\sum_{i=1}^{L} N_i \sigma_i^2}{N\sigma^2} \tag{10}$$

where up-script L represents the classification number of the influencing factors; N is the total number of samples; N_i is the total number of the i type factor; σ_i^2 is the variance of the i type factor; and σ is the variance of SUHI for different types of LZC. The range of q-value is presented as: $q \in [0, 1]$. The larger the q-value of the influencing factor, the stronger its impact on SUHI.

The interaction detector was used to identify the explanatory power of SUHI, explaining how factors impact on different LCZs when any two influencing factors work together. As shown in Table 4, the geographical detector (GD) explanatory power can be divided into five types.

Table 4. List of geographical detector explanatory types.

Types	Formula	Degree of Influence
nonlinear enhancement	q(X1∩X2) > q(X1) + q(X2)	Strong
independent	q(X1∩X2) = q(X1) + q(X2)	Relatively Strong
linear enhancement	q(X1∩X2) > Max(q(X1), q(X2))	Average
weakening	Min(q(X1), q(X2)) < q(X1∩X2) < Max(q(X1),q(X2))	Relatively weak
nonlinear attenuation	q(X1∩X2) < Min(q(X1),q(X2))	weak

3. Results

3.1. LCZ Maps

The characteristics of the surface landscape in the Guangzhou-Foshan metropolitan area were classified by LCZ generator and random forest. After several rounds of adjustment, the final Kappa coefficients turned out to be 0.88 (2013), 0.76 (2018), and 0.91 (2023) (Figure 3). Among built LCZ types, sparsely built (LCZ9) and Large lowrise (LCZ8) took up the largest proportion of land within the overall scope, while open highrise (LCZ4) and open midrise (LCZ5) had the largest proportion of land area in the central urban area. As for the factors in land cover LCZ types, dense tree (LCZ A) has the largest land occupation ratio.

Figure 4 and Table 5 illustrate the change of diverse LCZs in 2013, 2018 and 2023. This figure demonstrates a significant growth trend in highrise (LCZ4), open midrise (LCZ5) and sparsely built (LCZ9), with LCZ9 having the largest growth area, increasing from 1618.563 km^2 to 1755.408 km^2, leading to a total growth of 136.845 km^2. LCZ4 had the second largest growth area, with a total growth of 80.557 km^2, increasing from 450.274 km^2 to 530.831 km^2. LCZ5 was the object of the least growth of 74.152 km^2 in area, increasing from 786.609 km^2 to 860.761 km^2. On the contrary, Large lowrise (LCZ8), bush, scrub (LCZ C) and bare rock or paved (LCZ E) represented a remarkable reduced trend, with LCZ8 experiencing the most drastic drop from 1285.022 km^2 to 917.980 km^2, a total decrease of 367.042 km^2. LCZ E decreased the second most in area, from 152.330 km^2 to 90.305 km^2, marking a total decrease of 62.025 km^2. LCZ C had the least decrease of 39.849 km^2, from 138.346 km^2 to 98.515 km^2.

a. LCZ maps of Guangzhou-Foshan metropolitan area in 2013

b. LCZ maps of Guangzhou-Foshan metropolitan area in 2018

c. LCZ maps of Guangzhou-Foshan metropolitan area in 2023
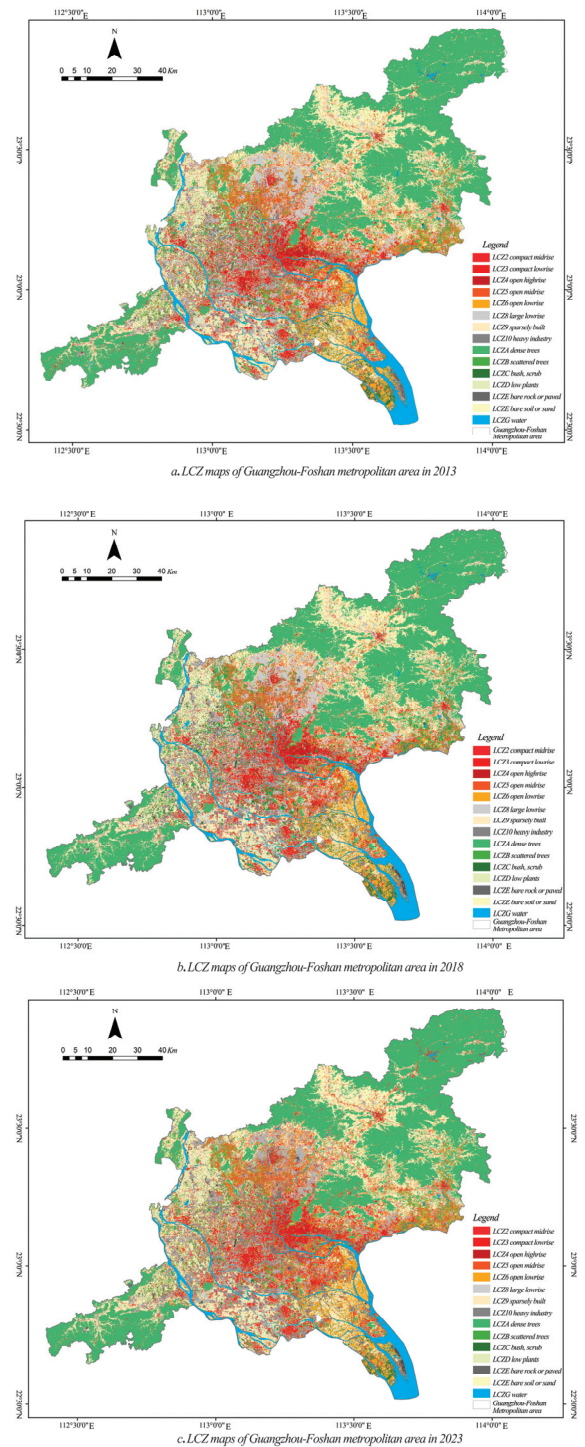
Figure 3. LCZ maps of Guangzhou-Foshan metropolitan area in 2013 (**a**), 2018 (**b**), 2023 (**c**).
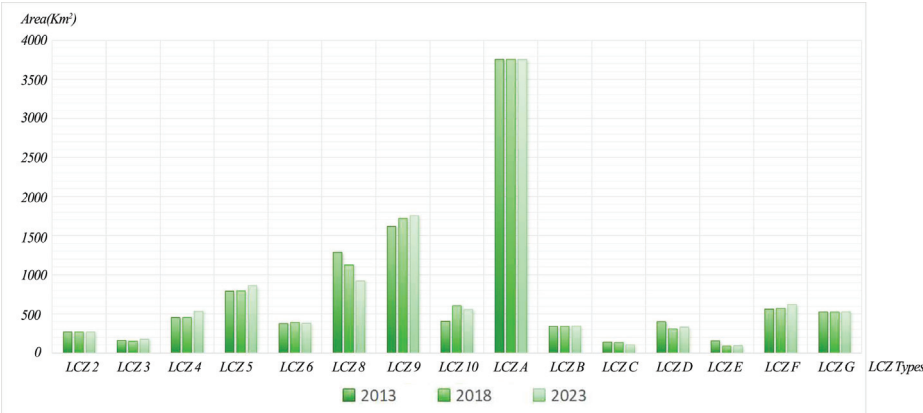
Figure 4. The trend of area variation for different LCZs in 2013, 2018 and 2023.

Table 5. Area variation of different types of LCZs in 2013, 2018 and 2023 (km^2).

Years	2013	2018	2023
LCZ Types	Area (km^2)		
2	267.162	267.806	267.381
3	157.042	151.017	174.357
4	450.274	450.236	530.831
5	786.609	791.185	860.761
6	375.630	388.973	377.779
8	1285.022	1125.337	917.980
9	1618.563	1718.923	1755.408
10	403.269	601.363	553.087
A	3753.009	3757.327	3757.472
B	337.218	338.616	346.711
C	138.346	133.454	98.515
D	397.150	304.506	329.785
E	152.330	83.679	90.305
F	558.028	567.559	619.909
G	524.774	524.445	524.145

3.2. LST and SUHI of Guangzhou-Foshan Metropolitan Area

The Guangzhou-Foshan metropolitan area presents a complete core-periphery urban structure, resulting in a significant decrease of LST from the center to the outer edge of the metropolitan area. Figure 5 represents the spatial-temporal distribution of LST in Guangzhou-Foshan metropolitan area in 2013, 2018 and 2023, from which it can be observed that the LST in the central urban areas is significantly higher than the LST in the surrounding suburban areas. The central urban areas mainly consist of compact lowrise (LCZ3), open highrise (LCZ4) and open midrise (LCZ5) urban morphology, represented by Liwan District, Tianhe District, Yuexiu District, and Baiyun District in Guangzhou city, as well as Nanhai District and Chancheng District in Foshan city.

Based on the LST calculation results above, this paper computed SUHII by Formula (7). This study divided SUHII into seven types based on previous researches referred to in the literature review and practical experience: Super strong heat island (VII, 7 K < SUHII), Strong heat island (VI, 5 K < SUHII < 7 K), Normal heat island (V, 3 K < SUHII < 5 K), Weak heat island (IV, 1 K < SUHII < 3 K), No heat island (III, −1 K < SUHII < 1 K), Weak cold island (II, −3 K < SUHII < −1 K), Strong cold island (I, −3 K > SUHII) [26,71]. Figure 6 presents the spatial-temporal distribution of SUHII in Guangzhou-Foshan metropolitan area in 2013, 2018 and 2023, by observing which it can be inferred that the SUHI appears

to be the strongest in the core area of the Guangzhou-Foshan metropolitan area, such as Liwan district, Yuexiu district in Guangzhou, and Nanhai district, Chancheng district in Foshan, with a radiate attenuation outwards.
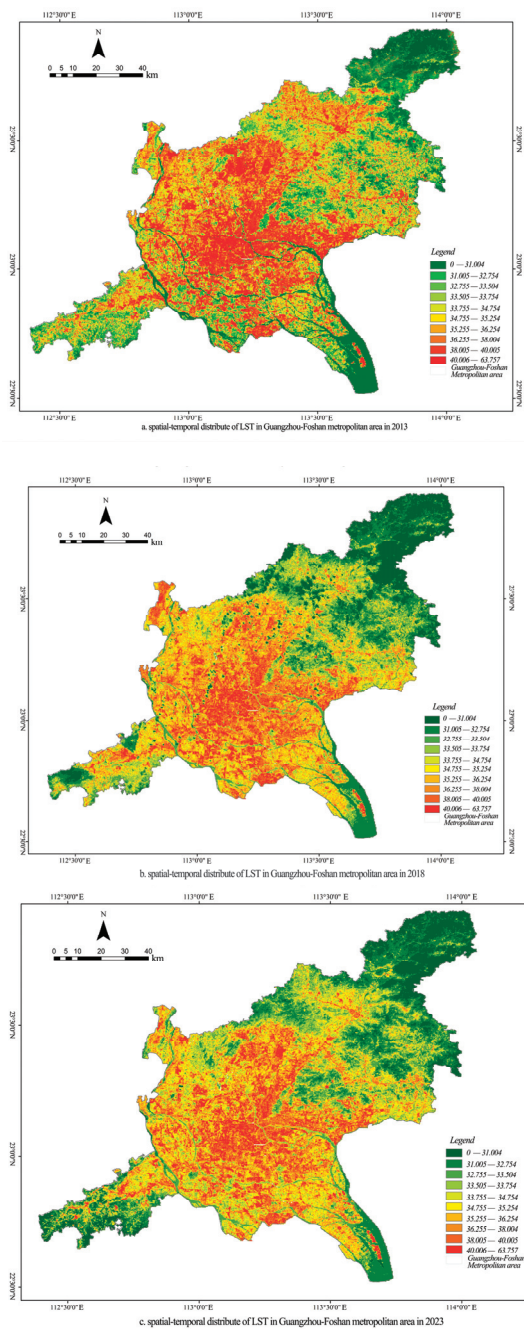

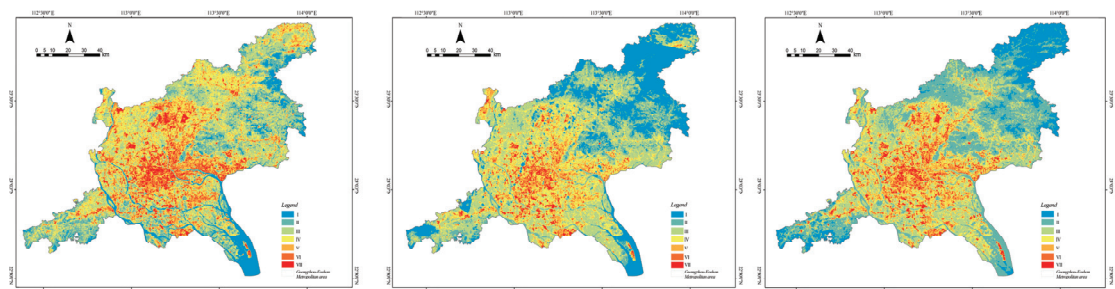**Figure 5.** Spatial-temporal distribution of LST in Guangzhou-Foshan metropolitan area in 2013 (**a**), 2018 (**b**), 2023 (**c**).

Figure 6. Spatial-temporal distribution of SUHI effect in Guangzhou-Foshan metropolitan area in 2013 (**left**), 2018 (**middle**), 2023 (**right**).

The analysis results above show that the urban central area of Guangzhou-Foshan metropolis experienced severe SUHI effects in the summers of 2013, 2018, and 2023. Despite the fact that, generally speaking, the overall SUHI effects of Guangzhou-Foshan metropolitan area have been alleviated, they are still intensifying in urban core functional areas, especially in high-density high-rise areas (Table 6). In the summer of 2013, the land area with SUHI effect was 5232.58 km^2, accounting for 45.94% of the total land area. Among different types of land area with SUHI effects, Type VII (Super strong heat island) had an area of 391.49 km^2, accounting for the largest proportion of 3.44%. Furthermore, in the summer of 2018, the area with SUHI effect was 4088.73 km^2, accounting for 35.90% of the total area, while Type VII (Super strong heat island) took up 399.46 km^2, accounting for a proportion of 3.51%. Whereas in the summer of 2023, the area with SUHI effects was 3901.32 km^2, accounting for 34.25%, with Type VII covering an area of 412.38 km^2, accounting for the proportion of 3.62%.

Table 6. The land area and proportion of the SUHI effect in the Guangzhou-Foshan metropolis.

SUHII Types	Area (2013) km^2	Percentage (2013)	Area (2018) km^2	Percentage (2018)	Area (2023) km^2	Percentage (2023)
VII (Super strong heat island)	391.49	3.44%	399.46	3.51%	412.38	3.62%
VI (Strong heat island)	814.76	7.15%	595.91	5.23%	562.59	4.94%
V (Normal heat island)	1515.06	13.30%	938.43	8.24%	1069.11	9.39%
IV (Weak heat island)	2511.27	22.05%	2184.93	19.18%	1857.24	16.31%
III (No heat island)	3261.69	28.64%	3510.9	30.83%	3054.96	26.82%
II (Weak cold island)	1749.15	15.36%	1656.36	14.54%	3130.38	27.49%
I (Strong cold island)	1145.99	10.06%	2103.42	18.73%	1302.75	11.44%

Figure 7a shows the distribution of blocks with extreme SUHI effects in the Guangzhou-Foshan metropolitan area from 2013 to 2023, and Figure 7b–f zoom in to display key blocks.

Figure 7b illustrates the SUHI effects of the important transportation hubs and their surrounding neighborhoods. As shown in the figure, there are two types of spaces that are more likely to be the object of SUHI effects: one type of space features blocks with a large area of hard paving, which is similar to the environment of Baiyun Airport; the other type of space is the urban central areas or urban functional areas featured by a large number of high-rise and compact buildings with diverse urban residential, commercial and recreational facilities.

As shown in Figure 7c, the SUHII value in the blocks around Yongqingfang, Beijing Road and the Pearl River New Town on the north side of the Pearl River front channel is relatively high. These blocks are mainly the central commercial and residential areas of Guangzhou city, characterized by dense road networks, large neighborhoods with high density, and numerous high-rise buildings. On the contrary, Figure 7d presents the blocks

of high SUHI effects in Nanhai district in Foshan city, mainly consisting of large urban villages mixed with industrial zones.

As shown in Figure 7e, the high SUHI effect areas in Panyu District, Guangzhou City present scattered distribution. Similar to the urban morphology of Figure 7d, these areas are also composed of scattered villages mixed with a large area of industrial factory buildings.

Figure 7f shows the urban morphology of the Shunde District Government in Foshan City, with high-density residential and commercial areas covering the land, resulting in high SUHI effects.
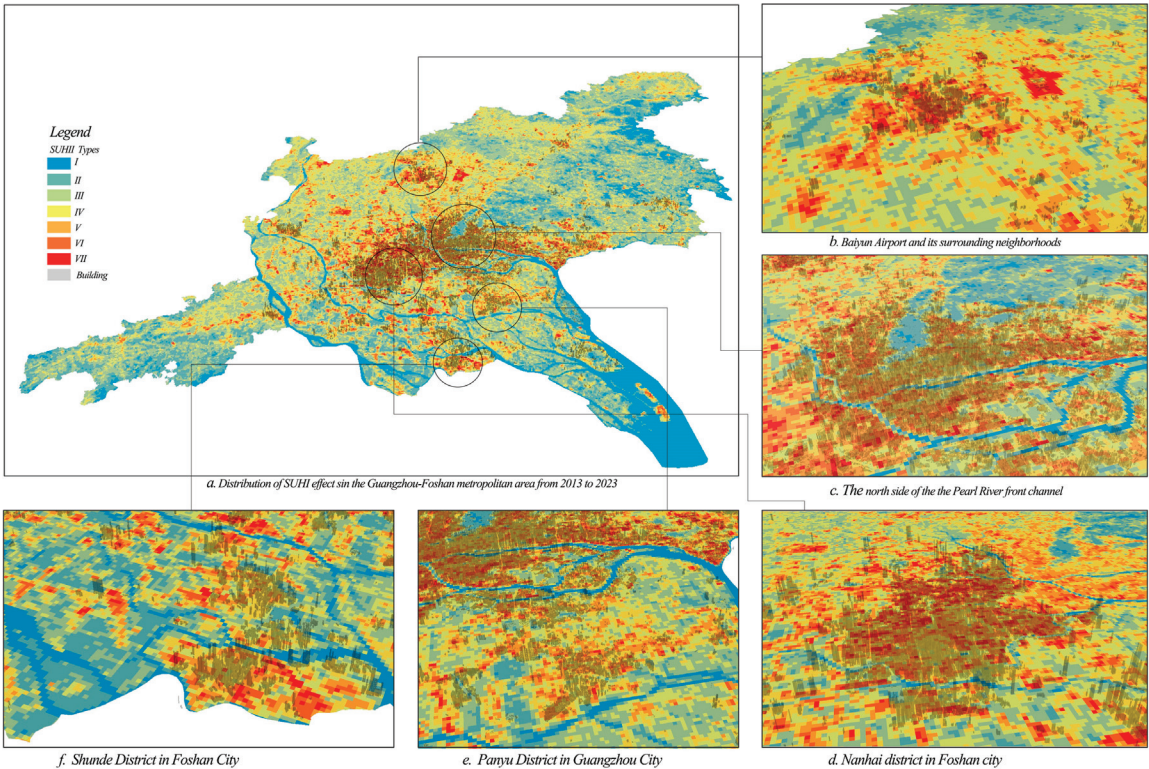
Figure 7. SUHI effects distribution in the Guangzhou-Foshan metropolitan area.

3.3. Analysis of SUHI Influential Factors

3.3.1. The Relationship between Local Climate Zones and SUHI Effects

As shown in Figure 8, the SUHI effects of built types LCZs are significantly higher than those of the land cover types. Among the built types, LCZ 8 (large lowrise) and LCZ10 (heavy industry), characterized by large areas of impervious surfaces, substantial building volumes, and a lack of green coverage, have the most significant SUHI effects. These areas are also known for their vast blocks (typically over 300 m × 300 m) and wide roadways. Moreover, the SUHI effect of LCZ3 (compact lowrise) and LCZ4 (open highrise) is also significant in the built type. The main urban morphology of LCZ3 in the Guangzhou-Foshan metropolitan area is urban villages, while LCZ4 is mainly high-density, high-plot ratio residential areas with typical building heights of 12 floors or more, experiencing its fastest development between 2005 and 2015.
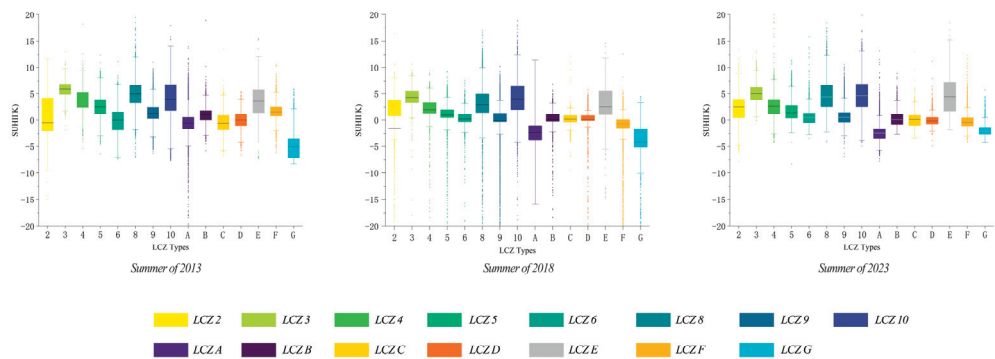
Figure 8. SUHII (K) of diverse LCZ types.

Among land cover types, the SUHI effect is more pronounced in LCZ E (bare rock or paved) and LCZ F (bare soil or sand). In the Guangzhou-Foshan metropolitan area, LCZ E is mainly composed of important transportation hubs, such as Guangzhou Baiyun Airport, Guangzhou South Station, Foshan Station, Foshan West Station, etc. The characteristic of this land cover type is that there are large areas of hard paving and large open squares with less green coverage. In contrast, the composition of LCZ F is much more complex. Through careful comparison, it is found that LCZ F includes pond fish farms, exposed farmland, and reorganized but not yet developed land.

From the comparison of the data collected in the summers of 2013, 2018, and 2023, it can be observed that the SUHI effects of LCZ2 (compact midrise) have been intensifying year by year, while the SUHI of LCZ3, LCZ4, and LCZ5 remained high. Such phenomenon indicates that the implementation of a series of greening-related policies such as park and community green space construction did not make significant impact on the alleviation of SUHI effects.

3.3.2. GWR Analysis of SUHI Effect Influential Factors

This study conducted a global regression analysis using GWR on the factors that may impact SUHI effects in 2013, 2018, and 2023. In the analysis results of GWR, the q-value, ranging from −1 to 1, represents the correlation between the factor under analysis and SUHI effects. The higher the absolute value, the greater the impact of the influencing factor on the SUHI effect. The *p*-value represents the significance of the influencing factors, with smaller values indicating a more significant impact. When the *p*-value is less than 0.05, the factor under analysis can be considered a significant influencing factor.

As shown in Figure 9, the q-values of NDVI and NDWI ranged from −0.66 to −0.1, indicating a significant negative impact on the SUHI effects of almost all types of LCZ, especially on LCZ2, LCZ4, LCZ5, and LCZ8. On the contrary, the q-value of NDBI ranging from 0.1 to 0.84 indicated a significant positive influence on the SUHI effects of diverse LCZ, particularly on LCZ3 and LCZ10.

Furthermore, factors such as RD, POI, and POP also had a significant positive impact on SUHI effects. To be more specific, RD had a significant positive impact on the SUHI effects of LCZ2, LCZ3, and LCZ4 in 2013, with q-values being 0.15, 0.19, and 0.14, respectively; in 2018, with q-values of 0.15 and 0.12, RD demonstrated a significant positive impact on LCZ2 and LCZ6; in 2023, the significant positive impact was on LCZ2, 3, 4, 5, 6, 8, and 10, with q-values ranging from 0.13 to 0.34. As for POI, it also had a positive impact on almost all types of LCZ in 2013, 2018, and 2023, with q-values ranging from 0.027 to 0.23. The impact of POP is similar to that of the two aforementioned factors, with a q-value range from −0.021 to 0.12.
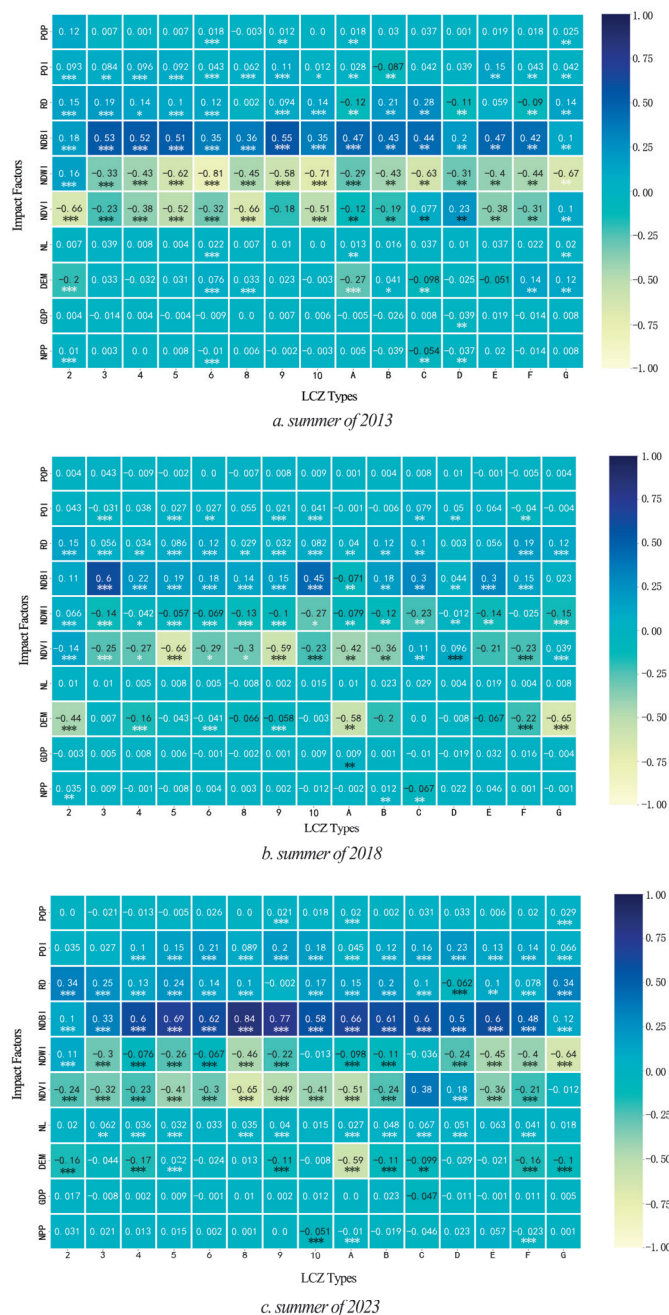
Figure 9. LCZ-based variables' coefficients on SUHII in 2013 (**a**), 2018 (**b**), and 2023 (**c**). (Note: * indicates significant at $p < 0.05$, ** indicates significant at $p < 0.01$, *** indicates significant at $p < 0.001$).

Finally, factors such as GDP, NPP, NL, and DEM also impacted the SUHI effects of different types of LCZ in some periods, but in a comparatively less significant way, with their q-values generally distributed between -0.001 and 0.07.

3.3.3. MGWR Analysis of SUHI Effect Influential Factors

On the basis of the GWR analysis in the previous section, further analysis was conducted on the LCZ of built types, utilizing the MGWR model to analyze the impact of different influencing factors on SUHI effects at different geographical locations in the Guangzhou-Foshan metropolitan area.

First of all, as shown in Figure 10, in 2013, the factors having the greatest impact on the SUHI effects in built type of LCZ were land cover factors (NDVI, NDBI, NDWI), among which NDVI and NDWI showed significant negative effects, while NDBI showed significant positive effects. The significance of the negative effect of NDVI and NDWI diverges from area to area, with a trend of greater negative impact in the core area and less negative impact in the peripheral area for LCZ 2, and a decreasing negative impact from east to west for LCZ 3. For LCZ 4 and LCZ 5, higher impact was exhibited in the northern part, with lower impact in the southern part of the metropolis. For LCZ 6–10, the impact demonstrated an outward decrease, with the significance of the impact lessening from the center of the urban block cluster to the peripheral area. As for NDBI, among the various built types of LCZs, the urban core such as the central business district had a high impact on the SUHI effects, while low impact was exhibited in the peripheral area. Moreover, urban environmental and socioeconomic factors such as POI and POP generally had a positive impact on the SUHI effects, with the overall trend showing higher impact in the urban core area and lower impact in the suburban or periphery area. Additionally, the RD factor belonging to urban environmental factors exhibited significant spatial heterogeneity, with an overall positive impact on the SUHI effects. Specifically speaking, it showed a significantly negative impact in the city center and a significantly positive impact in the outskirts or suburban areas.

Secondly, Figure 11 displays the results from the analysis of the impact factors of SUHI effects on different built types LCZs in 2018, using the MGWR model as the approach. Compared to the situation in 2013, land cover factors (NDVI, NDBI, NDWI) still had a significant impact on the SUHI effects of all built types LCZs. The main positive influencing factors included NDBI and POI, while the main negative influencing factors turned out to be NDVI, NDWI, and NPP. Different from the factors above, DEM exhibited different impact types in different locations, with a significant negative influence in the city center, but a significant positive effect in the suburban mountainous areas, especially in the northern part of the Guangzhou-Foshan metropolitan area. Similar to DEM, RD also exhibited significant spatial heterogeneity, with a negative influence in the city center and a positive influence in the port area in the southern part of the Guangzhou-Foshan metropolitan area.

To be more specific, the negative impact of NDVI and NDWI is more significant in the city center in LCZ 3–5. Nevertheless, such negative impact was not that significant in the city center of LCZ 2, 6, 7, 8, and 10, some of which were even the object of positive impact. Moreover, the impact of NDBI on LCZ5, 6, 8, and 9 is not as significant as its impact on other areas, while the impact of POI on the SUHI effects of LCZ 3, 5, 6, 9, and 10 is more significant than that of other areas, showing an influential situation where the south had greater impact than the north did and the west with greater impact than the east. As for the RD factor, it had a significant impact on the SUHI effects of built types LCZs, generally showing a negative impact in the central areas of the metropolis and a positive impact in the peripheral areas, with the port area in the southern part of the Guangzhou-Foshan metropolis circles having the most significant positive impact.

Finally, Figure 12 illustrates the results from the analysis of the driving mechanism of SUHI effects in 2023 through the application of the MGWR model. Compared with the analysis of 2013 and 2018 stated above, this analysis had the following similarities: (1) NDVI and NDWI had negative impacts on the SUHI effects of most LCZs; (2) NDVI and POI had significant positive impacts on the SUHI effects. The difference lies in: (1) the ability of NDVI and NDWI to alleviate SUHI effects is further weakened, especially for LCZ 2 and LCZ 3. NDVI and NDWI did not effectively slow down SUHI effects. (2) The positive impact of POI on SUHI effects is greater than NDBI, especially in the central urban area of the Guangzhou-Foshan metropolis, to be more specific, LCZ 4, LCZ 5, and LCZ 8.

(3) The negative effect of RD on SUHI effects is more significant in the central urban area, especially for LCZ 2, 3, 4, and 5.
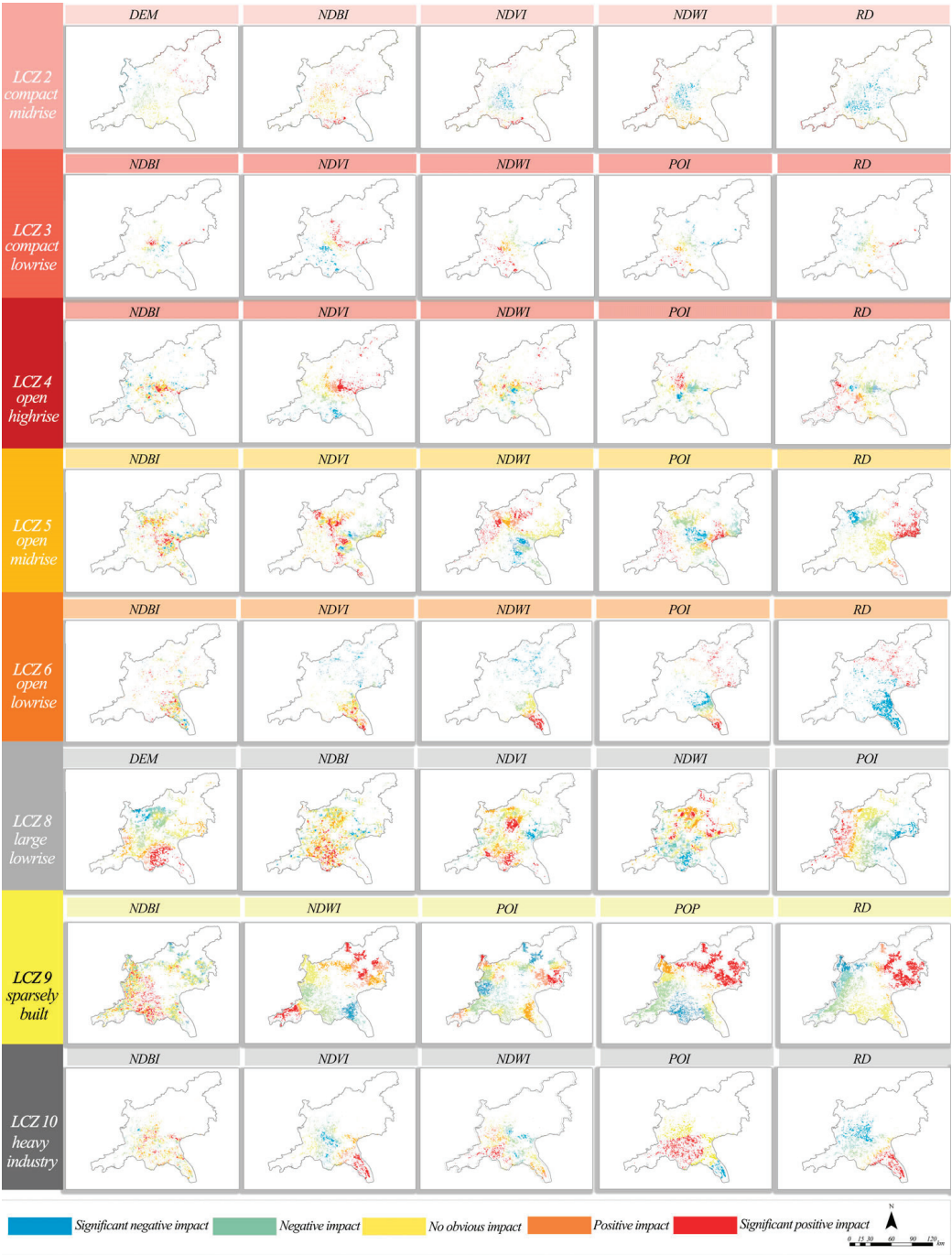

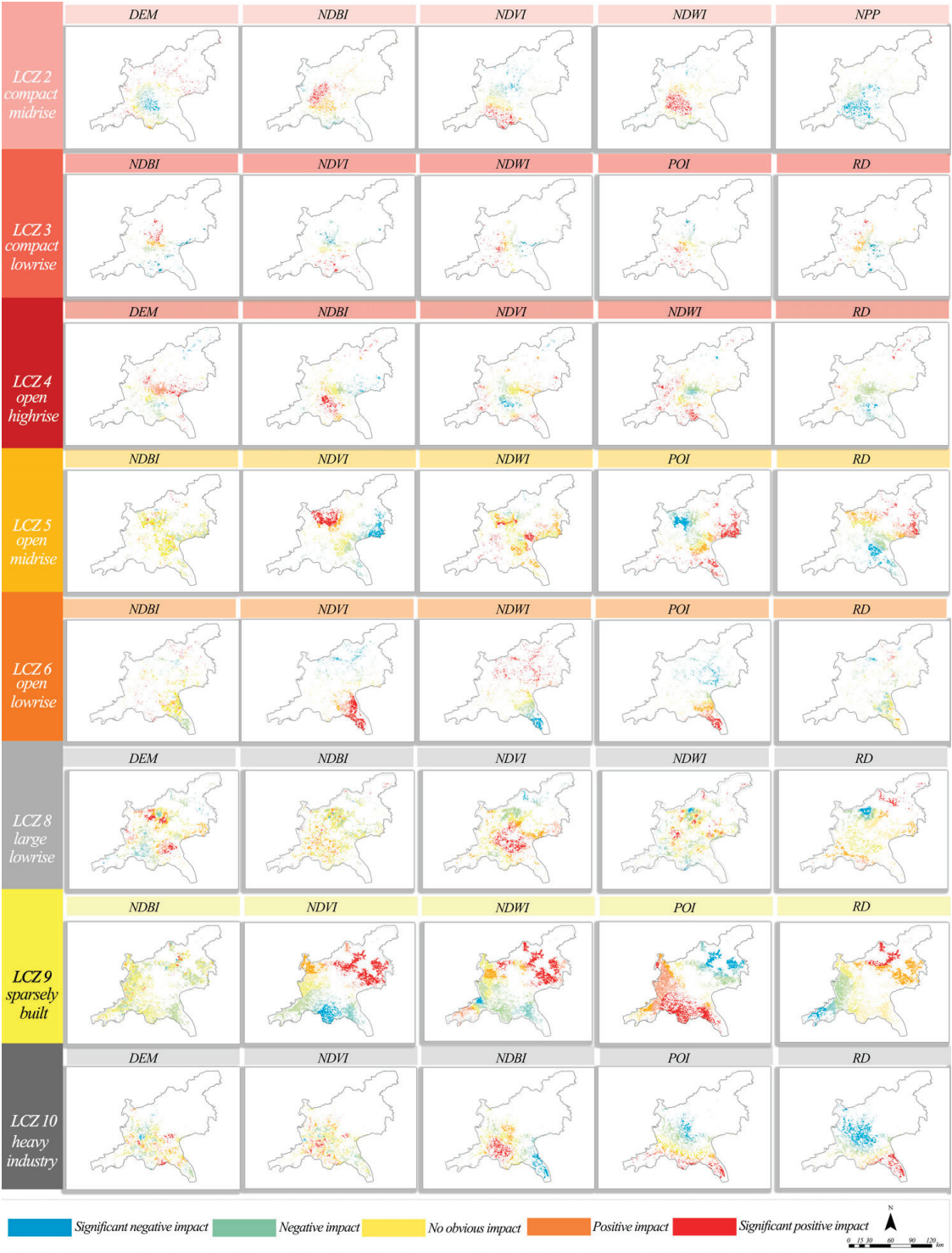**Figure 10.** MGWR analysis of SUHI effects influential factors of built type LCZs in 2013.

Figure 11. MGWR analysis of SUHI effects influential factors of built type LCZs in 2018.
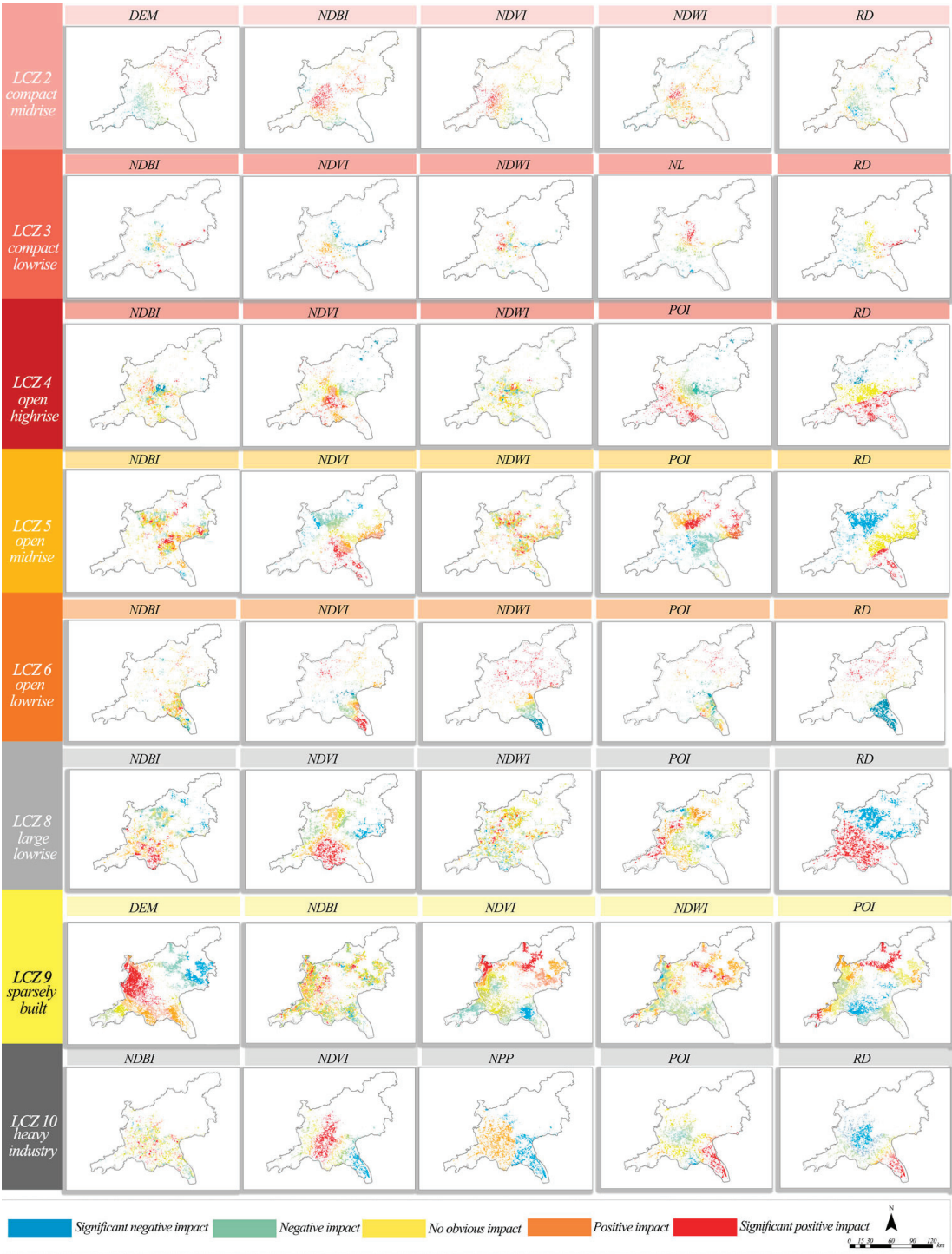
Figure 12. MGWR analysis of SUHI effects influential factors of built type LCZs in 2023.

To summarize, there were three findings through the analysis of the driving mechanisms of SUHI effects in 2013, 2018, and 2023: firstly, with time going by, the types of factors that affect the SUHI effects gradually increase and show a diversified trend; secondly, the spatial heterogeneity of land cover factors (NDVI, NDWI, NDBI) is significant, showing different impact effects at different locations in the Guangzhou-Foshan metropolis; thirdly, the explanatory power of the influencing factors reflects that the power of land cover factors was greater than that of urban environmental factors, which is also greater than that of social economic factors.

3.3.4. GD Analysis of SUHI Effects Influential Factors

The above analysis by GWR and MGWR has explored the impact of different influencing factors on the SUHI effects of different types of LCZ. The further exploration of the impact mechanism of SUHI effects was conducted using the GD model to explore the impact of different influencing factors and the impact of their interactions on the SUHI effects of different types of LCZ in 2013, 2018, and 2023 [37,72,73]. The result values (q-values) of the GD model are distributed between 0 and 1. The closer the q-value is to 1, the greater the impact on SUHI effects is. Unlike GWR and MGWR models described in the previous section, the GD model bears the disadvantage that it is not possible to determine whether the influencing factor has a positive or negative impact on SUHI effects, for there are no positive or negative q values in the GD model.

Figure 13 visually displays the q-values indicating the significance of the impact of individual influencing factors and that of their interactions on SUHI effects of diverse LCZ in 2013, 2018, and 2023. As shown in Figure 13a, in 2013, in terms of single factor impact, NDVI, NDBI, and NDWI had the highest impact on SUHI effect, with q-values of 0.371, 0.392, and 0.343, respectively. Considering the impact of interactions between factors on SUHI effects, the interaction between NDWI and NDBI had the most significant impact on SUHI effects, with a q-value of 0.598. Other significant interaction effects include: NDVI ∩ NDBI (0.582), NDVI ∩ NDWI (0.535), NDWI ∩ POI (0.532), NDBI ∩ POI (0.517), etc. These results indicated the fact that land cover factors, whether in terms of single factor influence or dual factor interaction, still played an important role in the driving mechanism of SUHI effects.

Figure 13b shows the results from the interaction detector of the GD model in 2018. In terms of single factor influence, POI demonstrated a significantly increased impact on the SUHI effects, with the q-value increasing from 0.305 in 2013 to 0.461 in 2018. The impact of NDVI on the SUHI effect is the second most significant one, with a q-value of 0.459. The q-values of NDVI and NDWI were both 0.351, following the q-values of POI and NDVI. In terms of dual factor interaction, similar to the situation in 2013, NDWI ∩ NDBI had the highest q-value of 0.798, while other interactions with less significant impact included NDVI ∩ NDWI (0.61), NDVI ∩ NDBI (0.6), POI ∩ NDWI (0.601), NL ∩ NDWI (0.577), RD ∩ NDVI (0.532), NDVI ∩ POI (0.523), RD ∩ NDBI (0.514), etc.

Figure 13c displays the results of GD analysis in 2023. In terms of single factor impact, compared to the factors in 2013 and 2018, the number of factors that affect SUHII is significantly larger in 2023, with the factors arranged from that of high q-value to that of low one as: POI (0.492), NDWI (0.478), NDVI (0.385), RD (0.382), NDBI (0.367), and DEM (0.341). In terms of factor interaction, the interaction effect between NDWI and POI is relatively significant, with a q-value of 0.638. The other interaction effects with lower q-values are RD ∩ NDWI (0.6), POI ∩ NDBI (0.594), POI ∩ NDVI (0.562), POI ∩ DEM (0.543), NDVI ∩ NDWI (0.537), DEM ∩ NDWI (0.534), etc. To summarize, the number of factors that have a significant impact on SUHI effects increased from the years 2013 and 2018 to 2023, with only land cover factors having a greater impact on SUHI in the past years while urban environmental factors and social economic factors gradually increased their impact to the significant level in 2023.

a. summer of 2013
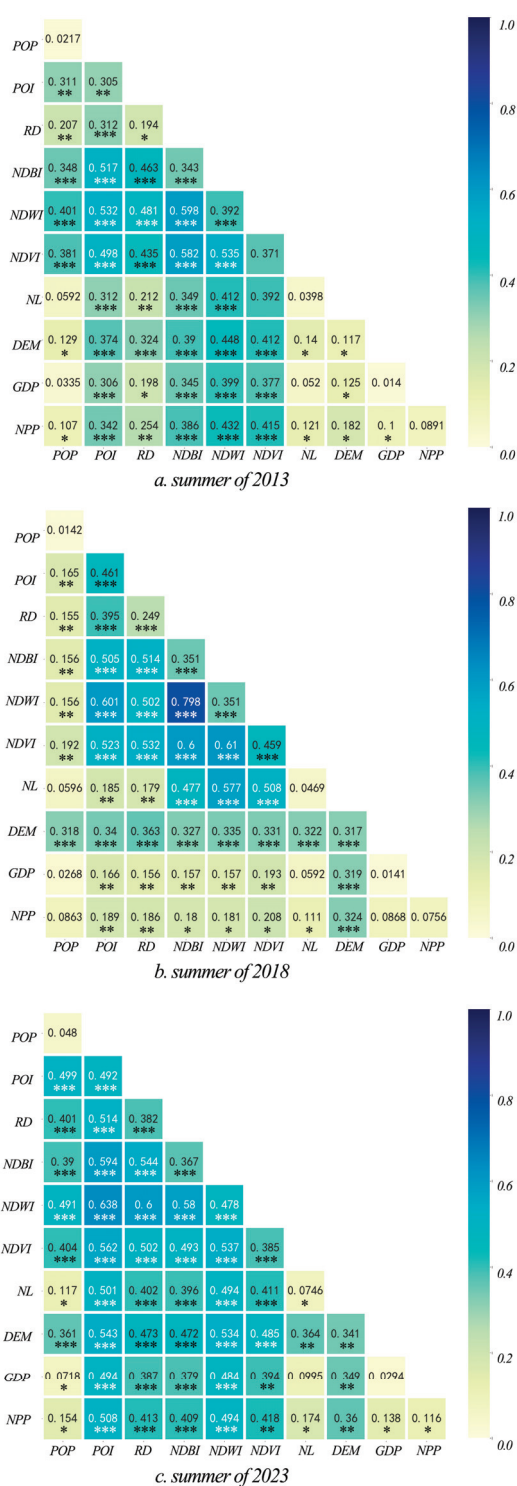
b. summer of 2018

c. summer of 2023

Figure 13. Contributions of influencing factors on SUHI effects. (Note: * indicates significant at $p < 0.05$, ** indicates significant at $p < 0.01$, *** indicates significant at $p < 0.001$).

4. Discussion

4.1. The Spatial Heterogeneity of the SUHI Effects

Determining the surface urban heat island (SUHI) effects in various locations within a metropolis is always a crucial consideration. When investigating the surface urban heat island effects in target areas, while field observations were employed to obtain land surface temperature (LST), remote sensing images were more commonly used, often in conjunction with the analysis of local climate zones (LCZs) [64]. In previous studies, different types of Local Climate Zones (LCZs) have demonstrated varying surface urban heat island intensities (SUHII) based on the time and location of the research. However, a common finding across these studies is that LCZs 2, 3, 8, and 10 consistently show high surface urban heat island intensities (SUHII) [74–76].

Based on the results presented above, the spatial heterogeneity of the SUHI effects in the Guangzhou-Foshan metropolis demonstrated a significant core-periphery pattern. Figure 9 shows that the SUHII in the central area of the Guangzhou-Foshan metropolis is significantly higher than that in the surrounding areas, with the peak values of SUHII in 2013, 2018 and 2023 being 16.05 K, 15.20 K and 18.49 K, respectively. Similar to the research conducted in Wuhan, Nanjing, Changzhou, Chongqing, and Hefei, the LCZ types contributing the most to the SUHI effects were LCZ 2, 3, 4, 5, 8, and 10 [19,77–80]. In the central part of the Guangzhou-Foshan metropolitan area, the SUHI effects were mainly driven by LCZ 2, 3, 4, and 5, which were primarily characterized by urban villages, residential areas, and old neighborhoods, such as the South Residential Block in Panyu District, old neighborhoods in Liwan District, and large urban villages in Yuexiu District. In the peripheral area of the Guangzhou-Foshan metropolis, the SUHI effects were mainly triggered by LCZ 8 and LCZ 10, with the potential triggers being their components like transportation hubs, village-level industrial zones, and industrial zones mixed with urban villages, such as Baiyun Airport and Nanhai Industrial zones.

What is more, according to Figure 8, within the Guangzhou-Foshan metropolitan area, the surface urban heat island intensity (SUHII) in northern mountainous regions is significantly higher than that in southern coastal areas for LCZs of the same type. Consistent with other studies, LCZ3, LCZ8, and LCZ10, which are situated in mountainous areas, demonstrate the highest surface urban heat island intensity (SUHII). To further investigate the influencing factors, we employed the MGWR model, which effectively analyzes geographic spatial heterogeneity, to examine the underlying impact mechanisms [64,81].

4.2. Analysis of Main Influential Factors of SUHI Effects

Existing research has utilized various quantitative analysis models to examine the causes of the SUHI effects across different Local Climate Zones (LCZs). Among these, Ordinary Least Squares (OLS) is the most commonly employed method, primarily focusing on the global impact of various influencing factors on the Surface Urban Heat Island Intensity (SUHII). As research has progressed, the spatial heterogeneity of the urban heat island effect has gained increasing attention, particularly in studies utilizing LCZs. Different types of LCZs in various geographical locations demonstrate distinct heat island intensities. Consequently, models capable of analyzing spatial heterogeneity, such as Geographically Weighted Regression (GWR) and Multiscale Geographically Weighted Regression (MGWR), have begun to be adopted [82–85].

In this study, three types of regression models, GWR, MGWR, and GD, were applied to the analysis of SUHI effects to explore the driving mechanism. The results from GWR and MGWR models were similar in that both models exhibited that land cover factors played the most important role in the SUHI effects, with NDVI and NDWI being the most significant negative factors affecting the SUHI effects, and NDBI being the most significant positive factor. Different from the significant impact of land cover factors, the influence of urban environment factors was comparatively less. Among urban environment factors, POI and RD had a relatively strong impact on the SUHI effects, while DEM only had a relatively significant impact on some built types LCZ, such as LCZ 2, LCZ 4, LCZ 8, and LCZ 10. The

spatial heterogeneity of the impact of DEM on SUHII in this study was relatively greater than that in the results of other researches [86,87]. Unlike other influencing factors, DEM had a non-linear impact on SUHII, mainly affecting mountainous areas with elevations above 98 m and coastal areas with elevations below 26 m. Furthermore, the analysis of the interactions between the influencing factors was conducted by the application of the GD model, the results of which showed that, in 2013 and 2018, the interaction results between NDWI and NDBI were the highest, with q-values of 0.598 and 0.798, respectively, while in 2023, the interaction results between NDWI and POI were the highest, with a q-value of 0.638. In summary, from 2013 to 2023, the impact of urban environmental factors and social economic factors on SUHI effects gradually increased, and their interactive impact values also gradually increased. The factors that influenced SUHI effects showed a diversified trend overall.

4.3. Policy Recommendations to Alleviate SUHI Effects

Based on the results and findings in this research, the following three policy recommendations can be proposed to mitigate the SUHII: firstly, since the results of this study showed that NDVI and NDWI had the highest negative impact on SUHII as single factors, especially for LCZ2 and LCZ3, it is necessary to introduce more related land types, such as small parks and water bodies in cities, especially pocket parks and lake water bodies. Based on previous research findings by scholars, it has been proven that such measures are effective in mitigating the SUHI effects [88–91]. Secondly, the results of the analysis on the factor interaction in this research showed that the interaction between NDVI and NDWI had the most significant negative effect on SUHI effects. Based on such finding and previous researches by other scholars, it is recommended to combine parks, important green patches, and water systems to form a blue-green network [92–95]. Thirdly, the Results part in Section 3.3 revealed the impact of urban environmental factors on SUHII, stating that the higher significance of the SUHI effect was related to the higher POI density, and that RD was negatively correlated with the SUHII in the central area of the city, and positively correlated with the SUHI effect outside the city. An on-site investigation revealed that most roads in the city center are lined with trees, effectively lowering LST. In contrast, the peripheral areas of the urban circle predominantly feature wide asphalt or hard-paved lanes, which lack sufficient greenery. Based on such findings, these relevant policies can be drawn: (1) In the city's central area, the density of the road network can be appropriately increased, with a recommended size for commercial blocks of 150 m × 150 m. Additionally, incorporating tall trees as roadside vegetation can enhance the shaded area along roads and help reduce surface land surface temperature (LST). In the city's peripheral areas, it is advisable to replace traditional road materials with permeable and cooling stone materials to minimize the exposure of asphalt pavement to direct sunlight. (2) The research findings indicate that the degree of POI agglomeration is positively correlated with the intensity of the urban heat island effect. Field verification reveals that areas with clustered POIs are often associated with continuous high-density urban development. Consequently, avoiding highly concentrated building construction can effectively mitigate the urban heat island effect. (3) Given their substantial SUHI effects, the compact lowrise and midrise areas (LCZ2 and LCZ3) in the central region of the Guangzhou-Foshan metropolitan area, along with the industrial district near the northern mountainous areas (LCZ8 and LCZ10), should be renovated and upgraded to enhance vegetation and water features. Alternatively, they could be demolished and rebuilt as part of urban renewal efforts to expand outdoor green spaces.

4.4. Limitation and Future Research Direction

This study consisted of three critical parts: firstly, the identification and division of LCZs based on remote sensing images; secondly, the calculation of SUHII derived from remote sensing surface temperature inversion; and thirdly, the identification of relevant factors and influencing mechanisms on SUHI effects.

However, there are still limitations in these parts, which require further improvement. Firstly, in the stage of LCZ recognition, this study mainly used the LCZ generator developed by WUDAPT, followed by precision adjustments through random forest [18,96,97]. However, the existing methods are prone to confuse LCZ 2 with LCZ 3 in built types, as well as confusing LCZ B with LCZ C in land cover types, for the remote sensing images of each pair are of high similarity. For further research, deep learning methods should be combined to improve the recognition accuracy of LCZs in the Guangzhou-Foshan metropolis. Secondly, the method of calculating SUHII in this study is mainly based on remote sensing inversion, only obtaining the LST. In subsequent research, the perceived temperature should be added as the dependent variable of the SUHI effects analysis. Meanwhile, research should be conducted to further explore the influencing factors that affect human beings on their perception of temperature in cities. Thirdly, in this study, the main factors affecting the SUHI effects were mainly two-dimensional factors such as NDVI or NDBI, lacking three-dimensional elements such as building materials, building volume, or building shape, etc. Therefore, further research could conduct analysis on the effects of three-dimensional influencing factors such as building height, shape, and material on the UHI effects [19,58]. What is more, since the relationship between the SUHII of different LCZs and influencing factors is non-linear, the GD model still has significant shortcomings in exploring the correlation of influencing factors. In the future, the random forest model in machine learning regression analysis and the YOLOv5 algorithm in deep learning will be used to deeply explore the influencing factors of SUHII [13,14,98,99].

5. Conclusions

A detailed analysis of the changes in local climate zones in the Guangzhou-Foshan metropolitan area from 2013 to 2023, as well as the influencing factors of the surface urban heat island (SUHI) effects in different types of LCZs, can provide quantitative support for future mitigation of the deterioration of urban thermal environment.

In this study, LCZ exhibited significant spatial heterogeneity and complex distribution in the Guangzhou-Foshan metropolitan area, in which LCZ 9 took up the largest proportion, yet its area kept increasing over time. In the central urban area, the proportion of LCZ 5 in the built types was the largest, and its area has been increasing annually. In the metropolitan area of Guangzhou-Foshan, the proportion of LCZ A in the land cover types was the largest, and its area remained relatively stable without annual increase or decrease.

The SUHI effects in the Guangzhou-Foshan metropolis exhibited a clear core-periphery pattern. A comparison between 2013, 2018, and 2023 showed that the overall SUHII in the Guangzhou-Foshan metropolitan area has been alleviated in general terms, but to a specific extent, the SUHII in the central urban area continued to increase, with the peak value of SUHII in 2023 significantly higher than that of 2013. Additionally, the analysis revealed that LCZ 8 had the highest positive impact on the SUHI effect, followed by LCZ 3; conversely, LCZ G had the greatest negative impact on the SUHI effect, followed by LCZ A.

In terms of single-factor influence, through the analysis of the GWR and MGWR regression models, it was found that land cover factors had the greatest impact on SUHII, with NDVI and NDWI showing significant negative effects and NDBI showing a significant positive effect. The comparison between the results from 2013 to 2023 showed that the factors influencing SUHII have become increasingly diverse, with factors such as POI and RD gradually becoming more influential. In terms of two-factor interactions, in 2013 and 2018, the interaction between NDBI and NDWI had the greatest impact on SUHII, while in 2023, the interactions between POI, RD, and land cover factors had a significant impact on the SUHII.

In conclusion, this study took the Guangzhou-Foshan Metropolitan Area as the research object, making a longitudinal comparison between the data collected at three different time periods in 2013, 2018, and 2023, applying multiple models. With the support of both quantitative and qualitative analysis, this study delved deeply into the driving mechanisms influencing the SUHI effects, providing suggestions for future policy-making.

Abbreviations

UHI	Urban heat island
SUHI	Surface urban heat island
SUHII	Surface urban heat island intensity
LST	Land surface temperature
LCZs	Local climate zones
POI	Points of interest
DEM	Digital elevation model
NDVI	Normalized Difference Vegetation Index
NDBI	Normalized Difference Built-up Index
NDWI	Normalized Difference Water Index
POP	Population Density
RD	Road density
GDP	Gross Domestic Product
NPP	Net Primary Productivity
NL	Night light
WUDAPT	World Urban Database and Access Portal Tools

References

1. Ward, K.; Lauf, S.; Kleinschmit, B.; Endlicher, W. Heat waves and urban heat islands in Europe: A review of relevant drivers. *Sci. Total Environ.* **2016**, *569*, 527–539. [CrossRef] [PubMed]
2. Cheval, S.; Amihaesei, V.A.; Chitu, Z.; Dumitrescu, A.; Falcescu, V.; Irasoc, A.; Micu, D.M.; Mihulet, E.; Ontel, I.; Paraschiv, M.G.; et al. A systematic review of urban heat island and heat waves research (1991–2022). *Clim. Risk Manag.* **2024**, *44*, 100603. [CrossRef]
3. Oke, T.R. City Size and Urban Heat Island. *Atmos. Environ.* **1973**, *7*, 769–779. [CrossRef]
4. Oke, T.R. The Energetic Basis of the Urban Heat-island. *Q. J. R. Meteorol. Soc.* **1982**, *108*, 1–24. [CrossRef]
5. Abougendia, S.M. Investigating surface UHI using local climate zones (LCZs), the case study of Cairo's River Islands. *Alex. Eng. J.* **2023**, *77*, 293–307. [CrossRef]
6. Chai, R.M. Relating Urban Morphology and Urban Heat Island During Extreme Heat Events in the Kansas City Metropolitan Area. Ph.D. Thesis, University of Kansas, Lawrence, KS, USA, 2018.
7. Bureau, P.R. *2023-World-Population-Data-Sheet-Booklet*; Population Reference Bureau: Washington, DC, USA, 2023.
8. Debbage, N.; Shepherd, J.M. The urban heat island effect and city contiguity. *Comput. Environ. Urban Syst.* **2015**, *54*, 181–194. [CrossRef]
9. Peng, W.; Wang, R.; Duan, J.; Gao, W.; Fan, Z. Surface and canopy urban heat islands: Does urban morphology result in the spatiotemporal differences? *Urban Clim.* **2022**, *42*, 101136. [CrossRef]

10. Wen, C.; Mamtimin, A.; Feng, J.; Wang, Y.; Yang, F.; Huo, W.; Zhou, C.; Li, R.; Song, M.; Gao, J.; et al. Diurnal Variation in Urban Heat Island Intensity in Birmingham: The Relationship between Nocturnal Surface and Canopy Heat Islands. *Land* **2023**, *12*, 2062. [CrossRef]

11. Yuan, D.; Zhang, L.; Fan, Y.; Sun, W.; Fan, D.; Zhao, X. Spatio-Temporal Analysis of Surface Urban Heat Island and Canopy Layer Heat Island in Beijing. *Appl. Sci.* **2024**, *14*, 5034. [CrossRef]

12. Mirabi, E.; Davies, P.J. A systematic review investigating linear infrastructure effects on Urban Heat Island (UHI$_{ULI}$) and its interaction with UHI typologies. *Urban Clim.* **2022**, *45*, 101261. [CrossRef]

13. Lin, J.; Wei, K.; Guan, Z. Exploring the connection between morphological characteristic of built-up areas and surface heat islands based on MSPA. *Urban Clim.* **2024**, *53*, 101764. [CrossRef]

14. Jung, W.; Kim, G. Reduction of Fine Dust and Alleviation of Heat Island Effect: An Analysis of Cold Air Flow in Pohang City, South Korea. *Land* **2024**, *13*, 347. [CrossRef]

15. Kang, S.; Lee, D.; Park, J.; Jung, J. Exploring Urban Forms Vulnerable to Urban Heat Islands: A Multiscale Analysis. *Sustainability* **2022**, *14*, 3603. [CrossRef]

16. Zhang, J.; Tu, L.; Wang, X.; Liang, W. Comparison of Urban Heat Island Differences in the Yangtze River Delta Urban Agglomerations Based on Different Urban-Rural Dichotomies. *Remote Sens.* **2024**, *16*, 3206. [CrossRef]

17. Badaro-Saliba, N.; Adjizian-Gerard, J.; Zaarour, R.; Najjar, G. LCZ scheme for assessing Urban Heat Island intensity in a complex urban area (Beirut, Lebanon). *Urban Clim.* **2021**, *37*, 100846. [CrossRef]

18. Muhammad, F.; Xie, C.K.; Vogel, J.; Afshari, A. Inference of Local Climate Zones from GIS Data, and Comparison to WUDAPT Classification and Custom-Fit Clusters. *Land* **2022**, *11*, 747. [CrossRef]

19. Xi, Y.; Wang, S.; Zou, Y.; Zhou, X.; Zhang, Y. Seasonal surface urban heat island analysis based on local climate zones. *Ecol. Indic.* **2024**, *159*, 111669. [CrossRef]

20. Yin, S.; Xiao, S.Y.; Ding, X.T.; Fan, Y.F. Improvement of spatial-temporal urban heat island study based on local climate zone framework: A case study of Hangzhou, China. *Build. Environ.* **2024**, *248*, 111102. [CrossRef]

21. Zhang, J.; Tu, L.; Shi, B. Spatiotemporal Patterns of the Application of Surface Urban Heat Island Intensity Calculation Methods. *Atmosphere* **2023**, *14*, 1580. [CrossRef]

22. Qin, Y.; Ghalambaz, S.; Sheremet, M.; Baro, M.; Ghalambaz, M. Deciphering Urban Heat Island Mitigation: A Comprehensive Analysis of Application Categories and Research Trends. *Sustain. Cities Soc.* **2024**, *101*, 105081. [CrossRef]

23. Shi, L.; Ling, F.; Foody, G.M.; Yang, Z.; Liu, X.; Du, Y. Seasonal SUHI Analysis Using Local Climate Zone Classification: A Case Study of Wuhan, China. *Int. J. Environ. Res. Public Health* **2021**, *18*, 7242. [CrossRef]

24. Han, J.; Liu, J.; Liu, L.; Ye, Y. Spatiotemporal Changes in the Urban Heat Island Intensity of Distinct Local Climate Zones: Case Study of Zhongshan District, Dalian, China. *Complexity* **2020**, *2020*, 8820338. [CrossRef]

25. Hu, J.; Yang, Y.; Pan, X.; Zhu, Q.; Zhan, W.; Wang, Y.; Ma, W.; Su, W. Analysis of the Spatial and Temporal Variations of Land Surface Temperature Based on Local Climate Zones: A Case Study in Nanjing, China. *IEEE J. Sel. Top. Appl. Earth Obs. Remote Sens.* **2019**, *12*, 4213–4223. [CrossRef]

26. Bechtel, B.; Demuzere, M.; Mills, G.; Zhan, W.; Sismanidis, P.; Small, C.; Voogt, J. SUHI analysis using Local Climate Zones-A comparison of 50 cities. *Urban Clim.* **2019**, *28*, 100451. [CrossRef]

27. Eldesoky, A.H.M.; Gil, J.; Pont, M.B. The suitability of the urban local climate zone classification scheme for surface temperature studies in distinct macroclimate regions. *Urban Clim.* **2021**, *37*, 100823. [CrossRef]

28. Kamath, H.G.; Martilli, A.; Singh, M.; Brooks, T.; Lanza, K.V.; Bixler, R.P.; Coudert, M.; Yang, Z.L.; Niyogi, D. Human heat health index (H3I) for holistic assessment of heat hazard and mitigation strategies beyond urban heat islands. *Urban Clim.* **2023**, *52*, 101675. [CrossRef]

29. Moon, S.Y.; Kim, J.; Chong, W.K.O.; Ariaratnam, S.T. Urban Green Space Layouts and Urban Heat Island: Case Study on Apartment Complexes in South Korea. *J. Urban Plan. Dev.* **2018**, *144*, 04018004. [CrossRef]

30. Li, D.; Yan, S.F.; Chen, G.Z. Effects of Urban Redevelopment on Surface Urban Heat Island. *IEEE J. Sel. Top. Appl. Earth Obs. Remote Sens.* **2023**, *16*, 2366–2373. [CrossRef]

31. Iamtrakul, P.; Padon, A.; Chayphong, S. Quantifying the Impact of Urban Growth on Urban Surface Heat Islands in the Bangkok Metropolitan Region, Thailand. *Atmosphere* **2024**, *15*, 100. [CrossRef]

32. Ramírez-Aguilar, E.A.; Souza, L.C.L. Urban form and population density: Influences on Urban Heat Island intensities in Bogota, Colombia. *Urban Clim.* **2019**, *29*, 100497. [CrossRef]

33. Murayama, Y.; Wang, R.C. Editorial: Special Issue on Geographical Analysis and Modeling of Urban Heat Island Formation. *Remote Sens.* **2023**, *15*, 4474. [CrossRef]

34. Meng, F.; Yan, S.L.; Tian, G.H.; Wang, Y.D. Surface urban heat island effect and its spatiotemporal dynamics in metropolitan area: A case study in the Zhengzhou metropolitan area, China. *Front. Environ. Sci.* **2023**, *11*, 1247046. [CrossRef]

35. Kim, H.; Seok, H.B.; Kim, Y.K. A Study on the Change of the Urban Heat Island Structure in Busan Metropolitan Area, Korea. *J. Environ. Sci. Int.* **2014**, *23*, 1807–1820. [CrossRef]

36. Yu, Z.W.; Yao, Y.W.; Yang, G.Y.; Wang, X.R.; Vejre, H. Spatiotemporal patterns and characteristics of remotely sensed region heat islands during the rapid urbanization (1995-2015) of Southern China. *Sci. Total Environ.* **2019**, *674*, 242–254. [CrossRef]

37. Song, Y.; Wang, J.; Ge, Y.; Xu, C. An optimal parameters-based geographical detector model enhances geographic characteristics of explanatory variables for spatial heterogeneity analysis: Cases with different types of spatial data. *GIScience Remote Sens.* **2020**, *57*, 593–610. [CrossRef]

38. Yu, H.; Fotheringham, A.S.; Li, Z.; Oshan, T.; Kang, W.; Wolf, L.J. Inference in Multiscale Geographically Weighted Regression. *Geogr. Anal.* **2020**, *52*, 87–106. [CrossRef]

39. Meng, L.; Zhu, C.G.; Pu, J.; Wen, B.; Si, W.T. Study on the Influence Mechanism of Intangible Cultural Heritage Distribution from Man-Land Relationship Perspective: A Case Study in Shandong Province. *Land* **2022**, *11*, 1225. [CrossRef]

40. Huang, Y.; Lang, W.; Chen, T.T.; Wu, J.M. Regional Coordinated Development in the Megacity Regions: Spatial Pattern and Driving Forces of the Guangzhou-Foshan Cross-Border Area in China. *Land* **2023**, *12*, 753. [CrossRef]

41. Ye, Y.Q.; Zhang, J.E.; Bryan, B.A.; Gao, L.; Qin, Z.; Chen, L.L.; Yang, J.Y. Impacts of rapid urbanization on ecosystem services along urban-rural gradients: A case study of the Guangzhou-Foshan Metropolitan Area, South China. *Ecoscience* **2018**, *25*, 235–247. [CrossRef]

42. Malakar, N.K.; Hulley, G.C.; Hook, S.J.; Laraby, K.; Cook, M.; Schott, J.R. An Operational Land Surface Temperature Product for Landsat Thermal Data: Methodology and Validation. *IEEE Trans. Geosci. Remote Sens.* **2018**, *56*, 5717–5735. [CrossRef]

43. Park, S.H.; Jung, H.S.; Shin, H.S. Time-series monitoring result of land surface temperature variation at Mt. Baekdu using Landsat images. In Proceedings of the Conference on Land Surface Remote Sensing II, Beijing, China, 13–16 October 2014.

44. Li, S.J.; Cao, X.; Zhao, C.C.; Jie, N.; Liu, L.L.; Chen, X.H.; Cui, X.H. Developing a Pixel-Scale Corrected Nighttime Light Dataset (PCNL, 1992-2021) Combining DMSP-OLS and NPP-VIIRS. *Remote Sens.* **2023**, *15*, 3925. [CrossRef]

45. Demuzere, M.; Kittner, J.; Bechtel, B. LCZ Generator: A Web Application to Create Local Climate Zone Maps. *Front. Environ. Sci.* **2021**, *9*, 637455. [CrossRef]

46. Vaidya, M.; Keskar, R.; Kotharkar, R. Classifying heterogeneous urban form into local climate zones using supervised learning and greedy clustering incorporating Landsat dataset. *Urban Clim.* **2024**, *53*, 101770. [CrossRef]

47. Zhao, N.; Ma, A.; Zhong, Y.; Zhao, J.; Cao, L. Self-Training Classification Framework with Spatial-Contextual Information for Local Climate Zones. *Remote Sens.* **2019**, *11*, 2828. [CrossRef]

48. Yang, Y.M.; Qiu, J.X.; Su, H.B.; Bai, Q.M.; Liu, S.H.; Li, L.; Yu, Y.L.; Huang, Y.X. A One-Source Approach for Estimating Land Surface Heat Fluxes Using Remotely Sensed Land Surface Temperature. *Remote Sens.* **2017**, *9*, 43. [CrossRef]

49. Cai, M.; Ren, C.; Xu, Y. Investigating the relationship between local climate zone and land surface temperature—A case study in Shanghai. In Proceedings of the Joint Urban Remote Sensing Event (JURSE), Dubai, United Arab Emirates, 6–8 March 2017.

50. Nasehi, S.; Yavari, A.; Salehi, E.; Emmanuel, R. Role of local climate zone and space syntax on land surface temperature (case study: Tehran). *Urban Clim.* **2022**, *45*, 101245. [CrossRef]

51. Quan, J.L. Diurnal land surface temperature characteristics of local climate zones: A case study in beijing, china. In Proceedings of the IEEE International Geoscience and Remote Sensing Symposium (IGARSS), Yokohama, Japan, 28 July–2 August 2019; pp. 7443–7446.

52. Hong, S.-O.; Kim, D.-H.; Byon, J.-Y.; Park, H.; Ha, J.-C. Analysis of the Effects of Advection and Urban Fraction on Urban Heat Island Intensity using Unified Model for Seoul Metropolitan Area, Korea. *Atmosphere* **2019**, *29*, 381–390. [CrossRef]

53. Bechtel, B.; Alexander, P.J.; Beck, C.; Boehner, J.; Brousse, O.; Ching, J.; Demuzere, M.; Fonte, C.; Gal, T.; Hidalgo, J.; et al. Generating WUDAPT Level 0 data—Current status of production and evaluation. *Urban Clim.* **2019**, *27*, 24–45. [CrossRef]

54. Alghamdi, A.S.; Alzhrani, A.I.; Alanazi, H.H. Local Climate Zones and Thermal Characteristics in Riyadh City, Saudi Arabia. *Remote Sens.* **2021**, *13*, 4526. [CrossRef]

55. Huang, F.; Jiang, S.D.; Zhan, W.F.; Bechtel, B.; Liu, Z.H.; Demuzere, M.; Huang, Y.; Xu, Y.; Ma, L.; Xia, W.J.; et al. Mapping local climate zones for cities: A large review. *Remote Sens. Environ.* **2023**, *292*, 113573. [CrossRef]

56. Perera, N.G.R.; Emmanuel, R. A "Local Climate Zone" based approach to urban planning in Colombo, Sri Lanka. *Urban Clim.* **2018**, *23*, 188–203. [CrossRef]

57. Xu, D.; Zhang, Q.; Zhou, D.; Yang, Y.J.; Wang, Y.Q.; Rogora, A.; Pitts, A. Local Climate Zone in Xi'an City: A Novel Classification Approach Employing Spatial Indicators and Supervised Classification. *Buildings* **2023**, *13*, 2806. [CrossRef]

58. Xu, Y.N.; Hou, W.; Zhang, C.X. Spatial Association Rules and Thermal Environment Differentiation Evaluation of Local Climate Zone and Urban Functional Zone. *Land* **2023**, *12*, 1701. [CrossRef]

59. Schonlau, M.; Zou, R.Y. The random forest algorithm for statistical learning. *Stata J.* **2020**, *20*, 3–29. [CrossRef]

60. dos Anjos, C.S.; Lacerda, M.G.; Andrade, L.D.; Salles, R.N. Classification of urban environments using feature extraction and random forest. In Proceedings of the IEEE International Geoscience and Remote Sensing Symposium (IGARSS), Fort Worth, TX, USA, 23–28 July 2017; pp. 1205–1208.

61. Sekertekin, A.; Bonafoni, S. Land Surface Temperature Retrieval from Landsat 5, 7, and 8 over Rural Areas: Assessment of Different Retrieval Algorithms and Emissivity Models and Toolbox Implementation. *Remote Sens.* **2020**, *12*, 294. [CrossRef]

62. Garcia, D.H.; Diaz, J.A. Modeling of the Urban Heat Island on local climatic zones of a city using Sentinel 3 images: Urban determining factors. *Urban Clim.* **2021**, *37*, 100840. [CrossRef]

63. Zhang, W.; Huo, H.; Geng, X.; Zhou, P.; Guo, L.; Li, Z.-L. Simulation of canopy urban heat island at a block scale based on local climate zones and urban weather generator: A case study of Beijing. *Int. J. Remote Sens.* **2023**. *early access*. [CrossRef]

64. Li, C.; Zhang, N.; Wang, Y.; Chen, Y. Modeling Urban Heat Islands and Thermal Comfort During a Heat Wave Event in East China With CLM5 Incorporating Local Climate Zones. *J. Geophys. Res.-Atmos.* **2023**, *128*, e2023JD038883. [CrossRef]

65. Lin, Z.; Xu, H.; Yao, X.; Yang, C.; Yang, L. Exploring the relationship between thermal environmental factors and land surface temperature of a "furnace city" based on local climate zones. *Build. Environ.* **2023**, *243*, 110732. [CrossRef]

66. Zhang, H.; Wang, C.; Yang, H.; Ma, Z. How do morphology factors affect urban heat island intensity? an approach of local climate zones in a fast-growing small city, Yangling, China. *Ecol. Indic.* **2024**, *161*, 111972. [CrossRef]

67. Liu, W.; Zhang, L.; Hu, X.; Meng, Q.; Qian, J.; Gao, J.; Li, T. Nonlinear effects of urban multidimensional characteristics on daytime and nighttime land surface temperature in highly urbanized regions: A case study in Beijing, China. *Int. J. Appl. Earth Obs. Geoinf.* **2024**, *132*, 104067. [CrossRef]

68. Sarricolea, P.; Smith, P.; Romero-Aravena, H.; Serrano-Notivoli, R.; Fuentealba, M.; Meseguer-Ruiz, O. Socioeconomic inequalities and the surface heat island distribution in Santiago, Chile. *Sci. Total Environ.* **2022**, *832*, 155152. [CrossRef] [PubMed]

69. Wu, Z.; Xu, Y.; Cao, Z.; Yang, J.; Zhu, H. Impact of Urban Agglomeration and Physical and Socioeconomic Factors on Surface Urban Heat Islands in the Pearl River Delta Region, China. *IEEE J. Sel. Top. Appl. Earth Obs. Remote Sens.* **2021**, *14*, 8815–8822. [CrossRef]

70. Chen, G.; Wei, Z. Exploring the impacts of built environment on bike-sharing trips on weekends: The case of Guangzhou. *Int. J. Sustain. Transp.* **2024**, *18*, 315–327. [CrossRef]

71. Bechtel, B.; See, L.; Mills, G.; Foley, M. Classification of Local Climate Zones Using SAR and Multispectral Data in an Arid Environment. *IEEE J. Sel. Top. Appl. Earth Obs. Remote Sens.* **2016**, *9*, 3097–3105. [CrossRef]

72. Liao, C.M.; Zuo, Y.F.; Law, R.; Wang, Y.Y.; Zhang, M. Spatial Differentiation, Influencing Factors, and Development Paths of Rural Tourism Resources in Guangdong Province. *Land* **2022**, *11*, 2046. [CrossRef]

73. Yuan, W.R.; Chen, L.K.; Chen, H.X.; Deng, S.F.; Ji, H.; Liang, F.S. Assessing habitat quality at Poyang Lake based on InVEST and Geodetector modeling. *Ecol. Evol.* **2023**, *13*, e10759. [CrossRef] [PubMed]

74. Lu, Y.; Yang, J.; Ma, S. Dynamic Changes of Local Climate Zones in the Guangdong-Hong Kong-Macao Greater Bay Area and Their Spatio-Temporal Impacts on the Surface Urban Heat Island Effect between 2005 and 2015. *Sustainability* **2021**, *13*, 6374. [CrossRef]

75. Xiang, Y.; Zheng, B.; Bedra, K.B.; Ouyang, Q.; Liu, J.; Zheng, J. Spatial and seasonal differences between near surface air temperature and land surface temperature for Urban Heat Island effect assessment. *Urban Clim.* **2023**, *52*, 101745. [CrossRef]

76. Zhao, Z.; Sharifi, A.; Dong, X.; Shen, L.; He, B.-J. Spatial Variability and Temporal Heterogeneity of Surface Urban Heat Island Patterns and the Suitability of Local Climate Zones for Land Surface Temperature Characterization. *Remote Sens.* **2021**, *13*, 4338. [CrossRef]

77. Wang, Z.H.; Xing, W.; Huang, Y.; Xie, T.A. Studying the Urban Heat Island Using a Local Climate Zone Scheme. *Pol. J. Environ. Stud.* **2016**, *25*, 2609–2616. [CrossRef] [PubMed]

78. Tian, W.S.; Yang, Y.J.; Wang, L.L.; Zong, L.; Zhang, Y.H.; Liu, D.Y. Role of local climate zones and urban ventilation in canopy urban heat island-heatwave interaction in Nanjing megacity, China. *Urban Clim.* **2023**, *49*, 101474. [CrossRef]

79. Ma, L.; Huang, G.A.; Johnson, B.A.; Chen, Z.J.; Li, M.C.; Yan, Z.Y.; Zhan, W.F.; Lu, H.; He, W.Q.; Lian, D.J. Investigating urban heat-related health risks based on local climate zones: A case study of Changzhou in China. *Sustain. Cities Soc.* **2023**, *91*, 104402. [CrossRef]

80. Shen, Y.; Zeng, C.; Cheng, Q.; Shen, H.F. Opposite Spatiotemporal Patterns for Surface Urban Heat Island of Two "Stove Cities" in China: Wuhan and Nanchang. *Remote Sens.* **2021**, *13*, 4447. [CrossRef]

81. Deng, X.D.; Gao, F.; Liao, S.Y.; Liu, Y.; Chen, W.Y. Spatiotemporal evolution patterns of urban heat island and its relationship with urbanization in Guangdong-Hong Kong-Macao greater bay area of China from 2000 to 2020. *Ecol. Indic.* **2023**, *146*, 109817. [CrossRef]

82. Guo, A.; Yang, J.; Xiao, X.; Xia, J.; Jin, C.; Li, X. Influences of urban spatial form on urban heat island effects at the community level in China. *Sustain. Cities Soc.* **2020**, *53*, 101972. [CrossRef]

83. Huang, Y.; Yuan, M.; Lu, Y. Spatially varying relationships between surface urban heat islands and driving factors across cities in China. *Environ. Plan. B-Urban Anal. City Sci.* **2019**, *46*, 377–394. [CrossRef]

84. Wang, L.; Hou, H.; Weng, J. Ordinary least squares modelling of urban heat island intensity based on landscape composition and configuration: A comparative study among three megacities along the Yangtze River. *Sustain. Cities Soc.* **2020**, *62*, 102381. [CrossRef]

85. Wang, X.; Zhou, T.; Tao, F.; Zang, F. Correlation Analysis between UBD and LST in Hefei, China, Using Luojia1-01 Night-Time Light Imagery. *Appl. Sci.* **2019**, *9*, 5224. [CrossRef]

86. Chen, P. Inequality in heat: The role of spatial patterns of urban green infrastructure. *Urban Clim.* **2024**, *53*, 101820. [CrossRef]

87. Lan, Y.L.; Zhan, Q.M. How do urban buildings impact summer air temperature? The effects of building configurations in space and time. *Build. Environ.* **2017**, *125*, 88–98. [CrossRef]

88. Wang, Y.S.; Zhan, Q.M.; Ouyang, W.L. How to quantify the relationship between spatial distribution of urban waterbodies and land surface temperature? *Sci. Total Environ.* **2019**, *671*, 1–9. [CrossRef] [PubMed]

89. Wu, C.Y.; Li, J.X.; Wang, C.F.; Song, C.H.; Chen, Y.; Finka, M.; La Rosa, D. Understanding the relationship between urban blue infrastructure and land surface temperature. *Sci. Total Environ.* **2019**, *694*, 133742. [CrossRef]

90. Xu, Z.Y.; Zhao, S.Q. Scale dependence of urban green space cooling efficiency: A case study in Beijing metropolitan area. *Sci. Total Environ.* **2023**, *898*, 165563. [CrossRef] [PubMed]

91. Zölch, T.; Maderspacher, J.; Wamsler, C.; Pauleit, S. Using green infrastructure for urban climate-proofing: An evaluation of heat mitigation measures at the micro-scale. *Urban For. Urban Green.* **2016**, *20*, 305–316. [CrossRef]

92. Asadi, A.; Arefi, H.; Fathipoor, H. Simulation of green roofs and their potential mitigating effects on the urban heat island using an artificial neural network: A case study in Austin, Texas. *Adv. Space Res.* **2020**, *66*, 1846–1862. [CrossRef]

93. Chenary, K.; Soltani, A.; Sharifi, A. Street network patterns for mitigating urban heat islands in arid climates. *Int. J. Digit. Earth* **2023**, *16*, 3145–3161. [CrossRef]

94. Irie, T. The cooling effect of green infrastructure in mitigating nocturnal urban heat islands: A case study of Yoyogi Park and Meiji Jingu Shrine in Tokyo. *Landsc. Res.* **2022**, *47*, 559–583. [CrossRef]

95. Qian, W.Q.; Li, X.Y. A cold island connectivity and network perspective to mitigate the urban heat island effect. *Sustain. Cities Soc.* **2023**, *94*, 104525. [CrossRef]

96. Wong, M.M.F.; Fung, J.C.H.; Ching, J.; Yeung, P.P.S.; Tse, J.W.P.; Ren, C.; Wang, R.; Cai, M. Evaluation of uWRF performance and modeling guidance based on WUDAPT and NUDAPT UCP datasets for Hong Kong. *Urban Clim.* **2019**, *28*, 100460. [CrossRef]

97. Zonato, A.; Martilli, A.; Di Sabatino, S.; Zardi, D.; Giovanni, L. Evaluating the performance of a novel WUDAPT averaging technique to define urban morphology with mesoscale models. *Urban Clim.* **2020**, *31*, 100584. [CrossRef]

98. Daemei, A.B.; Bradecki, T.; Pancewicz, A.; Razzaghipour, A.; Jamali, A.; Abbaszadegan, S.M.; Askarizad, R.; Kazemi, M.; Sharifi, A. An experimental analysis and deep learning model to assess the cooling performance of green walls in humid climates. *Front. Energy Res.* **2024**, *12*, 1447655. [CrossRef]

99. Tanoori, G.; Soltani, A.; Modiri, A. Machine Learning for Urban Heat Island (UHI) Analysis: Predicting Land Surface Temperature (LST) in Urban Environments. *Urban Clim.* **2024**, *55*, 101962. [CrossRef]

Thermal Footprint of the Urbanization Process: Analyzing the Heat Effects of the Urbanization Index (UI) on the Local Climate Zone (LCZ) and Land Surface Temperature (LST) over Two Decades in Seville

Nadia Falah [1], Jaime Solis-Guzman [1,*] and Nahid Falah [2]

[1]   ArDiTec Research Group, Department of Architectural Constructions II, Higher Technical School of Building Engineering, Universidad de Sevilla, Av. Reina Mercedes 4-a, 41012 Seville, Spain; nadfal@alum.us.es
[2]   Landkreis Harburg, Schloßplatz 6, 21423 Winsen (Luhe), Germany; n.falah@lkharburg.de
*   Correspondence: jaimesolis@us.es

Abstract: Urbanization is a multifaceted process characterized by changes in urban areas through various means, such as sprawl, ribbon development, or infill and compact growth. This phenomenon changes the pattern of the local climate zone (LCZ) and significantly affects the climate, vegetation dynamics, energy consumption, water resources, and public health. This study aims to discern the impacts of changes in urban growth on the LCZ and land surface temperature (LST) over a two-decade period. A comprehensive methodology that integrates statistical analysis, data visualization, machine learning, and advanced techniques, such as remote sensing technology and geospatial analysis systems, is employed. ENVI, GEE, and GIS tools are utilized to collect, process, and monitor satellite data and imagery of temporal and spatial variations in intensive or diffuse urbanization processes from 2003 to 2023 to analyze and simulate land use and land cover (LULC) changes, urbanization index (UI), LCZ patterns, and LST changes over the years and to make overlapping maps of changes to recognize the relation between LULC, LCZ, and LST. This study focuses on Seville's urban area, which has experienced rapid urbanization and a significant increase in average temperature during the last few decades. The findings of this study will provide actionable recommendations into the interplay between urban growth and climate and highlight the pivotal role of urban growth in shaping resilience and vulnerable areas based on microclimate changes. Urban planners can leverage these insights to predict alternatives for the future development of urban areas and define practical climate mitigation strategies.

Keywords: urbanization process; land use and land cover (LULC); local climate zone (LCZ); climate change; land surface temperature (LST); remote sensing (RS); Google earth engine (GEE)

1. Introduction

The onset of the 21st century has marked a significant acceleration in urbanization, with more than half of the world's population now residing in urban areas. This number is anticipated to rise to nearly 60% by 2030 [1,2]. Rapid urban expansion profoundly affects local urban environments and has become a major catalyst for increasing LULC changes. Characterized by long-term shifts in weather patterns, climate change exacerbates temperature instability and disrupts natural cycles [3].

Urban growth and intensification patterns are driven by factors such as population shifts [2], infrastructure development, industrialization [4–6], historical development, economic growth [7], and various environmental, geographical, and planning conditions, which cause changes in the multifaceted nature of urban systems.

All these elements shape urban morphology and texture and cause changes in LULC's current status [8–10]. LULC refers to the pattern of biological and physical cover over

the land's surface, including forests, water bodies, agricultural and vegetation lands, and urban areas, as well as the human activities associated with them. These changes in LULC create different types of urban growth with distinct characteristics [11,12], changing the pattern of microclimates over time [5,6]. A microclimate change is described as a long-term change in the average weather patterns that affect Earth's local climates [1,3], which is crucial for understanding the impact and role of urban growth patterns on climate, especially temperature variation patterns [3]. LCZs, as a standardized framework, categorize urban landscapes into different classes based on several factors, such as the physical and thermal properties of urban and natural landscapes [13]. These classes are influenced by urbanization processes, changes in LULC patterns, and climate change [14,15]. On one hand, the classification of LCZs involves analyzing surface structure, land cover, local climate conditions, function, and anthropogenic influence, with a particular focus on urban and peri-urban areas [16,17]. On the other hand, LST changes are influenced by landscape alterations, vegetation loss, LULC composition, urban materials and geometry, anthropogenic heat, natural settings, and geographic locations, the same as LCZ [13,16,18]. In many metropolitan areas, the temperature differential caused by an elevated LST, driven by a high percentage of impermeable surfaces, can escalate to around 5 °C [19–21]. This rise in LST predominantly results from the expansion of impermeable areas, which correlate closely with urban development-induced modifications in LULC. This trend is raising significant environmental and human health concerns [22–24]. Over the past few decades, urban areas have seen surface temperatures rise by approximately 0.87 °C, attributed to global climate change and human activities [4,19,20]. Predictions indicate the LST in urban areas will continue to increase [8,14,20]. Subsequently, evaluating the impact of LULC changes on LST is urgent for designing livable areas and creating healthy urban environments. Table 1 provides an overview of previous studies, summarizing key findings related to the effects of urbanization on land cover and temperature.

Table 1. Previous studies related to the LULC, LCZs, and LST.

Main Point	Studies
Studies emphasized the correlation between climate change, land alteration, and their consequences on LST outcomes.	[15,20,25–28]
Studies examined the urban growth and sprawl's impact on local climate. The effects on LST are crucial for evaluating sustainable urban development and understanding both the quantity and quality of these changes.	[3,7,12,24,29–31]
Studies explored the relationship between LCZs and LST, demonstrating that different LCZ types exhibit varying thermal behaviors and providing insights into how urban morphology influences local temperatures.	[14,16,19,32–34]
Studies defined the relationship between LULC changes and LCZ patterns and mentioned that changes in land use and cover directly influence the classification of LCZ and the integration of them allows for a more detailed analysis of urban heat islands (UHIs) by linking specific land cover types with their corresponding thermal effects.	[14,21,35–37]

According to Table 1, the indicators and lines of these studies include LULC, LCZs, and LST, which are defined as follows.

Main types of urban growth include the following:

- Compact growth or infill development: concentrating buildings within existing developed areas [8], focusing on vertical development.
- Ribbon development and infrastructure-led growth: occurring alongside transportation and communication routes [5], forming linear patterns of development.
- Sprawl or dispersed growth: the outward expansion of urban boundaries, often linked with suburban or exurban areas [12].

- Mixed development: involves varied types of development occurring over time within different parts of an urban area, reflecting a city area faced with multiple types of growth and development.
- LULC change: identified various land use types, such as built-up areas (BUAs), water bodies (WBs), agricultural lands, vegetation, forest lands (A/V/F), and barren soil (BS) [4,5,12]. LULC change detection entails the comparison of images taken at various times to detect and study alterations in the landscape and to observe urban growth and deforestation [12,38].
- LCZ: This classification system, introduced by Stewart and Oke [14], categorizes urban and rural areas based on surface cover, structure, and thermal properties, providing a standardized framework for comparing different urban areas. This system is widely used to study how various urbanization forms influence microclimates, particularly in relation to LST. Different physical classifications of LCZ are explained in the methodology section.
- LST: A critical factor in comprehending the thermal atmosphere and Earth's surface in urban areas [16,39] is associated with different patterns of urban growth. Many factors play crucial roles in the level of LST, such as solar radiation, vegetation cover, LULC, urban growth, topography, weather and climate condition, and human activities [19–21]. LST is a critical parameter in studying Earth's energy balance, urban heat islands, climate change, and environmental processes.

Due to the interplay and connection between urbanization, LULC, LCZ, and LST changes (Figure 1), the main points mentioned based on the literature review are included:
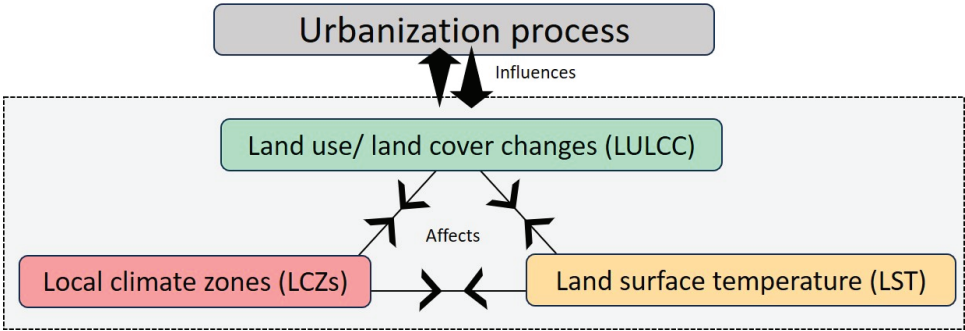
Figure 1. Relationship between urbanization process, LULCC, LCZ and LST.

- The urbanization process influences LULC changes (LULCCs), altering how land is used and covered.
- LULCCs then modify LCZ, affecting the classification of different urban and rural areas based on their structure and surface properties.
- The LCZ impacts LST by determining the thermal characteristics of different zones and LULC.
- Both the LCZ and LST contribute to the urban heat island effect (UHIE), where urban areas become noticeably warmer than their rural or surrounding areas due to the interplay between urbanization, LULC, and LST changes (Figure 1).

Therefore, this research aims to systematically review and evaluate the existing data linked to LULC, LCZ, and UI and investigate the adverse environmental impacts of urban growth, particularly in long-term local climate change patterns in Seville, Spain. It examines two decades of LULC distribution and changes, the types of urban growth, and UI patterns and density and evaluates LCZ changes, population trends and flow, and their effect on LST variations from 2003 to 2023.

Previous research has often focused on isolated aspects of urbanization, such as land use changes or short-term temperature variations. However, this study addresses both the long-term effects of urbanization on microclimate and the interaction between multiple factors, including urban growth patterns and climate resilience strategies. This research employs advanced methodologies such as remote sensing, geospatial analysis, and machine learning, which were not widely utilized in earlier studies. The integration of these technologies allows for a more comprehensive understanding of how Seville's urbanization has influenced its microclimate, particularly in terms of long-term LST changes. By applying multi-temporal satellite data and predictive modeling techniques, this study fills a significant gap in the literature, particularly in Mediterranean climates where urban growth patterns and climate dynamics are complex and interdependent and help to identify areas most vulnerable to temperature increases and other climatic changes due to urbanization, which is essential for developing strategies to mitigate the negative effects of urbanization and improve urban sustainability.

2. Materials and Methods

The methodology for analyzing the thermal footprint of urbanization involves a mixed-method approach (descriptive and analytic) and a multi-step process combining spatial, statistical, remote sensing techniques and historical documents. Therefore, the methodology of this research consists of three main sections. The Section 2.1 introduces the process and step-by-step structure of data collection, preparation, and the methods and techniques used in Section 2.2. In Section 2.2, all the formulas related to the indices affecting the research objectives are introduced and explained. Finally, in Section 2.3, the case study is presented.

2.1. Methods

The methodology is divided into two specific parts: firstly, classification, selection, and preparation that includes 4 separate sections. The first is the process of case study area and the period of time selection (mentioned in Section 2.3). The second specifies the criteria and indicators based on the literature review and the aims of this study (explained in Section 2.2). The third describes data collection and compilation and defines the sources of different types of data and the process of selection and evaluation of the data (defined in Section 2.1). The fourth outlines the collection methods for analysis (mentioned in Section 2.1). The second part, analyzing and modeling, includes 2 main sections. The first describes data pre-processing and preprocessing (defined in Sections 2.1 and 3.3). The second provides a statistical analysis and modeling, and the evaluation of current conditions is explained in the discussion part. The methodology is drawn in Figure 2, which explains these two specific parts of the method.

Advanced remote sensing (RS) technology and geospatial information system (GIS and statistical methods) satellite image data, which increase the visibility of the Earth's surface change [40,41], and statistics of documents of macro plans, reports, research, and projects from organizations and meteorological stations are utilized to analyze and examine the environmental characteristics. In the following sections, this paper introduces indices, models, and validation approaches that evaluate population movement, LULC, LCZ, and LST. The main dataset is multi-temporal Landsat satellite images from the USGS website [42] because this site provides data with high spatial resolution.

For data preprocessing, as a crucial step in preparing the satellite products, layer stacking, mosaicking, and clipping multi-band images, the brightness temperature was adjusted and DOS1 atmospheric correction was applied using methods that are explained in the second section of Figure 2. The multi-band images of Landsat 5 TM (path/row: 164/35, collection 2), with a reflectance resolution of 30 m and thermal resolution of 120 m, were acquired from 1 to 31 July 2003, and for Landsat 8 OLI/TIRS (path/row: 164/35), the reflectance resolution was 30 m and the thermal resolution was 100 m, with images collected between 1 and 31 July 2023 used for preprocessing; the satellite images' regions of interest

(ROI) were applied to ensure minimal cloud coverage (less than 10%) [42]. Supervised maximum likelihood classifier (MLC), K-mean clustering, and artificial neutral network (ANN) are the most common approaches to classify remote sensing images [41,43,44] and to calculate LULCCs; in this study, the support vector machine (SVM) system was used. To evaluate the correlation between indicators, the geographically weighted regression (GWR) equation was used in QGIS, and for assessment of the classification accuracy, overall accuracy and the kappa index were utilized, as they are mentioned in Figure 2. The images were calibrated using accurate classification methods (Section 4, part one, in Figure 2). In addition, this study utilized various software but with a focus on QGIS3.28.8, GIS 10.8.2, and ENVI 5.3 as powerful software for processing and analyzing satellite imagery, which allow for advanced image classification and change detection, and Google Earth Engine (GEE), a cloud-based platform designed for analyzing environmental data on a planetary scale using JavaScript programming language, suitable for large-scale mapping projects.
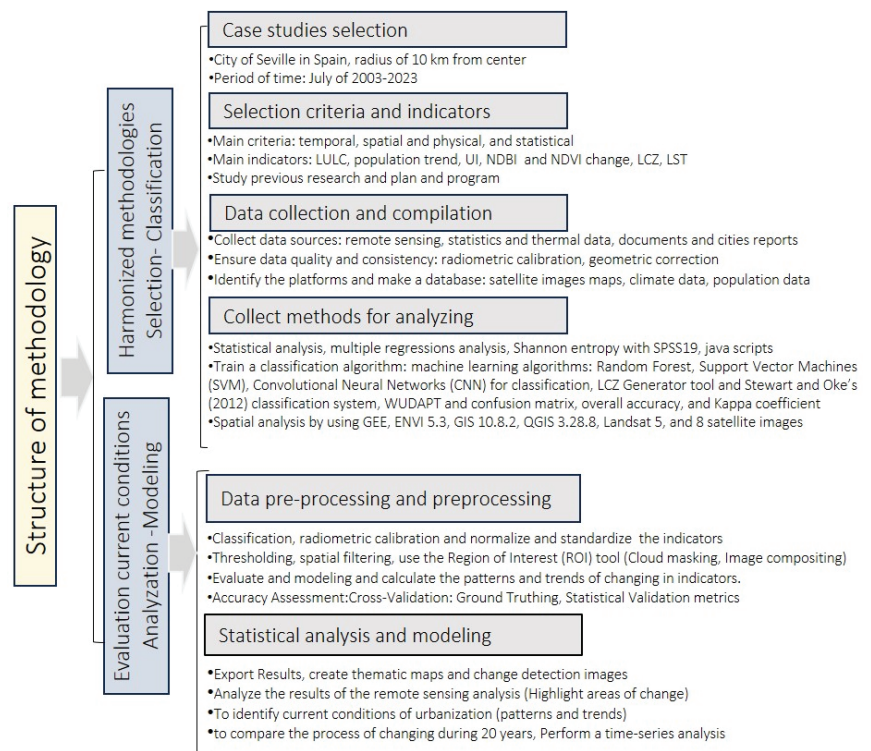
Figure 2. Methodology.

2.2. Define Indicators

As mentioned in the introduction, there are different types of indicators that can be used to establish a correlation between LULCC, LCZ, and LST. Based on the initial definitions and the relationship between the components, the following indicators have been examined as the main influencing factors: normalized difference vegetation index (NDVI), normalized difference built-up index (NDBI), and UI. NDBI identifies areas with built-up surfaces like roads and buildings, while NDVI indicates areas with healthy vegetation. The formulas employed and method explanations for them are explained in the following sections.

- LULCC: Change detection entails comparing two or more images acquired at different times to identify and analyze changes in the landscape [12,38] and the context of the

urban area, which is identified by different colors for the BUA levels for cities, villages, roads, industrial areas; WB levels for rivers, canals, and swamps, A/V/F area; and BS [4,9,12]. One common method for LULC change detection involves computing the LULC for each period and then subtracting one from the other [8]. For a given land cover type (e.g., urban), the area can be calculated using the formula in Equation (1).

$$\text{Area\_(Type,Time)} = \Sigma \ (\text{Pixels classified as Type}) \times \text{Area per Pixel} \qquad (1)$$

The change in a specific land cover type between two time periods (Time1 (2003) and Time2 (2023)) can be calculated as in Equation (2):

$$\Delta \ \text{Area\_Type} = \text{Area\_(Type,Time2)} - \text{Area\_(Type,Time1)} \qquad (2)$$

- UI: This clarifies the amount of urban areas in case studies [3,38]. The Shannon entropy model was employed to evaluate urbanization trends and study how the city expands and deforestation occurs [11,45] by measuring the extent of BUAs relative to natural landscapes or other land uses for comparing urbanization levels across regions or tracking urban growth. The structure of the model is as follows, in Equation (3):

$$H = \sum_{i=1}^{n} Pi * \ln(pi) \qquad (3)$$

In the formula above, the variables are defined as follows:

H = Shannon entropy value;
Pi = ratio of BUA;
i: area of the total BUA;
N = total area [46].

The value of the entropy is from zero to Ln, where (n) represents the amount of sprawl urban growth. A greater value of entropy indicates more dispersed urban growth [47].
- NDBI: A remote sensing index used to identify changes in BUA density or urban extent cover [4,8,12]. The formula for NDBI is typically derived from the reflectance values in the near-infrared and shortwave infrared of the land surface bands of the satellite data (Landsat) and is expressed in Equation (4).

$$NDBI = \frac{(SWIR - NIR)}{(SWIR + NIR)} \qquad (4)$$

In this formula, the variables are defined as follows:

SWIR is the shortwave infrared band;
NIR is the near-infrared band.

The resulting NDBI values range from -1 to 1. Positive values indicate a higher likelihood of BUAs, while negative values suggest non-BUAs, such as vegetation or water bodies. NDBI values closer to -1 typically represent areas with little to no built-up features, such as vegetation or water bodies [4]. An increase in NDBI values (moving toward 0) suggests an increase in BUAs or urbanization. Conversely, a decrease in NDBI values (moving away from 0 toward -1) indicates a decrease in BUAs or urbanization. It is crucial to note that the effectiveness of the NDBI for mapping BUAs may depend on the characteristics of the study area, the spatial resolution of the satellite imagery, temporal resolution, and the presence of factors such as shadows or mixed land cover types [8].

- NDVI: This is used to estimate vegetation health, density, and coverage [48], as well as the intensity of greenness and surface radiant temperature of the area. It is calculated using the reflectance values from the NIR and RED bands surface reflectance data of Landsat 5 TM (bands 4 and 3) and Landsat 8 OLI/TIRS satellite sensor (bands 5 and 4). NDVI operates on the concept that vibrant, healthy vegetation primarily

absorbs most of the visible light (specifically red) and reflects a significant amount of the near-infrared light [4]. Equation (5) is as follows:

$$NDVI = \frac{(NIR - RED)}{(NIR + RED)} \tag{5}$$

NIR: Near-infrared band;
RED: Red band.

The index value of NDVI ranges from −1 to 1. Positive and high NDVI values closer to +1 indicate a higher likelihood of denser and healthier vegetation, while low NDVI values closer to 0 and negative values suggest sparse or unhealthy vegetation, and negative NDVI values closer to −1 typically indicate non-vegetated surfaces, such as BS. A decrease in NDVI values, particularly in urban areas, indicates a reduction in the density of green spaces, likely due to increased urbanization [48].

- LCZ: This system was developed to provide a standardized method for describing and comparing the physical characteristics of different areas, particularly in the context of urban climate research [36,37]. The classification of LCZ defined by Stewart and Oke [14] is based on qualitative assessments of urban and rural landscapes. The 17 standard LCZ types are categorized into two main groups: urban LCZ types and natural LCZ types, as follows in Figure 3:
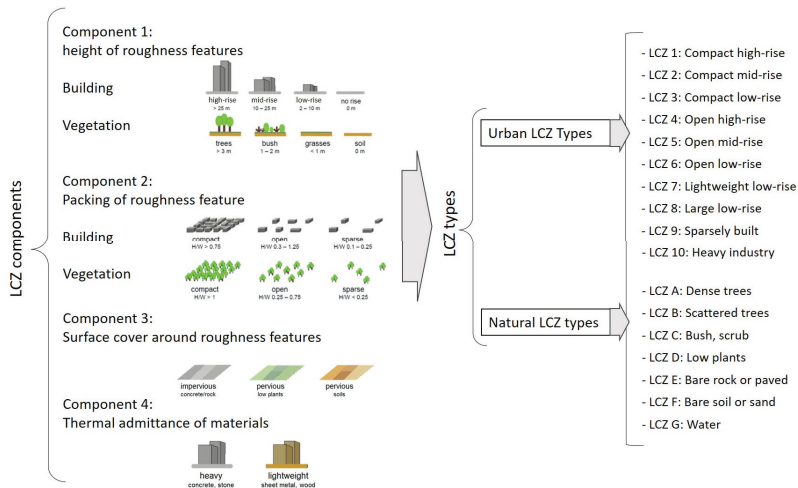
Figure 3. Urban and natural LCZ types based on Stewart and Oke [14].

There are mainly three types of LCZ classification methods: the remote-sensing-based method, including WUDAPT L0, LCZ Generator, and GEE; the GIS-based method; and the combined method [17,19,36]. Generally, the GIS-based method is applied for urban areas, estimating parameters such as building height, density, greening rate, and other spatial metrics, while the remote-sensing-based method is more suitable for natural coverage areas, calculating indices like surface cover, vegetation fraction, and albedo [21,49]. In this research, the primary LCZ classification process was carried out using the LCZ Generator, which provides templates for use with GIS during the sampling process. These templates were also used as auxiliary data to enhance the overall classification accuracy. The LCZ Generator follows WUDAPT's (World Urban Database and Access Portal Tools) default protocol [35,36], which has been sequentially improved over time to facilitate single-city LCZ mapping [21,49]. For the classification, WUDAPT_L0_Training_template [50] was used to generate L0 data. After collecting samples for the 17 LCZ classes, the remaining

steps were performed using the LCZ Generator according to the submission form on the website [17,36,50]. To ensure accuracy, the random forest (RF) algorithm was applied. This method classifies each pixel into an LCZ type based on decision trees and requires minimal training data. To validate the results, the classification process was performed using both the LCZ Generator and the GIS template for consistency, following the WU-DAPT_L0_Training_template [50]. By comparing the outputs of both systems, any potential errors were identified and addressed. The RF algorithm demonstrated high accuracy, and the classification results were confirmed to be consistent with minimal discrepancies.

- LST: This can be derived from thermal infrared data from satellite sensors [20,51]. The formula to convert the brightness temperature to LST uses the thermal band data from Landsat. This formula corrects for emissivity and atmospheric effects to estimate the actual LST [19,21]. The formula involves several steps, including the use of thermal infrared (TIR) imagery and the application of Planck's law and atmospheric correction models. Equation (6) is as follows:

$$\text{LST}(^{\circ}\text{C}) = \frac{T_B}{1 + \left(\lambda \times \frac{T_B}{\rho}\right) \times \ln\varepsilon} - 273.15 \tag{6}$$

T_B: At-satellite brightness temperature in Kelvin, and the final LST is in Celsius;
λ: Wavelength of emitted radiance;
ρ: Constant ($h*c/\sigma = 1.438 \times 10^{-2}$ mK);
ε: Surface emissivity.

High LST values suggest that the surface might occur in urban areas, deserts, or other regions with little vegetation or high heat-absorbing materials, like asphalt and concrete.

Low LST values indicate a surface typically found in areas with dense vegetation, water bodies, or regions with a higher moisture content.

2.3. Study Area

The study area of this research is the city of Seville and its urban settlement area. Seville, in Spain, is situated at 37.3891° N, 5.9845° W [51,52]. Spread over an area of 141.28 km^2, with an average elevation of 6 m above sea level, Seville experiences a Mediterranean climate characterized by hot, dry summers and mild, rainy winters. The average annual temperature in 2020 was around 19 °C, with summer highs often exceeding 35 °C, and every year, 40 °C is surpassed on several occasions [8,53]. Winters are mild, and the city receives about 550 mm of rainfall annually, mostly between October and April. This climate, along with rapid urbanization, influences the city's microclimate and UHIE. Seville is a city with a rich history and cultural heritage dating back to Roman times, and due to being inhabited for centuries, Seville, like many other cities worldwide, underwent significant rapid urban development and substantial urban expansion during the first decade of the 21st century. This period saw a strong boost from public and private investments, which translated into numerous infrastructure projects, urban developments, and economic initiatives [8,54–56].

3. Results

In this section, the main indicators that were mentioned in the methodology section are evaluated and overlapped for providing an understanding of the condition of the study area over a period of 20 years. The parameters include an evaluation of the history of the urban growth trend, population trend, UI trend, and LULCC, NDBI and NDVI, and LCZ and LST patterns from 2003 to 2023. In the first step, the history of urbanization in Seville was studied to find the main causes and reasons for change, and then the process of changing over time was evaluated with the help of previous plans, research studies, and historical documents.

3.1. History of Urban Growth Trend

This study meticulously examines the various facets of urban growth in Seville, incorporating insights from contemporary urban studies and previous plans, programs, and projects to provide a comprehensive overview of Seville's urban growth trends and their climatic ramifications from 2003 to 2023. Based on findings from previous research and under the new General Urban Development Plans (1988, 2006, and 2018), the process of urban growth in the previous century was influenced by various internal and external factors [5,8]. Some World Exhibitions and national and international events and projects, such as the Ibero-American Exposition 1929–1930 (from 1015 to 1029, 36.19% increase in BUA) and the World Exhibition—EXPO'92 (from 1981 to 1992, 40.79% increase in BUA) [53], had a huge effect of shaping the context of the city in 21 centuries. By examining the city's structure, Seville shows an ecological design with a central urban area and radial growth, in which newly developed areas are gradually integrated over several years [57].

In Figure 4, the map of urban growth from 1918 to 1995 (before the period of time that was evaluated in this research) displays rapid and varied types of urbanization and shows the direction of growth in the city of Seville. Initially, growth was circular and compact and involved infill development, but over the decades, it transitioned to ribbon and sprawl [8,55,56].
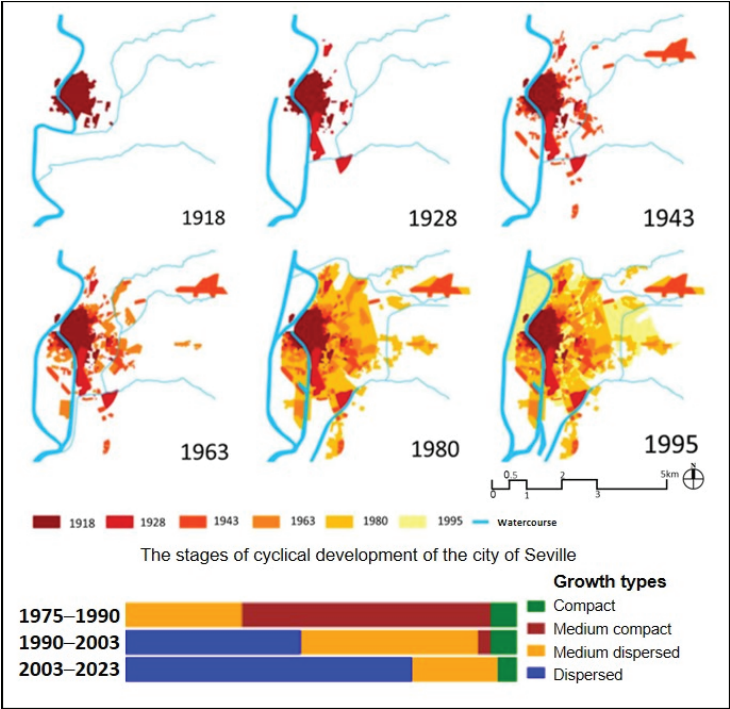
Figure 4. Visual representation of urban growth trends and changes in the city of Seville over the decades based on the master plan of the city, 2006 [8,54,55,57].

These data illustrate and prove the physical growth of the city of Seville before 2003, highlighting the importance of studying this historical data due to the rapid urbanization and high population growth rate in the previous century, the effects of which are still evident years later. In Figure 4, the amount of each type of urban growth is evaluated and classified from compact to medium compact, and from medium dispersed to totally dispersed or sprawl [8,52–54]. It is noted that there was a limitation in accessing the data;

therefore, for the previous century, only the period from 1975 to 2023 is mentioned (for a better understanding of the process of changing, the time of evaluation was extended).

Additionally, the preprocessing and processing images (Figure 5) clarify that the trend of dispersed or sprawl growth in the city was driven by the need to connect to settlements around the main city, resulting from rapid urbanization. Now, in the satellite image related to 2023, we are faced with an urban area, not just a city, based on the direction and pattern of sprawl and changes in urbanization in the study area. These changes demonstrate a network of connections between the city and surrounding urban areas. Therefore, in this study, the city of Seville and its first layer of settlement will be evaluated; in the satellite images, a buffer of 10 Km from the center of the city is analyzed.
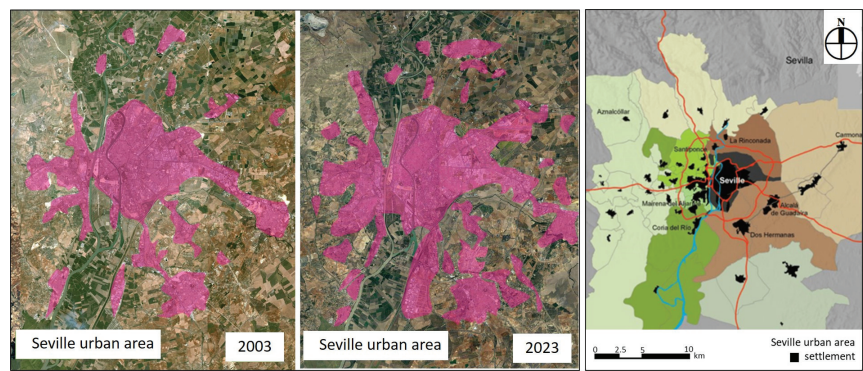
Figure 5. Schematic map of urban growth and expansion from 2003 to 2023 in the city and surrounding settlement [42,58].

3.2. Population Trend

Population trend is one the most important factors in defining types of urbanization and the growth rate. Shifting people, the same as an urbanization process, does not just happen only in the city, it is a process that has an effect on a larger scale area (metropolitan). The city of Seville faced a decline in population growth and experienced a negative growth rate in the city, especially during the last 5 years of 2003 to 2023 (Figure 6). The histogram below shows that Seville has bounced back after experiencing these losses, before 2000 and after 2021. This means the city is losing population, but the question of where people went remains. Therefore, the growth rate of the city and surrounding area in metropolitan Seville is calculated in Table 2, which shows, in comparison to the main city, that the settlement around the city has faced a huge number of changes in population [59].
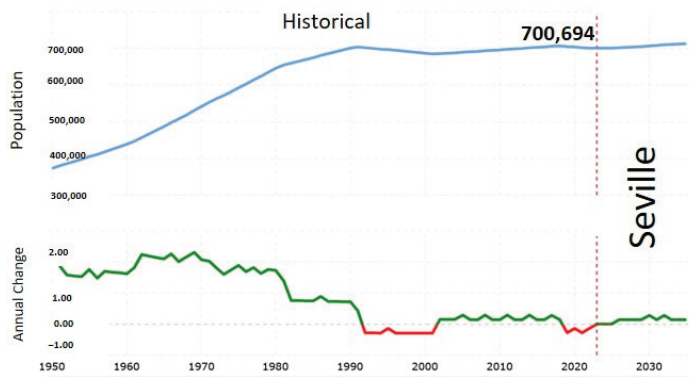
Figure 6. Population trend in the city of Seville over 20 years [59].

Table 2. City and urban area population growth rate [59].

City	Year	Population	Period	Growth Rate
Seville	2003 2023	686,845 700,694	2003–2023	+0.692%
Seville urban area	2003 2023	1,328,985 1,547,945	2003–2023	+10.94%

In the following section, based on linear model in SPSS.19 for the specified multi-year interval, the growth rate and population trend in the city and a comparison within the urban area was evaluated (Figure 7). The results show, in total, both the city and urban areas have positive growth rates; the growth rate in the urban area is almost 15 times bigger than that of the city. This finding indicates that the urban area (metropolitan area) is migrant-receptive, as there was a significant increase in the population and the direction of population movement was from the city to urban areas and suburbs. Seville acts as a source of migrants [8,51,59]; therefore, urban areas have experienced a considerable increase in population and physical growth. This phenomenon can prove the types of urban growth in the past, present, and future of the study area, which are explained in Figures 4 and 5. As mentioned before, these items were the main factors that indicate there is a need for analyzing not only the city but also the surrounding area because they have an effect on the pattern of changing in all of the evaluated indicators.
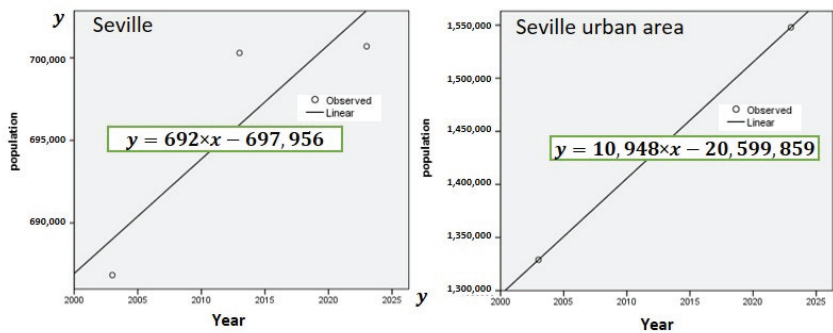
Figure 7. Formula for predicting changes in population trend; processed in SPSS 19.

These results are very important for understanding the patterns of UI, LULC, LCZ, and LST changes, especially in comparison with previous data. Before 2003, when the growth rate of the city was higher and the city was faced with a huge migration of people to city, the type of urbanization was more compact. After 2003, when the annual rate of population decreased in the city, the type of urbanization shifted from compact to dispersed urbanization (Figure 4).

3.3. Evaluation of LULC, NDBI, NDVI, and UI
3.3.1. LULC Evaluation

For the evaluation of urbanization patterns, the first item is the LULC maps (Figure 8 and Table 3). Seville's urban area experienced significant changes in the distribution of land use. In 2023, 42% of land in the urban area was covered by BUAs, compared with only 28% 20 years earlier and almost a 50% decrease in BS. This shows a very high rate of change in urbanization. There is also a substantial increase in areas designated as A/V/F and BUA (Table 3). The area increased from 208,288 m^2 in 2003 to 317,865 m^2 in 2023, showing +52% increase for A/V/F areas and a 51% increase relative to the total area for BUAs, and marking a significant decrease in BS areas (−45.8% compared to 2003).
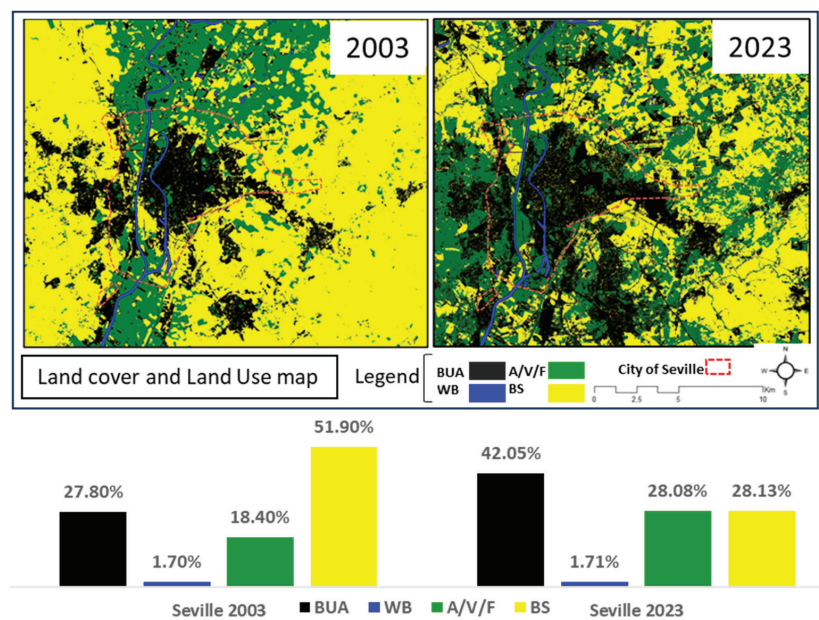
Figure 8. LULC change detection for 20 years; processed in ENVI and GIS, and normalized in SPSS.

Table 3. Comparing the amount of LULC changing trend.

Year	2003		2023	
Area	m^2	Percentage of Total	m^2	Percentage of Total
BUA	314,696	27.8%	476,006	42.1%
WB	19,244	1.7%	19,357	1.7%
A/V/F	208,288	18.4%	317,865	28.1%
BS	587,508	51.9%	318,431	28.1%
Total	1,132,000	100%	1,132,000	100%

Therefore, half of the BS land changed to BUA or A/V/F. In summary, the location of the area that changed to BUA proved the findings of the urban growth trend and population shifting and shows that the city is faced with ribbon and dispersed or sprawl types of urban growth in order to connect to other settlements and to the main roads in the urban area. Additionally, the increase in A/V/F in Seville suggests efforts to promote agriculture areas, possibly through afforestation or urban planning initiatives. As shown on the map, the most significant land use changes have occurred in the northern and northeastern areas, as well as the southeastern and southern areas. It can be said that the pattern of urban growth and changes has continued to follow the growth trends of previous years.

3.3.2. NDBI and NDVI

Over the past 20 years, the urban area of Seville has experienced an increase in mean NDBI values, showing a 0.19-point increase in Figure 8. There is a notable reduction in the blue areas (indicating they are not BUAs) in 2023 compared to 2003. This could reflect an expansion of urban areas where previously there were none or changes in the intensity of urbanized regions. The spread of yellow regions (indicating a low BUA intensity) in 2023 suggests urban changes. In general, based on these maps and histograms (Figure 9), the NDBI parameters are still moving toward 0. This shift does not solely signify a dispersed type of urban growth but indicates that BUAs, such as roads, buildings, and infrastructure (in infill, ribbon, and dispersed growth), are increasing, with more land being developed

and fewer areas remaining as undeveloped or vegetative cover. Urban areas, characterized by high NDBI values due to the presence of built-up structures, tend to have higher surface temperatures compared to surrounding rural or natural areas. In general, the maps show that the north, northwest, east, and south sections of the area are faced with changes more than other parts.
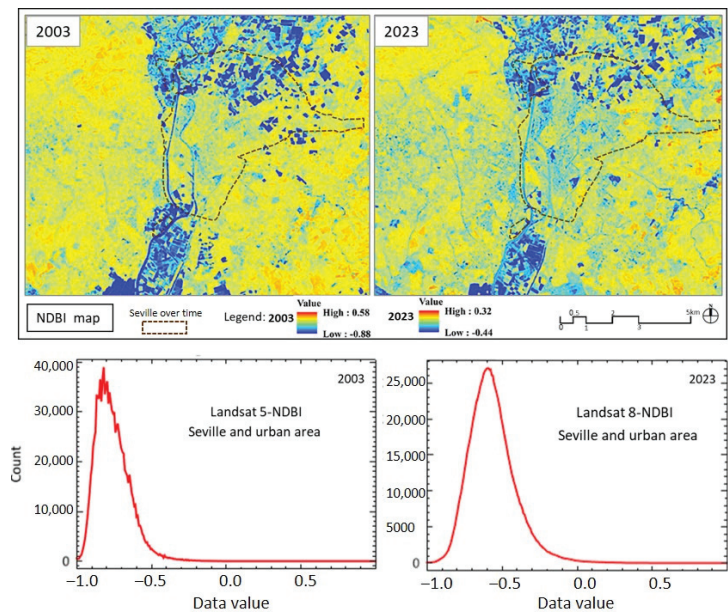
Figure 9. Map and the main data of NDBI index for the city of Seville and its urban area [42].

The main points illustrated in Figure 9 include the following:

- A 0.26-point decrease in the upper limit: More areas now have very high NDBI values, suggesting a rise in dense urbanization and construction.
- A 0.44-point increase in the lower limit: The shift from very low to moderate NDBI values suggests land use change, with natural areas being converted to urban or built-up regions.

In addition, the NDVI maps (Figure 10) show a visible reduction in NDVI values from 2003 to 2023, particularly in the northern and southern parts of Seville, which could be due to deforestation, land clearing for agriculture, or urban development. This shift to a lower NDVI value suggests that the overall vegetation health or density has slightly decreased.

The main points illustrated in Figure 10 include the following:

- A 0.17-point decrease in the upper limit: Fewer areas now have very high NDVI values (dense vegetation).
- A 0.21-point increase in the lower limit: The shift from very low to moderate NDVI values could suggest urban expansion over bare areas, leading to a less natural landscape overall.

Reviewing the NDBI and NDVI maps reveals areas where increased urbanization correlates with decreased vegetation. High values in the NDBI map alongside low NDVI values could indicate regions most affected by urban growth and also prove that although the A/V/F area increased, the quality and level of the health of the vegetation is faced with a reduction.
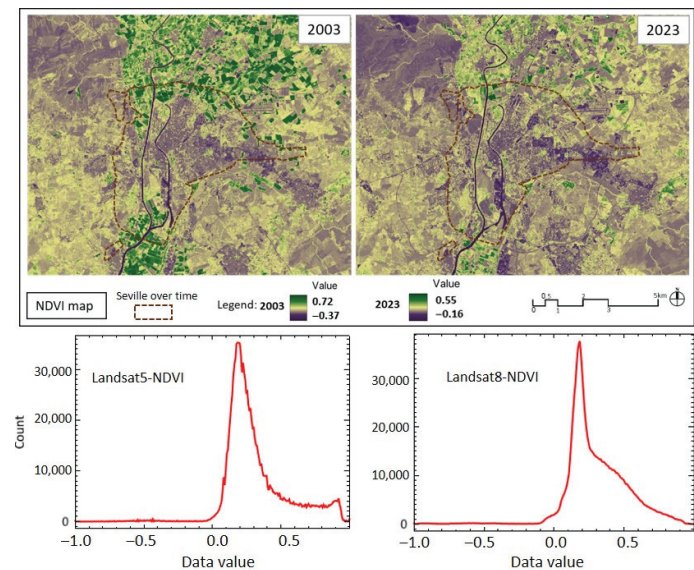
Figure 10. NDVI index for the city of Seville and its urban area [42].

3.3.3. UI

Urban/non-urban area changes or UI over time can be evaluated by the results of the LULCC, NDBI, and NDVI findings and by evaluation plans, projects, and previous research related to Seville. The extent of change in BUAs is revealed as an important dimension compared with the total area, and this parameter clarifies the types, direction, and limitations of urban growth and the urbanization process over 20 years. Figure 11 indicates that the city has faced a noticeable increase in sprawl urban growth and LULCCs. The percentage of BUAs in the total area has increased by 14.25%; when that is compared with other LULCC classes and with changes in BUAs in previous decades, it is quite noticeable that there is a shift toward growing urban footprints around the main city, following population movement. This map shows that within the current boundaries of the city, the extent of urban development and BUAs has significantly expanded, indicating that 42.05% of the land within the city is occupied by BUAs, which has increased by 14.25% over 20 years.

As was mentioned in the methodology section, the Shannon entropy method, which is often used to measure the distribution and intensity of land use, such as BUAs, was utilized in this study area. Based on Table 4, if entropy has decreased, it indicates that urban development has become concentrated in specific areas, such as along transportation routes or in designated development zones, while other areas have seen less development. The entropy value for 2023 was less negative than that for 2003, indicating possible urban sprawl or concentrated development, which is obvious in Figure 11.

Table 4. Calculation of Shannon entropy for the years 2003 and 2023 in Seville.

Year	BUA (m^2)	Pi	(Ln)Pi	H$_i$ = Pi × Ln(Pi)	ΣPi × Ln(Pi)
2003	314,696	0.2784	−1.2788	−0.3560	−0.3560
2023	476,006	0.4206	−0.8662	−0.3643	−0.3643
Total, area			399,734		
ΔH			H$_{2023}$ − H$_{2003}$ = −0.3643 − (−0.3560) = −0.0083		
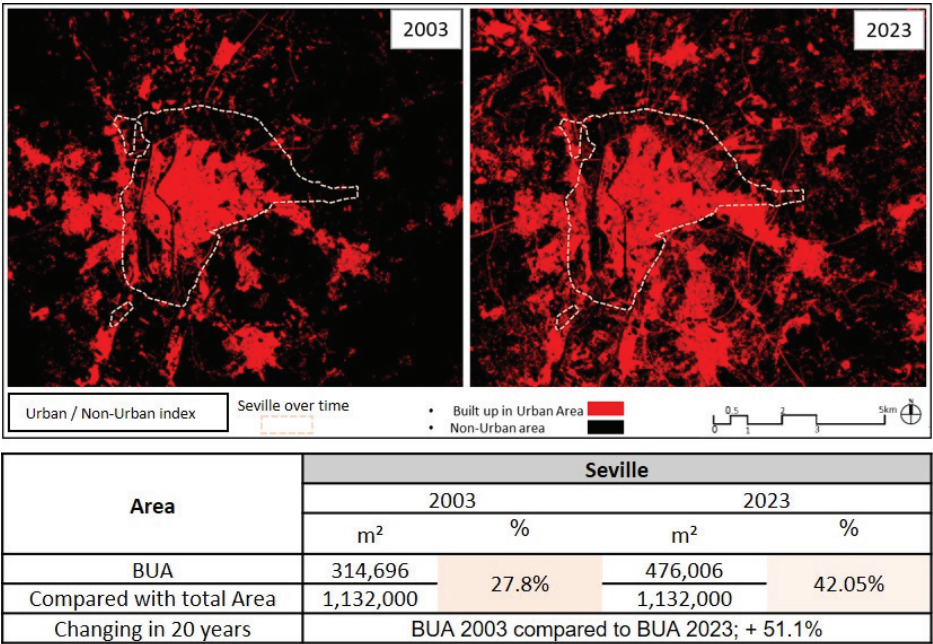
Figure 11. Urban/non-urban area index in 2003 and 2023. Based on ENVI and ARCGIS.

A slight decrease in the entropy value between 2003 and 2023 means that development increased in specific areas of the city, and these areas were being built-up and developed more compared to the past. The areas with a huge amount of change in LULC are in the north and northeast of the urban area (Figure 11).

For better clarification of the types of changes, based on GEE and using JavaScript programming language, UI indexes were generated for 2003 and 2023, and then the maps were overlapped and the types and direction of changes in LULC classes were calculated. The results exactly proved the finding of Shannon entropy (Table 4). In addition, the period of the time was divided into 2003 to 2013 and 2013 to 2023 to better identify the extent of the changes and their trends. The first decade (2003–2013) was more focused on BUAs and agricultural transitions, whereas the second decade (2013–2023) showed a broader spread of changes across BUAs and all land cover types. In Figure 12, the BUA changes indicate significant urbanization and expansion of BUAs, which seems particularly evident in both decades but is more pronounced in the second period (2013–2023). This could reflect infrastructure expansion or city development policies pushing urban sprawl pattern. BS changes (yellow) are evident, especially in the latter decade (2013–2023), suggesting either land clearance, deforestation, or areas prepared for future construction or development. A/V/F changes represent fluctuations in agriculture, forests, or vineyards. While there are pockets of these changes, they seem less dominant in the overall transition compared to BUAs, suggesting more focus on urban growth than agricultural expansion or reforestation. WB changes indicate water body changes, but the minimal representation of this category suggests that water-related changes were less significant in this timeframe.

In general, the northern and southern zones of the highlighted region in Seville appear to have experienced the most intense changes. In particular, the expansion of BUAs is evident in the southern peripheries, potentially indicating suburbanization or the development of new residential or industrial zones. Inner city areas, particularly those within the marked boundary, show less change, suggesting that urban densification or expansion has primarily occurred in the outskirts, while the central city area remains stable.
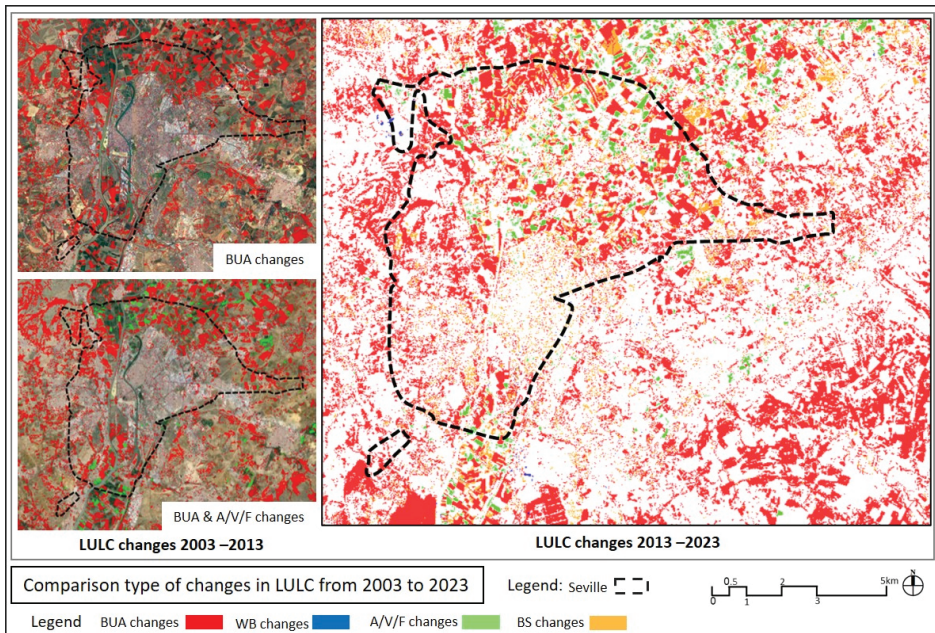
Figure 12. Comparison of types of changes in LULC over time.

These changes, particularly the significant rise in BUAs, likely point to urban development and land preparation for future projects. Therefore, there is a need for evaluation of city reports and development plans. One of the main datapoints that helps categorize the changes is the city data from open-access resources and city documents. The city's strategic plans were studied, and two maps were made demonstrating what the development process would be like in the future (Figure 13). These two maps are development planning and classification of urban developable and non-developable areas, based on online GIS data of Seville [60]. The map of development and UI map from satellite images show the same pattern, meaning the number of changes in UI is based on predicted plans and projects of the city master plan, respecting legal, environmental, and historical opportunities and constraints, which is because of urban planning laws and regulations that have influenced land use changes and the direction of growth.

The development planning map (Figure 13A) shows different stages of urban planning across the city, including areas that are still being processed, those that have received final approval (pink), and areas where development has been annulled due to legal reasons (purple). It highlights zones of significant interest where urban development is either ongoing or proposed. The classification map (B) provides a detailed categorization of land into developable and non-developable zones based on its potential for urban development and its conservation status [61,62]. Developable areas are shown in colors like yellow and orange, indicating land that can be urbanized, while green areas represent non-developable zones, such as protected natural or rural areas.

There is a clear distinction between urban expansion zones (developable land) and protected or rural zones (non-developable land). These maps, together, illustrate the planning status and how urban planning is structured in terms of both the approval process and land categorization, helping to visualize which areas will undergo future development and which are preserved. These maps also provide a comprehensive view of urban development strategy, highlighting the complexities of managing growth and showing which areas are prioritized for urbanization and which are protected from it.

The combination of Figures 12 and 13 indicates that the areas designated as "development zones" in the proposed plan have experienced the highest levels of change in both BS and BUAs. Notably, these changes became more pronounced during the second decade of the period under review. These maps are based on current data from the city of Seville, obtained through up-to-date sources and modeled in conjunction with satellite imagery.
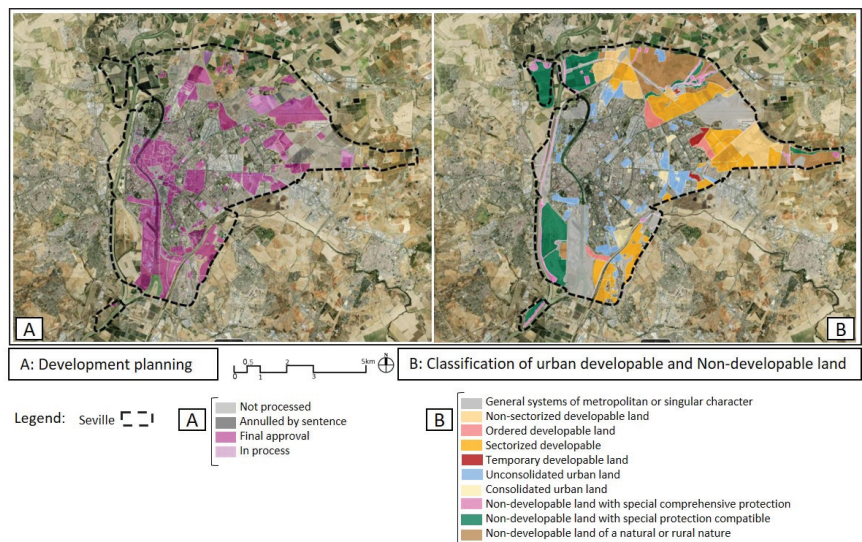
Figure 13. Map of development planning and classification of urban developable types [60].

3.3.4. LCZ

As was mentioned in the methodology section, to compare the LCZs of Seville between 2003 and 2023, several factors should be considered, including changes in urbanization, vegetation cover, industrial expansion, and infrastructural developments [14,35,36]. Seville has become more urbanized, especially with the rise of mid-rise and high-rise buildings. New areas have been developed, and suburban zones have become more compact. In 2003, the densely built environment in the city center and lack of greenery was obvious, and focus on climate mitigation in urban design was less pronounced, but over the past 20 years, the city has introduced efforts to introduce more green spaces through tree planting, construct sustainable buildings, and incorporate smart infrastructure to control climate changes, to expand LCZs A and B (Figure 3), and to limit excessive temperature rise in LCZs 1–3. The general data of the LCZ maps is defined by the LCZ Generator [50] (Table 5):

Table 5. General data of LCZ map; LCZ Generator [36,50].

Submission Information	Submission Date	Representative Date
Seville LCZ map	23 July 2024 16 July 2024	12 December 2023 12 September 2003

Figure 14 shows the LCZ distribution in Seville in 2003 and 2023. The colors represent different LCZ classes, such as urban areas, vegetation, bare soil, water bodies, etc. In 2003, the urban region was more concentrated in a central location with less surrounding urban sprawl, but over 20 years, there are visible changes in the land cover, with a likely transition of some natural zones into more developed or urbanized regions and a visible increase in red zones (LCZs 1 and 2), indicating a significant rise in built-up or dense urban areas between 2003 and 2023.
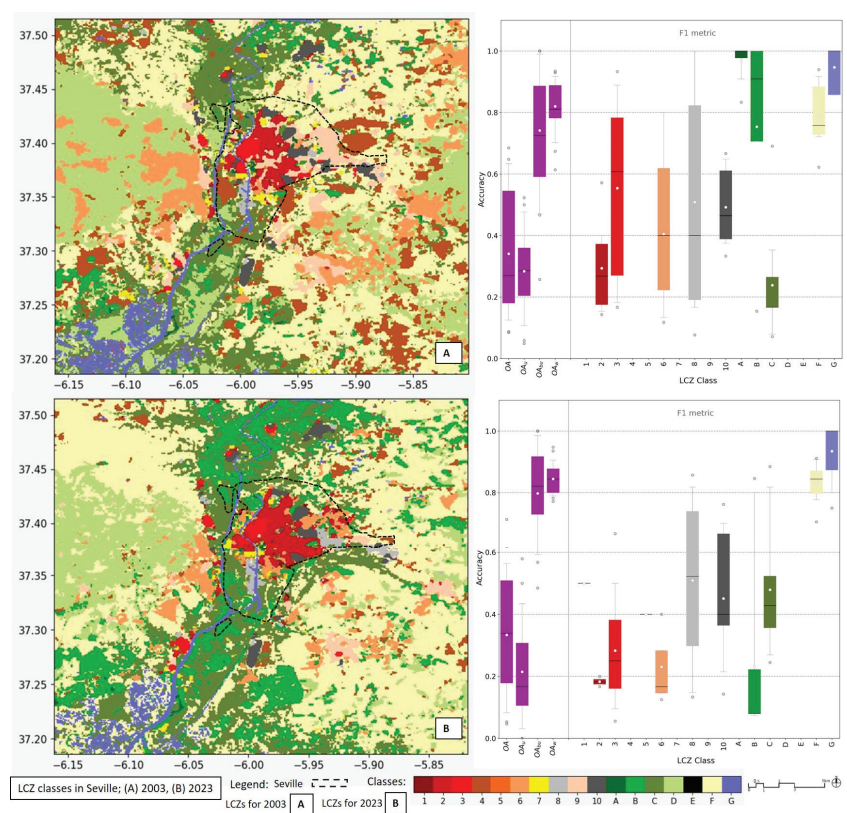
Figure 14. LCZ map; analyzed in QGIS and LCZ Generator [42,50,58].

The area and classes with the most significant changes based on the findings of the LCZ maps and maps of UI and urban development and the results of the master and strategic plans of Seville are shown in Table 6.

Table 6. Main changes in LCZ classes in Seville urbanization and built environment (2003 vs. 2023).

LCZ Classes	2003	2023
LCZ 1 (compact high-rise)	Limited to a few business districts.	Further urban development and modernization added areas like Torre Sevilla and new commercial centers.
LCZ 2 (compact mid-rise)	Central part of Seville, especially historic areas like Santa Cruz and El Arenal, retained their mid-rise, compact structures.	The central part has remained largely unchanged, as historical preservation laws protect this area.
LCZ 8 (large low-rise)	Industrial areas were still in expansion, but significant growth was underway.	Large low-rise zones have expanded significantly due to the growth of the Seville industrial park and commercial warehousing sectors
LCZ 9 (sparsely built)	Areas on the outskirts, with large plots of land, are still undeveloped.	Urban expansion and developments have reduced sparsely built areas.
LCZ 10 (heavy industry)	Industrial areas were concentrated in specific zones (on the outskirts).	Industrial expansion, in the Zona Franca and areas near the port, reflect Seville's growing industrial economy.
LCZ A (dense trees)	Parks, such as Parque de María Luisa, were well-maintained.	The expansion of green spaces and urban forestry projects slightly expanded LCZ A.
LCZ B (scattered trees)	Tress were commonly found in residential neighborhoods and near the Guadalquivir River.	Expansion of urban gardens and street trees as part of Seville's environmental policies increases this type of LCZ.

The box plots on the right side show the accuracy and F1 metrics for different LCZ classes (Figure 14). Each color in the box plot corresponds to a different LCZ class, as shown in the map legend. The higher the box plot, the more accurately the LCZ class has been predicted or classified. It can be seen that some LCZ classes, like urban areas, might have higher accuracy compared to others. This metric combines precision and recall, providing an overall measure of classification performance. High F1 values in the box plots mean that certain LCZ classes, such as those in purple and blue, have been classified with greater consistency.

3.3.5. LST

LST, as a primary indicator for the evaluation of climate change and environmental conditions, is classified based on a period of 20 years. Figure 15 indicates that the entire urban area has experienced an excessive increase in mean temperature because of urban expansion, LCZ changes, and a dense population. The maps in Figure 15 show how different types of land cover absorb and retain heat.
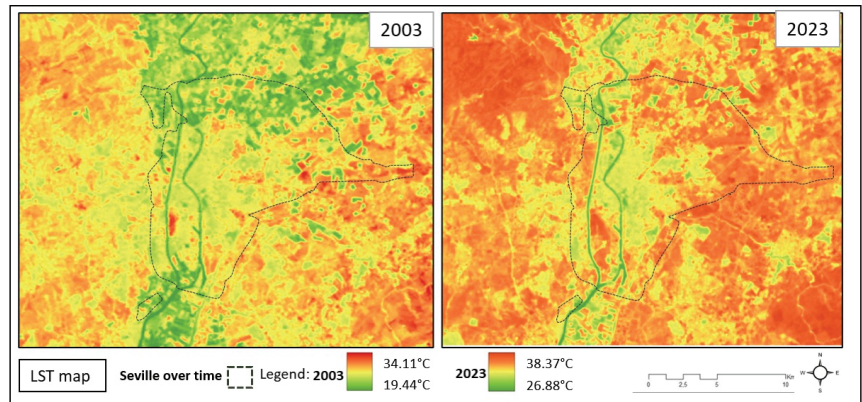
Figure 15. Analysis of LST (°C) pattern over time and changes in LST mean.

The LST maps were calculated using RS-based Landsat 5 TM, Collection 2 (band 6) for 2003 and Landsat 8 TIRS (band 10) for 2023, with temperatures expressed in Celsius. The data were obtained from satellite images collected between 1 July and 31 July for both years. The final LST map is the result of combining multiple satellite images captured over this time period to create a comprehensive representation of typical summer conditions. In ENVI, standard pre-processing techniques, including atmospheric correction and layer stacking, were applied to ensure accurate and consistent LST calculations [42].

Mostly built areas are hotter than other areas, and agriculture land increases thermal comfort, but the number of changes in the A/F/V area is significantly noticeable. The central part of Seville, marked by green areas, and the historical area indicate lower temperatures compared to the surrounding regions. This suggests that the core urban area, despite being densely built-up, has managed to avoid the same level of temperature increase as the outlying areas.

To gain a clearer insight into the pattern of changes, data trends from 1993 to 2023 were evaluated and are displayed in Figure 16. The graph shows a consistent upward trend in the mean LST in July, from 30.13 °C in 1993 to 38.37 °C in 2023 [61,62]. This highlights a near 8 °C rise in surface temperatures over 30 years. In total, the annual average increase rate from 2003 to 2013 is 0.198 °C per year; from 2013 to 2023 is 0.228 °C per year; and the overall rate (from 1993 to 2023) is 0.275 °C per year. The compound annual growth rate (CAGR) is calculated based Equation (7):

$$CAGR = \left(\frac{Value\ at\ the\ end}{Value\ at\ the\ begining} \right)^{\frac{1}{Number\ of\ Years}} - 1 \qquad (7)$$

Value at the end: temperature in 2023;
Value at the beginning: temperature in 2003;
Number of Years: between 2003 and 2023 (20 years).

	V/F/A	BUA/ IS	WB	BS
2003	29.9	33.5	24.8	34
2023	36.5	39.9	33	40.5

Mean LST of the LULC classes in Seville urban area

	1993	2003	2013	2023
LST	30.13	34.11	36.09	38.37

Mean LST in Seville urban area from 1993 to 2023
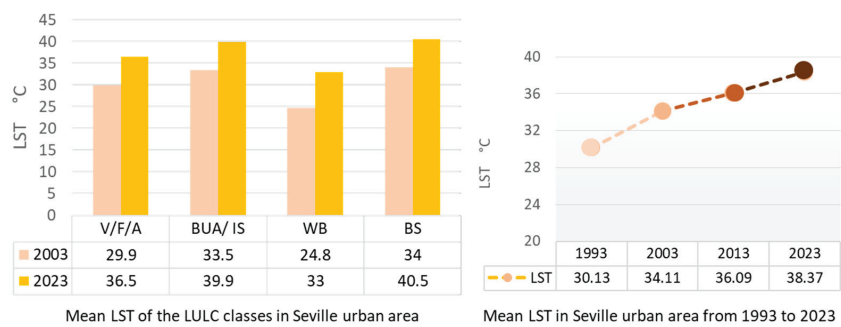
Figure 16. Mean of LST (°C) and LULCC in urban area in July 2003 and 2023.

The CAGR for the LST in Seville from 2003 to 2023 is 0.59% per year; that is higher than the global average for urban areas [61,62]. The global urban LST has increased by approximately 0.38% per year during a similar timeframe [61].

In Figure 16, each category shows an increase in the LST. The BS category experienced the highest increase, with the LST rising from 34 °C in 2003 to 40.5 °C in 2023, a 6.5 °C increase, followed by BUA; the locations of these hotspot areas are specified in Figure 15. As the LST increases, the NDVI declines, leading to more extensive areas of stress and possibly desertification or reduced agricultural productivity over time. This relationship highlights the environmental changes happening in Seville, possibly due to climate change, urbanization, or other anthropogenic factors, and clarifies that Seville is experiencing a relatively rapid increase in LST due to rapid urbanization process in past decades. In connection with Figures 11 and 13, that means this amount of change and increase in hotspot areas is the result of the proposed city plans from previous years [60].

4. Discussion

This section uses overlapping maps and thermal images to illustrate the direct correlation between urban expansion, the LCZ, and increased LST. These visuals highlight that urbanized (BUAs) and barren soil (BS) areas tend to be warmer, while vegetated and WB zones are cooler. Figure 15 specifically shows that in 2023, BS areas experienced the most significant temperature increase over the last 20 years, with all the LULC categories generally showing rising LSTs. These findings correlate urban expansion with temperature increases, in comparison with the 20-year LCZ maps, and, particularly, an increase in density in the central (not the historical part of the city) part and expanding outwards corresponds with reductions in BS areas. It is evident that areas that have undergone changes in the density patterns of their urban fabric, as well as those where classification or LULC has shifted based on the land context, have experienced the most significant changes in LST. These changes are illustrated in Figure 14 in the LCZ section. The city center of Seville, with its compact mid-rise (LCZ 2) and low-rise (LCZ 3) buildings, was already experiencing higher temperatures compared to the surrounding areas, especially in summer. New developments, particularly the increase in high-rise buildings (LCZ 1) and expansion in industrial zones (LCZ 10), have contributed to higher LSTs in these areas. The addition of more high-rise buildings has led to significant increases in LST in areas like Torre Sevilla and the Triana district, where tall buildings trap heat. The LST in

these areas is significantly higher compared to low-rise or suburban zones due to reduced vegetation and the heat-retention properties of concrete and asphalt (Figure 15). While the LST in low-rise zones (LCZ 3 and LCZ 6) has remained high, urban greening efforts and changes in construction materials have slightly mitigated temperature increases in some neighborhoods. Industrial expansion (LCZ 8 and LCZ 10) has contributed to an increase in LST. These areas are now some of the hottest zones in Seville, with large heat-retaining surfaces and minimal vegetation (e.g., asphalt, concrete). In addition, the LST of urban areas, based on UI (Figures 11 and 12), was compared with the LST of non-urban areas to understand the impact of urbanization on local temperatures. This is reflected in the UI maps (Figure 11) and LST maps (Figure 15), showing more red areas (BUAs) in 2023 compared to 2003, indicating an increase in the temperature. Therefore, there is a need for an urbanization pattern map based on overlapping UI maps over time (Figure 17). This map shows Seville's urban growth trends, pattern directions, and limitations, and reveals significant urban growth through sprawl and ribbon development, particularly at the city's borders and in suburban areas, with dense infill development in central urban areas.
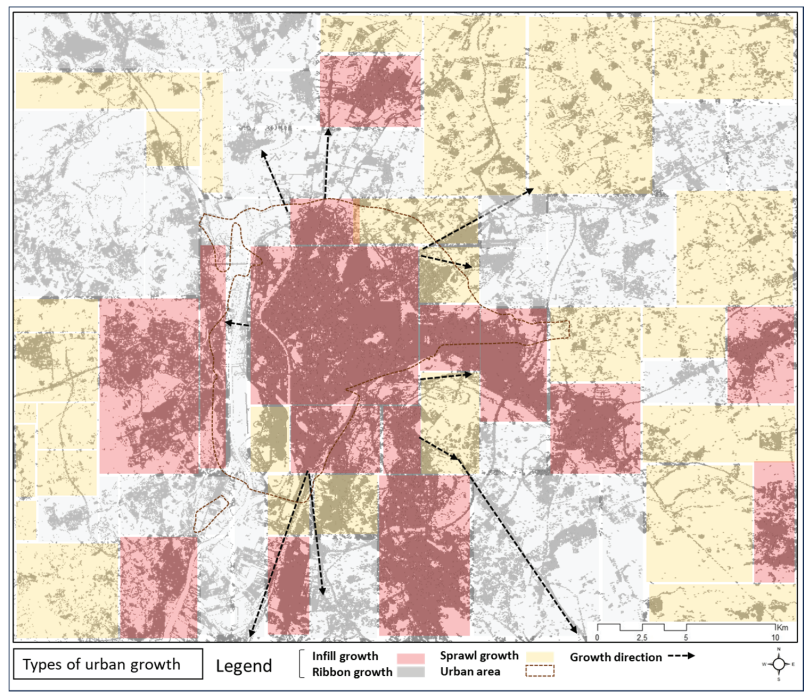
Figure 17. The pattern of urbanization process and direction of urban growth.

4.1. The Pattern of the Urbanization Process

Figure 17 highlights the role of LULC patterns in shaping local temperature regimes and indicates a trend toward a mixed development pattern over a 20-year period. The map also shows an increasing of urban dispersion, based on the characteristics of BUAs, and a reduction in BS, influenced by factors such as infrastructure and network enhancements, which have shifted residential patterns from the city to more affordable suburban areas, and historical conservation, whose efforts have limited changes in Seville's historical core, preserving its character [53,54].

The central, eastern, and northern parts of Seville are the main hotspots experiencing the most significant temperature increases, while the historical center, areas near the river, and the western and southern regions also see warming, but to a lesser extent compared to

the core urban areas. Comparing maps of the LST and LULCC show that the study area has experienced rapid urbanization, and the highest average temperature changes happen in these mentioned areas. These areas are shown based on their distances from the center of the city, with a radiance of 10 Km (Figure 18), which proves that the parts of the urban area that had significant increases in LST are the areas with significant LULCC, NDBI, and NDVI changes. For instance, areas with low NDVI values are predicted to often exhibit higher LST values due to the lack of vegetation cover and increased heat absorption by built-up surfaces. Another point that must be mentioned is related to the population trend (Figure 6). The city of Seville faced an almost zero growth rate in recent years, while the urban area has had a significant growth rate; therefore, the pattern of change around the city based on the growth rate in the urban area and the result of the city's development strategies is acceptable.
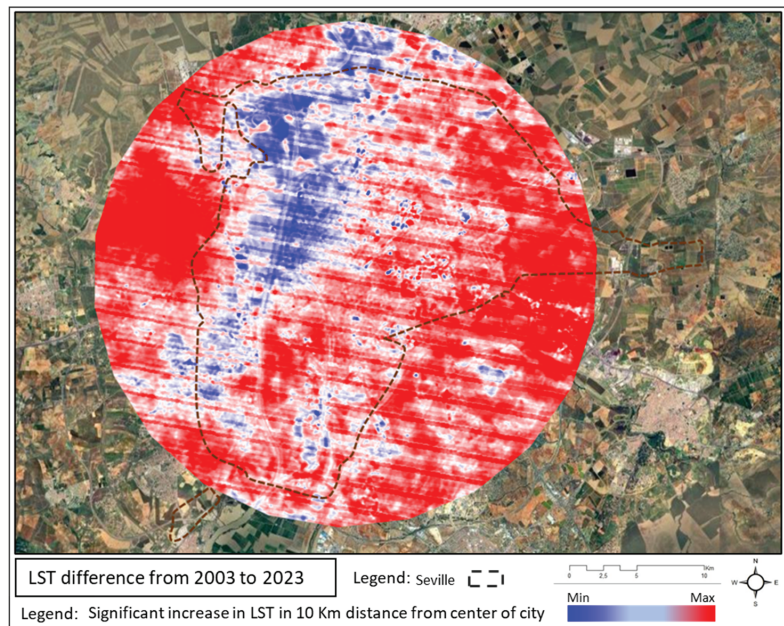
Figure 18. Area with significant changes in LST (2003–2023).

Figure 17 provides a visual representation of different types of urban growth within the city and surrounding area, based on historical trends and LCZ changes and the findings of Figure 13, that overlap, using GIS and raster databases. The growth directions show the main directions in which the city's urban expansion is occurring, pointing toward the outskirts or less developed areas of the province along major transport routes. This highlights a linear expansion pattern that can influence transportation and housing policies. The presence of infill growth in central areas suggests attempts to utilize available space efficiently, whereas the sprawl growth around the periphery indicates ongoing expansion, possibly at the cost of greenfield or agricultural land.

Evaluating Figure 17 with Figure 13, these main points must be mentioned:

- Areas (city) marked as "in process" or "final proposal" in map 12.A align with regions showing infill or sprawl growth in the current map, indicating where future developments are targeted or planned.
- Areas marked as "annulled by sentence" could correlate with areas that are not experiencing significant growth in the current map, suggesting that regulatory restrictions have halted developments.

- The distinction between developable and non-developable land in the urbanization process (map 13.B) is directly linked to the growth types indicated here. For example, areas marked non-developable due to environmental protection might be adjacent to but do not overlap with sprawl growth areas.
- The "consolidated urban land" regions from map 13.B likely correspond to the "urban area" and "infill growth" sections in this map.

These maps collectively provide a multi-faceted view of urban development dynamics, understanding the types of growth, the stages of development, and the classification of land use. Such detailed mapping aids in assessing the balance between development needs and environmental conservation, crucial for crafting policies that guide urban expansion in a manner that is both economically viable and ecologically responsible. In essence, these maps form a foundational tool for decision-makers to visualize and strategize urban growth, ensuring that development is aligned with broader sustainability and resilience goals.

4.2. The Pattern of LST Changes over 20 Years

These urbanization trends correlate with changes in the LST and highlight the impact of urban development on local climates. Based on Figure 12 that was obtained from the overlay of the UI, with the aim of making a more precise comparison with LST change patterns, a map of the LST differences over time was created by overlaying the maps of Figure 15 via programming in GEE platform.

Figure 18 is a comprehensive map that shows which part of the city is faced with a significant amount of changes in temperature. This does not mean each area has high or low temperature; it identifies the areas that have experienced the most significant temperature changes due to urban development. This map shows the areas that are at risk, sensitive, and vulnerable in the future in terms of temperature changes, particularly the northern and southeastern peripheries, where urban sprawl and industrial growth have led to significant increases in LST. These areas are most at risk due to the lack of green infrastructure and the dominance of impervious surfaces.

Seville has experienced an overall increase in the average LST over the past 20 years, partly due to urban expansion and climate change. The city's growing compact built areas, particularly in high-rise and mid-rise zones, have led to higher temperatures in these areas. The expansion of compact BUAs, classified as LCZ 1, LCZ 2, and LCZ 10 (high-rise, mid-rise, and industrial zones) now show the highest LST values compared to 2003 (Figure 14). These zones experience hotter surface temperatures, especially during the summer. The expansion of green zones (LCZ A and B) in 2023 and urban greening policies have slightly mitigated LST increases in some areas. In 2003, suburban areas of Seville had lower LSTs compared to the city center. By 2023, due to suburban expansion (LCZ 6 and LCZ 9), these areas also showed a rise in LST. New developments in areas like Sevilla Este have led to a mix of LST trends, where built environments contribute to increased heat, but new green spaces help offset some of the warming. All these indicators, compared to the trend of urban growth in the period before the timeframe studied (Figure 4), demonstrate the direct effects of urban sprawl on changes in LCZs and LST. The correlation between urbanization and LST is evident throughout this study, demonstrating how unplanned urban expansion can lead to undesirable temperature increases and environmental degradation. To achieve sustainable urban growth, these findings underscore the importance of incorporating climate-responsive planning strategies. For example, encouraging infill development and mixed-use zoning can limit urban sprawl while optimizing land use. Additionally, integrating renewable energy sources, improving public transportation systems, increasing the proportion of green buildings, limiting industrial expansion near residential zones, and promoting compact vertical growth instead of horizontal sprawl can significantly reduce Seville's overall carbon footprint and will help maintain thermal balance.

In summary, this paper confirms the results of previous research on urbanization and surface temperature changes. Although no prior study has comprehensively addressed the simultaneous analysis of LST, LCZ, and the urbanization index, this research builds

upon the findings from studies on UHI, LCZ, and urban growth patterns. Given Seville's specific climatic and temperature conditions, numerous studies have examined its thermal characteristics, and this paper integrates these components while further confirming the trends in the city's strategic development plans. This research highlights the links between urbanization and surface temperature, advancing the insights from previous studies.

5. Conclusions

This study examines the thermal impacts of urbanization on LCZs and LSTs in Seville over the past two decades. The findings emphasize that urban planning must integrate green infrastructure and sustainable land use to mitigate the environmental impacts of urban growth. The key recommendations include the expansion of green spaces, especially in vulnerable northern and southeastern areas, where urban sprawl and industrial development have led to significant temperature increases. Additionally, enforcing stricter zoning laws to limit sprawl and encourage compact, vertical growth will help reduce the long-term effects of UHI.

This study also highlights the need for continuous evaluation of urban plans and strategies to understand their long-term impacts on LCZ and LST patterns. The results confirm that changes in land use, particularly in built-up areas (BUA), have led to significant temperature rises, with an average increase of 6.4 °C in these areas. Predictive models for LCZ and LST changes should be developed to help urban planners to implement climate-resilient policies for managing sustainable growth.

Seville's experience provides a model for global urban environmental management, demonstrating how cities can adopt land-use policies that address the negative effects of urbanization and promote sustainable development. Regular assessment of city plans and strategic actions is necessary to understand their impact on the local climate and LST. Enhancing green infrastructure and promoting sustainable development in sensitive areas are essential measures to counteract the negative consequences of rapid urbanization.

This research also concludes that, in addition to global climate change, urban development and the shift from compact to sprawling growth patterns have significantly contributed to the rise in surface temperatures in Seville. Therefore, it is crucial to review and adjust the city's strategic plans to mitigate these environmental impacts. Future research should focus on developing predictive models to assess the direct and indirect effects of LULCCs on LST and guide urban planning in vulnerable areas by adopting climate-resilient infrastructure.

The analysis of Seville's urbanization process underscores the importance of understanding how land use and cover changes can influence local climate dynamics. This study's results indicate that the increase in temperature within BUAs is more significant than in other land types, with the total temperature rise in Seville being 4.26 °C, and 6.4 °C specifically in BUAs. This rise in temperature is closely linked to urban development trends and the transition from compact growth to dispersed urban growth.

In conclusion, Seville's urban development trends, while aligned with global climate patterns, also highlight the role of local urban planning decisions in shaping temperature increases. To effectively manage these challenges, cities must regularly revise their strategic plans to ensure they are compatible with environmental sustainability goals. Future research should focus on further refining the models used in this study and applying them to other cities to enhance global urban resilience against climate change.

Author Contributions: Conceptualization, N.F. (Nadia Falah), N.F. (Nahid Falah) and J.S.-G.; methodology, N.F. (Nadia Falah) and N.F. (Nahid Falah); software, N.F. (Nadia Falah) and N.F. (Nahid Falah); validation, N.F. (Nadia Falah) and J.S.-G.; formal analysis, N.F. (Nadia Falah) and J.S.-G.; investigation, N.F. (Nadia Falah) and N.F. (Nahid Falah); resources, N.F. (Nadia Falah), N.F. (Nahid Falah) and J.S.-G.; data curation, N.F. (Nadia Falah) and J.S.-G.; writing—original draft preparation N.F. (Nadia Falah), N.F. (Nahid Falah) and J.S.-G.; writing—review and editing, N.F. (Nadia Falah) and J.S.-G.; visualisation, N.F. (Nadia Falah) and N.F. (Nahid Falah); supervision, J.S.-G. All authors have read and agreed to the published version of the manuscript.

Abbreviations

LST	Land surface temperature
LCZ	Local climate zones
LULC	Land use and land cover
UI	Urbanization index
RS	Remote sensing
GEE	Google Earth Engine
GIS	Geographic information system
ENVI	Environmental visual imaging software
BUA	Built-up area
WB	Water body
A/V/F	Agricultural/vegetation/forest
BS	Barren soil
MLC	Maximum likelihood classifier
SVM	Support vector machine
GWR	Geographically weighted regression
NDVI	Normalized difference vegetation index
NDBI	Normalized difference built-up index
ANN	Artificial neural network
TIR	Thermal infrared
ROI	Region of interest
TA	Training area
WUDAPT	World Urban Database and Access Portal Tools
CAGR	Compound annual growth rate
SPSS	Statistical Package for the Social Sciences
UHIE	Urban heat island effect
USGS	United States Geological Survey

References

1. Almulhim, A.I.; Bibri, S.E.; Sharifi, A.; Ahmad, S.; Almatar, K.M. Emerging Trends and Knowledge Structures of Urbanization and Environmental Sustainability: A Regional Perspective. *Sustainability* **2022**, *14*, 13195. [CrossRef]
2. United Nations World Urbanization Prospects—Population Division—United Nations. Available online: https://population.un.org/wup/Country-Profiles/ (accessed on 4 December 2023).
3. Yan, H.; Liu, Z. A New Perspective on the Evaluation of Urbanization Sustainability: Urban Health Examination. *Sustainability* **2023**, *15*, 9338. [CrossRef]
4. Zheng, Y.; Tang, L.; Wang, H. An Improved Approach for Monitoring Urban Built-up Areas by Combining NPP-VIIRS Nighttime Light, NDVI, NDWI, and NDBI. *J. Clean. Prod.* **2021**, *328*, 129488. [CrossRef]
5. Lopez-Carreiro, I.; Monzon, A. Evaluating Sustainability and Innovation of Mobility Patterns in Spanish Cities. Analysis by Size and Urban Typology. *Sustain. Cities Soc.* **2018**, *38*, 684–696. [CrossRef]
6. World Bank. Urban Development Overview. Available online: https://www.worldbank.org/en/topic/urbandevelopment/overview (accessed on 5 December 2023).
7. Feng, Y.; Wang, R.; Tong, X.; Zhai, S. Comparison of Change and Static State as the Dependent Variable for Modeling Urban Growth. *Geocarto Int.* **2021**, *37*, 6975–6998. [CrossRef]
8. Gago, E.J.; Berrizbeitia, S.E.; Torres, R.P.; Muneer, T. Effect of Land Use/Cover Changes on Urban Cool Island Phenomenon in Seville, Spain. *Energies* **2020**, *13*, 3040. [CrossRef]
9. López-Casado, D.; Fernández-Salinas, V. The Expression of Illegal Urbanism in the Urban Morphology and Landscape: The Case of the Metropolitan Area of Seville (Spain). *Land* **2023**, *12*, 2108. [CrossRef]
10. Hewitt, R.J.; Shadman Roodposhti, M.; Bryan, B.A. There's No Best Model! Addressing Limitations of Land-Use Scenario Modelling through Multi-Model Ensembles. *Int. J. Geogr. Inf. Sci.* **2022**, *36*, 2352–2385. [CrossRef]
11. Liu, Y.; Hu, Y.; Long, S.; Liu, L.; Liu, X. Analysis of the Effectiveness of Urban Land-Use-Change Models Based on the Measurement of Spatio-Temporal, Dynamic Urban Growth: A Cellular Automata Case Study. *Sustainability* **2017**, *9*, 796. [CrossRef]

12. Falah, N.; Karimi, A.; Harandi, A.T. Urban Growth Modeling Using Cellular Automata Model and AHP (Case Study: Qazvin City). *Model. Earth Syst. Environ.* **2020**, *6*, 235–248. [CrossRef]
13. Wang, Z.; Ishida, Y.; Mochida, A. Effective Factors for Reducing Land Surface Temperature in Each Local Climate Zone Built Type in Tokyo and Shanghai. *Remote Sens.* **2023**, *15*, 3840. [CrossRef]
14. Stewart, I.D.; Oke, T.R. Local Climate Zones for Urban Temperature Studies. *Bull. Am. Meteorol. Soc.* **2012**, *93*, 1879–1900. [CrossRef]
15. Pramanik, S.; Punia, M. Land Use/Land Cover Change and Surface Urban Heat Island Intensity: Source–Sink Landscape-Based Study in Delhi, India. *Environ. Dev. Sustain.* **2020**, *22*, 7331–7356. [CrossRef]
16. Bai, Y.; Liu, L.; Yang, J.; Wang, J.; Zou, Q. Drivers of Land Surface Temperatures from the Perspective of Urban Functional Zones. *IEEE J. Sel. Top. Appl. Earth Obs. Remote Sens.* **2024**, *17*, 926–937. [CrossRef]
17. Huang, F.; Jiang, S.; Zhan, W.; Bechtel, B.; Liu, Z.; Demuzere, M.; Huang, Y.; Xu, Y.; Ma, L.; Xia, W.; et al. Mapping Local Climate Zones for Cities: A Large Review. *Remote Sens. Environ.* **2023**, *292*, 113573. [CrossRef]
18. Yan, J.; Yin, C.; An, Z.; Mu, B.; Wen, Q.; Li, Y.; Zhang, Y.; Chen, W.; Wang, L.; Song, Y. The Influence of Urban Form on Land Surface Temperature: A Comprehensive Investigation from 2D Urban Land Use and 3D Buildings. *Land* **2023**, *12*, 1802. [CrossRef]
19. Yang, J.; Ren, J.; Sun, D.; Xiao, X.; Xia, J.; Jin, C.; Li, X. Understanding Land Surface Temperature Impact Factors Based on Local Climate Zones. *Sustain. Cities Soc.* **2021**, *69*, 102818. [CrossRef]
20. Wang, S.; Ma, Q.; Ding, H.; Liang, H. Detection of Urban Expansion and Land Surface Temperature Change Using Multi-Temporal Landsat Images. *Resour. Conserv. Recycl.* **2018**, *128*, 526–534. [CrossRef]
21. Cai, M.; Ren, C.; Xu, Y.; Lau, K.K.L.; Wang, R. Investigating the Relationship between Local Climate Zone and Land Surface Temperature Using an Improved WUDAPT Methodology—A Case Study of Yangtze River Delta, China. *Urban Clim.* **2018**, *24*, 485–502. [CrossRef]
22. Abu Bakar, A.H.; Cheen, K.S. A Framework for Assessing the Sustainable Urban Development. *Procedia Soc. Behav. Sci.* **2013**, *85*, 484–492. [CrossRef]
23. Zhang, W. Evaluation Method of Urban Sustainable Development Based on Entropy Method. *Adv. Eng. Res.* **2017**, *130*, 1086–1089. [CrossRef]
24. Yang, B.; Xu, T.; Shi, L. Analysis on Sustainable Urban Development Levels and Trends in China's Cities. *J. Clean. Prod.* **2017**, *141*, 868–880. [CrossRef]
25. Gabaldón-Leal, C.; Lorite, I.J.; Mínguez, M.I.; Lizaso, J.I.; Dosio, A.; Sanchez, E.; Ruiz-Ramos, M. Strategies for Adapting Maize to Climate Change and Extreme Temperatures in Andalusia, Spain. *Clim. Res.* **2015**, *65*, 159–173. [CrossRef]
26. Dorr, E.; François, C.; Poulhès, A.; Wurtz, A. A Life Cycle Assessment Method to Support Cities in Their Climate Change Mitigation Strategies. *Sustain. Cities Soc.* **2022**, *85*, 104052. [CrossRef]
27. Das, B.; Khan, F.; Mohammad, P. Impact of Urban Sprawl on Change of Environment and Consequences. *Environ. Sci. Pollut. Res.* **2023**, *30*, 106894–106897. [CrossRef]
28. Abulibdeh, A. Analysis of Urban Heat Island Characteristics and Mitigation Strategies for Eight Arid and Semi-Arid Gulf Region Cities. *Environ. Earth Sci.* **2021**, *80*, 259. [CrossRef]
29. Yu, J.; Hagen-Zanker, A.; Santitissadeekorn, N.; Hughes, S. A Data-Driven Framework to Manage Uncertainty Due to Limited Transferability in Urban Growth Models. *Comput. Environ. Urban Syst.* **2022**, *98*, 101892. [CrossRef]
30. Zhang, W.; Yang, J.; Yang, L.; Niyogi, D. Impacts of City Shape on Rainfall in Inland and Coastal Environments. *Earths Future* **2022**, *10*, e2022EF002654. [CrossRef]
31. Wang, Y.; Yuan, G.; Yan, Y.; Zhang, X. Evaluation of Sustainable Urban Development under Environmental Constraints: A Case Study of Jiangsu Province, China. *Sustainability* **2020**, *12*, 1049. [CrossRef]
32. Sliuzas, R.; Kuffer, M.; Kemper, T. Assessing the quality of Global Human Settlement Layer products for Kampala, Uganda. In Proceedings of the 2017 Joint Urban Remote Sensing Event (JURSE), Dubai, United Arab Emirates, 6–8 March 2017; ISBN 9781509058082.
33. Khoshnoodmotlagh, S.; Daneshi, A.; Gharari, S.; Verrelst, J.; Mirzaei, M.; Omrani, H. Urban Morphology Detection and It's Linking with Land Surface Temperature: A Case Study for Tehran Metropolis, Iran. *Sustain. Cities Soc.* **2021**, *74*, 103228. [CrossRef]
34. Quan, S.J.; Dutt, F.; Woodworth, E.; Yamagata, Y.; Yang, P.P.J. Local Climate Zone Mapping for Energy Resilience: A Fine-Grained and 3D Approach. *Energy Procedia* **2017**, *105*, 3777–3783. [CrossRef]
35. Demuzere, M.; Kittner, J.; Martilli, A.; Mills, G.; Moede, C.; Stewart, I.D.; Van Vliet, J.; Bechtel, B. A Global Map of Local Climate Zones to Support Earth System Modelling and Urban Scale Environmental Science. *Earth Syst. Sci. Data* **2022**, *14*, 3835–3873. [CrossRef]
36. Demuzere, M.; Kittner, J.; Bechtel, B. LCZ Generator: A Web Application to Create Local Climate Zone Maps. *Front. Environ. Sci.* **2021**, *9*, 637455. [CrossRef]
37. Xu, Y.; Ren, C.; Cai, M.; Wang, R. Issues and Challenges of Remote Sensing-Based Local Climate Zone Mapping for High-Density Cities. In Proceedings of the 2017 Joint Urban Remote Sensing Event, JURSE 2017, Dubai, United Arab Emirates, 6–8 March 2017; Institute of Electrical and Electronics Engineers Inc.: Piscataway, NJ, USA, 2017.
38. Hosseini, S.H.; Hajilou, M. Drivers of Urban Sprawl in Urban Areas of Iran. *Pap. Reg. Sci.* **2018**, *98*, 1137–1159. [CrossRef]
39. Wang, S.; Jiao, X.; Wang, L.; Gong, A.; Sang, H.; Salahou, M.K.; Zhang, L. Integration of Boosted Regression Trees and Cellular Automata-Markov Model to Predict the Land Use Spatial Pattern in Hotan Oasis. *Sustainability* **2020**, *12*, 1396. [CrossRef]

40. Shafizadeh-Moghadam, H.; Asghari, A.; Taleai, M.; Helbich, M.; Tayyebi, A. GIScience & Remote Sensing Sensitivity Analysis and Accuracy Assessment of the Land Transformation Model Using Cellular Automata Sensitivity Analysis and Accuracy Assessment of the Land Transformation Model Using Cellular Automata. *GISci. Remote. Sens.* **2017**, *54*, 639–656. [CrossRef]

41. West, H.; Quinn, N.; Horswell, M. Remote Sensing for Drought Monitoring & Impact Assessment: Progress, Past Challenges and Future Opportunities. *Remote Sens. Environ.* **2019**, *232*, 111291. [CrossRef]

42. USGS Home—GloVis. Available online: https://glovis.usgs.gov/ (accessed on 26 October 2024).

43. Zhang, Y.; Peng, C.; Li, W.; Fang, X.; Zhang, T.; Zhu, Q.; Chen, H.; Zhao, P. Monitoring and Estimating Drought-Induced Impacts on Forest Structure, Growth, Function, and Ecosystem Services Using Remote-Sensing Data: Recent Progress and Future Challenges. *Environ. Rev.* **2013**, *21*, 103–115. [CrossRef]

44. Aburas, M.M.; Ho, Y.M.; Ramli, M.F.; Ash'aari, Z.H. The Simulation and Prediction of Spatio-Temporal Urban Growth Trends Using Cellular Automata Models: A Review. *Int. J. Appl. Earth Obs. Geoinf.* **2016**, *52*, 380–389. [CrossRef]

45. Long, Y.; Yang, Y.; Lei, X.; Tian, Y.; Li, Y. Integrated Assessment Method of Emergency Plan for Sudden Water Pollution Accidents Based on Improved Topsis, Shannon Entropy and a Coordinated Development Degree Model. *Sustainability* **2019**, *11*, 510. [CrossRef]

46. Mehrgan, M. Cities Dealing with Space Structure Analysis of Lorestan State (Iran) Using Entropy Model at Urban, Province, Township, District and National Levels. *J. Geogr. Reg. Plan.* **2013**, *6*, 1–9. [CrossRef]

47. Zachary, D.; Dobson, S. Urban Development and Complexity: Shannon Entropy as a Measure of Diversity. *Plan. Pract. Res.* **2021**, *36*, 157–173. [CrossRef]

48. Gui, X.; Wang, L.; Yao, R.; Yu, D.; Li, C. Investigating the Urbanization Process and Its Impact on Vegetation Change and Urban Heat Island in Wuhan, China. *Environ. Sci. Pollut. Res.* **2019**, *26*, 30808–30825. [CrossRef] [PubMed]

49. Wang, R.; Ren, C.; Xu, Y.; Lau, K.K.L.; Shi, Y. Mapping the Local Climate Zones of Urban Areas by GIS-Based and WUDAPT Methods: A Case Study of Hong Kong. *Urban Clim.* **2018**, *24*, 567–576. [CrossRef]

50. LCZ Generator. Available online: https://lcz-generator.rub.de/ (accessed on 26 October 2024).

51. Tu, D.T.; Ha, N.T.T.; Ngan, N.T.M. Monitoring Influence of Urbanization on Urban Thermal Environment Using Multi-Temporal LANDSAT Imagery: Application to Da Nang City. *Vietnam. J. Earth Sci.* **2016**, *37*, 318–327. [CrossRef]

52. Jover, J.; Díaz-Parra, I. Gentrification, Transnational Gentrification and Touristification in Seville, Spain. *Urban Stud.* **2020**, *57*, 3044–3059. [CrossRef]

53. Petrović Krajnik, L.; Krajnik, D.; Petrović, V. World Exhibitions and Changes in the Urban Morphology of Seville. *Archit. City Environ.* **2020**, *15*, 1–25. [CrossRef]

54. Christodoulou, A.; Christidis, P. Evaluating Congestion in Urban Areas: The Case of Seville. *Res. Transp. Bus. Manag.* **2021**, *39*, 2210–5395. [CrossRef]

55. Parralejo, J.-J.; Díaz-Parra, I. Gentrification and Touristification in the Central Urban Areas of Seville and Cádiz. *Urban Sci.* **2021**, *5*, 40. [CrossRef]

56. Alba-Rodríguez, M.D.; Solís-Guzmán, J.; Marrero, M. Evaluation Model of the Economic-Environmental Impact on Housing Recovery. Application in the City of Seville, Spain. *Sustain. Cities Soc.* **2022**, *83*, 103940. [CrossRef]

57. Borrallo-Jiménez, M.; LopezdeAsiain, M.; Herrera-Limones, R.; Arcos, M.L. Towards a Circular Economy for the City of Seville: The Method for Developing a Guide for a More Sustainable Architecture and Urbanism (GAUS). *Sustainability* **2020**, *12*, 7421. [CrossRef]

58. Google Earth. Available online: https://earth.google.com/web/@0,-25.604,0a,22251752.77375655d,35y,0h,0t,0r/data=CgRCAggBOgMKATBCAggASg0I_____ARAA (accessed on 26 October 2024).

59. World Population Review Seville Population. 2023. Available online: https://worldpopulationreview.com/world-cities/seville-population (accessed on 4 December 2023).

60. Idesevilla Maps. Available online: https://idesevilla.maps.arcgis.com/apps/webappviewer/index.html?Id=d6b1424e6c2d4386ad228323bb70483f (accessed on 26 October 2024).

61. CDS (Beta). Available online: https://cds.climate.copernicus.eu/ (accessed on 26 October 2024).

62. Aemet. Agencia Estatal de Meteorología—AEMET. Gobierno de España. Available online: https://www.aemet.es/es/portada (accessed on 26 October 2024).

Numerical Study on the Summer High-Temperature Climate Adaptation of Traditional Dwellings in the Western Plains of Sichuan, China

Rongjia Li [1], Qiushan Li [1,*], Ishikawa Mikiko [2] and Kabilijiang Wumaier [1]

[1] Sichuan University–The Hong Kong Polytechnic University Institute for Disaster Management and Reconstruction (IDMR), Sichuan University, Chengdu 610207, China; 2021226200008@stu.scu.edu.cn (R.L.); kabil@scu.edu.cn (K.W.)

[2] Department of Integrated Science and Engineering for Sustainable Society, Faculty of Science and Engineering, Chuo University, Tokyo 112-8551, Japan; ishikawa.27@g.chuo-u.ac.jp

* Correspondence: liqiushan@scu.edu.cn; Tel.: +86-156-8099-7814

Abstract: Ongoing global climate change, marked by sustained warming and extreme weather events, poses a severe threat to both the Earth's ecosystems and human communities. Traditional settlements that underwent natural selection and evolution developed a unique set of features to adapt to and regulate the local climate. A comprehensive exploration of the spatial patterns and mechanisms of the adaptation of these traditional settlements is crucial for investigating low-energy climate adaptation theories and methods as well as enhancing the comfort of future human habitats. This study used numerical simulations and field measurements to investigate the air temperature, relative humidity, wind speed, wind direction, and thermal comfort of traditional settlements in Western Sichuan Plain, China, and uncovered their climate suitability characteristics to determine the impact mechanisms of landscape element configurations (building height, building density, tree coverage, and tree position) and spatial patterns on microclimates within these settlements. The results revealed the structural and layout strategies adopted by traditional settlements to adapt to different climatic conditions, providing valuable insights for future rural protection and planning and enhancing climate resilience through natural means. These findings not only contribute to understanding the climate adaptability of Earth's ecosystems and traditional settlements but also offer new theories and methods to address the challenges posed by climate change.

Keywords: nature-based solution; traditional settlement; Linpan in western Sichuan; microclimate; ENVI-met

1. Introduction

In recent years, the urban heat island (UHI) effect, which is driven by global warming and intensive urbanization, has significantly elevated regional summer temperatures, leading to an increase in the duration and frequency of extreme high-temperature events [1,2]. The impact of urban microclimates on outdoor human comfort, building energy consumption, and heat wave dispersion has been demonstrated [3–5]. As the UHI effect extends towards urban outskirts and rural areas, studies have revealed the substantial risks of high temperatures to the health and safety of outdoor rural residents [6]. Its negative consequences, including reduced thermal comfort [7], increased morbidity rates [8], deteriorating air quality [9], and additional cooling energy consumption [10,11], pose significant challenges to rural residents and their living environments.

Current microclimate research is predominantly focused on urban areas spanning various scales [12]. In contrast, research on the microclimates of rural settlements is relatively limited. Compared with urban areas, rural infrastructure is often more vulnerable and disadvantaged in addressing the impacts of climate change. Rural settlements rely

heavily on their external environment and, without the use of mechanical equipment, optimize their location, architectural design, and crop layout to adapt to local climates. Such longstanding indigenous wisdom is a nature-based solution (NbS) that addresses challenges such as UHIs and heat waves by providing cooling services [13,14]. Introduced by the World Bank in 2008 and subsequently incorporated into the United Nations Framework Convention on Climate Change by the World Wide Fund for Nature, NbSs rely on nature-derived and nature-dependent approaches to efficiently solve diverse challenges and simultaneously ensure economic, social, and environmental benefits. Currently, NbSs primarily utilize ecosystems and their services to address social challenges such as climate change, food security, and natural disasters [15]. China's historical planning principles, which emphasize alignment with nature, are a manifestation of NbSs that integrate local traditional wisdom. Improving rural living environments and constructing ecologically livable and beautiful villages are crucial tasks in implementing rural revitalization strategies. Therefore, studying the climate adaptability of traditional rural settlements and exploring NbSs is of paramount importance.

However, existing research on microclimates in rural settlements faces challenges in terms of differences and comparability between Western and Chinese rural settlements. The climate in China boasts a wide range of latitudinal and longitudinal spans, featuring diverse climate types such as tropical, subtropical, and temperate monsoons, temperate continental, and high-altitude cold climates. In contrast, European countries primarily experience temperate maritime, temperate continental, and Mediterranean climates, whereas North American countries are characterized by temperate continental and subarctic coniferous forest climates. This diversity makes the direct application of results from studies on Western rural areas to Chinese rural areas challenging. Owing to the larger residential land area in Western countries and scattered distribution of rural residences, most studies have concentrated on small towns. However, the significant differences in scale, layout, and materials between Western and Chinese rural settlements have weakened the applicability of these studies [16].

The Dujiangyan Water Conservancy Project in Western Sichuan, China, is a famous World Heritage site owing to its irrigation engineering, which has been used for flood control and irrigation since its construction 2200 years ago. Abundant water and flat land helped develop the local agriculture and provide natural conditions for farming in the Land of Abundance [17]. In the process of adapting to nature, the "Chuanxi Linpan" was formed, a traditional settlement that facilitates life and production. This refers to a composite rural residential environment that integrates farmsteads on the Chengdu Plain and hilly areas with surrounding tall trees, bamboo groves, rivers, and peripheral farmland, forming a complex living environment that combines production, daily life, and the landscape [18]. As shown in Figure 1, typically organized around clans, it has courtyard houses, tall arbors, shrubs, and bamboos and externally connects to the fields with a river system, reflecting the Taoist view of ecology [19].
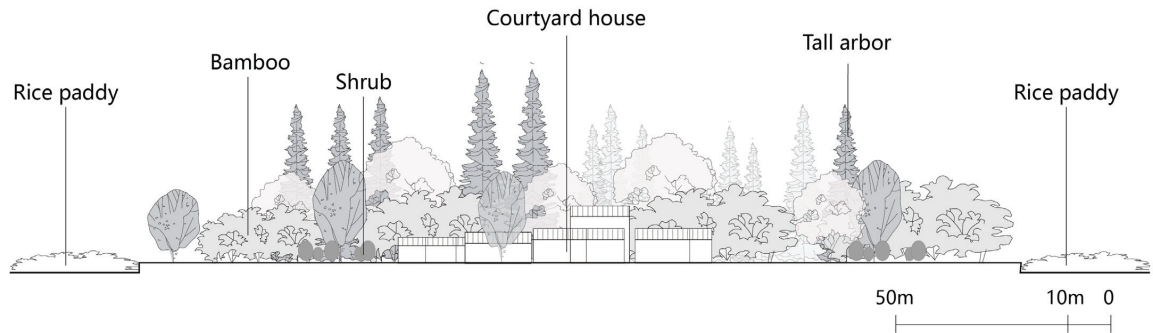

Figure 1. Layout of a Linpan (traditional settlement) in Western Sichuan.

Owing to the absence of hills to block the wind in the Chengdu Plain, tall trees and bamboo protect against the wind. Typically, rural homes often adopt a linear, L-shaped, or concave-shaped layout, and each household has its own courtyard; three to ten households form a small Linpan, ten to thirty households form a medium Linpan, and over thirty households constitute a large Linpan [20]. In addition to the built structures, the open space within a Linpan serves as a transitional semi-open area. This space encompasses natural elements such as the sky, earth, and plants, and their interactions create a distinctive ecological environment in the Chengdu Linpan. This, in turn, generates a mild and comfortable microclimate for the residents [21].

Linpans are not only unique in their form but have also accumulated ecological wisdom over their millennia of development. Their passive design and low-energy consumption are considered NbSs. The arrangement of a long cornice forms a space under the eaves that considers factors such as rain, shade, and ventilation. Deciduous trees provide shade from direct summer sunlight and guarantee access to sunlight during winter. Moreover, recent studies, such as the assessment of land ecological security in the Chengdu Plain Region from 2000 to 2020 by Zhang et al. (2023), highlight the importance of integrating NbSs into regional planning to enhance ecological resilience and sustainability. The ecological strategies embedded in Linpans align with the findings of Zhang et al., emphasizing the critical role of NbSs in maintaining ecological security and promoting sustainable development in traditional and modern settlements alike [22,23].

With the advancement of computer technology and computational fluid dynamics (CFD) software, numerical analysis and computer simulations have become pivotal tools for studying microclimates in human habitats [24]. Among these tools, ENVI-met stands out as a three-dimensional small-scale CFD model that is widely used to simulate microclimatic phenomena within the urban canopy and boundary layers based on interactions among surfaces, buildings, vegetation, and air. It has been extensively and successfully applied to assess microclimates and the human biometeorological impacts of different urban climate design strategies [25]. Microclimate analysis primarily focuses on climate characteristics at the scale of urban blocks, with heights and widths within 0.1 km, and includes meteorological elements such as atmospheric temperature, ground temperature, humidity, wind speed, and thermal radiation near buildings [26]. Furthermore, existing research indicates that variables such as street orientation, building density, floor area ratio, green space density, impervious surface ratio, and sky view factor can considerably influence the local climate [27–30].

Through their study of outdoor thermal comfort in Tunisia, Achour-Younsi and Kharrat [31] proposed that aspect ratio and street orientation are crucial factors influencing urban street canyons. Giridharan et al. [32] analyzed daytime UHI effects in densely populated areas of Hong Kong and found that increasing the surface albedo and floor area ratio and decreasing the sky view factor reduced the UHI index. Furthermore, reducing the impact of buildings is more significant in mitigating the UHI effect, decreasing its temperature increase and duration by approximately 30% [33]. In contrast, artificial surfaces such as walls and impermeable roads have been found to significantly enhance the UHI effect [34]. In terms of vegetation environment, Morakinyo et al. [35] found that leaf area index, tree height, and trunk height most significantly improve outdoor thermal comfort, but the beneficial daytime effects of trees diminish with increasing urban density. Amani-Beni et al. [36] determined that increasing vegetation cover under trees and irrigating grass can effectively reduce temperatures during summer. Yang [37] found that vegetation positively affects the surrounding thermal environment through shading, reflecting shortwave radiation, and transpiration. Increasing the tree coverage provides a more comfortable microclimate than increasing shrubs, making trees a priority when selecting variables [38]. Furthermore, Abdi et al. [39], Atwa et al. [40], and Sahar et al. [41] investigated the mechanisms influencing outdoor microclimates through the types, density, arrangement, and windward direction of different tree species. Wu et al. [42] evaluated four spatial tree layouts in the ENVI-met

model of a high-rise residential area in Beijing and found that different spatial arrangements produced different effects by influencing the location of building shadows.

In this study, the microclimate of a traditional settlement, Linpan, in the Chengdu Plain, China, is simulated using hourly monitoring data from meteorological stations, and field measurements were used to validate the model. This study aimed to assess the key factors and indicators influencing the climatic suitability of Linpans by changing the spatial layouts of buildings and trees within them. The main objectives of this research are as follows: (i) elucidate the microclimate environment formed within a Linpan, explore its self-adaptive ability in high-temperature weather, and assess its outdoor thermal comfort; (ii) simulate multiple scenarios for the first time that change the building height, building density, tree coverage, and tree position inside a Linpan using ENVI-met 5.5 software to investigate the influence of a Linpan's configuration on climatic elements such as air temperature, relative humidity, wind speed, and wind direction; and (iii) design strategies for the effective control of thermal comfort to provide a reference for traditional settlement planning.

2. Study Area

The research subject of this study was a traditional settlement in JuYuan Town, Dujiangyan City, QuanShui Village, Cluster 7 (30.971119° N, 103.695207° E) (Figure 2). This settlement has 15 residences clustered together, surrounded by a green barrier made up of tall trees and bamboo, and represents a typical Chengdu Linpan. The Linpan covers an area of approximately 29,328 m^2, making it medium-sized. The predominant tree species are camphor trees, metasequoias, ginkgo trees, paulownias, and bamboo clusters. The architectural forms within this Linpan include one-character, L-shaped, and three-sided enclosed structures. Buildings on the north side face south, whereas those on the south side, which are more compact, primarily face north. This layout reflects the adaptable characteristics of the Linpan arrangement based on local conditions. Meteorological data were measured at a point 1.5 m away from the forest plate from 16 July 2023, 00:00, to 17 July 2023, 00:00. These measurements were used to validate the simulation results (Figure 3E).

Figure 2. Elevated view of the study area.
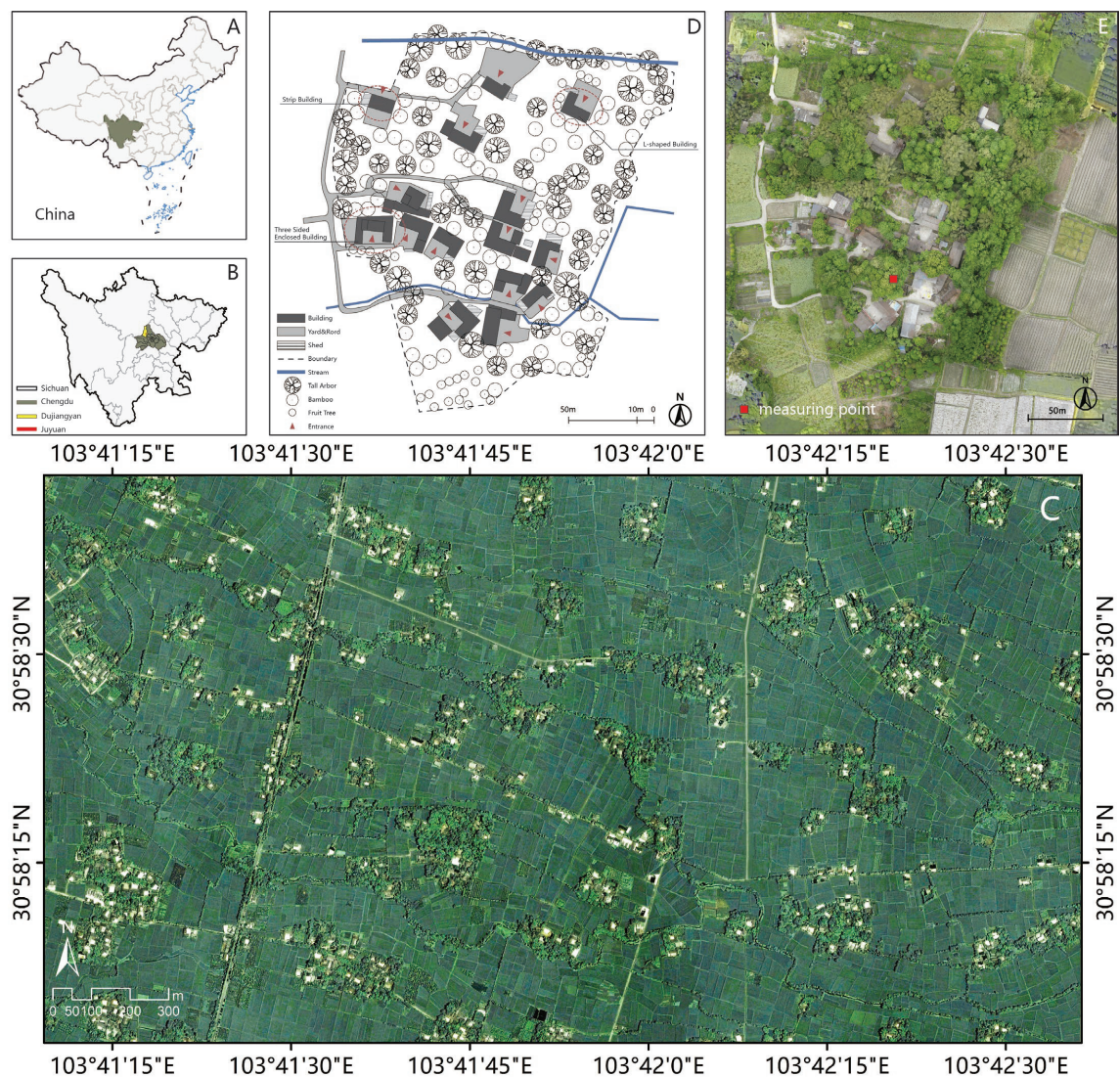
Figure 3. Location map and layout plan of the study area. (**A**) The location of Sichuan Province in China; (**B**) The location of the Linpan distribution area in Sichuan Province; (**C**) Aerial photo of the distribution of Linpan in the field; (**D**) Data model of the simulated Linpan; (**E**) Actual photo of the simulated Linpan (obtained by author used drone photography).

3. Data and Methods

3.1. Simulation Data

For the microclimate simulation, ENVI-MET software was utilized due to its established effectiveness in such analyses. ENVI-MET is a three-dimensional, non-hydrostatic model specifically designed for simulating surface-plant-air interactions in urban environments. It is particularly adept at analyzing the impact of building structures and landscape elements on microclimates, including parameters such as air temperature, humidity, and wind patterns. The extensive validation of ENVI-MET in similar studies underscores its reliability for assessing the microclimatic effects of traditional settlements and their land-

scape configurations. The strong agreement between the simulated results and the on-site measurements further supports the model's accuracy and credibility in this study. Following the temperature classification method [43], this study defines summer as the period from June to August. The focal month chosen for the investigation was July, specifically targeting days with high temperatures and minimal cloud cover. Consequently, 16 July 2023, a day with a peak temperature of 33.7 °C and 4% cloud cover, was selected as the validation date. Meteorological data (air temperature, relative humidity, wind speed, wind direction, wind angle, visibility, hourly precipitation, average total cloud cover, etc.) in Dujiangyan City, encompassing a 24 h timeframe from 00:00 on 16 July 2023, to 00:00 on 17 July 2023, were sourced from Huiju Data (hz.hjhj-e.com).

3.2. Software Simulation

As shown in Table 1, two distinct input files were defined. First, the environmental elements within the study area, including three-dimensional models of buildings, vegetation, artificial surfaces, water bodies, and soil. Ultimately, a three-dimensional unit model measuring 246 × 236 × 25 m was established, with the dimensions of each unit set to 1 × 1 × 1 m. A 20 m grid extension was also applied externally to the simulation area to mitigate the complex boundary layer effects and enhance stability in proximity to the primary research elements. Second, the climate configuration parameters encompassing the time and climatic environment for model simulation. Hourly air temperature, relative humidity, wind speed, and wind direction data for 16 July 2023, from 00:00 to 24:00, were input for the simulation, which began at 0:00 on the day and was analyzed at 14:00. This time was selected to avoid errors associated with the numerical software and consider the impact of surface radiation during the time of the daily peak air temperature [44]. The measured and simulated values were linearly fitted, and the coefficient of determination and root mean square error were calculated to jointly evaluate the accuracy of the model.

Table 1. Input model data.

Element	Sub-Element	Input Value
Environmental elements	Location	Dujiangyan
	Coordinate Position	30.97° N, 103.69° E,
	Model Dimensions	246 × 236 × 24
	Grid Cell Size	Dx = 1 m, Dy = 1 m, Dz = 1 m
Simulation Date and Time	Start Date	16 July 2023
	Start Time	0:00
	Total Simulation	24 h
Meteorology	Boundary Condition	Simple Forcing
	Air Temperature	Hourly Data From Weather Station
	Relative Humidity	Hourly Data From Weather Station
	Wind Speed	1.6 m/s
	Wind Direction	135° (Southeast)

In the vegetation selection simulation, the Linpan was predominantly characterized by bamboo clusters and tall deciduous trees. Because of the dense and relatively small leaves of bamboo groves coupled with the curvature of the main trunk beyond a certain height, precise morphological control was challenging in the modeling process. To simplify the simulation and account for the substantial impact of individual parameters, deciduous tall trees were selected as surrogates for bamboo. The height distribution of vegetation in the study area primarily ranges from 9 to 15 m. As the cooling effect is more pronounced with a continuous increase in tree height, especially within the range of 8–12 m [45,46], a representative tree height of 12 m was selected for the simulation. This choice was made to streamline the model while acknowledging the significant influence of a singular parameter on the overall simulation. Local 12 m trees were selected for modeling, and LAD values of different heights were assigned according to tree characteristics (Figure 4).
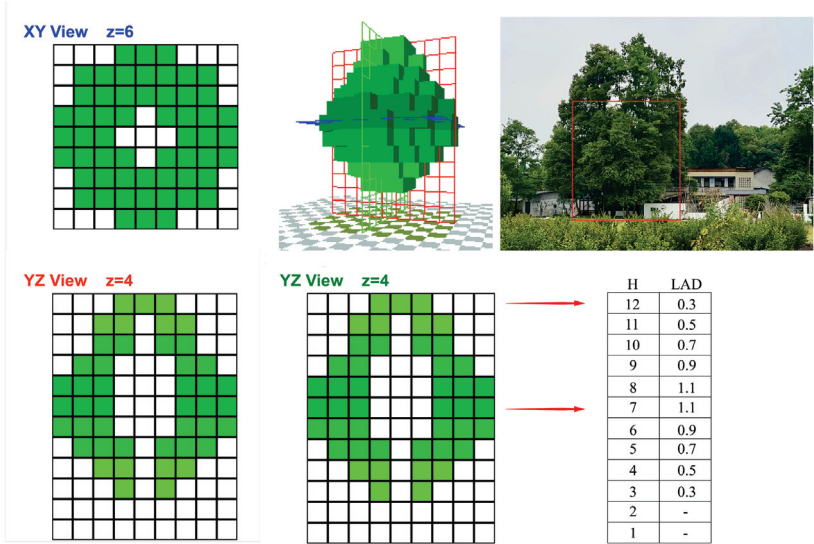
Figure 4. Construction of the Arbor Model.

The physiologically equivalent temperature (PET) is a thermal comfort assessment standard that integrates geographical information [47], climatic parameters, solar radiation, and clothing impact. Thermal comfort levels, classified based on PET, are shown in Table 2.

Table 2. Physiologically equivalent temperature standards.

Physiological Equivalent Temperature (°C)	Human Perception	Physical Stress Levels
<4	Very Cold	Extreme Cold Stress
4–8	Cold	Strong Cold Stress
8–13	Cool	Moderate Cold Stress
13–18	Slightly Cool	Mild Cold Stress
18–23	Comfortable	Non-Heat Stress
23–29	Slightly Warm	Mild Heat Stress
29–35	Warm	Moderate Heat Stress
35–41	Hot	Intense Heat Stress
>41	Very Hot	Extreme Heat Stress

3.3. ENVI-Met Modeling and Validation

This study used unmanned aerial vehicle imagery and on-site reconnaissance observations to analyze the components of the Linpan. Then, an ENVI-MET microclimatic simulation model was developed. By manipulating the four key factors of building height, building density, arbor coverage, and arbor distribution, nine distinct scenarios were devised based on the characteristics of the Linpan. This approach was used to investigate the impact of morphological variations on traditional settlements, as detailed in Table 3.

Table 3. Modeling scenario settings.

No.	Factors	Characteristics	Model Diagram
1	Original	Modeling of the site's architecture, surface, vegetation, and water system elements according to the results of the site survey	SC_origin

Table 3. *Cont.*

No.	Factors	Characteristics	Model Diagram
2	Building Height	Height increase of one floor on top of the original forest plate, i.e., one additional single story building (3 m) per building on top of the original forest plate	SC_B_add1
3		Height increase of two floors on top of the original forest plate, i.e., two additional building single floors (6 m) per building on top of the original forest plate	SC_B_add2
4	Building Density	Low building density, i.e., removal of L-shaped buildings, monolithic buildings, and all small individual blocks in the original forested area	SC_B_spa
5		Medium building density, i.e., removal of L-shaped buildings in the original forested area	SC_ B_med
6	Arbor Coverage	Sparse arbor coverage, reducing arbor to a density of about 40% from the original forested area	SC_P_spa
7		Sparse arbor coverage, reducing arbor to a density of about 80% from the original forested area	SC_P_den
8	Arbor Distribution	Full enclosure of the forest plate by trees, i.e., plants surround the building	SC_P_full
9		Arborvitae upwind and semi-enclosed, arborvitae located windward and upwind	SC_P_up
10		Arborvitae downwind and semi-enclosed, arborvitae located downwind of the windward side	SC_P_down

4. Results

A comparison of the simulation results with the measured data revealed a strong hourly correlation between air temperature and relative humidity (Figure 5). At 16:00, a brief spike in air temperature and a decrease in relative humidity occurred, which was hypothesized to be related to the height of the sun descending into the gaps not covered by trees and buildings. After 17:00, the air temperature and relative humidity returned to normal, owing to the sun's further descent, avoiding direct exposure due to obstruction by buildings and vegetation.
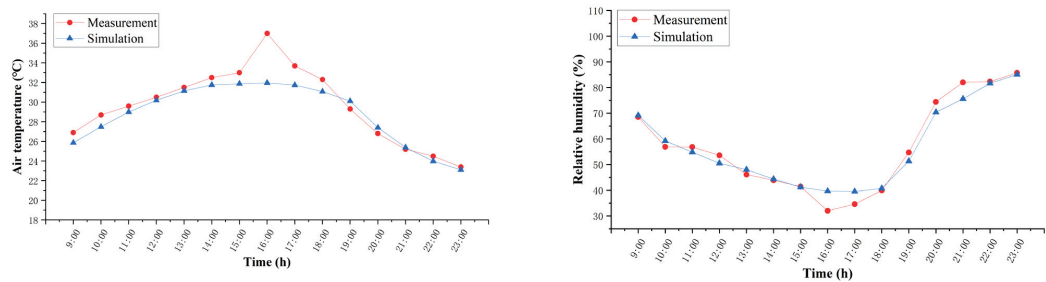
Figure 5. Comparison of simulated results and measured data for temperature and relative humidity.

Figure 6 shows that the coefficient of determination for air temperature and relative humidity are 0.89 and 0.97, respectively, and the root mean square error is 1.04 °C and 2.79%, respectively. According to Tsoka et al. [48], the root mean square error should be <4.3 °C for air temperature and <10.2% for relative humidity. When the root mean square error is smaller and the coefficient of determination is closer to 1, the correlation between the two data groups is more credible; therefore, this ENVI-MET simulation result is considered to be of analytical reference significance.

The simulation results indicate that building height, building density, tree coverage, and tree arrangement all impact the microclimate of traditional settlements. In the visualization of results, air temperature is controlled at a starting point of 29.5 °C, increasing in 0.5 °C intervals; relative humidity is controlled at a starting point of 37.5%, increasing in 1.5% intervals; wind speed is controlled at a starting point of 0.1 m/s, increasing in 0.1 m/s intervals; and wind direction is controlled at a starting point of 0°, increasing in 45° intervals.
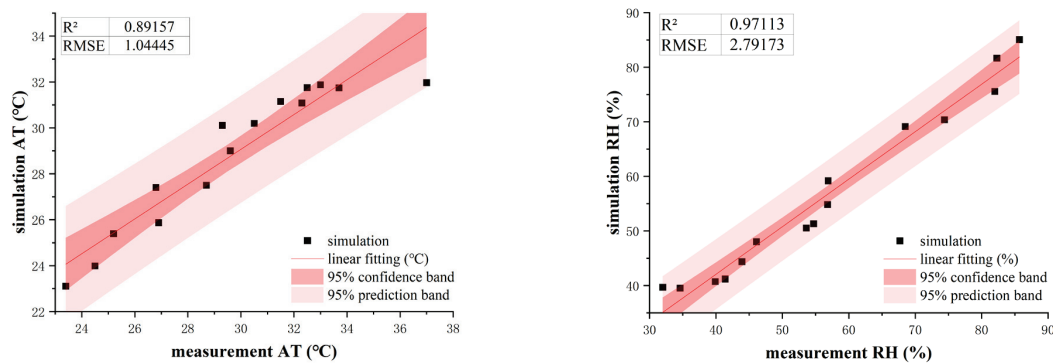
Figure 6. Linear fitting of simulation results to measured data.

4.1. Influence of Building Height on Microclimate

As the building height increased, the overall temperature variation in the settlement remained insignificant, ranging from 0.05 °C–0.46 °C. In contrast, a more noticeable de-

crease in temperature, approximately 0.6 °C–0.87 °C, was observed around the buildings (Figure 7). An upward trend in relative humidity around the buildings was also evident, increasing by >1.6%, whereas the overall relative humidity of the settlement increased by approximately 0.32–1.6%. The wind speed significantly decreased, forming a large stagnant zone (0–0.2 m/s) around the buildings. Simultaneously, the wind speed in narrow gaps and passages between buildings exhibited a noticeable enhancement, increasing by approximately 0.03–0.19 m/s. The wind direction showed an increased variation area, with the degree of change decreasing with distance from the buildings.
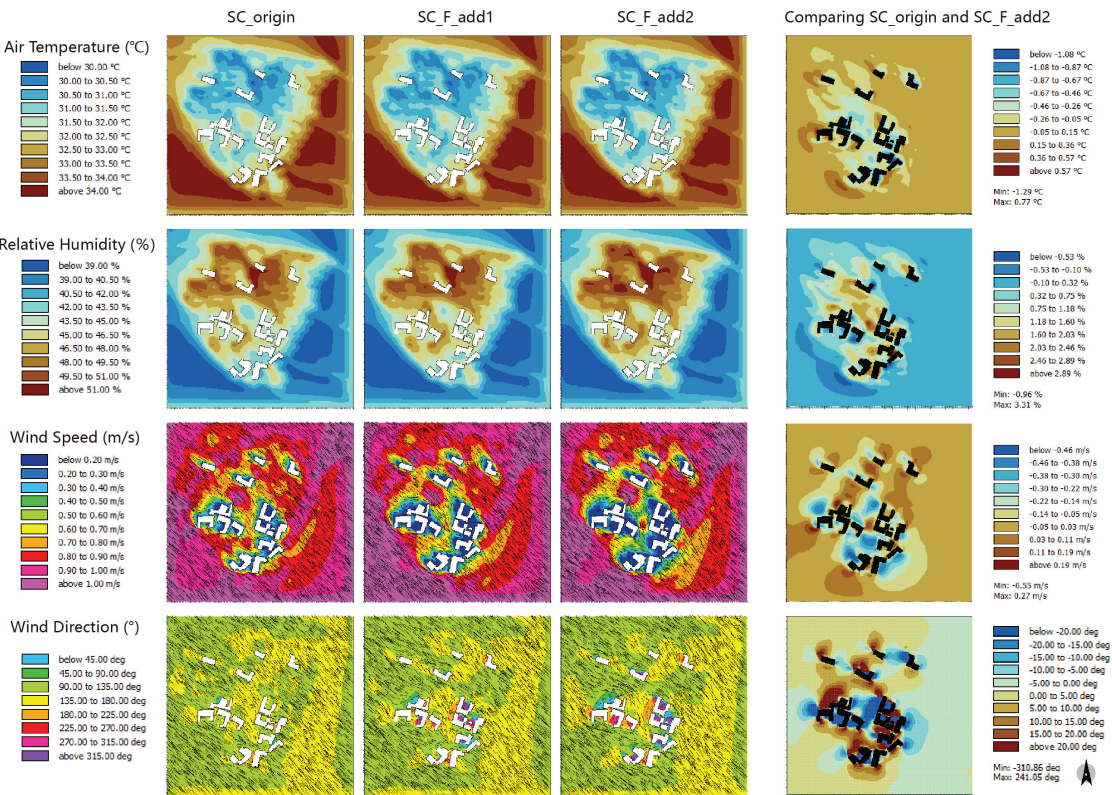
Figure 7. Impact of changes in building height on the microclimate.

4.2. Influence of Building Density on Microclimate

By reducing building density, the temperature within the settlement slightly increased, rising by approximately 0.24 °C–0.8 °C. The high temperatures extended inward along the southeastern wind direction (Figure 8). Changes in humidity within the settlement were insignificant; however, a slight decrease in humidity ranging from 0.15–0.85% was observed at the location where buildings were removed. The wind speed did not significantly change around the preserved buildings, but it increased when the buildings were removed, indicating an influx of air. Although changes in wind direction were not pronounced, the wind direction tended to become more consistent around the removed buildings, especially in the courtyards.
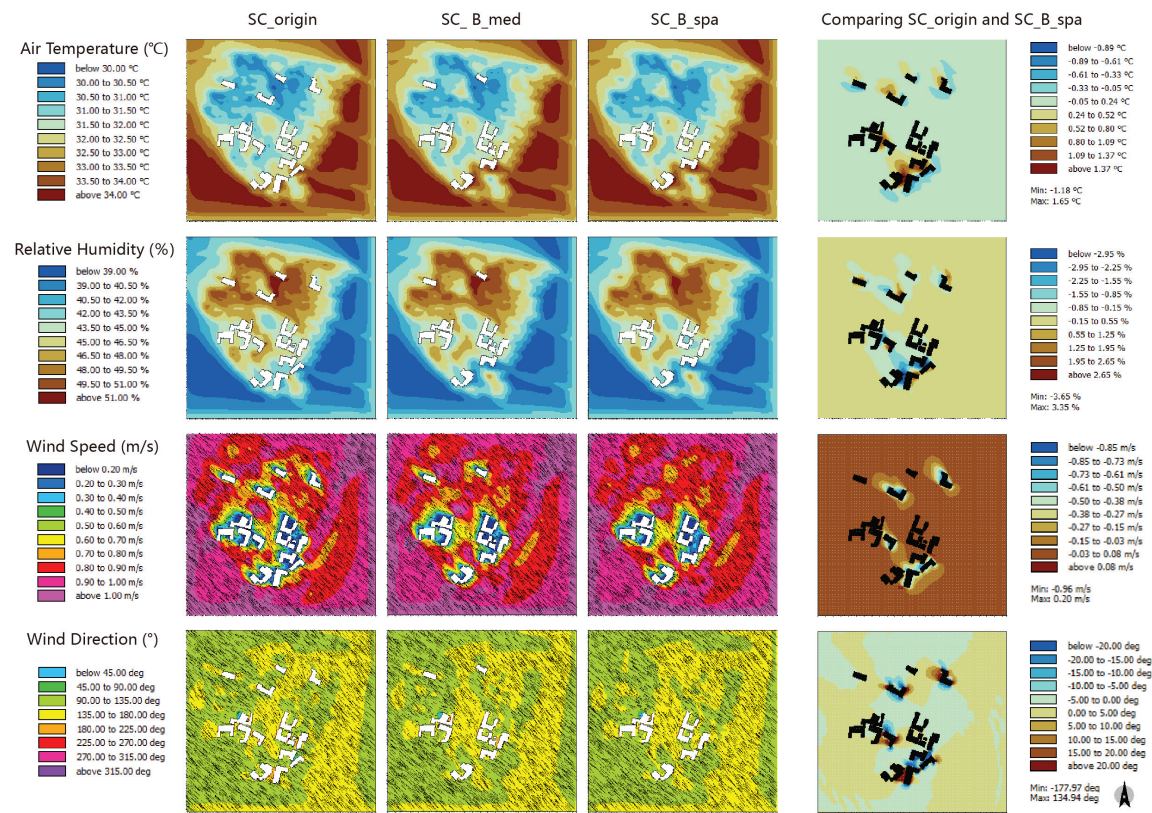
Figure 8. Impact of building density changes on microclimate.

4.3. Influence of Arbor Coverage on Microclimate

The investigation of the impact of tree coverage on the microclimate involved incremental increases (40%, 60%, and 80%). The results revealed a notable reduction in the temperature within the settlement, exhibiting a general decrease of >0.66 °C, with the maximum reduction reaching 2.27 °C (Figure 9). Concurrently, the relative humidity within the settlement considerably increased, by >2.02%, with a maximum increase of 7.05%. The wind speed was noticeably reduced, exhibiting an overall decrease of >0.03 m/s, and in specific areas decreasing by 0.22 m/s. Alterations in wind direction were not pronounced, with only slight variations within 15° observed in areas covered by trees.
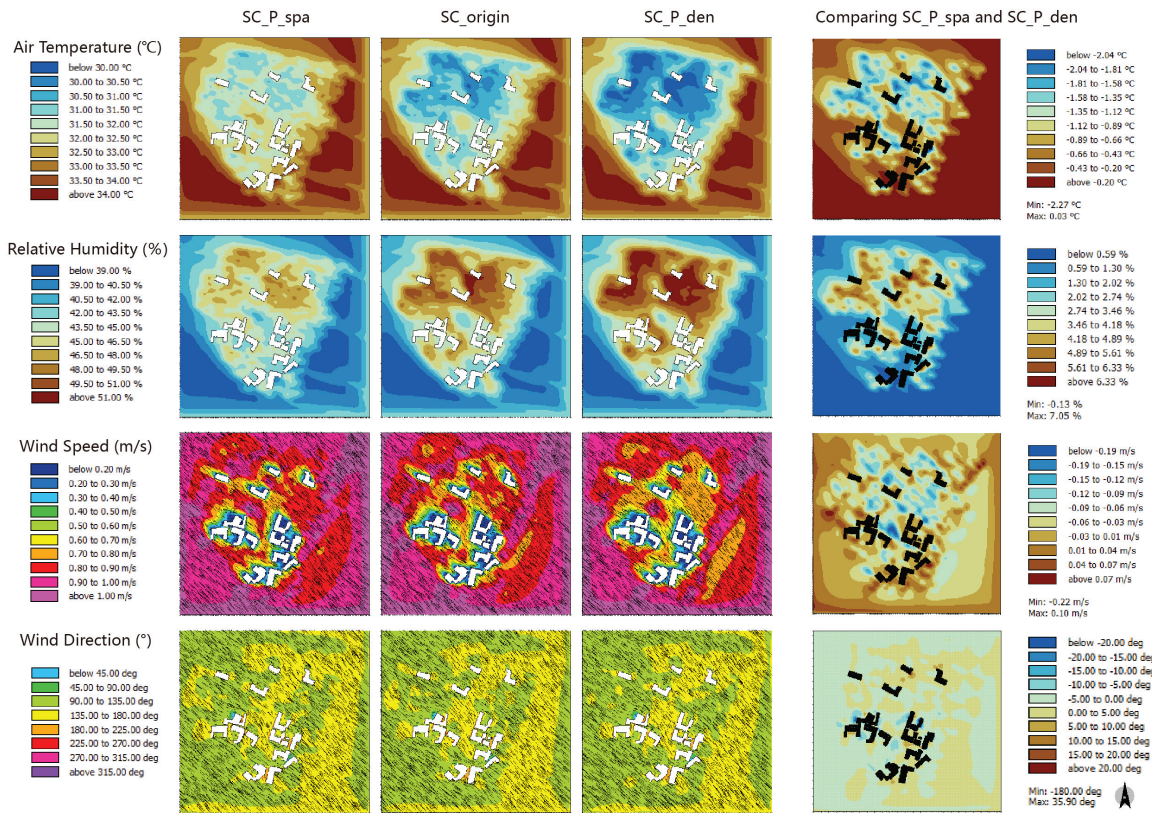
Figure 9. Impact of arbor density changes on the microclimate.

4.4. Influence of Arbor Position on Microclimate

The temperature distribution was varied by modifying the arrangement of the tree enclosures. However, areas with reduced temperatures generally aligned with the position of trees and their downwind directions. Under fully enclosed conditions, a significant temperature reduction was observed around the enclosed trees, contributing to the cooling effects in the upwind direction within the settlement. However, a slight temperature rebound occurred downwind. Under semi-enclosed conditions, trees positioned upwind had a limited range of blocking effects against heat waves, similar to that in the fully enclosed state. Meanwhile, in the downwind direction, heat waves tended to accumulate within the settlement (Figure 10). The distribution of relative humidity also varied, aligning with the position of the trees. It significantly increased in the outer periphery of the settlement under fully enclosed conditions. Meanwhile, wind speed accelerated around areas with tree distribution, and the acceleration effect extended to a certain distance, resulting in the formation of a wind zone around the tree arrangement. The wind direction was minimally affected by the distribution of trees, having slight variations within 30°, which were likely associated with the height of the tree canopy.
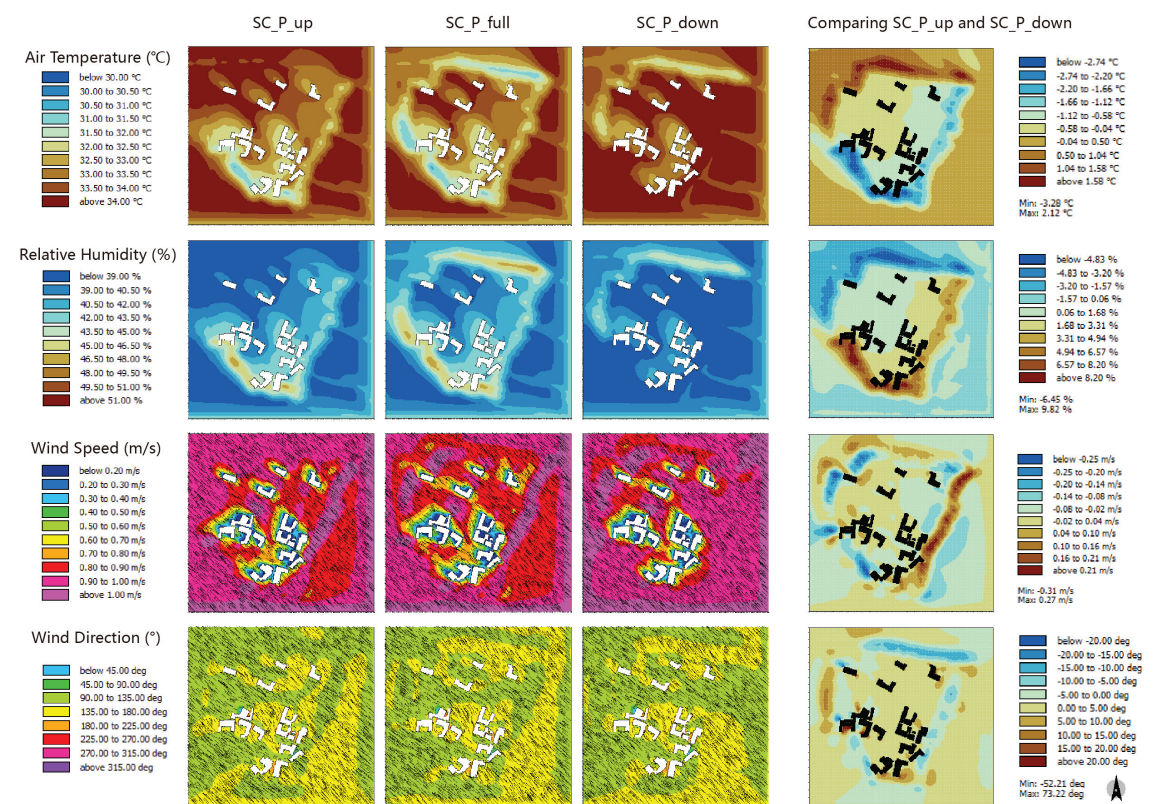
Figure 10. Impact of arbor positioning on the microclimate.

According to the calculated results, the PET value for each scenario reached its highest at 14:00. The graph exhibits a bimodal shape because of the difference between the inside and outside PET values. When the external environment is "very hot" (PET > 41 °C), most of the internal area is also "warm" (29–35 °C). In the simulation, the Linpan can effectively regulate extreme highs. Figure 11 illustrates the ten scenarios, with variations in the height and distribution density of buildings and trees within the Linpan settlement, exhibiting its enhanced adaptability to extreme heat. In scenarios 1–7, distinct temperature concentration areas emerged within the simulation, emphasizing the noteworthy temperature distinction between the Linpan settlement and its external surroundings. The spatial distribution map revealed that the cooling impact within the Linpan settlement primarily resulted from the shading effects produced by buildings and trees. As the building height increased, the shaded area expanded; the shadow positioned northeast of the building led to a significant temperature reduction. Simultaneously, an increase in tree coverage expanded the region of optimal temperatures, although the overall positioning of trees appeared to exert a less visible influence on climate adaptability compared with the initial seven scenarios.
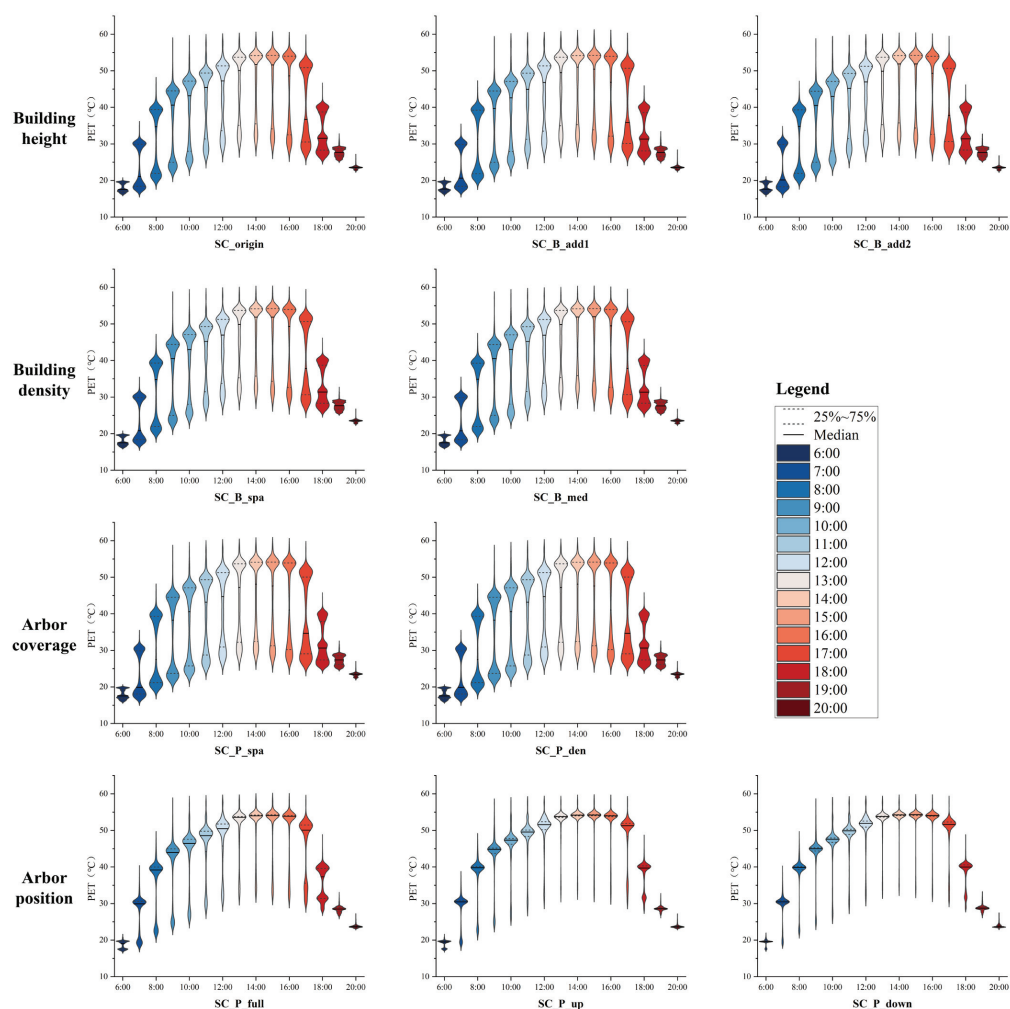
Figure 11. 24 h simulations of PET thermal comfort under nine scenarios.

5. Discussion

The simulation results clearly indicate that Linpans have a cooling effect on the summer environment, with varying degrees of internal influence. These results underscore key factors affecting the Linpan microclimate, as simulated under different scenarios. The outcomes, grounded in benchmark samples and theoretical insights, discuss strategies for Linpan restoration and planning that align with natural processes.

Increasing building height has been shown to impede hot air, induce cooling, and enhance humidity. However, the larger volume of structures can lead to stagnant air around buildings, negatively impacting internal ventilation. Existing research highlights that increased building density tends to correlate with decreased overall wind speed. An optimal building height can create shaded areas, contributing to harmonious rural esthetics; hence, the indiscriminate pursuit of excessively low or high building heights may compromise quality of life and psychological well-being [49]. Furthermore, towering structures may not align with the resident population, resulting in the wasteful utilization of construction resources. Insights from traditional eave designs, which provide shade

and manage rainwater, suggest that such features can mitigate temperature extremes and enhance outdoor and indoor comfort.

Changes in building density and height similarly affect microclimates. Both approaches—raising building height and increasing density—expand shaded areas, reducing solar radiation and thus cooling and humidifying the environment. However, this increased volume can also weaken wind speed. In narrow spaces between buildings, wind flow is restricted, leading to higher wind pressure and speed [50]. Effective urban planning in forested areas should incorporate ventilation corridors aligned with prevailing seasonal wind directions to optimize natural light and airflow.

Tree coverage also plays a crucial role in cooling and humidity enhancement, similar to the effects of increased building height. However, excessive tree coverage (over 60%) can reduce wind speed and potentially worsen thermal comfort in still, warm areas [51,52]. In urban settings, higher structures are often promoted to increase shaded areas and lower temperatures. Conversely, in rural areas, strategic tree planting can improve shade, ventilation, and humidity regulation. Effective planning should involve placing trees around buildings and along roadsides while selecting appropriate species to balance summer shade and winter sunlight [53]. Deciduous broad-leaved trees, like ginkgo and dove trees, offer shade in summer and allow sunlight in winter.

The arrangement of trees corresponded to zones affected by temperature reduction and humidity increase. A continuous and dense planting pattern notably hindered external heat waves. However, when this layout was applied to the downwind side of a forested settlement, it impeded the outward flow of internal heat, leading to an increase in the internal temperature [54]. Therefore, the primary roles of tree layout include resisting external heat waves, dissipating internal heat, and introducing wind during calm weather conditions. The arrangement of trees should therefore align with prevailing wind directions to ensure effective heat management and airflow. This strategy also requires a specific analysis of the prevailing wind directions within the settlement to determine the precise arrangement of trees based on the dominant wind directions during summer and winter. For instance, in Dujiangyan City, where northwesterly and southeasterly winds predominate, tree planting should focus on these directions to avoid obstructing wind channels [55].

6. Conclusions

This study investigated the impact of increased building height and tree coverage on the microclimate within traditional rural settlements, emphasizing the positive role of NbSs. Based on ecological principles, these solutions aim to improve the quality of human living environments, mitigate the impacts of extreme weather events on human life, enhance air quality, and promote residential comfort. The findings underscore that while augmenting building height and tree coverage exerts a discernible influence on the microclimate, certain drawbacks also emerge. Elevated buildings can lower temperatures and increase relative humidity but also create stagnant wind areas around the structures, reducing internal ventilation. Increased tree coverage fosters cooling and enhances humidity but may impede airflow, potentially diminishing wind speed. Both heightened buildings and increased tree coverage contribute to the enlargement of shaded regions within settlements.

While various spatial arraignments were observed to influence microclimates, the simulation groups revealed that the cooling effect generated by buildings is less significant compared to that induced by trees. This discrepancy arises from the fact that buildings reflect radiation, which influences shaded areas, whereas trees adeptly sidestep this phenomenon. In summary, NbSs enhance the microclimate in traditional residential settings by enlarging the shaded zones and mitigating direct solar radiation. However, these solutions also hinder wind dynamics, resulting in diminished wind speed. Therefore, in future planning and design endeavors for forested settlements, a judicious equilibrium of these factors is imperative to achieve optimal microclimate effects.

It is imperative to note that the simulation did not account for detailed architectural features, such as eaves, which are crucial for understanding the characteristics of under-

eave spaces. Traditional spatial arrangements, which have largely fallen out of use, offered significant environmental benefits compared to contemporary practices. Historical living environment layouts, including tree-lined avenues and shaded public spaces, have been shown to enhance environmental quality and comfort [56]. These factors merit thorough exploration and analysis in future research. Furthermore, the technical methods used in this study can be applied more broadly, and the basic strategies mentioned in our findings can serve as a baseline for human habitat planning. However, specific localized strategies may vary depending on different models, reflecting the unique characteristics of each area.

Author Contributions: Conceptualization, R.L., Q.L. and I.M.; Methodology, R.L. and Q.L.; Software, R.L.; Validation, R.L.; Formal analysis, R.L.; Investigation, R.L. and Q.L.; Resources, R.L. and Q.L.; Data curation, R.L. and Q.L.; Writing—original draft, R.L.; Writing—review & editing, Q.L.; Visualization, R.L.; Supervision, Q.L., I.M. and K.W.; Project administration, Q.L. and K.W.; Funding acquisition, Q.L. All authors have read and agreed to the published version of the manuscript.

Data Availability Statement: The original contributions presented in the study are included in the article, further inquiries can be directed to the corresponding author.

Conflicts of Interest: The authors declare no conflict of interest.

References

1. Brysse, K.; Oreskes, N.; O'Reilly, J.; Oppenheimer, M. Climate change prediction: Erring on the side of least drama? *Glob. Environ. Chang.-Hum. Policy Dimens.* **2013**, *23*, 327–337. [CrossRef]
2. Morakinyo, T.E.; Ouyang, W.L.; Lau, K.K.L.; Ren, C.; Ng, E. Right tree, right place (urban canyon): Tree species selection approach for optimum urban heat mitigation—Development and evaluation. *Sci. Total Environ.* **2020**, *719*, 137461. [CrossRef]
3. Santamouris, M. Cooling the cities—A review of reflective and green roof mitigation technologies to fight heat island and improve comfort in urban environments. *Sol. Energy* **2014**, *103*, 682–703. [CrossRef]
4. Xu, L.Y.; Xie, X.D.; Li, S. Correlation analysis of the urban heat island effect and the spatial and temporal distribution of atmospheric particulates using TM images in Beijing. *Environ. Pollut.* **2013**, *178*, 102–114. [CrossRef] [PubMed]
5. Santamouris, M.; Cartalis, C.; Synnefa, A.; Kolokotsa, D. On the impact of urban heat island and global warming on the power demand and electricity consumption of buildings—A review. *Energy Build.* **2015**, *98*, 119–124. [CrossRef]
6. Li, X.D.; Chow, K.H.; Zhu, Y.M.; Lin, Y. Evaluating the impacts of high-temperature outdoor working environments on construction labor productivity in China: A case study of rebar workers. *Build. Environ.* **2016**, *95*, 42–52. [CrossRef]
7. Shashua-Bar, L.; Pearlmutter, D.; Erell, E. The influence of trees and grass on outdoor thermal comfort in a hot-arid environment. *Int. J. Climatol.* **2011**, *31*, 1498–1506. [CrossRef]
8. Wang, D.; Lau, K.K.L.; Ren, C.; Goggins, W.; Shi, Y.; Ho, H.C.; Lee, T.C.; Lee, L.S.; Woo, J.; Ng, E. The impact of extremely hot weather events on all-cause mortality in a highly urbanized and densely populated subtropical city: A 10-year time-series study (2006–2015). *Sci. Total Environ.* **2019**, *690*, 923–931. [CrossRef]
9. Lai, L.W.; Cheng, W.L. Air quality influenced by urban heat island coupled with synoptic weather patterns. *Sci. Total Environ.* **2009**, *407*, 2724–2733. [CrossRef]
10. Akbari, H.; Pomerantz, M.; Taha, H. Cool surfaces and shade trees to reduce energy use and improve air quality in urban areas. *Sol. Energy* **2001**, *70*, 295–310. [CrossRef]
11. Sipei, M.; Jinkui, W. Analysis of Earth Dwellings' Architectural Climate Adaptability in South of Sichuan, China. *Hous. Sci.* **2016**, *36*, 27–30. [CrossRef]
12. Yi, W.; Meixia, S.; Suming, G. Research Progress and Prospects of Outdoor Microclimate in Chinese Cities Based on Bibliometrics and Content Analysis. *Landsc. Archit. Acad. J.* **2023**, *40*, 92–98.

13. Kabisch, N.; Frantzeskaki, N.; Pauleit, S.; Naumann, S.; Davis, M.; Artmann, M.; Haase, D.; Knapp, S.; Korn, H.; Stadler, J.; et al. Nature-based solutions to climate change mitigation and adaptation in urban areas: Perspectives on indicators, knowledge gaps, barriers, and opportunities for action. *Ecol. Soc.* **2016**, *21*, 39. [CrossRef]

14. Lafortezza, R.; Chen, J.Q.; van den Bosc, C.K.; Randrup, T.B. Nature-based solutions for resilient landscapes and cities. *Environ. Res.* **2018**, *165*, 431–441. [CrossRef] [PubMed]

15. Zhifang, W.; Yuqing, J.; Zhibin, H.; Hongpeng, F. A Review of Nature-based Solutions Research Perspectives and Enlightenments Thereof to the Application in China. *Landsc. Archit.* **2022**, *29*, 12–19. [CrossRef]

16. Han, F.; Cai, J. The evolution and reconstruction of peri-urban rural habitat in China. *Geogr. Res.* **2011**, *30*, 1271–1284.

17. Longquanshan Irrigation District Management Division of Dujiang Weir of Sichuan Province. Studies on heritage and development of water civilization from the respect of Dujiang Weir, China. *China Water Resour.* **2020**, *3*, 60–62.

18. Mikiko, I.; Li, Q.; Sae, Y. Study on Green Space Planning after the Great Sichuan Earthquake, and Restoration of Linpan in Agricultural Area of Dujiangyan. Sichuan Province, China. *City Plan. Inst. Jpn.* **2020**, *55*, 753–760. [CrossRef]

19. Fang, Z. Basic Study on the Linpan Culture at Western Sichuan Plain. Ph.D. Thesis, Chongqing University, Chongqing, China, 2012.

20. Kai, P.; Lingli, M. Research on the Protection of Native Landscape Features of Linpan in Western Sichuan Based on the Extraction of Landscape Genes: Taking the Linpan of Longquan Community in Juyuan Town as an Example. *Dev. Small Cities Towns* **2022**, *40*, 49–58+96.

21. Qian, W.; Meiling, L.; Hua, Z. Micrometeorology influence of Linpan on its adjacent environment in summer. *Ecol. Sci.* **2021**, *40*, 139–148. [CrossRef]

22. Gou, S.Q.; Li, Z.R.; Zhao, Q.; Nik, V.M.; Scartezzini, J.L. Climate responsive strategies of traditional dwellings located in an ancient village in hot summer and cold winter region of China. *Build. Environ.* **2015**, *86*, 151–165. [CrossRef]

23. Zhang, L.; Peng, W.; Zhang, J. Assessment of Land Ecological Security from 2000 to 2020 in the Chengdu Plain Region of China. *Land* **2023**, *12*, 1448. [CrossRef]

24. Chen, Y.H.; Wu, J.T.; Yu, K.; Wang, D.D. Evaluating the impact of the building density and height on the block surface temperature. *Build. Environ.* **2020**, *168*, 106493. [CrossRef]

25. Salata, F.; Golasi, L.; Volloaro, R.D.; Vollaro, A.D. Urban microclimate and outdoor thermal comfort. A proper procedure to fit ENVI-met simulation outputs to experimental data. *Sustain. Cities Soc.* **2016**, *26*, 318–343. [CrossRef]

26. Li, J.W.; Liu, N.Y. The perception, optimization strategies and prospects of outdoor thermal comfort in China: A review. *Build. Environ.* **2020**, *170*, 106614. [CrossRef]

27. Xu, Y.; Ren, C.; Ma, P.F.; Ho, J.; Wang, W.W.; Lau, K.K.L.; Lin, H.; Ng, E. Urban morphology detection and computation for urban climate research. *Landsc. Urban. Plan.* **2017**, *167*, 212–224. [CrossRef]

28. Prasad, P.S.; Satyanarayana, A.N. Assessment of universal thermal climate index (UTCI) using the WRF-UCM model over a metropolitan city in India. *Int. J. Biometeorol.* **2024**, 1–4. [CrossRef] [PubMed]

29. Tong, S.; Wong, N.H.; Jusuf, S.K.; Tan, C.L.; Wong, H.F.; Ignatius, M.; Tan, E. Study on correlation between air temperature and urban morphology parameters in built environment in northern China. *Build. Environ.* **2018**, *127*, 239–249. [CrossRef]

30. Zhang, J.; Cui, P.; Song, H.H. Impact of urban morphology on outdoor air temperature and microclimate optimization strategy base on Pareto optimality in Northeast China. *Build. Environ.* **2020**, *180*, 107035. [CrossRef]

31. Achour-Younsi, S.; Kharrat, F. Outdoor thermal comfort: Impact of the geometry of an urban street canyon in a Mediterranean subtropical climate—Case study Tunis, Tunisia. In Proceedings of the Conference on Urban Planning and Architectural Design for Sustainable Development (UPADSD), Lecce, Italy, 14–16 October 2015; pp. 689–700.

32. Giridharan, R.; Ganesan, S.; Lau, S.S.Y. Daytime urban heat island effect in high-rise and high-density residential developments in Hong Kong. *Energy Build.* **2004**, *36*, 525–534. [CrossRef]

33. Liu, Y.; Li, Q.; Yang, L.; Mu, K.K.; Zhang, M.Y.; Liu, J.P. Urban heat island effects of various urban morphologies under regional climate conditions. *Sci. Total Environ.* **2020**, 743. [CrossRef] [PubMed]

34. Mohajerani, A.; Bakaric, J.; Jeffrey-Bailey, T. The urban heat island effect, its causes, and mitigation, with reference to the thermal properties of asphalt concrete. *J. Environ. Manag.* **2017**, *197*, 522–538. [CrossRef] [PubMed]

35. Morakinyo, T.E.; Kong, L.; Lau, K.K.L.; Yuan, C.; Ng, E. A study on the impact of shadow-cast and tree species on in-canyon and neighborhood's thermal comfort. *Build. Environ.* **2017**, *115*, 1–17. [CrossRef]

36. Amani-Beni, M.; Zhang, B.; Xie, G.D.; Xu, J. Impact of urban park's tree, grass and waterbody on microclimate in hot summer days: A case study of Olympic Park in Beijing, China. *Urban. For. Urban. Green.* **2018**, *32*, 1–6. [CrossRef]

37. Yang, Y.J.; Zhou, D.; Wang, Y.P.; Ma, D.X.; Chen, W.; Xu, D.; Zhu, Z.Z. Economical and outdoor thermal comfort analysis of greening in multistory residential areas in Xi'an. *Sustain. Cities Soc.* **2019**, *51*, 101730. [CrossRef]

38. Karimi, A.; Sanaieian, H.; Farhadi, H.; Norouzian-Maleki, S. Evaluation of the thermal indices and thermal comfort improvement by different vegetation species and materials in a medium-sized urban park. *Energy Rep.* **2020**, *6*, 1670–1684. [CrossRef]

39. Abdi, B.; Hami, A.; Zarehaghi, D. Impact of small-scale tree planting patterns on outdoor cooling and thermal comfort. *Sustain. Cities Soc.* **2020**, *56*, 102085. [CrossRef]

40. Atwa, S.; Ibrahim, M.G.; Murata, R. Evaluation of plantation design methodology to improve the human thermal comfort in hot-arid climatic responsive open spaces. *Sustain. Cities Soc.* **2020**, *59*, 102198. [CrossRef]

41. Sodoudi, S.; Zhang, H.W.; Chi, X.L.; Müller, F.; Li, H.D. The influence of spatial configuration of green areas on microclimate and thermal comfort. *Urban. For. Urban. Green.* **2018**, *34*, 85–96. [CrossRef]

42. Wu, Z.F.; Chen, L.D. Optimizing the spatial arrangement of trees in residential neighborhoods for better cooling effects: Integrating modeling with in-situ measurements. *Landsc. Urban Plan.* **2017**, *167*, 463–472. [CrossRef]

43. Bai, X.Y.; Yu, Z.W.; Wang, B.Y.; Zhang, Y.T.; Zhou, S.Q.; Sha, X.H.; Li, S.H.; Yao, X.H.; Geng, X.L. Quantifying threshold and scale response of urban air and surface temperature to surrounding landscapes under extreme heat. *Build. Environ.* **2024**, 247. [CrossRef]

44. Mughal, M.O.; Li, X.X.; Yin, T.G.; Martilli, A.; Brousse, O.; Dissegna, M.A.; Norford, L.K. High-Resolution, Multilayer Modeling of Singapore's Urban Climate Incorporating Local Climate Zones. *J. Geophys. Res. Atmos.* **2019**, *124*, 7764–7785. [CrossRef]

45. Yang, Y.J.; Zhou, D.; Wang, Y.P.; Meng, X.Z.; Gu, Z.L.; Xu, D.; Han, X.X. Planning method of centralized greening in high-rise residential blocks based on improvement of thermal comfort in summer. *Sustain. Cities Soc.* **2022**, *80*. [CrossRef]

46. Zhao, Y.F.; Chen, Y.H.; Li, K.N. A simulation study on the effects of tree height variations on the facade temperature of enclosed courtyard in North China. *Build. Environ.* **2022**, *207*, 108566. [CrossRef]

47. Tseliou, A.; Tsiros, I.X.; Lykoudis, S.; Nikolopoulou, M. An evaluation of three biometeorological indices for human thermal comfort in urban outdoor areas under real climatic conditions. *Build. Environ.* **2010**, *45*, 1346–1352. [CrossRef]

48. Tsoka, S.; Tsikaloudaki, A.; Theodosiou, T. Analyzing the ENVI-met microclimate model's performance and assessing cool materials and urban vegetation applications—A review. *Sustain. Cities Soc.* **2018**, *43*, 55–76. [CrossRef]

49. Zarghami, E.; Ghanbaran, A.; Karimimoshaver, M.; Saadativaghar, P. Effect of Height and Color of Tall Buildings on the Perceived Psychological Restoration of Residents. *J. Archit. Plan. Res.* **2019**, *36*, 321–342.

50. Baangood, R.S.; Hassan, A.S. Impact of Courtyard and Narrow Streets on Thermal Comfort of Traditional Buildings in Mukalla City. *Int. Trans. J. Eng. Manag. Appl. Sci. Technol.* **2017**, *8*, 115–126.

51. Bo-rong, L. Studies of Greening's Effects on Outdoor Thermal Environment. Ph.D. Thesis, Tsinghua University, Beijing, China, 2005.

52. Chow, W.T.L.; Akbar, S.; Heng, S.L.; Roth, M. Assessment of measured and perceived microclimates within a tropical urban forest. *Urban For. Urban Green.* **2016**, *16*, 62–75. [CrossRef]

53. Teshnehdel, S.; Akbari, H.; Di Giuseppe, E.; Brown, R.D. Effect of tree cover and tree species on microclimate and pedestrian comfort in a residential district in Iran. *Build. Environ.* **2020**, *178*, 106899. [CrossRef]

54. Potchter, O.; Cohen, P.; Bitan, A. Climatic behavior of various urban parks during hot and humid summer in the Mediterranean city of Tel Aviv, Israel. *Int. J. Climatol.* **2006**, *26*, 1695–1711. [CrossRef]

55. Cheng, H.; Liu, C.C.; Kang, L.Q. Experimental study on the effect of plant spacing, number of rows and arrangement on the airflow field of forest belt in a wind tunnel. *J. Arid Environ.* **2020**, *178*, 104169. [CrossRef]

56. Caneva, G.; Bartoli, F.; Zappitelli, I.; Savo, V. Street trees in italian cities: Story, biodiversity and integration within the urban environment. *Rend. Lincei Sci. Fis. Nat.* **2020**, *31*, 411–417. [CrossRef]

Article

Role of Social Infrastructure in Social Isolation within Urban Communities

Yeo-Kyeong Kim and Donghyun Kim *

Department of Urban Planning and Engineering, Pusan National University, Busan 46241, Republic of Korea; clara13@naver.com
* Correspondence: donghyun-kim@pusan.ac.kr; Tel.: +82-51-510-2448

Abstract: Social isolation is a global problem with far-reaching consequences. Nevertheless, various solutions can address it. Building social infrastructure is important for preventing isolation. In this study, we aimed to understand the impact of urban infrastructure on social isolation using social surveys and statistical data from South Korea. A multilevel logistic model identified the infrastructure characteristics required to solve social isolation by adding regional-level data to individual-level data. The analysis showed that, at the individual level, gender, age, marital status, and household income were significant, whereas at the regional level, the ratio of single-person households, access to traditional markets, and the capital region status areas were significant. The findings suggest that social infrastructure can impact social isolation. Hence, it is important to plan urban spaces and design infrastructure to help alleviate social isolation.

Keywords: social isolation; multilevel logistic model; social infrastructure; urban community

1. Introduction

As the number of people experiencing social isolation worldwide rises, so do the efforts of various governments. Unlike in the past, social isolation has been recognized as a crucial issue requiring policy intervention, with the UK and Japan appointing a Minister for Loneliness in 2018 and 2021, respectively. Given that social isolation can lead to poor health [1] and people dying alone (a phenomenon known as lonely deaths), it is important to explore interventions to address the risks deriving from social isolation.

On 1 April 2021, South Korea's Ministry of Government Legislation passed the Act on the Prevention and Management of Lonely Deaths. This legislation establishes an institutional basis for the systematic prevention and management of lonely deaths nationally. A basic preventive plan must be formulated and implemented every five years. The Act includes matters related to creating a social environment, such as a community's social network programs using libraries or community facilities. These policies are important because they recognize the influence of the social environment, rather than just individual factors, on social isolation, although their practical effects have not yet been seen. According to Carstensen et al. [2], organizing spaces with different functions and activities can help alleviate social and physical isolation among urbanites.

Social isolation is recognized as an urban problem, not just an individual problem. Most studies have aimed to identify individual characteristics associated with social isolation, focusing on specific age, gender, and class groups as units of analysis. However, individual behaviors associated with social isolation are influenced by urban environmental factors such as a lack of social networking space. To overcome the limitations of considering only individual characteristics and not environmental influences on social isolation, some studies have considered the influence of the urban environment on the formation of social relationships. Zavaleta et al. [3] described social isolation as a state of deprivation of social connectedness, and, according to Mouratidis [4], social relationships are affected by the planning of urban environments.

Social isolation has gained increased attention as an important social issue since coronavirus disease 2019 (COVID-19) [5]. Social isolation is an individual phenomenon, but it interacts with environmental factors surrounding the individual. Individuals' social relationships are weakening, especially in urbanized environments. Face-to-face contact and forming social relationships between individuals can depend on the accessibility and type of space in which they engage in their daily activities [6]. Recent studies [7] discuss how certain neighborhoods have better social infrastructure conducive to forming social relationships, which may lead to health disparities between neighborhoods. While this study focuses on South Korea, which has a high rate of aging and suicide, the general relationship between individuals, their surroundings, and social infrastructure may also apply elsewhere.

This study aimed to combine individual- and regional-level factors affecting social isolation in a multilayered structure and determine how regional factors impact social isolation. We used a sample of 89,768 respondents from the 2020 Social Survey of South Korea, considering both individual factors that influence social isolation, as in previous studies, and regional factors in the 59 municipalities where the respondents lived.

This study is structured as follows. First, we examine the conceptual definition of social isolation and the theoretical background underlying personal and regional characteristics. Second, we describe how, based on the data, we used a multilevel logistic model to analyze social isolation, considering personal and regional factors. Third, we present the results of the analysis to identify personal and regional characteristics that influence social isolation. Fourth, we pinpoint the reasons for the significant factors in the analysis; we also derive implications from the findings.

2. Literature Reviews

2.1. Social Isolation

Social isolation is associated with loneliness and refers to a state in which an individual has minimal contact with others or has limited participation in community life [8], is deprived of social connectedness [3], and lacks personal relationships [9]. A concept similar to social isolation is social exclusion, which Bäckman and Nilsson [10] described as a situation or process in which individuals or groups cannot fully participate in society owing to factors such as unemployment, poverty, or poor health. Social exclusion refers to discrimination regarding social activities, such as financial poverty and labor market exclusion. In contrast, social isolation focuses on emotional isolation from family and friends within a social network. The social infrastructure of a city is related to social isolation because social infrastructure has attributes based on the social network.

Several studies have examined how social isolation can be measured and its associated factors. Chatters et al. [1] explored the frequency of contact with one's family and friends to gauge social isolation using the following questions: "How often do you see, write to, or talk on the phone with family or relatives who do not live with you? Would you say almost every day, at least once a week, a few times a month, at least once a month, a few times a year, hardly ever, or never?" Prior studies have linked social isolation to loneliness and confirmed the former by measuring the latter. Gyasi et al. [11] suggested that social isolation can be measured by responding to questions such as "Do you feel left out?", "Do you feel isolated?", and "Do you feel that you lack friendships?" with responses of sometimes or often. Social isolation can be measured in two ways: (1) objectively by ascertaining whether a person is isolated from others based on measures such as contact and (2) by assessing whether the person perceives himself/herself as isolated.

Several personal characteristics influence social isolation. First, age is significant, with older people being particularly vulnerable, and their risk of social isolation increases as their opportunities to add new social relationships decrease [12]. However, a recent study found that younger people report twice as many lonely and isolated days, even with larger social networks [13], confirming that social isolation is a problem that can be experienced at any age. Gender and income are also significant factors. Generally, men are

more vulnerable to social isolation because they have fewer social resources and limited interactions with others compared to women. At the same time, higher income is associated with a lower likelihood of isolation from one's family [1].

Metropolitan areas are more vulnerable to social isolation. Warner and Andrews [14] found that as urban high-rise development increases and more parents and children live in urban centers, they experience physical and social barriers that prevent them from forming deeper social connections with their neighbors. Warner and Andrews [14] interviewed residents and found that the high density of high-rise living makes it difficult to visit acquaintances and maintain existing social ties owing to the increased cost of parking and that spaces such as outdoor common areas and indoor walkways are not conducive to forming new relationships. Chile et al. [15] also found in an interview study of social isolation among inner-city high-rise residents in Auckland, New Zealand, that 43% of respondents reported feeling isolated in the city center. Large cities with dense high-rise residential areas are more vulnerable to social isolation. Therefore, it is necessary to consider the environment of large cities as a factor when we analyze social isolation.

2.2. Social Infrastructure

According to Popova [16], the concept of infrastructure is broadly divided into social infrastructure and economic and production infrastructure; social infrastructure consists of healthcare, education, culture, and tourism. Grum and Kobal Grum [17] defined social infrastructure as things that play an important role in people's daily lives; they are important elements that satisfy the needs and overall development of individuals and society alike and contribute to non-social interactions. Social infrastructure relates to various services, facilities, and public spaces for the community, relationships, and networks between community members, and creates opportunities for social integration and participation [6,18]. Smith et al. [19] suggested that because the COVID-19 pandemic required physical distancing, which has led to increased social isolation, remote services and programs should be developed to provide the infrastructure to prevent social isolation. Stender and Nordberg [5] emphasize the role of social networks in public spaces as social infrastructure, which they argue became even more prominent during the COVID-19 pandemic.

Social infrastructure that supports social interactions also reduces social isolation. Ward Thompson et al. [20] found that parks and open spaces offer support for neighborhood contact and the preservation of connections within communities, which in turn mitigates social isolation; Ward Thompson et al. [20] also revealed a link between the percentage of green space and reduced stress levels. Social infrastructure can contribute to forming social networks, mitigating social isolation, and positively impacting mental health by reducing stress. Johansson-Pajala et al. [21] stated that information and communication technologies (ICTs) are a good means of preventing and addressing social isolation and loneliness among older people, as they can develop social networks that offer proper support. ICTs have been studied as a new type of infrastructure that helps resolve the issue of social isolation in modern society. Jiménez et al. [22] indicated that older adults who received face-to-face ICT training experienced reduced social isolation and loneliness, which increased their overall well-being. Therefore, considerations should be included to facilitate the implementation of ICT programs in community settings.

With the increasing awareness of the importance of social infrastructure, South Korea is trying to introduce infrastructure to improve livelihood. Currently, infrastructure is well distributed in South Korea. Still, there is a shortage of cultural, sports, and leisure facilities and a minimization of the importance of the distance between facilities and residences [23]. In South Korea, infrastructure includes traditional markets, which have long been central to the living environment; they serve various socioeconomic functions and influence small communities [11,24]. Cultural and sports centers, leisure facilities, and traditional markets are vital pieces of social infrastructure in South Korea.

There are two main takeaways from the literature on social isolation and social infrastructure. First, the factors that influence social isolation can be divided into individual biological, behavioral, and socioeconomic factors, which work in combination. Urban environmental factors are important in shaping social relationships among socioeconomic factors. Urban environmental factors can be further categorized into residential and neighborhood factors, and even within the same urban environmental factors, there are differences in the degree of impact depending on the region and the area under study. Second, social infrastructure contributes to resolving social isolation. In traditional urban planning discussions, social infrastructure refers to physical facilities such as roads, railways, and schools. Still, recent discussions have emphasized the networked nature of social infrastructure, which can contribute to interactions between people. The role of infrastructure in influencing individual behavior and networks is based on this discussion. In this study, we investigated variables based on the influencing factors of social isolation discussed in the literature. We integrated two factors with different units of analysis into a single model to examine the relationship between them.

3. Materials and Methods

3.1. Data and Variables

The scope of the study included 59 municipalities in four cities—Seoul, Busan, Daegu, and Incheon—which are representative metropolitan areas in South Korea where people are at risk of social isolation. The social survey of Busan, Daegu, and Incheon used in this study identified social concerns, including social isolation, individual characteristics, and subjective perceptions of people related to quality of life. In the case of Seoul, a similar survey was conducted under the name of the Urban Policy Indicators Survey (Seoul Survey), which was used in the analysis.

The data and variables in Table 1 are organized as follows. We focused on adults aged 20 and older who responded to a social survey. They were divided into five age groups (20s, 30s, 40s, 50s, and over 60), by gender (women and men), and three educational levels (middle school or lower, high school or lower, and university or higher). The three educational levels were divided into graduated, attended, completed, dropped out, took leave of absence, and graduated from school. Economic activity was divided into those who were economically active and those who were not. In the case of Seoul, only the occupation category was available, so we classified unemployed, student, and housewife as non-economic activities. Housewives' domestic work can be considered labor. Still, as it does not trigger interaction with others, which is the core of social isolation research, we classified it as a non-economic activity.

We obtained data on regional influences from the Korean Statistical Information Service (KOSIS) [24–28]. The cultural and sports facilities variable is the sum of the number of cultural and sports facilities converted to the number of facilities per 10,000 inhabitants for each municipality and 0 for no facilities. The parks and welfare facilities variable was created by dividing the number of facilities in each municipality by the population and turning the number of facilities into facilities per 10,000 people. However, in the case of traditional markets, data that separated each city and district's areas were unavailable; therefore, the time taken to access traditional markets was used. For the ratio of multifamily units, the number of multifamily houses was divided by the total number of houses, and for the ratio of single-person households, the total number of single-person households was divided by the total number of households. Seoul and Incheon were classified as capital regions, whereas Busan and Daegu were classified as non-capital regions.

<div align="center">**Table 1.** Data and variables.</div>

Type	Variable (Name)	Definition	Source
Dependent	Social isolation	Do you have someone to help you in times of need? 1 = No (social isolation), 0 = Yes	Social Survey [25], Seoul Survey [26]
Independent (Individual Level)	Gender (*Gender*)	1 = Man, 0 = Woman	Social Survey [25], Seoul Survey [26]
	Age (*Age*)	2 = 20s, 3 = 30s, 4 = 40s, 5 = 50s, 6 = 60 and above	
	Education (*Education*)	1 = Middle school or lower, 2 = High school or lower, 3 = University or higher	
	Marital status (*Marriage*)	1 = Non-married, 0 = Married	
	Economic activity (*Economic*)	1 = No, 0 = Yes	
	Average monthly household income (*Income*)	1 = Less than KRW 1 million, 2 = KRW 1 million to less than KRW 2 million, 3 = KRW 2 million to less than KRW 3 million, 4 = KRW 3 million to less than KRW 4 million, 5 = KRW 4 million to less than KRW 5 million, 6 = More than KRW 5 million	
Independent (Regional Level)	Ratio of single-person households (*Singleperson*)	$\frac{Number\ of\ single-person\ households}{Total\ households}$	Population Census [27]
	Number of parks per 10,000 people (*Park*)	$\frac{Number\ of\ parks \times 10,000}{Total\ population}$	Urban planning statistics [28]
	Number of culture and sports facilities per 10,000 people (*CulSpo*)	$\frac{Number\ of\ culture\ and\ sports\ facilities \times 10,000}{Total\ population}$	Urban planning statistics [28]
	Number of welfare facilities per 10,000 people (*Welfare*)	$\frac{Number\ of\ welfare\ facilities \times 10,000}{Total\ population}$	Urban planning statistics [28]
	Access to traditional markets (*Market*)	Travel time (min) to traditional markets (average of car, public transit, and walking)	Transportation accessibility index [29]
	Number of places of worship per 10,000 people (*Religion*)	$\frac{Number\ of\ places\ of\ worship \times 10,000}{Total\ population}$	Building energy usage [30]
	Capital region status (*Capital*)	1 = No 0 = Yes (Seoul, Incheon, and Gyeonggi)	
	Ratio of multifamily units (*Apart*)	Total multifamily units divided by total housing units	Housing census [31]

3.2. Multilevel Logistic Model

As a measure of the dependent variable—social isolation—we used the response to the question "Is there anyone you can turn to for help in times of need?" from the social survey. The response was presented as a binary variable—yes or no— with yes indicating that the respondent was not socially isolated. The independent variables were divided into individual and regional.

Previous studies on individual variables have used age, gender, residence, marital status, educational level, employment status, and monthly income level as covariates that may affect social isolation [11]. Similarly, age, gender, race/ethnicity, family income, educational level, marital status, and household status have been used as socioeconomic variables [32]. In addition, social infrastructure based on social networks is discussed as a regional-level variable that can influence social isolation [5,6,33]. Based on previous research, we used age, gender, household income, educational level, marital status, and economic activity as variables that could be obtained from social survey data. For the regional variables, we used the social infrastructure elements of time to reach a traditional market and the number of parks, cultural/sports facilities, welfare facilities, and places of worship per 10,000 people in the municipality. Additionally, we used the ratios of multifamily units, single-person households, and the capital region status.

We employed a multilevel logistic model for the analysis (Figure 1). The goal of logistic regression is to predict the probability of a phenomenon occurring in an individual based on the value of a certain binary dependent variable. A multilevel logistic model considers the statistical dependence of an individual's probability on their region of residence [32]. Such a model is appropriate because the dependent variable in this study had a binary nature of 1 and 0, and we aimed to identify the characteristics of the social infrastructure in the region of residence that affected social isolation in addition to individual characteristics. The equations used in this study are as follows:

$$log(p_i) = logodds = log\left(\frac{p_i}{1 - p_i}\right) = M + E_r \tag{1}$$

$$Logit(p_i) = M + \beta_1 Gender_i + \beta_2 Age_i + \beta_3 Education_i + \beta_4 Marriage_i + \beta_5 Economic_i + \beta_6 Income_i + E_r \tag{2}$$

$$\begin{aligned} Logit(p_i) = M + \ &\beta_1 Gender_i + \beta_2 Age_i + \beta_3 Education_i + \beta_4 Marriage_i \\ &+\beta_5 Economic_i + \beta_6 Income_i + \beta_7 Singleperson_r + \beta_8 Park_r \\ &+\beta_9 CulSpo_r + \beta_{10} Wlfare_r + \beta_{11} Markt_r + \beta_{12} Religion_r \\ &+\beta_{13} Capital_r + \beta_{14} Apart_r + E_r \end{aligned} \tag{3}$$

p_i : probability that a phenomenon occurs for individual i
M : overall mean probability expressed on the logistic scale
E_r : regional level residual
i : individual level
r : regional level (municipality)
$\beta_1, \beta_2, \beta_3, \beta_4, \beta_5, \beta_6$: regression coefficients (individual level)
$\beta_7, \beta_8, \beta_9, \beta_{10}, \beta_{11}, \beta_{12}, \beta_{13}, \beta_{14}$: regression coefficients (regional level)

We used Stata 16 (StataCorp., College Station, TX, USA) software for all analyses. The analysis sequence was as follows. First, we performed basic statistical analysis of each variable to identify its characteristics, and we derived the variance inflation factor to check for multicollinearity. We calculated the intraclass correlation coefficient (ICC) to determine the dependent variable's explanatory power at the regional level. After conducting a multilevel logistic model analysis, we re-derived the ICC value to determine the explanatory power of the regional-level variables. Finally, we obtained the marginal effects.
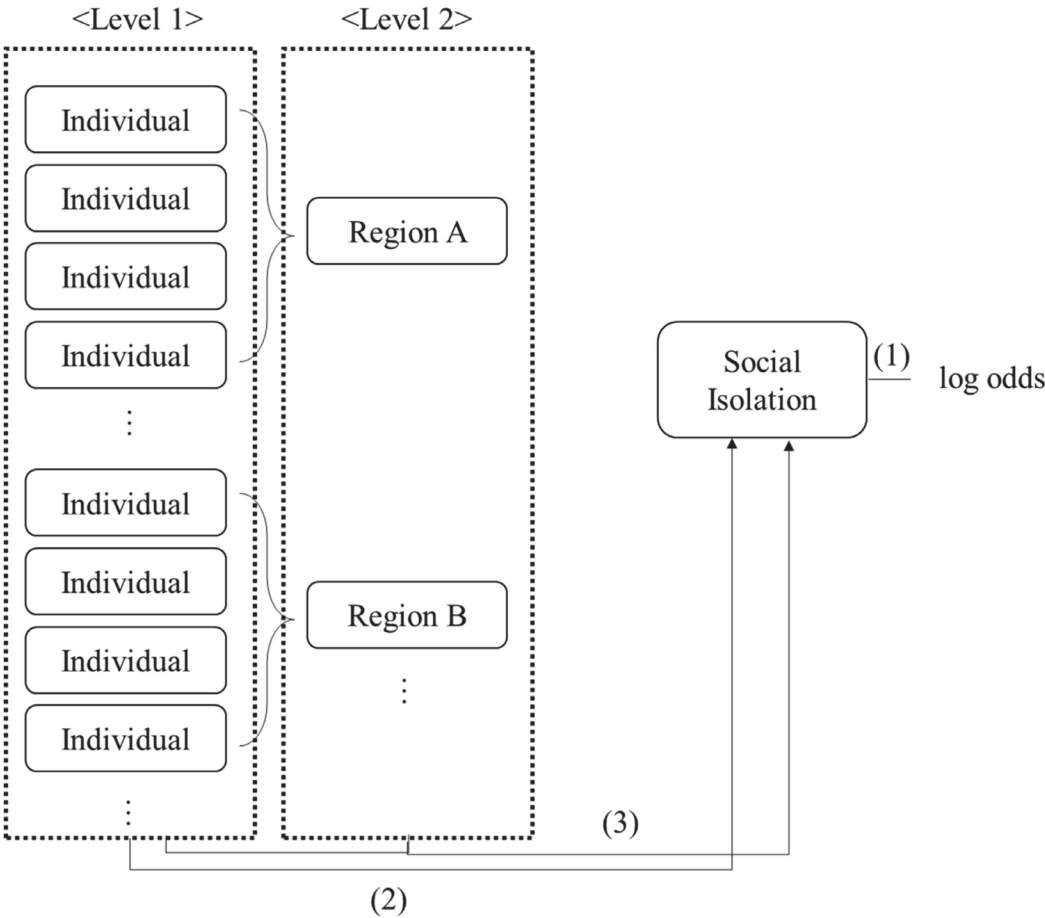
Figure 1. Analytic model flow. Note: Parentheses indicate the number of equation.

4. Results

We found the variance inflation factor values to be a maximum of 3.48 for all variables; as the values were not greater than 10, there was no multicollinearity problem.

Table 2 presents the basic statistical analysis. The total number of respondents was 89,768; women comprised 51.2% of the sample, and people aged 60 and above amounted to 32.5%. Regarding educational level, 54.1% of the respondents had a university degree or higher, and married people composed 66.9% of the sample. The economic activity rate was 62.4%, and the proportion of an average monthly household income of more than KRW 5 million was 31.3%. As for regional characteristics, the ratio of single-person households was about 0.3, and there were 2.3 parks per 10,000 people, while there were 0.12 cultural/sports facilities and 0.24 welfare facilities per 10,000 people, respectively. There were about four places of worship per 10,000 people. In addition, 44.1% of the respondents lived in the non-capital region. On average, the multifamily ratio was 0.835.

As the multilevel model was analyzed by determining whether the Level 2 independent variables (this study's regional variable) affected the dependent variable, it was necessary to check the ICC value using first-level individual factors (Table 3). A value close to 0 indicated no difference between regions. In this study, the ICC value is 0.117. This means that the region explained 11.7% of the variance in social isolation.

Table 2. Basic statistics.

Type	Variables	Obs.	Mean	Std. Dev.	Min	Max
Dependent	Social isolation	89,768	0.176	0.381	0	1
Independent (Individual Level)	*Gender*	89,768	0.488	0.500	0	1
	Age	89,768	4.482	1.352	2	6
	Education	89,768	2.376	0.751	1	3
	Marriage	89,768	0.331	0.471	0	1
	Economic	89,768	0.376	0.484	0	1
	Income	89,768	4.026	1.753	1	6
Independent (Regional Level)	*Singleperson*	59	0.327	0.058	0.234	0.497
	Park	59	2.375	2.040	0	13.033
	CulSpo	59	0.121	0.147	0	1.195
	Welfare	59	0.246	0.158	0	0.817
	Market	59	9.044	12.248	4.005	120
	Religion	59	4.145	2.727	1.225	17.994
	capital	59	0.441	0.497	0	1
	Apart	59	0.835	0.124	0.246	0.970

Table 3. First-level individual factors and multilevel model analysis.

Variables	Coef.	Robust Std. Err.	z	P > |z|	[95% Confidence Interval]	
Gender	0.237	0.034	6.96	0	0.171	0.304
Age	0.051	0.019	2.63	0.009	0.013	0.089
Educational level	−0.023	0.044	−0.53	0.598	−0.110	0.064
Marital status (Marriage)	0.199	0.078	2.56	0.01	0.047	0.352
Economic activity (Economic)	0.012	0.041	0.29	0.775	−0.069	0.092
Average monthly household income (Income)	−0.178	0.018	−9.81	0	−0.213	−0.142

Note: residual intraclass correlation (ICC) at the regional level is 0.117 with 0.024 standard error. Pseudo R^2 is 0.3311 in the individual level model.

The ICC value after constructing the multilevel logistic model, as depicted in Table 4, was 0.059, which means that the regional factors explained about 5.8% of the previous 11.7%, and approximately 5.9% remained; this implies that the regional variables explained around half of the regional influence of social isolation, so the variables were set appropriately. Also, it was necessary to examine the marginal effects to interpret the multilevel logistic model; therefore, we derived the marginal effects (Table 5). The results are as follows.

The first level of the individual variables showed that gender, age, marital status, and average monthly household income were significant. Men were 3.3% more likely to be socially isolated than women (Coef. = 0.238, P > |z| = 0.000, [95% confidence interval (CI)] = [0.171, 0.305], dy/dx = 0.033). Increased age was associated with 0.7% higher odds of being socially isolated (Coef. = 0.051, P > |z| = 0.008, [95% CI] = [0.013, 0.090], dy/dx = 0.007). Being non-married compared to married was associated with a 2.7% greater likelihood of being socially isolated (Coef. = 0.199, P > |z| = 0.011, [95% CI] = [0.046, 0.351], dy/dx = 0.027). Finally, an increase in income was associated with a 2.4% decrease in the odds of being socially isolated (Coef. = −0.179, P > |z| = 0.000, [95% CI] = [−0.214, −0.143], dy/dx = −0.024).

Table 4. Multilevel logistic model results.

	Variables	Coef.	Robust Std. Err.	z	P > |z|	[95% Confidence Interval]	
Individual Level	Gender	0.238	0.034	6.98	0.000	0.171	0.305
	Age	0.051	0.019	2.64	0.008	0.013	0.090
	Education	−0.024	0.044	−0.55	0.584	−0.111	0.063
	Marriage	0.199	0.078	2.56	0.011	0.046	0.351
	Economic	0.012	0.041	0.29	0.775	−0.069	0.092
	Income	−0.179	0.018	−9.86	0.000	−0.214	−0.143
Regional Level	Singleperson	3.163	1.403	2.25	0.024	0.414	5.913
	Park	0.043	0.025	1.73	0.084	−0.006	0.091
	CulSpo	−0.371	0.597	−0.62	0.534	−1.542	0.800
	Welfare	−0.353	0.644	−0.55	0.584	−1.614	0.909
	Market	−0.022	0.005	−4.44	0.000	−0.032	−0.012
	Religion	−0.015	0.023	−0.65	0.518	−0.059	0.030
	Capital	−0.602	0.116	−5.19	0.000	−0.829	−0.374
	Apart	0.840	0.836	1.01	0.315	−0.798	2.478
	Prob > chi^2 = 0.0000						

Note: residual intraclass correlation (ICC) at the regional level is 0.059 with 0.018 standard error.

Table 5. Multilevel logistic model's marginal effects.

	Variables	dy/dx	Delta-Method Std. Err.	z	P > |z|	[95% Confidence Interval]	
Individual Level	Gender	0.033	0.005	7.15	0.000	0.024	0.041
	Age	0.007	0.003	2.61	0.009	0.002	0.012
	Education	−0.003	0.006	−0.55	0.582	−0.015	0.009
	Marriage	0.027	0.010	2.6	0.009	0.007	0.048
	Economic	0.002	0.006	0.29	0.774	−0.009	0.013
	Income	−0.024	0.003	−9.59	0.000	−0.029	−0.019
Regional Level	Singleperson	0.433	0.188	2.31	0.021	0.065	0.801
	Park	0.006	0.003	1.73	0.084	−0.001	0.012
	CulSpo	−0.051	0.081	−0.62	0.532	−0.210	0.109
	Welfare	−0.048	0.088	−0.55	0.582	−0.220	0.124
	Market	−0.003	0.001	−4.53	0.000	−0.004	−0.002
	Religion	−0.002	0.003	−0.64	0.52	−0.008	0.004
	Capital	−0.082	0.016	−5.09	0.000	−0.114	−0.051
	Apart	0.115	0.114	1.01	0.315	−0.109	0.339

At the regional level, the ratios of single-person households, access to traditional markets, and the capital region status were significant. An increase in the ratio of single-person households was associated with a 43% increase in the risk of social isolation (Coef. = 3.163, P > |z| = 0.024, [95% CI] = [0.414, 5.913], dy/dx = 0.433). In the case of access to traditional markets, a 0.3% reduction in the probability of being socially isolated was found for each additional hour of travel time (Coef. = −0.022, P > |z| = 0.000, [95% CI] = [−0.032, −0.012], dy/dx = −0.003). Finally, regarding the capital region status, there was an 8.2% decrease in the probability of being socially isolated in the non-capital region compared to the capital region (Coef. = −0.602, P > |z| = 0.000, [95% CI] = [−0.829, −0.374], dy/dx = −0.082).

5. Discussion

The analysis revealed that the risk of social isolation increased for older people, men, unmarried people, and low-income individuals. Like previous studies, we found that men were more likely to be socially isolated than women and that older people were more likely to be socially isolated. However, social isolation in older adults can be prevented by pro-

moting communication and mutual help among neighbors [34]. Chatters et al. [1] found that women are more invested in and connected to social networks, including family and friends, which can prevent social isolation, even in old age. In contrast, older men may be more vulnerable to social isolation because they have fewer social resources and limited social interactions [1]. Health factors such as physical discomfort, as well as reduced income and anxiety in retirement, may contribute to limited social interaction. As an older society will have more seniors who may be at risk of social isolation, local governments need to expand their welfare workforce and foster related industries to provide a variety of services.

We also observed an increased risk of social isolation for unmarried individuals because, unlike married people, they are unable to form new social networks through their spouses and children, as well as through their spouses' families and friends. Notwithstanding, Sarkisian and Gerstel [35] indicated that being unmarried has a positive impact, with more frequent contact with parents, siblings, neighbors, and friends for support and increased social connectedness versus being married. Hence, it is likely that in a modern society with a growing unmarried population, there are more social connections between unmarried people than in the past, when being married was the norm. As such, rather than simply being unmarried increasing the risk of social isolation, other factors are likely to have a greater impact on this phenomenon. Therefore, it is necessary to identify the status and situation of the unmarried population to distinguish between those who are at risk of social isolation and those who are not and to develop strategies to reduce social isolation tailored to their unique circumstances.

When household income is low, a lack of resources to undertake a range of social activities to build social connections limits choices and participation. As a result, one's social network of relationships shrinks, increasing the risk of social isolation. Urban planning should endeavor to provide facilities that are accessible to all so that low-income people can naturally form social networks in the city, even if they do not participate in activities specifically for this purpose. For example, when installing facilities such as libraries, it is necessary to maximize the community element, and when organizing operational programs, it is necessary to support activities such as discussion groups and reading clubs that allow various people to mingle.

At the regional level, parks, culture and sports facilities, welfare facilities, and places of worship (generally considered elements of social infrastructure that contribute to community building), as well as the ratio of multifamily units, were not significant. In contrast, the ratio of single-person households, access to traditional markets, and the status of the capital region were significant. The risk of social isolation increased with a higher proportion of single-person households. In line with the fact that family and friends are the most important primary groups in any society and are expected to fulfill people's social needs and sense of belonging [1], single-person households are distant from their most important social networks, thus increasing the risk of social isolation. Therefore, creating a network of interactive ties among single-person households is important. This requires organizing the social infrastructure of cities to increase opportunities for natural contact and provide spaces for dialogue at the urban level.

Short travel times to traditional markets were associated with greater social isolation. The formation of traditional markets has generally involved a long historical process, making them more likely to be in older, less-developed areas. Newly formed areas do not have a traditional market, and large-scale commercial facilities are built, distancing people from existing traditional markets. Older neighborhoods are more likely to be inhabited by socially vulnerable groups, such as older adults living alone, at greater risk of social isolation. This leads to a higher risk of social isolation when there is good access to traditional markets, as demonstrated in this study. In this regard, the role of traditional markets as a key part of the social infrastructure can be reconfigured to maximize their effectiveness. Rather than creating communities by building new facilities in deteriorating areas, using existing markets can help reduce social isolation by revitalizing small communities and promoting social interaction.

In terms of the capital region, the results showed that their residents were more prone to social isolation than residents of the non-capital region. This outcome can be attributed to overcrowding, increased competition, and declining quality of life due to increased commuting distances. Overcrowding caused by increased migration from the non-capital region to the capital region has increased competition in all aspects of life, including education, employment, and income. Those who fall behind are pushed to the outskirts of the capital region and face longer commutes, which reduces the time they must engage in social interaction. This problem is also linked to a decline in quality of life, contributing to the overall issue of social isolation. To solve this fundamental problem, it is necessary to realize balanced regional development in the non-capital regions so that the populations of the capital region can be dispersed to the non-capital regions. When the population is dispersed, and competition is reduced, people have more physical and mental space, which can help alleviate social isolation by increasing social interaction.

Finally, although we thought having many multifamily housing units would bring more people together and allow for social interaction, this was not the case. This was also observed by Kang et al. [36], who indicated that apartments—the main type of housing in South Korea—are isolated from the rest of the external environment, strengthening the internal community but isolating individuals from the outside world. Kang et al. [36] also revealed that social capital (such as cooperation with one's neighbors) decreases when apartment complexes increase in scale. As a result, people living in apartments are isolated from the surrounding community by not using the external social infrastructure, and their relationships with their neighbors deteriorate as the size of the complex increases, leading to social isolation. Urban planning policies should ensure the openness of apartments to solve these problems. First, it is necessary to widen public pathways to provide spaces for apartment residents and outsiders to have natural contact. Second, they must ensure they do not duplicate the surrounding infrastructure when installing community facilities inside apartments. This would allow apartment residents to actively engage in community activities with the outside world, reducing social isolation risk.

Owing to the social survey used in this study, the questions differed by the local government of the metropolitan city; we did not select the metropolitan cities of Ulsan, Daejeon, or Gwangju. Another limitation is that more control variables could not be used for the target sample. As social isolation has been linked to physical and mental health conditions [11], it is necessary to control for these variables; however, we could not do so because the social survey in all target cities did not include this question. In addition, although we used the municipality as the regional level of analysis, a smaller level may have been more appropriate because people tend to use nearby facilities. Nevertheless, owing to the data collection limitations, we could not conduct neighborhood-level analysis, and it is necessary to explore ways to solve this problem in future research.

6. Conclusions

To examine the impact of social infrastructure on the social isolation of urban residents, we used a multilevel logistic model with individual characteristics as the first level and the region they live in as the second level. The results showed that being male, older, unmarried, and having a lower income increased the risk of social isolation. As for regional characteristics, the impact of social infrastructure was greater in areas with more single-person households and better access to traditional markets. In contrast, the presence of parks, cultural/sports facilities, social welfare facilities, and multifamily housing was not significantly associated with social isolation.

Our findings have several implications for future research. First, previous studies have mostly considered social isolation and individual or regional characteristics separately based on multinomial models; however, this study is significant in that it reflects the complex interactions of diverse factors affecting social isolation by simultaneously considering each sample and the region where the respondents lived. Moreover, this study suggests ways to improve the social infrastructure in South Korea. Parks, cultural/sports facilities,

welfare facilities, and places of worship are typical elements of social infrastructure that should promote cohesive local communities and reduce social isolation; however, we did not find the presence of these facilities significant. These results confirm the inadequacy of the current configuration of facilities and indicate the need to plan and establish future social infrastructure to increase social interaction among local communities.

Finally, we propose urban planning implications for mitigating social isolation in cities. For urban planning to help alleviate the social isolation of citizens in cities, it is necessary to change the focus of social infrastructure provision in cities. This means shifting the focus from quantitative expansion to considering the networked nature of social infrastructure. The networked nature of social infrastructure requires increasing access to facilities and ensuring that the programs and content of the facilities are designed to increase interaction between people. Such a city's social infrastructure can function as a universal facility for all citizens and improve the health of its inhabitants.

Author Contributions: Conceptualization, Y.-K.K. and D.K.; methodology, Y.-K.K.; formal analysis, Y.-K.K.; writing—original draft preparation, Y.-K.K. and D.K.; writing—review and editing, Y.-K.K. and D.K.; supervision, D.K.; funding acquisition, D.K. All authors have read and agreed to the published version of the manuscript.

Data Availability Statement: All data were provided by Statistics Korea.

References

1. Chatters, L.M.; Taylor, H.O.; Nicklett, E.J.; Taylor, R.J. Correlates of objective social isolation from family and friends among older adults. *Healthcare* **2018**, *6*, 24. [CrossRef] [PubMed]
2. Carstensen, T.A.; Skytt-Larsen, C.B.; Busck, A.G.; Søraa, N.G. Constructing common meeting places: A strategy for mitigating the social isolation of disadvantaged neighbourhoods? *Urban. Plan.* **2022**, *7*, 486–498. [CrossRef]
3. Zavaleta, D.; Samuel, K.; Mills, C.T. Measures of social isolation. *Soc. Indic. Res.* **2017**, *131*, 367–391. [CrossRef]
4. Mouratidis, K. Urban planning and quality of life: A review of pathways linking the built environment to subjective well-being. *Cities* **2021**, *115*, 103229. [CrossRef]
5. Stender, M.; Nordberg, L.W. Learning from Covid-19: Social infrastructure in disadvantaged housing areas in Denmark. *Urban. Plan.* **2022**, *7*, 432–444. [CrossRef]
6. Latham, A.; Layton, J. Social infrastructure and the public life of cities: Studying urban sociality and public space. *Geogr. Comp.* **2019**, *13*, e12444. [CrossRef]
7. Klinenberg, E. *Palaces for the People: How Social Infrastructure Can Help Fight Inequality, Polarization, and the Decline of Civic Life*; Crown: New York, NY, USA, 2018.
8. Grenade, L.; Boldy, D. Social isolation and loneliness among older people: Issues and future challenges in community and residential settings. *Aust. Health Rev.* **2008**, *32*, 468–478. [CrossRef]
9. Eckhard, J. Indicators of social isolation: A comparison based on survey data from Germany. *Soc. Indic. Res.* **2018**, *139*, 963–988. [CrossRef]
10. Bäckman, O.; Nilsson, A. Pathways to social exclusion—A life-course study. *Eur. Sociol. Rev.* **2011**, *27*, 107–123. [CrossRef]
11. Gyasi, R.M.; Adu-Gyamfi, S.; Obeng, B.; Asamoah, E.; Kisiangani, I.; Ochieng, V.; Appiah, K. Association between physical activity participation and perceived social isolation at older ages: Do social participation, age and sex differences matter? *Arch. Gerontol. Geriat.* **2021**, *96*, 104441. [CrossRef]
12. Abbott, K.M.; Bettger, J.P.; Hampton, K.N.; Kohler, H.P. The feasibility of measuring social networks among older adults in assisted living and dementia special care units. *Dementia* **2015**, *14*, 199–219. [CrossRef] [PubMed]
13. Child, S.T.; Lawton, L. Loneliness and social isolation among young and late middle-age adults: Associations with personal networks and social participation. *Aging Ment. Health* **2019**, *23*, 196–204. [CrossRef] [PubMed]
14. Warner, E.; Andrews, F.J. "Surface acquaintances": Parents' experiences of social connectedness and social capital in Australian high-rise developments. *Health Place* **2019**, *58*, 102165. [CrossRef]
15. Chile, L.M.; Black, X.M.; Neill, C. Experience and expression of social isolation by inner-city high-rise residents. *Hous. Care Support* **2014**, *17*, 151–166. [CrossRef]
16. Popova, Y. Relations between wellbeing and transport infrastructure of the country. *Procedia Eng.* **2017**, *178*, 579–588. [CrossRef]
17. Grum, B.; Kobal Grum, D. Concepts of social sustainability based on social infrastructure and quality of life. *Facilities* **2020**, *38*, 783–800. [CrossRef]

18. Vaznoniene, G.; Kiaušiene, I. Social infrastructure services for promoting local community wellbeing in Lithuania. *Eur. Countrys.* **2018**, *10*, 340–354. [CrossRef]
19. Smith, M.L.; Steinman, L.E.; Casey, E.A. Combatting social isolation among older adults in a time of physical distancing: The COVID-19 social connectivity paradox. *Front. Public Health* **2020**, *8*, 403. [CrossRef]
20. Ward Thompson, C.; Aspinall, P.; Roe, J.; Robertson, L.; Miller, D. Mitigating stress and supporting health in deprived urban communities: The importance of green space and the social environment. *Int. J. Environ. Res. Public Health* **2016**, *13*, 440. [CrossRef] [PubMed]
21. Johansson-Pajala, R.M.; Gusdal, A.; Eklund, C.; Florin, U.; Wågert, P.V.H. A codesigned web platform for reducing social isolation and loneliness in older people: A feasibility study. *Inform. Health Soc. Care* **2023**, *48*, 109–124. [CrossRef]
22. Jiménez, F.N.; Brazier, J.F.; Davoodi, N.M.; Florence, L.C.; Thomas, K.S.; Gadbois, E.A. A technology training program to alleviate social isolation and loneliness among homebound older adults: A community case study. *Front. Public Health* **2021**, *9*, 750609. [CrossRef] [PubMed]
23. Kim, Y.; Oh, J.; Kim, S. The transition from traditional infrastructure to living SOC and its effectiveness for community sustainability: The case of South Korea. *Sustainability* **2020**, *12*, 10227. [CrossRef]
24. Park, C.H.; Koo, J.H. An analysis of the influential relationship between cultural promotion activities and social capital in the traditional market: A comparative view with routine merchant activities. *J. Asian Archit. Build. Eng.* **2014**, *13*, 71–78. [CrossRef]
25. Micro Data Integrated Service-Social Survey (Busan, Daegu, and Incheon). Available online: https://mdis.kostat.go.kr/index.do (accessed on 1 July 2024).
26. The Seoul Research Data Service-Seoul Survey. Available online: https://data.si.re.kr/node/65072 (accessed on 1 July 2024).
27. Korean Statistical Information Service-Population Census. Available online: https://kosis.kr/statisticsList/statisticsListIndex.do?vwcd=MT_ZTITLE&menuId=M_01_01&outLink=Y&entrType=#content-group (accessed on 1 July 2024).
28. Korean Statistical Information Service-Urban Planning Statistics. Available online: https://kosis.kr/statisticsList/statisticsListIndex.do?vwcd=MT_ZTITLE&menuId=M_01_01&outLink=Y&entrType=#content-group (accessed on 1 July 2024).
29. Korean Statistical Information Service-Transportation Accessibility Index. Available online: https://kosis.kr/statisticsList/statisticsListIndex.do?vwcd=MT_ZTITLE&menuId=M_01_01&outLink=Y&entrType=#content-group (accessed on 1 July 2024).
30. Korean Statistical Information Service-Building Energy Usage. Available online: https://kosis.kr/statisticsList/statisticsListIndex.do?vwcd=MT_ZTITLE&menuId=M_01_01&outLink=Y&entrType=#content-group (accessed on 1 July 2024).
31. Korean Statistical Information Service-Housing Census. Available online: https://kosis.kr/statisticsList/statisticsListIndex.do?vwcd=MT_ZTITLE&menuId=M_01_01&outLink=Y&entrType=#content-group (accessed on 1 July 2024).
32. Merlo, J.; Chaix, B.; Ohlsson, H.; Beckman, A.; Johnell, K.; Hjerpe, P.; Råstam, L.; Larsen, K. A brief conceptual tutorial of multilevel analysis in social epidemiology: Using measures of clustering in multilevel logistic regression to investigate contextual phenomena. *J. Epidemiol. Community Health* **2006**, *60*, 290–297. [CrossRef] [PubMed]
33. Klinenberg, E. Social isolation, loneliness, and living alone: Identifying the risks for public health. *Am. J. Public Health* **2016**, *106*, 786–787. [CrossRef]
34. Kono, A.; Tadaka, E.; Kanaya, Y.; Dai, Y.; Itoi, W.; Imamatsu, Y. Development of a community commitment scale with cross-sectional survey validation for preventing social isolation in older Japanese people. *BMC Public Health* **2012**, *12*, 903. [CrossRef]
35. Sarkisian, N.; Gerstel, N. Does singlehood isolate or integrate? Examining the link between marital status and ties to kin, friends, and neighbors. *J. Soc. Pers. Relat.* **2016**, *33*, 361–384. [CrossRef]
36. Kang, S.; Lee, Y.; Koo, J.H. Spatially neighborhood and socially non neighborhood: Illustrating social capital perception of neighbors around the apartment complex. *J. Asian Archit. Build. Eng.* **2022**, *22*, 1284–1299. [CrossRef]

Article

Residential Satisfaction of Subsidized Housing Estates in Post-Reform China: Roles of the Built and Social Environments

Qijing Tang, Zongcai Wei * and Shaoqi Huang

School of Architecture, State Key Laboratory of Subtropical Building and Urban Science, South China University of Technology, Guangzhou 510641, China; 202220104804@mail.scut.edu.cn (Q.T.); 202121007061@mail.scut.edu.cn (S.H.)

* Correspondence: weizongcai@scut.edu.cn; Tel.: +86-15820228781

Abstract: Residential satisfaction has been heavily discussed worldwide amid the increasing emphasis on the social dimension of sustainability. However, consensus has not been reached regarding its determinants, and little research has focused on the subsidized housing estates (SHEs) in post-reform China. Using data collected from field observations in Guangzhou, this study developed a conceptual framework on the basis of the ACSI and Campbell's models and employed structural equation modeling to investigate what and how factors pertaining to both the built and social environments influenced residential satisfaction of SHEs. Generally, SHE residents were moderately satisfied with their housing estates, although challenges persisted in estate management and security, suggesting that the performance of China's subsidized housing policies were acceptable. Echoing existing arguments, this empirical investigation revealed the substantial positive roles played by both the built and social environments in shaping residential satisfaction. Specifically, the livable built environment characterized by large housing size and well-equipped neighborhoods, coupled with the friendly social environment marked by intimate neighborly relationships and diverse community activities, correlated with an elevated level of residential satisfaction of SHEs. Importantly, residents' subjective perceptions of the built environment emerged as the most influential factor, which acted a significant mediating role, linking both objective attributes and individual expectations to residential satisfaction. This underscored the necessity of integrating public opinions into the planning process to meet SHE residents' actual desires. These findings not only extended the scholarly discourse on residential satisfaction, especially among disadvantaged groups in low-income housing estates, but also advanced urban sustainable development by providing references for enhancing SHE performance.

Keywords: residential satisfaction; subsidized housing estate; built environment; social environment; post-reform China

1. Introduction

The increasingly prevalent emphasis on the social dimension of sustainability has sparked heated discussions about residential satisfaction worldwide. The concept of 'residential satisfaction' encompasses a broad scope and has been employed across various multidisciplinary and interdisciplinary contexts, including sociology, psychology, architecture, and urban planning [1–3]. Generally, residential satisfaction, conceptualized as a synthesis of residents' evaluations of housing and community livability, as well as the subjective feelings toward their living environment [4,5], is commonly regarded as a significant component of individuals' quality of life [6–9]. As a relatively abstract concept, residential satisfaction not only depends on objective attributes, such as housing conditions and public facilities within the neighborhood, but also reflects the expectations and needs of residents, influenced by individual factors, such as income and age [10–12]. Despite planners' efforts to propose a set of livability/sustainability principles, it is widely acknowledged that the

lack of consideration for inputs emanating from the end-users contributes to the failure of many public and private housing projects [13–15]. Therefore, it is of considerable significance to conduct empirical research into the factors influencing residential satisfaction at the individual level, to enhance residents' well-being and further advance sustainable development [16].

In comparison to Western countries, post-reform China faces distinct housing challenges, posing an inevitable hurdle in its pursuit of socially sustainable development. With the backdrop of market reform and housing commodification since the 1980s, China's residential landscape has transitioned from a dualistic one of traditional and work-unit neighborhoods, to a heterogeneous one, featuring emerging types, such as urban villages and gated communities [17]. There has been a stratified and differentiated pattern of housing opportunities for residents in post-reform China as a result of the combined influence of both incomplete housing market structures and institutional factors, such as planning and policies [18]. Consequently, housing problems for low-income households, characterized as inadequacies and lack of public facilities, have become increasingly pronounced [19]. In response to this potential social instability, subsidized housing, provided and operated by local authorities, has emerged as a new housing type in post-reform urban China, and as a consequence, ambitious construction plans have been released [20]. Since the large-scale implementation of subsidized housing campaigns in 2008, the central government and local authorities have built over 80 million sets of government-subsidized and renovation housing in China, improving the living conditions of more than 200 million people with difficulties [21]. Then, whether the housing conditions of those vulnerable groups have been greatly improved, are they satisfied with their current subsidized housing estates (SHEs)? It is necessary to assess the residential satisfaction of SHEs from the perspective of actual beneficiaries to evaluate the performance of post-reform China's SHE construction plans, and to promote sustainable development.

Residential satisfaction has long been discussed in the field of housing and urban studies. Extant studies have explored the level of residential satisfaction and its influencing factors in various countries and regions, which provided us with valuable insights into this subject. First, residential satisfaction is evaluated by individuals' comparisons between their actual and desired living conditions and is widely acknowledged as a significant predictor of their overall quality of life [10]. Second, both the built environment (i.e., housing characteristics, the accessibility to public facilities and services, and the provision of public spaces) and the social environment (i.e., community activities, social relations, and social spirit) are proven to be instrumental in influencing residential satisfaction [1,22,23]. Third, it is evident that residential satisfaction is a highly contextual construct, varying across different urban settings [13,24].

In spite of these viewpoints provided by the extant studies, consensus has not yet been reached regarding its influencing factors and the underlying mechanism, especially in post-reform China, where SHE policy focuses on solving housing shortages, rather the quality aspects. First, despite recognizing the variation in residents' satisfaction across groups and housing types [25], and although increasing studies have explored factors influencing residential satisfaction globally, there has been a relatively limited number of studies shedding light on specific housing types, such as SHEs for low- and lower–middle-income groups, in post-reform China, a context characterized by a rapidly evolving planning system. Over the past 15 years, there has been a rapid expansion of SHE projects in China [26], attracting growing scholarly interest in the evolution [27] and implementation [15] of the nationwide policy for constructing large-scale SHEs. However, research on residential satisfaction of China's SHEs, which represents the quality aspects and performance from the perspective of actual beneficiaries, appears to be less reported in the existing literature, with only a few exceptions, such as focusing on tenants in public rental housing [28]. Considering the gradually improved planning system in post-reform China [15], more research is required to grasp the determinants in improving the quality aspects of housing estates and to provide planning implications. Second, previous studies mostly relied on questionnaires

to obtain residents' subjective perceptions of the residential environment [29], often neglecting the integration of both objective attributes and subjective perceptions of the built environment [30]. In particular, most models used in extant studies failed to distinguish the built and social environment factors when exploring the influencing factors of residential satisfaction [31], thus leaving the underlying mechanisms between the two aspects and residential satisfaction unclear. Additionally, commonly used methods, such as the linear regression and ordered logit model used in previous studies to identify factors associated with residential satisfaction [32], are insufficient to fully capture the multidimensional nature of residential satisfaction, as discussed in [33]. Therefore, there is a pressing need to develop an analytical framework to identify the relationship between both the built and social environments and residential satisfaction of China's SHEs.

To bridge the aforementioned gaps in the literature, this study attempts to refine the prevailing models to identify the determinants of residential satisfaction of China's SHEs. Using data collected from field observations across 11 SHEs in Guangzhou in 2018, this study focuses on the following three questions:

Q1: To what extent do residents living in SHEs have residential satisfaction?

Q2: Which elements related to the built and social environments, including both objective and subjective factors, are instrumental to residential satisfaction of SHEs?

Q3: How can urban planners and housing authorities help to improve residential satisfaction of SHEs?

The study develops a conceptual framework on the basis of current prevailing models and conducts multidimensional analysis by using the method of structural equation modeling (SEM). The hypotheses put forward and tested in this study are that (1) both the built and social environment factors have significant influence on residential satisfaction, and (2) residents' subjective perceptions of the built environment act as mediators among objective attributes, expectations, and residential satisfaction. It is hoped that this study will not only enrich the literature by gaining a fuller understanding of residential satisfaction, but also contribute to the implications for public housing in post-reform China, where ambitious SHE construction plans are being carried out, and further facilitate socially sustainable development.

The reminder of this paper is organized as follows. Section 2 describes the materials and methods of this study, including the analysis framework, case selection, data collection, and analytical methods. Section 3 presents the results of the descriptive analysis and SEM analysis. Section 4 provides scholarly discussions and policy implications. Finally, Section 5 offers a summary of the key findings and concluding remarks of this study.

2. Literature Review

A wealth of research on residential satisfaction exists in the field of housing and urban studies, with the appearance of several notable theories and multiple empirical studies. Despite varying and diverse understandings of residential satisfaction [34], it commonly refers to individuals' perceptions, feelings, and consciousness regarding their place of residence [35], evaluating whether their needs, expectations, and desires are being met by housing and the surrounding environment [9,22,36]. Owing to its broad nature, the concept of residential satisfaction has given rise to several theories, with the three most prevalent ones being the "housing needs theory" [37], the "housing deficit theory" [38], and the "psychological construct theory" [34], respectively. Subsequently, a great deal of studies about residential satisfaction have been conducted, which can be classified into four categories: residential satisfaction of specific demographic groups, such as black adults [39], migrants [11,40], and the elderly [41,42], residential satisfaction of individuals at specific stages of life, such as housewives [1] and individuals at different stages of the life cycle [43], residential satisfaction concerning specific housing preferences [44], and residential satisfaction regarding a particular building performance or specific neighborhood, such as council housing [45], redeveloped neighborhoods [12,46], and affordable housing [2,47,48].

The literature is replete with explorations of influencing factors of residential satisfaction. It is generally believed that residential satisfaction is highly related to both the physical and social aspects of the residential environment [1,22,23]. First, the physical aspect of the residential environment, encompassing the built environment at the housing and community levels, has been verified to be an important factor influencing residential satisfaction. For one thing, housing characteristics, such as housing size, building orientation, lighting, and ventilation, are verified to significantly correlate with residential satisfaction [49–51]. Specifically, more pleasant designs, such as larger housing sizes and better housing forms, are usually associated with an increased level of residential satisfaction [52]. Particularly, investigations of public housing inhabitants in both Wuhan, China, and Kuala Lumpur, Malaysia, found that there was a significant and positive correlation between housing unit size and residential satisfaction [47,53]. Community characteristics regarding the public facilities and services are also dominant determinants of residential satisfaction. It has been observed by many scholars that a better-equipped and more convenient neighborhood, which is characterized by higher accessibility of necessary public facilities and services, such as healthcare and commercial facilities, transportation, and public spaces, is conducive to create a desirable and preferable residential environment, and further improve residents' satisfaction [54–56]. Notably, a study conducted in a highly dense resettlement neighborhood in Suzhou, China, concluded that it was not the residential unit (housing characteristics) but the urban environment (public facilities) that mostly impacted residential satisfaction [57].

Second, the social aspect of the residential environment has also been widely considered to play a significant role in influencing residential satisfaction. To be specific, social relations among neighbors and community spirit are important predictors of residential satisfaction [58,59]. For instance, assessment of residential satisfaction of public housing in Ogun State, Nigeria, revealed that increased residential satisfaction was attributed to strong social cohesion and active participation in the development of residences [24]. Similarly, scholars have stressed the importance of creating intangible community settings to enhance the social network among neighbors for socially sustainable community regeneration [51]. To sum up, the social environment pertaining to community activities, interactions among residents, and neighborly relationships effectively contributes to promoting a sense of belonging and community integration, and further increasing residents' satisfaction with living in the community [3,24,60,61].

In light of the extant literature, residential satisfaction is a multidimensional synthesis of residents' intricate cognitive construct to their living environment [1,5,62], and various models have been developed to explore its influencing factors and to further identify the inherent mechanism. One of the most prevailing models was established by Campbell [36], and it was refined and applied in several subsequent empirical studies [30,55,63,64]. This model highlighted the strong association between residential satisfaction and both objective attributes and subjective perceptions of the residential environment. Objective attributes of the environment are filtered through perceptions and evaluations to affect satisfaction [64]. Notably, subjective perceptions, such as the perceived convenience of the housing estates, are usually regarded as stronger predictors of residential satisfaction than objective ones [32,59]. Another prevalent model is adapted from the American Consumer Satisfaction Index (ACSI). In the proposed ACSI model [65], overall customer satisfaction has two antecedent constructs, including customer expectations and perceived quality. Specifically, the expectations, which represent both the prior consumption experience and the forecast of the supplier's ability to deliver quality in the future, are largely rational [66], and they naturally exert a direct and positive association with a cumulative evaluation of the satisfaction [67]. Despite the wide application of the ACSI model in the field of residential satisfaction, the extant studies primarily focused on the community service [67,68] and public participation [69].

In summary, the existing literature has provided rich insights, but a fuller picture of residential satisfaction and its influencing mechanism of SHEs remains to be revealed. It can

be concluded from the foregoing review that residential satisfaction varies across regions and demographic groups, yet there has been relatively little focus on the socially vulnerable, low-income residents in post-reform China. Also, factors related to the built and social environments of the housing estates are recognized as determinants of residential satisfaction. Many researchers have developed models to identify these correlations, but the intricate interplay between objective attributes and subjective perceptions of the built environment, as well as the combined effect of the built and social environments on residential satisfaction, has not been thoroughly explored. To fill in these research gaps, this study assesses residential satisfaction and explores the influencing factors of SHEs in Guangzhou, China.

3. Materials and Methods

3.1. Conceptual Framework

In light of extant studies, residential satisfaction refers to the perception of feelings and consciousness of one's place of residence [35], assessing both the physical and social aspects of the residential environment [1,23,70]. From this integrating perspective, this study proposed a conceptual framework.

First, based on the psychological construct theory, this study combined the ACSI model and Campbell's model to examine the impacts of the built environment on residential satisfaction of SHEs. Theoretically, residents perceive the attributes of the residential environment, and compare these characteristics with certain standards generated from individual past experiences, needs, and expectations. Therefore, residential satisfaction considerably depends on the results of the comparisons between residents' current residential conditions and the reference standard. As a result, a higher level of residential satisfaction is closely correlated with a greater degree of congruence between current and expected conditions [34,54]. In general, from the perspective of the built environment, residential satisfaction is related to three sets of factors, namely, objective attributes, subjective perceptions of the residents, as well as their expectations and aspirations [31].

On the one hand, from the lens of the ACSI model (Figure 1), scholars have confirmed that residents' perceptions of the residential environment was the extent to which the housing estates met their expectations and would further exert impacts on the level of satisfaction [14]. Theoretically, customer satisfaction stems from the relationship between the supply and demand of the product, which exists in many fields, e.g., between the government and the public, or between the market and the public [71]. Inspired by the ACSI model, residential satisfaction of SHEs, considered as a criterion for assessing the performance of SHEs constructed by the government, is the product of the comparison between the perceived characteristics of the residential environment and the residents' expectations. On the other hand, as one of the most prevailing frameworks, Campbell's model (Figure 2) is capable of exploring the impacts and in-depth mechanisms of both objective attributes and subjective perceptions of the built environment on residential satisfaction. According to this model, residential satisfaction results from a process from objective stimuli to cognitive responses.

Second, considering the impacts of the social aspects of the residential environment, a structure of "community activity participation–cognition of neighborly relationship–evaluation of residential satisfaction" was formulated. Inspired by established research, this study argues that the social environment of the estates is the result of community participation and social activities, as well as an incubator for neighborly relationships [72], both of which exert a beneficial effect on residential satisfaction. Additionally, the neighborly relationship is also influenced by residents' participation in community activities, where the more active they are in community activities, the more positive the cognitive response to the neighborly relationship [73].

To summarize, based on the psychological construct theory and existing studies, we developed a conceptual framework integrating both the physical and social aspects of the residential environment, as shown in Figure 3. In this study, we focused on the role of both the built and social environment factors that influence residents' satisfaction

with the housing estates. It was hypothesized that the objective attributes, residents' subjective perceptions, and their expectations of various aspects of the built environment are three key determinants, and the social factors also have a significant influence on residential satisfaction of SHEs. According to the conceptual framework, objective attributes of the built environment and residents' participation in community activities are two exogenous variables, whereas residents' expectations for the built environment, their subjective perceptions of both the built environment and neighborly relationships, as well as residential satisfaction are endogenous variables. The specific hypotheses are proposed in the following.
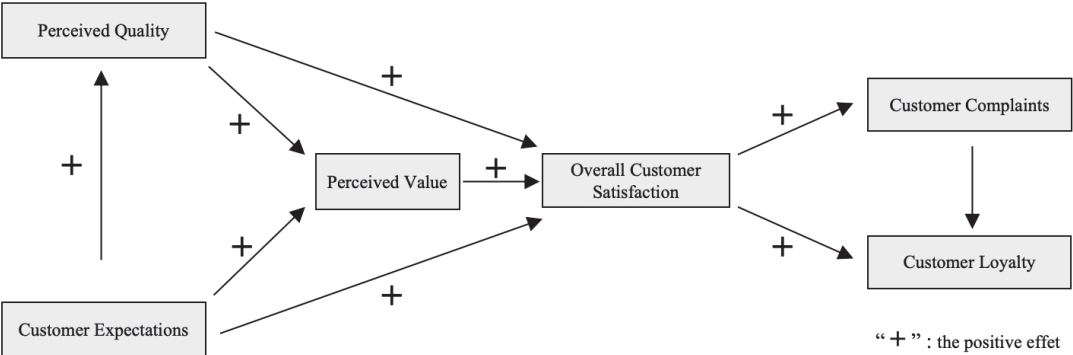
Figure 1. The American Customer Satisfaction Index (ACSI) model [65].
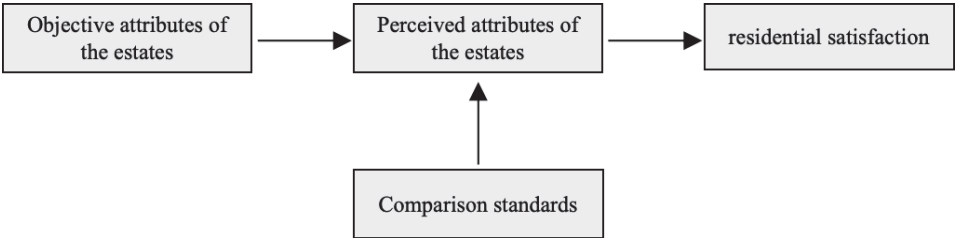
Figure 2. Campbell's model [36].
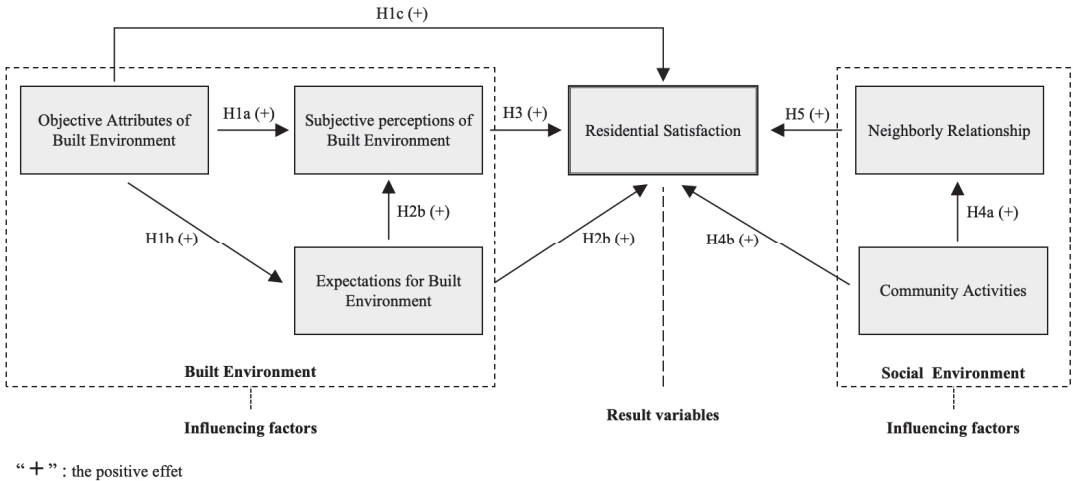
Figure 3. The conceptual framework for residential satisfaction of SHEs in this study.

H1. *Objective attributes of the built environment have a positive impact on residents' subjective perceptions (H1a), expectations (H1b), and residential satisfaction (H1c) of SHEs.*

H2. *Residents' expectations for the built environment have a positive impact on their perceptions (H2a) and residential satisfaction (H2b) of SHEs.*

H3. *Residents' subjective perceptions of the built environment have a positive impact on residential satisfaction directly, since quality perceptions act as agents between both expectations and satisfaction, and objective attributes and satisfaction.*

H4. *Residents' participation in community activities has a positive impact on their cognition of neighborly relationships (H4a) and residential satisfaction (H4b).*

H5. *Residents' cognition of neighborly relationships has a positive impact on residential satisfaction.*

In order to assess these variables, we specified the observed indicators that are associated with each variable based on the literature. The observed variables and their sources are presented in Table 1, and detailed descriptions are provided in Table A1.

Table 1. Variables used in the analysis and their sources.

Latent Variables	Observed Variables	Sources
Residential Satisfaction	Overall residential satisfaction (RS1)	Tao et al., 2014 [74]
	Estate management (RS2)	Ibem et al., 2013 [9] Tao et al., 2014 [74]
	Safety condition (RS3)	Tao et al., 2014 [74] Gou et al., 2018 [75]
	Aspiration to stay in SHEs for the long term (RS4)	Kwon et al., 2013 [76] Li et al., 2019 [53] Du et al., 2020 [72]
Objective Attributes of the Built Environment	Housing size (OBE1)	Li et al., 2019 [53]
	Accessibility to public transportation (OBE2)	Cao et al., 2015 [55]
	Accessibility to public facilities/services (OBE3)	Cao et al., 2015 [55]
	Accessibility to public spaces (OBE4)	Cao et al., 2015 [55]
Subjective Perceptions of the Built Environment	Convenience of public transportation (SBE1)	Li et al., 2019 [53]
	Satisfaction with the provision of public facilities/services within the SHEs (SBE2)	Addo, 2016 [77]
	Satisfaction with the provision of public facilities/services outside the SHEs (SBE2)	Gan et al., 2016 [70]
	Satisfaction with the provision of community open space (SBE3)	Chan et al., 2008 [78] Karuppannan et al., 2011 [79]
	Satisfaction with the provision of public space (SBE4)	Chan et al., 2008 [78] Karuppannan et al., 2011 [79]
Expectations for the Built Environment	Expectations of accessibility to places of work (EBE1)	Jiboye, 2012 [14] Jansen, 2014 [80] Tao et al., 2014 [74]
	Expectations of accessibility to large public facilities (EBE2)	Jiboye, 2012 [14] Jansen, 2014 [80]

Latent Variables	Observed Variables	Sources
Participation in Community Activities	Participation in technical training (CA1)	Hur et al., 2008 [64] Kale, 2019 [73] Du et al., 2020 [72]
	Participation in recreational activities (CA2)	Hur et al., 2008 [64] Du et al., 2020 [72]
	Participation in volunteer activities (CA3)	Hur et al., 2008 [64] Du et al., 2020 [72]
	Participation in discussions on community development issues (CA4)	Hur et al., 2008 [64] Du et al., 2020 [72]
Cognition of Neighborly Relationship	Friends made (NR1)	Tao et al., 2014 [74] Liu et al., 2015 [81]
	Casual interactions (NR2)	Liu et al., 2015 [81]
	Social contacts (NR3)	Vemuri et al., 2011 [61]
	Reciprocity (NR4)	Vemuri et al., 2011 [61] Liu et al., 2015 [81]

3.2. Case Selection and Data Collection

Guangzhou is a pioneer city in the construction of SHEs, making it an appropriate case study for an in-depth analysis of SHE residential satisfaction and its influencing factors. The origin of subsidized housing development in Guangzhou could be traced back to the Healthy Housing Scheme introduced in 1986, even earlier than the similar policy, named Comfortable Housing, promulgated by the central government in 1995. During the nearly past four decades, the development of subsidized housing in Guangzhou has undergone three major stages [82]. In the first development stage (1986–1997), the coverage of the subsidized housing policy was limited, principally benefiting households who working in government departments or public institutions, thus neglecting a significant portion of low-income families. The second development stage (1998–2006) marked a period of transition to extend the coverage of subsidized housing from workers in government departments or public institutions to the urban registered families with housing hardships. In the third and current development stage (2007–present), the coverage of SHEs in Guangzhou has broadened to include the low- and lower-middle-income families, signifying the establishment of an ideal subsidized housing system featuring different types of subsidized housing for residents across various income levels. As the vanguard city in SHE construction, Gunagzhou's experience has been considered exemplary and has been emulated by numerous cities in China [20]. Furthermore, the issue of residential satisfaction that arose in Guangzhou's SHEs is similar to those of other post-reform Chinese cities, justifying the appropriateness of conducting an investigation into Guangzhou's SHEs.

To provide a thorough understanding of residential satisfaction of SHEs and to further facilitate the comprehension of social reality, this study chose SHE cases from the aforementioned development stages. Accordingly, at least three SHEs were selected for each development stage. Since more SHEs were built during the third development stage compared to the other two stages, five SHEs were selected from this development stage. Consequently, a total of 11 SHEs were selected for field observations (Figure 4).

Data utilized in this study were collected through a structured questionnaire survey conducted from August to December 2018 in the 11 SHEs in Guangzhou, China. The random sampling method was employed to ensure better representativeness. Owing to the prohibition of door-to-door visits, three methods were used. First, with the help of community resident committees and property management companies, a notice of the date and time, as well as the research objectives was put up at the entrances of every housing block one week before the survey. Second, the questionnaire was undertaken at different

times during weekends (from early morning to noon and from late afternoon to evening) to enable a balanced and diverse group of respondents, considering that most residents work during weekdays. Third, the survey was conducted at the entrances of every housing block inside the housing estates.
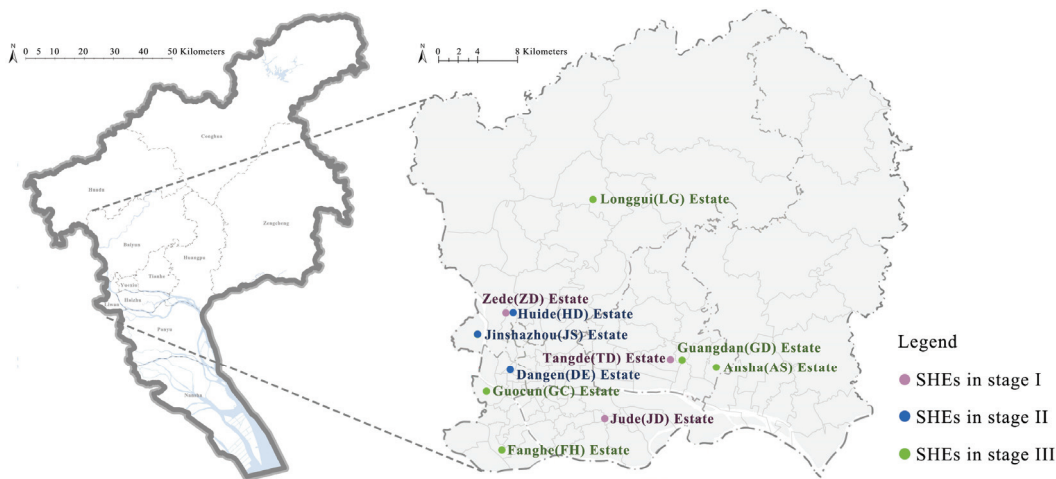
Figure 4. Locations of the 11 selected SHE cases in Guangzhou.

Ultimately, this study collected 1078 questionnaires, 907 of which were valid for further statistical analyses. The socioeconomic characteristics of the respondents in the 11 SHE cases are presented in Table 2. A few more male than female residents were surveyed, which generally mirrored the population structure pattern of Guangzhou (male 52.83%, female 47.17%) [83]. The age structure of the respondents differed from the actual population in China, since only the adults (age above 18 years) were counted in this survey. Since the percentage of residents living in Guangzhou with the education level of secondary school or above was 78.76% [83], and the average monthly household expense in Guangzhou was approximately 3500 yuan in 2018 [84], these SHEs were justified to be socially disadvantaged communities, since they had high percentages of both a low education level (secondary school or below, 81.26%) and low monthly household expenses (less than 5000 yuan, 97.13%).

Table 2. Socioeconomic characteristics of the respondents (N = 907).

	Frequency	Percent
Gender		
Male	503	55.46%
Female	404	44.54%
Age		
18–30	52	5.73%
31–40	67	7.39%
41–50	190	20.95%
51–60	390	43.00%
61 years and above	208	22.93%
Education level		
Primary school or below	180	19.85%
Secondary school	557	61.41%
College or above	170	18.74%

Table 2. *Cont.*

	Frequency	**Percent**
Monthly household expense		
2000 or below	488	53.80%
2000–5000	393	43.33%
5000 or above	26	2.87%
Living allowance recipient		
Yes	104	11.47%
No	803	88.53%

3.3. Analytical Methods

We employed SEM as the analytical method because of the multidimensional nature of residential satisfaction and the complexity of its influencing factors. SEM is a combination of both confirmatory factor analysis (CFA) and path analysis. CFA identifies the indicators (observed variables) of each latent variable [85], and path analysis captures and quantifies the regression effects among multiple latent variables [86]. For the detailed introduction and mathematical presentation of the SEM, please refer to Byrne (2010) [87] and Kline (2015) [88]. Traditional multiple regression analysis can only identify a single relationship between the independent and dependent variables, and that the interactions between variables are not sufficiently clear, while SEMs are able to estimate the paths of multiple observed and latent variables at the same time. One distinct advantage of SEMs is that they can capture both direct, indirect, and total effects of the variables. Therefore, the method of SEM was used to explore factors associated with residential satisfaction of SHEs.

4. Results

4.1. Descriptive Analysis

The overall residential satisfaction of SHEs was found to be undesirable but acceptable. The score of the indicator was 3.47 on a five-point Likert scale (Table 3). A notable portion (40.90%) of respondents were neutral in terms of their residential satisfaction, while 49.94% expressed satisfaction (including both satisfied and very satisfied), a significantly higher percentage compared to those who reported dissatisfaction (9.04%; including both very dissatisfied and dissatisfied). The results were generally consistent with those of Tao et al. (2014) concerning Chinese migrant workers [74], but the satisfaction levels in this study were higher, likely attributed to the fact that the overall residential satisfaction levels in Tao's study were derived from the comparison with the satisfaction in respondents' hometowns.

Table 3. Residential satisfaction of SHEs.

Dimensions	**Total**	**Stage I**	**Stage II**	**Stage III**
Safety condition	2.69	2.79	2.92	2.54
Estate management	3.00	2.70	3.03	3.11
Willingness to reside in the long term	3.94	3.54	4.03	4.07
Overall residential satisfaction	3.47	3.38	3.70	3.40

The dimension "Willingness to reside in the long term" stood out positively. Residents were observed to have a strong sense of community due to the significantly higher score of 3.94 of the dimension "Willingness to reside in the long term", compared with the other two dimensions (Table 3). A majority of the respondents expressed strong willingness (27.45%) or willingness (48.63%) to reside in their current housing estate for the long term. Notably, residents living in SHEs of Stage III exhibited the strongest inclination for long-term residency, contrasting with those in stage I, who showed the weakest willingness. The respectively high quality of housing in the newly built SHEs might provide a reasonable explanation (interviews with residents of the LG Estate).

However, challenges persisted in estate management. Residents found difficulty receiving support from residents' organizations and management companies, resulting in their low satisfaction with the estate management, with the score of 3.00. Residents were reluctant to seek assistance and obtained limited support from relevant residents' organizations and management companies. This was mainly because the residents of SHEs had an unfavorable relationship with residents' organizations and management companies in terms of maintaining the built environment, and they had little trust in these organizations (interviews with three residents of JD Estate).

Worse yet, residents expressed a lack of a strong sense of safety. The score of perceived safety in SHEs was only 2.69, which was the lowest among the four indicators regarding residential satisfaction. Residents living in SHEs of Stage III had a weaker sense of safety than those of the early two stages. The underlying reasons for the weak safety conditions within the SHEs might be attributed to ineffectual property management and the complicated socioeconomic composition of SHE residents. First, the property management, especially the security guard, was ineffectual and failed to play a significant role in preventing antisocial behaviors. As residents of FH Estate complained, the frequent safety issues, such as theft, lessened their sense of safety. Second, the SHEs in Guangzhou accommodate many disadvantaged people from the entire city, many of whom came from socially disadvantaged backgrounds. Particularly, those residents with criminal records or serious mental health issues sometimes committed antisocial behaviors that heavily disturbed other residents and weakened the sense of safety, as a director of the residents' committee in JS Estate reported.

4.2. Structural Equation Modeling (SEM) Analysis

4.2.1. Modeling Procedure

First, we conducted the reliability and validity analyses. The overall Cronbach's Alpha coefficient for the entire questionnaire was 0.800, exceeding the recommended threshold of 0.700, thus confirming the reliability of the questionnaire. The Kaiser–Meyer–Olkin test (0.874) and Bartlett's test ($p = 0.000$) suggested that the data are suitable for factor analysis. Then, the confirmatory factor analysis (CFA) was conducted to confirm whether the observed variables reliably measured the latent constructs, as hypothesized [89]. After removing the observed variable with a factor loading below 0.4 [90], the final model exhibited acceptable results. Measurements of latent factors and their unstandardized and standardized factor loading are presented in Table 4. Specifically, the composite reliability (CR) of each latent variable, representing the internal consistency of construct indicators, ranged from 0.690 to 0.867 in the model, all exceeding 0.6 [91], indicating the high internal consistency of the construct indicators. The average variance extracted (AVE), representing the average amount of variance that latent variables explain in their measured variables, ranged from 0.367 to 0.793, all exceeding the threshold value of 0.36 [92], indicating the acceptable convergent validity of the model. Additionally, the *p*-values of the unstandardized parameters of the measurement model were all less than 0.001, which met the significance requirement. To summarize, the model was capable of reflecting the influencing mechanisms of residential satisfaction.

Furthermore, we examined the model's goodness of fit by applying Bollen–Stine bootstrapping (N = 3000) to re-estimate Chi-square, and to mitigate the statistical biases resulting from the non-normality of the data [93]. As recommended by Hu and Bentler (1998) [94], the Chi-square/the degrees of freedom (χ^2/df), probability value of Bollen–Stine, comparative fit index (CFI), goodness-of-fit index (GFI), adjusted goodness-of-fit index (AGFI), and root-mean-square error of approximation (RMSEA) were used to test the model's goodness of fit. Ultimately, all fit indices of the final model were acceptable (Table 5), implying a relatively good fit between the hypothesized model and the observed data and ensuring the subsequent explanation of the model results.

Table 4. Factor structures of identified latent factors and results of CFA.

Items	Unstandardized Parameter Estimates				Standardized Parameter Estimates		CFA	
	Unstd.	S.E.	C.R.	*p*	Std.	SMC	CR	AVE
Residential satisfaction							0.690	0.362
RS1	1.000	-	-	-	0.664	0.441		
RS2	1.377	0.088	15.735	***	0.691	0.477		
RS3	0.991	0.073	13.495	***	0.558	0.311		
RS4	0.85	0.073	11.647	***	0.468	0.219		
Objective Attributes of the Built Environment							0.776	0.478
OBE1	1.000	-	-	-	0.473	0.224		
OBE2	1.005	0.078	12.825	***	0.650	0.423		
OBE3	200.231	14.609	13.706	***	0.927	0.859		
OBE4	406.83	32.011	12.709	***	0.638	0.407		
Subjective Perceptions of the Built Environment							0.828	0.500
SBE1	1.000	-	-	-	0.442	0.195		
SBE2	1.620	0.127	12.749	***	0.787	0.619		
SBE3	1.477	0.116	12.764	***	0.790	0.624		
SBE4	1.319	0.107	12.381	***	0.722	0.521		
SBE5	1.243	0.100	12.454	***	0.734	0.539		
Expectations for the Built Environment							0.867	0.763
EBE1	1.000				0.863	0.745		
EBE2	1.051	0.054	19.643	***	0.884	0.781		
Community Activities							0.729	0.404
CA1	1.000				0.620	0.384		
CA2	1.904	0.145	13.100	***	0.609	0.371		
CA3	1.472	0.105	13.979	***	0.731	0.534		
CA4	0.869	0.069	12.563	***	0.570	0.325		
Neighborly Relationship							0.691	0.367
NR1	1.000				0.548	0.300		
NR2	0.915	0.076	12.091	***	0.791	0.626		
NR3	0.674	0.061	11.084	***	0.523	0.274		
NR4	0.829	0.075	11.035	***	0.519	0.269		

Note: *** $p < 0.001$. Unstd. = unstandardized factor loading; S.E. = standard error; C.R. = critical ratio; Std. = standardized factor loading; SMC = squared multiple correlation; CR = composite reliability; AVE = average variance extracted.

Table 5. Model goodness of fit.

Model Goodness of Fit	χ^2/df	RMSEA	GFI	AGFI	CFI
Corrected value by Bollen–Stine	1.015	0.004	0.972	0.962	0.996
Ideal value [94]	<3.000	<0.080	>0.900	>0.900	>0.950
Fitting evaluation	Ideal	Ideal	Ideal	Ideal	Ideal

The final model is shown in Figure 5, demonstrating the interconnections between the endogenous and exogenous variables, and Table 6 presents the outcomes of the final model for direct, indirect, and total effects.

Table 6. Values of standardized direct, indirect, and total effects of SEM path analysis.

		Objective Attributes of the Built Environment	Subjective Perception of the Built Environment	Expectations for the Built Environment	Community Activities	Neighborly Relationship
Subjective perceptions of the Built Environment	Total	0.314		0.368		
	Direct	0.158		0.368		
	Indirect	0.157				

Table 6. *Cont.*

		Objective Attributes of the Built Environment	Subjective Perception of the Built Environment	Expectations for the Built Environment	Community Activities	Neighborly Relationship
Expectations for the Built Environment	Total	0.426				
	Direct	0.426				
	Indirect					
Neighborly Relationship	Total				0.173	
	Direct				0.173	
	Indirect					
Residential Satisfaction	Total	0.135	0.749	0.373	0.153	0.128
	Direct	−0.142	0.749	0.098	0.131	0.128
	Indirect	0.277		0.275	0.022	

Note: A blank cell means insignificant effects between variables at a 0.05 level.

Figure 5. SEM model results.

4.2.2. The Impact of the Built Environment on Residential Satisfaction

According to the final model (Figure 5), residential satisfaction resulted from a process of objective stimuli, expectation, and subjective perceptions in terms of the built environment. First, consistent with Campbell's model, individuals perceived the objective residential built environment through a subjective judgement process, ultimately leading to the evaluation of residential satisfaction. As expected, the better the objective attributes of the built environment, the higher the subjective perceptions among residents, thereby yielding a higher level of residential satisfaction, which supported Hypothesis 1 and Hypothesis 4. Specifically, the effect of subjective perceptions of the built environment on residential satisfaction was notably significant (0.749), surpassing that of all other latent variables, underscoring its paramount importance. However, the direct effect of objective attributes of the built environment on residential satisfaction was negative, with a value of −0.142, contrary to Hypothesis 3. One of the possible reasons for this directly negative effect might be the actual needs of SHE residents. To be specific, it was observed that most (65.93%) of them were aged over 50. For older residents, the scope of activities tended to be contracted, and their living needs were fewer in comparison. Consequently, an excessively large housing area and an abundance of public facilities might be counterproductive to their living. Another possible explanation might be the common mentality that people tended to enjoy life once conditions were permitted [95]. SHE residents living in poor conditions might have provided low satisfaction scores, but above a certain level of comfort they tended to be satisfied. Therefore, the improvement of the objective attributes of

the built environment did not directly enhance residential satisfaction, but it positively affected residents' subjective cognition and perceptions, thus promoting residential satisfaction. The results coincided with the findings of an empirical study on the influence of the community-built environment on the residential satisfaction of the elderly [96].

Second, in alignment with the "expectation–perception–satisfaction" framework proposed by Fornell et al. (1996) [65], residents' expectations for the built environment exerted positive impacts on both subjective perceptions and residential satisfaction, and subjective perceptions further exhibited a beneficial effect on residential satisfaction, confirming Hypotheses 4, 5, and 6, respectively. For products such as housing, residents' expectations were relatively stable since they were rooted in long-term assessments of the housing market's consistent performance. As the survey showed, SHE residents' expectations for the built environment were moderate and rational, with more than 40% of the respondents holding neutral expectations, and most of them expressed that the built environment had improved considerably compared to where they used to live. As a resident of JS Estate stated: "Some improvements in the provision of public services and facilities have gradually emerged in our housing estates. I am quite satisfied with the current environment." In accordance with the psychological construct theory, it could be inferred that the residential conditions of SHE residents were perceived as superior to the ones they had previously experienced, and closely congruent with the reference conditions; therefore, they tended to express satisfaction, and there was a positive correlation between SHE residents' expectations and satisfaction [97]. Noteworthily, SHEs represent a form of Chinese government intervention in the marketized economy [20], providing basic security for low-income residents. Undoubtedly, this imbues them with a "halo effect", further elucidating the observed significant positive correlation between expectations and satisfaction of SHE residents [65].

Additionally, objective attributes of the built environment were found to have a positive influence on expectations, which confirmed Hypothesis 2. As expected, the better the actual built environment, the higher the expectations the residents had. This was mainly due to a psychological process of cognitive restructuring [80]. SHE residents might lower their expectations ("I don't need much") since they were forced to be satisfied with what they had ("what I have is fine") and to make the best of a situation that they could not change.

4.2.3. The Contribution of the Social Environment to Residential Satisfaction

A favorable social environment, characterized by abundant community activities and close networks among residents, was validated to improve residential satisfaction. First, active participation in community activities was found to increase residential satisfaction, aligning with previous studies [72,98,99]. The model results indicated that the total effect of community activities on residential satisfaction was 0.153, with the direct effect being stronger at 0.131, and the indirect effect of influencing perceptions of neighborly relationships to increase residential satisfaction was relatively weaker but still significant and positive (0.022), thereby confirming Hypotheses 7 and 8. Community activities, such as technical training, recreational activities, volunteer engagements, and discussions on community development issues, could improve residential satisfaction by enhancing "interest connections" and nurturing residents' sense of belongings. As articulated by one resident: "Given that I am retired now, I spend most of my time in the housing estate. We, the retired residents, gather every day to chat, exercises, and play cards or mahjong at the cultural corridor of the center of this community".

Second, the neighborly relationship was found to be significantly and positively associated with residential satisfaction, consistent with the findings of previous studies [2,45,74,100], thereby confirming Hypothesis 9. Stronger neighborly relationships contributed to higher levels of residential satisfaction. To be specific, for each unit increase in neighborly relationship, residential satisfaction increased by 0.128 units accordingly (Table 6). On the one hand, the maintenance of social network, trust, and mutual assistance among neighbors could foster senses of intimacy and safety among residents [61]. On the other hand, casual

interactions, social contacts with neighbors, and mutual assistance could significantly enhance residents' sense of identity and sense of belonging [101], which would in turn improve residential satisfaction [81]. Notably, the path coefficients of the indicator related to residents' willingness to have casual interactions with each other (NR2) was significantly higher than the other three observed variables, indicating its strong correlation with SHE residents' neighborly relationships. This might be attributed to the fact that financial constraints hindered in-depth social contacts and interactions among residents, as noted in interviews with residents of the FH Estate.

5. Discussion

5.1. The Influencing Mechanism of Residential Satisfaction of SHEs

This study explored the impacts of both the built and social environments on residential satisfaction of SHEs. The conceptual framework developed in this study distinguished the factors of the physical and social aspects of the residential environment, and the results indicated that elements related to both the built environment (i.e., housing size, transportation, public facilities, public spaces, and open spaces) and the social environment (i.e., neighborly relationships and community activities) were instrumental to residential satisfaction of SHEs. These findings echoed the suggestion proposed by Canter and Rees (1982) that the separation of the physical and social aspects of the residential environment was of significance in any analysis concerning residential satisfaction [22]. Figure 6 presents what and how factors regarding both the built and social environments influenced residential satisfaction of SHEs.
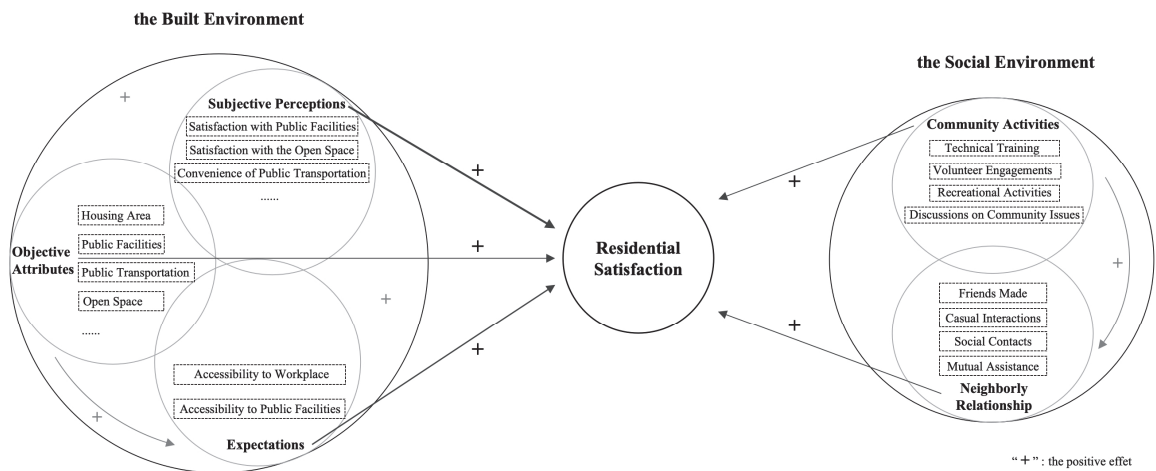

Figure 6. The determinants of residential satisfaction of SHEs.

First, residential satisfaction of SHEs was positively influenced by objective attributes, residents' expectations, and subjective perceptions of the built environment. The findings supported the combination of the two classic frameworks of Campbell's model and the ACSI model. On the one hand, despite a slightly negative direct effect, objective attributes of the built environment positively affected residents' subjective perceptions, which in turn affected residential satisfaction of SHEs. This illustrated the mechanism through which estate design and neighborhood planning influenced residential satisfaction. On the other hand, the results empirically validated the structural framework of "expectation–perception–satisfaction" in the ACSI model in explaining the residential satisfaction of SHEs. A similar conclusion was also proposed by Emami and Sadeghlou in 2021 [71], contending that residential satisfaction was the positive or negative psychological outcome of individuals' subjective evaluative processes between what was expected and what was

perceived. To improve SHE residential satisfaction, it is essential to elevate residents' expectations and perceived quality of the built environment.

Importantly, the findings unveiled the role of residents' subjective perceptions in mediating among the objective attributes, expectations, and residential satisfaction of the built environment. The findings echoed both the psychological construction theory [34] and Jiboye's argument [14], and further reinforced the relevance of the two aforementioned models, suggesting that subjective perceptions were responses to the extent to which the objective attributes of housing estates' built environments met residents' expectations, exerting the greatest impact on their residential satisfaction. Similar effects were also observed in the empirical study of the residential satisfaction of the elderly in Hefei, China [96], which proposed to place increased stress on residents' subjective perceptions of the built environment to meet their actual needs. In essence, a high level of residential satisfaction was not thoroughly contingent upon complete congruence between the actual residential built environment and the theoretically ideal one; rather, it was the subjective perceptions of the built environment that were more decisive. Underlying factors that might influence subjective perceptions included comparison processes [95,102] and psychological processes, such as expectation revision and cognitive adaption [34,80]. For the low-income SHE residents, it was of high possibility that they previously lived in significantly lower-quality built environments, or that their relatives or friends have experienced similar situations (as indicated in interviews with residents in the LG Estate and FH Estate). Therefore, in the process of such comparisons and cognitive restructuring, they subjectively perceived satisfaction with the current residential built environment, and such subjective perceptions profoundly affected their overall residential satisfaction.

Second, an enhanced social environment was closely related to increased residential satisfaction of SHEs. Specifically, a clear mechanism involving "community activity participation–development of neighborly relationship–evaluation of residential satisfaction", regarding the influence of the social environment on residential satisfaction, was identified. There was a two-by-two relationship among these three variables, and all three relationships were positively connected. Supporting the hypotheses, residents who participated more frequently in community activities tended to develop closer relationships with neighbors, and further presented higher levels of residential satisfaction. This result strongly supported the conclusion that the social capital in low-income communities, encompassing social networks that facilitate social cohesion and the development of residents within the neighborhood [103,104], contributed substantively to residential satisfaction [45]. Indeed, there have been a number of empirical studies that confirmed these effects, such as studies of residential satisfaction of low-income communities in Ogun State, Nigeria [24], Beijing, China [81], and Seoul, South Korea [105]. Some scholars have even concluded from surveys of residential satisfaction in public housing in Madrid that the psycho-social aspects, such as neighborly relationships and the sense of attachment, would exert stronger effects on residential satisfaction than physical features of the built environment [1]. Despite that the extent of the impacts might vary across different contexts, factors related to the social environment could indeed influence residential satisfaction. Therefore, it is necessary to enhance the social environment to improve residential satisfaction, especially for low-income neighborhoods in rapidly urbanizing countries such as China.

5.2. Policy Implications for Improving Residential Satisfaction of SHEs

Additional efforts should be made to improve the quality of the built environment to decent standards, which can greatly enhance residential satisfaction. As hypothesized, the built environment exerted a substantial impact on the residential satisfaction of SHEs, with factors such as open space, transportation, and public facilities playing pivotal roles. It is suggested that housing authorities should pay attention to the improvement of greening, open space, and public facilities within and surrounding the estates, beyond the mere provision of accommodation units [106]. Furthermore, the implementation, post-construction maintenance, and management are also critical factors in enhancing the quality

of the built environment. During the investigation of SHEs, deviations from the original planning scheme, the lag period of actual provision of public facilities and services, and unmaintained neighborhood amenities were observed. Therefore, achieving high-quality built environments necessitates improvements across various aspects, from housing to community surroundings, and from design to management throughout the entire process.

More emphasis should be placed on creating a livable and favorable built environment that is sought by the public in the operation of urban planning. Considering the largest positive impact observed from residents' subjective perceptions of the built environment, it is necessary to integrate public opinions into the planning process. This is a feasible measure to ensure that residents' actual needs and expectations are thoroughly investigated and addressed by housing authorities and planners. However, urban planning in China is typically operated as a technical tool to fulfill the political aspirations of local governments under the top-down administration [15], often leading to outcomes contrary to public expectations. To counteract this, it is crucial to establish and enhance an effective mechanism for public participation. This participatory approach is particularly important for residents of SHEs, who represent socially vulnerable groups with low incomes, and a significant portion of whom are elderly individuals. Their real requirements and expectations regarding the built environment must be thoroughly investigated and considered. By integrating their voices into the planning process, residential environment of SHEs can be not only functional but also genuinely livable and favorable, ultimately improving residents' satisfaction.

Attention should also be paid to the improvements of the social environment of SHEs, as this contributes to enriching residents' spiritual life and promoting social cohesion, and thus improving residential satisfaction. The positive impacts of the social environment on residential satisfaction highlight the need to cultivate a sense of intimacy and safety among SHE residents, which in turn bolsters their sense of belonging to the estates. To be specific, during the design phase, it is suggested to create public spaces that facilitate informal interactions and community activities. For instance, cultural corridors and communal gardens with pleasant spatial scales should be created and thoughtfully designed to provide spatial support for social contacts among neighbors. During the governance and management phase, residents' organizations and management companies of SHEs should strengthen their active roles in revitalizing residents' networks. This can be achieved by organizing and encouraging residents to actively participate in various community activities, fostering a stronger sense of community engagement and promoting residential satisfaction.

6. Conclusions

Residential satisfaction represents one important domain of individuals' general quality of life, particularly for low- and lower–middle-income residents residing in SHEs, and it also serves as a vital indicator to assess the performance of SHE projects. Extant studies highlighted that the determinants of residential satisfaction tended to vary by housing types, tenure, countries, and cultures [37]. Since existing empirical studies, which focused on the well-being of low-income residents in affordable housing programs, were mostly conducted in European and American cities, where mature planning systems exist, it is imperative to shed light on post-reform China, which has recently experienced large-scale expansion of SHE projects and where the planning systems are gradually improving [15]. Moreover, the impacts of factors related to the social environment on residential satisfaction of SHEs was not well explored in the existing literature. Therefore, taking advantage of field observations in 11 SHEs in Guangzhou, we developed an analytical framework and employed SEM to capture the effects of both the built and social environments on residential satisfaction of SHEs. This study provided a fuller picture of residential satisfaction and its determinants, especially for understanding residential satisfaction among disadvantaged groups in developing countries, and contributed to the debate over the assessment and improvement of the performance of China's SHE projects.

According to the survey, the overall residential satisfaction of SHEs was found to be undesirable but acceptable, with the dimension of "Willingness to reside in the long term" ranking first. The results suggested that China's recent implementation of subsidized housing policies has yielded some positive outcomes, proving to be an effective measure in addressing the housing needs of low-income groups and tackling the increasingly severe problem of housing unaffordability in post-reform China. However, the limited services provided by management companies and insufficient support from residents' organizations have led to residents' negative remarks on both management and security issues within the SHEs. Additionally, the complicated sociodemographic characteristics of SHE residents have presented challenges in further enhancing residential satisfaction.

This empirical study in Guangzhou echoed those in previous arguments that both the physical and social aspects of the residential environment are closely related to residential satisfaction, and further illustrated the mechanisms under which the built environment affected residential satisfaction. The results of the SEM indicated that both a desirable built environment, such as pleasant housing designs and well-equipped neighborhoods, and a friendly social environment, characterized by intimate neighborly relationships and diverse community activities, could contribute to the improvement of residential satisfaction in SHEs. Furthermore, this study developed Campbell's model and the ACSI model in terms of the influencing mechanisms of the built environment on residential satisfaction. Specifically, objective attributes affected both residents' perceived evaluations and expectations, which in turn affected residential satisfaction. Residents' expectations also positively related to their cognitive evaluation of residential environments. Overall, residents' subjective perceptions served as mediators among the objective attributes and expectations and exerted the greatest impacts on residential satisfaction.

This study implicated that policymakers in China should recognize the multidimensional nature of residential satisfaction of SHEs to meet the actual housing needs of low-income groups and to further facilitate urban sustainable development. In addition to the provision of basic sheltering, policies for SHE projects should strive to improve the quality of the built environment to meet decent standards, such as optimizing the allocation of public service facilities surrounding the housing estates. Further consideration should also be given to SHE residents' pursuit of spiritual life. To foster favorable social environments and promote neighborhood social cohesion, residents' organizations should encourage residents to participate in diverse community activities. Additionally, it is necessary to strengthen the mechanisms for public participation to better grasp residents' actual requirements and expectations, even in completed SHE projects.

However, there are several limitations. First, city-level contextual factors, such as the scale, the location, and the socioeconomic characteristics, may have significant impacts on residential satisfaction of SHEs. Nevertheless, this study only investigated specific SHEs in Guangzhou, a pioneer mega-city in the construction of SHEs, limiting its applicability to other cities. Future studies should also focus on those cities with disadvantaged performance in SHE development. Second, focusing on the built and social environments, the model developed in this study did not cover individual socioeconomic attributes, such as age, level of income, and general outlook on life [64], which would affect residential satisfaction. Additionally, the geographical characteristics of the housing estates (e.g., geographical location) were not fully considered in this study. Presumably, adding such factors into the model would help gain a fuller understanding of residential satisfaction of SHEs. Third, a longitudinal research design and panel data may serve as effective tools to deeply illuminate the influencing mechanisms through investigating how the life course and processes of gentrification or land use change affect individuals' residential satisfaction over time [3]. Despite its limitations, this study still contributes to the literature with insights on the effects of the built and social environments on residential satisfaction of SHEs, which will facilitate socially sustainable development by providing references for enhancing SHE performance.

Appendix A

Table A1. Variables used in the analysis and their descriptions.

Latent Variables	Observed Variables	Description
Residential Satisfaction	Overall residential satisfaction (RS1)	Residents' overall satisfaction with their current residence: very dissatisfied, dissatisfied, neutral, satisfied, very satisfied.
	Estate management (RS2)	Satisfaction with the estate management: very dissatisfied, dissatisfied, neutral, satisfied, very satisfied.
	Safety condition (RS3)	Perceived safety within the SHEs: very unsafe, unsafe, neutral, safe, very safe.
	Aspiration to stay in SHEs for the long term (RS4)	"I would like to continue to live in this housing estate": strongly disagree, disagree, neutral, agree, strongly agree.
Objective Attributes of the Built Environment	Housing size (OBE1)	Housing area per capita (m^2).
	Accessibility to public transportation (OBE2)	Distance to the subway/bus station (m).
	Accessibility to public facilities/services (OBE3)	Distance to the nearest public facilities/services (m).
	Accessibility to public spaces (OBE4)	Distance to the nearest public spaces (m).
Subjective Perceptions of the Built Environment	Convenience of public transportation (SBE1)	Convenience of public transportation: very dissatisfied, dissatisfied, neutral, satisfied, very satisfied.
	Satisfaction with the provision of public facilities/services within the SHEs (SBE2)	Satisfaction with the provision of public facilities/services within the SHEs: very dissatisfied, dissatisfied, neutral, satisfied, very satisfied.
	Satisfaction with the provision of public facilities/services outside the SHEs (SBE2)	Satisfaction with the provision of public facilities/services outside the SHEs: very dissatisfied, dissatisfied, neutral, satisfied, very satisfied.
	Satisfaction with the provision of community open space (SBE3)	Satisfaction with the provision of community open space: very dissatisfied, dissatisfied, neutral, satisfied, very satisfied.
	Satisfaction with the provision of public space (SBE4)	Satisfaction with the provision of public space: very dissatisfied, dissatisfied, neutral, satisfied, very satisfied.

Table A1. *Cont.*

Latent Variables	Observed Variables	Description
Expectations for the Built Environment	Expectations of accessibility to places of work (EBE1)	"I HOPE that the distance from my house to places of work does not differ from that of most people in the city": strongly disagree, disagree, neutral, agree, strongly agree.
	Expectations of accessibility to large public facilities (EBE2)	"I HOPE that the distance from my house to large public facilities does not differ from that of most people in the city": strongly disagree, disagree, neutral, agree, strongly agree.
Participation in Community Activities	Participation in technical training (CA1)	Self-reported involvement in technical training in the last year: none, 1–2, 3–6, 7–12, >12.
	Participation in recreational activities (CA2)	Self-reported involvement in recreational activities in the last year: none, 1–2, 3–6, 7–12, >12.
	Participation in volunteer activities (CA3)	Self-reported involvement in volunteer activities in the last year: none, 1–2, 3–6, 7–12, >12.
	Participation in discussions on community development issues (CA4)	Self-reported involvement in discussions on community development issues in the last year: none, 1–2, 3–6, 7–12, >12.
Cognition of Neighborly Relationship	Friends made (NR1)	Number of friends made in the housing estates: none, 1–4, 5–9, 10–20, more than 20.
	Casual interactions (NR2)	"When I meet neighbors on the street, I say 'hi' or chat with them": strongly disagree, disagree, neutral, agree, strongly agree.
	Social contacts (NR3)	Frequency of social contacts with neighbors: less than once a month, 2–3 times a month, once a week, 2–3 times a week, every day.
	Reciprocity (NR4)	"I help my neighbors or seek help from them, if necessary": strongly disagree, disagree, neutral, agree, strongly agree.

References

1. Amérigo, M.; Aragones, J.I. A theoretical and methodological approach to the study of residential satisfaction. *J. Environ. Psychol.* **1997**, *17*, 47–57. [CrossRef]
2. Riazi, M.; Emami, A. Residential satisfaction in affordable housing: A mixed method study. *Cities* **2018**, *82*, 1–9. [CrossRef]
3. Biswas, B.; Sultana, Z.; Priovashini, C.; Ahsan, M.N.; Mallick, B. The emergence of residential satisfaction studies in social research: A bibliometric analysis. *Habitat Int.* **2021**, *109*, 102336. [CrossRef]
4. Hui, E.C.M.; Yu, K.H. Residential mobility and aging population in Hong Kong. *Habitat Int.* **2009**, *33*, 10–14. [CrossRef]
5. Permentier, M.; Bolt, G.; Van Ham, M. Determinants of neighbourhood satisfaction and perception of neighbourhood reputation. *Urban Stud.* **2011**, *48*, 977–996. [CrossRef]
6. Lee, E.; Park, N.K. Housing Satisfaction and Quality of Life among Temporary Residents in the United States. *Hous. Soc.* **2010**, *37*, 43–67. [CrossRef]
7. Sirgy, M.J.; Cornwell, T. How Neighborhood Features Affect Quality of Life. *Soc. Indic. Res.* **2002**, *59*, 79–114. [CrossRef]
8. Wang, D.; Wang, F. Contributions of the Usage and Affective Experience of the Residential Environment to Residential Satisfaction. *Hous. Stud.* **2016**, *31*, 42–60. [CrossRef]
9. Ibem, E.O.; Amole, D. Residential Satisfaction in Public Core Housing in Abeokuta, Ogun State, Nigeria. *Soc. Indic. Res.* **2012**, *113*, 563–581. [CrossRef]
10. Galster, G.; Hesser, G. Residential satisfaction: Compositional and contextual correlates. *Environ. Behav.* **1981**, *13*, 735–758. [CrossRef]
11. Barcus, H. Urban-rural migration in the USA: An analysis of residential satisfaction. *Reg. Stud.* **2004**, *38*, 643–657. [CrossRef]

12. Jiang, W.; Feng, T.; Timmermans, H.; Li, H. A gap-theoretical path model of residential satisfaction and intention to move house applied to renovated historical blocks in two Chinese cities. *Cities* **2017**, *71*, 19–29. [CrossRef]
13. Ogu, V.I. Urban residential satisfaction and the planning implications in a developing world context: The example of Benin City, Nigeria. *Int. Plan. Stud.* **2002**, *7*, 37–53. [CrossRef]
14. Jiboye, A.D. Post-occupancy evaluation of residential satisfaction in Lagos, Nigeria: Feedback for residential improvement. *Front. Archit. Res.* **2012**, *1*, 236–243. [CrossRef]
15. Wei, Z.; Chen, T. Dilemma of pursuing livability in China's urban planning: The case of Longguicheng housing estate in Guangzhou. *J. Hous. Built Environ.* **2023**, *39*, 557–572. [CrossRef]
16. Wei, Z.; Chen, T. Review on Social Sustainability of Subsidized Housing Estates in China and Its Planning Strategy: Towards an Analytical Framework. In Proceedings of the ICCREM, Xi'an, China, 23–24 September 2023; pp. 323–336.
17. Wu, F. Introduction: Leaving the soil. In *Creating Chinese Urbanism: Urban Revolution and Governance Change*; UCL Press: London, UK, 2022; p. 19.
18. Wei, Z.; Liu, Y.; He, S.; Mo, H. Housing differentiation in transitional urban China. *Cities* **2020**, *96*, 102469. [CrossRef]
19. Piekałkiewicz, M. Why do economists study happiness? *Econ. Labour Relat. Rev.* **2017**, *28*, 361–377. [CrossRef]
20. Wei, Z.; Chiu, R.L.H. Livability of subsidized housing estates in marketized socialist China: An institutional interpretation. *Cities* **2018**, *83*, 108–117. [CrossRef]
21. The State Council the People's Republic of China. Available online: http://english.www.gov.cn/statecouncil/ministries/202109/01/content_WS612ed2bbc6d0df57f98df761.html (accessed on 23 March 2024).
22. Canter, D.; Rees, K. A multivariate model of housing satisfaction. *Int. Rev. Appl. Psychol.* **1982**, *31*, 185–207. [CrossRef]
23. Mesch, G.S.; Manor, O. Social ties, environmental perception, and local attachment. *Environ. Behav.* **1998**, *30*, 504–519. [CrossRef]
24. Ibem, E.O.; Aduwo, E.B. Assessment of residential satisfaction in public housing in Ogun State, Nigeria. *Habitat Int.* **2013**, *40*, 163–175. [CrossRef]
25. Azimi, N.; Esmaeilzadeh, Y. Assessing the relationship between house types and residential satisfaction in Tabriz, Iran. *Int. J. Urban Sci.* **2017**, *21*, 185–203. [CrossRef]
26. Fang, Y.; Liu, Z.; Chen, Y. Housing inequality in urban China: Theoretical debates, empirical evidences, and future directions. *J. Plan. Lit.* **2020**, *35*, 41–53. [CrossRef]
27. Chen, J.; Yang, Z.; Wang, Y.P. The new Chinese model of public housing: A step forward or backward? *Hous. Stud.* **2014**, *29*, 534–550. [CrossRef]
28. Li, J.; Stehlik, M.; Wang, Y. Assessment of barriers to public rental housing exits: Evidence from tenants in Beijing, China. *Cities* **2019**, *87*, 153–165. [CrossRef]
29. Smrke, U.; Blenkus, M.; Socan, G. Residential satisfaction questionnaires: A systematic review. *Urbani Izziv* **2018**, *29*, 67–82. [CrossRef]
30. Shen, Y.; Fu, X. Impacts of built environment and perceived neighborhood characteristics on residents' satisfaction: Evidence from the Shanghai suburbs. *Prog. Geogr.* **2019**, *5*, 686–697.
31. Ibem, E.O.; Ayo-Vaughan, E.A.; Oluwunmi, A.O.; Alagbe, O.A. Residential satisfaction among low-income earners in government-subsidized housing estates in Ogun State, Nigeria. In *Urban Forum*; Springer: Dordrecht, The Netherlands, 2019; Volume 30, pp. 75–96.
32. Lu, M. Determinants of residential satisfaction: Ordered logit vs. regression models. *Growth Chang.* **1999**, *30*, 264–287. [CrossRef]
33. Yuan, Y.; Ding, K.; Cao, X.; Wu, X. A review of neighborhood satisfaction. *Urban Dev. Stud.* **2018**, *10*, 105–111.
34. Galster, G.C. Evaluating indicators for housing policy: Residential satisfaction vs marginal improvement priorities. *Soc. Indic. Res.* **1985**, *16*, 415–448. [CrossRef]
35. Cutter, S.L. Residential satisfaction and the suburban homeowner. *Urban Geogr.* **2013**, *3*, 315–327. [CrossRef]
36. Campbell, A.; Converse, P.E.; Rodgers, W.L. *The Quality of American Life: Perceptions, Evaluations, and Satisfactions*; Russell Sage Foundation: New York, NY, USA, 1976.
37. Rossi, P.H. *Why Families Move: A Study in the Social Psychology of Urban Residential Mobility*; Free Press: Glencoe, IL, USA, 1955; p. 220.
38. Morris, E.W.; Winter, M. A theory of family housing adjustment. *J. Marriage Fam.* **1975**, *37*, 79–88. [CrossRef]
39. Jagun, A.; Brown, D.R.; Milburn, N.G.; Gary, L.E. Residential satisfaction and socioeconomic and housing characteristics of urban black adults. *J. Black Stud.* **1990**, *21*, 40–51. [CrossRef]
40. Lin, S.; Li, Z. Residential satisfaction of migrants in Wenzhou, an "ordinary city" of China. *Habitat Int.* **2017**, *66*, 76–85. [CrossRef]
41. Rioux, L.; Werner, C. Residential satisfaction among aging people living in place. *J. Environ. Psychol.* **2011**, *31*, 158–169. [CrossRef]
42. Fernández-Portero, C.; Alarcón, D.; Padura, Á.B. Dwelling conditions and life satisfaction of older people through residential satisfaction. *J. Environ. Psychol.* **2017**, *49*, 1–7. [CrossRef]
43. Osman, F.O.; Moustafa, Y.M.; Fahmy, A.A. Residential satisfaction in gated communities according to stages in the life cycle with reference to Cairo, Egypt. *J. Eng. Appl. Sci.* **2021**, *68*, 41. [CrossRef]

44. Ge, J.; Hokao, K. Research on residential lifestyles in Japanese cities from the viewpoints of residential preference, residential choice and residential satisfaction. *Landsc. Urban Plan.* **2006**, *78*, 165–178. [CrossRef]
45. Amérigo, M.; Aragonés, J.I. Residential satisfaction in council housing. *J. Environ. Psychol.* **1990**, *10*, 313–325. [CrossRef]
46. Fang, Y. Residential satisfaction, moving intention and moving behaviours: A study of redeveloped neighbourhoods in inner-city Beijing. *Hous. Stud.* **2006**, *21*, 671–694. [CrossRef]
47. Mohit, M.A.; Ibrahim, M.; Rashid, Y.R. Assessment of residential satisfaction in newly designed public low-cost housing in Kuala Lumpur, Malaysia. *Habitat Int.* **2010**, *34*, 18–27. [CrossRef]
48. Kim, S.; Hwang, J.; Lee, M.H. Effect of housing support programs on residential satisfaction and the housing cost burden: Analysis of the effect of housing support programs in Korea based on household attributes. *Land* **2022**, *11*, 1392. [CrossRef]
49. Zhan, D.; Meng, B.; Zhang, W.Z. A Study on Residential Satisfaction and Its Behavioral Intention in Beijing. *Geogr. Res.* **2014**, *33*, 336–348.
50. Niu, J.; Zhao, M. Analysis on factors influencing of yurts residence satisfaction based on structural equation model. *Sci. Technol. Dev.* **2018**, *14*, 750–756.
51. Chen, J.; Pellegrini, P.; Wang, H. Comparative Residents' Satisfaction Evaluation for Socially Sustainable Regeneration—The Case of Two High-Density Communities in Suzhou. *Land* **2022**, *11*, 1483. [CrossRef]
52. Chen, L.; Zhang, W.; Yang, Y.; Yu, J. Disparities in residential environment and satisfaction among urban residents in Dalian, China. *Habitat Int.* **2013**, *40*, 100–108. [CrossRef]
53. Li, J.; Li, D.; Ning, X.; Sun, J.; Du, H. Residential satisfaction among resettled tenants in public rental housing in Wuhan, China. *J. Hous. Built Environ.* **2019**, *34*, 1125–1148. [CrossRef]
54. Huang, Z.; Du, X. Assessment and determinants of residential satisfaction with public housing in Hangzhou, China. *Habitat Int.* **2015**, *47*, 218–230. [CrossRef]
55. Cao, X.J. How does neighborhood design affect life satisfaction? Evidence from Twin Cities. *Travel. Behav. Soc.* **2016**, *5*, 68–76. [CrossRef]
56. Zarghami, E.; Olfat, M.; Fatourehchi, D. An investigation into the relationship between quality of life of the elderly in relation to physical spaces in order to select an ideal residence. *J. Hous. Built Environ.* **2018**, *8*, 8–9. [CrossRef]
57. Chen, J.; Pellegrini, P.; Xu, Y.; Ma, G.; Wang, H.; An, Y.; Feng, X. Evaluating residents' satisfaction before and after regeneration. The case of a high-density resettlement neighbourhood in Suzhou, China. *Cogent Soc. Sci.* **2022**, *8*, 2144137. [CrossRef]
58. Milić, J.; Zhou, J. Residential satisfaction among young people in post-socialist countries: The case of Serbia. *J. Hous. Built Env.* **2018**, *33*, 715–730. [CrossRef]
59. Parkes, A.; Kearns, A.; Atkinson, R. What makes people dissatisfied with their neighbourhoods? *Urban Stud.* **2002**, *39*, 2413–2438. [CrossRef]
60. Adriaanse, C.C.M. Measuring residential satisfaction: A residential environmental satisfaction scale (RESS). *J. Hous. Built Environ.* **2007**, *22*, 287–304. [CrossRef]
61. Vemuri, A.W.; Morgan, G.J.; Wilson, M.A.; Burch, J.W.R. A tale of two scales: Evaluating the relationship among life satisfaction, social capital, income, and the natural environment at individual and neighborhood levels in metropolitan Baltimore. *Environ. Behav.* **2011**, *43*, 3–25. [CrossRef]
62. Weidemann, S.; Anderson, J.R. A conceptual framework for residential satisfaction. In *Home Environments*; Altman, I., Werner, C.M., Eds.; Plenum Press: London, UK, 1985; Volume 8.
63. Amérigo, M. A model of residential satisfaction. In *Socio-Environmental Metamorphoses: Builtscape, Landscape, Ethnoscape*; Aristides, M., Karaletsou, K., Eds.; Aristotle University of Thessaloniki: Salonica, Greece, 1992; Volume V, pp. 411–417.
64. Hur, M.; Nasar, J.L.; Chun, B. Neighborhood satisfaction, physical and perceived naturalness and openness. *J. Environ. Psychol.* **2010**, *30*, 52–59. [CrossRef]
65. Fornell, C.; Johnson, M.D.; Anderson, E.W.; Cha, J.; Bryant, B.E. The american customer satisfaction index: Nature, purpose, and findings. *J. Mark.* **1996**, *60*, 7–18. [CrossRef]
66. Anderson, E.W. Cross-category variation in customer satisfaction and retention. *Mark. Lett.* **1994**, *5*, 19–30. [CrossRef]
67. Van Ryzin, G.G.; Muzzio, D.; Immerwahr, S.; Gulick, L.; Martinez, E. Drivers and consequences of citizen satisfaction: An application of the American customer satisfaction index model to New York City. *Public Adm. Rev.* **2004**, *64*, 331–341. [CrossRef]
68. Kuo, Y.C.; Huh, Y.; Hwang, B.G. A Comparative analysis of residents' satisfaction with apartment building management and maintenance services in South Korea and Taiwan. *Qual. Quant.* **2022**, *56*, 395–412. [CrossRef]
69. Sun, S.; Chen, R.; Qin, S.; Liu, L. Evaluating the Public Participation Processes in Community Regeneration Using the EPST Model: A Case Study in Nanjing, China. *Land* **2022**, *11*, 1405. [CrossRef]
70. Gan, X.; Zuo, J.; Wen, T.; She, Y. Exploring the adequacy of massive constructed public housing in China. *Sustainability* **2019**, *11*, 1949. [CrossRef]
71. Emami, A.; Sadeghlou, S. Residential satisfaction: A narrative literature review towards identification of core determinants and indicators. *Hous. Theory Soc.* **2021**, *38*, 512–540. [CrossRef]
72. Du, T.; Zeng, N.; Huang, Y.; Vejre, H. Relationship between the dynamics of social capital and the dynamics of residential satisfaction under the impact of urban renewal. *Cities* **2020**, *107*, 102933. [CrossRef]
73. Kale, A. Building attachments to places of settlement: A holistic approach to refugee wellbeing in Nelson, Aotearoa New Zealand. *J. Environ. Psychol.* **2019**, *65*, 101315. [CrossRef]

74. Tao, L.; Wong, F.K.; Hui, E.C. Residential satisfaction of migrant workers in China: A case study of Shenzhen. *Habitat Int.* **2014**, *42*, 193–202. [CrossRef]

75. Gou, Z.; Xie, X.; Lu, Y.; Khoshbakht, M. Quality of life (QoL) survey in Hong Kong: Understanding the importance of housing environment and needs of residents from different housing sectors. *Int. J. Environ. Res. Public Health* **2018**, *15*, 219. [CrossRef] [PubMed]

76. Kwon, H.J.; Beamish, J.O. Older adults in multifamily housing: Residential satisfaction and intention to move. *Fam. Consum. Sci. Res. J.* **2013**, *42*, 40–54. [CrossRef]

77. Addo, I.A. Assessing residential satisfaction among low income households in multi-habited dwellings in selected low income communities in Accra. *Urban Stud.* **2016**, *53*, 631–650. [CrossRef]

78. Chan, E.; Lee, G.K. Critical factors for improving social sustainability of urban renewal projects. *Soc. Indic. Res.* **2008**, *85*, 243–256. [CrossRef]

79. Karuppannan, S.; Sivam, A. Social sustainability and neighbourhood design: An investigation of residents' satisfaction in Delhi. *Local Environ.* **2011**, *16*, 849–870. [CrossRef]

80. Jansen, S.J.T. Why is Housing Always Satisfactory? A Study into the Impact of Cognitive Restructuring and Future Perspectives on Housing Appreciation. *Soc. Indic. Res.* **2014**, *116*, 353–371. [CrossRef]

81. Liu, Z.; Liao, L.; Niu, C. Residential satisfaction of community social capital: An empirical study of middle and low-income residents in urban Beijing. *Hum. Geogr.* **2015**, *30*, 21–27.

82. Wei, Z.; Chen, T.; Chiu, R.L.; Chan, E.H. Policy transferability on public housing at the city level: Singapore to Guangzhou in China. *J. Urban Plan. Dev.* **2017**, *143*, 05017010. [CrossRef]

83. The People's Government of Guangzhou Municipality. Available online: https://www.gz.gov.cn/zwgk/sjfb/tjgb/content/post_7286236.html (accessed on 9 May 2024).

84. Guangzhou Statistics Bureau. Available online: http://tjj.gz.gov.cn/zzfwzq/tjgb/content/post_8542999.html (accessed on 9 May 2024).

85. Hoyle, R.; Isherwood, J. Reporting results from structural equation modeling analyses in Archives of Scientific Psychology. *Arch. Sci. Psychol.* **2013**, *1*, 14–22. [CrossRef]

86. Wright, S. Correlation and causation. *J. Agric. Res.* **1921**, *20*, 557–585.

87. Byrne, B.M. *Structural Equation Modeling with AMOS: Basic Concepts, Applications, and Programming*; Routledge: New York, NY, USA, 2010.

88. Kline, R. *Principles and Practice of Structural Equation Modeling*, 5th ed.; Guilford Publications: New York, NY, USA, 2005.

89. Hair, J.; Black, W.; Babin, B.; Anderson, R.; Tatham, R. *Multivariate Data Analysis*, 6th ed.; Pearson Prentice Hall: Old Bridge, NJ, USA, 2006.

90. Stevens, J. *Applied Multivariate Statistics for the Social Sciences*, 4th ed.; Lawrence Erlbaum Associates: Mahwah, NJ, USA, 1996.

91. Fornell, C.; Larcker, D.F. Evaluating structural equation models with unobservable variables and measurement error. *J. Mark. Res.* **1981**, *18*, 39–50. [CrossRef]

92. Wei, Z.; Tang, Q.; Zhen, F. Spatial and social heterogeneities of residents' online shopping behaviors within a large Chinese city: The case of Weifang. *Appl. Geogr.* **2024**, *167*, 103289. [CrossRef]

93. Fisher, M.J.; King, J. The self-directed learning readiness scale for nursing education revisited: A confirmatory factor analysis. *Nurse Educ. Today* **2010**, *30*, 44–48. [CrossRef] [PubMed]

94. Hu, L.; Bentler, P. Fit indices in covariance structure modeling: Sensitivity to underparameterized model misspecification. *Psychol. Methods* **1998**, *3*, 424. [CrossRef]

95. Veenhoven, R. Developments in satisfaction-research. *Soc. Indic. Res.* **1996**, *37*, 1–46. [CrossRef]

96. Han, H.; Xu, Y.; Wang, W.; Xu, W.; Chen, Q.; Yang, C. The influence of community built environment on the residential satisfaction of the elderly: A case study of Hefei City, Anhui Province. *Hum. Geogr.* **2022**, *37*, 118–128.

97. Shen, H. On the testing model of customers' satisfaction in budget-type hostels based on the framework of ACSI. *Tour. Trib.* **2011**, *26*, 58–62.

98. McGuinn, K.K.; Mosher-Ashley, P.M. Participation in recreational activities and its effect on perception of life satisfaction in residential settings. *Act. Adapt. Aging* **2001**, *25*, 77–86. [CrossRef]

99. Kahana, E.; Lovegreen, L.; Kahana, B.; Kahana, M. Person, environment, and person-environment fit as influences on residential satisfaction of elders. *Environ. Behav.* **2003**, *35*, 434–453. [CrossRef]

100. Salleh, A.G. Neighbourhood factors in private low-cost housing in Malaysia. *Habitat Int.* **2008**, *32*, 485–493. [CrossRef]

101. Ghafourian, M.; Hesari, E. Evaluating the model of causal relations between sense of place and residential satisfaction in Iranian Public Housing (the case of Mehr housing in Pardis, Tehran). *Soc. Indic. Res.* **2018**, *139*, 695–721. [CrossRef]

102. Christoph, B. The relation between life satisfaction and the material situation: A re-evaluation using alternative measures. *Soc. Indic. Res.* **2010**, *98*, 475–499. [CrossRef]

103. Brisson, D.; Usher, C.L. The effects of informal neighborhood bonding social capital and neighborhood context on homeownership for families living in poverty. *J. Urban Aff.* **2007**, *29*, 65–75. [CrossRef]

104. Curley, A.M. Relocating the poor: Social capital and neighborhood resources. *J. Urban Aff.* **2010**, *32*, 79–103. [CrossRef]

105. Lee, K.Y.; Jeong, M.G. Residential environmental satisfaction, social capital, and place attachment: The case of Seoul, Korea. *J. Hous. Built Environ.* **2021**, *36*, 559–575. [CrossRef]

106. Mo, H.; Wei, Z. Evolution of Community Planning in China under the context of Improving the Quality of Residential Environments: Case Study on Subsidized Housing Estates in Guangzhou. *South Archit.* **2021**, *5*, 38–43.

Spatial Characteristics of Multidimensional Urban Vitality and Its Impact Mechanisms by the Built Environment

Aibo Jin, Yunyu Ge and Shiyang Zhang *

School of Landscape Architecture, Beijing Forestry University, Beijing 100083, China; jinaibo@bjfu.edu.cn (A.J.); geyunyu717@bjfu.edu.cn (Y.G.)
* Correspondence: zhangshiyang@bjfu.edu.cn

Abstract: Urban vitality, intricately connected to urban morphology, has long been a cornerstone of urban planning and design. The accelerated pace of urbanization has created abundant living and working spaces, but it has also brought about a series of issues such as traffic congestion, environmental pollution, insufficient public spaces, and uneven urban development, leading to a decline in urban vitality. The spatial distribution patterns of urban vitality and their influencing factors are diverse and vary across different cities, necessitating a multidimensional exploration of the relationship between urban vitality and the built environment. Utilizing the central urban area of Beijing as a case study, this research leverages multi-source urban spatial data to delineate the spatial characteristics of social, economic, cultural, and comprehensive vitality. Furthermore, a comprehensive set of built-environment indicators is developed across five dimensions to analyze their correlation with urban vitality. The results indicate: (1) There is a significant spatial clustering of various vitality types in Beijing, with a pronounced correlation between high-density population aggregation and vigorous economic activities. (2) Subdistricts exhibiting high social vitality display an "n"-shaped distribution around the Second Ring Road. In contrast, those with high economic vitality are concentrated along Chang'an Street and various district commercial centers. High cultural vitality subdistricts are distributed in a northwest–southeast trajectory from the Fourth Ring Road to the Second Ring Road, and subdistricts with high comprehensive vitality exhibit a concentric distribution radiating outwards from the center. (3) Social vitality is most closely related to comprehensive vitality, and the various vitality types in Beijing's central urban area develop relatively evenly. (4) The built environment significantly affects all types of urban vitality. Factors such as floor area ratio, POI density, POI mixing degree, and intersection density are fundamental to enhancing urban vitality, whereas the greening rate somewhat inhibits it. (5) Future spatial planning should utilize the radiating effect of high-vitality subdistricts to optimize population distribution, enhance POI mixing, increase metro station density, and strengthen critical urban structures for synergistic economic and cultural development. This study provides a foundation and promotion strategies for optimizing the layout and enhancing vitality at the subdistrict scale within Beijing's central urban area.

Keywords: urban vitality; built environment; spatial distribution; promotion strategies; Beijing's central area

1. Introduction

As urbanization accelerates, the rapid increase in population in urban centers has significantly altered urban spatial structures. Concurrently, the disorderly expansion of cities has led to numerous urban issues, such as environmental pollution, traffic congestion, and imbalances in public service provision. These issues have collectively contributed to a decline in urban spatial vitality [1,2]. China, having transitioned from an industrial to a post-industrial society, is now shifting towards high-quality development [3]. Under the pressure of intensified land use in urban centers, China has undertaken extensive renewal of traditional neighborhoods, old communities, and urban villages, significantly impacting

the integrity and sustainability of current urban systems [4]. With the growing demand for an improved quality of life, enhancing urban livability has become a key objective in contemporary urban planning [5,6]. Urban vitality is closely linked to spatial quality and it directly influences livability [7]. High urban vitality indicates greater attractiveness, which can draw talent and capital, thereby increasing competitiveness and providing more benefits and opportunities for residents [8]. Urban vitality also serves as an effective measure of spatial quality and distribution characteristics [9–11]. However, due to the diverse structures and functions of different cities, the relationship between urban vitality and the built environment lacks a unified pattern. Therefore, in-depth research and exploration into enhancing urban spatial vitality are crucial for achieving sustainable urban development, improving residents' quality of life, and strengthening overall urban competitiveness.

Since the 1960s, scholarly interest in urban vitality has steadily grown [12]. Originating from Jane Jacobs, the concept underscores the vibrancy infused into cities through pedestrian activities on streets, social interactions among urban dwellers, and the dynamic interplay between people and places, particularly evident in the bustling public life of streets, squares, and parks [13]. Kevin Lynch defines urban vitality as a dimension of urban form that sustains human life needs and social functions, embracing the continuity, safety, and stability of the entire ecosystem [14]. Maas conceptualizes urban vitality as a reflection of urban spatial quality, encompassing the continual presence of people in streets and public spaces, their diverse activities and opportunities, and the material environments that facilitate such engagements [15]. Montgomery posits that vibrant human activities are pivotal in nurturing urban vitality, with successful urban locales often boasting vibrant public spaces conducive to a myriad of human endeavors [2]. Yang et al. suggest that urban vitality manifests in spaces' capacity to attract a variety of human activities [16]. The 2024 Beijing Municipal Government Work Report proposed the development goal of strengthening urban fine governance and enhancing urban vitality by scientifically harnessing the laws of development in mega-cities. Despite nuances in scholars' definitions, urban vitality consistently emerges as a vital ingredient in fostering high-quality urban living, with the built environment playing a pivotal role in shaping this vitality. Consequently, investigating the nexus between urban vitality and the built environment holds paramount significance, offering critical insights into the spatial dynamics and challenges of contemporary urban development, and providing foundational support for urban design and management endeavors aimed at enhancing vitality.

Assessing urban vitality has long been a significant challenge, with past approaches primarily focusing on two dimensions: human activity intensity and built environment indicators [17–19]. Regarding human activity intensity, Jane Jacobs pioneered field research methods to measure and validate the degree of population aggregation in urban areas [9,13]. In terms of built environment indicators, Jacobs argued that diverse urban areas should exhibit high functional mix, small-scale streets, a mix of old and new buildings, and high pedestrian flow density [13]. Similar viewpoints include Jan Gehl's emphasis on the integrated, cohesive, and open characteristics of urban built environments [20], and Montgomery's assertion that appropriate density, human-scale dimensions, and the presence of public spaces and parks are vital guarantees of urban vitality [2,21]. The urban built environment serves as a tangible manifestation of the region's social, economic, and cultural development levels [22], and its diverse connotations have spurred the development of various urban vitality assessment methods, which can be broadly categorized as field research [23,24] and big data analytics [25–34]. At the city scale, field research often faces challenges such as data collection difficulties and heterogeneity. Currently, many studies rely on Internet Points of Interest (POI) provided by various online platforms to reflect the distribution characteristics of different types of venue and regional urban vitality [35,36]. However, due to their lack of timeliness and objectivity, POI data often provide a one-sided view of urban vitality and may not accurately represent actual human activity levels [26]. The utilization of multiple data sources effectively integrates the advantages of traditional research and modern technological methods, enhancing the comprehensiveness and accu-

racy of evaluation, and has become the prevailing trend in urban vitality assessment [37]. Combining satellite remote sensing, social media, and traffic flow data for comprehensive evaluation not only provides dynamic information with strong temporal continuity and wide coverage but also fully reflects the multidimensional characteristics of urban vitality, thus facilitating a deeper understanding of the complex relationship between urban vitality and urban development.

In recent years, scholars such as Si et al. and Liu et al. have undertaken a nuanced classification of urban vitality, delineating it into three principal dimensions: social vitality, economic vitality, and cultural vitality [34,38,39]. This classification underscores social vitality as the linchpin, economic vitality as the foundational element, and cultural vitality as the intrinsic quality inherent in urban vigor. Such conceptual refinement reflects a broader trend towards acknowledging the multifaceted nature of urban dynamism. Notably, recent investigations into the vitality of critical Chinese metropolitan centers like Shanghai and Chengdu have adopted this tripartite framework to develop comprehensive indicator systems, integrating diverse built environment factors [33,40]. With the advent of big data technology, a plethora of Location-Based Services (LBS) data types have been integrated into studies on urban vitality, facilitating the visualization of population distribution dynamics. These datasets encompass heat map data [25–29], social media check-in data [30,31], mobile phone signaling data [32], and taxi arrival data, among others [33], offering insights into the social vibrancy of diverse urban demographics across varying temporal contexts. The concentrated presence of small-scale dining establishments is recognized as an indicator of vibrant urban locales, reflecting the daytime economic vigor of urban centers [41,42]. Moreover, nocturnal light emissions captured via satellite imagery serve as a surrogate for GDP in specific contexts, capturing the economic vitality of regions with predictive accuracy scaling with spatial resolution [43,44]. Furthermore, the spatial dispersion of urban cultural amenities such as libraries, museums, and art galleries serves as an objective manifestation of cultural vibrancy within urban landscapes [33,34].

The urban built environment is considered a key factor influencing urban vitality. Cervero R. et al. proposed a "3D" model consisting of density, diversity, and design dimensions to assess the relationship between the built environment and transportation [45]. Building upon this, Ewing R. et al. added dimensions of public transportation accessibility and availability [46], although there is some controversy regarding the specific selection of factors [33]. Gomez-Varo et al. constructed a multidimensional index system, including density, functional diversity, social opportunities, architectural diversity, accessibility, and boundary vacuum to evaluate the vitality of a low-income area in Barcelona and provide recommendations for public policy improvements [47]. Li X. et al. explored factors contributing to or inhibiting urban vitality in Wuhan from six aspects: facilities and land use, neighborhood attributes, urban form, location, landscape, and accessibility [12]. Xia, C. et al. validated the impact of three-dimensional measures such as walkability and comfort in the built environment on urban vitality, in contrast with two-dimensional measures like accessibility, proximity, and mixture across 15 major cities in China [48]. Most scholars have evaluated the influence of these indicators on urban vitality using linear methods such as analytic hierarchy process, principal component analysis, and grey relational analysis, which may not fully capture the complex relationships between urban vitality and urban elements [11]. Exploring the spatial heterogeneity of different urban built environment indicators' effects on urban vitality is crucial as it helps urban planners and decision-makers understand how various environmental factors manifest different impacts in different areas. Analyzing this spatial heterogeneity can identify which environmental features exhibit more significant effects in promoting or inhibiting urban vitality, thereby enabling more refined and targeted urban planning.

As fundamental administrative units, the quality of the living environment in subdistricts directly affects residents' quality of life and the overall urban living environment [38]. Therefore, this study selects the subdistricts in Beijing's central urban area as the primary research unit, as they can finely capture urban dynamics and human activity character-

istics. We employ population heat map data, nighttime light data, and the density of cultural facilities' POIs to represent social, economic, and cultural vitality, respectively. Additionally, we construct a comprehensive index system of the urban built environment, including land use intensity, service outlets, blue–green spaces, accessibility, and location to analyze their impact mechanisms using the Geographic Weighted Regression (GWR) model. The research aims to comprehensively investigate the relationship between the built environment and urban vitality in mega-cities in China from the perspective of urban structure and landscape. The objectives of the study are: (1) to scientifically analyze the spatial distribution patterns of urban vitality in Beijing's central area and the relationships between different types of vitality, (2) to explore the mechanisms of how the urban built environment affects urban vitality at the neighborhood scale, and (3) proposing strategies for sustainably enhancing urban vitality in Beijing's central area.

2. Study Area and Data Sources

2.1. Study Area

This study focuses on Beijing's central area, comprising six administrative districts: Dongcheng, Xicheng, Chaoyang, Haidian, Fengtai, and Shijingshan (excluding Beijing Capital International Airport). Covering approximately 1378 km^2, this area has a permanent population of 10.93 million, accounting for 50.2% of Beijing's total population according to the Seventh National Population Census. As outlined in the Beijing Urban Master Plan 2016–2035 (Master Plan), Beijing's central area serves as the concentrated hub for the national political, cultural, international communication, and scientific and technological innovation centers. It is pivotal to the goal of creating a world-class, harmonious, and livable city (Figure 1).
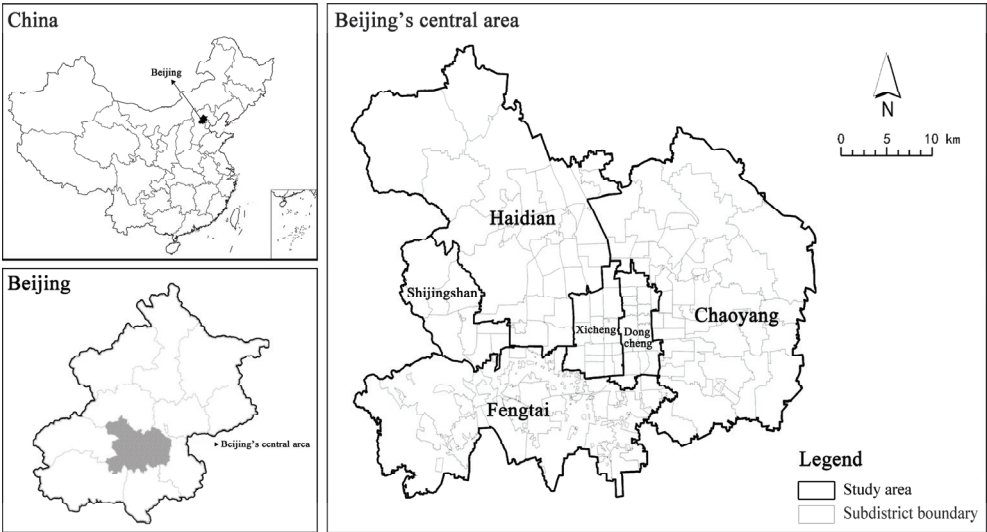

Figure 1. Location of the study area.

Subdistricts and townships are the fundamental administrative units in China's hierarchy, providing a detailed perspective on urban governance and development. To address grassroots governance in urban–rural integration areas, Beijing has established regional offices within its administrative divisions. These offices manage urban affairs and facilitate the transition of highly urbanized townships to subdistrict offices [49]. Research at this level allows for a detailed observation of the impacts and challenges of urban policies, especially in densely populated and rapidly urbanizing central areas, offering precise and practical support for urban planning and governance.

With the recent issuance of the Beijing Garden City Special Plan (2023–2035), Beijing Municipality will further enhance the urban built environment based on vital urban structures such as the north–south central axis and the "Three Mountains and Five Gardens" area. Urban structure significantly shapes the spatial pattern of the built environment. In Beijing's central urban area, key elements include urban axes, major transportation systems, and natural blue–green substrates [50]. The north–south central axis stretches from the Yanshan Mountains to Beijing Daxing International Airport, while the east–west axis extends from Tiananmen Square to the Chaobai River. The transportation network is supported by five ring roads surrounding Beijing Old Town (BOT). The blue–green system is characterized by the interconnected Beiyun River and Yongding River water systems, linked by natural and artificial waterways. Additionally, the urban park belt within and beyond the Fifth Ring Road, along with the suburban park belt, forms a continuous green buffer zone (Figure 2).
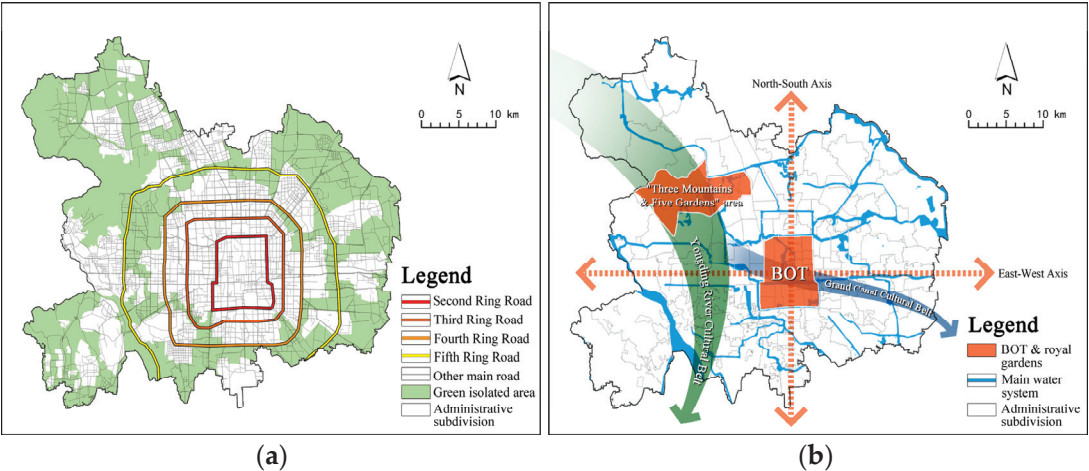
Figure 2. (**a**) Urban transport and green space structure; (**b**) urban rivers, axes, and cultural belts.

Based on the "Master Plan", this study examines 100 subdistricts, 31 regions, and 2 towns within the Beijing's central area as research units. The goal is to explore the spatial patterns of its diverse vitality and identify the influencing factors. By doing so, this study aims to offer direct references and insights for enhancing urban grassroots governance.

2.2. Data Sources

The measurement of Urban Social Vitality (SV) is sourced from Baidu Heatmap data for Beijing's central area. To avoid disruptions from holidays and other special occasions on social vitality, this study chose two typical dates for measuring social vitality. These dates were carefully selected to ensure they represented regular days without any significant external influences that could skew the data. By doing so, the study aimed to obtain a more accurate and consistent measure of social vitality, providing a clearer picture of everyday social interactions and activities. Data were collected on 23 January 2022 (weekend) and 24 January 2022 (weekday) at hourly intervals from 7:00 to 21:00. To characterize SV, we computed the average heat density values from 30 time points.

Urban Economic Vitality (EV) was assessed using night-time light data from the LJ1-01 high-resolution remote sensing imagery of Beijing (http://www.lmars.whu.edu.cn, accessed on 5 May 2022) [51]. The imagery was resampled using the nearest neighbor method, and the data from each sampled grid within the research units were aggregated to represent EV.

Urban Cultural Vitality (CV) was evaluated using data from the Amap online map (https://lbs.amap.com/, accessed on Amap Software Co., Ltd). These data include venues such as museums, exhibition centers, libraries, concert halls, theaters, and art galleries, which are considered essential cultural elements. The density of POI was used to assess CV [52].

Given the spatial characteristics of Beijing's central urban area, the study selected a built environment indicator system, detailed in Table 1. Building vector data, diverse POI data, including bus stops, metro stations, and urban centers, as well as road network data, were acquired from Amap. Blue–green space data were derived from the GLC_FCS30 product (https://data.casearth.cn, accessed on Aerospace Information Research Institute, Chinese Academy of Sciences), which provided 30 m resolution land use and land cover data.

Table 1. Built environment variables in Beijing's central area.

Dimension	Variable	Illustrate
Land use intensity	Building density	Sum of built-up area within the unit/Unit area
	Floor area ratio	Total built-up area within the unit/Sum of building footprint areas within the unit
Service outlets	POI density	Total count of POIs within the unit/Unit area
	POI mixing degree	$E = -\sum_{i=0}^{n} P_i log_2 P_i$ where E denotes the information entropy, and P_i represents the proportion of the *i*-th category of POI in the unit [53]
Blue–green space	Greening rate	Total area of green and blue spaces within the unit/Unit area
Accessibility	Road network density	Total length of the road network within the unit/Unit area
	Bus stop density	Total count of bus stops within the unit/Unit area
	Metro station density	Total count of metro stations within the unit/Unit area
	Intersection density	Total count of road intersections within the unit/Unit area
Location	Distance from the administrative center	Linear distance from the spatial centroid of the unit to Tiananmen Square

Note: The original POI types collected are screened, deduplicated, and reclassified into six categories: residential, commercial services, commercial offices, public facilities, roads and transportation facilities, and parks and scenic spots to calculate the POI density and POI mixing degree.

3. Methods

By exploring the spatial distribution of different types of urban vitality and their correlation with the built environment, a technical roadmap encompassing data representation, indicator construction, and quantitative evaluation was constructed (Figure 3). Firstly, the SV, EV, and CV of Beijing's central area were characterized separately and, after normalizing the three types of vitality, their average represented comprehensive vitality (COV). Secondly, the spatial distribution characteristics of individual vitality and their spatial correlations with COV were examined. Thirdly, a built environment indicator system was constructed, comprising ten indicators across five dimensions, including land use intensity, service outlets, blue–green spaces, accessibility, and location. Subsequently, the relationship between different urban area vitality and various factors of the built environment were analyzed. Finally, promotion strategies at the urban spatial pattern level were proposed through comparison with existing studies.
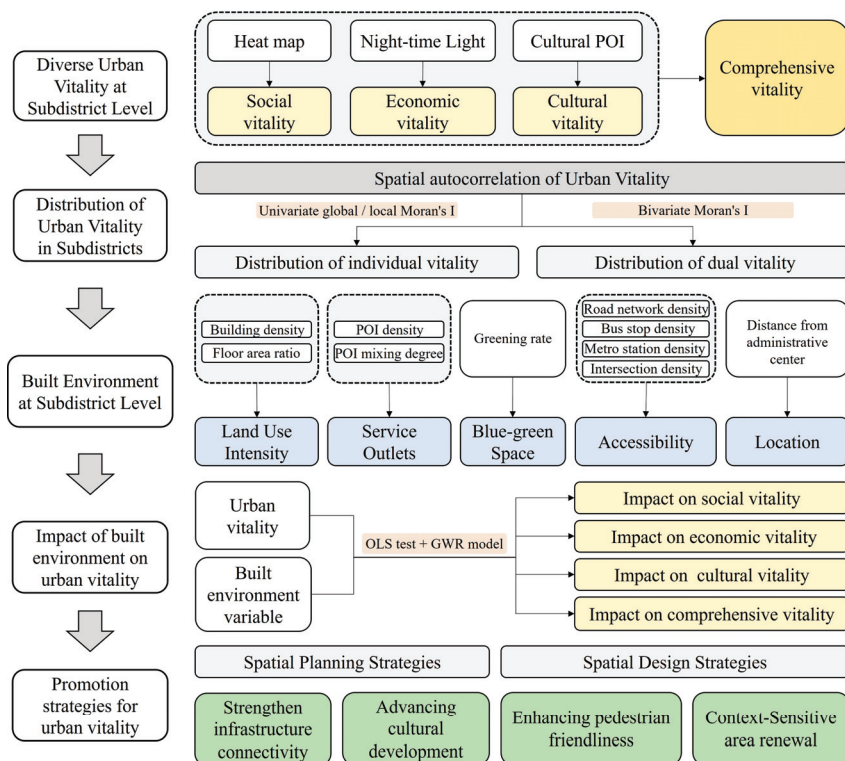
Figure 3. Conceptual framework of the study.

3.1. Spatial Autocorrelation

Spatial autocorrelation was employed to uncover whether a notable interdependence existed between a geospatial unit and an attribute of its neighboring spatial units [54]. The study utilized Moran's I to gauge its spatial autocorrelation.

(1) Univariate global autocorrelation. To ascertain the presence of spatial global dependence among different vitality types within the study area, the global Moran index test was conducted, with the calculation formula as follows:

$$I = \frac{\sum_{i=1}^{n} \sum_{j=1}^{n} W_{ij} \left(Y_i - \overline{Y} \right) \left(Y_j - \overline{Y} \right)}{S^2 \sum_{i=1}^{n} \sum_{j=1}^{n} W_{ij}} \tag{1}$$

$$Z = \frac{1 - E(I)}{\sqrt{Var(I)}} \tag{2}$$

where: n is the number of spatial units in the study area; Y_i and Y_j are the observed values of an attribute of spatial units i and j; W_{ij} is the spatial weight matrix established on the basis of the adjacent relationship W_{ij} of spatial units i and j; S^2 is Y_i the variance of; Z is the normal standardized statistic of Moran's I; $E(I)$ is the expectation of Moran's I; $Var(I)$ is the variance of Moran's I.

(2) Univariate local autocorrelation was conducted to determine the presence of local spatial agglomeration or differentiation of different vitality types within the study area. The calculation formula is as follows:

$$I_i = \frac{Y_i - \overline{Y}}{S^2} \sum_{j=1}^{n} W_{ij}(Y_j - \overline{Y}) \tag{3}$$

(3) Bivariate spatial autocorrelation assesses the degree of correlation between the value of a positional variable and other variables by utilizing the weighted average of all adjacent positions. This method enables the exploration of spatial correlation between different vitality types [54]. The calculation formula is as follows:

$$I_{lm}^i = z_l^i \sum_{j=1}^n W_{ij} z_m^j = \frac{X_l^i - \overline{X_l}}{\sigma_l} \sum_{j=1}^n W_{ij} \frac{X_m^j - \overline{X_m}}{\sigma_m} \tag{4}$$

where: X_l^i is the observed value of attribute l of space unit i; X_m^j is the observed value of attribute m of spatial unit j; σ_l and σ_m are the variance of the observed value of attribute l and m, respectively.

Furthermore, to emphasize the spatial characteristics of individual vitality and composite vitality at the urban street scale, as well as the spatial correlation between individual vitality measures, we utilized LISA (Local Indicators of Spatial Association) cluster maps for visualization. LISA cluster maps are particularly useful for identifying clusters of high or low values, revealing patterns of spatial association or disassociation. By employing LISA cluster maps, we could visually dissect the intricate spatial dynamics of urban vitality. These maps allowed us to pinpoint specific areas within the urban fabric where vitality metrics were exceptionally high or low, thus highlighting zones of potential intervention or further study.

3.2. Geographically Weighted Regression

Due to sample size limitations and the presence of multicollinearity among variables, the OLS model may compromise the accuracy of regression results. Additionally, it fails to detect spatial heterogeneity issues at the local level. Therefore, by screening the respective variable factors and selecting those with probabilities < 0.05 or robust probabilities < 0.05 in the OLS model analysis, and with variance inflation factors (VIF) < 10, variables were chosen to construct the GWR model. This model was utilized to analyze the strength of associations between different urban regions and vitality with their respective variable factors. Extending upon the linear regression model, the GWR model adapts the regression equation to local spatial elements, providing a better reflection of how independent variables influence dependent variables as spatial locations vary [55]. Its calculation formula is as follows:

$$y_i = \beta_0(u_i, v_i) + \sum_{i=1}^k \beta_0(u_i, v_i) x_{ik} + \varepsilon_i \tag{5}$$

where: x_{ik} is the value of the k-th independent variable at the i-th point; ε_i is the residual; (u_i, v_i) is the spatial coordinate of the i-th sample point; $\beta_0(u_i, v_i)$ is the continuous function $\beta_0(u, v)$ the value at point i. This study employed the Akaike Information Criterion (AIC), a widely recognized statistical tool known for its high degree of fit, to select the optimal bandwidth parameter. The AIC is particularly valued for its ability to balance model complexity and goodness of fit, thus preventing overfitting. By using AIC, the study aimed to achieve a balance between model variance and bias. This method ensures that the chosen bandwidth parameter is neither too large, which could lead to an overly simplistic model that misses important patterns in the data, nor too small, which could result in an overly complex model that captures noise rather than the underlying trend. The application of AIC in this context helps to identify the most appropriate model that generalizes well to new data, ensuring both robustness and reliability in the study's findings.

4. Results

4.1. Spatial Characteristics of Vitality in Beijing's Central Area

4.1.1. Single versus Integrated Vitality Spatial Characteristics

Figure 4 illustrates the spatial distribution of SV, EV, CV, and COV at the subdistrict scale in Beijing's central area. Subdistricts with high SV exhibit an "n"-shaped distribution

along the Second Ring Road. In contrast, those with high EVs are concentrated along Chang'an Avenue and various commercial centers in each district—subdistricts with high CV form a belt-like distribution from the northwest to the southeast. Specifically, Chongwenmen, Chaoyangmen, and Hujialou are the top three subdistricts with the highest SV in the core area, hosting significant urban nodes such as Beijing Railway Station, the Central Business District (CBD), and embassy areas. Jianwai and Jianguomen Subdistricts, located in the eastern part of Chang'an Avenue, have the highest EV. In contrast, Yayuncun and Jinrongjie Subdistricts are the high EV centers in the northern and western parts of the city, respectively. Unlike SV, EV does not uniformly decrease from the center outward but instead exhibits five areas of high EV aggregation between the Second Ring Road and the Fourth Ring Road. The region with the highest CV forms a strip along the eastern side of the central axis, from the Jianguomen Subdistrict in the north to the Dashilar and Qianmen Subdistricts in the south. This area encompasses 17 historical and cultural blocks designated in the regulatory plan of the core area of the capital, reflecting a relatively high coverage of cultural facilities. The western region of the city, with a relatively high CV, connects the "Three Mountains and Five Gardens" area and two cultural cores. Jiuxianqiao Subdistrict in the northeast and Yongdinglu Subdistrict in the west are isolated areas with high CV, with the former being the location of the famous 798 Art Zone.
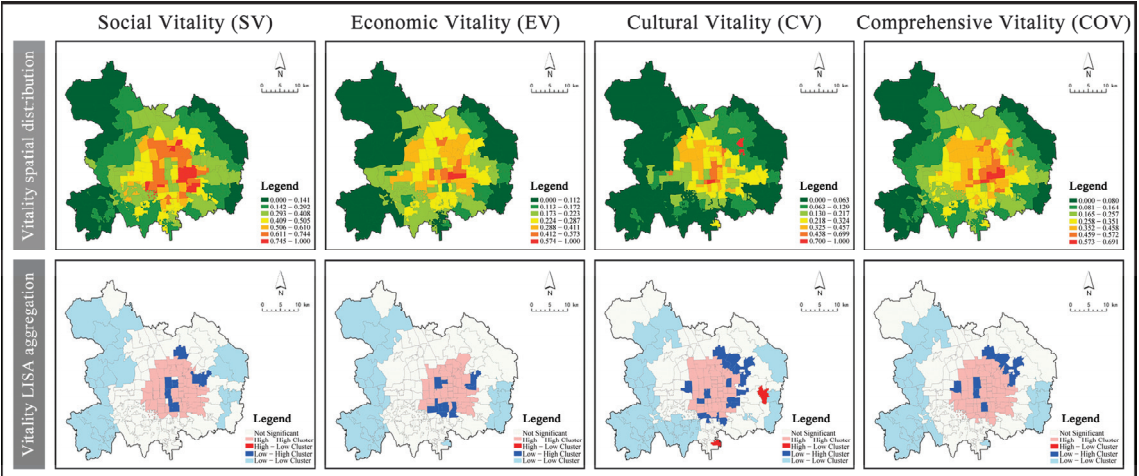
Figure 4. Vitality spatial distribution and LISA aggregation.

The overall distribution of COV in the subdistricts is similar to that of SV. Apart from the subdistricts in the city center, such as Xichanganjie, Shichahai, and Tiantan Subdistricts, which exhibit low vitality due to political and historical remnants, extensive green spaces, and water bodies, the distribution of COV also shows a concentric layout decreasing from the center outward. The areas with the highest COV in the city are located from the central axis to the east along the "East Chang'an Avenue—Tonghui River" corridor, with Jianwai Subdistrict having the highest COV. The higher vitality concentric zones are generally delineated by the Third Ring Road to the west, the Fourth Ring Road to the north and east, and the Second Ring Road to the south, roughly corresponding to the boundaries of the core area of the capital designated in the "Master Plan". The mid-range COV areas exhibit multiple finger-like extensions outward, mainly along the extensions of East and West Chang'an Avenue, the southern extension of the central axis, and the northwest extension along the Airport Expressway. The areas with lower COV are primarily located in the green isolation zones where the suburban park belt is situated according to the "Master Plan".

Using Local Indicators of Spatial Association (LISA) cluster maps, we can discern the clustering patterns of various types of vitality in Beijing's central area. These maps

specifically highlight the distribution of Low–High (LH) and High–Low (HL) clusters, which visually represent the heterogeneous distribution of subdistrict vitality.

For SV, an LH cluster formed along the central axis within the Second Ring Road. This area includes the highest national administrative organs and significant historical and cultural landmarks, such as Shichahai, Beihai, Zhongnanhai, and Tiantan. Additionally, historical cultural districts like Nanluoguxiang and Dashilar are situated here. Two other LH clusters are located near the northeast Fourth Ring Road, encompassing large green spaces within the subdistricts, known as the "green isolated area". In terms of EV, the absence of a well-developed economic radiation relationship in the eastern and southern directions has resulted in the formation of LH clusters in these areas. The LH clusters near the BOT are primarily due to the lower nighttime lighting data from traditional residential areas. Regarding CV, LH clusters are more dispersed. Within the Third Ring Road and its interior, there are several LH clusters of CV. The largest of these is centered around the "Datun–Wangjing" Subdistrict in the northwest.

Notably, there are two HL clusters in the CV: the Sanjianfang Regional Office in the east, which hosts the Communication University of China, an essential cultural industry area in Chaoyang District, and the Donggaodi Subdistrict in the south, marking the southern endpoint of the central axis. The Donggaodi Subdistrict also has the highest building density in Fengtai District, featuring relatively complete cultural facilities. Combining SV, EV, and CV data, a large-scale LH cluster emerged in the northeastern part of the mid-range COV area. This indicates significant differences in COV within and outside the northeastern Fourth Ring Road, suggesting a key area for future vitality enhancement efforts. A comprehensive global spatial autocorrelation analysis of urban vitality in Beijing's central area reveals significant spatial dependency across all forms of vitality, as evidenced by the Z score (Table 2). Notably, the spatial clustering of COV surpasses that of the three individual types of vitality, while SC demonstrates slightly higher spatial clustering than both CV and EV.

Table 2. Global spatial autocorrelation results of urban vitality.

Vitality Type	Social Vitality (SV)	Economic Vitality (EV)	Cultural Vitality (CV)	Comprehensive Vitality (COV)
Moran's I	0.480	0.418	0.461	0.604
Z score	19.757	17.754	19.224	24.757

Note: SV, EV, CV, and COV all passed the significance level test ($p < 0.001$).

4.1.2. Spatial Correlation between Individual Types of Vitality

Table 3 details the interrelations among the individual forms of vitality. Notably, the spatial autocorrelation between SV and EV is the highest, indicating a robust spatial association between high-density population concentration and intense economic activities in the central urban area of Beijing. The correlation between SV and CV is slightly lower, suggesting that while cultural elements attract population concentrations, their pull is somewhat weaker compared to economic factors. The weakest correlation is observed between CV and EV, highlighting that cultural and economic activities are less spatially intertwined.

Table 3. Spatial autocorrelation results of various activity bivariate variables.

Variable 1	Variable 2	Moran's I
Social vitality	Economic vitality	0.582
Social vitality	Cultural vitality	0.427
Cultural vitality	Economic vitality	0.405

This analysis underscores the pronounced spatial association between areas with high population density and intense economic activities in Beijing's central urban area. While the

spatial distribution of cultural elements may not draw population aggregation as strongly as economic factors, they still wield significant influence. Certain areas with a dense concentration of cultural facilities demonstrate a notable catalyzing effect on economic activities, indicating that cultural elements can enhance economic vibrancy in their vicinity.

Figure 5 illustrates the spatial distribution of the correlation between single vitality indices at the subdistrict scale in Beijing's central area. The relationship between SV and EV is characterized by two main categories: HH and LL clusters. HH clusters are primarily concentrated at the intersection of Chang'an Street and the eastern Second Ring Road, indicating areas of both high population density and intense economic activity. In contrast, LL clusters are predominantly found along the eastern and western peripheries of the central urban area, where both population density and economic activity are lower.
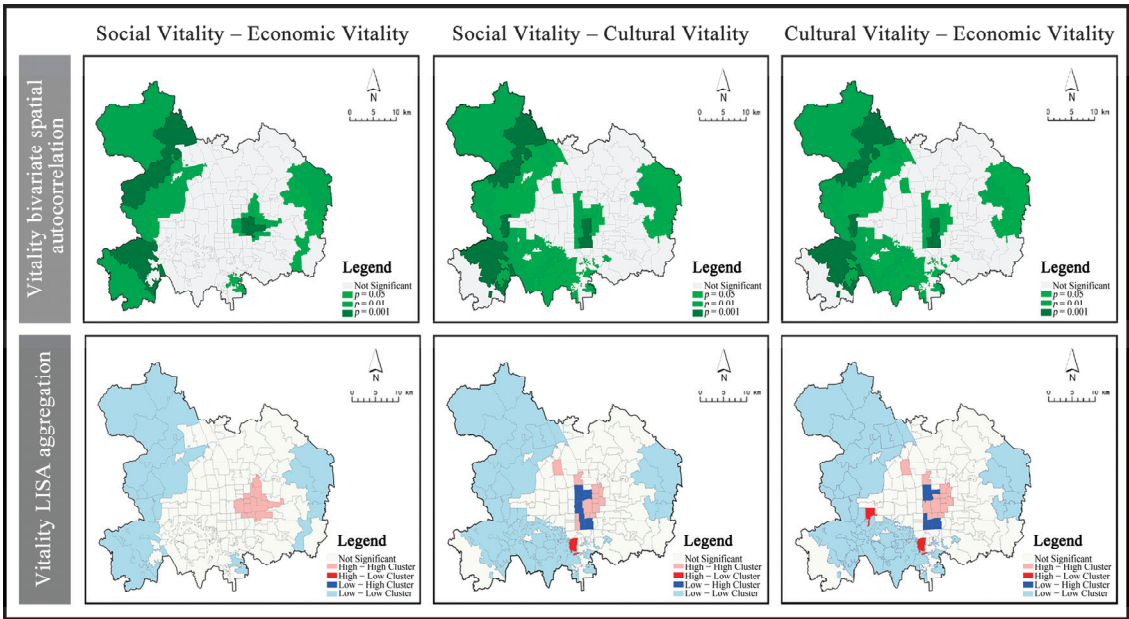
Figure 5. Vitality bivariate spatial autocorrelation and LISA aggregation.

The relationship between SV and CV is more complex than that between SV and EV. HH clusters are prevalent in several subdistricts south of Chang'an Street in Dongcheng District, as well as in Desheng Subdistrict, Chunshu Subdistrict, and Taoranting Subdistrict in Xicheng District, and Zhongguancun Subdistrict in Haidian District. These areas are characterized by high levels of both population density and cultural activity. LL clusters are situated outside the Fifth Ring Road in Haidian District and Shijingshan District, significant portions of Fengtai District, and subdistricts beyond the East Fifth Ring Road in Chaoyang District, where both cultural and population density are low. LH clusters representing areas with low population density but high CV exhibit a distribution pattern similar to SV within the Second Ring Road. Notably, the Majiabao Subdistrict in the south constitutes an HL cluster area, indicating high population density but lower CV.

The clustering patterns and significantly correlated regions between EV–CV and SV–CV show remarkable similarity. However, in comparison to EV–CV, SV–CV features LH clusters centered around Beihai Park and Temple of Heaven Park in the north and south, respectively, exhibiting distribution characteristics akin to EV. Additionally, there is one HL cluster area located in Babaoshan Subdistrict in Shijingshan District, highlighting an area of high CV but lower population density.

4.2. Impact of Built Environment on Multidimensional Urban Vitality

Filtering the built environment factors that significantly impact each vitality dimension, the analysis results are presented in Tables 4–7. By comparing with the OLS model analysis results, it was found that the reduction in Akaike Information Criterion corrected (AICc) for each GWR model was >3, and the residuals of each GWR model exhibited a random spatial distribution, demonstrating the reliability of the GWR model analysis results. The spatial correlations between various types of vitality and their significantly associated built environment factors are illustrated in Figures 6–9.

Table 4. Descriptive statistics of GWR regression coefficients for social vitality.

Variable	Max	Median	Min	Average	Standard Deviation
Floor area ratio	0.290	0.262	0.191	0.259	0.018
POI density	0.401	0.365	0.343	0.372	0.012
POI mixing degree	0.213	0.187	0.159	0.186	0.012
Greening rate	−0.135	−0.147	−0.158	−0.146	0.007
Metro station density	0.133	0.123	0.118	0.124	0.004
Distance from administrative center	−0.213	−0.224	−0.249	−0.225	0.008
Correction R^2	0.879				

Table 5. Descriptive statistics of GWR regression coefficients for economic vitality.

Variable	Max	Median	Min	Average	Standard Deviation
Floor area ratio	0.293	0.233	0.019	0.209	0.072
POI density	0.475	0.295	0.161	0.296	0.067
Metro station density	0.188	0.132	0.081	0.137	0.030
Intersection density	0.208	0.158	0.056	0.145	0.049
Correction R^2	0.786				

Table 6. Descriptive statistics of GWR regression coefficients for cultural vitality.

Variable	Max	Median	Min	Average	Standard Deviation
Building density	0.873	0.593	0.233	0.597	0.127
Road network density	0.368	0.281	−0.163	0.201	0.165
Metro station density	0.136	−0.126	−0.210	−0.111	0.056
Intersection density	0.395	0.266	0.137	0.269	0.058
Distance from administrative center	0.633	0.281	−0.324	0.269	0.224
Correction R^2	0.802				

Table 7. Descriptive statistics of GWR regression coefficients for comprehensive vitality.

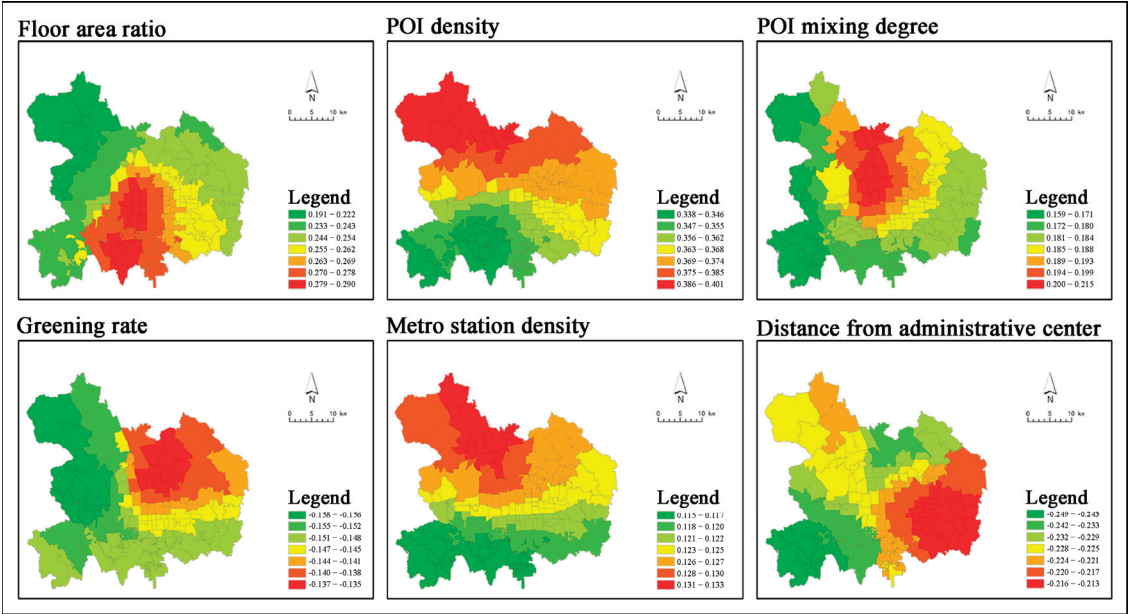| Variable	Max	Median	Min	Average	Standard Deviation
Building density	0.344	0.237	0.169	0.242	0.050
Floor area ratio	0.248	0.160	0.100	0.164	0.036
POI density	0.420	0.333	0.288	0.332	0.028
POI mixing degree	0.172	0.160	0.110	0.155	0.015
Greening rate	0.038	−0.075	−0.101	−0.060	0.039
Intersection density	0.197	0.138	0.096	0.138	0.027
Correction R^2	0.904				

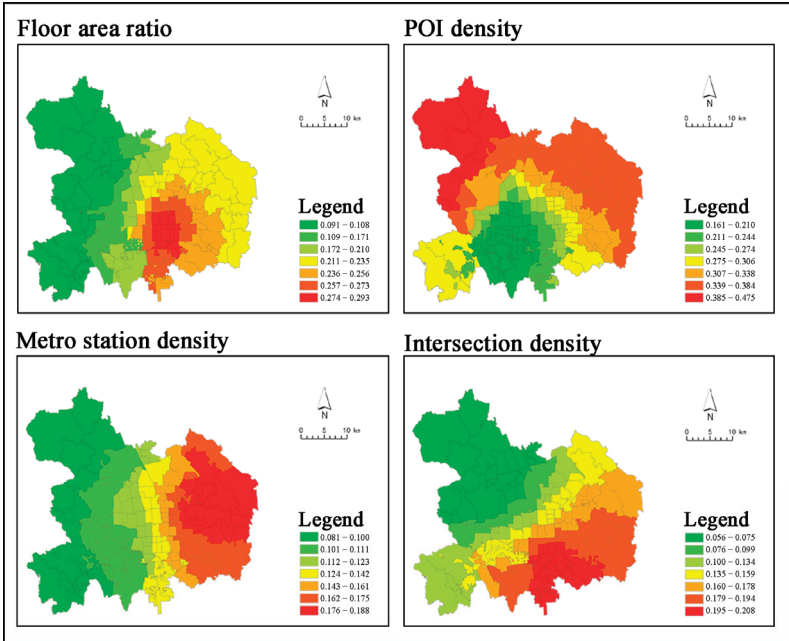**Figure 6.** Correlation between social vitality and the built environment.

Figure 7. Correlation between economic vitality and built environment.
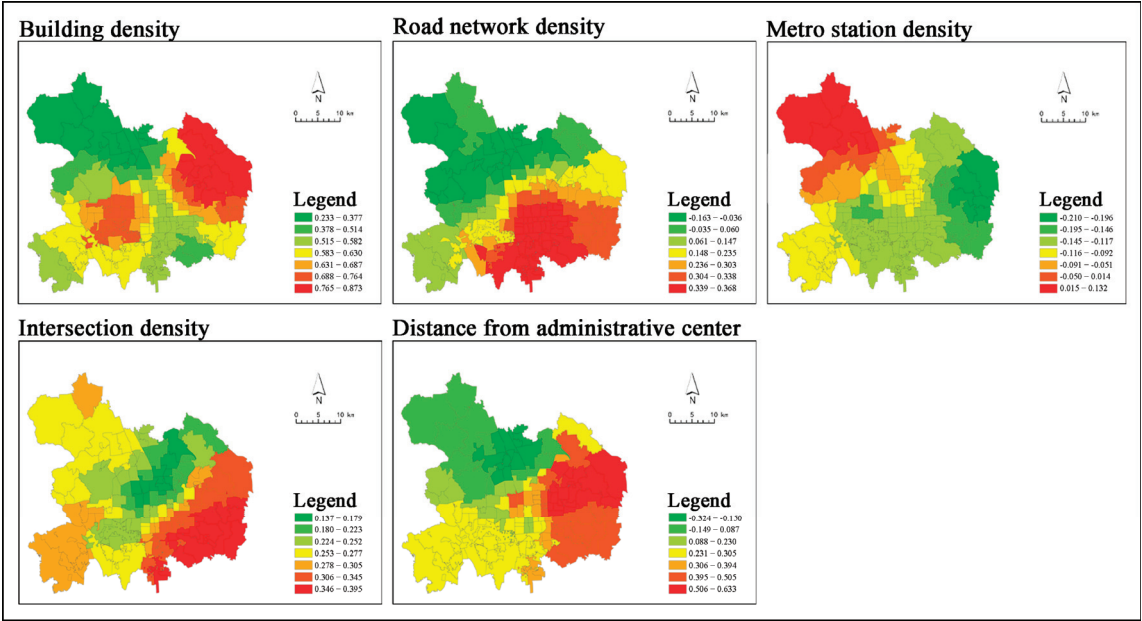
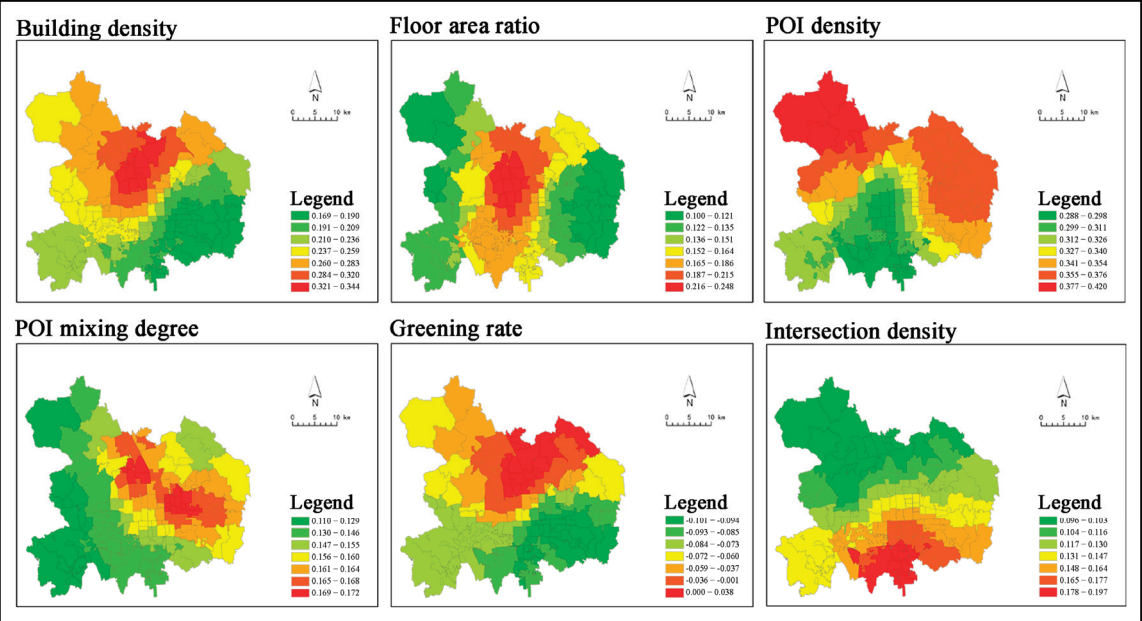**Figure 8.** Correlation between cultural vitality and built environment.

Figure 9. Correlation between comprehensive vitality and built environment.

4.2.1. Correlation between Social Vitality and Built Environment

SV exhibited significant positive correlations with four categories of environmental factors: floor area ratio, POI density, POI mixing degree, and metro station density. Conversely,

SV showed significant negative correlations with two categories of built environment factors: greening rate and distance from administrative center.

The strongest correlation was observed between SV and POI density, particularly pronounced in the northern part of the city, displaying a decreasing trend from north to south. The relationship between the floor area ratio and SV was consistently positive. However, it varied widely in standard deviation, with the highest correlations found in the western part of Xicheng District and the eastern part of Fengtai District, gradually diminishing outward from the BOT area. The correlation between POI mixing degree and SV, although weaker compared to POI density, was highest along the Qinghe Station–Beijing North Station corridor, decreasing gradually towards the surrounding areas. Negative correlations were observed between the greening rate and SV, with an increasing trend from the northeast region outward. The correlation between metro station density and SV was the weakest, declining from the northeast of Haidian District towards the south. The distance from the administrative center exhibited negative correlations with SV, with significantly lower associations in the eastern region compared to the western region. The highest correlation was observed in the southern part of Chaoyang District. In contrast, the lowest correlations were found in the western part of Fengtai District and the northern part of Chaoyang District.

4.2.2. Correlation between Economic Vitality and Built Environment

For EV, four influencing factors—floor area ratio, POI density, metro station density, and intersection density—exerted significant effects. Floor area ratio consistently correlated positively with EV, with the highest correlation observed in the BOT area and its immediate southern vicinity. This correlation followed an east–high to west–low trend along the central axis. POI density demonstrated the strongest association with EV, with the lowest correlation observed in the western and southern parts of BOT, indicating a radial increase from this center to the outer layers. Metro station density exhibited the weakest correlation with EV, showing a decreasing trend from east to west. Intersection density also showed a decreasing trend from southeast to northwest in its relationship with EV, highlighting the spatial distribution patterns affecting EV in these regions.

4.2.3. Correlation between Cultural Vitality and Built Environment

For CV, five influencing factors—building density, road network density, metro station density, intersection density, and distance from the administrative center—exerted significant effects. Building density exhibited the strongest association with CV, with the highest correlation observed in the northern part of Chaoyang District and the western part of the BOT area. This correlation gradually decreased from these two centers towards the periphery. Road network density showed a complex relationship with CV, displaying a negative association in the northwest region and a positive association in the southeast. This presented an increasing trend along the diagonal from northeast to southwest. Metro station density demonstrated the weakest correlation with CV, showing a positive association in the northwest region and negative associations in the east and south. There was a trend of increasing correlation along the diagonal from northeast to southwest. Intersection density correlated positively with CV, with the highest correlation observed in the southeastern part of the region adjacent to areas with the lowest correlation. Distance from the administrative center exhibited the highest correlation with CV in the northern part of Chaoyang District and a negative correlation in the northwest region, indicating a nuanced spatial relationship between CV and proximity to administrative center.

4.2.4. Correlation between Comprehensive Vitality and Built Environment

For COV, six influencing factors—building density, floor area ratio, POI density, POI mixing degree, greening rate, and intersection density—exerted significant effects. Except for the greening rate, all other factors exhibited positive associations with COV across all subdistricts. POI density emerged as the most closely associated factor with COV. The areas

around Shangzhuang in the northernmost part of the Haidian District and the Zizhuyuan Subdistrict in the northwest of the Second Ring Road showed the strongest correlations. In contrast, subdistricts outside the Fifth Ring Road in the southern part of Fengtai District exhibited the weakest correlations, with a decreasing trend from the northwest to the south. Building density showed generally higher correlations with COV in the west and lower correlations in the east. A series of moderately vital subdistricts were distributed along the G5 expressway and the western Second Ring Road, with areas in Shijingshan District having the highest correlation and areas around BOT having the lowest.

Additionally, some subdistricts in the northeastern part of Chaoyang District also exhibited high correlations. The floor area ratio showed the closest correlation with COV along the subdistricts around the north–south central axis of the city, gradually decreasing from the center towards the periphery. POI mixing degree exhibited the closest correlation with COV along the subdistricts from the Xiaoyue River to the Tonghui River, gradually decreasing towards the sides. The positive association between POI mixing degree and COV was generally higher in the east and lower in the west, with the highest correlation observed around BOT. The greening rate showed a trend of higher correlation in the south and lower in the north. Intersection density exhibited the weakest correlation with COV, generally showing a trend of higher correlation in the south and lower in the north.

5. Discussion

5.1. Determinants of Urban Vitality Spatial Distribution

Multi-source data enable more efficient evaluation of urban vitality for urban planners and policymakers [56]. SV is influenced by the aggregation of populations at different times of the day [57], resulting in a characteristic circular distribution pattern with higher concentrations in the center and lower concentrations towards the periphery. This aggregation is diverse, closely reflecting human activity patterns and displaying the strongest spatial autocorrelation across various city zones. EV, determined by nighttime light brightness, is closely tied to regional planning and industrial layout [58]. However, varied commercial districts in different regions lead to generally higher spatial clustering of EV compared to CV. CV, influenced by the distribution of cultural POIs, closely aligns with historical and cultural heritage, and is often prioritized in urban cultural heritage preservation plans [59]. Consequently, high-CV areas are concentrated in historically significant subdistricts. However, the more balanced distribution of cultural heritage in the BOT area results in relatively lower CV clustering, despite a higher number of cultural POIs. COV, constrained by green isolation area, exhibits significant differences within and outside the northeast Fourth Ring Road. This area's proximity to CV's high clusters suggests that EV alone does not determine urban COV.

Comparing the spatial distribution of the two types of vitality, SV better reflects the underlying circular symmetry of Beijing's central urban area, indicating that the traditional urban structure continues to influence contemporary human activity trends profoundly. Essential urban functions lay the foundation for SV, as Beijing's central urban area hosts crucial national functions such as politics, culture, international exchanges, and technological innovation. This leads to a more concentrated clustering of urban functional groups and, hence, more pronounced spatial aggregation of SV [33]. EV still exhibits significant disparities from the current economic spatial structure outlined in urban planning. The ten major urban fringe clusters in the modern urban area, such as Dongba, Fudingzhuang, and Fatou, designated in the "Master Plan", do not demonstrate prominent EVs in their vicinity. Instead, EVs remain reliant on early-developed commercial centers such as Chang'an Street and CBD. CV derives from three aspects of current urban planning: heritage preservation, industrial zone transformation, and infrastructure support. These aspects give rise to three constituent elements—historical and cultural heritage, modern cultural hubs, and cultural infrastructure—that collectively influence the layout of urban SV and EV. Consequently, CV's spatial arrangement is closely intertwined with the urban axis and the blue–green foundation.

5.2. Impact Mechanism of Built Environment on Urban Multidimensional Vitality

The floor area ratio significantly influences both SV and EV, reflecting the overall building height and scale of subdistricts. This provides ample space for constructing concentrated offices and large commercial complexes [60]. In Beijing, due to factors like cultural heritage preservation, the floor area ratio within the Second Ring Road is relatively low. Consequently, the capacity to accommodate people and economic activities is much less compared to areas outside the Second Ring Road, such as the CBD and Financial Street. The relationship between floor area ratio and EV varies across urban spaces, indicating differences in human activities between day and night. This confirms previous research by Xia et al. on land use intensity and urban vitality in Beijing [43]. Furthermore, contrary to the findings of Lu et al. [31], the correlation between COV and building density in Beijing's central urban area is positive. This discrepancy is related to the study's definition of COV, which underscores the complementarity between COV, SV, and EV.

Service outlets, indicated by POI density, have a significant impact on Beijing's EV. Higher POI density reflects the dense aggregation of commercial service outlets, whereas more extensive residential and public service facilities result in lower POI density [61]. A high POI mixing degree indicates greater functional diversity, which is essential for high vitality. However, excessive richness and randomness can hinder urban vitality, aligning with previous research findings [62,63]. Regarding blue–green spaces, the greening rate has a suppressive effect on both SV and EV, showing that these spaces accommodate fewer people compared to built environments. Larger green spaces typically represent lower land development intensity, which is not conducive to large-scale commercial activities within these areas. However, they can enhance the quality of the surrounding built environment [64]. The Olympic Forest Park, for instance, has positively impacted the overall vitality of surrounding subdistricts, highlighting the potential positive role of urban blue–green spaces in densely populated areas.

In terms of accessibility, high intersection density offers diverse walking options, promoting business emergence and efficient service provision for cultural facilities [65]. However, the relationship between COV and intersection density in Beijing's central urban area does not match, suggesting that measuring COV at more minor street block scales is challenging, consistent with Liu et al.'s findings on Shanghai's comprehensive vitality [40]. Metro station density indicates public transportation accessibility, facilitating population aggregation [66]. However, high land values near metro stations prioritize commercial development over small-to-medium-sized cultural facilities, negatively impacting CV.

Finally, the suppression of SV by the distance from the administrative center reflects a decreasing population aggregation pattern in Beijing. Despite a high density of cultural facilities in historical and cultural districts, the central urban area of Beijing needs to exhibit a comparative advantage in cultural facility density. Regions such as the area between the Second and Fourth Ring Roads in the northwest, and subdistricts like Yongdinglu and Jiuxianqiao outside the Fourth Ring Road, show higher CV despite their distance from Tiananmen Square. This results in a negative correlation between CV and the distance from the administrative center.

5.3. Promotion Strategy

In the future, spatial planning should continue to rely on the radiating effect of high-vitality subdistricts in the east and west to optimize the population distribution structure in Beijing's central area. This can be achieved by upgrading the POI mixing degree and increasing metro station density in areas outside the Third Ring Road, such as the Western Third Ring Road, Western Fourth Ring Road, and areas beyond the Eastern Fourth Ring Road to enhance population aggregation. Additionally, EVs in commercial districts such as Zhongguancun and the "Sanyuanqiao–Wangjing" area can be enhanced through improvements in POI density, walkability, and environmental quality. Leveraging the economic influence of financial districts and CBD along Chang'an Street can help achieve balanced development of economic centers in different directions within Beijing's

central area. Furthermore, there should be a focus on enhancing cultural facilities in the southern area of ZhuShiKou, as well as the northern, eastern, and southwestern areas between the Second and Fourth Ring Roads to promote the synergistic development of economy and culture in the eastern CBD area. Based on the distribution characteristics of various types of vitality, the study also found that the north–south central axis, Chang'an Street, the Grand Canal (from Kunming Lake to Tonghui River), and the urban express ring road play important structural roles in facilitating different types of vitality. Therefore, it is recommended to strengthen the connection and radiating effect of these critical urban structures in urban planning and layout.

In terms of spatial design, to effectively promote urban vitality in Beijing's central area, urban planners should prioritize pedestrian-friendly environments and mixed-use developments [67]. This includes designing well-connected street networks that enhance walkability and community interaction, and accommodating users of all ages and abilities through thoughtful sidewalk layouts and traffic-calming measures [68]. Enhancing neighborhood aesthetics with landscape design and lighting encourages nighttime walking, while integrating residential, commercial, and recreational activities reduces reliance on motorized transport [69]. Additionally, improving access to parks and recreational facilities fosters community vitality [70]. Tailoring specific measures to the unique urban fabric of each area is essential, from increasing service outlets in BOT areas to refining pedestrian environments in historic neighborhoods and micro-updating methods like clearing occupied roads, ensuring the smooth operation of national administrative departments, and protecting cultural heritage sites [71]. For other areas, full consideration should be given to public suggestions. Through collaborative development, redevelopment approaches, and targeted renewal measures, the efficiency of both above-ground and underground spaces should be improved. This can be achieved by maximizing the utilization of ground-floor spaces of buildings along streets to increase the number and diversity of commercial facilities, while also focusing on enhancing the pedestrian environment and connectivity of urban streets at all levels. Attention should be paid to the balance between green space and construction intensity. Efforts should be directed towards improving the ecological environment through vertical greening, three-dimensional greening, and green micro-updating methods, among others, to ensure a balanced development of the built environment.

5.4. Limitations

This study has several limitations that should be acknowledged. In terms of data acquisition, our study utilized heat maps from a regular weekday and a weekend day within a week to depict social vitality. In future research, it will be essential to collect data over more days and different seasons to avoid the limitations posed by seasonal differences and an insufficient number of days. Additionally, enriching the types of data used in the study is crucial. We will integrate survey and interview data, as well as mobile signaling data, to explore the comprehensive distribution of urban social vitality. Furthermore, our method of portraying economic vitality is constrained by the scale of our study units and the inherent inaccuracies of using nighttime light data as an economic proxy. Moving forward, research endeavors could enhance this method by amalgamating data on the density of operational restaurants, the count of commercial establishments, and other pertinent metrics to offer a more holistic depiction of regional economic vitality [72,73]. In terms of scale, although focusing on subdistricts facilitates direct alignment with grassroots administrative units, it may need to clearly identify localized high-vitality areas, especially for larger subdistricts. Subsequent research could benefit from juxtaposing subdistricts with smaller-scale grid data to address this issue. Regarding dimensionality, the study should have considered the issue of the mixture of old and new buildings mentioned by Jacobs, thus overlooking the impact of environmental history on vitality. Additionally, in terms of accuracy, Beijing's rich urban history results in significant textural differences across different regions, suggesting the possibility of conducting classification discussions in future research.

6. Conclusions

This study offered urban planners and policymakers an efficient framework for evaluating urban vitality, particularly in the culturally rich central districts of Beijing, through its innovative use of multi-source data. By analyzing 133 subdistricts, the research integrated socioeconomic and cultural metrics, and employed bivariate spatial autocorrelation analysis to examine the distribution patterns of social, economic, and cultural vigor. The findings confirmed a previously hypothesized weak correlation between urban vitality and development intensity. Significant spatial clustering of various types of urban vitality was observed, with the most pronounced clustering found in overall vitality, followed by social, cultural, and economic vitality. This underscored the existence of distinct population, economic, and cultural centers within Beijing's urban space. High social vitality was mainly correlated with the central city areas outlined in the master plan, forming a notable "n"-shaped distribution around the Second Ring Road. Economic vitality centered around the CBD and commercial hubs along Chang'an Avenue, while cultural vitality exhibited a northwest–southeast distribution. Interestingly, the overall vitality displayed a concentric distribution that decreased from the urban center to the peripheries, influenced by political, cultural, and historical elements in the center, and by urban greening efforts in the outer areas. Furthermore, the study highlighted the built environment's substantial influence on urban vitality. Factors such as floor area ratio, POI density, diversity, and intersection density were crucial in fostering an environment conducive to urban vitality. Additional influences included population density, metro station proximity, and specific locational attributes, with green space ratios moderating high vitality zones. Overall, the study indicated a balanced spatial development of urban vitality across Beijing, providing valuable insights for future urban development initiatives.

References

1. Botta, F.; Gutiérrez-Roig, M. Modelling urban vibrancy with mobile phone and OpenStreetMap data. *PLoS ONE* **2021**, *16*, e0252015. [CrossRef] [PubMed]
2. Montgomery, J. Making a city: Urbanity, vitality and urban design. *J. Urban Des.* **1998**, *3*, 93–116. [CrossRef]
3. Xie, R.; Yao, S.; Han, F.; Zhang, Q. Does misallocation of land resources reduce urban green total factor productivity? An analysis of city-level panel data in China. *Land Use Policy* **2022**, *122*, 106353. [CrossRef]
4. Batty, M. Empty buildings, shrinking cities and ghost towns. *Environ. Plan. B Plan. Des.* **2016**, *43*, 3–6. [CrossRef]
5. Deng, C.; Ma, J. Viewing urban decay from the sky: A multi-scale analysis of residential vacancy in a shrinking US city. *Scape Urban Plan.* **2015**, *141*, 88–99. [CrossRef]
6. Huang, Z.; He, C.; Zhu, S. Do China's economic development zones improve land use efficiency? The effects of selection, factor accumulation and agglomeration. *Landsc. Urban Plan.* **2017**, *162*, 145–156. [CrossRef]
7. Landry, C. Urban vitality: A new source of urban competitiveness. *Archis* **2000**, *12*, 8–13.
8. Wu, J.; Ta, N.; Song, Y.; Lin, J.; Chai, Y. Urban form breeds neighborhood vibrancy: A case study using a GPS-based activity survey in suburban Beijing. *Cities* **2018**, *74*, 100–108. [CrossRef]
9. Delclòs-Alió, X.; Gutiérrez, A.; Miralles-Guasch, C. The urban vitality conditions of Jane Jacobs in Barcelona: Residential and smartphone-based tracking measurements of the built environment in a Mediterranean metropolis. *Cities* **2019**, *86*, 220–228. [CrossRef]

10. Marquet, O.; Miralles-Guasch, C. Neighbourhood vitality and physical activity among the elderly: The role of walkable environments on active ageing in Barcelona, Spain. *Soc. Sci. Med.* **2015**, *135*, 24–30. [CrossRef]
11. Huang, X.; Jiang, P.; Li, M.; Zhao, X. Applicable Framework for Evaluating Urban Vitality with Multiple-Source Data: An Empirical Research of the Pearl River Delta Urban Agglomeration by Using Bpnn. *Land* **2022**, *11*, 1901. [CrossRef]
12. Li, X.; Li, Y.; Jia, T.; Zhou, L.; Hijazi, I.H. The six dimensions of built environment on urban vitality: Fusion evidence from multi-source data. *Cities* **2022**, *121*, 103482. [CrossRef]
13. Jacobs, J. *The Death and Life of Great American Cities*; Random House: New York, NY, USA, 1961.
14. Lynch, K. *Good City Form*; The MIT Press: Cambridge, UK, 1984.
15. Maas, P.R. *Towards a Theory of Urban Vitality*; University of British Columbia: Vancouver, BC, USA, 1984.
16. Chen, Y.; Yu, B.; Shu, B.; Yang, L.; Wang, R. Exploring the spatiotemporal patterns and correlates of urban vitality: Temporal and spatial heterogeneity. *Sustain. Cities Soc.* **2023**, *91*, 104440. [CrossRef]
17. Delclòs-Alió, X.; Miralles-Guasch, C. Looking at Barcelona through Jane Jacobs's eyes: Mapping the basic conditions for urban vitality in a Mediterranean conurbation. *Land Use Policy* **2018**, *75*, 505–517. [CrossRef]
18. Kim, Y.-L. Seoul's Wi-Fi hotspots: Wi-Fi access points as an indicator of urban vitality. *Comput. Environ. Urban Syst.* **2018**, *72*, 13–24. [CrossRef]
19. Jin, X.; Long, Y.; Sun, W.; Lu, Y.; Yang, X.; Tang, J. Evaluating cities' vitality and identifying ghost cities in China with emerging geographical data. *Cities* **2017**, *63*, 98–109. [CrossRef]
20. Gehl, J. *Life between Buildings: Using Public Space*; Island Press: Washington, DC, USA, 1971.
21. Ye, Y.; Zeng, W.; Shen, Q.; Zhang, X.; Lu, Y. The visual quality of streets: A human-centred continuous measurement based on machine learning algorithms and street view images. *Environ. Plan. B Urban Anal. City Sci.* **2019**, *46*, 1439–1457. [CrossRef]
22. Li, X.; Liu, H. The Influence of Subjective and Objective Characteristics of Urban Human Settlements on Residents' Life Satisfaction in China. *Land* **2021**, *10*, 1400. [CrossRef]
23. Zumelzu, A.; Barrientos-Trinanes, M. Analysis of the effects of urban form on neighborhood vitality: Five cases in Valdivia, Southern Chile. *J. Hous. Built Environ.* **2019**, *34*, 897–925. [CrossRef]
24. Sallis, J.F.; Cerin, E.; Conway, T.L.; Adams, M.A.; Frank, L.D.; Pratt, M.; Salvo, D.; Schipperijn, J.; Smith, G.; Cain, K.L. Physical activity in relation to urban environments in 14 cities worldwide: A cross-sectional study. *Lancet* **2016**, *387*, 2207–2217. [CrossRef]
25. Wu, C.; Ye, X.; Ren, F.; Du, Q. Check-in behaviour and spatio-temporal vibrancy: An exploratory analysis in Shenzhen, China. *Cities* **2018**, *77*, 104–116. [CrossRef]
26. Chen, L.; Zhao, L.; Xiao, Y.; Lu, Y. Investigating the spatiotemporal pattern between the built environment and urban vibrancy using big data in Shenzhen, China. *Comput. Environ. Urban Syst.* **2022**, *95*, 101827. [CrossRef]
27. Yang, J.; Cao, J.; Zhou, Y. Elaborating non-linear associations and synergies of metro access and land uses with urban vitality in Shenzhen. *Transp. Res. Part A Policy Pract.* **2021**, *144*, 74–88. [CrossRef]
28. Fan, Z.; Duan, J.; Luo, M.; Zhan, H.; Liu, M.; Peng, W. How Did Built Environment Affect Urban Vitality in Urban Waterfronts? A Case Study in Nanjing Reach of Yangtze River. *ISPRS Int. J. Geo-Inf.* **2021**, *10*, 611. [CrossRef]
29. Liu, S.; Lai, S.-Q.; Liu, C.; Jiang, L. What influenced the vitality of the waterfront open space? A case study of Huangpu River in Shanghai, China. *Cities* **2021**, *114*, 103197. [CrossRef]
30. Huang, B.; Zhou, Y.; Li, Z.; Song, Y.; Cai, J.; Tu, W. Evaluating and characterizing urban vibrancy using spatial big data: Shanghai as a case study. *Environ. Plan. B Urban Anal. City Sci.* **2020**, *47*, 1543–1559. [CrossRef]
31. Lu, S.; Shi, C.; Yang, X. Impacts of built environment on urban vitality: Regression analyses of Beijing and Chengdu, China. *Int. J. Environ. Res. Public Health* **2019**, *16*, 4592. [CrossRef] [PubMed]
32. Tu, W.; Zhu, T.; Xia, J.; Zhou, Y.; Lai, Y.; Jiang, J.; Li, Q. Portraying the spatial dynamics of urban vibrancy using multisource urban big data. *Comput. Environ. Urban Syst.* **2020**, *80*, 101428. [CrossRef]
33. Li, Q.; Cui, C.; Liu, F.; Wu, Q.; Run, Y.; Han, Z. Multidimensional urban vitality on streets: Spatial patterns and influence factor identification using multisource urban data. *ISPRS Int. J. Geo-Inf.* **2021**, *11*, 2. [CrossRef]
34. Shi, J.; Miao, W.; Si, H.; Liu, T. Urban Vitality Evaluation and Spatial Correlation Research: A Case Study from Shanghai, China. *Land* **2021**, *10*, 1195. [CrossRef]
35. He, Q.; He, W.; Song, Y.; Wu, J.; Yin, C.; Mou, Y. The impact of urban growth patterns on urban vitality in newly built-up areas based on an association rules analysis using geographical 'big data'. *Land Use Policy* **2018**, *78*, 726–738. [CrossRef]
36. Qin, L.; Zong, W.; Peng, K.; Zhang, R. Assessing Spatial Heterogeneity in Urban Park Vitality for a Sustainable Built Environment: A Case Study of Changsha. *Land* **2024**, *13*, 480. [CrossRef]
37. Liu, L.; Dong, Y.; Lang, W.; Yang, H.; Wang, B. The Impact of Commercial-Industry Development of Urban Vitality: A Study on the Central Urban Area of Guangzhou Using Multisource Data. *Land* **2024**, *13*, 250. [CrossRef]
38. Liu, H.; Li, X. Understanding the Driving Factors for Urban Human Settlement Vitality at Street Level: A Case Study of Dalian, China. *Land* **2022**, *11*, 646. [CrossRef]
39. Zhe, C.; Ma, S. Research on the Vitality of Urban Streets. *Archit. J.* **2009**, *S2*, 121–126.
40. Liu, D.; Shi, Y. The Influence Mechanism of Urban Spatial Structure on Urban Vitality Based on Geographic Big Data: A Case Study in Downtown Shanghai. *Buildings* **2022**, *12*, 569. [CrossRef]
41. Ye, Y.; Li, D.; Liu, X. How block density and typology affect urban vitality: An exploratory analysis in Shenzhen, China. *Urban Geogr.* **2018**, *39*, 631–652. [CrossRef]

42. Wang, X.; Zhang, Y.; Yu, D.; Qi, J.; Li, S. Investigating the spatiotemporal pattern of urban vibrancy and its determinants: Spatial big data analyses in Beijing, China. *Land Use Policy* **2022**, *119*, 106162. [CrossRef]

43. Xia, C.; Yeh, A.G.-O.; Zhang, A. Analyzing spatial relationships between urban land use intensity and urban vitality at street block level: A case study of five Chinese megacities. *Landsc. Urban Plan.* **2020**, *193*, 103669. [CrossRef]

44. Gibson, J.; Olivia, S.; Boe-Gibson, G.; Li, C. Which night lights data should we use in economics, and where? *J. Dev. Econ.* **2021**, *149*, 102602. [CrossRef]

45. Cervero, R.; Kockelman, K. Travel demand and the 3Ds: Density, diversity, and design. *Transp. Res. Part D Transp. Environ.* **1997**, *2*, 199–219. [CrossRef]

46. Ewing, R.; Cervero, R. Travel and the built environment: A synthesis. *Transp. Res. Rec.* **2001**, *1780*, 87–114. [CrossRef]

47. Gómez-Varo, I.; Delclòs-Alió, X.; Miralles-Guasch, C. Jane Jacobs reloaded: A contemporary operationalization of urban vitality in a district in Barcelona. *Cities* **2022**, *123*, 103565. [CrossRef]

48. Zhang, A.; Li, W.; Wu, J.; Lin, J.; Chu, J.; Xia, C. How can the urban landscape affect urban vitality at the street block level? A case study of 15 metropolises in China. *Environ. Plan. B Urban Anal. City Sci.* **2021**, *48*, 1245–1262. [CrossRef]

49. Zhang, K.; Sun, P. A Study on the Adjustment of Primary-Level Administrative Divisions in the Context of Urbanization: On the Basis of the Practice of Regional Offices in Beijing. *J. Beijing Adm. Inst.* **2022**, *4*, 18–24.

50. Tian, G.; Wu, J.; Yang, Z. Spatial pattern of urban functions in the Beijing metropolitan region. *Habitat Int.* **2010**, *34*, 249–255. [CrossRef]

51. Li, X.; Zhao, L.; Li, D.; Xu, H. Mapping urban extent using Luojia 1-01 nighttime light imagery. *Sensors* **2018**, *18*, 3665. [CrossRef]

52. Montalto, V.; Moura, C.J.T.; Langedijk, S.; Saisana, M. Culture counts: An empirical approach to measure the cultural and creative vitality of European cities. *Cities* **2019**, *89*, 167–185. [CrossRef]

53. Yue, Y.; Zhuang, Y.; Yeh, A.G.; Xie, J.-Y.; Ma, C.-L.; Li, Q.-Q. Measurements of POI-based mixed use and their relationships with neighbourhood vibrancy. *Int. J. Geogr. Inf. Sci.* **2017**, *31*, 658–675. [CrossRef]

54. Zhang, J.; Zhang, K.; Zhao, F. Research on the regional spatial effects of green development and environmental governance in China based on a spatial autocorrelation model. *Struct. Change Econ. Dyn.* **2020**, *55*, 1–11. [CrossRef]

55. Torun, A.Ö.; Göçer, K.; Yeşiltepe, D.; Argın, G. Understanding the role of urban form in explaining transportation and recreational walking among children in a logistic GWR model: A spatial analysis in Istanbul, Turkey. *J. Transp. Geogr.* **2020**, *82*, 102617. [CrossRef]

56. Niu, H.; Silva, E.A. Crowdsourced data mining for urban activity: Review of data sources, applications, and methods. *J. Urban Plan. Dev.* **2020**, *146*, 04020007. [CrossRef]

57. Mouratidis, K.; Poortinga, W. Built environment, urban vitality and social cohesion: Do vibrant neighborhoods foster strong communities? *Landsc. Urban Plan.* **2020**, *204*, 103951. [CrossRef]

58. Zhang, Y.; Shang, K.; Shi, Z.; Wang, H.; Li, X. Spatial pattern of the vitality of Chinese characteristic towns: A perspective from nighttime lights. *Land* **2022**, *11*, 85. [CrossRef]

59. Yan, W.-J.; Liu, S.-T. Built Equality and Sustainable Urban Cultural Space: A Case Study of Quanzhou, China. *Buildings* **2023**, *13*, 2337. [CrossRef]

60. Belmiro, C.; Neto, R.d.M.S.; Barros, A.; Ospina, R. Understanding the land use intensity of residential buildings in Brazil: An ensemble machine learning approach. *Habitat Int.* **2023**, *139*, 102896. [CrossRef]

61. Huang, C.; Xiao, C.; Rong, L. Integrating point-of-interest density and spatial heterogeneity to identify urban functional areas. *Remote Sens.* **2022**, *14*, 4201. [CrossRef]

62. Lan, F.; Gong, X.; Da, H.; Wen, H. How do population inflow and social infrastructure affect urban vitality? Evidence from 35 large-and medium-sized cities in China. *Cities* **2020**, *100*, 102454. [CrossRef]

63. Liu, S.; Zhang, L.; Long, Y. Urban vitality area identification and pattern analysis from the perspective of time and space fusion. *Sustainability* **2019**, *11*, 4032. [CrossRef]

64. Chen, Y.; Xu, Z.; Byrne, J.; Xu, T.; Wang, S.; Wu, J. Can smaller parks limit green gentrification? Insights from Hangzhou, China. *Urban For. Urban Green.* **2021**, *59*, 127009. [CrossRef]

65. Long, Y.; Huang, C. Does block size matter? The impact of urban design on economic vitality for Chinese cities. *Environ. Plan. B Urban Anal. City Sci.* **2019**, *46*, 406–422. [CrossRef]

66. Li, S.; Lyu, D.; Huang, G.; Zhang, X.; Gao, F.; Chen, Y.; Liu, X. Spatially varying impacts of built environment factors on rail transit ridership at station level: A case study in Guangzhou, China. *J. Transp. Geogr.* **2020**, *82*, 102631. [CrossRef]

67. Balsas, C.J. Exciting walk-only precincts in Asia, Europe and North-America. *Cities* **2021**, *112*, 103129. [CrossRef]

68. Christiansen, L.B.; Cerin, E.; Badland, H.; Kerr, J.; Davey, R.; Troelsen, J.; van Dyck, D.; Mitáš, J.; Schofield, G.; Sugiyama, T.; et al. International comparisons of the associations between objective measures of the built environment and transport-related walking and cycling: IPEN adult study. *J. Transp. Health* **2016**, *3*, 467–478. [CrossRef] [PubMed]

69. Morris, J.; Colombo, S.; Angus, A.; Parsons, D.; Brawn, M.; Stacey, K.; Hanley, N. The value of public rights of way: A choice experiment in Bedfordshire, England. *Landsc. Urban Plan.* **2009**, *93*, 83–91. [CrossRef]

70. Mu, B.; Liu, C.; Mu, T.; Xu, X.; Tian, G.; Zhang, Y.; Kim, G. Spatiotemporal fluctuations in urban park spatial vitality determined by on-site observation and behavior mapping: A case study of three parks in Zhengzhou City, China. *Urban For. Urban Green.* **2021**, *64*, 127246. [CrossRef]

71. Tian, M.; Li, Z.; Xia, Q.; Peng, Y.; Cao, T.; Du, T.; Xing, Z. Walking in China's historical and cultural streets: The factors affecting pedestrian walking behavior and walking experience. *Land* **2022**, *11*, 1491. [CrossRef]

72. Xia, C.; Zhang, A.; Yeh, A.G. The varying relationships between multidimensional urban form and urban vitality in Chinese megacities: Insights from a comparative analysis. *Ann. Am. Assoc. Geogr.* **2022**, *112*, 141–166. [CrossRef]

73. Fan, Y.; Kuang, D.; Tu, W.; Ye, Y. Which Spatial Elements Influence Waterfront Space Vitality the Most?—A Comparative Tracking Study of the Maozhou River Renewal Project in Shenzhen, China. *Land* **2023**, *12*, 1260. [CrossRef]

Article

The Improving of Sky Gardens' Environmental Quality from a Health Promotion Perspective

Yan Li [1] and Hongwu Du [2,3,*]

[1] College of Architecture and Urban Planning, Tongji University, Shanghai 200092, China; 23310340@tongji.edu.cn
[2] School of Architecture, South China University of Technology, Guangzhou 510641, China
[3] State Key Laboratory of Subtropical Building and Urban Science, Guangzhou 510641, China
[*] Correspondence: hongwudu@scut.edu.cn

Abstract: The quality of landscape space directly influences public health behaviors, making public assessments of the qualities of the sky garden landscape crucial for optimizing it. This article focuses on three types of typical high-rise building sky garden (plaza-park, rest-stay, and move-pass type) and establishes an evaluation framework for their health promotion characteristics (24 indicators in 7 dimensions) based on existing restorative environment research. Then, questionnaires (354 valid responses) and quantitative calculations were employed to assess the public's perception of demand in health behaviors and the spatial supply of different sky garden types. Ultimately, the data were processed to propose targeted interventions and recommendations to enhance health benefits using the comprehensive importance-performance analysis method. The results show the following: (1) The public seems to have widely accepted sky gardens in the context of high-density urban environments (near 6.92, below the mean of 7.09). They place greater emphasis on spatial indicators that cater to relaxation activities and show heightened sensitivity toward public facilities (7.32–8.00) that contribute to physical and mental health-related activities. (2) The health promotion performance of different types of sky garden shows significant variation, with the rest-stay sky gardens at the embodied scale demonstrating the greatest competitive advantage. (3) The development of sky gardens has significant potential, and different types of sky garden need to specifically lever-age their characteristics as complementary public spaces.

Keywords: sky gardens; health promotion; importance-performance analysis; high-density environment; sustainable healthy living environment

1. Introduction

1.1. Background of the Study

Urbanization is an evolutionary process in which human beings seek survival and development and expand the use of space. The high density of the urban environment is the result of population explosion and realistic choice under urbanization [1]. A large number of studies have confirmed that natural landscapes and open spaces have health promotion effects such as relieving stress, improving mood, and enhancing cognitive abilities [2,3]. However, high-density urban spaces greatly limit the exposure of urban residents to ground-level green environments [4–6]. Therefore, exploring the complex relationship between the spatial environment and the public's physical and psychological health in a high-density urban environment is one of the important issues facing current research and practice in high-rise buildings. Sky gardens, as important natural environments in high-rise buildings, have become potential resources for nature-based solutions in urban environments [7], and it is important to explore their health promotion.

Sky gardens are the contemporary interpretation of Le Corbusier's concept of "streets in the sky" [8] and are one of the most important components of urban green infrastructures [9]. Existing studies confirm the sustainability value of sky gardens and the role of

complementing ground-level green spaces [10–12] by integrating the public realm, natural landscapes, and community facilities in high-rise buildings [13]. Compared to parks, green spaces, and other public spaces, sky gardens are mostly privately owned public spaces [6], and it is relatively difficult to measure and evaluate the difference between the supply and demand of their spatial health quality. However, there is some consistency in health-promoting environmental factors, and restorative environment research provides a feasible angle for studying the relationship between sky gardens and human well-being [14].

Schröpfer Thomas et al. systematically investigated the integration of green spaces in buildings among contemporary architecture and urban design practice through a series of international in-depth case studies, producing new typologies for high-density environments that include public spaces, sky terraces, sky bridges, vertical parks, roof gardens, and other 'green' components [15]. Notwithstanding, it is evident that most studies concerning people's satisfaction with health promotion in sky gardens are usually conducted in more advanced countries, especially Singapore [8,16,17]. Again, such studies have extensively reported the environmental, social, urban, architectural, and economic benefits of large-scale, urban-iconic sky gardens, such as rooftop gardens and podium gardens [4,5,8,10,17–21]. To a certain extent, the small-scale and other functions of sky gardens scattered in high-rise buildings, such as sky courtyards, sky terraces, and sky-bridges, have been neglected. Therefore, for policymakers and planners, it is necessary to accurately understand the public demand for different types of sky garden in order to propose targeted health-promoting planning and design strategies to better meet the public's cognition and demand preferences for sky gardens, especially for sky gardens that are widely scattered within high-rise buildings and at small-to-medium scales.

Importance-performance analysis (IPA) is a measure that has been gradually introduced into the management of natural and built environments to understand the difference between public expectations and their experience [22]. The method is based on the collected survey data and the calculation and comparison of performance and importance scores of different variables to discover the potential strengths and weaknesses of the services and to prioritize their development [23]. Studying public perceptions of health promotion in sky gardens can help policymakers and planners to properly understand the relationship between people and the environment, rather than separately studying human activities or environmental factors [24]. In turn, a better understanding and experience of sky gardens can encourage people to support and participate in various public affairs related to sky gardens [8,17].

1.2. Literature Review

1.2.1. Trends and Transformations

Design with nature is a classic topic in the field of urban design [25]. Since the 1960s, massive urban renewal movements have attracted much attention and reflection, and urbanists, landscape architects, and others have begun to explore the construction of urban habitats centered on human experience and perception [26–31]. The concept of "natural environmental health promotion" can be traced back to Ian McHarg's *The Place of Nature in The City of Man* [26], which suggests the need to critically examine the place of nature in the city, and fully utilize it to provide well-being benefits for city dwellers and improve the qualities of the urban environment. It echoes previous thinkers concerned with urban issues, such as Ebenezer Howard's garden cities of tomorrow [29], Frederick Law Olmsted's city park movement [30], and Patrick Geddes's comprehensive vision of nature in urban planning [31].

European countries began to explore the development path of green urbanism in the 1990s, influenced by urban issues and diseases caused by urbanization and industrialization, and by the ideas and methods of ecologism that design with nature. Vertical green spaces, such as rooftop greening, living gardens, sky terraces, green walls, and urban farms [32] have become important extensions of urban green infrastructures, and their proportion in cities has been gradually increasing by space flexibility and healthiness,

the closeness with people's daily lives, and the iconicity in spatial form [33]. Recently, researchers and scholars have found that vertical green spaces have great potential for physical and psychological health promotion [14]. They have also called for associating wellness environments with people's daily lives in order to promote more social interaction and enhance the belonging of space [8,17], thus reaching harmonious coexistence between high-density and green environments [15]. Green urbanism is one of the ideal models to alleviate urban problems, promote public health, improve urban ecology, and achieve sustainable urban development [34]. Green urbanism in highly dense urban environments has more important reality and practicability.

Compact cities and high-intensity development and construction have intensified, and the densification of the urban environment has accelerated the shift of public space from the ground to the sky. Sky gardens, as part of the urban green infrastructure in densified cities [5,35], are gradually forming a paradigm of compact open green spaces with a mix of density and natural and social spaces [15]. Sky gardens have become transitional and social spaces in high-rise buildings with the characteristics of spatial flexibility, functional diversity, and composite value [36]. This not only vertically divides the different vertical areas of high-rise buildings [37] but also meets the increasing demand for public space and the health promotion of users [8]. In high-density urban environments, sky gardens have gradually attracted attention and are widely established [7,38]. It has become the key element in building livable and resilient urban environments through reducing harm (e.g., air pollution, noise), restoring capacities (e.g., attention restoration, physiological stress relief), and building capacities (e.g., physical activity, social cohesion) [39]. Sky gardens have grown exponentially with the incentives of sustainable development and privately open public spaces (POPS), and with the strong promotion of architects they have shown various potential in compact urban environments [40]. Also, the lack of urban green space due to different drivers, such as urban intensification, has accelerated the process of implementing sky gardens and other vertical green spaces [41]. Indeed, the greening of buildings through vertical green spaces might well develop into one of the major architectural movements of the twenty-first century, and, in times to come, become a norm rather than a trend [32].

1.2.2. Spatial Features for Health Promotion

Health promotion research in built environments has been receiving academic attention for a long time, and spatial features have been extensively studied from multiple perspectives, including physiological, psychological, emotional, and cognitive ones. To understand the key elements of sky gardens for health promotion, this study takes reference from the dominant theories of restorative environment research—the attention restoration theory (ART) and the stress reduction theory (SRT) of restorative environment research [42,43]. The specific restorative factors are key to the fulfillment of restorative effects [44]. The restorative properties in different dimensions are fulfilled by stimulating positive emotions, reducing stress and distraction, and providing social support [33,39]. In addition, preference is strongly associated with judgments of restoration likelihood [45]. Therefore, the literature on preferences for built environments can guide the identification of physical attributes that affect restorative experience.

Humans have innate or evolved preferences for nature [46], which is one of the basic psychological demands of human beings [47]. The positive restorative effects of green vegetation on emotions, cognition, and mental health were already confirmed in the 1970s [48–50]. Natural elements relieve human physiological stress through visual–emotional responses [51], and viewing greenery alone also has positive effects on mood and performance [52], helping to alleviate visual fatigue in workspaces. Water features are also seen as a positive restorative component, and people prefer to be in water-rich areas to relieve stress [53], which positively affects their emotional status [54]. In addition to natural and water elements, other recreational infrastructures are also important for the public in relation to psychological restoration: sport facilities and pathways, playgrounds, sitting

features, lighting, drinking fountains and swimming areas, and silence and tranquility areas [55,56]. Furthermore, spatial forms have an important influence on spatial preferences, such as void-to-solid ratio (VSR), the scale of green space. There is an inverted U-shaped relationship between preference and the spatial VSR [57]; large-scale green spaces have visually broad views [58] and city residents are also willing to pay for housing with more green space [59]. Therefore, natural elements, water features and landscapes, public facilities, and form features are important dimensions to explore the health-promoting effects of the internal environment in sky gardens.

Some scholars have further explored the external supportive effects that influence the health-promoting experience of spatial environments. Studies have found that sky gardens are widely distributed in urban centers [16]. Central urban areas have high inclusiveness, overtime openness, and physical and visual accessibility [60], which provide activity support for the health-promoting experiences of accessing sky gardens. High-quality urban environments are more likely to attract the public to visit the adjacent public space, with increased accessibility, activity numbers, duration, and range of use [61], thus further enhancing the health promotion potential of sky gardens. Skyscape is one of the external environmental features perceived by the public in the internal environment of sky gardens [16], and distant skyscapes positively influence emotional states [62]. Skyscape-evoked restorative ratings are like those for ground-level spaces with street trees, but the most restorative and popular are those with the most sky [63]. High-rise buildings are an important carrier for the development of sky gardens in high-density cities [4,5,40], and there are potential impacts on the performance of sky gardens' health benefits. In contrast, people expect more open space in high-rise buildings with high floor area ratio (FAR) to satisfy their needs for rest and recreation [6]. Building height, outlines [64], spatial configuration, and layout [65] can also affect the fulfillment of health promotion, especially for stressed individuals. Therefore, the skyscape is an extension of the internal environment, the high-rise building is the carrier of sky gardens, and the surrounding urban environment encourages participation in activities that support accessing the health-promoting experience in sky gardens; these are important dimensions for exploring the analysis of the external environment of sky gardens for public health promotion.

1.3. Aim and Research Questions

The quality of landscape space directly influences public health behaviors, and sky garden spatial characteristics fulfill certain aspects of the public's health needs in high-density cities. Health perception assessments from the public, who experience the sky garden landscape, are crucial for optimizing the qualities of sky gardens. Numerous studies have extensively investigated the possibilities of health promotion in natural environments and urban public spaces [48–50]. However, most of the studies on sky gardens focus on only one or two dimensions [8,17,18,66] and lack a comprehensive framework to integrate people's multidimensional perceptions to assess the difference between the supply of and the demand for the health promotion qualities of sky gardens.

The objective of this study is to investigate the demand and supply of the health promotion qualities of sky gardens in high-rise buildings. It is hypothesized that health promotion demand and supply are influenced by the type of sky garden. This study seeks to answer the following research questions:

(1) What are the perceived needs for health promotion in sky gardens by the public?
(2) What are the differences in the health promotion supply status across different types of sky garden?
(3) What are the focuses of interventions for health promotion in different types of sky garden?

2. Methodology

We developed a comprehensive quantitative framework for assessing the difference between supply and demand for health promotion qualities in sky gardens (Figure 1). For

this reason, we measure the quality of sky gardens in seven dimensions: the surrounding environment, high-rise, skyscape, geometric form, greenscape, waterscape, and public facility. The analysis content mainly includes the following four parts: (1) Identifying the types of sky garden and typical cases based on previous studies (3 types, 12 sky gardens); (2) Clarifying the environmental characteristics affecting health promotion in sky gardens and the calculation method (7 dimensions, 24 indicators); (3) Collecting data on the demand (importance) and supply (performance) characteristics of health promotion in sky gardens through questionnaire surveys (354 valid responses) and quantitative analysis (288 spatial data); (4) Importance-expression analysis to compare the differences in the demand and supply of various types of sky garden, and targeted development recommendations for the optimization of the indicators.
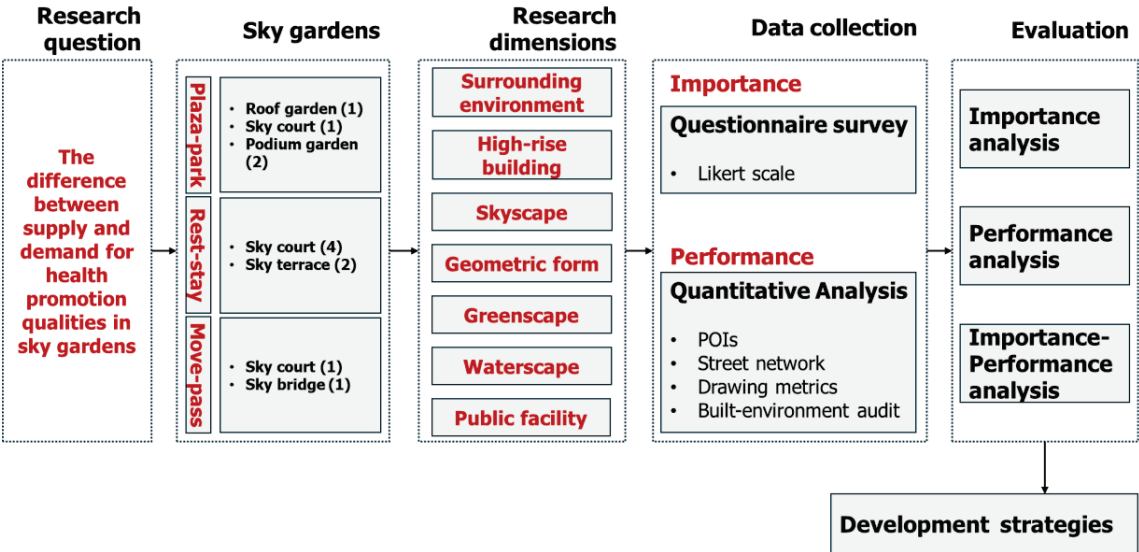
Figure 1. Analytical framework.

2.1. Study Location

This study selected a total of 157 typical sky garden spaces in 46 high-rise buildings within Shenzhen, Hong Kong, and Singapore, which are widely known or have received professional awards (Figure 2). Most of these are concentrated in the urban center with compact space and limited land [16]. Sky gardens can be classified into three types, and the differences between the types were verified [67]: plaza-park type with podium gardens and rooftop gardens, rest-stay type with sky courts and sky terraces, and move-pass type with sky bridges. Plaza-park sky gardens have a large spatial scale, are regular in shape, and have high landscape richness; rest-stay sky gardens are distributed higher in high-rises, have moderate scales, and have high landscape richness; and move-pass sky gardens are linear in shape and are related to transport functions. Then, based on two indicators, namely the "open space ratio" (sky garden area/total floor area) and the "void-to-solid ratio" (sky garden façade area/floor façade area), 12 cases were selected from widely known or professionally awarded sky gardens (Table 1, Figure 3).
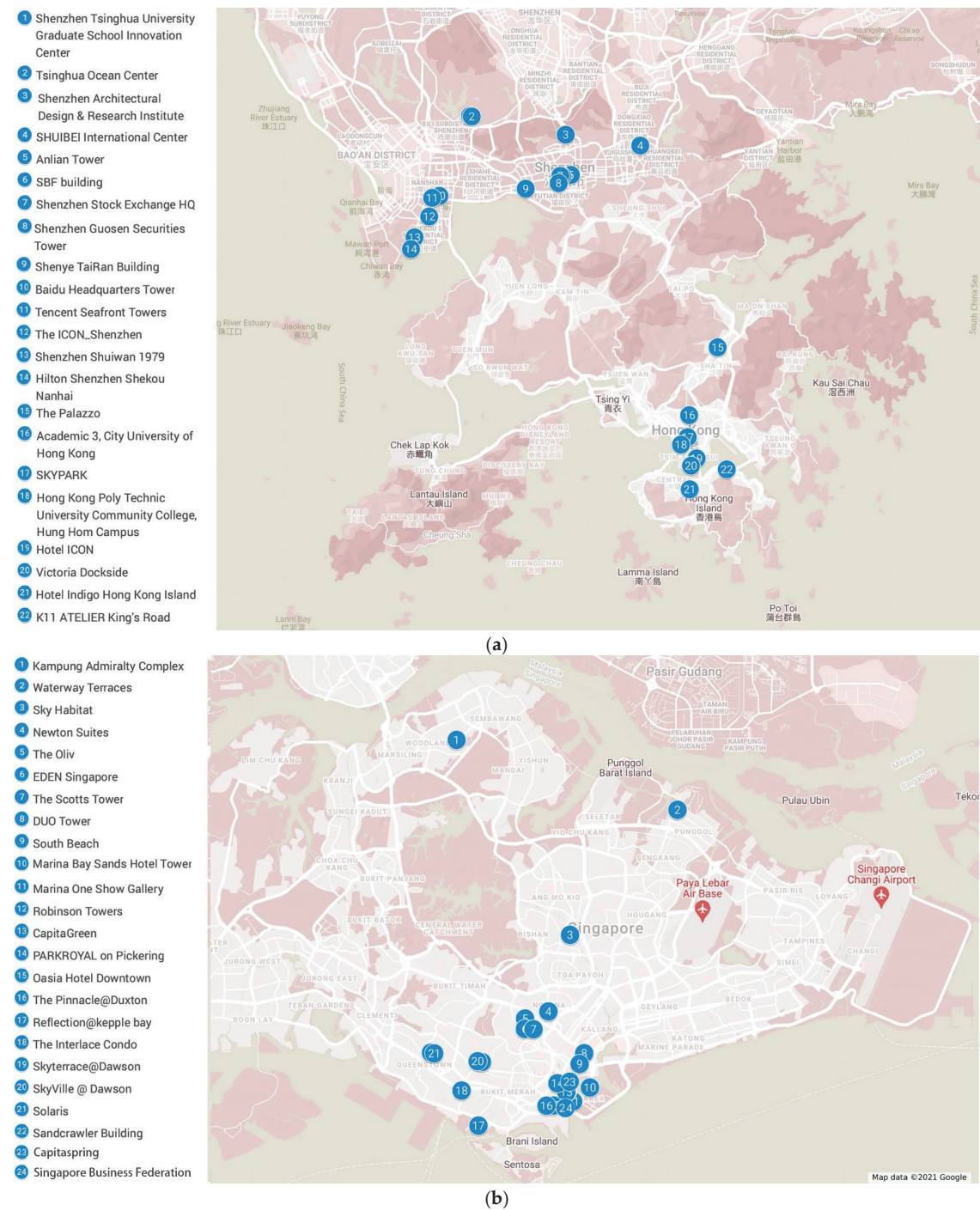
1. Shenzhen Tsinghua University Graduate School Innovation Center
2. Tsinghua Ocean Center
3. Shenzhen Architectural Design & Research Institute
4. SHUIBEI International Center
5. Anlian Tower
6. SBF building
7. Shenzhen Stock Exchange HQ
8. Shenzhen Guosen Securities Tower
9. Shenye TaiRan Building
10. Baidu Headquarters Tower
11. Tencent Seafront Towers
12. The ICON_Shenzhen
13. Shenzhen Shuiwan 1979
14. Hilton Shenzhen Shekou Nanhai
15. The Palazzo
16. Academic 3, City University of Hong Kong
17. SKYPARK
18. Hong Kong Poly Technic University Community College, Hung Hom Campus
19. Hotel ICON
20. Victoria Dockside
21. Hotel Indigo Hong Kong Island
22. K11 ATELIER King's Road

(**a**)

1. Kampung Admiralty Complex
2. Waterway Terraces
3. Sky Habitat
4. Newton Suites
5. The Oliv
6. EDEN Singapore
7. The Scotts Tower
8. DUO Tower
9. South Beach
10. Marina Bay Sands Hotel Tower
11. Marina One Show Gallery
12. Robinson Towers
13. CapitaGreen
14. PARKROYAL on Pickering
15. Oasia Hotel Downtown
16. The Pinnacle@Duxton
17. Reflection@kepple bay
18. The Interlace Condo
19. Skyterrace@Dawson
20. SkyVille @ Dawson
21. Solaris
22. Sandcrawler Building
23. Capitaspring
24. Singapore Business Federation

(**b**)

Figure 2. Distribution of 157 typical sky gardens in 46 high-rise buildings in Shenzhen, Hong Kong, and Singapore: (**a**) Shenzhen and Hong Kong; (**b**) Singapore.

Table 1. General information on the three types of 12 sky gardens.

Type	Building Name	Garden Type	OSR	VSR	FAR	Scale/m²
Plaza-park	01—SkyVille @ Dawson	Podium garden	1.00	1.00	3.9	3659.9
	02—The Pinnacle@Duxton	Roof garden	0.63	0.87	8.4	2923.0
	03—Hilton Shenzhen Shekou Nanhai	Podium garden	0.31	0.45	2.4	2252.6
	04—Capitaspring	Sky court	0.79	0.28	12.8	1862.3
Rest-stay	05—Singapore Business Federation Center	Sky court	0.68	0.68	11.9	198.7
	06—Oasia Hotel Downtown	Sky court	0.38	0.51	8.4	1071.4
	07—Baidu Headquarters East Tower	Sky court	0.10	0.43	10.8	222.9
	08—Shuiwan1979	Sky terrace	0.01	0.13	11.0	24.7
	09—DUO Tower	Sky court	0.40	0.27	6.0	1208.7
	10—Newton Suites	Sky terrace	0.06	0.19	2.8	34.6
Move-pass	11—PARKROYAL COLLECTION Pickering	Sky court	0.15	0.47	4.3	993.1
	12—SkyTerrace @ Dawson	Sky bridge	0.26	0.32	4.7	328.2
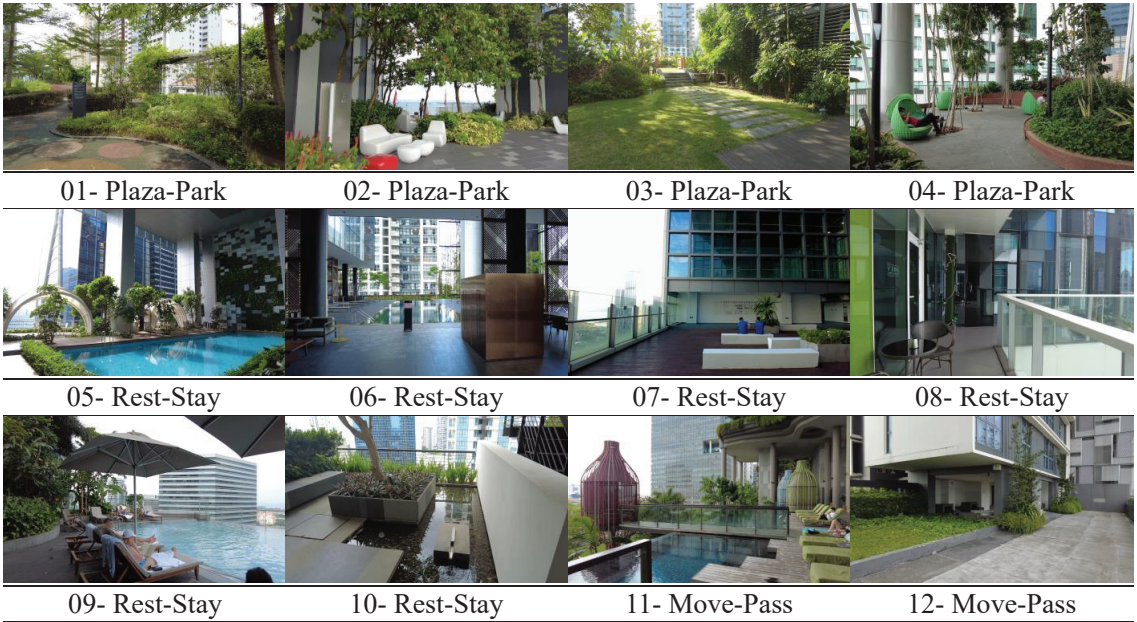
Figure 3. The three types of 12 sky garden scenarios.

2.2. Research Methods

2.2.1. Measuring Sky Garden Space Quality via Seven Dimensions

To determine the dominant spatial characteristics of health promotion to be included in the main study, an explorative pilot study was carried out in two stages.

First, spatial composition was conducted using computer vision API and manual identification of sky garden images from the internet. According to principal component analysis, the main spatial elements of sky gardens consist of seven principal components: urban landscape, skyscape, high-rise, public facility, natural landscape, waterscapes, and cultural activity [16].

Secondly, a meta-analysis of the literature was conducted, combining typical spatial elements that promote health from previous restorative environment studies. "Restorative", "healing", "health promoting", "therapeutic", "healthy", "salutogenic", "supportive environment", "environment", "landscape", and "garden" were used as keywords to search in the Web of Science and CNKI databases. Fifty-three articles, including environmental elements and indicators of health promotion, were selected. The environmental studies on health promotion focused on 19 elements, including greenery/vegetation, architecture, natural environment, waterscapes, streets/roads, public facilities, colors, rocks and mountains, environmental attributes/phenomena, people, urban/man-made natural landscapes, urban landscapes, vehicles, scale/forms, animals, sky, sounds, indoor spaces, and agricultural landscapes.

Since recreational activities mostly rely on public facilities, considering the spatial scale and form of sky gardens as the focus of this study, and following the comprehensive exploration of the two stages mentioned above, a total of seven dimensions and 24 indicators were selected. We introduced a comprehensive framework to assess the health-promoting quality of sky gardens through multidimensional perception (Figure 4), and specific indicators are detailed in the following text.
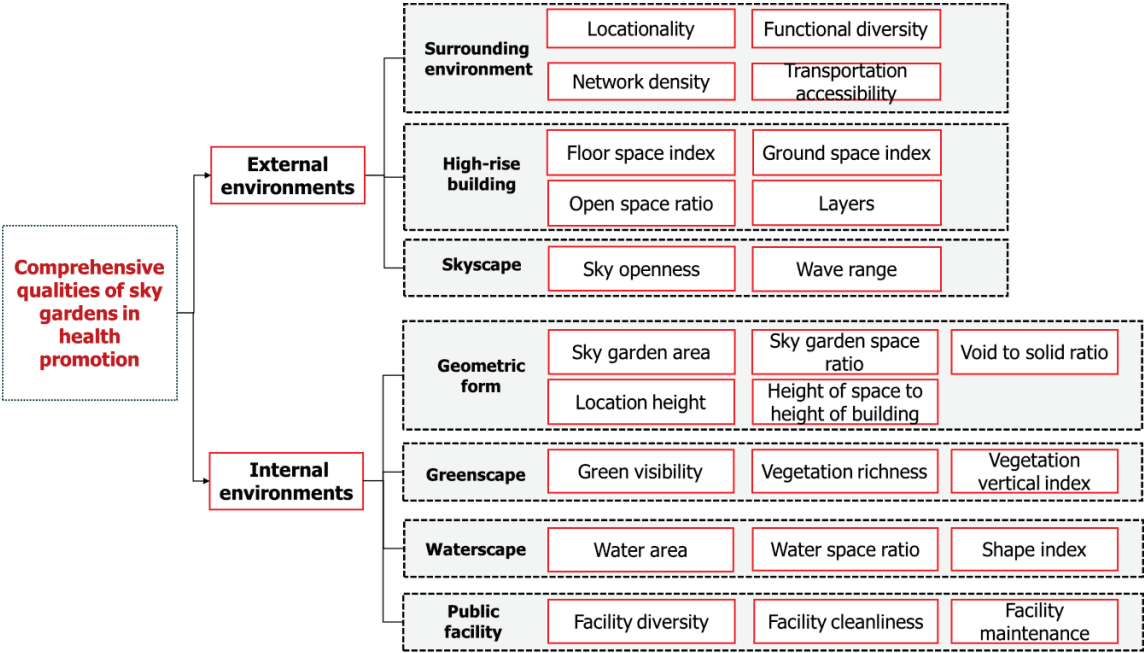
Figure 4. Twenty-four spatial indicators in the seven dimensions of health promotion in sky gardens.

- Surrounding environment

As described in Section 1.2.2, we selected the locationality, functional diversity, network density, and transportation accessibility based on previous studies to characterize the supportive effect provided by the surrounding environment for the public to access sky gardens to serve their health values. Of these, locationality and functional diversity can influence the attractiveness and uniqueness of sky gardens, making more people likely to visit them; network density and transportation accessibility directly affect the convenience of sky gardens, attracting public access and thus supporting healthy activities. This part of the research data mainly includes street network data and POI data. Previous studies have confirmed the alternative public space value of sky gardens [16], but their service radius is slightly shorter than that of the public space in the city. Thus, regarding the service radius

of public space in residential neighborhoods (≤400–500 m), the calculation radius is set to 500 m, and POIs and street network data are selected from this region.

Locationality: the linear distance of the sky garden from the city center.

Functional Diversity: the degree of mixing the POIs types within the area where the sky garden is located.

$$\text{Functional Diversity} = -\sum_i^n (Pi \times \ln Pi) \tag{1}$$

In this equation, Pi represents the proportion of urban facilities belonging to the i-th type of functional categories, and the PoIs are categorized into eight: leisure, living, sporting, shopping and commerce, scenery, culture and education, traffic, and public facilities.

Network density: the development level of road infrastructure in the surrounding environment of sky gardens.

$$\text{Network density} = \frac{L}{\text{Area}} \tag{2}$$

In this equation, L is the total length of the road within a 500 m radius of the building where the sky garden is located (km) and Area is the total area within 500 m radius of the building where the sky garden is located (km^2).

Transportation accessibility: The linear distance between the high-rise building where the sky garden is located and the nearest metro/bus station. It is one of the important influencing factors to attract people visiting the sky garden.

- High-rise building

High-rise buildings are the important spatial composition of sky gardens [16], providing important opportunities for sky garden development [4]. To describe the density metrics of high-rise buildings where sky gardens are located, the spacemate diagram proposed by Meta Berghauser Pont and Per Haupt was used [68,69], which decomposed the density metrics into the floor space index (FSI), ground space index (GSI), open space ratio (OSR), and layers (L). The formula is as follows:

$$\text{FSI} = \frac{\text{Gross Floor Area}}{\text{Plan Area}}, \tag{3}$$

$$\text{GSI} = \frac{\text{Built Area}}{\text{Plan Area}}, \tag{4}$$

$$\text{OSR} = \frac{\text{Plan Area} - \text{Built Area}}{\text{Gross Floor Area}}, \tag{5}$$

$$\text{L} = \frac{\text{Gross Floor Area}}{\text{Built Area}}. \tag{6}$$

- Skyscape

The sky scope and shape seen by people differ due to the changes of vertical position in sky gardens. Therefore, sky openness and wave range indicators are selected in this paper to quantify the sky view in the sky garden.

Sky openness is the proportion of the sky that can be seen in a sky garden. Using the "histogram" function of Photoshop software, the ratio was calculated of the sky area pixels to the total pixels in the image. In this paper, 90 images of typical sky gardens chosen to represent the whole environment of the sky gardens are selected from subsequent field studies. The sky openness is calculated by the 90 images' mean values for the sky gardens, respectively.

$$\text{Sky openness} = \sum_i^{90} \frac{PCi(\text{Sky})}{PCi(\text{Picture})}/90 \tag{7}$$

The sky wave range is the degree of fluctuation of the skyline [70]. The highest and lowest points of the skyline are the sky wave range. ΔL is calculated as the distance between

the lowest points based on the skylines, and then ΔH, the height difference between the lowest point and the highest point, is calculated. ΔL/ΔH indicates the sky wave range. The larger ΔL value indicates that the sky is more visible and the visual depth is farther; the larger ΔH value indicates that the sky contour lines are more diverse and pleasing to the viewers. The formula is as follows [71]:

$$\text{Wave range} = \frac{(\Delta L1 + \Delta L2)}{(\Delta H1 + \Delta H2)}, \tag{8}$$

where ΔL1 is the horizontal distance from the lowest point of the skyline to the highest point on the left, ΔL2 is the horizontal distance from the lowest point of the skyline to the highest point on the right, ΔH1 is the vertical distance from the lowest point of the skyline to the highest point on the left, and ΔH2 is the vertical distance from the lowest point of the skyline to the highest point on the right.

- Geometric form

The sky garden space supports relaxation, viewing, socializing, and other healthy behaviors within the high-rise building. Typically, the greater the spatial range of activity, the greater the health-promoting behaviors [69]; the more visible the façade void, the easier it is to be perceived [72]. In addition, different from ground-level green spaces, the vertical position of sky gardens in high-rise buildings directly affects the viewpoint from which people perceive the surroundings. Therefore, sky garden area (SGA), sky garden area ratio (SGSR), void-to-solid ratio (VRS), location height (LH), and height of space to height of building (HSB) were selected as important indicators to measure the internal geometry form of the sky garden.

$$\text{SGSR} = \frac{\text{Space Area}}{\text{Floor Area}} \tag{9}$$

$$\text{VSR} = \frac{Void}{Solid} \tag{10}$$

$$\text{HSB} = \frac{\text{Height}}{\text{Height of Building}} \tag{11}$$
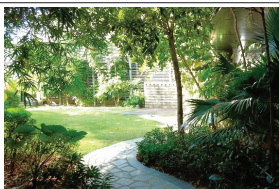
- Greenscape
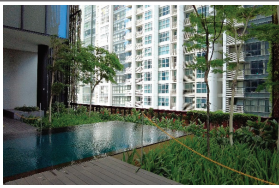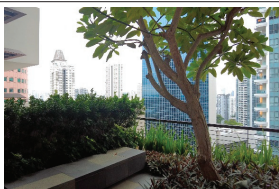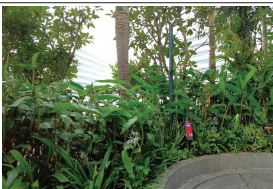
We selected greenery visibility, vegetation richness, and vegetation vertical index to characterize the quality of the greenscape of the sky gardens in terms of overall greenness, vegetation species, and vertical distribution, respectively. Greenery visibility is the proportion of green vegetation in people's view. It is calculated using the same method as sky openness.

Vegetation richness is the degree of abundance and mixture. Vegetation communities are generally grouped into three categories: woodland, shrub, and herbaceous, while vegetation richness is influenced by both the plant structure and the natural attributes [73]. Therefore, nine types of vegetation communities are defined in this paper based on three levels of vegetation structural and vegetation naturalness, low, medium, and high, with corresponding scores (Table 2). Vegetation richness measurements were conducted through the virtual built-environment audit. Five auditors majoring in architecture were selected and trained in rating to reduce statistical inaccuracy. Due to the large scale of the sky gardens (>800 m^2), typical spatial joints were classified according to the morphology, and the vegetation richness of multiple joints in each sky garden was scored and averaged.

The vegetation vertical index is the difference in the vertical spatial distribution of vegetation. Vegetation outlines were drawn according to the vegetation communities, the ratio of the highest to the height of the screen was calculated as the vertical index of each community, and then the mean value of the vertical index of vegetation at each node was calculated.

Table 2. The vegetation richness: the criteria (planting structure and species character) used to define nine types and scores.

	Structural Similarity to Natural Vegetation		
	Least Natural	**Moderately Natural**	**Most Natural**
Least natural	Simple, singer layer, isolated trees or shrubs. 1 score	Two vegetation layers, least naturalness. 2 score	Three vegetation layers, least naturalness. 3 score
moderately natural	Simple, largely singer layer, intermediate naturalness. 2 score	Two vegetation layers, intermediate naturalness. 4 score	Three vegetation layers, intermediate naturalness. 6 score
most natural	Simple, largely singer layer, most naturalness. 3 score	Two vegetation layers, most naturalness. 6 score	Three vegetation layers, most naturalness. 9 score

(Row label on left side: Species character similarity to natural vegetation)

- Waterscape

The waterscape is one of the important landscape elements to promote environmental health. Water area, water space ratio (water area/sky garden area), and shape index were selected as quantitative indicators of waterscape. The shape index of the water area mainly depends on the water area and the number of shape characterizing points (NSCP). The NSCP is an index characterizing two-dimensional geometric shapes by the minimum number of points necessary to describe their boundary. The NSCP is calculated by counting the number of a polygon's vertices. To buffer for inaccuracy of the digitizing process and to eliminate minor shape irregularities, the threshold value for valid vertex angles was set to 160°. To describe the landscape as a whole for individual study sites, the area-weighted mean was calculated as a measure of the landscape shape index. The formula is as follows [74]:

$$\text{Shape index} = \text{NSCP} * \text{Water Area} \tag{12}$$

- Public facility

Facility diversity, facility cleanliness, and facility maintenance directly affect the likelihood of people visiting the space and the stay time. Firstly, the diversity, cleanliness, and

maintenance of the 23 facilities in the six dimensions (see Appendix A for details) within the sky gardens were summarized. The five auditors scored various elements of the facility, and values were averaged in the virtual built-environment audit [75,76]. The specific steps are as follows: (1) Facility diversity: the auditor scores the facility evaluation elements in the sky garden image on dichotomous scales, which means that the presence of feature is scored as 1 and the absence is scored as 0; (2) the auditor evaluates the facility elements present in the sky garden on a scale of 1 to 5 in terms of cleanliness and maintenance according to the detailed auditing criteria; (3) the average of facility diversity, cleanliness, and maintenance for each sky garden is calculated.

2.2.2. Importance-Performance Analysis

● Approaches to synthesize IPA Matrix

This study employs the importance-performance analysis (IPA) method to understand the differences between the public's expectations and the actual performance of environmental characteristics in sky gardens for health promotion. The spatial characteristics of sky gardens for health promotion are measured by 24 indicators across the seven dimensions outlined earlier. The standard IPA diagram integrates the importance and expressiveness measures into two-dimensional, four-quadrant diagrams, with performance as the horizontal axis and importance as the vertical axis [23]. The first quadrant is "keep up the good work", the second quadrant is "concentrate here", the third quadrant is "low priority", and the fourth quadrant is "possible overkill". The thresholds in the IPA diagram directly influence the quadrant distribution [22,77] and may lead to inconsistent results [78]. Therefore, we used the mean value, diagonal, and coordinates-origin approaches to synthesize and discuss the spatial indicator importance and performance of the sky garden (Figure 5).
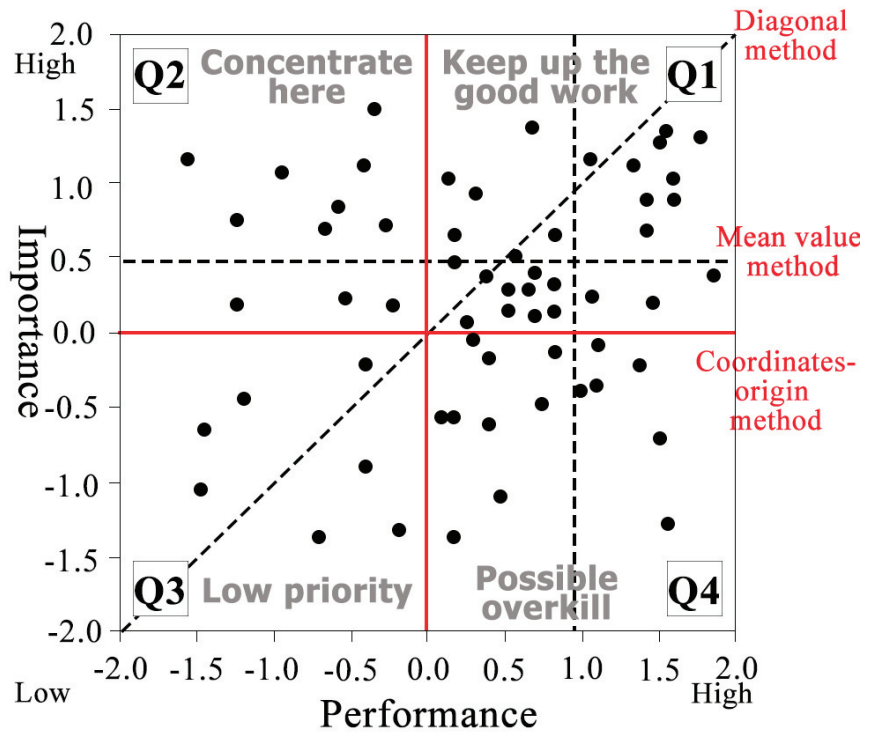

Figure 5. Graphical comparison of mean value, diagonal, and coordinates−origin approaches in identifying the IPA matrix.

● Subjects

Individual differences influence spatial preferences, while experts and relevant professionals demonstrate good consistency and discrimination in corresponding research [79]. The expert evaluation, which relies entirely on professionals, has been questioned because of some differences with the evaluation of the public. Therefore, this study combines evaluations from both experts and the public. Given that the selected cases needed to consider the typicality of various types of sky garden, which are widely distributed across cities and even countries, conducting on-site surveys was challenging. Therefore, we opted for online surveys to obtain more comprehensive data. In total, there were 375 individuals, including 170 males and 206 females (Table 3).

Table 3. The evaluation subjects.

Group	Description	Planned Participant	Actual Participant
Expert Group	Architectural design-related fields, PhD, university teachers, and professionals engaged in high-density environment, sky garden space design related work	20	27
Relevant Professional Group	Designers in architectural design	130	163
Public Group	The public and non-professionals in the field of architectural design	150	186
	Sum	300	376

● Data collection

Before the data collection commenced, a field survey was conducted to discover the activity patterns of the sky garden users. The data collection for this study includes two parts: perception data from the public regarding the importance of health promotion in sky gardens and spatial performance data related to the health promotion of sky gardens. (1) Importance data of health promotion in sky gardens. In the questionnaire design phase, a pre-survey was conducted to test the applicability of the questionnaire. Based on the results, adjustments were made to the questionnaire text to align with respondents' reading habits and to facilitate understanding. The formal questionnaire was divided into two parts. The first part asked the subjects about their demographic characteristics and activities. The second part uses a 10-point Likert scale to ask subjects about the importance of health promotion in various dimensions of sky gardens. (2) Performance data of health promotion in sky gardens. Based on the selected sky gardens, spatial performance data representing health promotion in sky gardens were collated by calculating 24 indicators in seven dimensions in Section 2.2.

2.2.3. Questionnaire Analysis

In this research, 376 questionnaires were recalled, and 354 valid questionnaires were finally obtained by deleting incomplete and overtime-filled questionnaires. Then the reliability and validity of the questionnaire data were tested. The results (Table 4) indicate that Cronbach's alpha value is 0.96, indicating that the questionnaire's reliability was at a high level. The Kaiser–Meyer–Olkin (KMO) value is 0.93, which is located between the high scoring range (>0.9), and significance is 0.000, which is less than 0.05. In conclusion, the data reliability and internal consistency results of this questionnaire demonstrate high reliability and meet the requirements of the validity test indicators, providing support for the reliability of subsequent analyses.

Table 4. Results of questionnaire reliability and validity analysis.

	Valid	354		Cronbach's alpha	0.96
Cases	Excluded	0	Bartlett's test of sphericity	Approx Chi-Square	748.67
	Total	354		df	276
KMO of sampling adequacy	0.93			Sig.	0.000

3. Results

3.1. Subjects' Demographic Profile

From the basic information of the subjects in the first part of the valid questionnaire, 45.1% were male and 54.9% were female, which is an equal gender distribution. The age distribution ranges from 0 to over 60 years old, with 18–30 year-olds accounting for approximately 80% of the total population. Educational background is dominated by bachelor's (38.93%) and master's (39.73%) degrees, totaling more than 2/3 of the whole. In terms of the types of sky garden visited, the survey adopted a multiple-choice approach. The results show that 21.60% had not visited any sky gardens, while those who have visited two types (21.33%) and three types (22.40%) of sky gardens account for approximately half (43.73%). Among these, rooftop gardens (47.20%), podium gardens (43.20%), and sky terraces (39.47%) are the most frequently visited sky garden types. The analysis above shows that the sampled survey has good representativeness and comprehensiveness (Table 5, Figure 6).

Table 5. Subjects' basic information variable description and statistics.

Variable	Variable Description	Mean	S.D.	Variance
Gender	Male = 1, Female = 2.	1.55	0.498	0.248
Age	18–25 years = 1, 26–30 years = 2, 31–40 years = 3, 41–50 years = 4, 51–60 years = 5, over 60 years = 6.	2.90	0.976	0.953
Education	PhD = 1, master = 2, bachelor = 3, college = 3, high school = 4, junior high school and below = 5.	2.42	0.880	0.774
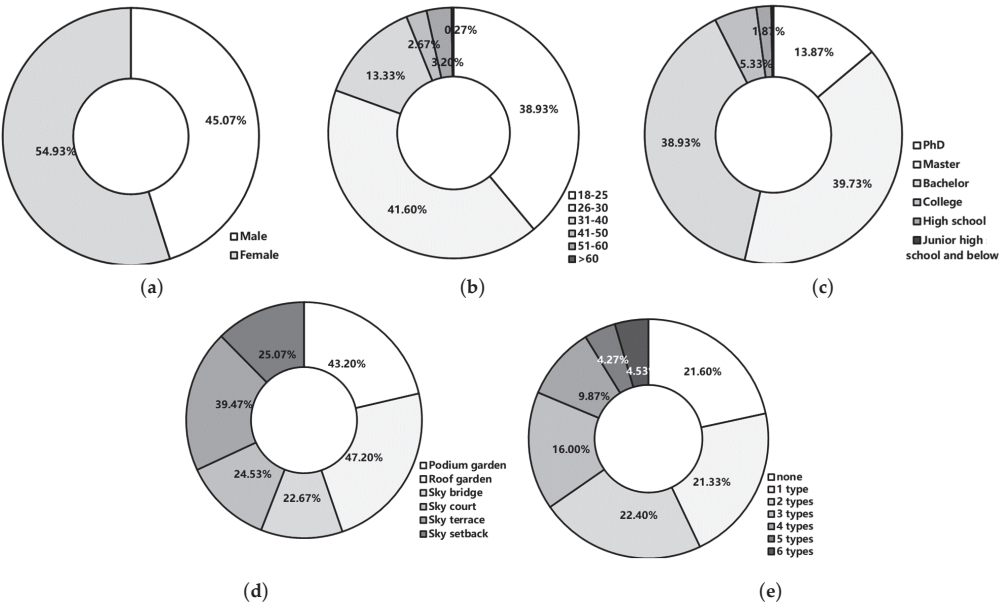
Figure 6. Subjects' demographic profile. (**a**) Gender statistics; (**b**) Age statistics; (**c**) Education statistics; (**d**) Statistics on the types of sky garden visited; (**e**) Statistics on the number of types of sky garden visited.

3.2. Importance Analysis of Public Perceptions on Health Promotion in Sky Gardens

The evaluation results of the importance of each spatial indicator of the sky garden were statistics, and the bar graph of the indicator importance was drawn (Figure 7). The results indicate that the public evaluated the importance of sky gardens the highest in terms of the indicators for facility cleanliness and maintenance, green visibility and vegetation

richness in the greenscape dimension, and sky openness in the skyscape dimension. The traffic accessibility in the dimension of the surrounding environment, open space ratio in the dimension of high-rise buildings, sky garden area, sky garden area ratio and location height in the dimension of geometric form, and vegetation vertical index in the dimension of greenscape were evaluated highly.
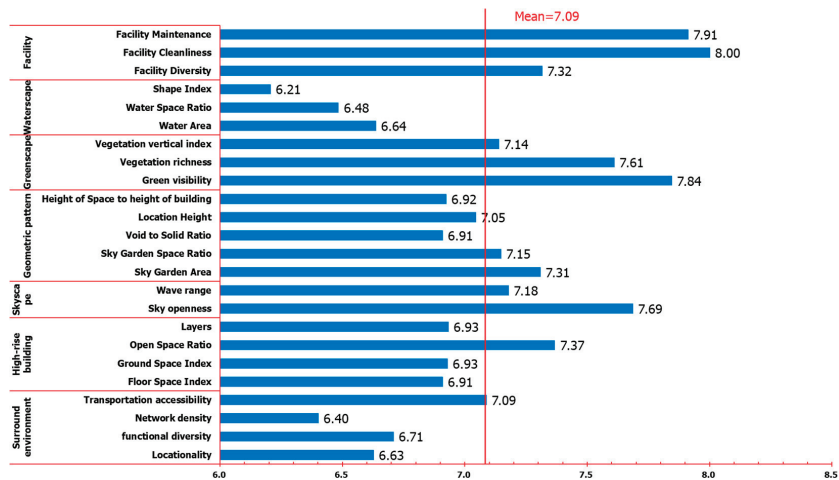

Figure 7. Importance values of 24 indicators of sky gardens.

Considering the above results, transportation accessibility, public facilities, greenscape, and skyscape are the most crucial dimensions affecting the public's engagement in health behaviors. Convenient transportation plays a crucial role in encouraging the public to visit nearby sky gardens, providing essential support for enhancing the health promotion experience associated with accessing these spaces. Public facilities serve as the crucial material foundation for highlighting health promotion attributes, solidifying the recreational environment status, and enhancing the vitality of shared spaces in sky gardens. The expansive skyscape with its distant, peaceful attributes, can alleviate people's physical and mental stress and help them to quickly recover to better states. Waterscape has not been listed in the public requirements for sky gardens, while spatial scale and greenery are in high demand for sky gardens. It is widely accepted that sky gardens are within the urban habitat context of high-density cities; density indicators associated with high-rise buildings have a relatively low impact on health promotion, such as FSI, GSI, L, and location height, which refers to the height of the space relative to the height of the building. Overall, the public places greater emphasis on spatial indicators that cater to activities such as relaxation, being close to nature, and enjoying panoramic views in sky gardens. Furthermore, there is greater sensitivity towards public facilities that contribute to activities related to physical and mental health.

3.3. Performance Analysis of Public Perceptions on Health Promotion in Sky Gardens

According to the comprehensive quantitative framework of health benefits for sky gardens, the data of spatial indicators were calculated and normalized over the same range (0, 1). Subsequently, radar diagrams were drawn to compare and analyze the similarities and differences in the performance of three types of sky garden. It is noted that the differences in performance between internal and external spatial indicators are more significant within each type of sky garden (Figure 8). The three types of sky garden show relatively consistent performance in external environmental indicators such as locationality, transportation accessibility, sky wave range, floor space index, and open space ratio. This indicates a certain convergence in the external environmental characteristics of sky gardens, suggesting the distribution in densely populated, compact urban environments. As for the

internal environmental indicators, plaza-park sky gardens have excellent performance in scale size, green visibility, vegetation richness, and vegetation vertical index. Rest-stay sky gardens perform well in vegetation richness, water space ratio, and facility cleanliness and maintenance. Move-pass type sky gardens have outstanding performance in sky garden area ratio and void-to-solid ratio indicators.
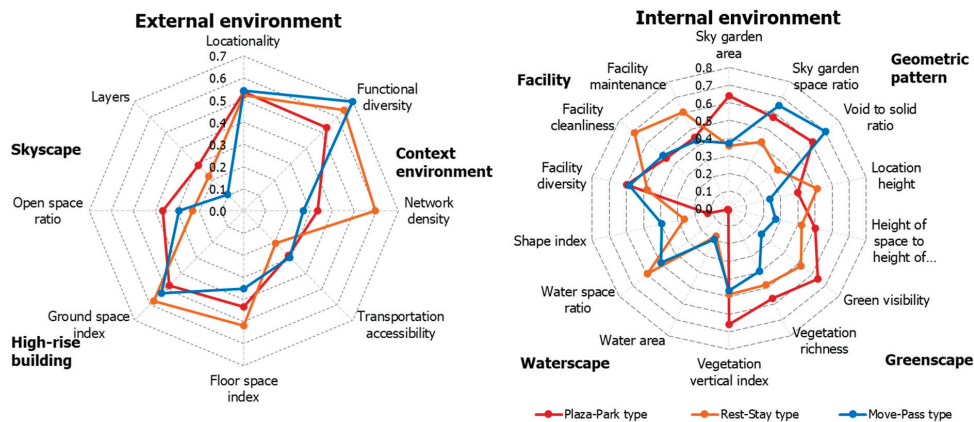

Figure 8. Performance radar diagrams of three sky garden spatial indicators.

Based on the performance of spatial indicators that ranked in the top 25%, it is evident that various types of sky garden display distinct characteristic tendencies (Figure 9). Plaza-park sky gardens with high-performance indicators are mainly focused on geometric form, greenscape, and public facility dimensions, which can satisfy people's diversified behavioral needs in sky gardens. Rest-stay sky gardens are concentrated in public facilities, waterscape scenery, and greenscape dimensions. Due to their limited spatial area and surrounding dense environment, differentiation in internal natural landscapes and public facilities is the focus of their spatial creation. Move-pass sky gardens focus on geometric form, surrounding environment, and public facility dimensions. Despite their relatively small size, these sky gardens have high spatial openness and visibility that play a positive role in spatial identification and perception. Additionally, neither the sky openness nor the wave range were included in the top 25% of indicators for all types of sky garden. This may be related to obstruction of the sky views by surrounding high-rise buildings, internal vegetation, and facilities, resulting in a relatively poor performance of these indicators.
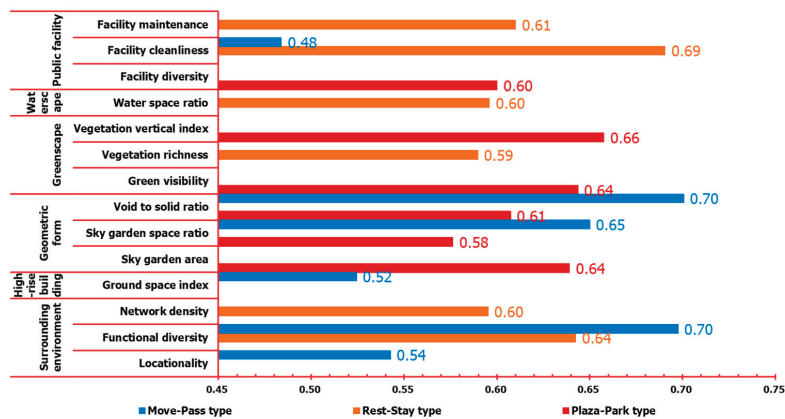
Figure 9. Top 25% spatial indicators of performance in health promotion in three types of sky garden.

3.4. Importance-Performance Analysis Matrix on Health Promotion in Sky Gardens

Standardized spatial indicator performance and importance data affecting health promotion in sky gardens, using the mean value, diagonal, coordinates-origin methods, to generate IPA matrix and discuss the spatial indicators for each dimension to the status of different types of sky garden (Figure 10). The specific steps are as follows: first, determine the approximate distribution of the indicator quadrants through the mean value, diagonal, and coordinates-origin methods, respectively. Then, the high threshold of the quadrant is used as a baseline to determine the indicator's position. For areas with differences between the quadrant division of the mean value and coordinates-origin, the priorities for their development are further clarified by considering the standard errors of the indicators and the actual status of the sky gardens. Taking facility cleanliness of plaza-park sky gardens as an example, the point is on the second and third quadrants in the coordinates-origin method and mean value method analyses, and above the 45° line in the diagonal method, indicating the indicator belongs to "concentrate here", "low priority". Then, consider the standard error line of the facility cleanliness indicator, which can be in the first and second quadrants of the coordinates-origin method and mean value method analyses, and above the 45° line in the diagonal method. Based on the facility cleanliness of the plaza-park sky gardens, the point was finally placed in the second quadrant, which is the "concentrate here" indicator. Continuing with the analysis, the spatial indicator placement areas for each type of sky garden are analyzed individually, and the results are as follows (Table 6):

Table 6. Table of corrected attributes of spatial indicators for three types of sky garden.

	Plaza-Park Sky Gardens	Rest-Stay Sky Gardens	Move-Pass Sky Gardens
Q1 Keep up the good work	13, 16, 17, (1), (18)	3, 7, 8, 16, 23, (20)	2, 13, (1), (20)
Q2 Concentrate here	2, 23	1, 13, 17, 18, 21, (2), (9)	16, 17, (18), (23)
Q3 Low priority	14, 15, 19, 21, 24, (3), (8), (20)	5, 10, 11, 12, 22, (4), (19), (24)	6, 9, 10, 14, 15, 24, (3), (7), (11), (22)
Q4 Possible overkill	4, 5, 6, 9, 10, 11, 12, 22, (7)	(6), (14), (15)	4, 5, 12, 19, 21, (8)

Note: The numbers have the same meanings as in Figure 10. Indicators in parentheses represent the comprehensive consideration of standard error lines and the specific spatial status of sky gardens.
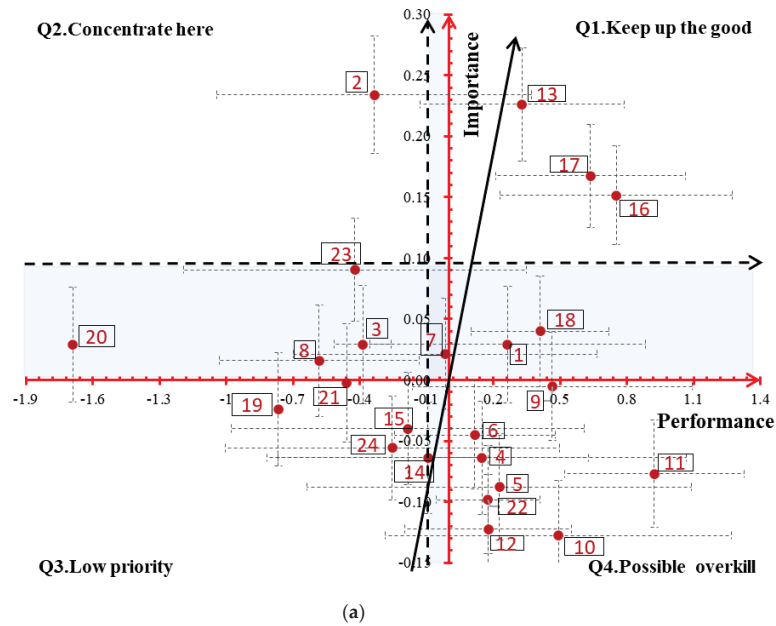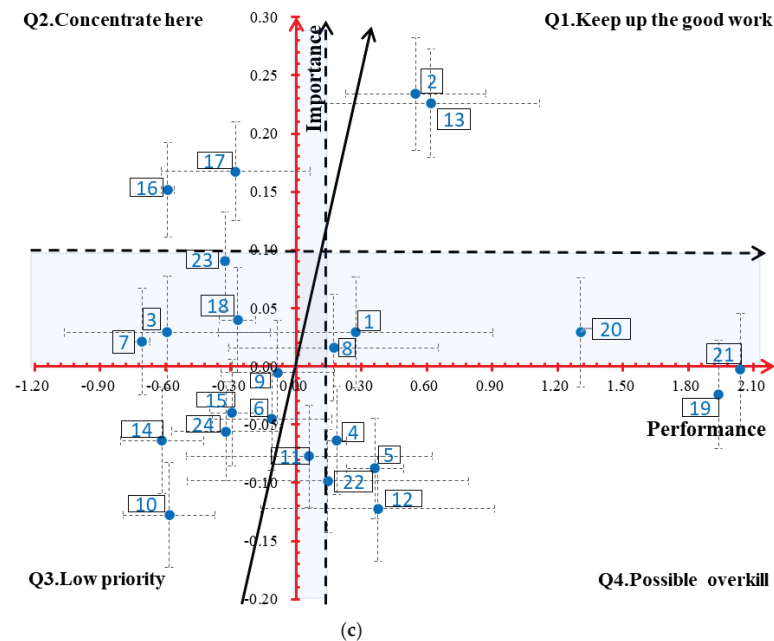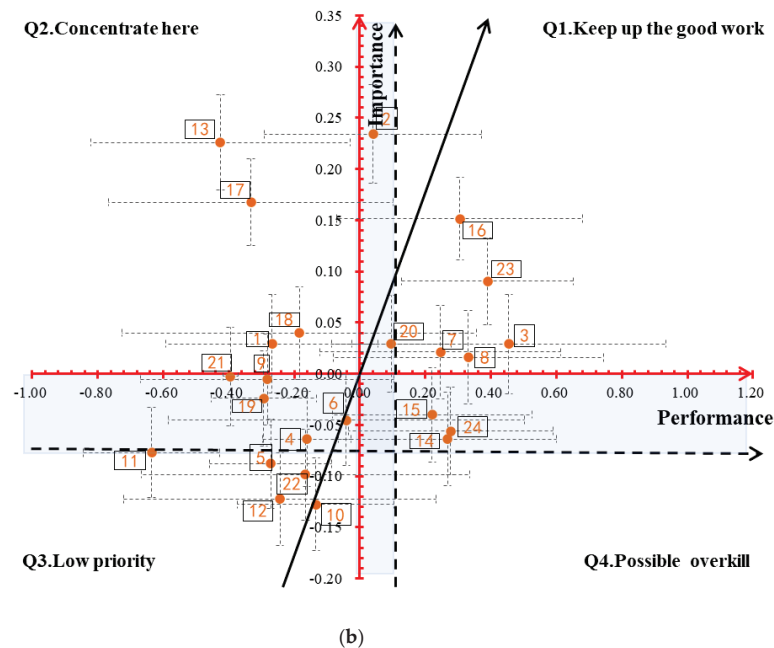

(**a**)

Figure 10. *Cont.*

Figure 10. IPA matrix of 24 spatial indicators for three types of sky garden. (**a**) Plaza-park sky gardens; (**b**) Rest-stay sky gardens; (**c**) Move-pass sky gardens. Notes: 1 = Locationality, 2 = Functional diversity, 3 = Network density, 4 = Transportation accessibility, 5 = Sky openness, 6 = Wave range, 7 = Floor space index, 8 = Ground space index, 9 = Open space ratio, 10 = Layers, 11 = Sky garden area, 12 = Sky garden space ratio, 13 = Void-to-solid ratio, 14 = Location height, 15 = Height of space to height of building, 16 = Green visibility, 17 = Vegetation richness, 18 = Vegetation vertical index, 19 = Water area, 20 = Water space ratio, 21 = Shape index, 22 = Facility diversity, 23 = Facility cleanliness, 24 = Facility maintenance.

(1) "Keep up the good work" area. These indicators represent the major strengths and potential competitive advantages of sky gardens. The results indicate that the indicators of void-to-solid ratio, green visibility, vegetation richness, and vegetation vertical index for plaza-park sky gardens; the network density, green visibility, facility cleanliness, and water space ratio for rest-stay sky gardens; and the function diversity, void-to-solid ratio, and water space ratio for move-pass sky gardens, all fall within this area.

(2) "Concentrate here" area. These indicators play crucial roles in promoting public health, but their spatial performance is relatively low and urgently needs improvement and enhancement. The function diversity and facility cleanliness of plaza-park sky gardens, the void-to-solid ratio, vegetation richness, vegetation vertical index, and waterscape shape index of rest-stay sky gardens, and the greenscape indicators and facility cleanliness of move-pass sky gardens are in urgent need of optimization and improvement. Therefore, plaza-park sky gardens need to prioritize improving the facility cleanliness, rest-stay sky gardens need to enhance spatial permeability and the hierarchy of green landscape, while move-pass sky gardens need to increase the greenscape richness and facility cleanliness.

(3) "Low priority" area. The attributes that fall into this quadrant are not performing exceptionally well but are relatively unimportant to the public; they represent minor weaknesses and poor performance is not a major problem. Compared to that, the vertical location height and waterscape demand of plaza-park sky gardens, facility diversity and skyscape of rest-stay sky gardens, and location height and height of space to height of building of move-pass sky gardens are within this area.

(4) "Possible overkill" area. Attributes are of low importance but perform strongly, indicating that limited resources may be a waste and are inefficiently used and can be reallocated. The plaza-park sky gardens in terms of transportation accessibility, skyscape, high-rise buildings (open space ratio, layers), and geometric form (sky garden area, sky garden space ratio); the indicators of height of space to height of building in rest-stay sky gardens; and transportation accessibility, sky openness, water area, and waterscape shape index of move-pass sky gardens fall into this quadrant.

In summary: (1) Transportation accessibility is good for all types of sky garden in their locations. This indicator is "possible overkill" in plaza-park and move-pass sky gardens, while it is a "low priority" improvement for rest-stay sky gardens. (2) Rest-stay sky gardens' public facilities are optimal. In plaza-park sky gardens, the facility diversity is "possible overkill", facility cleanliness falls into the "concentrate here" area, and facility maintenance is a "low priority" attribute. In rest-stay sky gardens, facility cleanliness serves as "keep up the good work" indicator, facility diversity and maintenance belong to the "low priority" area. In move-pass sky gardens, facility cleanliness has the "concentrate here" attribute, while facility diversity and maintenance are "low priority" for health promotion. (3) Plaza-park sky gardens have the highest quality in greenscape. All greenscape indicators in plaza-park sky gardens fall into the "keep up the good work" area. In rest-stay sky gardens, green visibility is the "keep up the good work" indicator, while the vegetation richness and vegetation vertical index need improvement. In move-pass sky gardens, all three indicators need enhancement. (4) Skyscape shows varying degrees of overkill in different types of sky garden. Plaza-park sky gardens of sky openness and wave range are overkill indicators. For rest-stay sky gardens, sky openness is a "low priority" attribute, while sky wave range is an overkill indicator. the situation is the opposite for the move-pass and the rest-stay sky gardens. Overall, rest-stay sky gardens have the greatest competitive advantage, which is possibly due to their embodied scale, but their spatial permeability and interface openness need to be raised. Plaza-park sky gardens, while large in scale, still have certain gaps in richness, diversity, and alignment with public demands, such as vegetation richness, waterscapes, and facility cleanliness. It may also cause some emotional barriers to people due to the increase of vertigo or agoraphobia at greater heights [17]. Move-pass sky gardens are limited by their transportation function, resulting in moderate levels of both public demand and supply.

4. Discussion

4.1. Opportunities and Strategies for Sky Garden Development

High-density cities have many opportunities to realize the potential of sky gardens. The previous texts confirm that there are already significant foundations in public awareness regarding the positive values of sky gardens for public physical and mental health and social interaction. Additionally, government policies have attempted to encourage the development of the roof and podium greening of high-rise buildings in order to tackle the inadequate ground-level open spaces [80], expand the green network [5,81], and promote carbon peaking and carbon neutrality action [82,83]. Additionally, research and demonstration projects on sky gardens provide the objective and scientific basis for multiple benefits [84–86]. Research findings on materials, techniques, and maintenance of vertical greening have been disseminated to the public through popular science methods. Recently, the pilot implementation of the research and demonstration of vertical garden green ecological architecture has begun. This plan specifies the inclusion of sky garden (green space) plants and facilities, the use of vertical open spaces, and related management and services in property service contracts [87]. Sky garden development has taken root in high-density environments, with expectations of a significant emergence of new sky gardens in due course.

To foster the systematic development of sky gardens, the following broad strategies could be adopted: (1) governments could incentivize construction through reward policies and establish an accreditation system to ensure delivery quality; (2) strict standards and regulations for sky garden materials and methods should be promptly instituted to ensure quality and durability. For sky garden construction, the following should be applied: (1) More attention could be paid to high-density, compact urban environments. On one hand, this study found that people are accepting sky gardens in the context of high-density urban environments. On the other hand, the scarcity of ground-level green spaces in these areas underscores the importance of utilizing sky gardens as supplementary public spaces [8], thereby enhancing users' spatial experiences and overall well-being. (2) In practical application, precedence could be afforded to the development of rest-stay sky gardens. These spaces offer significant health-promoting advantages, come with relatively lower construction costs, and provide convenient spots for the occupants of high-rise buildings for daily relaxation and work breaks [8,17].

4.2. Utilizing the Qualities of Complementary Public Spaces

Population growth and migration towards urban centers, along with the resulting urbanization process, have accelerated the density, scale, and functional diversity of high-rise building development [36]. This also inevitably demands more open spaces within high-rise buildings, and sky gardens serve as practical significance and operability solutions to complement public spaces as pocket parks in dense urban environments [17]. The previous studies indicate that the public places greater emphasis on activities in sky gardens, such as relaxation, being close to nature, and enjoying panoramic views, and they are more sensitive to public facilities that promote physical and mental well-being. Rich natural landscapes [51,52], expansive sky views [62], waterscapes [53], and diverse public facilities [55,56] all have positive effects on mental and physical well-being. Sky gardens play a significant role in promoting public health, especially in high-density urban areas, as supported by empirical evidence.

Different types of sky garden exhibit distinct disparities in their health-promoting effects, which can be reinforced by leveraging their spatial attributes to enhance their qualities as complementary public spaces. Plaza-park sky gardens have high similarity in attributes with ground-level public spaces [17]. These gardens are more likely to benefit from landscape typologies, functions, and facility selections and combinations, and they are best positioned to cater to the diverse and abundant health needs of the public. Thus, plaza-park sky gardens could focus on the overall quality of vegetation types, layout, and public facilities, aiming to enhance visitor initiative and prolong exposure to natural environments by increasing landscape complexity. Rest-stay sky gardens primarily cater to the daily relaxation needs of

high-rise building occupants [36]. Therefore, they can fully utilize their small size and flexible usage characteristics by being distributed throughout high-rise buildings. In terms of spatial interface permeability, rest-stay sky gardens need enhancement. By reducing view-blocking materials and controlling vegetation density, they can provide natural environments while effectively promoting social interactions. The first two types of sky garden mainly cater to static leisure activities, while move-pass sky gardens primarily support dynamic viewing activities. Their spatial form is predominantly linear [66], and they also serve a transportation function. The public's attention to its health promotion and its performance are both low. To improve this, rest areas can be appropriately incorporated into their transportation function, enriching spatial usability and attracting public engagement.

To further enhance the characteristics of sky gardens as complementary public spaces, it is necessary to specifically increase the utilization frequency. Research has confirmed that high-quality urban environments are more likely to attract the public to visit the adjacent open space, with increased accessibility, activity numbers, duration, and range of use [61]. To enhance the health-promoting potential of sky gardens, the supportive role of the surrounding environment can be amplified by the following: (1) By improving transportation accessibility, the frequency of sky garden usage can be increased; (2) By enhancing the functional diversity of the surrounding environment, "accidentally visit" can be attracted from other functional spaces; (3) By improving the openness of sky gardens in high-rise buildings, both physically and socially, the visitation rate of the public to sky gardens can be increased through higher spatial visibility.

5. Conclusions

This study aims to emphasize the differences in the multidimensional spatial characteristics of different types of sky garden by selecting representative, diverse, and typical cases. The research results provide a general understanding of the public's health promotion needs and supplies in different types of sky garden. The results show the following: (1) The public seems to have widely accepted sky gardens in the context of high-density urban environments (near 6.92, below the mean of 7.09). They place greater emphasis on spatial indicators that cater to relaxation activities and show heightened sensitivity toward public facilities (7.32–8.00) that contribute to physical and mental health-related activities. (2) The health promotion performance of different types of sky garden shows significant variation, with the rest-stay sky gardens at the embodied scale demonstrating the greatest competitive advantage. (3) The development of sky gardens has significant potential, and different types of sky garden need to specifically leverage their characteristics as complementary public spaces. Since the primary purpose of this study was to explore the overall demand of the public for health promotion in sky gardens, we did not categorize the sky gardens in the importance analysis. In future research, we will further clarify the different health experience needs of sky gardens and consider incorporating longitudinal assessments to evaluate the long-term effects of regular exposure to sky gardens on physiological and psychological well-being. Furthermore, health benefit analysis of landscape spaces could be conducted by more rigorous evidence-based studies using technologies such as virtual reality and wearable biosensors. Meanwhile, textual, image, and video data from social media platforms can provide insights into people's perceptions and feedback regarding landscape spaces. It helps to assess people's feelings and evaluations from a humanistic perspective, thus adding another dimension to the assessment of landscape space optimization.

Data Availability Statement: Data are contained within the article.

Appendix A. Examples of Virtual Built-Environment Audit on Facility Diversity, Tidiness, and Maintenance of Sky Garden

Table A1. Facility diversity virtual built-environment audit.

	Building Name	PARKROYAL COLLECTION Pickering					
General Information	Sky Garden Type	Rest-Stay Sky Garden					
	Sky Garden NO.	11					
	Auditor NO.	01	02	03	04	05	Mean
Basic facility	Hard seat						
	Soft seat	1	1	1	1	1	1
	Table	1	1	1	1	1	1
	Trash bin	1	1	1	1	1	1
	Deck chair	1	1	1	1	1	1
Athletic facility	Fitness equipment (outdoor)						
	Fitness equipment (indoor)	1	1	1	1	1	1
	Swimming pool	1	1	1	1	1	1
	Shower zone						
	Public facility for children						
Access for disabled	Handrail			1	1		1
	Ramp						
Safety facility	Envelope (railing/glass/bush)	1	1	1	1	1	1
	Fire hydrant	1	1	1		1	1
	Indication signage	1	1	1	1	1	1
	Lifesaving appliance	1	1	1	1	1	1
Shading facility	Beach umbrella						
	Sunshade tent						
	Empty space	1	1	1	1	1	1
Landscape facility	Sculpture	1	1	1		1	1
	Decoration pendant						
	Landmark	1	1	1	1		1
	Pool	1	1	1			1

Note: Facility diversity: 1—present, 0 or null—not present.

Table A2. Facility cleanliness virtual built-environment audit.

	Building Name	PARKROYAL COLLECTION Pickering					
General Information	Sky Garden Type	Rest-Stay Sky Garden					
	Sky Garden NO.	11					
	Auditor NO.	01	02	03	04	05	Mean

Table A2. *Cont.*

Basic facility	Hard seat						
	Soft seat	5	4	5	5	4	4.6
	Table	5	4	3	5	5	4.4
	Trash bin	5	4	3	5	5	4.4
	Deck chair	5	3	4	5	4	4.2
Athletic facility	Fitness equipment (outdoor)						
	Fitness equipment (indoor)	5	4	4	5	5	4.6
	Swimming pool	5	4	5	5	5	4.8
	Shower zone						
	Public facility for children						
Access for disabled	Handrail			3	4		3.5
	Ramp						
Safety facility	Envelope (railing/glass/bush)	5	4	4	4	5	4.4
	Fire hydrant	5	3	4		5	4.3
	Indication signage	5	3	4	4	5	4.2
	Lifesaving appliance	4	3	4	4	5	4.0
Shading facility	Beach umbrella						
	Sunshade tent						
	Empty space	4	4	4	5	5	4.4
Landscape facility	Sculpture	4	4	5			4.3
	Decoration pendant						
	Landmark	4	4	5	4		4.3
	Pool	3	4	3			3.3

Notes: Facility cleanliness: 5—very clean, 4—somewhat clean, 3—normal, 2—less clean, 1—dirty.

Table A3. Facility maintenance virtual built-environment audit.

General Information	Building Name	PARKROYAL COLLECTION Pickering					
	Sky Garden Type	Rest-Stay Sky Garden					
	Sky Garden NO.	11					
	Auditor NO.	01	02	03	04	05	Mean
Basic facility	Hard seat						
	Soft seat	5	4	5	5	4	4.6
	Table	5	4	4	5	5	4.6
	Trash bin	5	3	4	5	5	4.4
	Deck chair	5	3	3	5	4	4.0
Athletic facility	Fitness equipment (outdoor)						
	Fitness equipment (indoor)	5	4	4	5	5	4.6
	Swimming pool	5	4	4	5	5	4.6
	Shower zone						
	Public facility for children						
Access for disabled	Handrail			4	4		4.0
	Ramp						

Table A3. *Cont.*

Safety facility	Envelope (railing/glass/bush)	5	4	4	4	5	4.4
	Fire hydrant	5	3	3		5	4.0
	Indication signage	5	3	4	4	5	4.2
	Lifesaving appliance	5	3	4	4	5	4.2
Shading facility	Beach umbrella						
	Sunshade tent						
	Empty space	4	3	4	5	5	4.2
Landscape facility	Sculpture	4	4	5		5	4.5
	Decoration pendant						
	Landmark	4	4	5	4		4.3
	Pool	3	4	3			3.3

Note: Facility maintenance: 5—very good, 4—somewhat good, 3—normal, 2—less good, 1—bad.

References

1. Oldfield, P. *The Sustainable Tall Building a Design Primer*; Routledge: New York, NY, USA, 2019.
2. Stigsdotter, U.K.; Ekholm, O.; Schipperijn, J.; Toftager, M.; Kamper-Jørgensen, F.; Randrup, T.B. Health promoting outdoor environments-Associations between green space, and health, health-related quality of life and stress based on a Danish national representative survey. *Scand. J. Public Health* **2010**, *38*, 411–417. [CrossRef]
3. Bratman, G.N.; Daily, G.C.; Levy, B.J.; Gross, J.J. The benefits of nature experience: Improved affect and cognition. *Landsc. Urban Plan* **2015**, *138*, 41–50. [CrossRef]
4. Tian, Y.; Jim, C.Y. Development potential of sky gardens in the compact city of Hong Kong. *Urban For. Urban Green.* **2012**, *11*, 223–233. [CrossRef]
5. Tian, Y.; Jim, C.Y.; Tao, Y. Challenges and Strategies for Greening the Compact City of Hong Kong. *J. Urban Plan. Dev. -ASCE* **2012**, *138*, 101–109. [CrossRef]
6. Németh, J. Defining a Public: The Management of Privately Owned Public Space. *Urban Stud.* **2009**, *46*, 2463–2490. [CrossRef]
7. Seddon, N.; Chausson, A.; Berry, P.; Girardin, C.A.J.; Smith, A.; Turner, B. Understanding the value and limits of nature-based solutions to climate change and other global challenges. *Philos. Trans. R. Soc. B Biol. Sci.* **2020**, *375*, 20190120. [CrossRef] [PubMed]
8. Samant, S.; Hsi-En, N. A tale of two singapore sky gardens. *Ctbuh J.* **2017**, *3*, 26–31.
9. Shafique, M.; Kim, R.; Rafiq, M. Green roof benefits, opportunities and challenges—A review. *Renew. Sustain. Energy Rev.* **2018**, *90*, 757–773. [CrossRef]
10. Tien, P.W.; Calautit, J.K. Numerical analysis of the wind and thermal comfort in courtyards "skycourts" in high rise buildings. *J. Build. Eng.* **2019**, *24*, 100735. [CrossRef]
11. Mohammadi, M.; Calautit, J.K. Numerical Investigation of the Wind and Thermal Conditions in Sky Gardens in High-Rise Buildings. *Energies* **2019**, *12*, 1380. [CrossRef]
12. Yuliani, S.; Hardiman, G.; Setyowati, E. Green-Roof: The Role of Community in the Substitution of Green-Space toward Sustainable Development. *Sustainability* **2020**, *12*, 1429. [CrossRef]
13. Yeang, K. *Reinventing the Skyscraper: A Vertical Theory of Urban Design*; Wiley-Academy: Chichester, UK; Hoboken, NJ, USA, 2002; pp. 218–219.
14. Lotfi, Y.A.; Refaat, M.; El Attar, M.; Abdel Salam, A. Vertical gardens as a restorative tool in urban spaces of New Cairo. *Ain Shams Eng. J.* **2020**, *11*, 839–848. [CrossRef]
15. Schröpfer, T.; Menz, S. *Dense and Green Building Typologies: Research, Policy and Practice Perspectives*; Springer: Singapore, 2019.
16. Li, Y.; Du, H. Research on the spatial characteristics of sky gardens based on networked pictures: A case study of Singapore. *J. Asian Archit. Build.* **2022**, *21*, 2247–2261. [CrossRef]
17. Hadi, Y.; Heath, T.; Oldfield, P. Gardens in the sky: Emotional experiences in the communal spaces at height in the Pinnacle@Duxton, Singapore. *Emot. Space Soc.* **2018**, *28*, 104–113. [CrossRef]
18. Li, Y.; Du, H.; Sezer, C. Sky Gardens, Public Spaces and Urban Sustainability in Dense Cities: Shenzhen, Hong Kong and Singapore. *Sustainability* **2022**, *14*, 9824. [CrossRef]
19. Knaus, M.; Haase, D. Green roof effects on daytime heat in a prefabricated residential neighbourhood in Berlin, Germany. *Urban For. Urban Green.* **2020**, *53*, 126738. [CrossRef]
20. Liu, S.; Huang, G. The Ventilation Improvement Assessment of Sky Gardens-A Case Study of Hysan Place. *Iop Conf. Ser. Earth Environ. Sci.* **2020**, *440*, 52033. [CrossRef]
21. Tony, I. Sky Garden Design in High-density High-rise Residential Development. In Proceedings of the Sustainable Building 2013 Hong Kong Regional Conference, Hongkong, China, 12–13 September 2013; pp. 1–8.

22. Sever, I. Importance-performance analysis: A valid management tool? *Tour. Manag.* **2015**, *48*, 43–53. [CrossRef]
23. Martilla, J.A.; James, J.C. Importance-Performance Analysis. *J-Mark.* **1977**, *41*, 77–79. [CrossRef]
24. Gai, S.; Fu, J.; Rong, X.; Dai, L. Importance—Performance analysis and improvement of an urban park's cultural ecosystem services based on users' perspectives: A Beijing case study. *J. Asian Archit. Build.* **2023**, *22*, 726–739. [CrossRef]
25. McHarg, I.L. *Design with Nature*; Wiley: Hoboken, NJ, USA, 1969.
26. McHarg, I.L. The Place of Nature in the City of Man. *Ann. Am. Acad. Political Soc. Sci.* **1964**, *352*, 1–12. [CrossRef]
27. Calthorpe, P. *The Next American Metropolis*; Princeton Architectural Press: New York, NY, USA, 1993; Volume 23.
28. Fuller, M.; Moore, R. *An Analysis of Jane Jacobs's The Death and Life of Great American Cities*; Macat Library: London, UK, 2017.
29. Howard, E.; Osborn, F.J.; Mumford, L. *Garden Cities of Tomorrow*; Routledge: New York, NY, USA, 2013.
30. Beveridge, C.E.; Rocheleau, P. *Frederick Law Olmsted*; Rizzoli International Publications: New York, NY, USA, 1995.
31. Geddes, P. *Cities in Evolution: An Introduction to the Town Planning Movement and to the Study of Civics*; Williams: London, UK, 1915.
32. Tan, P.Y.; Köhler, M.; Peck, S.; Velazquez, L. *Vertical Garden City: Singapore*; Straits Times Press: Singapore, 2014.
33. Briz, J.; Köhler, M.; de Felipe, I. *Multifunctional Urban Green Infrastructure*; WGIN: Hong Kong, 2019.
34. Shuhua, L.; Kang, N.; Shulin, S.; Rongliang, Y.; Yanan, Y. The Theory of Green Healthy City. *Chin. Landsc. Archit.* **2020**, *36*, 14–19.
35. Raji, B.; Tenpierik, M.J.; van den Dobbelsteen, A. The impact of greening systems on building energy performance: A literature review. *Renew. Sustain. Energy Rev.* **2015**, *45*, 610–623. [CrossRef]
36. Pomeroy, J. *The Skycourt and Skygarden: Greening the Urban Habitat*; Routledge: New York, NY, USA; Taylor & Francis Group: Abingdon-on-Thames, UK, 2014.
37. Yeang, K. *The Green Skyscraper: The Basis for Designing Sustainable Intensive Buildings*; Prestel Verlag: Munich, Germany; London, UK; New York, NY, USA, 1999.
38. Haaland, C.; van den Bosch, C.K. Challenges and strategies for urban green-space planning in cities undergoing densification: A review. *Urban For. Urban Green.* **2015**, *14*, 760–771. [CrossRef]
39. Markevych, I.; Schoierer, J.; Hartig, T.; Chudnovsky, A.; Hystad, P.; Dzhambov, A.M.; de Vries, S.; Triguero-Mas, M.; Brauer, M.; Nieuwenhuijsen, M.J.; et al. Exploring pathways linking greenspace to health: Theoretical and methodological guidance. *Environ. Res.* **2017**, *158*, 301–317. [CrossRef] [PubMed]
40. Tian, Y.; Jim, C.Y. Factors influencing the spatial pattern of sky gardens in the compact city of Hong Kong. *Landsc. Urban Plan.* **2011**, *101*, 299–309. [CrossRef]
41. Irga, P.J.; Braun, J.T.; Douglas, A.N.J.; Pettit, T.; Fujiwara, S.; Burchett, M.D.; Torpy, F.R. The distribution of green walls and green roofs throughout Australia: Do policy instruments influence the frequency of projects? *Urban For. Urban Green.* **2017**, *24*, 164–174. [CrossRef]
42. Kaplan, R.; Kaplan, S. *The Experience of Nature: A Psychological Perspective*; Cambridge University Press: Cambridge, UK, 1989.
43. Ulrich, R.S. View through a window may influence recovery from surgery. *Science* **1984**, *224*, 420–421. [CrossRef] [PubMed]
44. Zhang, Y.; Tzortzopoulos, P.; Kagioglou, M. Healing built-environment effects on health outcomes: Environment-occupant-health framework. *Build. Res. Inf.* **2019**, *47*, 747–766. [CrossRef]
45. Nordh, H.; Hartig, T.; Hagerhall, C.M.; Fry, G. Components of small urban parks that predict the possibility for restoration. *Urban For. Urban Green.* **2009**, *8*, 225–235. [CrossRef]
46. Balling, J.D.; Falk, J.H. Development of visual preference for natural environments. *Environ. Behav.* **1982**, *14*, 5–28. [CrossRef]
47. Shiqi, W.; Hongyuan, M. Research on Biophilic Design: Theory, Method and Trend. *Landsc. Archit.* **2021**, *28*, 83–89.
48. Ulrich, R.S. Visual landscapes and psychological well-being. *Landsc. Res.* **1979**, *4*, 17–23. [CrossRef]
49. Ulrich, R.S. Natural versus urban scenes: Some psychophysiological effects. *Environ. Behav.* **1981**, *13*, 523–556. [CrossRef]
50. Hartig, T.; Evans, G.W. Restorative effects of natural environment experiences. *Environ. Behav.* **1991**, *23*, 3–26. [CrossRef]
51. Ulrich, R.S. Human responses to vegetation and landscapes. *Landsc. Urban Plan.* **1986**, *13*, 29–44. [CrossRef]
52. Seiji, S.; Suzuki, N. Effects of the Foliage Plant on Task Performance and Mood. *J. Environ. Psychol.* **2002**, *22*, 265–272.
53. Nutsford, D.; Pearson, A.L.; Kingham, S.; Reitsma, F. Residential exposure to visible blue space (but not green space) associated with lower psychological distress in a capital city. *Health Place* **2016**, *39*, 70–78. [CrossRef] [PubMed]
54. Nichols, W.J. *Blue Mind: The Surprising Science That Shows How Being Near, in, on, or under Water Can Make You Happier, Healthier, more Connected, and Better at What You Do*; Little, Brown: Boston, MA, USA, 2014.
55. Nordh, H.; Østby, K. Pocket parks for people—A study of park design and use. *Urban For. Urban Green.* **2013**, *12*, 12–17. [CrossRef]
56. Nordh, H.; Alalouch, C.; Hartig, T. Assessing restorative components of small urban parks using conjoint methodology. *Urban For. Urban Green.* **2011**, *10*, 95–103. [CrossRef]
57. Alkhresheh, M.M. Preference for void-to-solid ratio in residential facades. *J. Environ. Psychol.* **2012**, *32*, 234–245. [CrossRef]
58. Vartanian, O.; Navarrete, G.; Chatterjee, A.; Fich, L.B.; Gonzalez-Mora, J.L.; Leder, H.; Modroño, C.; Nadal, M.; Rostrup, N.; Skov, M. Architectural design and the brain: Effects of ceiling height and perceived enclosure on beauty judgments and approach-avoidance decisions. *J. Environ. Psychol.* **2015**, *41*, 10–18. [CrossRef]
59. Jim, C.Y.; Chen, W.Y. External effects of neighbourhood parks and landscape elements on high-rise residential value. *Land Use Policy* **2010**, *27*, 662–670. [CrossRef]
60. Whyte, J.; Ewenstein, B.; Hales, M.; Tidd, J. Visualizing Knowledge in Project-Based Work. *Long-Range Plan.* **2008**, *41*, 74–92. [CrossRef]

61. Ribeiro, A.I.; Tavares, C.; Guttentag, A.; Barros, H. Association between neighbourhood green space and biological markers in school-aged children. Findings from the Generation XXI birth cohort. *Environ. Int.* **2019**, *132*, 105070. [CrossRef]
62. Kaplan, R. The nature of the view from home: Psychological benefits. *Environ. Behav.* **2001**, *33*, 507–542. [CrossRef]
63. Masoudinejad, S.; Hartig, T. Window view to the sky as a restorative resource for residents in densely populated cities. *Environ. Behav.* **2020**, *52*, 401–436. [CrossRef]
64. Lindal, P.J.; Hartig, T. Architectural variation, building height, and the restorative quality of urban residential streetscapes. *J. Environ. Psychol.* **2013**, *33*, 26–36. [CrossRef]
65. Sahlin, E.; Ahlborg, G.; Tenenbaum, A.; Grahn, P. Using Nature-Based Rehabilitation to Restart a Stalled Process of Rehabilitation in Individuals with Stress-Related Mental Illness. *Int. J. Environ. Res. Public Health* **2015**, *12*, 1928–1951. [CrossRef]
66. Lee, D.; Park, C. Typology of skybridges in Asia. *J. Asian Archit. Build.* **2022**, *21*, 663–676. [CrossRef]
67. Li, Y.; Du, H. Research on the restorative benefits of sky gardens in high-rise buildings based on wearable biosensors and subjective evaluations. *Build. Environ.* **2024**, *260*, 111691.
68. Berghauser Pont, M.; Haupt, P. *Spacemate: The Spatial Logic of Urban Density*; Delft University Press Science: Delft, The Netherlands, 2004.
69. Pont, M.B.; Haupt, P. The relation between urban form and density. *Urban Morphol.* **2007**, *11*, 62–65. [CrossRef]
70. Stamps, A.I.; Nasar, J.L.; Hanyu, K. Using pre-construction validation to regulate urban skylines. *J. Am. Plan. Assoc.* **2005**, *71*, 73–91. [CrossRef]
71. Xinyi, N.; Kaike, L. A quantitative approach to visual impact analysis of city skyline. *Urban Plan. Forum* **2013**, *3*, 99–105.
72. Tao, Y.; Lau, S.S.Y.; Gou, Z.; Zhang, J.; Tablada, A. An investigation of semi-outdoor learning spaces in the tropics: Spatial settings, thermal environments and user perceptions. *Indoor Built Environ.* **2019**, *28*, 1368–1382. [CrossRef]
73. Hoyle, H.; Hitchmough, J.; Jorgensen, A. All about the 'wow factor'? The relationships between aesthetics, restorative effect and perceived biodiversity in designed urban planting. *Landsc. Urban Plan.* **2017**, *164*, 109–123. [CrossRef]
74. Moser, D.; Zechmeister, H.G.; Plutzar, C.; Sauberer, N.; Wrbka, T.; Grabherr, G. Landscape patch shape complexity as an effective measure for plant species richness in rural landscapes. *Landsc. Ecol.* **2002**, *17*, 657–669. [CrossRef]
75. Edwards, N.; Hooper, P.; Trapp, G.S.; Bull, F.; Boruff, B.; Giles-Corti, B. Development of a public open space desktop auditing tool (POSDAT): A remote sensing approach. *Appl. Geogr.* **2013**, *38*, 22–30. [CrossRef]
76. Liao, C.; Hsueh-Sheng, C.; Tsou, K. Explore the spatial equity of urban public facility allocation based on sustainable development viewpoint. In Proceedings of the REAL CORP 2009: CITIES 3.0—Smart, Sustainable, Integrative Strategies, Concepts and Technologies for Planning the Urban Future, Catalonia, Spain, 22–25 April 2009; pp. 137–145.
77. Bacon, D.R. A Comparison of Approaches to Importance-Performance Analysis. *Int J Market Res* **2003**, *45*, 55–71. [CrossRef]
78. Azzopardi, E.; Nash, R. A critical evaluation of importance–performance analysis. *Tour. Manag.* **2013**, *35*, 222–233. [CrossRef]
79. Vodak, M.C.; Roberts, P.L.; Wellman, J.D.; Buhyoff, G.J. Scenic Impacts of Eastern Hardwood Management. *For. Sci.* **1985**, *31*, 289–301.
80. Buildings Department; Lands Department; Department, Planning Joint Practice Note No. 1. 2001. Available online: https://www.pland.gov.hk/pland_sc/tech_doc/joint_pn/index.html (accessed on 18 October 2021).
81. Zaid, S.M.; Perisamy, E.; Hussein, H.; Myeda, N.E.; Zainon, N. Vertical Greenery System in urban tropical climate and its carbon sequestration potential: A review. *Ecol. Indic.* **2018**, *91*, 57–70. [CrossRef]
82. China Academy of Building Technology Development Research and Demonstration of Vertical Garden Green Ecological Architecture. Available online: http://www.cstid.org.cn/xwdt/002003/20220930/9f73fb92-5756-40fc-b5d2-f2de1c0b72ed.html (accessed on 8 June 2024).
83. The State Council of the People's Republic of China Action Plan for Carbon Dioxide Peaking Before 2030. Available online: https://www.mee.gov.cn/zcwj/gwywj/202110/t20211026_957879.shtml?type=bgxz (accessed on 8 June 2024).
84. Jim, C.Y.; Tsang, S.W. Biophysical properties and thermal performance of an intensive green roof. *Build. Environ.* **2011**, *46*, 1263–1274. [CrossRef]
85. Wong, N.H.; Tan, C.L.; Kolokotsa, D.D.; Takebayashi, H. Greenery as a mitigation and adaptation strategy to urban heat. *Nat. Rev. Earth Environ.* **2021**, *2*, 166–181. [CrossRef]
86. Vijayaraghavan, K. Green roofs: A critical review on the role of components, benefits, limitations and trends. *Renew. Sustain. Energy Rev.* **2016**, *57*, 740–752. [CrossRef]
87. Housing & Urban-Rural Development Bureau of Shaoxing Notice on Issuing the "Implementation Plan for the Pilot of Vertical Ecological Buildings (Trial)". Available online: https://www.sxyc.gov.cn/art/2024/2/1/art_1229445656_1895232.html (accessed on 12 June 2024).

Identifying Land Use Functions in Five New First-Tier Cities Based on Multi-Source Big Data

Wangmin Yang [1], Yang Ye [1], Bowei Fan [1], Shuang Liu [2] and Jingwen Xu [1,*]

[1] College of Resources, Sichuan Agricultural University, Chengdu 611130, China; yangwangmin@stu.sicau.edu.cn (W.Y.); yeyang@stu.sicau.edu.cn (Y.Y.); 201608171@stu.sicau.edu.cn (B.F.)

[2] Institute of Mountain Hazards and Environment, Chinese Academy of Sciences, Chengdu 610299, China; liushuang@imde.ac.cn

[*] Correspondence: 11893@sicau.edu.cn; Tel.: +86-182-15673015; Fax: +86-028-82690983

Abstract: With the continuous development of big data technology, semantic-rich multi-source big data provides broader prospects for the research of urban land use function recognition. This study relied on POI data and OSM data to select the central urban areas of five new first-tier cities as the study areas. The TF-IDF algorithm was used to identify the land use functional layout of the study area and establish a confusion matrix for accuracy verification. The results show that: (1) The common feature of these five cities is that the total number and area of land parcels for residential land, commercial service land, public management and service land, and green space and open space land all account for over 90%. (2) The Kappa coefficients were all in the range [0.61, 0.80], indicating a high consistency of accuracy evaluation. (3) Chengdu and Tianjin have the highest land use function mixing degree, followed by Xi'an, Nanjing, and Hangzhou. (4) Among the five new first-tier cities, Hangzhou and Nanjing have the highest similarity in land use function structure layout. This study attempts to reveal the current land use situation of five cities, which will provide a reference for urban development planning and management.

Keywords: POI data; TF-IDF; urban function identification; spatial analysis

1. Introduction

Thanks to the high-speed development of the economy driven by reform and open policy, China has experienced the largest urbanization process in human history [1]. Although the rapid urbanization process improves people's material conditions, it also brings many problems to urban planning and development, such as the single function of urban fringe areas and excessive traffic congestion within the city, which brings inconvenience to people's daily life and travel [2]. Disorderly urban expansion also poses threats to the natural ecological environment and disrupts ecological balance, resulting in economic, social, and ecological problems [3]. Therefore, the functional zoning of cities is essential for their scientific and reasonable construction and planning. China's latest policies emphasize the importance of urbanization and stress the need to identify and divide the functions of urban land use. This approach not only facilitates rational construction and planning of the city but also contributes to the optimization of urban layout, efficient distribution of urban resources, and the formation of a more efficient and orderly urban structure layout. This provides a solid foundation for the steady progress of urbanization [4–7].

The traditional methods of identifying urban land use functions rely on data from population census, land census, industrial statistics, and socio-economic statistics. However, these sources often involve confidentiality, making them challenging to access and resulting in lengthy update cycles. This greatly reduces the practicality of experiments, leading to research that often remains at a macro level, and is difficult to widely apply. With the advent of the network era and the rapid development of communication technologies, big data has emerged as a valuable resource. This includes various types of data such as remote

sensing images and environmental and meteorological data obtained through professional scientific research equipment. These big data have advantages such as high accuracy, wide coverage, strong timeliness, and low acquisition cost [8]. Compared with traditional remote sensing images, the network big data obtained through communication devices has better timeliness and microscale, including POI (point-of-interest) data, GPS (global positioning system) trajectory data, mobile phone signaling data, and bus card swiping data that can be obtained from users' daily lives [9]. Currently, more and more scholars are analyzing urban space by mining big data, focusing on exploring urban economic activities, resident mobility, and resident traffic trajectories from a micro perspective. For example, Frias Martinez et al. used Twitter's social media activity data to analyze urban land use functions in Manhattan, London, and Madrid using clustering analysis [10]; Jiang et al. used the frequency of POI data in the Boston metropolitan area to identify land types in cities and estimate employment distribution density based on this data [11]; Hu et al. used Landsat remote sensing image data and POI data to achieve the division of functional land in Beijing [12]; Ye et al. combined social media data with street level remote sensing image data to identify urban land use functions in Beijing [13]; Liu et al. used time series data of taxi travel trajectories to identify the functional layout of land use in Chengdu City [14]; Sun et al. achieved recognition of land use functions in Beijing by analyzing text information on Sina Weibo [15]; and Huang et al. divided the urban functional areas of Beijing and Wuhan by combining nighttime lighting data and daytime multi-perspective remote sensing image data [16]. With the progress and development of technology, the acquisition and analysis methods of big data are becoming increasingly perfect, which can further explore urban spatial layout and intuitively reflect urban spatial structure.

With the maturation of big data mining technology, many sample data and precise positioning information have been excavated in cities. The integration of big data with urban spatial analysis and the comprehensive analysis of hidden information has emerged as a research hotspot [17]. For example, Yuan et al. used the time, location, and type of crowd activity to represent the potential activity trajectory of the crowd and combined it with POI data kernel density analysis to identify the urban function of Beijing [18]; Feng et al. combined the Logic regression model with POI data to extract the urban functional zoning of the Wuhan urban area [19]; Zhai et al. combined the Place2vec model with the K-means clustering algorithm to partition the functional layout of land use in Wuxi City, with an overall accuracy of 74.24% [20]; Yan et al. used the KD-Tree clustering algorithm and Tyson polygon algorithm combined with POI data to accurately partition urban functional areas [21]; and Sun et al. used Word2vec, LDA, and Block2vec models to identify land use functions in the central urban area of Wuhan, which also confirmed that the Word2vec model has the best recognition accuracy [22]. In addition, the TF-IDF (term frequency inverse document frequency) quantification method based on machine learning has also received the attention of some scholars [23–25]. The TF-IDF algorithm is a weighting technique used for key information in data mining. This method has unique advantages in analyzing policy texts at the macro level and extracting keywords of different importance levels [26].

Theoretical research on urban land use functions has reached a relatively mature stage, and technical methods have undergone significant transformation. However, current research on identified urban functional zoning has primarily focused on applying new urban planning technologies, evaluating current layout features, and identifying functional issues. There is a lack of in-depth analysis of the identification results and insufficient connection with regional urban planning policies and development models. As a result, there is a challenge in providing feedback for future planning and design, as well as offering guidance for urban formulation and management. Urban function identification based on POI data often stems from surveying and mapping, cartography, and related disciplines. In the current era of land spatial planning, it is essential to conduct research on land use functions from the perspective of urban planning [27]. Moreover, current research primarily relies on manual comparative statistical analysis for the accuracy evaluation of

the final recognition results, which is significantly influenced by the researcher's personal subjective will. The new first-tier cities are a list of 337 prefecture-level-and-above cities in China, evaluated and analyzed by First Financial News based on five major indicators: commercial resource agglomeration, urban hub, urban human activity, lifestyle diversity, and future plasticity. These new first-tier cities have strong representativeness, and their development process can be seen as a microcosm of China's urbanization process to a certain extent. However, current research on new first-tier cities predominantly focuses on cultural, commercial, financial, and other fields, with limited attention to the functional layout of urban land use. Furthermore, existing research on the functional structure layout of urban land use is primarily confined to the study of individual cities, with inadequate comprehensive analysis and research on the functional layout of land use across multiple cities.

This study is grounded in OSM data and POI data to identify the current land use functions in the central urban areas of five new first-tier cities. The aim is to enhance understanding of the current situation and distribution pattern of land use functions in major Chinese cities and to provide a reference basis for optimizing the allocation of urban and national spatial planning. Furthermore, building upon the results of urban land use function identification, this study conducts an analysis from three perspectives: urban functional spatial elements, urban functional mixing degree, and urban structural similarity, to ascertain whether there is a certain regularity in the land use functions of these five new first-tier cities. The objective is to establish a data foundation and provide theoretical support for the formulation of planning policies for underdeveloped cities in China, thereby ensuring the steady and smooth progress of urbanization in the country.

2. Overview of the Study Area

The research areas are the central urban areas within the ring highways of Chengdu, Nanjing, Hangzhou, Xi'an, and Tianjin (Figure 1). These five cities have outstanding performance in terms of GDP (gross domestic product), number of permanent residents, concentration of commercial resources, and urban hub, all of which are extremely strong new first-tier cities. The selected central urban area concentrates most of the city's construction land and permanent population, making it a key area for urban planning and construction. And the urban functional distribution within this area is concentrated, with high spatial heterogeneity and suitable block scale, making it an ideal area for identifying and analyzing the current urban land use functions.
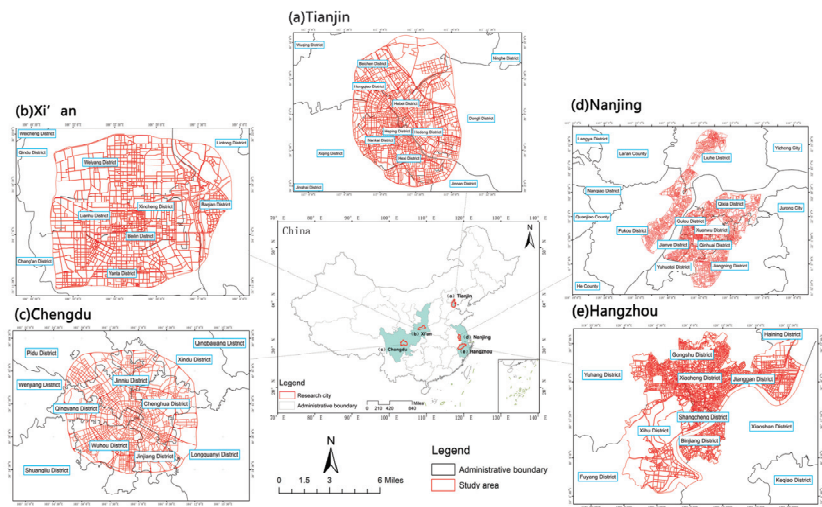

Figure 1. Research areas of the five cities.

3. Data Sources and Processing

3.1. Data Sources

This study uses OSM (OpenStreetMap) data as the base map of the study area, which is an open-source world map that can be freely edited by Internet users. Users can access and download data for free through an open license agreement (www.openstreetmap.org). This study uses POI data from Amap (https://lbs.amap.com), which was crawled on its API platform in December 2022 to ensure that the POI data utilized in this research is highly current. The total number of raw POI data for the five cities reached more than 1,735,000 items. And the land use status of the five cities on the Gaode satellite map was referenced as the real value to construct the confusion matrix to test the precision of identifying urban functions. The technical pathway is illustrated in Figure 2.
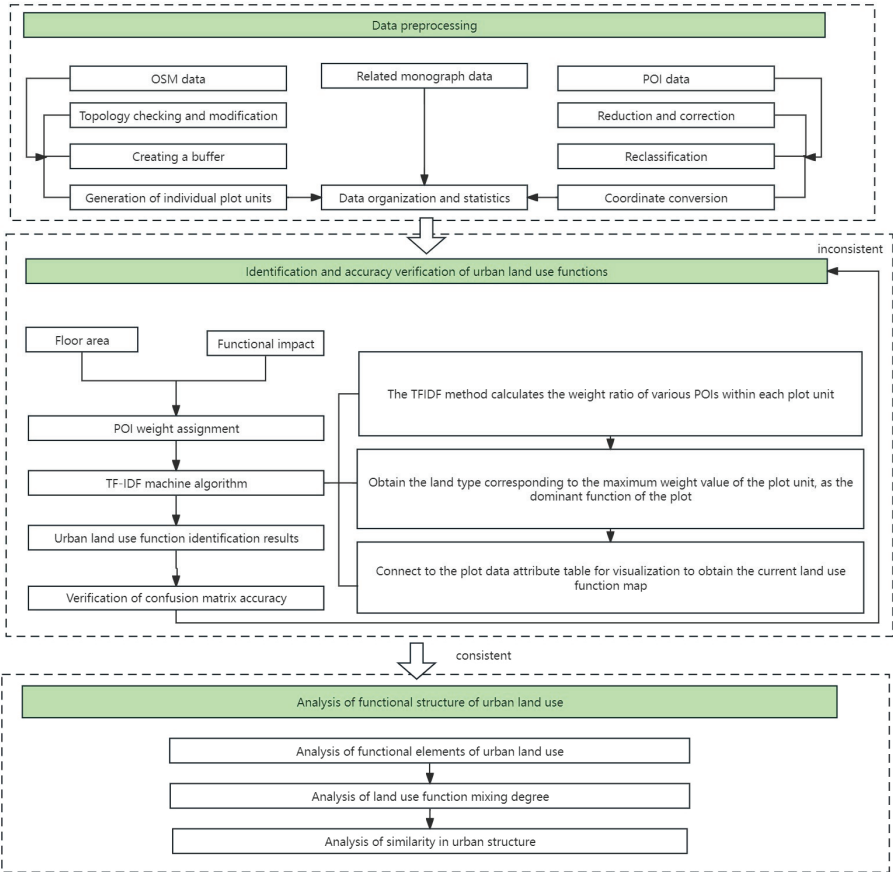
Figure 2. Flowchart of the research.

3.2. Data Preprocessing

3.2.1. OSM Data Preprocessing

(1) Topology checking and modification.

The original data volume of OSM data is huge and contains many disconnected, cluttered, and duplicated roads. Topology checking and modification of road line elements in ArcMap is performed to remove and fix the problematic roads by establishing topology rules such as no overlapping, no suspension points, no pseudo-nodes, no self-intersections, and so on.

(2)   Creating a buffer.

Delete suburban rural roads, pedestrian roads, bicycle lanes, unknown roads, and some internal roads based on road attribute information. Then, use highways, expressways, urban main roads, urban secondary roads, and some internal roads as the main line elements. Refer to China's "Urban Road Engineering Design Specification" (CJJ37-2019) to determine the grade width of different roads, and establish buffer zones on this basis. The specific width of the buffer is shown in Table 1.

Table 1. Urban road buffer widths.

Road Class	Name of Road	Buffer Width (m)
Primary Road	freeway	60
Secondary Road	speedway trunk road of city	45
Tertiary roads	secondary urban road	30
Fourth-class road	Internal roads	20

(3)   Generation of individual plot units.

After generating buffer zones for different roads, independent plot units are obtained by removing the road space. The smaller and fragmented parcel units are removed by combining the actual city conditions and satellite electronic maps. Finally, the base map of the five new first-tier cities is obtained for this study.

3.2.2. Preprocessing of POI Data

(1)   Data Reduction and Correction.

The original POI data of Amap is huge in volume, and there are problems such as missing information and duplicated information, and some information features are not significant. Firstly, POI data with missing coordinate information is directly deleted. Then, POI data with the same coordinate information and name are regarded as duplicated data, and only one piece of data is simplified and retained. Finally, POI data such as public toilets and bus stops, which are not significant in terms of functional features, are selected for deletion.

(2)   Data Reclassification.

The classification standard of POI data of Amap is relatively standardized among the POI data of many websites, but it also has the problems of rigid classification, duplication of classification, and overly detailed criteria of subtables, which lead to the fact that the POI data of Amap cannot be effectively connected with the actual land use function of the city, and it is challenging to establish a standardized framework for the future planning and construction of the city. Therefore, this study reclassified the POI data of five new first-tier cities based on multiple classification criteria, totaling eight primary classifications [28]. For details, see Table 2.

(3)   Data coordinate conversion.

The original POI data obtained directly used the GCJ-02 coordinate system. It is necessary to unify the spatial coordinates and convert the coordinate system of POI data to the coordinate system of OSM data. After the conversion is completed, the POI data are vectorized and then converted to projected coordinates. Finally, a shape file of POI data points is generated.

Table 2. List of classifications after POI reclassification.

Functional Site Type	Secondary Category	POI Detailed Category
Public administration and public service facilities	Administrative offices	Party and government organs; social organizations; police stations; institutions
	Cultural facilities	Book exhibitions; cultural events
	Healthcare	Hospitals; primary care; public health
	Education	Higher education; secondary vocational; primary and secondary schools; kindergartens; other education
	Scientific research	Research organizations
	Sports	Public gymnasiums
Commercial service land	Commercial land	Shopping centers; supermarkets; convenience stores
		Regular restaurants; fast food restaurants
		Hotels; hostels
	Commercial and financial land	Commercial office buildings; corporate companies
	Recreational land	Theaters
	Other commercial service land	Hairdressing and cosmetology; training institutions
Serviced land	Supply of land for facilities	Land for water supply; land for electricity supply; land for communications
	Land for environmental facilities	Drainage land; sanitation land
	Land for security facilities	Firefighting land; flood control land
Green spaces and open spaces	——	Parks and squares; heritage sites
Industrial and mining area	Industrial site	Industrial parks
Residential land	——	Living area
Transportation	Transportation site	Train station; bus station
Warehousing land	Land for logistics and warehousing	Logistics warehousing

4. Research Methodology

4.1. Urban Land Use Function Identification

4.1.1. POI Weight Assignment Methods

Due to the lack of information on the area occupied by physical objects and the level of public understanding in POI data, it is difficult to objectively reflect the importance of physical objects in their respective regions, which in turn affects the determination of dominant functions in that region [29,30]. In the process of quantifying the importance of different types of POI data, it is necessary to comprehensively consider indicators such as their quantity, function, scale, and public understanding. Given the difficulty in collecting relevant information and quantifying some indicators, this study used two indicators, land area and functional impact, to assign weight values to POI data [31]. The land area refers to the designated construction land within the land use boundary, requiring measurement, approval, and planning by the relevant management authorities. It primarily encompasses the land requisition area and the net land area of construction projects, including the main buildings, supporting facilities, activity areas, roadways, and green spaces. Additionally, the environmental awareness of urban residents can reflect the functional impact and significance of various types of POI entities over a specific period, which can be gauged through public awareness. This study determines the land area of different POI data and their functional impact based on standards such as the "Retail Format Classification Standard (GB/T18106-2021)" and the relevant research by Zhao et al. [32]. The

functional impact of each type of POI data is determined (Table 3), and then weighted values are calculated.

Table 3. POI data area and functional influence reference table.

Functional Site Type	Secondary Category	POI Detailed Category	Reference Footprint (hm^2)	Functional Influence
Public administration and public service facilities	Administrative offices	Party and government organs; social organizations; police stations; institutions	0.8; 0.1; 0.5	0.3550
	Cultural facilities	Book exhibitions; cultural events	0.2; 1	0.6760
	Healthcare	Hospitals; primary care; public health	6; 2; 0.1	0.7460
	Education	Higher education; secondary vocational; primary and secondary schools; kindergartens; other education	10; 3; 1.5	0.6760
	Scientific research	Research organizations	0.5	0.5010
	Sports	Public gymnasiums	1	0.5060
Commercial service land	Commercial land	Shopping centers; supermarkets; convenience stores	1; 0.2	0.5220
		Regular restaurants; fast food restaurants	0.1; 0.05	0.8140
		Hotels; hostels	5; 0.3	0.9260
	Commercial and financial land	Commercial office buildings; corporate companies	0.2	0.3520
	Recreational land	Theaters	2	0.2260
	Other commercial service land	Hairdressing and cosmetology; training institutions	0.2; 0.1	0.1250
Serviced land	Supply of land for facilities	Land for water supply; land for electricity supply; land for communications	0.5	0.0000
	Land for environmental facilities	Drainage land; sanitation land	0.5	0.0000
	Land for security facilities	Firefighting land; flood control land	0.5	0.0000
Green spaces and open spaces	——	Parks and squares; heritage sites	10	0.7520
Industrial and mining area	Industrial site	Industrial parks	5	0.2690
Residential land	——	Living area	8	0.7890
Transportation	Transportation site	Train station; bus station	50	0.0000
Warehousing land	Land for logistics and warehousing	Logistics warehousing	2	1.0000

Referring to the method adopted by Li et al. [33] in urban land functional zoning, first assign values to the reference land area corresponding to different types of POIs (Table 4), and then assign values to the functional impact of each type of POI (Table 5).

Table 4. POI floor area assignment table.

Area (m^2)	0–100	100–1000	1000–3000	3000–5000	5000–10,000	>10,000
Assignment	1	10	30	50	80	100

Table 5. Functional impact assignment table.

Functional Impact	0	0.3057	0.3350	0.5010	0.5069	0.6548	0.7460	0.8146
Assignment	0	30.6	33.5	50.1	50.7	65.5	74.6	81.4

Five different weighting ratios of 1:9, 3:7, 5:5, 7:3, and 9:1 were set for the floor space and functional influence. Through the precision test of the sampled plots, it was found that the average precision was the highest when the weighting ratio was 5:5. The weighting ratio of 5:5 was set for the POI for the assignment of weights with the weighting formula as follows:

$$W_{i,j} = 0.5 \times A_{i,j} + 0.5 \times I_{i,j} \tag{1}$$

where $W_{i,j}$ is the weight value of the ith POI data in parcel j, $A_{i,j}$ is the footprint assignment of the ith POI data in parcel j, and $I_{i,j}$ is the functional influence assignment of the ith POI data in parcel j.

4.1.2. TF-IDF Machine Algorithm

In order to highlight the unique POI types within each plot unit and reduce the interference of general POI types, the identification method used in this study is the TF-IDF statistical method. TF-IDF machine algorithm is a statistical method commonly used in information retrieval and text processing [34]. In the study of urban functional land use, all the constituent land parcels of the study area are considered as a collection of documents, with each individual land parcel being treated as a document, and the POI data distributed in the land parcels are regarded as different words. By utilizing the TF-IDF algorithm to calculate and determine which type of POI data has the highest TF-IDF value in the individual land parcels, it signifies the most "important" type of POI and also reflects the dominant function of the land parcel [35]. Considering that the simple structure of IDF does not effectively reflect the importance and distribution of words in the specific calculation process, this study adopts POI data endowed with weight values for calculation for the purpose of enhancing the algorithm's effectiveness in identifying the urban land use functions. The calculation can be performed using the following formula.

$$TF_{i,j} = \frac{n_{i,j}}{\sum_k n_{k,j}} \tag{2}$$

$$IDF_i = \log \frac{|D|}{|\{j : t_i \in d_j\}|} \tag{3}$$

$$TF - IDF_{i,j} = TF_{i,j} \times IDF_i \tag{4}$$

where i denotes the POI data and j denotes the parcel unit where the POI data is located. $n_{i,j}$ denotes the frequency of POI data i in parcel unit j; $\sum_k n_{k,j}$ denotes the total frequency of all the POI data occurrences in parcel unit j; D denotes the total number of parcel units; and $\{j : t_i \in d_j\}$ denotes the total number of parcel units containing POI data i.

The specific method includes three key steps. Firstly, the preprocessed POI data and road network are spatially connected in ArcGIS to obtain the corresponding number of various POIs for each plot unit. The spatially connected attribute table is exported, and POI categories are merged according to the methods in the literature. Then, the names and quantities of each POI category for each spatial unit are read and written into the document. Secondly, according to the TF-IDF algorithm, read the documents corresponding to each spatial unit and calculate and output the weight results for each category of each document (Namely, spatial unit). Finally, the category with the highest weight can be considered as the dominant function of the plot.

4.2. Verification of the Accuracy of Urban Land Use Function Identification Results

After obtaining the land use function layout of the five new first-tier cities, if we want to analyze and evaluate them, the analysis and evaluation need to be based on the recognition results with sufficient accuracy. This study randomly selected a certain number of parcel units for each different land use type as the identification results and the corresponding Gaode satellite map of the cities as the actual results; meanwhile, it used the method of constructing confusion matrix to test the accuracy of the land use function identification results of the five new first-tier cities, supplemented by the manual visual comparison test method, in which the land use function identification results of the five new first-tier cities' downtowns are contrasted with the land use functions of the Gaode satellite electronic maps by manual visual comparison.

A confusion matrix is constructed to contain four indexes: user accuracy (UA), Producer accuracy (PA), overall accuracy (OA), and Kappa coefficient, in which the Kappa coefficient is used to assess the precision of the recognition results [36]. The confusion matrix consists of N rows and N columns, where the rows represent the recognition results and the columns of the matrix represent the actual results. In this study, a certain number of randomly selected parcel units for each different land use type are used as the recognition results, and their city counterparts of the Gaode electronic satellite map are used as the actual results. The following is the calculation formula:

$$UA = \frac{X_{ii}}{\sum_{j=1}^{N} X_{ij}} \times 100\% \tag{5}$$

$$PA = \frac{X_{ii}}{\sum_{j=1}^{N} X_{ji}} \times 100\% \tag{6}$$

$$OA = \frac{\sum_{i=1}^{N} X_{ii}}{M} \times 100\% \tag{7}$$

$$Kappa = \frac{M \times \sum_{i=1}^{N} X_{ii} - \sum_{i=1}^{N} \left(\sum_{j=1}^{N} X_{ij} \times \sum_{j=1}^{N} X_{ji} \right)}{M^2 - \sum_{i=1}^{N} \left(\sum_{j=1}^{N} X_{ij} \times \sum_{j=1}^{N} X_{ji} \right)} \tag{8}$$

where M denotes the overall number of sampled parcel units, N denotes the number of land types, X_{ij} represents the total number of correctly identified parcels, $\sum_{j=1}^{N} X_{ij}$ denotes the sum of the number of parcels in row i, and $\sum_{j=1}^{N} X_{ji}$ denotes the sum of the number of parcels in column i.

4.3. Functional Mix of Urban Land Use

With the rise of the concept of intensive land use, government departments will also consider the degree of functional mixing in functional areas when formulating urban planning [37]. The mixing of land use functions within a certain range helps to realize the efficient use of urban land. The degree of land use mixing reflects the degree of mixing of functions in a parcel of land by calculating the proportion of various types of POI data within the parcel unit. This study further analyzes the current status of urban land use functions in the urban centers of five new first-tier cities by calculating the degree of mixing of land use functions in the downtown of the five new first-tier cities. The equation used to determine the extent of land use mixing is shown below [38]:

$$M = -\sum_{i=1}^{n} (p_i \times \ln p_i) \tag{9}$$

where M is the functional mixing degree of the site, n denotes the number of POI data types in the parcel, and p_i denotes the proportion of POI data of type i in the parcel to all POI data. For each parcel unit, the site mixing degree values were categorized into low, lower, general, high, and higher.

4.4. Similarity of Urban Land Use Structure

VSM (vector space mode) was developed in the late 1960s when G Salton et al. [39] proposed a model that was first used in SMART information retrieval systems and has now become a commonly used model in natural language processing [40]. This model transforms text into high-dimensional vectors, with feature terms as its basic unit. Each dimension of a vector corresponds to a feature item of the text, and the dimension also represents the weight value of the feature item in the text, and the degree of the weight value also indicates the importance of the feature item in its text. When comparing the similarity between two documents, the inner product between vectors is usually used in calculations. In this study, the document was considered as a city, and the feature items were considered as the type of land use. Referring to the algorithm proposed by Li et al. [41],
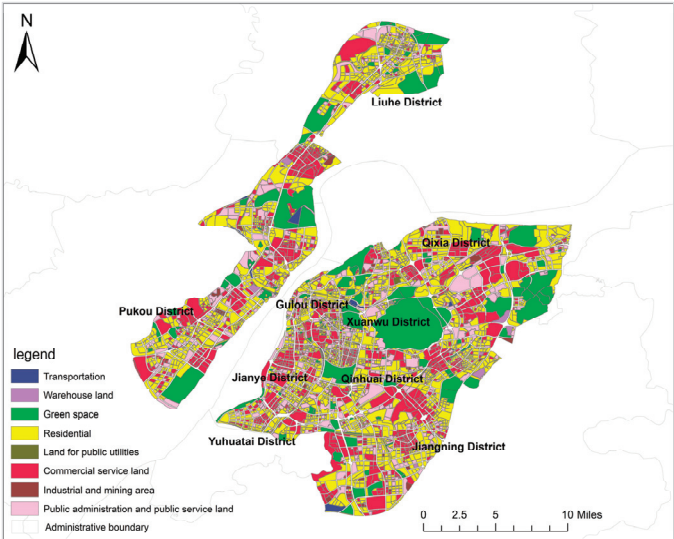
Figure 4. Results of functional identification of land use in Nanjing's central urban area.

As can be seen from Figure 5, residential land and green space occupy most of the study area in Hangzhou. In addition, most of the green space, represented by Hangzhou West Lake Scenic Spot, Wuchao Mountain National Forest Park, and Xixi National Wetland Park, is concentrated in the West Lake district, while residential land and commercial service land are concentrated in Gongshu District, Shangcheng District, and Binjiang District.
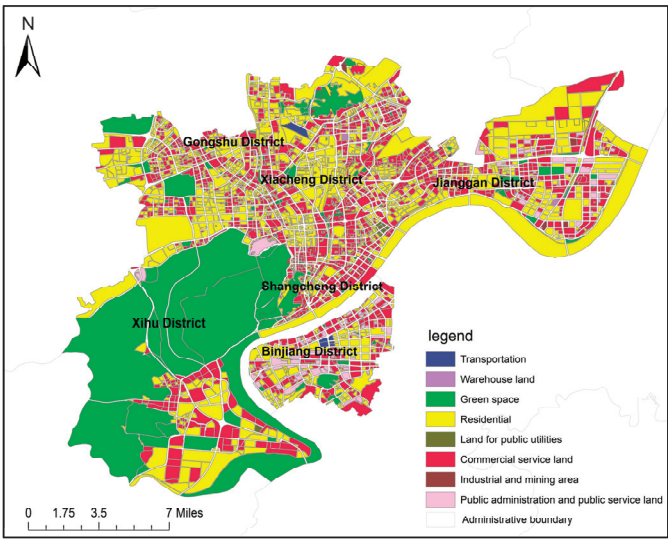
Figure 5. Results of land use function identification in Hangzhou's central urban area.

Figure 6 shows that residential land occupies most of the land in the center of Xi'an. Further observation reveals that residential land, commercial service land, and public administration and public service land are distributed in each administrative district, while green space is mainly distributed in Weiyang District, Lianhu District, Beilin District, and Baqiao District.
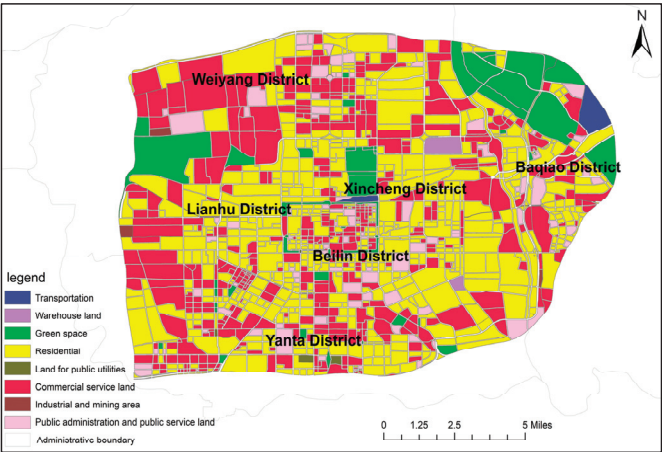
Figure 6. Results of land use function identification in Xi'an's central urban area.

As can be seen from Figure 7, residential land occupies most of downtown Tianjin. Meanwhile, residential land, commercial service land, and public management and public service land are more evenly distributed, while green space is mostly distributed in Dongli District, Nankai District, and Beichen District and concentrated at the edges of the study area. Meanwhile, the number of internal areas is relatively small.
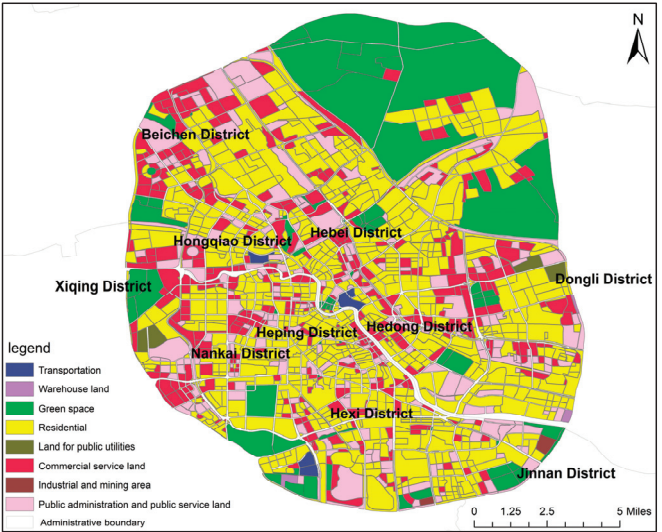

Figure 7. Results of land use function identification in Tianjin's central urban area.

5.2. Verification of the Accuracy of the Results of Site Function Identification

After using the TF-IDF machine algorithm on the OSM data and POI data of the five new first-tier cities, their respective land use function identification results are obtained. To verify the accuracy of the identification results, 30 plots are indiscriminately picked for each land use function to establish the confusion matrix. The Kappa coefficients of the confusion matrices of the five new first-tier cities are 0.68, 0.70, 0.73, 0.73, and 0.72, respectively (Table 6). They are in the range of 0.61 to 0.80, which means that the results of

the identification results show high consistency in comparison with the actual situation of the cities and can be continued to carry out the subsequent analysis and evaluation.

Table 6. Overall accuracy of the five new first-tier cities and the Kappa coefficient.

City	Overall Accuracy (%)	Kappa
Chengdu	78.00	0.72
Xi'an	74.37	0.68
Tianjin	76.00	0.70
Hangzhou	78.67	0.73
Nanjing	78.67	0.73

5.3. Comprehensive Analysis of Urban Functional Land Use Elements

The statistical results of land use function identification for eight types of land parcels in the central urban areas of five cities are as follows:

From Figure 8a, in the research area of Chengdu, among the 1420 plot units and a total area of 485.02 km^2, residential land has the highest number of plot units, with 685 (185.08 km^2). The commercial land plot is second, with 387 (72.46 km^2). Additionally, there are 199 (64.64 km^2) and 49 (128.36 km^2) plots of land for public management and public services, as well as for green spaces and open spaces.

As described in Figure 8b, in the research area of Nanjing, among the 5289 plot units and a total area of 649.92 km^2, residential land has the highest number of plot units, with 2691 (251.78 km^2). The commercial land plot is second, with 1368 (153.55 km^2). Furthermore, there are 944 (90.98 km^2) and 165 (140.61 km^2) plots of land for public management and public services, as well as for green spaces and open spaces.

As shown in Figure 8c, among the 3959 plot units and a total area of 541.30 km^2 in the Hangzhou research area, residential land has the highest number of plot units, with 2086 (212.42 km^2). The commercial land parcels are second, with 1499 (122.75 km^2). There are 166 (190.15 km^2) and 145 (12.38 km^2) plots of land for green spaces and open spaces, as well as for public management and services.

In Figure 8d, among the 1396 plot units and a total area of 335.87 km^2 in the research area of Xi'an, residential land has the highest number of plot units, with 738 (163.76 km^2). The commercial land parcels come in second place, with 443 (109.21 km^2). There are 104 (20.32 km^2) and 66 (36.05 km^2) plots of land for public management and public services, as well as for green spaces and open spaces.

As illustrated in Figure 8e, among the 1920 plot units and a total area of 374.23 km^2 in the Tianjin research area, residential land has the highest number of plot units, with 1070 (173.01 km^2). The commercial land parcels come in second place, with 439 (57.68 km^2). There are 280 (53.33 km^2) and 74 (84.43 km^2) plots of land for public management and public services, as well as for green spaces and open spaces. In addition, the number of land parcels for public facilities, industrial and mining, warehousing, and transportation in the five cities is relatively small and decreasing in sequence.

Comparing the number of plots and area of the eight different land use types in these five new-tier cities, it is found that their common characteristics, which are the total number of plots and area of the four land use types, namely, residential, commercial service land, public management and public service land, and green space, account for more than 90%, which is also in line with the functions that are carried by the downtown of the cities (Figure 9). Looking at the ratio of the number of plots and area of these four types of land in the five new first-tier cities, it is clear that residential land is the first land type in the five cities in terms of the number of plots and area of land. As for the proportion of land, the situation varies from city to city, but in general, it can be seen that the commercial service land and green space are larger, followed by the public management and public service land.
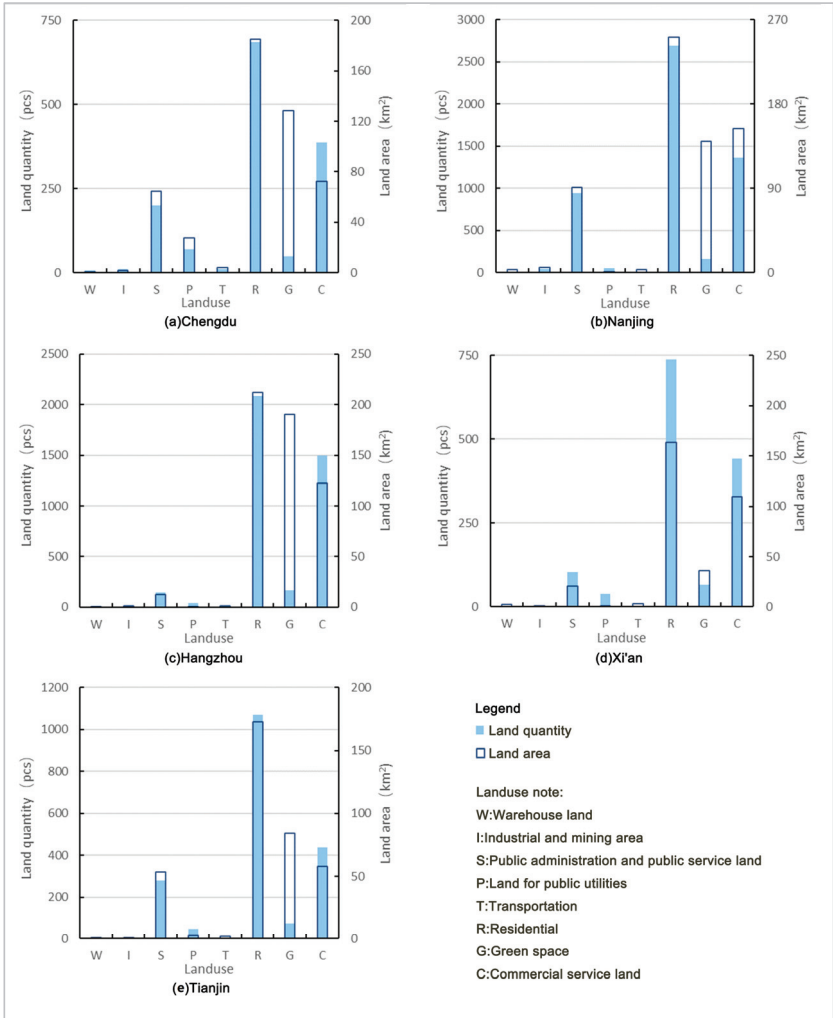
Figure 8. Quantity and area of land use in five new first-tier cities.

5.4. Comprehensive Analysis of the Functional Mix of Urban Land Use

In Figure 10a, the mixed degree of functional land in the study area of Chengdu is relatively high. The land use units with mixed degrees of "high" and "higher" account for nearly 50% of the study area, mainly concentrated in Wuhou District, Qingyang District, Jinniu District, Chenghua District, and Jinjiang District, which are part of the five districts in the city, as well as Xindu District and Pidu District. Due to the policy of constructing urban forest parks, the land mix in Longquanyi District is relatively low. The plot units with "low" and "lower" mixing degrees account for about 20% of the study area and are relatively scattered, mainly carrying the functions of residential land.

In Figure 10b, the overall land use function mixing degree in Nanjing is relatively low, with only about 20% of the study area being occupied by land units with "high" and "higher" mixing degrees, mainly concentrated in Gulou District and Qinhuai District. The land mix of land units in Xuanwu District, Pukou District, Qixia District, and Liuhe District is mostly "low" and "average", mainly carrying green space and open space land and

residential land, such as Zhongshan Scenic Area, Xuanwu Lake Park, Pearl Spring Scenic Area, Niushoushan Tourism Area, etc.
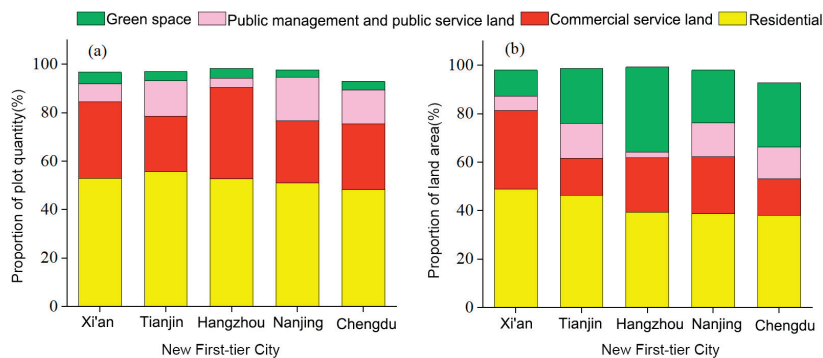

Figure 9. Number and size of land parcels for major land use functions in new first-tier cities. Note: (**a**) represents the proportion of land parcels with main land use functions in new first-tier cities; (**b**) represents the proportion of land area for the main land use functions in new first-tier cities.

In Figure 10c, the overall land mix in Hangzhou City is not high, especially in the West Lake District, as well as the riverside areas of Shangcheng District and Jianggan District. The vast majority of the West Lake area is the West Lake Scenic Area, while the remaining riverside areas follow the ecological protection policies of Hangzhou City, and their land use functions are relatively single. The north side of the research area in Hangzhou basically only carries residential and commercial service functions, so the land mix is also relatively low.

In Figure 10d, plot units with "high" and "higher" mixing degrees occupy nearly one-third of the research area in Xi'an and are mostly distributed in Lianhu District, Xincheng District, and Beilin District within the Second Ring Road. These areas mainly carry urban functions such as residential, commercial services, public management, and public services. In the research area of Xi'an City, most of the areas with "low" and "average" mixing degrees are distributed in the West Third Ring Road, where the development level is relatively backward and the functions carried by the plot units are relatively few. In addition, the land mix in the Chanba Ecological Area on the east side of Baqiao District is relatively low.

In Figure 10e, the degree of land use mixing in the study area of Tianjin shows a clear dispersion pattern. The old urban areas of Tianjin, Hexi District, Hedong District, Hebei District, Heping District, Nankai District, and Hongqiao District, have a reasonable planning layout, with land units of different degrees of mixing arranged in a staggered manner. While carrying land functions such as residential, commercial services, public management, and public services, they meet the living needs of citizens. It will not cause excessive concentration of land use functions, leading to traffic congestion problems. In addition, the plots with a low degree of mixing are mostly located in the northern expansion section of the outer ring road. Due to their low level of development, they mainly carry residential and green space functions, and the overall functional land mixing is the lowest.

In Figure 11, the similarities in land use function mix among the five new first-tier cities are as follows: (1) In the proportion of the number of land plots with varying degrees of land mix to the land area, the number of land plots with a high degree of land mix to the land area is mostly the smallest part. (2) Chengdu, Tianjin, and Xi'an show a clear pattern of dispersion in the functional mix of the five classes of land use, among which Chengdu and Tianjin have a higher overall functional mix of land use, and Xi'an has a lower overall functional mix of land use. (3) Nanjing and Hangzhou both have a low degree of functional mixing due to a relatively significant amount of scenic spots and cultural heritage sites in

their urban study areas. (4) The plot units with a high and higher degree of mixing only account for about 20% of the study area.
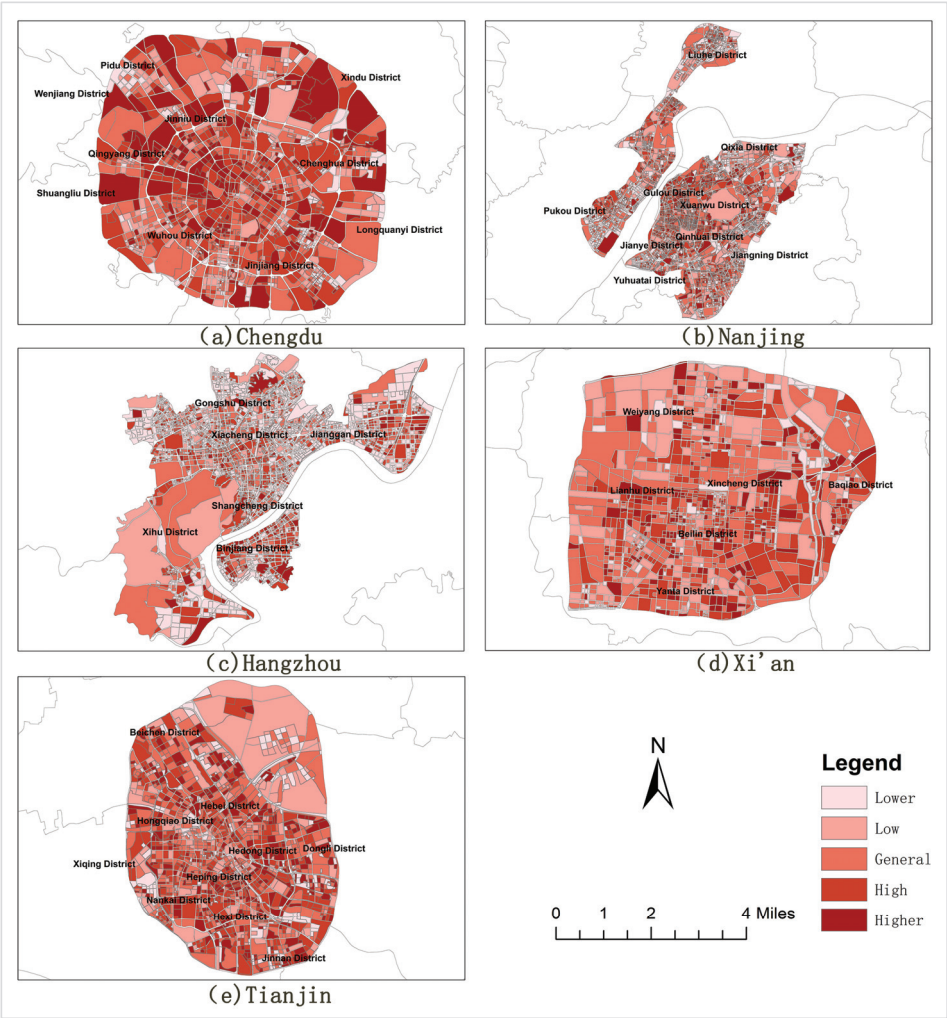

Figure 10. Land use mixing degree in five new first-tier cities.

5.5. Similarity Analysis of Urban Land Use Structure

From Table 7 and Figure 12, we can see that in the downtown of the five new first-tier cities, Hangzhou and Nanjing have the highest degree of similarity in the layout of the functional structure of urban land use. Xi'an and Tianjin have the second highest degree of similarity, and Chengdu and Nanjing have the lowest degree of similarity in the layout of functional structure of urban land use.

In addition, the similarity of the functional structure of land use between these five new first-tier cities, from high to low, is as follows: Hangzhou–Nanjing, Tianjin–Xi'an, Tianjin–Nanjing, Xi'an–Hangzhou, Xi'an–Nanjing, Chengdu–Xi'an, Tianjin–Hangzhou, Tianjin–Chengdu, Chengdu–Hangzhou, Chengdu–Nanjing.
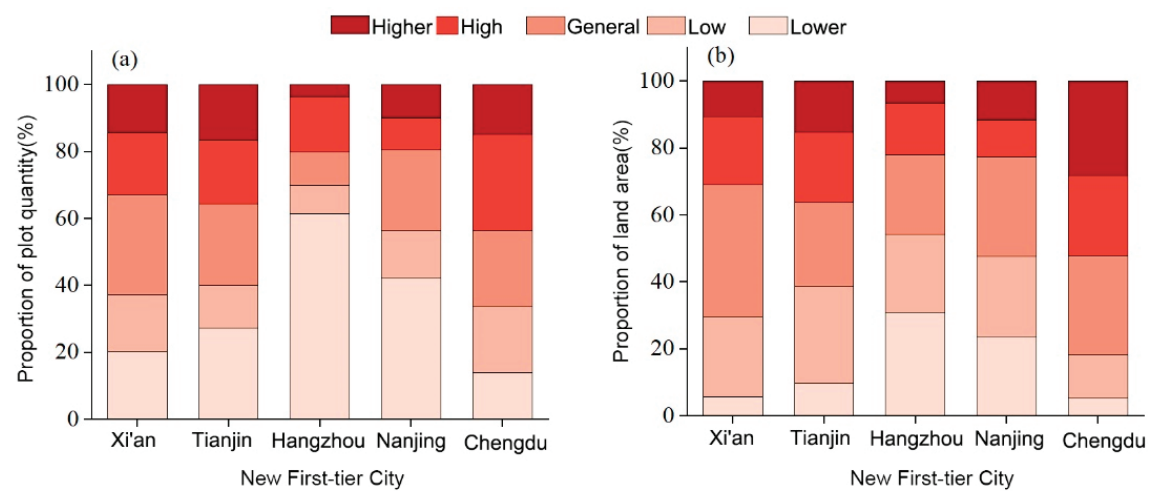
Figure 11. Number and Size of plots with different degrees of functional mix in new first-tier cities. Note: (**a**) represents the proportion of land parcels with varying degrees of functional mix in new first-tier cities; (**b**) represents the proportion of land use area in new first-tier cities with varying degrees of functional mix.

Table 7. Similarity of land use functional structure among the five new first-tier cities.

Cities	Chengdu	Xi'an	Tianjin	Hangzhou	Nanjing
Chengdu	-	-	-	-	-
Xi'an	0.59	-	-	-	-
Tianjin	0.36	0.76	-	-	-
Hangzhou	0.29	0.72	0.56	-	-
Nanjing	0.19	0.66	0.74	0.81	-

As the two cities with the highest structural similarity, Hangzhou and Nanjing exhibit a close resemblance in their POI data, particularly under the detailed category classification. The number of POI data in the two cities is very similar, contributing to their higher structural similarity in the final calculation result. Conversely, the structural similarity between the remaining cities diminishes as the proximity of the type and number of POI data diverges. Consequently, the evaluation index of urban land using function similarity can effectively illustrate the degree of similarity in land use functions between cities in terms of quantity and type, thereby facilitating a comprehensive exploration of the general pattern of land use function structure in the five new first-tier cities. As the four land use types occupy the majority of land use in the study area of the five new first-tier cities, residential land is similar in quantity and occupies the largest area, and commercial service land is similar in quantity, but there are differences in types. Green space is similar in type but different in number. Public management and public services land are similar in number and type.
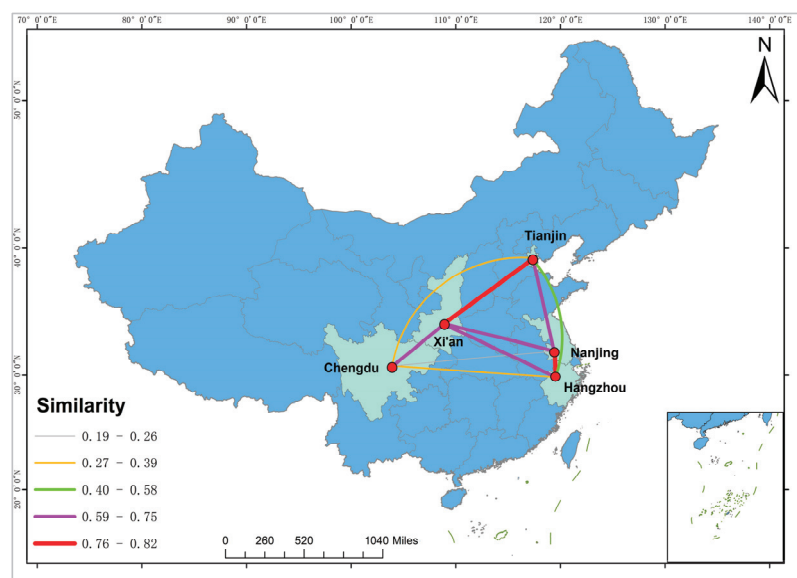
Figure 12. Similarity of land use structure in five new first-tier cities.

6. Discussion

6.1. Feasibility Analysis of Methods

Previous studies have demonstrated the advantages of multi-source big data in urban land use research and refinement [42]. Among these, POI data represents urban functions in daily life in spatial point form, encompassing spatial information such as longitude, latitude coordinates, and addresses of geographic entities, along with various attribute information like main categories, administrative divisions, and names. Compared to other big data sources, POI data is closely related to land use types, has fewer privacy concerns, is easily obtainable, and relatively straightforward to process. It significantly reduces the cost of preliminary research, effectively reflects urban spatial structure, and finds wide application in the identification and analysis of urban functional areas [11,12,43]. For a more accurate analysis of urban functional zoning, a need for refined research units arises. Li et al. used grid data to generate research units to identify functional areas in the central urban area of Wuhan, which is a simple and fast division method [33]. However, urban blocks typically have irregular polygonal shapes, and using grid data may not accurately reflect the actual block situation. OSM (OpenStreetMap) road network data, with its high positioning accuracy and basic spatial information, including longitude, latitude, road types, and names, provide a more realistic division of block units, making it a valuable data source in land use analysis [44–46]. This study, based on OSM and POI data, breaks through the limitations of traditional static data by utilizing the TF-IDF quantitative analysis method in machine learning to identify urban land use functions. This approach reduces manual intervention and provides a more scientific and objective reflection of urban land use. Comparison with previous studies reveals relatively consistent identification results for land use functions in these five cities. For example, Yu et al. identified the urban functional areas in Chengdu and observed that the primary functional zones were distributed in concentric circles centered around the city center. Residential land dominated the main urban areas, with mixed functional areas comprising 50% of the total area, aligning closely with the findings of this study [47]; Ding et al. identified the functional areas in the central urban area of Nanjing and discovered that residential land comprised 42.3% of the study area, a slight variance from the 50.88% residential land in this study. This difference may be attributed to the broader scope of our study area, leading to a greater diversity of

functional elements and a larger proportion of various land uses [48]. Wu et al. developed an urban functional area identification model using the kernel density estimation method and delineated six single/mixed functional areas within Tianjin City. The distribution of different land types exhibits a gradually dispersing pattern from the city center to the periphery, which is largely in line with the findings of this work [49]. In conclusion, the availability of OSM and POI data makes this method easily applicable to other cities.

6.2. Current Situation Analysis

The study found that residential land in five cities occupies most of the major urban areas. This is because the urbanization level of these cities is relatively high, and a large number of rural populations are gathering in the central urban areas, leading to an increasing demand for urban residential land. In addition, due to historical reasons, Hangzhou, Nanjing, and Chengdu implemented the plan of evacuating residential functions to the periphery earlier in the process of urban development. Therefore, their proportion of residential land is lower than that of the central urban areas of Xi'an and Tianjin. For the element of green space and open space land, as Hangzhou is located along the southern edge of the Yangtze River Delta and the Qiantang River Basin with abundant water and forest resources, it not only has natural landscapes such as West Lake and Xixi Wetland, but its unique natural endowment also facilitates the creation and development of various green spaces and parks between cities, resulting in the highest proportion of green space and open space land. Although Xi'an, as one of the four ancient capitals of China, has cultural relics such as the Daming Palace and the Weiyang Palace, its complex terrain and variable climate result in the lowest proportion of green space and open space land.

By integrating the findings of land use function identification, it was observed that the majority of land units with low functional diversity in the study area of the five new first-tier cities are characterized by diverse urban landscapes. This can be attributed to two potential reasons: (1) These land units may contain buildings and facilities with singular functions, such as commercial, residential, or industrial areas. The lack of comprehensive planning and design results in a singular and less dynamic urban landscape, contributing to the low degree of functional diversity in these land units; (2) Constraints imposed by land ownership and planning management. Divergent interests and planning objectives among different landowners and planning managers may lead to the fragmentation and decentralization of internal functions within land units.

6.3. Shortcomings and Prospects

First of all, there is still room for further improvement in the processing of POI data. From the initial deletion processing to the subsequent weight assignment, there are certain human influence factors. To address this problem, deep learning algorithms can be used to further reduce POI data to ensure its authenticity and objectivity and minimize the occurrence of duplicate superimposition. OSM has low density and a lack of data in suburban and rural areas, resulting in excessive division of functional units and poor local recognition results.

Secondly, when analyzing and evaluating the five new first-tier cities, there is potential to enrich the indicators used, particularly for comprehensive comparative analysis among these cities. In the future, it would be beneficial to include indicators such as location entropy and nearest-neighbor distance to further assess the current status of urban land use functions and explore their patterns. This approach will enable the formulation of more objective and comprehensive problem assessments and optimization suggestions.

Thirdly, when selecting research subjects, for a more extensive exploration of the current state of urbanization in China, it would be advantageous to encompass a broader range of cities for a more comprehensive analysis. This broader perspective will allow for an exploration of the current state of urbanization in China from a more macroscopic viewpoint.

Finally, this study identified certain similarities in their land use functions. However, due to the different policies and historical conditions implemented in different cities, it is difficult to promote this land use feature throughout China and even the world. Future research could involve a comprehensive evaluation of various land use functional layouts to determine the optimal layout for urban planning.

7. Conclusions

Identification of central urban land use functions in the five new first-tier cities involves processing OSM and POI data for each city and utilizing the TF-IDF machine algorithm for function identification. Influenced by geographical conditions, resource endowments, and planning policies, differences in the functional layout of land use are observed among these cities. However, common characteristics among the five cities include residential land, commercial service land, public management and public service land, green land, and open land, with the total number and area of these land types accounting for over 90%.

The accuracy verification of central urban land use function identification results of the five new first-tier cities involved constructing a confusion matrix to test the accuracy of land use function identification. The Kappa coefficients, falling within the range of [0.61, 0.80], indicate a high level of consistency in accuracy evaluation. This further verifies the feasibility of urban land function identification based on multi-source big data. Most of the plot units with low functional mixing in the research area of the five new first-tier cities are distributed with various urban landscapes.

The evaluation of central urban land use in the five new first-tier cities involves assessing the present situation of urban land use function through land use mix degree and urban structure similarity degree. Chengdu and Tianjin exhibit the highest land use function mixing degree, followed by Xi'an, Nanjing, and Hangzhou. In Chengdu, Tianjin, and Xi'an, the mixing degree of five levels of land use functions shows an obvious dispersion pattern, while Nanjing and Hangzhou have high mixed land use function plots concentrated in several administrative regions. According to the calculation results of urban structure similarity, Hangzhou and Nanjing have the highest similarity of land use function structure layout, followed by Xi'an and Nanjing, with the lowest similarity observed between Chengdu and Nanjing. The similarity of land use function structure layout is higher when cities are closer in terms of the type and quantity of land use functions.

Conflicts of Interest: The authors declare no conflicts of interest.

References

1. Ni, P.F.; Xu, D.H. China's Urbanization for 2035. *Reform* **2022**, *8*, 98–110.
2. Yang, X.; Lu, X. Driving factors of urban land urbanization in China from the perspective of spatial effects. *China Popul. Resour. Environ.* **2021**, *31*, 156–164.
3. Yang, Y. A Study on Identification of Urban Functional Zones and Evolution of Spatial Structure—A Case of Changchun City. Ph.D. Dissertation, Jilin University, Changchun, China, 2022.

4. Pan, C.; Wu, S.; Li, E.; Li, H.; Liu, X. Identification of urban functional zones in Macau Peninsula based on POI data and remote information sensors technology for sustainable development. *Phys. Chem. Earth Parts A/B/C* **2023**, *131*, 103447. [CrossRef]
5. Wang, Q.; Liu, X.; Li, Y. Spatial Structure, City Size and Innovation Performance of Chinese Cities. *China Ind. Econ.* **2021**, *398*, 114–132.
6. Qiu, B.; Ye, M.; Ning, K. Twelve Inflection Points Focusing on the Second Half of Urbanization in China. *Urban Dev. Stud.* **2021**, *9*, 1006–3862.
7. Wang, K. Green Transformation and Development of China's Urbanization. *City Plan. Rev.* **2021**, *36*, 9–16.
8. Dan, X. Research on Functional Area Division and Spatial Distribution of Chengdu Based on Multi-source Data. Master's Thesis, Yunnan University, Kunming, China, 2021.
9. Xue, B.; Xiao, X.; Li, J.; Zhao, B.; Fu, B. Multi-source Data-driven Identification of Urban Functional Areas: A Case of Shenyang, China. *Chin. Geogr. Sci.* **2022**, *33*, 21–35. [CrossRef]
10. Frias-Martinez, V.; Frias-Martinez, E. Spectral clustering for sensing urban land use using Twitter activity. *Eng. Appl. Artif. Intell.* **2014**, *35*, 237–245. [CrossRef]
11. Jiang, S.; Alves, A.; Rodrigues, F.; Ferreira, J., Jr.; Pereira, F.C. Mining point-of-interest data from social networks for urban land use classification and disaggregation. *Comput. Environ. Urban Syst.* **2015**, *53*, 36–46. [CrossRef]
12. Hu, T.; Yang, J.; Li, X.; Gong, P. Mapping Urban Land Use by Using Landsat Images and Open Social Data. *Remote Sens.* **2016**, *8*, 151. [CrossRef]
13. Ye, C.; Zhang, F.; Mu, L.; Gao, Y.; Liu, Y. Urban function recognition by integrating social media and street-level imagery. *Environ. Plan. B Urban Anal. City Sci.* **2020**, *48*, 1430–1444. [CrossRef]
14. Liu, X.; Tian, Y.; Zhang, X.; Wan, Z. Identification of Urban Functional Regions in Chengdu Based on Taxi Trajectory Time Series Data. *ISPRS Int. J. Geo-Inf.* **2020**, *9*, 158. [CrossRef]
15. Sun, Y.; Yin, H.; Wen, J.; Sun, Z. Urban Region Function Mining Service Based on Social Media Text Analysis. *Int. J. Softw. Eng. Knowl. Eng.* **2021**, *31*, 563–586. [CrossRef]
16. Huang, X.; Yang, J.; Li, J.; Wen, D. Urban functional zone mapping by integrating high spatial resolution nighttime light and daytime multi-view imagery. *ISPRS J. Photogramm. Remote Sens.* **2021**, *175*, 403–415. [CrossRef]
17. Liu, B.; Deng, Y.; Li, M.; Yang, J.; Liu, T. Classification Schemes and Identification Methods for Urban Functional Zone: A Review of Recent Papers. *Appl. Sci.* **2021**, *11*, 9968. [CrossRef]
18. Yuan, N.J.; Zheng, Y.; Xie, X.; Wang, Y.; Zheng, K.; Xiong, H. Discovering Urban Functional Zones Using Latent Activity Trajectories. *IEEE Trans. Knowl. Data Eng.* **2015**, *27*, 712–725. [CrossRef]
19. Feng, R.; Dong, X.; Liang, T.; Wang, L. Identification of Urban Functional Areas Based on Logistic Regression Model. *Geomat. Spat. Inf. Technol.* **2018**, *41*, 109–112.
20. Zhai, W.; Bai, X.; Shi, Y.; Han, Y.; Peng, Z.-R.; Gu, C. Beyond Word2vec: An approach for urban functional region extraction and identification by combining Place2vec and POIs. *Comput. Environ. Urban Syst.* **2019**, *74*, 1–12. [CrossRef]
21. Shicheng, Y.; Jingli, W.; Chengming, L.; Zhaoxin, D.; Hao, L. Urban Functional Area Division Considering POI and Land Use Data. *J. Geomat. Sci. Technol.* **2021**, *38*, 181–186.
22. Zhihao, S.; Hongzan, J.; Hao, W.; Zhenghong, P.; Lingbo, L. Block2vec: An approach for identifying urban functional regions by integrating sentence embedding model and points of interest. *ISPRS Int. J. Geo-Inf.* **2021**, *10*, 339.
23. Lai, G.; Zhao, G.; Yang, M. Identification of Urban Functional Areas and Measurement of Mixing Degree Based on Classification Modeling and TF-IDF Algorithm. *Geomat. Spat. Inf. Technol.* **2023**, *46*, 89–93.
24. Yang, M.; Cao, S.; Zhang, H.; Wu, S.; Zhang, D. Using Point of Interest Data and Satellite Observation for Urban Functional Zone Mapping. *Sens. Mater.* **2023**, *35*, 269–284. [CrossRef]
25. Miao, R.; Wang, Y.; Li, S. Analyzing Urban Spatial Patterns and Functional Zones Using Sina Weibo POI Data: A Case Study of Beijing. *Sustainability* **2021**, *13*, 647. [CrossRef]
26. Li, L.; Ma, S.J.; Wang, Y.P. Smart city and public cultural resources demand based on big data: A case study of Tianjin Library. *Int. J. Innov. Manag. Technol.* **2020**, *11*, 57–62. [CrossRef]
27. Gao, X. Identification and Optimization of Xi'an Urban Land Use Function Based on POI Data. Master's Thesis, Northwest University, Xi'an, China, 2021.
28. Cheng, Y.; Zhao, M. On the Land-use Classification System in the Context of Territorial Spatial Planning: Classification Structure and Application Rationale. *Urban Plan. Forum* **2021**, *4*, 367–377.
29. Bao, H.; Ming, D.; Guo, Y.; Zhang, K.; Zhou, K.; Du, S. DFCNN-Based Semantic Recognition of Urban Functional Zones by Integrating Remote Sensing Data and POI Data. *Remote Sens.* **2020**, *12*, 1088. [CrossRef]
30. Renato, A.; Ana, A.; Carlos, B. POI mining for land use classification: A case study. *ISPRS Int. J. Geo-Inf.* **2020**, *9*, 493.
31. Luo, G.; Ye, J.; Wang, J.; Wei, Y. Urban Functional Zone Classification Based on POI Data and Machine Learning. *Sustainability* **2023**, *15*, 4631. [CrossRef]
32. Zhao, W.; Li, Q.; Li, B. Extracting hierarchical landmarks from urban POI data. *J. Remote Sens.* **2011**, *15*, 973–988.
33. Qiang, L.; Xinqi, Z.; Yi, C. Research on function identification and distribution characteristics of Wuhan supported by big data. *Sci. Surv. Mapp.* **2020**, *45*, 119–125.
34. Zhuo, H.W.; Dong, W.; Qing, L.I. Keyword Extraction from Scientific Research Projects Based on SRP-TF-IDF. *Chin. J. Electron.* **2021**, *30*, 652–657. [CrossRef]

35. Zhou, L.; Liu, M.; Zheng, Z.; Wang, W. Quantification of Spatial Association between Commercial and Residential Spaces in Beijing Using Urban Big Data. *ISPRS Int. J. Geo-Inf.* **2022**, *11*, 249. [CrossRef]

36. Wei, X.; Hu, M.J.; Wang, X.J. The differences and influence factors in extracting urban green space from various resolutions of data: The perspective of blocks. *Remote Sens.* **2023**, *15*, 1261. [CrossRef]

37. Lv, Q.; Lin, Y.; Zhao, J.; Qin, B. The correlation between the prediction of land mixing degree and the evolution of land mixed use in Kunming. *J. Lanzhou Univ. Nat. Sci.* **2022**, *58*, 548–559.

38. Liu, X.; Long, Y. Automated identification and characterization of parcels (AICP) with OpenStreetMap and Points of Interest. *Environ. Plan. B* **2015**, *43*, 498–510.

39. Salton, G.; Wong, A.; Yang, C.S. A vector space model for automatic indexing. *Commun. ACM* **1975**, *18*, 613–620. [CrossRef]

40. Yan, L.; Ge, L.N.; Hu, Z. Attribute-based multi-keyword ranking search scheme based on blockchain. *Appl. Res. Comput.* **2023**, *40*, 1952–1956+1963.

41. Li, T.; Zheng, X.; Zhang, C.; Wang, R.; Liu, J. Mining Spatial Correlation Patterns of the Urban Functional Areas in Urban Agglomeration: A Case Study of Four Typical Urban Agglomerations in China. *Land* **2022**, *11*, 870. [CrossRef]

42. Kuang, W.H. Spatio-temporal patterns of intra-urban land use change in Beijing, China between 1984 and 2008. *Chin. Geogr. Sci.* **2012**, *22*, 210–220. [CrossRef]

43. Krause, C.M.; Zhang, L. Short-term travel behavior prediction with GPS, land use, and point of interest data. *Transp. Res. Part B Methodol.* **2019**, *123*, 349–361. [CrossRef]

44. Kulawiak, M.; Dawidowicz, A.; Pacholczyk, M.E. Analysis of server-side and client-side Web-GIS data processing methods on the example of JTS and JSTS using open data from OSM and geoportal. *Comput. Geosci.* **2019**, *129*, 26–37. [CrossRef]

45. Brovelli, M.A.; Zamboni, G. A New Method for the Assessment of Spatial Accuracy and Completeness of OpenStreetMap Building Footprints. *ISPRS Int. J. Geo-Inf.* **2018**, *7*, 289. [CrossRef]

46. Jokar Arsanjani, J.; Mooney, P.; Zipf, A.; Schauss, A. Quality assessment of the contributed land use information from Open-StreetMap versus authoritative datasets. In *OpenStreetMap in GIScience: Experiences, Research, and Applications*; Springer: Cham, Switzerland, 2015; pp. 37–58.

47. Yu, B.; Wang, Z.; Mu, H.; Sun, L.; Hu, F. Identification of Urban Functional Regions Based on Floating Car Track Data and POI Data. *Sustainability* **2019**, *11*, 6541. [CrossRef]

48. Ding, Y.W.; Xu, H.W.; Wang, C.H. Research on Urban Functional Area Recognition Integrating OSM Road Network and POI Data. *Geogr. Geo-Inf. Sci.* **2020**, *36*, 57–63.

49. Wu, K.P. *Research on Spatial Structure Identification and Distribution Characteristics of Urban Functional Areas Based on POI Data*; Tianjin Chengjian University: Tianjin, China, 2023.

Article

Commuting Pattern Recognition of Industrial Parks Using Mobile Phone Signaling Data: A Case Study of Nanjing, China

Xinguo Yuan [1,2], Xingping Wang [1], Yingyu Wang [3], Juan Li [3], Yang Zhang [1,3,*], Zhan Gao [2] and Gai Zhang [2]

[1] School of Architecture, Southeast University, Nanjing 210096, China; yuanxg@jspdg.com (X.Y.); wxpsx@seu.edu.cn (X.W.)

[2] Jiangsu Provincial Planning and Design Group, Nanjing 210019, China; gz_jup@163.com (Z.G.); klonana@foxmail.com (G.Z.)

[3] College of Geography and Planning, Chengdu University of Technology, Chengdu 610059, China; wangyingyu@stu.cdut.edu.cn (Y.W.); lijuan@stu.cdut.edu.cn (J.L.)

* Correspondence: zhangyang2021@seu.edu.cn

Abstract: As a novel industrial space to cope with global competition, industrial parks have gradually become important growth poles to promote regional development and provide a large number of employment opportunities. This study utilizes mobile phone signaling data to identify the commuting origins and destinations (OD) of different industrial parks in Nanjing while comparing the distribution of the working population, residential population, and commuting patterns across varying types and levels of industrial parks. The level of coordination of the employment–residential system in each park is quantified by calculating the resident commuting index (HSC_i), employee commuting index (WSC_i), and their coupling coordination degree. Additionally, geographic detectors are employed to identify the influencing factors and interaction effects that impact the employment–residential balance in industrial parks. Results show that industrial parks located in the central urban area attract more residential and working populations. The commuting volume of national and municipal as well as high-tech industrial parks is higher than other types of industrial parks. Most industrial parks experience more inward than outward commuting, and there is an uneven distribution of commuting flows, resulting in a network-like pattern of "central dense, peripheral sparse". Various industrial parks exhibit a highly coupled job–housing system, and those with high HSC_i tend to have high WSC_i as well. The coupling coordination of industrial parks ranged from 0.16 to 0.93, with 13 being primary coordination or above and 3 being disordered. Industrial parks are classified into three types: employment-oriented, residential-oriented, and employment–residential balanced, with the residential-oriented type being predominant. The density of public transportation stops, park area, and land use mix are the primary factors affecting the employment–residential balance. Industrial parks with larger scale, better land allocation, and higher service facility levels are more likely to achieve coordination in the employment–residential system. Our work utilizes mobile signaling data to characterize the commuting patterns of industrial parks, providing insights for industrial park planning and promoting the integration of industry and city.

Keywords: commuting; industrial parks; mobile phone signaling data; geodetector; Nanjing

1. Introduction

An industrial park is a defined area with designated geographical boundaries established by governments or enterprises to drive industrial development and promote regional growth [1]. Before the 1930s, in a market economy with perfect competition and no government intervention in business investment and operations, entrepreneurs typically placed factories in locations with lower costs. With the role of agglomeration economies, industrial zones formed spontaneously and spread from the birthplace of the Industrial Revolution in late 18th-century England to various parts of the world after the revolution. [2]. Starting from the mid-1930s, many countries implemented industrial regional development policies

that reinforced government intervention and regulation in economic affairs. In developed countries, it has become customary to construct new industrial parks on the periphery of urban centers, as well as to revive dilapidated or declining industrial and inner-city locales [3]. Export processing zones emerged in some developing countries and regions towards the end of the 1950s, and industrial parks were widely adopted as a means of development. As developed countries like Europe and the United States upgraded their industrial structures, certain labor-intensive and technology-intensive industries in their mature stages were gradually transferred to developing countries. This further catalyzed the construction of industrial parks in these countries, enabling some developing countries to transform into emerging industrialized countries. Since the 1980s, emerging industrial areas have become a popular strategy for urban development and growth, as countries worldwide adopt new strategies to cope with global competition and promote capital accumulation and urbanization [4].

To adapt to both domestic and international changes, China has implemented development zones as a targeted approach to promote emerging industries by creating economic spaces that benefit from special preferential policies. These industrial parks emerged alongside the country's gradual opening up and were established through government-led industrial agglomeration. Throughout their development, China's industrial parks have thrived under government support, leveraging integrated resources such as land, capital, and labor. Consequently, they are larger in scale compared to those in other countries [5]. Throughout their development, China's industrial parks have benefited from the government's special preferential policies, which have integrated and utilized related resources such as land, capital, and labor. As a result, they are larger in scale than those in other countries [5]. Against the background of industrial transformation and upgrading, industrial parks are gradually shifting from industrial economy to service economy, and the form of parks is constantly evolving to adapt to the current economic development environment. Industrial parks rely on independent innovation to drive economic development and engage in multi-level collaborative innovation with enterprises, universities, research institutions, governments, and other innovative entities, thereby promoting the emergence of various new urban spaces such as new districts, science and technology parks, and university towns, gradually assuming the role of an economic engine in regional development [6]. However, these industrial parks often lack necessary supporting facilities, and their functional and industrial structures are too singular, leading to the formation of "island economies" and hindering their sustainable development and integration with surrounding cities [7]. In response, China's "National New Urbanization Plan (2014–2020)" proposes the integration of industry and city to coordinate the planning and construction of production, office, residential, and commercial areas. This measure aims to strengthen the urban functional transformation of existing industrial parks and promote the transformation from single production function to urban comprehensive function. The integration of industry and city is regarded as an important driving force to accelerate the development of industrial parks at the present stage and a powerful means to promote high-quality development in China.

Commuting is typically influenced by the spatial separation between residential and employment areas [8]. During the initial stage of industrial park development, these parks were often situated in suburban areas far from city centers, serving only as emerging industrial spaces in the suburbs of major cities, creating suburban "islands" that relied on the central city for their existence [9]. Although industrial parks provided public service facilities for employee residence and daily life, their primary focus continued to be on the construction of economic spaces, leading to an obvious imbalance between work and residence. In the later stages of development, industrial parks gradually transformed from single economic spaces to industrial communities that integrated social spaces, allocating significant amounts of housing and infrastructure for employees. However, the construction of urban functions still lagged behind [10], resulting in the phenomenon of pendulum commuting. Against the backdrop of integrated development of industry and city, the

construction of industrial parks has shifted from separation to integration of industry and city. With the transformation and upgrading of industry, this process typically manifests as a shift from traditional manufacturing to productive service sectors, such as finance and technological innovation, resulting in the displacement of a large number of employees and triggering a reorganization of the social structure [11]. This, in turn, results in changes in job demand, causing drastic changes in the number and types of employment and affecting personal choices of work and residence. This is accompanied by a series of commuting problems, such as spatial mismatch and separation of work and residence [12]. Commuting, as one of the most critical activities in the daily lives of urban residents, plays a vital role in realizing personal labor value, cultivating social networks, and ensuring the smooth operation of the city's economy [13,14]. Therefore, it is particularly important to clarify the commuting mode of industrial parks and its influencing factors. Especially in the context of advocating for the integration of industry and city, clarifying the commuting patterns of industrial parks can help make better planning decisions, leading to the optimization of park spatial structure, reduction in excessive commuting, and promotion of job–housing balance in industrial parks.

Scholars have extensively researched commuter behavior, traditionally relying on data from population censuses and travel survey questionnaires. These data provide detailed socio-demographic attributes of individuals, enabling comparisons of commuting characteristics across income levels, genders, and occupations [15,16], spatial analysis of the relationship between work and residential locations [17], and the study of the impact of urban form, land use, and other factors on commuting patterns [18]. For example, Wang et al. (2010) [19] analyzed the commuting time and direction characteristics of Beijing residents through a questionnaire survey and found that there was a serious residency–workplace separation phenomenon. However, these data sources have several limitations, including low update frequency, small sample sizes, and limited spatial resolution, which hinder their ability to accurately capture individual mobility behaviors related to residential, work, and commuting activities [20,21]. Moreover, sample size limitations make it challenging to represent comprehensive population mobility behaviors, especially when examining the spatial structure characteristics of large-scale urban commuting [22]. However, with the rapid development of information and communication technology, location-aware devices, such as mobile phone signaling data [23], taxi GPS trajectory data [24], and smart card data [25], make it possible to collect extensive human space–time movement trajectory data. Among them, mobile phone signaling data are communication data between mobile phone users and base stations, which are real-time, accurate, and have a wide coverage. In recent years, it has been commonly used in research on urban commuting issues. Supported by various big data sources, scholars have conducted research on commuting problems at different scales, ranging from streets [26], cities [27], and larger metropolitan areas [28,29], to the analysis of job–residence space characteristics [30], commuting characteristics analysis [31], jobs–housing balance measurement [32], and commuting impact factor analysis [33]. Analytical methods, such as job–housing ratio [34,35], spatial mismatch index [36], self-sufficiency (internal employment ratio) [37–39], and excess commuting [39,40], have been established. With the help of geographical weighted regression model (GWR) [41], random forest (RF) and gradient boosting decision tree (GBDT) [42], geographical detector model (GDM) [33], and other methods, the factors influencing employment–housing relationship or commuting characteristics, such as urban built environment, residents' socio-economic attributes, and relevant policies and systems for housing and employment, have been explored. However, research on commuting patterns within specific areas, such as industrial parks, is still relatively rare.

China's industrial parks can be classified according to their functions, including economic and technological development zones (ETDZ), high-tech industrial development zones (HTID), export processing zones, bonded zones, border economic cooperation zones, and free trade zones. They can also be categorized by administrative level, such as national, provincial, and municipal industrial parks. National industrial parks, especially ETDZs

and HTIDs, have made remarkable contributions to China's sustainable development over the past four decades since the launch of the reform and opening-up policy. As of the end of June 2021, the GDP created by only 230 national economic development zones and 169 national high-tech zones in China exceeded one-fifth of China's GDP during the same period, and the total tax revenue was close to one-fourth of China's total tax revenue during the same period [43]. Obviously, industrial parks, especially national economic development zones and high-tech zones, have become the main platform for China's industrial development and an important growth pole for regional development [44]. These industrial parks have high economic output and provide a large number of job opportunities, but during their development there is often a mismatch between employment and housing, resulting in a spatial mismatch between work, residence, and excessive commuting.

Therefore, this article utilizes mobile signaling data to investigate the commuting patterns and factors affecting industrial park workers in Nanjing, China. This study aims to provide scientific support for planning decisions that optimize the spatial structure of industrial parks to reduce excessive commuting. The article is structured as follows: Section 2 introduces the study area and research methods, including the process of identifying commuting origin–destination (OD) pairs, measuring commuting indicators for industrial parks, identifying influencing factors, and selecting variables. In Section 3, a case study of Nanjing City is presented, which explores the commuting characteristics of various industrial parks and the level of jobs–housing balance and analyzes the main factors that impact industrial park commuting. Section 4 discusses the commuting patterns and influencing factors of industrial parks, as well as thoughts on future industrial park planning and construction. Finally, Section 5 summarizes the main conclusions and limitations of this study.

2. Data and Methods

2.1. Study Area

Nanjing is an important central city in eastern China, located in the lower reaches of the Yangtze River between 31°14′ N and 32°37′ N and 118°22′ E to 119°14′ E, and is the capital of Jiangsu Province. It has 11 districts (Xuanwu, Qinhuai, Jianye, Gulou, Pukou, Qixia, Yuhuatai, Jiangning, Liuhe, Lishui, and Gao chun) and one national new district (Jiangbei New District), covering a total area of 6587 km^2, as depicted in Figure 1a. The central urban area, with a total area of 804 km^2, is highly urbanized. By the end of 2023, the permanent population of Nanjing is expected to reach 9.547 million, with a GDP of CNY 1.742 trillion.

Nanjing, one of the most important cities for modern industrial development in China, was quick to establish the Nanjing High-tech Industrial Development Zone in 1988, leveraging its strategic location and advantages in high-level universities and research institutions. The zone received national recognition as a high-tech industrial development zone by the State Council in 1991, followed by the establishment of the Nanjing Economic and Technological Development Zone and Jiangning Development Zone in 1992. According to incomplete statistics, presently, Nanjing boasts a total of 102 parks across economic and technological development zones, high-tech industrial development zones, science and technology innovation platforms, scenic tourist areas, modern service industry clusters, new cities, and other types, including 17 national, 12 provincial, and 73 municipal parks. For this study, we selected 16 industrial parks with a focus on manufacturing, high-tech industries, and 2.5 industries, based on clear boundaries, appropriate scale, and spatial separation. We excluded parks with overlapping boundaries, small areas, inclusion within other parks, and with only scattered residential populations. Table 1 provides information on the level, type, area, development orientation, and dominant industries of each selected industrial park. The development of industrial parks in Nanjing has been rapid and is gradually maturing, and the development process has undergone a transformation from traditional industries to modern service and high-tech industries, followed by the emergence of specialty industries like "data + AI", special robots, new energy, and so on. Moreover, with a large number and diverse types of industrial parks covering different levels and categories, Nanjing provides

ideal conditions for studying the commuting patterns in industrial parks. Thus, the study of industrial parks in Nanjing as a case area is representative.
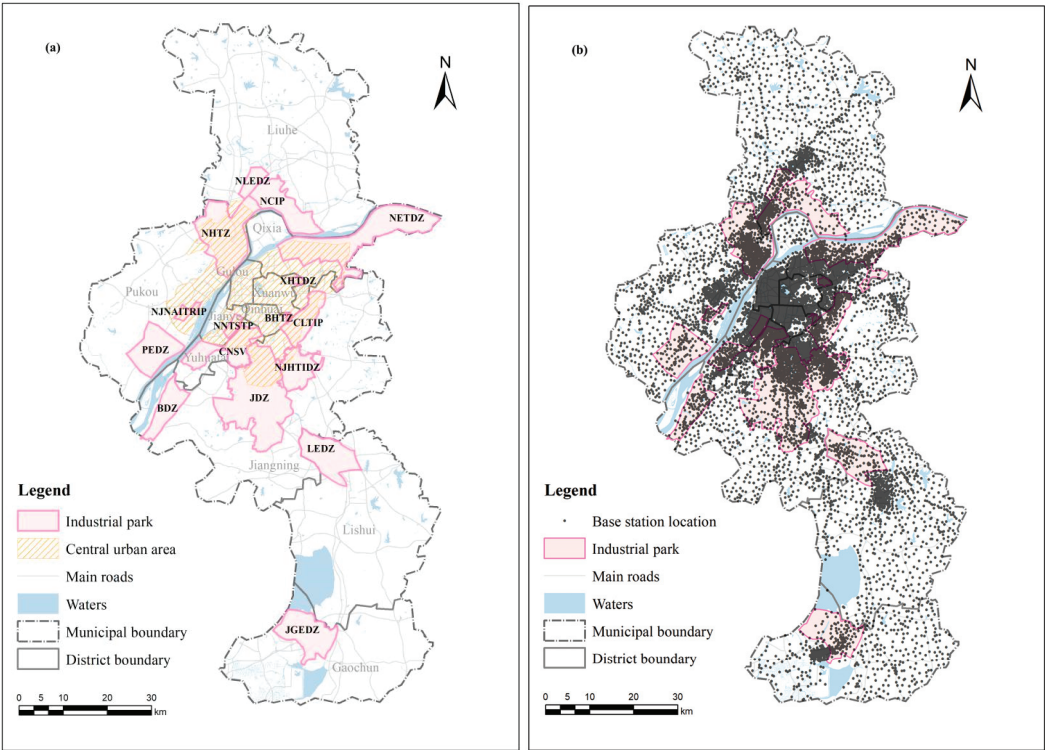

Figure 1. Location map of the study area. (**a**) Industrial parks in Nanjing. (**b**) Mobile communication base stations in Nanjing.

Table 1. Development of major industrial parks in Nanjing.

No.	Name	Level	Type	Area (km^2)	Development Orientation	Leading Industries
1	Jiangning Development Zone (JDZ)	National	Economic Development Zone	242.12	Modern international high-tech industrial new town	Green smart car, smart grid, new generation information technology, high-end equipment, intelligent environmental protection, life sciences, modern logistics, etc.
2	Nanjing Economic and Technological Development Zone (NETDZ)		Economic Development Zone	199.04	First-class international high-tech industrial new town	Optoelectronic display, biomedicine, high-end equipment, modern logistics, science and technology services, etc.
3	Nanjing High-Tech Zone (NHTZ)		High-tech Development Zone	145.78	World-class high-tech park	New-generation information technology, artificial intelligence, biomedicine, etc.
4	Nanjing Chemical Industry Park (NCIP)		Chemical Park	85.30	Key petrochemical bases	Petrochemicals, basic organic chemical materials, fine chemicals, polymer materials, new chemical materials, life medicine, etc.

Table 1. *Cont.*

No.	Name	Level	Type	Area (km²)	Development Orientation	Leading Industries
5	Xuzhuang High-Tech Development Zone (XHTDZ)	Provincial	High-tech Development Zone	4.08	Modern Service Industry Cluster	Incubation R&D, closed development, education and training, and public support, etc.
6	Baixia High-Tech Zone (BHTZ)		High-tech Development Zone	2.07	A Science and Technology Innovation Cluster with Strong Influence in the Yangtze River Delta	High-tech R&D and incubation zone, advanced manufacturing industry, modern service industry, headquarters economy, etc.
7	BinjiangDevelopment Zone (BDZ)		Economic Development Zone	55.02	A first-class development zone of international standard	Information and Communication Technology, Green Intelligent Vehicles, High-end Intelligent Equipment, Modern Service Industry, Health Industry, etc.
8	Pukou Economic Development Zone (PEDZ)		Economic Development Zone	81.58	A modern riverside new town featuring advanced manufacturing and port logistics	Biomedicine, high-tech textile and electronic information, etc.
9	Jiangsu Gaochun Economic Development Zone (JGEDZ)		Economic Development Zone	93.36	A new district with modern manufacturing as its main function	Machinery manufacturing, electronic information, new materials, green food, software industry, etc.
10	Nanjing Luhe Economic Development Zone (NLEDZ)		Economic Development Zone	22.08	Yangtze River Delta Modern Industrial Cluster	Electric vehicle industry, environmental protection equipment industry, new energy electric industry, urban industry, trade and logistics industry, etc.
11	Lishui Economic Development Zone (LEDZ)		Economic Development Zone	90.77	Nanjing manufacturing base and food processing production base	Food and medicine, automobiles and parts, machinery and electronics, new materials, etc.
12	Nanjing Jiangning Hi-Tech Industrial Development Zone (NJHTIDZ)	Municipal	High-tech Development Zone	61.71	A new technological city with balanced functions	New medicine and life health, new energy vehicles, software and information services, etc.
13	Nanjing Jiangbei New Area Industrial Technology Research and Innovation Park (NJNAITRIP)		High-tech Development Zone	10.20	World Influential Industrial Science and Technology Innovation Center	Intelligent manufacturing embedded hardware and software, Internet +, satellite navigation, etc.
14	China (Nanjing) Software Valley (CNSV)		High-tech Development Zone	74.28	Urban regional software centers	Communications software, outsourcing of services and information services, etc.
15	Chi-Lin Technology Innovation Park (CLTIP)		High-tech Development Zone	54.56	A modern eco-technology innovation city with complex functions	Integrated circuits, software and information services, intelligent equipment manufacturing, artificial intelligence, etc.
16	Nanjing New Town Science and Technology Park (NNTSTP)		High-tech Development Zone	10.45	Core area of modern service industry	Software and information services, technology services, artificial intelligence, etc.

2.2. Data Processing

This article focuses primarily on mobile phone signaling data as the main data source, which records the spatial and temporal information of mobile phone users' activities in the power-on state. China Mobile, the largest telecommunications service provider in China, provided the mobile signaling data, which were collected on 12 June 2019. According to the

"China Mobile Limited 2023 Annual Report", China Mobile had a user base of 991 million as of December 2023, accounting for approximately 70% of China's population and holding a market share of over 50%. Its wide coverage allows for the characterization of population features that are similar to those of the entire region. The data are provided by operators and has been cleaned and integrated to include fields such as phone identification code (ID), timestamps (start_time and end_time), base station number (base), base station longitude (lng), and base station latitude (lat). Figure 1b illustrates the spatial distribution of mobile base stations in Nanjing. The signal data undergo preprocessing to derive daily effective trajectory data for each user. This process involves removing duplicate and missing entries and merging drift and ping-pong data to extract individual activity sequences, which include fields such as ID, timestamps, base, lng, lat, and dwell time. Additionally, this article includes data on Nanjing industrial parks, land use, POI, and road network, obtained from official websites of various industrial parks, land use change investigation, Gaode Map, and Open Street Map, respectively. Considering data availability and the consistency of collection timing, all these data were gathered in 2020. These data sources are used to reflect the characteristics of industrial park attributes, land use, public service facilities, and transportation facilities in Nanjing. The detailed information of the data is shown in Table 2.

Table 2. Sources and types of data.

Data Name	Data Sources	Data Formats
Mobile phone signaling data	China Mobile	csv
POI data	Gaode Map (https://lbs.amap.com/) (accessed on 31 December 2020)	shp
Road network	OpenStreet Map (https://www.openstreetmap.org/) (accessed on 31 December 2020)	shp
Industrial park data	Refer to the official website of the industrial park and manually vectorize	excel
Land use data	Survey data of land use change in Nanjing in 2020	shp

2.3. Methods

2.3.1. Jobs–Housing Community Identification

The recognized process of commuting OD is shown in Figure 2. The first step is to identify stopping points. Initially, the trajectory points are assessed based on the time difference and speed between adjacent points. If the time difference exceeds 40 min, the point is classified as a definite stopping point; if it falls between 10 and 40 min, it is considered a possible stopping point; otherwise, it is labeled a displacement point. Additionally, a new field called "stay type" is added to each trajectory point to indicate its type. Next, it is determined whether adjacent continuous stopping points should be merged. All points are categorized as definite stopping points, possible stopping points, or displacement points. If two consecutive trajectory points are identified as stopping points and the distance between them is less than 800 m, they are merged. This process is repeated for all continuous stopping points until no points in Pi meet the merging conditions. The third step involves checking whether definite stopping points need to be merged. If fewer than two definite stopping points remain after the second step, the process proceeds to step four. If there are more than two stopping points, the spatial relationship between adjacent definite stopping points is evaluated. If the spatial constraint is satisfied, the two stopping points are merged; otherwise, no action is taken. In the fourth step, the final determination is based on the distance between each possible stopping point and the preceding and following definite stopping points. For each possible stopping point, its distance from the previous definite stopping point is calculated to determine if it satisfies the spatial constraint dqi. If it does, the point is identified as a stopping point; otherwise, it

is classified as a displacement point. Finally, the commuting origin (O) and destination (D) points are obtained.
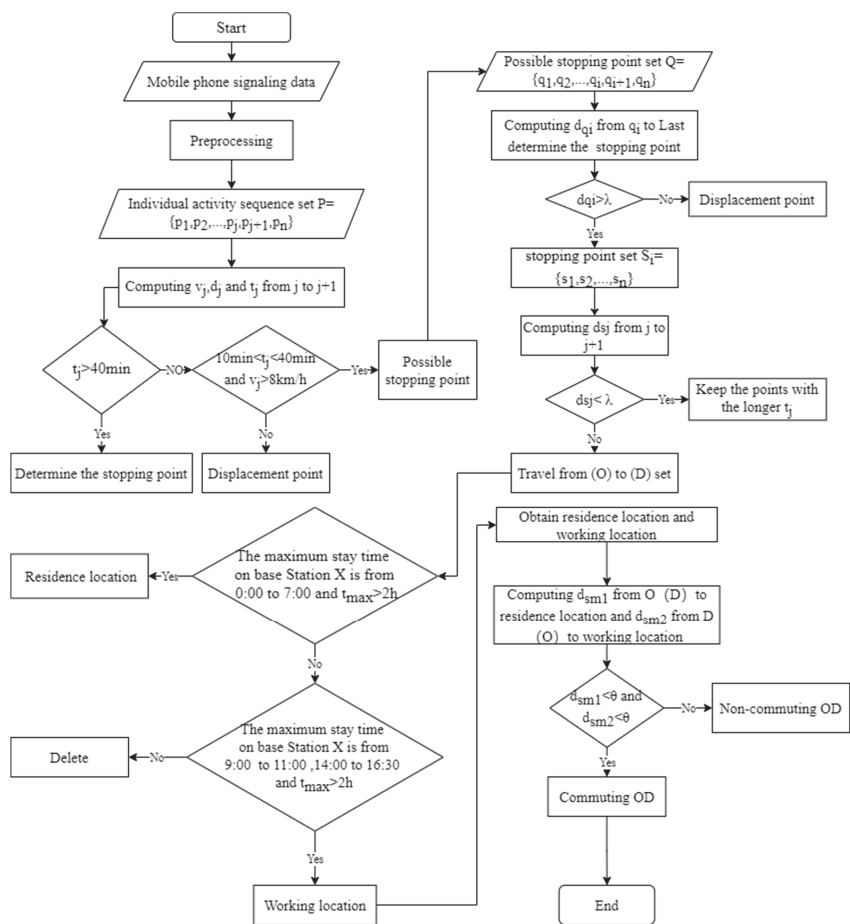

Figure 2. Identification process of a jobs–housing community.

Next, the user's residence and work locations are identified. Firstly, data during working days are selected based on the analysis of the user's spatio-temporal travel map and the residential characteristics of residents. To determine the user's place of residence, we look for the base station where the user has the longest stay time between 0:00 and 7:00 with an average daily stay time of exceeding two hours. For work location identification, we only consider the most common 8-hour work system and employment centers formed by employed people with fixed workplaces, accounting for differences in employment and travel patterns. Data are processed according to this rule, selecting 9:00–11:00 and 14:00–16:30 on working days to identify the point with the maximum daily stay time and a daily average stay time of more than two hours at a base station. To eliminate the possibility of mistaking a permanent residence for a work location, we exclude any base station within 400 m of the mobile phone user's home during the day and night. Commuting patterns non-routine commuting patterns, such as cases where the residence and work locations are the same or the work location is not fixed, are excluded from consideration.

Finally, commuting origins and destinations (OD) are identified by calculating the distance between the user's residence base station and work base station, along with the

potential origins (O) and destinations (D) for each trip. A distance threshold of 800 m is established; if the distance between the user's residence base station and O, as well as the distance between the work base station and D, both satisfy the condition of being less than 800 m, this trip is classified as a commuting OD. Otherwise, it is classified as a non-commuting OD.

2.3.2. Jobs–Housing Balance Evaluation

A well-balanced community should strive to be "self-contained", where residents work within the same area to minimize long-distance travel and car usage and to promote regional sustainability [45]. However, in reality, residents and workers in a region do not always overlap completely. A single evaluation perspective may overlook important residential or occupational characteristics that are relevant to the region. As a result, Home-based Self-Containment (HSC) and Work-based Self-Containment (WSC) were developed to assess the employment–residential relationship of both sides within the designated evaluation unit [46]. Therefore, based on relevant research, this paper uses two indicators, HSC_i (resident commuting index) and WSC_i (employee commuting index), to measure the job–housing balance of industrial parks from both the perspectives of employment and residence [26,39]. The formula for calculation is as follows:

$$HSC_i = 1 - \frac{\text{Outward commuting}}{\text{Total number of residents locally}}$$

$$WSC_i = 1 - \frac{\text{Inward commuting}}{\text{Total number of workers locally}}$$

The formula includes two indicators: HSC_i and WSC_i. HSC_i represents the contribution of the residential population in industrial parks to non-outward commuting, while WSC_i represents the contribution of the employed population in industrial parks to non-inward commuting. These indicators aim to investigate whether the residential or employed population in the industrial park chooses to work or live outside the park. A higher HSC_i indicates that more residential population in the industrial park works inside the park, while a higher WSC_i reflects that more employed population in the industrial park lives inside the park. These indicators demonstrate the industrial park's ability to provide job opportunities and living facilities, as well as the convenience of commuting for the residential and employed population in the local area. A region's employment and residential relationships can only be considered balanced when both HSC_i and WSC_i are relatively high.

Coupling coordination models are commonly used to examine the interactions and coordination among multiple systems. The extent of interaction between these systems is quantified by the "coupling degree" [47]. The closer the relationship between systems, the higher the coupling degree, leading to greater mutual influence. The "coordination degree" measures the consistency and cooperation among subsystems or components within a system. A higher coordination degree indicates a more harmonious internal operation and greater alignment of goals. The "coupling coordination degree" assesses the quality of coupling in the interactions between systems, reflecting the overall effectiveness of their coordination [48,49]. In this study, we will utilize the coupling coordination model to assess the relationship between employment and residence in industrial parks. The model is structured as follows [50]:

$$D = \sqrt{C \times T}$$

The coupling coordination degree, denoted as D, ranges from 0 to 1. A D value of 1 signifies that the systems have achieved the highest degree of coupling, while a value

of 0 indicates the lowest degree of coupling. The coupling degree, represented by C, is calculated using the following formula [51]:

$$C = 2\sqrt{\frac{U_1 \times U_2}{(U_1 + U_2)^2}}$$

The values of HSC$_i$ and WSC$_i$ are denoted by U$_1$ and U$_2$, respectively, and the correlation coefficient C ranges between 0 and 1. The coordination index, T, is calculated using the formula T = aU$_1$ + bU$_2$, where a and b are the contribution coefficients of HSC$_i$ and WSC$_i$, respectively. As both subsystems are equally significant, a and b are both set to 0.5. Based on previous studies [52–54], the coupling coordination degree is classified into 10 levels (Table 3).

Table 3. Classification criteria of coupling coordination degree.

D-Value Interval	[0.0~0.1)	[0.1~0.2)	[0.2~0.3)	[0.3~0.4)	[0.4~0.5)	[0.5~0.6)	[0.6~0.7)	[0.7~0.8)	[0.8~0.9)	[0.9~1.0]
Level of coordination	1	2	3	4	5	6	7	8	9	10
Type of coordination	Extreme disorder	Severe disorder	Moderate disorder	Mild disorder	Borderline disorder	Sue for coordination	Primary coordination	Moderate coordination	Good coordination	Excellent coordination

2.3.3. Exploring the Factors Influencing Commuting

The geographical detector model (GDM) is a spatial statistical analysis method that enables the exploration of correlations and degrees of influence between geographic phenomena [55]. GDM is primarily employed to comprehend complex relationships in spatial data and to identify the interactions between spatial variables [56]. The outcomes of GDM are quantified using q-values, as demonstrated in the formula [57]:

$$q_x = 1 - \sum_{h=1}^{L} N_h \sigma^2_h / N\sigma^2$$

The spatial correlation between X and Y is measured using q_x, while h ranges from 1 to L, where L denotes the layer of factor X (sub-region or sub-category). N and N$_h$ represent the sample size of the study area and each layer h, respectively. Additionally, σ^2 and $\sigma^2 h$ represent the variance of Y in the entire area and each layer (h), respectively. The q_x value ranges from 0 to 1, indicating the degree of influence of X on Y. A higher q-value indicates greater consistency between the coupling coordination of the industrial park and the corresponding factor's spatial distribution, suggesting that X$_n$ has a more significant impact on the coupling coordination. This study takes the dependent variable (Y) as the coupling and coordination results and selects eleven independent variables (X) from four aspects: park attributes, land use, public service facilities, and transportation facilities, combined with previous research on commuting impact factors (Table 4) [33,58]. GDM was utilized to explore the factors influencing commuting within industrial parks in Nanjing [59].

Table 4. Types of dependent variables.

Type	Variable	Variable Name	Unit	Measuring Method
	Y	Coupling coordination level	/	The coupling coordination degree is calculated by the coupling coordination degree model and divided into 10 levels by combining the division interval of the coupling coordination degree value.

Table 4. *Cont.*

Type	Variable	Variable Name	Unit	Measuring Method
Park Attributes	X1	Park grade	/	Combined with the data on the official website of each industrial park, it is divided into three levels: national industrial parks, provincial industrial parks, and municipal industrial parks.
	X2	Park area	km^2	Combined with the data from the official website of each industrial park, the scope of each industrial park is identified, and the size of the area is calculated with the help of ArcGIS.
	X3	Compatibility of dominant industry type and residence	/	Combining the data from the official website of each industrial park and judging based on the type of industrial park, the Economic Development Zone has the highest compatibility, the High and New Technology Industrial Development Zone is medium, and the Chemical Industrial Park Development Zone is the lowest.
	X4	Number of companies and research institutions	/	Obtained from POI data statistics.
	X5	Permanent residents	/	Based on the mobile phone signaling data, the population that meets the conditions of long-term residence (average daily length of stay is longer than 480 min, and the number of days of residence in the sample is not less than 9 days) or long-term work (average daily length of stay is longer than 480 min, and the number of days of work in the sample is not less than 9 days) is counted as the permanent population of the base station.
Land use	X6	Land use mix	/	Based on the 2020 Nanjing Land Use Change Survey data, the Shannon Diversity Index metric is used [60], using the formula: Diversity $= -\Sigma P_j \ln P_j (j = 1, 2, \cdots, n)$, where Pj indicates the proportion of the jth type in the industrial park, and the land use types include 17 categories, such as arable land, parkland, woodland, grassland, and wetland.
	X7	Percentage of residential land	/	The area of residential land in each industrial park is calculated based on the data of the Nanjing Land Use Change Survey in 2020 and divided by the area of the industrial park.
Public service facilities	X8	Integrated medical density	per km^2	The number of general hospitals in each industrial park, including health stations, was obtained by counting the number of general hospitals in the industrial park based on POI data and dividing it by the area of the industrial park.
	X9	Secondary and below density	per km^2	Based on the POI data, the number of secondary schools and below in the industrial estates, excluding vocational schools, was counted and divided by the area of the industrial estates.
Transportation facilities	X10	Density of public transport stops	per km^2	The number of public transport stops in industrial parks is counted based on POI data and divided by the area of the industrial park.
	X11	Road network density	km/km^2	The total length of roads at all levels in each park is calculated from the road network data and divided by the area of the industrial park.

The interaction detector is a tool utilized to identify and evaluate the interaction effect between distinct explanatory variables. It assesses whether the joint effect of two factors increases or weakens the explanatory power of the dependent variable, or whether these factors possess independent effects on the dependent variable.

3. Results

3.1. Characteristics of Commuting

3.1.1. Distribution of Employment and Residential Population

Referring to Figure 3, the ranking of the residential population in different industrial parks corresponds with that of the working population, indicating a positive correlation between the two. The top six industrial parks, each with a population exceeding 100,000, significantly outperform other parks. NHTZ leads with a residential population of over 500,000, while NJNAITRIP has the smallest residential population, with fewer than 10,000 residents. JDZ and NHTZ also have the largest working populations, both surpassing 300,000, whereas BHTZ has the smallest working population at 13,402.
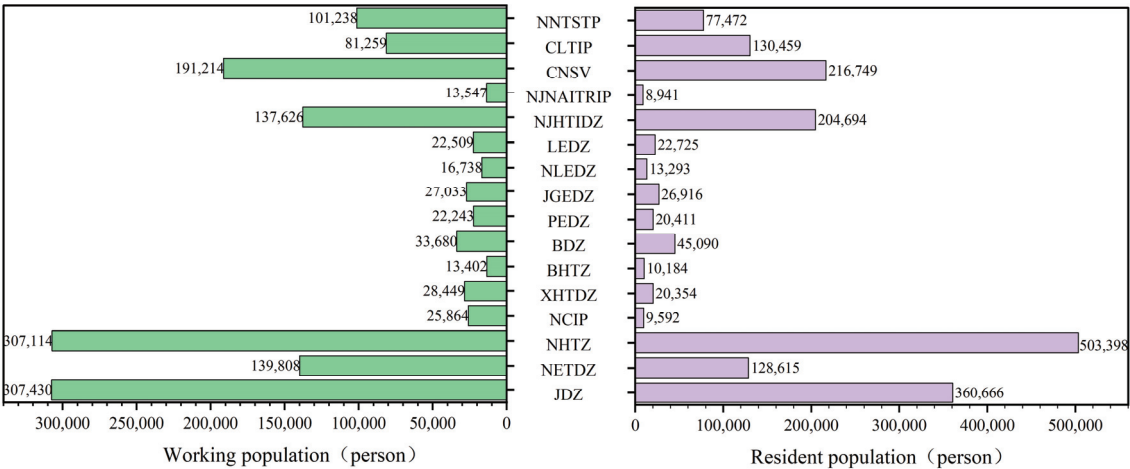
Figure 3. Residential and working population in various industrial parks.

JDZ, NHTZ, CNSV, and NJHTIDZ, which are situated in the heart of Nanjing, have a larger residential and working population compared to industrial parks located further from the central urban area. The primary reason for this is that the central urban area is highly urbanized, with a high population density and advanced economic and industrial functions. The built environment is more developed, and land development is more intensive, making it a crucial area for carrying out urban core functions. Therefore, industrial parks situated in the central urban area have better industrial development and urban functions, thus attracting more residential and working populations.

3.1.2. Commuting Disparities across Different Industry Parks

The amount of outward and inward commuting in industrial parks is shown in Figure 4. NHTZ stands out with the largest outward commuting volume, exceeding 20,000 commuting trips, while NCIP has the smallest outward commuting volume, with only 177 commuting trips. JDZ has the largest inward commuting volume, with over 20,000 commuting trips, and BDZ has the smallest inward commuting volume, with 1367 commuting trips. Interestingly, thirteen industrial parks have larger inward commuting numbers than outward commuting numbers, while only three industrial parks, namely NHTZ, NJHTIDZ, and CLTIP, have larger outward commuting numbers. This pattern is mainly due to the weak degree of employment self-sufficiency in most industrial parks,

resulting in a mismatch between jobs and housing. As a result, they are unable to fulfill their internal employment needs and must seek job opportunities in other industrial parks.
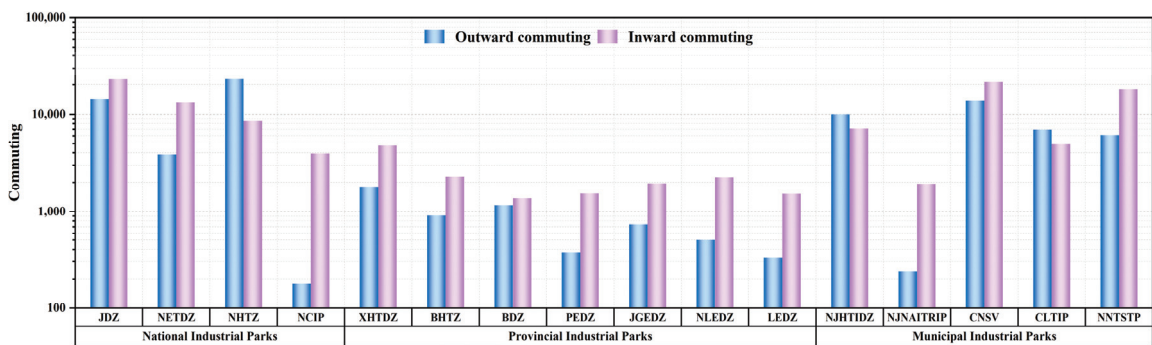

Figure 4. Comparison of commute quantity in different industrial parks.

Generally, national and municipal industrial parks experience higher volumes of both outward and inward commuting, while provincial industrial parks tend to have lower commuting volumes. As depicted in Figure 4, commuting volumes in most national and municipal industrial parks surpass those of provincial industrial parks. This is largely attributed to their larger scale and the more favorable policy conditions and development opportunities that higher-level parks enjoy. Additionally, the type of industrial park influences people's employment choices. High-tech industrial development zones have the highest commuting volume, with high numbers of both outward and inward commuting, followed by economic development zones, whereas chemical industrial parks have the lowest volume. Moreover, there are disparities in the gap between outward and inward commuting due to the different dominant industries and functional types in different types of industrial parks. For example, high-tech industrial development zones are primarily innovation centers and bases for high-tech research and development, while economic development zones are mainly new urban areas that balance production and living functions. Chemical parks focus primarily on production functions, resulting in different functional needs and employment opportunities that affect commuting in industrial parks. Therefore, compared to others, the living function of high-tech industrial parks is weaker, leading to a higher volume of outward commuting than inward commuting in NHTZ, NJHTIDZ, and CLTIP.

3.1.3. Spatial Distribution of Commuting Flow Disparities across Different Industry Parks

Figure 5 provides a clear visualization of the outward and inward commuting flows in each industrial park. The scale distribution of outward and inward commuting flows is uneven, with a higher proportion of small-scale commuters and a lower proportion of large-scale commuters. Short-distance commuting remains dominant, and large-scale commuting flows are mostly concentrated on the shortest straight-line distance between industrial parks that are far apart. Commuting flows of different scales are intertwined between industrial parks and are highly concentrated in the central urban area, with an overall spatial distribution that resembles a network shape of "dense in the center and sparse on the periphery". Regarding outward commuting flows, NETDZ, JDZ, CNSV, NJHTIDZ, CLTIP, and NNTSTP are the main destinations for outward commuting populations, and most of them involve large-scale commuting flows due to their favorable geographical location. Inward commuting flows are primarily attracted to JD Z, CNSV, NNTSTP, NCIP, NETDZ, and NJHTIDZ, again due to their central location and complete residential and employment functions. It is worth noting that JGEDZ, which is located far from the center, has fewer outward commuting flows, and residents in the industrial park tend to commute less to

work outside the park. Nonetheless, some workers still choose to commute long distances to work in the park, although short-distance commuting remains dominant, providing employment opportunities for the residents near the industrial park and covering a large area of Gaochun District.
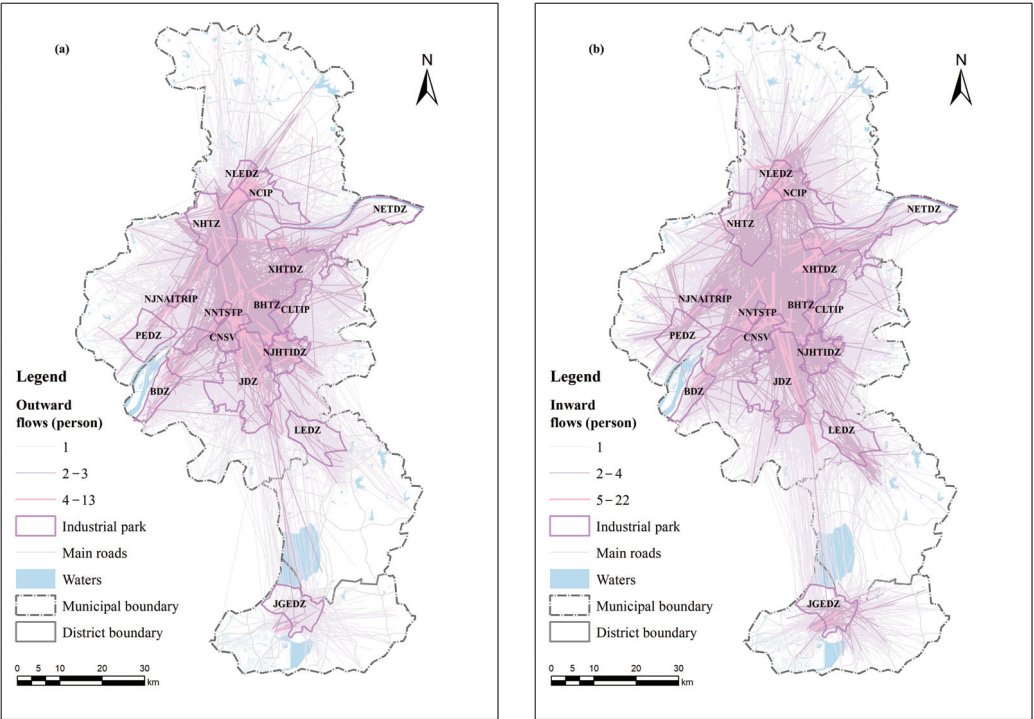

Figure 5. Spatial distribution of commuting across different industrial parks. (**a**) Outward flows and (**b**) inward flows.

3.2. Level of Jobs–Housing Balance

3.2.1. HSC$_i$ and WSC$_i$ Value

Overall, the HSC$_i$ and WSC$_i$ values for the 16 industrial parks were relatively high, with both exceeding 0.80, indicating that these parks can better satisfy the needs of local residents for work and housing (Figure 6). HSC$_i$ values range from 0.91 to 0.99, with the highest values of HSC$_i$ being observed in NETDZ, NCIP, BDZ, PEDZ, JGEDZ, LEDZ, and NJNAITRIP. Among these, seven parks, including two national, four provincial, and one municipal industrial park, all scored above 0.96, indicating strong employment self-sufficiency. This means that a larger population residing in these industrial parks can find work within the park. The smallest HSC$_i$ values were observed in BHTZ, XHTDZ, and NNTSTP, all below 0.93, indicating that the majority of the population residing in these three industrial parks work outside the area, with weak employment self-sufficiency.

The WSC$_i$ results range from 0.82 to 0.97, with high values distributed in NHTZ, BDZ, NJHTIDZ, and CLTIP. Of these, one national industrial park, one provincial industrial park, and two municipal industrial parks, all scoring above 0.93. This indicates that these four industrial parks have strong self-sufficiency in terms of residence, meaning that a large proportion of the population working in these parks can settle within the parks. Conversely, the WSC$_i$ in BHTZ, XHTDZ, and NNTSTP are still the smallest, consistent with HSC$_i$, all below 0.85. This suggests that the self-sufficiency of residents in these four industrial parks

is weak, meaning that the population working in these parks mostly comes from outside the area. Additionally, their small size greatly influences this trend.
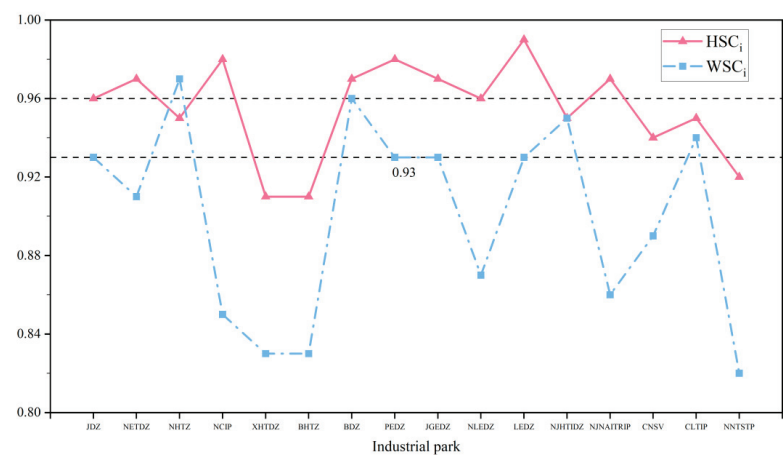

Figure 6. Jobs–housing balance in Nanjing Industrial Park.

As depicted in Figure 7, the areas with high HSC_i and WSC_i values do not entirely overlap, but they are adjacent in space. Industrial parks with higher HSC_i and WSC_i values are mainly situated on the periphery or outskirts of the central urban area. Furthermore, low-value areas are often adjacent to high-value areas, which could be industrial parks with superior living and working conditions. These parks have similar or comparable industrial distribution to smaller industrial parks in the surrounding region, but due to more comprehensive functions, better infrastructure, and more favorable development conditions, workers tend to congregate in these industrial parks, resulting in a relatively unbalanced between job and housing in smaller industrial parks. However, it is important to note that although NJNAITRIP has a small area, it is situated in the central urban region on the north bank of the Yangtze River and is not adjacent to any larger industrial parks. Consequently, the park's inhabitants naturally prefer convenient commuting, which contributes to its designation as a high-value area for HSC_i.

3.2.2. Coupling Coordination Degree of Jobs–Housing

As shown in Figure 8, except for NCIP, BHTZ, and NNTSTP, C values of other industrial parks exceed 0.8, indicating a high level of coupling and strong interaction between systems in Nanjing's industrial parks. The distribution of the system's D value in each park ranges from 0.16 to 0.93, with an average of 0.68. The T value between each park varies significantly, and the overall curve is below the C and D value curves, with a maximum of 0.87 and a minimum of 0.04. Coordination levels range from severe disorder to excellent coordination, with 13 industrial parks having a coordination level of 5 (borderline imbalance) or above, including BDZ, PEDZ, and LEDZ, with BDZ scoring the highest coupling coordination degree of 0.93. These industrial parks often have higher coordination indices, indicating better coordination between systems and more harmonious internal operations. Three industrial parks are below level 5, indicating an imbalanced state, with BHTZ having the lowest coupling coordination degree of only 0.16. National industrial parks have a relatively higher coupling coordination degree, while the coupling coordination degree of provincial and municipal industrial parks varies greatly.
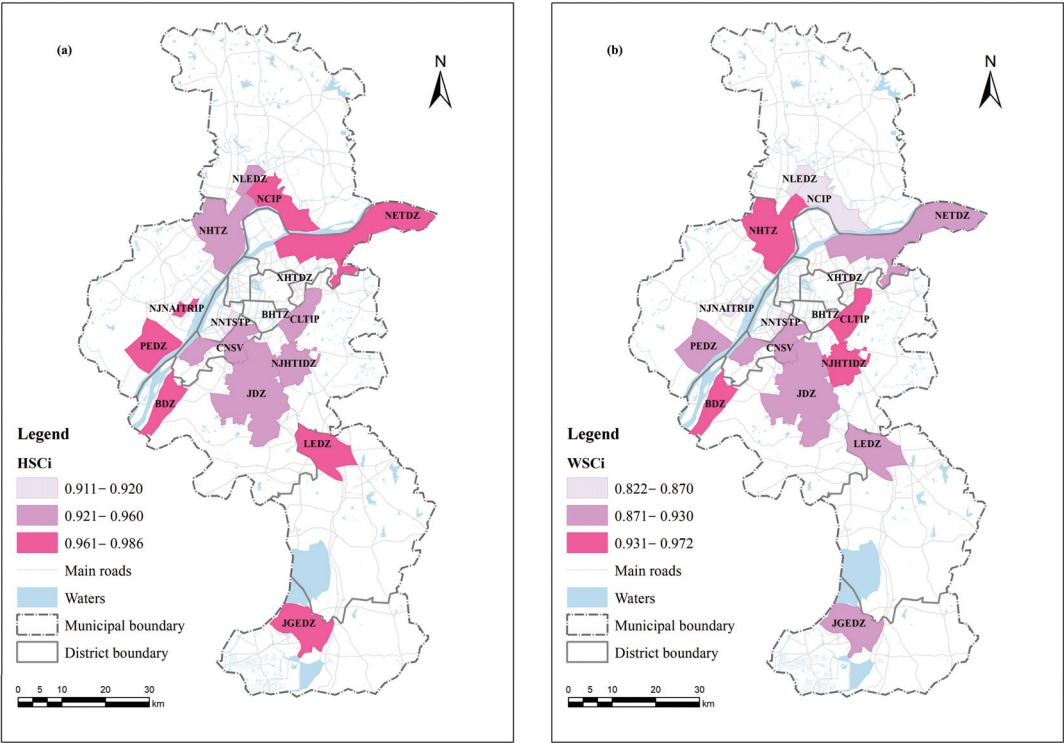
Figure 7. Spatial distribution of HSC_i and WSC_i in Nanjing Industrial Park. (**a**) HSC_i. (**b**) WSC_i.
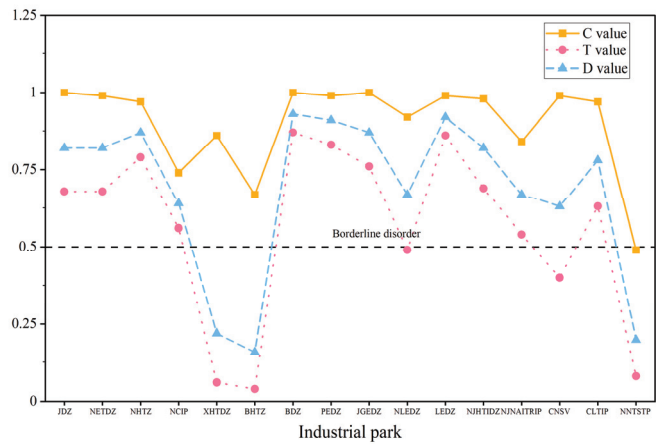

Figure 8. Trend diagram of coupling coordination degree.

3.3. Factors Affecting Commuting

3.3.1. Divergence and Factor Detection

After running the GDM, we obtained the factor detection results shown in Figure 9. The factors with the highest q values are X10 (density of public transportation stations), X2 (park area), and X6 (land use mix). These three factors have the strongest spatial correlation with the coupling coordination degree of work and residence in industrial

parks. The density of public transportation stations and park area are good indicators of the development level and current scale of the industrial park, while the land use mix can reduce the commuting needs of employees by obtaining the land value within the same size range. X9 (density of junior high schools and below) follows closely, as schools are essential residential supporting facilities that can attract more families to settle down. They are also a major consideration for people choosing to work and live in the industrial park. Furthermore, X11 (density of road network) also has a significant q value, as the density of road network is an important factor in measuring transportation convenience, which has a significant impact on the coupling coordination degree of work and residence in industrial parks. The three factors with the lowest q values are X5 (resident population), X1 (park level), and X4 (number of companies and research institutions), indicating that these factors have a relatively small impact on the coupling coordination degree of work and residence in industrial parks.
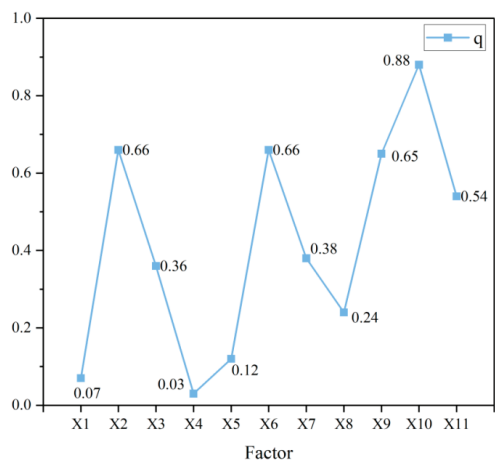

Figure 9. Results of geographical detector factors.

3.3.2. Interaction Detection

The results of the interaction detector reveal that the impact of each factor is not independent. Instead, they exhibit a dual-factor or nonlinear enhancement, wherein the interaction between any two factors is greater than the explanatory power of a single factor. This suggests that the work–residence relationship in Nanjing's industrial parks is formed by the interplay of multiple factors. To visualize this, we used a heat map in Origin to reflect the interaction detection effect of the impact factors on the coordination degree of work–residence coupling in Nanjing's industrial parks. Figure 10 illustrates that the darker the red, the stronger the interaction effect, with the strongest being X1 (park grade)∩X10 (density of public transportation stations), reaching 0.95. Additionally, X3 (compatibility between dominant industries and residence)∩X10 (density of public transportation stations) reached 0.934, and X2 (park area)∩X9 (density of secondary schools and below), X2 (park area)∩X7 (residential land use ratio), and X6 (land use mix)∩X7 (residential land use ratio) also reached 0.926. In the factor detection results, the interaction between the significant factors X10 (density of public transportation stations), X2 (park area), X6 (land use mix), and other factors is relatively strong, and the interaction between X10 (density of public transportation stations) and all factors is the most frequent. This further indicates that the coherence of the employment and residential systems is the result of the synergy of employment units, transportation convenience, park size, and housing conditions, and the explanatory power after interaction is higher.
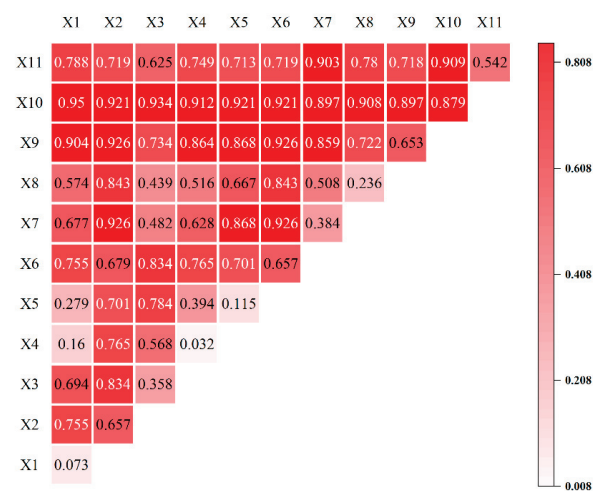
Figure 10. Driving factors interact with heat maps.

4. Discussion

4.1. Commuting Pattern of Industry Parks in Nanjing

Based on the HSC_i and WSC_i values of Nanjing's industrial parks and by considering the relative size of the two and the results of coupling coordination, these parks can be classified into three categories based on commuting patterns: employment-oriented, residence-oriented, and employment–residential balanced industrial parks (Figure 11).
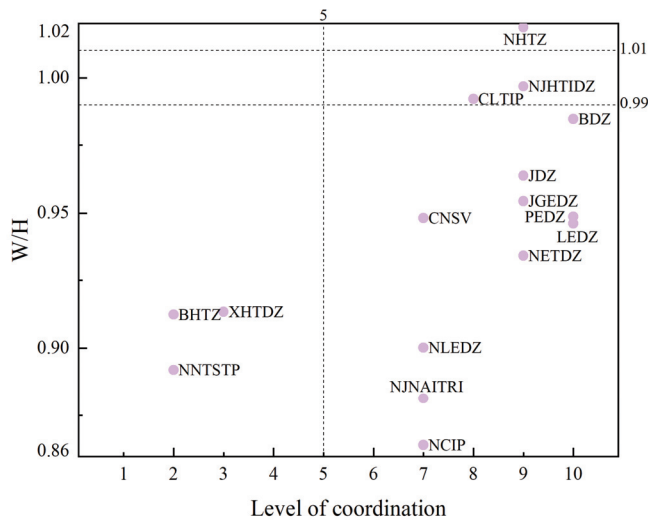

Figure 11. Quadrant map of commuting patterns.

The employment-oriented park is the NHTZ. Its WSC_i is higher than the HSC_i, suggesting that many employees in the park do not live in this region and that "residence" is scarcer than "employment". Employment-oriented parks primarily serve workers from outside the park, offering more job opportunities and attracting more commuters, making them more employment-focused. The coupling coordination between employment and residence is well coordinated, indicating a high degree of balance between the two.

The residential-oriented industrial parks include JDZ, NETDZ, NCIP, XHTDZ, BHTZ, BDZ, PEDZ, JGEDZ, NLEDZ, LEDZ, NJNAITRIP, CNSV, and NNTSTP. These parks exhibit a higher HSCi than WSCi, suggesting that the job opportunities within them are inadequate to meet the demands of local residents, who must therefore look for employment outside the parks. "Employment" is scarcer than "residence" in these areas. Residential-oriented industrial parks primarily cater to the needs of park employees and, compared to other parks, offer fewer job opportunities and have fewer commuters, making them more geared towards residential purposes. Among them, three are national, all provincial, and three municipal industrial parks. The overall coordination of employment and residential functions in industrial parks is relatively balanced, with ten parks at a primary coordination level or above, but three are in a state of disorder.

The employment–residential balanced industrial parks are CLTIP and NJHTIDZ. Their HSC_i and WSC_i are similar and at a medium level, indicating that the residents within the park can basically find employment opportunities within the park itself. Employment–residential balanced industrial parks have a strong level of self-sufficiency, with a relatively balanced population of working and living residents. Both of them are municipal industrial parks with intermediate and good coordination degrees, respectively. The coupling coordination degree of employment and residence is generally good.

4.2. Factors Influencing the Jobs–Housing Balance

Based on the findings of geographic detectors, the factors that impact the employment–residential balance in industrial parks can be classified into three categories: park size, land allocation, and level of service facilities. Among these factors, park size has an impact on both work and residential commuting within the industrial park. On one hand, larger industrial parks can accommodate more enterprises, thus providing more job opportunities and reducing external commuting, leading to improved commuting indices for the residents and addressing employment issues within the park. On the other hand, larger industrial parks can incorporate multiple functions, including production and living, effectively addressing the housing needs of the working population within the park.

The impact of land allocation is primarily reflected in factors such as land use mix and the proportion of residential land use. Both of these factors are the combined results of industrial park construction and related land use policies. Land use mix indicates the allocation status within industrial parks, and the richer the types of land use, the more comprehensive the functional types of industrial parks. This improves the quality of life for residents in the industrial park, attracts more workers, and helps to promote the balance between work and residence. Additionally, a higher proportion of residential land use signifies a greater allocation of housing within the industrial park. This allows the park to offer more housing options, accommodate a larger population, and effectively improve the commuting index, thereby reducing long-distance commutes.

The level of service facilities is primarily indicated by the density of public transportation stops, schools, road networks, and comprehensive medical facilities. The density of public transportation stops and road networks significantly affects the transportation conditions of industrial parks. Conversely, the density of schools and comprehensive medical facilities impacts the overall service level of these parks, thereby influencing commuting distances and times. Improved transportation conditions and service facilities within industrial parks will attract a larger working and residential population, promoting a better balance between employment and living conditions.

The results of the interactive detector indicate that the combined effect of two or more factors significantly influences the employment–residential relationship in industrial parks, more so than any single factor alone. The interactions of various influencing factors reveal that the relationship between work and residence in industrial parks is complex and intertwined. This complexity arises from the direct impact of these individual factors on the employment–residential relationship, which in turn enhances the influence of other factors. The interrelatedness of these factors can indirectly affect the employment–residential

relationship, ultimately amplifying their overall impact. For example, the q value of the interaction between park grade and the density of public transportation stops is as high as 0.95, underscoring the significant effect of this interaction on the employment–residential relationship. Higher park grades, greater development, and more robust infrastructure can attract larger residential and employment populations, effectively alleviating commuting issues, reducing long-distance travel, and promoting a better balance between employment and residence in industrial parks.

4.3. Inspiration for Industrial Park Planning

In many industrial parks, rush hour traffic congestion has become a significant transportation and social issue, posing an important obstacle to achieving sustainable development. The study of commuting patterns in Nanjing's industrial parks has led to several recommendations for the planning and construction of these parks. Firstly, it is necessary to promote the diversified development of industries in various industrial parks, especially the diversified development of chemical industry parks, to create diverse employment opportunities and meet the differentiated employment needs of the residents. Residential-oriented industrial parks should adopt this strategy to increase job positions and offer more employment options, thereby effectively reducing outward commuting. When employment opportunities within industrial parks can fully meet the needs of the resident population, residents are more likely to choose to work within the parks to reduce commuting costs. Secondly, it is particularly important to improve the overall level of service facilities in industrial parks. While meeting the production and development needs of industrial parks, it is crucial to enrich and improve the functional types of the parks, providing high-quality living environments and public services for both the working population and surrounding residents. For example, meeting the needs of families with children for schooling, reducing commuting time, facilitating medical treatment, etc. This will attract more residential population, and workers in the park will choose to live in the park, reducing the need for long-distance commuting. For employment-oriented industrial parks, it is essential to adopt these strategies to enhance their urban functions, thus making their functional types more comprehensive. This can also improve the quality of life for the residents in these industrial parks and provide more living conveniences for the surrounding communities. Additionally, it is essential to optimize land allocation and improve land layout, increase the degree of land use mix, and enhance the urban functions of industrial parks. By integrating industry with urban development, functional land should be allocated around industrial areas to create comprehensive new cities that combine industrial and residential facilities. Furthermore, the supply of supporting facilities must be tailored to meet industry demands. Strengthening the provision of land that aligns with the spatial preferences of the industrial population is crucial, as is improving the compatibility of land use to satisfy the needs of diverse groups. By implementing these strategies, industrial parks can evolve from purely industrial zones into integrated industrial communities and ultimately into comprehensive new cities.

5. Conclusions

This study utilizes mobile signaling data to identify commuting OD in various industrial parks and compares the distribution of working and residential populations, as well as commuting spatial distribution differences among different types and levels of industrial parks. Two commuting index indicators, HSC_i and WSC_i, are used to measure the employment–residence balance in industrial parks. Moreover, a coupling coordination degree model is employed to measure the interaction relationship and coordination degree of the employment–residence system in each industrial park. Lastly, using geographic detectors, this study explores the influencing factors of commuting balance in industrial parks and examines the interactive effects of various factors. This study summarizes the commuting patterns of industrial parks in Nanjing, analyzes their main influencing factors, and provides relevant suggestions for the future planning and construction of industrial

parks. This study has three main findings: (1) The residential and working populations are primarily concentrated in industrial parks located in the central urban area of Nanjing. Inward commuting is more prevalent than outward commuting in most industrial parks. National and municipal industrial parks exhibit a higher degree of inward and outward commuting as compared to provincial industrial parks. High-tech industrial development zones demonstrate the highest level of commuting, followed by economic development zones, while chemical industrial parks exhibit the least. The distribution of outward and inward commuting flows is uneven, with a larger proportion of small-scale commuters accounting for total commuting, primarily in short-distance commuting. Different scales of commuting flows are intertwined among various industrial parks, with a highly concentrated central urban area generally forming a network-like distribution with a "central dense, peripheral sparse" pattern. (2) The job–housing systems in various industrial parks are in a highly coupled stage, and those with high HSCi are more likely to have high WSCi. Both residents and employees enjoy favorable living and working conditions, with housing and job opportunities better suited to their needs within these industrial parks. The coupling coordination of industrial parks ranges from 0.16 to 0.93, with coordination levels ranging from excellent coordination to severe disorder. Nanjing's industrial parks are categorized into three types: employment-oriented, residential-oriented, and employment–residential balanced, with the residential-oriented type being predominant. (3) The balance between employment and residential in industrial parks is the outcome of multiple factors interacting in three areas: park size, land allocation, and level of service facilities. Among these factors, the density of public transportation stops, park area, and land use mix have greater explanatory power. Conversely, the impact ranking of industrial park level, number of companies and research institutions, and permanent population is the lowest. Industrial parks with larger scale, more housing opportunities, and higher levels of service facilities are more likely to achieve coordination in the employment–residential system. For different commuting modes, industrial park planning and construction can be strengthened by realizing diversified development of industrial parks, improving the overall level of service facilities, and optimizing land allocation to promote the integration of industry and the city.

This study utilizes mobile phone signaling data to identify commuting patterns, which provides a more precise spatial resolution and larger sample size than traditional small-scale travel surveys. This approach offers detailed commuting flows from home to work, making it more suitable for studying the relationship between work and residential areas. Moreover, examining commuting patterns in specific areas, such as industrial parks, can provide valuable insights into their transformation and upgrading as well as solutions to commuting problems. This will further promote the integration of industry and cities, enhance residents' well-being, and facilitate the high-quality development of industrial parks. However, this study has some limitations. The mobile base station coverage range selected for this study is between 100 m and 3 km, making it challenging to identify work and residential areas within the same coverage, which could result in lower commuting resolution and possible errors. Therefore, in the next step, multi-source big data, such as Tencent location data, can be combined to further investigate commuting patterns in industrial parks. This will help to gain a deeper understanding of issues like spatial mismatch and separation between work and residential areas, leading to a more comprehensive understanding of commuting patterns in industrial parks.

Data Availability Statement: The data presented in this study are available upon request from the corresponding author.

Conflicts of Interest: The authors declare no conflicts of interest.

References

1. Porsia, E. Industrial estates in Europe and the Middle East United Nations Industrial Development Organization. *G. Econ. Ann. Econ.* **1972**, *31*, 725.
2. Weber, A.; Friedrich, C.J. *Alfred Weber's Theory of the Location of Industries*; University of Chicago Press: Chicago, IL, USA, 1929.
3. Peddle, M.T. Planned industrial and commercial developments in the United States: A review of the history, literature, and empirical evidence regarding industrial parks and research parks. *Econ. Dev. Q.* **1993**, *7*, 107–124. [CrossRef]
4. Wei, C.; Shen, J.; Fan, J.H. Rescaling: Role Changing of the state and spatial production strategy of region in the globalization era. *City Plan. Rev.* **2011**, *35*, 28–35.
5. Yeung, Y.-m.; Lee, J.; Kee, G. China's special economic zones at 30. *Eurasian Geogr. Econ.* **2009**, *50*, 222–240. [CrossRef]
6. Li, W.B.; Chen, H. Analysis of City-Industry Integration and Planning Strategies. *Urban Planning Forum.* **2012**, *2012*, 99–103. [CrossRef]
7. Wang, X.C. Study on Spatial Structure Transformation of Suburban Industrial Development Zone. *Planners* **2011**, *27*, 93–98.
8. Hu, Y.; Wang, F.; Wilmot, C.G. Commuting variability by wage groups in Baton Rouge, 1990–2010. *Pap. Appl. Geogr.* **2017**, *3*, 14–29. [CrossRef]
9. Wang, X.C. Exploring the Mechanisms and Dynamics of the Transformation of China's Development Zones. *Mod. Econ. Res.* **2010**, *2010*, 15–19. [CrossRef]
10. Hutton, T.A. The new economy of the inner city. *Cities* **2004**, *21*, 89–108. [CrossRef]
11. Hamnett, C. Gentrification and the middle-class remaking of inner London, 1961-2001. *Urban Stud.* **2003**, *40*, 2401–2426. [CrossRef]
12. Fan, Y.L.; Allen, R.; Sun, T.S. Spatial mismatch in Beijing, China: Implications of job accessibility for Chinese low-wage workers. *Habitat Int.* **2014**, *44*, 202–210. [CrossRef]
13. Jing, Y.; Hu, Y.J.; Niedzielski, M.A. Neighborhood divides: Where you live matters for commuting and its efficiency. *Cities* **2023**, *132*, 11. [CrossRef]
14. Deng, Y.L.; Zhao, P.J. Quantifying residential self-selection effects on commuting mode choice: A natural experiment. *Transport. Res. Part D-Transport. Environ.* **2022**, *104*, 14. [CrossRef]
15. Sang, S.H.; O'Kelly, M.; Kwan, M.P. Examining Commuting Patterns: Results from a Journey-to-work Model Disaggregated by Gender and Occupation. *Urban Stud.* **2011**, *48*, 891–909. [CrossRef]
16. Dai, D.D.; Zhou, C.S.; Ye, C.D. Spatial-temporal Characteristics and Factors Influencing Commuting Activities of Middle-class Residents in Guangzhou City, China. *Chin. Geogr. Sci.* **2016**, *26*, 410–428. [CrossRef]
17. Han, H.R.; Yang, C.F.; Wang, E.R.; Song, J.P.; Zhang, M. Evolution of jobs-housing spatial relationship in Beijing Metropolitan Area: A job accessibility perspective. *Chin. Geogr. Sci.* **2015**, *25*, 375–388. [CrossRef]
18. Song, Y.; Shao, G.F.; Song, X.D.; Liu, Y.; Pan, L.; Ye, H. The Relationships between Urban Form and Urban Commuting: An Empirical Study in China. *Sustainability* **2017**, *9*, 1150. [CrossRef]
19. Wang, E.R.; Song, J.P.; Xu, T. From "spatial bond" to "spatial mismatch": An assessment of changing jobs-housing relationship in Beijing. *Habitat Int.* **2011**, *35*, 398–409. [CrossRef]
20. Iqbal, M.S.; Choudhury, C.F.; Wang, P.; González, M.C. Development of origin-destination matrices using mobile phone call data. *Transp. Res. Part C-Emerg. Technol.* **2014**, *40*, 63–74. [CrossRef]
21. Yue, Y.; Lan, T.; Yeh, A.G.O.; Li, Q.Q. Zooming into individuals to understand the collective: A review of trajectory-based travel behaviour studies. *Travel Behav. Soc.* **2014**, *1*, 69–78. [CrossRef]
22. Yuan, Y.; Raubal, M. Extracting dynamic urban mobility patterns from mobile phone data. In Proceedings of the Geographic Information Science: 7th International Conference, GIScience 2012, Columbus, OH, USA, 18–21 September 2012; Proceedings 7, pp. 354–367.
23. Song, C.M.; Qu, Z.H.; Blumm, N.; Barabási, A.L. Limits of Predictability in Human Mobility. *Science* **2010**, *327*, 1018–1021. [CrossRef]
24. Liu, Y.; Kang, C.G.; Gao, S.; Xiao, Y.; Tian, Y. Understanding intra-urban trip patterns from taxi trajectory data. *J. Geogr. Syst.* **2012**, *14*, 463–483. [CrossRef]
25. Huang, J.; Levinson, D.; Wang, J.O.; Zhou, J.P.; Wang, Z.J. Tracking job and housing dynamics with smartcard data. *Proc. Natl. Acad. Sci. USA* **2018**, *115*, 12710–12715. [CrossRef]
26. Wang, J.; Zhou, C.J.; Rong, J.; Liu, S.Y.; Wang, Y. Community-detection-based spatial range identification for assessing bilateral jobs-housing balance: The case of Beijing. *Sustain. Cities Soc.* **2022**, *87*, 11. [CrossRef]
27. Zheng, M.N.; Liu, F.; Guo, X.C.; Lei, X.Y. Assessing the Distribution of Commuting Trips and Jobs-Housing Balance Using Smart Card Data: A Case Study of Nanjing, China. *Sustainability* **2019**, *11*, 5346. [CrossRef]
28. Yao, Z.Y.; Kim, C. Analyzing the multiscale patterns of jobs-housing balance and employment self-containment by different income groups using LEHD data: A case study in Cincinnati metropolitan area. *Comput. Environ. Urban Syst.* **2022**, *96*, 13. [CrossRef]

29. Pinter, G.; Felde, I. Commuting Analysis of the Budapest Metropolitan Area Using Mobile Network Data. *ISPRS Int. J. Geo-Inf.* **2022**, *11*, 466. [CrossRef]

30. Wang, H.H.; Zeng, W.H.; Cao, R.X. Simulation of the Urban Jobs-Housing Location Selection and Spatial Relationship Using a Multi-Agent Approach. *ISPRS Int. J. Geo-Inf.* **2021**, *10*, 16. [CrossRef]

31. Yang, X.P.; Fang, Z.X.; Yin, L.; Li, J.Y.; Zhou, Y.; Lu, S.W. Understanding the Spatial Structure of Urban Commuting Using Mobile Phone Location Data: A Case Study of Shenzhen, China. *Sustainability* **2018**, *10*, 1435. [CrossRef]

32. Liu, H.; Kwan, M.P.; Hu, M.X.; Wang, H.; Zheng, J.M. Application of the local colocation quotient method in jobs-housing balance measurement based on mobile phone data: A case study of Nanjing City. *Comput. Environ. Urban Syst.* **2024**, *109*, 11. [CrossRef]

33. Wang, J.F.; Luo, G.W.; Huang, Y.J.; Liu, M.; Wei, Y. Spatial Characteristics and Influencing Factors of Commuting in Central Urban Areas Using Mobile Phone Data: A Case Study of Nanning. *Sustainability* **2023**, *15*, 9648. [CrossRef]

34. Horner, M.W.; Mefford, J.N. Investigating urban spatial mismatch using job–housing indicators to model home–work separation. *Environ. Plan. A* **2007**, *39*, 1420–1440. [CrossRef]

35. Cervero, R. Jobs-housing balancing and regional mobility. *J. Am. Plan. Assoc.* **1989**, *55*, 136–150. [CrossRef]

36. Martin, R.W. Spatial mismatch and the structure of American metropolitan areas, 1970–2000. *J. Reg. Sci.* **2004**, *44*, 467–488. [CrossRef]

37. Martinus, K.; Biermann, S. Strategic Planning for Employment Self-Containment in Metropolitan Sub-Regions. *Urban Policy Res.* **2018**, *36*, 35–47. [CrossRef]

38. Zhou, X.G.; Yeh, A.G.O.; Yue, Y. Spatial variation of self-containment and jobs-housing balance in Shenzhen using cellphone big data. *J. Transp. Geogr.* **2018**, *68*, 102–108. [CrossRef]

39. Zhang, P.; Zhou, J.P.; Zhang, T.R. Quantifying and visualizing jobs-housing balance with big data: A case study of Shanghai. *Cities* **2017**, *66*, 10–22. [CrossRef]

40. Hu, Y.J.; Wang, F.H. Decomposing excess commuting: A Monte Carlo simulation approach. *J. Transp. Geogr.* **2015**, *44*, 43–52. [CrossRef]

41. Wang, D.G.; Cao, X.Y. Impacts of the built environment on activity-travel behavior: Are there differences between public and private housing residents in Hong Kong? *Transp. Res. Part A-Policy Pract.* **2017**, *103*, 25–35. [CrossRef]

42. Tao, T.; Wang, J.Y.; Cao, X.Y. Exploring the non-linear associations between spatial attributes and walking distance to transit. *J. Transp. Geogr.* **2020**, *82*, 11. [CrossRef]

43. Ren, H.; Zhen, J.; Ye, J.F.; Liu, B.; Zhong, D.T. *The 2017 Blue Book on the Sustainable Development of Industrial Parks in China*; Tongji University Press: Shanghai, China, 2017; p. 233.

44. Zhen, J.; Ren, H.; Tang, K.Y. Sustainable Development of Industrial Parks in China: Process, Morphology, and Logic. *Urban Plan. Forum* **2022**, 66–73. [CrossRef]

45. Giuliano, G. *Is Jobs-Housing Balance a Transportation Issue?* University of California Transportation Center: Berkeley, CA, USA, 1991.

46. Zhang, H.; Xu, S.; Liu, X.; Liu, C. Near "real-time" estimation of excess commuting from open-source data: Evidence from China's megacities. *J. Transp. Geogr.* **2021**, *91*, 102929. [CrossRef]

47. Cai, J.; Li, X.P.; Liu, L.J.; Chen, Y.Z.; Wang, X.W.; Lu, S.H. Coupling and coordinated development of new urbanization and agro-ecological environment in China. *Sci. Total Environ.* **2021**, *776*, 11. [CrossRef]

48. Wang, R.; Tan, J.L. Exploring the coupling and forecasting of financial development, technological innovation, and economic growth. *Technol. Forecast. Soc. Chang.* **2021**, *163*, 11. [CrossRef]

49. Illingworth, V. *The New Penguin Dictionary of Geology*; Foreign Language Press: Beijing, China, 1996.

50. Naikoo, M.W.; Shahfahad; Talukdar, S.; Ishtiaq, M.; Rahman, A. Modelling built-up land expansion probability using the integrated fuzzy logic and coupling coordination degree model. *J. Environ. Manag.* **2023**, *325*, 17. [CrossRef] [PubMed]

51. Chen, Q.; Chen, W.X.; Wu, D.; Zheng, L.; Li, J.F. Spatiotemporal evolution and influencing factors of tourism development efficiency in the Yangtze River Economic Belt, China. *J. Clean. Prod.* **2022**, *379*, 11. [CrossRef]

52. Xu, M.X.; Hu, W.Q. A research on coordination between economy, society and environment in China: A case study of Jiangsu. *J. Clean. Prod.* **2020**, *258*, 10. [CrossRef]

53. Geng, Y.Q.; Wei, Z.J.; Zhang, H.; Maimaituerxun, M. Analysis and Prediction of the Coupling Coordination Relationship between Tourism and Air Environment: Yangtze River Economic Zone in China as Example. *Discret. Dyn. Nat. Soc.* **2020**, *2020*, 15. [CrossRef]

54. Liu, X.L.; Vu, D.; Perera, S.C.; Wang, G.F.; Xiong, R. Nexus between water-energy-carbon footprint network: Multiregional input-output and coupling coordination degree analysis. *J. Clean. Prod.* **2023**, *430*, 13. [CrossRef]

55. Song, Y.Z.; Wang, J.F.; Ge, Y.; Xu, C.D. An optimal parameters-based geographical detector model enhances geographic characteristics of explanatory variables for spatial heterogeneity analysis: Cases with different types of spatial data. *GISci. Remote Sens.* **2020**, *57*, 593–610. [CrossRef]

56. Wang, J.F.; Hu, Y. Environmental health risk detection with GeogDetector. *Environ. Modell. Softw.* **2012**, *33*, 114–115. [CrossRef]

57. Qiao, P.W.; Yang, S.C.; Lei, M.; Chen, T.B.; Dong, N. Quantitative analysis of the factors influencing spatial distribution of soil heavy metals based on geographical detector. *Sci. Total Environ.* **2019**, *664*, 392–413. [CrossRef] [PubMed]

58. Luo, G.W.; Ye, J.Y.; Wang, J.F.; Wei, Y. Urban Functional Zone Classification Based on POI Data and Machine Learning. *Sustainability* **2023**, *15*, 4631. [CrossRef]

59. Wang, H.Y.; Qin, F.; Xu, C.D.; Li, B.; Guo, L.P.; Wang, Z. Evaluating the suitability of urban development land with a Geodetector. *Ecol. Indic.* **2021**, *123*, 13. [CrossRef]
60. D'Agata, A.; Alaimo, L.S.; Cudlín, P.; Salvati, L. Easy come, easy go: Short-term land-use dynamics vis a vis regional economic downturns. *Socio-Econ. Plan. Sci.* **2023**, *88*, 10. [CrossRef]

MDPI

MDPI